SINGLE-SITE MOLYBDENUM(IV) MEDIATED BOND CLEAVAGE REACTIONS AND LIGAND PARAMETERIZATION USING A CR(VI) NITRIDO PLATFORM

By

Stephen Andrew DiFranco

A DISSERTATION

Submitted to
Michigan State University
in partial fulfillment of the requirements
for the degree of

Chemistry-Doctor of Philosophy

2013

ABSTRACT

SINGLE-SITE MOLYBDENUM(IV) MEDIATED BOND CLEAVAGE REACTIONS AND LIGAND PARAMETERIZATION USING A CR(VI) NITRIDO PLATFORM

By

Stephen Andrew DiFranco

The following pages comprise various studies in the area of organometallic chemistry of the transition metals and may be separated into two main projects; exploration of novel molybdenum(IV) bispyrrolide complexes with implications toward the mechanism(s) of catalytic dinitrogen fixation, and electronic and steric parameterization of ligands using a chromium(VI) nitride complexes.

Chapter 1 discusses a novel $2e^-$ reduction the N-N bond in disubstuted hydrazines that proceeds via a Mo-hydrazido(1-) moetiy to produce a Mo(VI) nitride and a free secondary amine from N-N bond cleavage. Kinetic studies on this and an analogous Zr(IV) system are presented. The related N-O bond cleavage of *o*-benzyl hydrazine is also reported. Such single-site bond cleavage reactions may be operative in the enzymatic reduction of dinitrogen, and my find use in future catalytic systems toward the same end. Chapter 2 focuses on the reactivity of the same molybdenum(IV) bispyrrolide with alcohols, giving either mono or multiple substitutions resulting in Mo(IV) alkoxides, or radical C-O bond cleavage commensurate with Mo(VI) bisoxo and C-C bond formation. Additional reactivity and structural studies of molybdenum(IV) bispyrrolides are presented in Chapter 3.

Chapter 4 presents the synthesis of 28 new chromium nitride complexes of the form $NCr(NPr^i_2)_2X$ where X is a halide or anionic ligand bound through O, N or S. A method for

using Spin Saturation Magnetization Transfer to measure the kinetics of diisopropylamide rotation is discussed. These barriers of rotation are indicative of the donor ability of the X ligand, and have been reported as the Ligand Donor Parameter (LDP) of each compound. Structural analysis is included of each compound, as it steric analysis using two different systems. Additionally, correlations to Hammett parameters, pK_a's, ^{13}C NMR data, electronic spectra, and the angular overlap model are presented. Chapter 5 explores similar $NCr(NPr^i_2)_2X$ compounds where X is cyclopentadienyl and related compounds. Further substitution induces a hapticity shift in the bound Cp. Chapter 6 presents a new set of compounds based on the $NCr(NPr^i_2)_2X$ platform where X is an organometallic ligand bound through carbon. Synthesis, structures, LDP's and steric analysis are presented. Chapter 7 discusses synthesis of cationic Cr(VI) nitridos of the form $[NCr(NPr^i_2)_2L][A]$ where L is a neutral $2e^-$ donor and A is a weakly coordinating anion. LDP's and a correction for anion effects are presented. Temperature dependent equilibrium in cation formation is reported. Structural and steric analysis of many of the compounds are included. Chapter 8 focuses on the synthesis and structure of a 3-ferrocenyl substituted pyrrolide ligand. Structural, steric and LDP analysis is discussed.

In total a series of 58 ligands bound through O, N, P, S and C and halides have been parameterized via the LDP methodology. This list spans both neutral and anionic ligands. Crystal structures and steric analysis for many of these are included as to comprise a comprehensive map of ligation toward transition metals.

ACKNOWLEDGEMENTS

While the following gives an account of the scientific progress made during my tenure at Michigan State University I would find it incomplete without dedicating at least a few pages to those that helped make it all possible. I would like to start by thanking my family. Their love and encouragement throughout the years has allowed me to go places and do things I never thought I could. I just hope that I can pay dividends on their investment in my future.

Next, I would like to thank Dr. Brenna Flannery for her love and support, and being my best friend and sounding board throughout this process.

I would like to thank my advisor, Aaron Odom for giving me a great opportunity to join his lab and explore my passion for chemistry. The lessons learned in his lab are invaluable to my past and future successes. His patience and guidance will not soon be forgotten.

Likewise, I would like to thank those who served on my committee, Prof. Jim McCusker, Prof. Babak Borhan, Prof. Mitch Smith, and Prof. Viktor Poltavets, for their continuing guidance, support and providing me perspective throughout my graduate career.

I am indebted to the Odom lab members who have come before me; Bala Kapil, Doug, Supriyo, Eyal, and Sam. You have taught me to think and act like a scientist. A large thank you to Amila and Nick for being such wonderful colleagues. I will miss your companionship and the long hours together in the lab. I also wish to thank Medha and other students from around the department, especially the McCusker and Poltavets lab members.

I would like to acknowledge the role of the support staff in the Department of Chemistry for their technical assistance, especially that of Dr. Dan Holmes and Kermit Johnson who were vital to the success of the LDP project.

Lastly, I would like to thank Dr. Richard Staples for the many hours spent together in the XRD lab. The technical support you have provided me is secondary only to mentorship you offer. In the words of our craft—without you I would have crashed from solution long ago.

–Steve.

TABLE OF CONTENTS

LIST OF TABLES

LIST OF FIGURES

LIST OF SCHEMES

LIST OF ABBREVIATIONS

$\%V_{bur}$	Percent Buried Volume
anth	2-anthrycenyl
AOM	Angular Overlap Model
BOC	*tert*-butyloxycarbonyl
CC^tBu	3,3-dimethylbut-1-yn-1-ide
$CCSi(Pr^i_3)$	(triisopropylsilyl)ethyn-1-ide
COD	1,5-cyclooctadiene
Cp	cyclopentadienyl
BAr^F_4	tetrakis(3,5-bis(trifluoromethyl)phenyl)borate
d	day
DBN	1,5-diazabicyclo[4.3.0]non-5-ene
dip	2,6-diisopropylphenyl
DMAP	4-dimethylaminopyridine
DME	dimethoxyethane
DMSO	dimethyl sulfoxide
Fc	ferrocenyl
GC	Gas Chromatograph
Flu	fluorenyl
$G_m(L)$	Solid angle
h	hour
H_2dpma	N-((1H-pyrrol-2-yl)methyl)-N-methyl-1-(1H-pyrrol-2-yl)methanamine
H_2dpmames	1-(5-mesityl-1H-pyrrol-2-yl)-N-((5-mesityl-1H-pyrrol-2-yl)methyl)-N-methylmethanamine
HMPA	hexamethylphosphoramide

ind	indenyl
LDP	Ligand Donor Parameter
NHC	1,3-dimethylimidazol-3-ium-2-ide
min	minute
mes	mesityl
NMR	Nuclear Magnetic Resonance
NPr^{i}_{2}	diisopropylamide
Ad	1-adamantyl
Bn	benzyl
OBu^{t}_{F6}	1,1,1,3,3,3-hexafluoro-2-methylpropan-2-olate
OPht	1,3-dioxoisoindolin-2-olate
OTf	trifluoromethanesulfonate
Pyr	pyrrolyl
Pyr^{C6F5}	3-(perfluorophenyl)pyrrol-1-ide
$Pyr^{C6H3(CF3)2}$	3-(3,5-bis(trifluoromethyl)phenyl)pyrrol-1-ide
Pyr^{Fc}	3-ferrocenyl pyrrolyl
$PzB(Et)_3$	2-(triethylboranyl)--pyrazolyl
quin	quinuclidine
SST or SSMT	Spin Saturation Magnetization Transfer
$^{t}BuNC$	2-isocyano-2-methylpropane
THF	tetrahydrofuran
tol	tolyl

Chapter 1: Single-Site N–N Bond Cleavage by Mo(IV) to Produce a Terminal Nitrido

ABSTRACT

$Mo(NMe_2)_4$ and the tridentate, dipyrrolyl ligand H_2dpma^{mes} were found to form 5-coordinate $Mo(NMe_2)_2(dpma^{mes})$ (**1**), which exhibits spin-crossover behaviour in solution. The complex is a ground state singlet with a barrier of 1150 cm^{-1} for production of the triplet in d_8-toluene. The complex reacts with 1,1-disubstituted hydrazines or *O*-benzylhydroxylamine to produce nitrido $MoN(NMe_2)(dpma^{mes})$. The mechanism of the 1,1-dimethylhydrazine reaction with **1** was examined along with the mechanism of substitution of NMe_2 with H_2NNMe_2 in a diamagnetic zirconium analogue. The proposed mechanism involves production of a hydrazido(1–) intermediate, $Mo(NMe_2)(NHNMe_2)(dpma^{mes})$, which undergoes an α,β-proton shift and N–N bond cleavage with metal oxidation to form the nitrido. This conversion from hydrazido(1–) to nitrido is less discussed in the dinitrogen activation literature but is somewhat analogous to the proposed mechanism for O–O bond cleavage in some peroxidases.

1. 1 Introduction

The reduction of dinitrogen is arguably one of the most important reactions ever discovered[1] and is the starting point for the production of the vast majority of nitrogen-containing compounds with applications from fertilizers to pharmaceuticals. In accordance with the importance of the reaction, numerous studies have been carried out on the biological systems responsible (nitrogenases),[2] the industrial process[3] for production of ammonia (Haber-Bosch), and other systems capable of nitrogen reduction.[1]

The naturally occurring systems can, but do not always, contain molybdenum in the active site of the cofactor but do include an iron-sulfur cluster.[4]

The mechanism of the N–N cleavage has been divided into two general forms depending largely on the sites of protonation, which have been dubbed the distal and alternating mechanisms. In Scheme 1.1 are some of the steps commonly attributed to these cycles.[5]

Frequently in molybdenum- and tungsten-based systems, the cleavage of the nitrogen-nitrogen single bond required in these reactions is proposed to occur through a hydrazido(2–)[6] intermediate that becomes protonated to an ammonium imido (hydrazidium) complex (Distal Cycle of Scheme 1.1). If the metal center has the two electrons required for N–N bond cleavage, this can occur through simple N–N bond scission in Mo(IV) and W(IV) hydrazidium intermediates.

Conversely, some molecular iron-based systems for nitrogen reduction often have been suggested to proceed through diazene intermediates (Alternating Cycle of Scheme 1.1).[7]

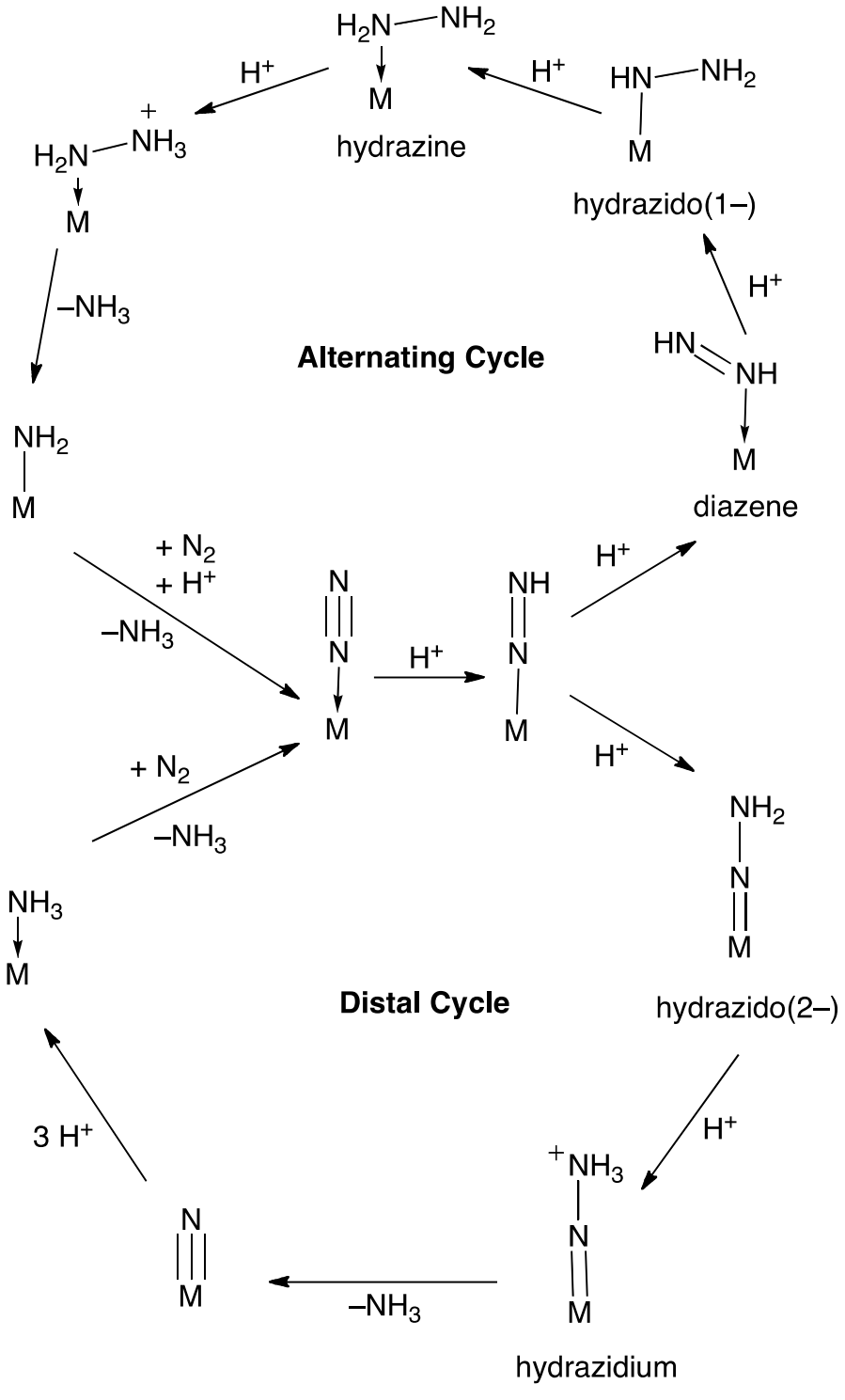

Scheme 1.1: Two catalytic cycles often discussed for N–N bond cleavage. The exact steps for electron transfer are left ambiguous.

In this report, we demonstrate facile single-site cleavage of an N–N bond through

production of a Mo(IV) hydrazido(1–). The data suggest that molybdenum systems can proceed from hydrazido(1–) to nitrido without the intermediacy of a hydrazido(2–) by way of α,β-proton migration. Consequently, pathways that include complexed diazene,[8] hydrazido(1–), and nitrido without the intermediacy of hydrazido(2–) appear to be viable for Mo-based N–N bond cleavage.

1.2 Synthesis and Characterization of Compounds

The ancillary ligand chosen was a sterically more substantial version of the pyrrole-based *N*,*N*-di(pyrroyl-α-methyl)-*N*-methylamine, dpma, which we have employed in several catalytic and stiochiometric studies previously.[9] For this chemistry, mesityl groups were installed[10] into the remaining α-positions of the pyrroles. The synthesis of the new ligand, H_2dpma^{mes}, is shown in Figure 1.1 along with the synthesis and structure of the molybdenum dimethylamido derivative prepared by transamination on $Mo(NMe_2)_4$.[11]

The structure of 5-coordinate **1** is very nearly halfway between trigonal bipyramidal (tbp) and square pyramidal (sp). The largest angle subtended at molybdenum is 164.9(1)° (α) for N3-Mo1-N5 and the second largest is 129.1(1)° (β) for N1-Mo1-N2. The value for τ from τ = (α – β)/60 = 0.60, where a value of 1 is for tbp and a value of 0 is for sp.[12]

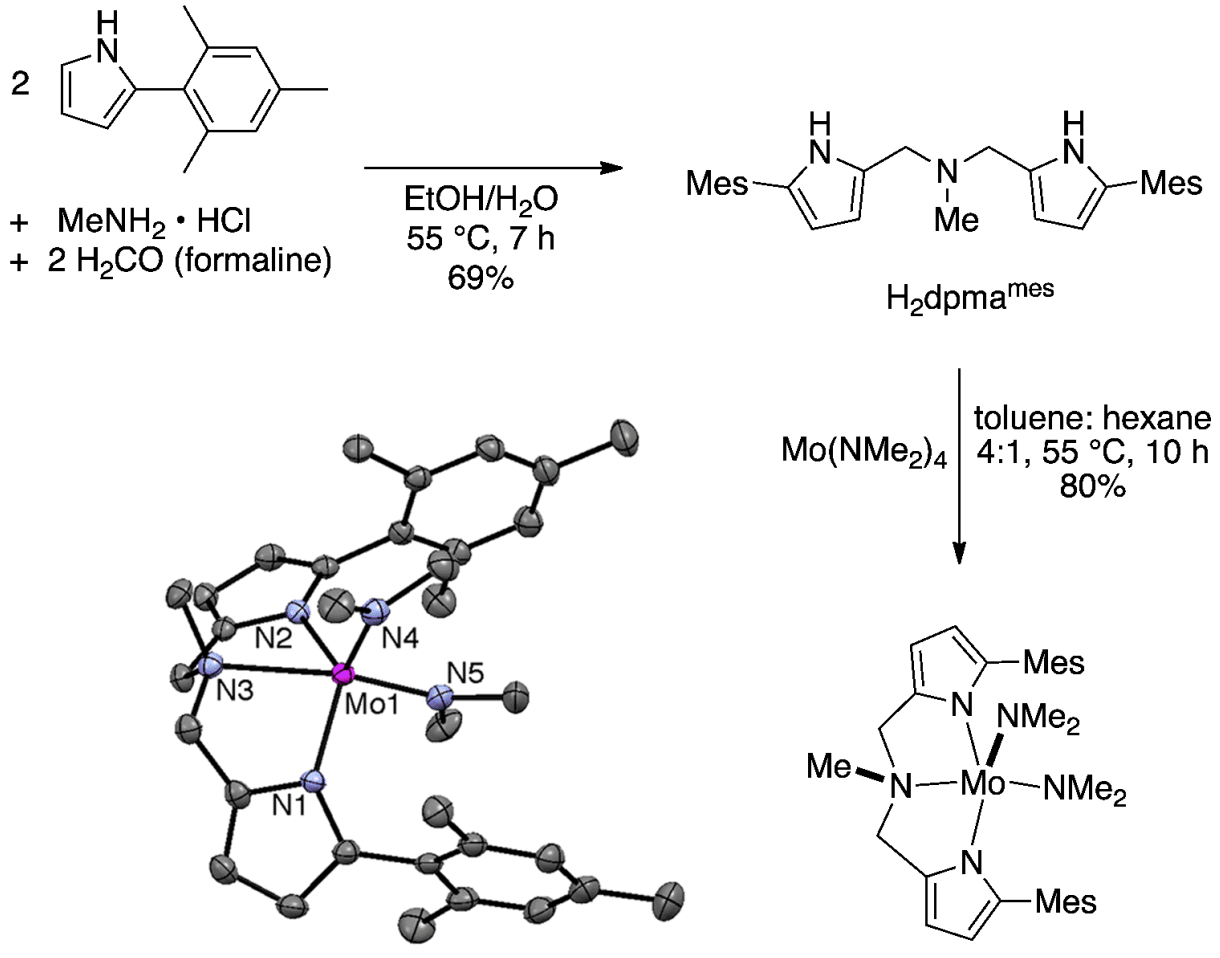

Figure 1.1: Synthesis and structure of $Mo(NMe_2)_2(dpma^{mes})$ (**1**). Hydrogens and a toluene solvent molecule found in the lattice are omitted from the structure. For interpretation of the references to color in this and all other figures, the reader is referred to the electronic version of this dissertation.

Due to weaker donation of the pyrroles to the Mo center relative to the dimethylamidos,[13] metal–N(pyrrole) distances are usually significantly longer than metal–NMe_2 distances, and that is the case here. The average Mo–N(pyrrole) distance in the structure was determined to be 2.091(2) Å. The average Mo–NMe_2 distance was 1.917(2) Å. The much weaker donor nitrogen of the $dpma^{mes}$ had an Mo(1)-N(3) distance of 2.401(2) Å.

Magnetic susceptibility measurements in solution (Evan's method at 29.7 °C in d_8-toluene)[14] provided a μ_{eff} = 1.18 μ_B, well below the spin-only moment for high-spin d^2 of 2.87 μ_B and well below the value for the high spin *tert*-butylisonitrile adduct of the same compound **1**•$CNBu^t$ (vide infra). SQUID magnetometry on **1** in the solid state suggests the compound is a ground-state singlet. Even at room temperature, the compound exhibited no detectable paramagnetism as a solid. This suggests that the compound has a thermally accessible triplet state in solution but not in the solid state, likely because an isomerization is required to access the higher spin state.

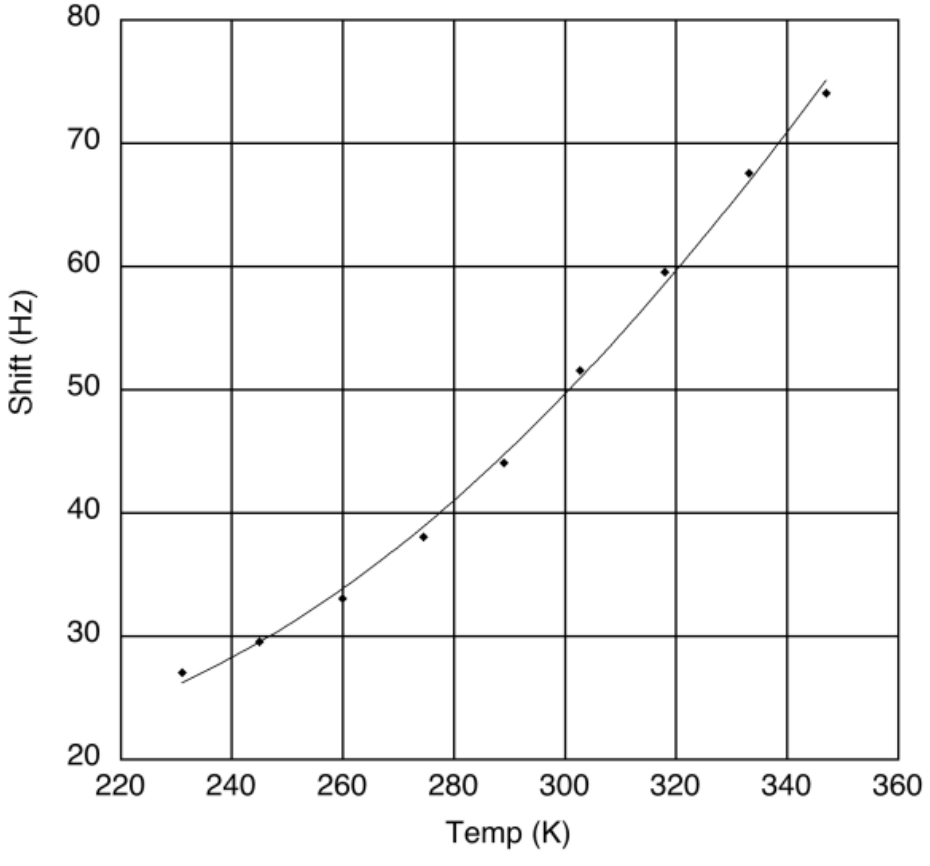

Figure 1.2: Fit of the Me_3SiPh methyl group chemical shifts to Equation 1. The values for the fit parameters are C = $(2.31 \pm 0.61)\times10^6$, $\Delta G = 3278 \pm 202$ cal/mol, and $\delta' = 18.3 \pm 2.0$ Hz.

Examination of the magnetism in solution was done over the accessible temperature range (~230-350 K), bound on the lower end by the solubility of the compound and on the higher end by its stability in solution. The data were fit using the expression of Gütlich and coworkers (Eqn. 1).[15] In our case, none of the resonances in the ^{1}H NMR could be followed over the entire temperature range due to broadening. Consequently, we used an internal standard of $PhSiMe_3$ in the solution with a capillary containing d_8-toluene and reference $PhSiMe_3$ to follow the contact shift due to the paramagnetic species.

$$\delta = \frac{C}{T\left(1+e^{\Delta G_{SC}/RT}\right)} + \delta' \quad (1)$$

The value δ is the difference in ppm between the chemical shift of the methyl groups in the $PhSiMe_3$ reference (inside the capillary) and $PhSiMe_3$ in solution with **1**. In Eqn 1, C is a constant, T is the temperature in Kelvin, and R is the Gas Constant. In this case ΔG_{SC}, the free energy associated with the spin crossover may contain components associated with the unidentified isomerization.

Fitting the data to this equation gives the plot shown in Figure 1.2. From the fit, ΔG_{SC} = 3.3 kcal/mol (1150 cm^{-1}). This is similar to values reported by Rothwell and coworkers for a large series of W(IV) complexes that exhibited spin crossover in solution.[16] For these cyclometallated 2,6-diphenylphenol compounds, $W(OC_6H_3Ph\text{-}C_6H_4\text{-})_2L_2$, the energy difference varied from 358-1205 cm^{-1}, where L was a host of different pyridine derivatives. Similarly, Schrock and co-workers have reported singlet-triplet spin crossover for the Mo(IV) species $[(Me_3SiNCH_2CH_2)_3N]MoNMe_2$.[17] The ΔG_{SC} value reported for this related system was ~1800

cm^{-1} based on reported enthalpy and entropy values.

Interestingly, there are now three different magnetic behaviours for reported Mo(IV) bis(dimethylamido) complexes bearing derivatives of the dpma ligand. In our paper using the less substituted pyrrolyl-based ligand,[18] 6-coordinate $Mo(NMe_2)_2(HNMe_2)$(dpma) was reported as a paramagnetic complex with a magnetic moment close to the spin-only value for two unpaired electrons. For this study, we confirmed that measurement on a freshly prepared sample; the value for this Mo(IV) 6-coordinate compound was found to be 2.48-2.40 μ_B from 210-300 K. Schrock and coworkers recently reported a related 5-coordinate compound $Mo(NMe_2)_2(tpa^{Ar})$, where tpa^{Ar} = tris[2-(3,5-trifluoromethylphenyl)pyrrolylmethyl)amine.[19] In this compound, which is structurally similar to **1**, two pyrrolyl substituents are bound to the metal center and the third is a "dangling" *NH*-pyrrole group. Interestingly, this compound is reported to have a mixture of broad and sharp lines in the NMR that were "slightly paramagnetically shifted". Consequently, this complex, contrary to **1**, seems to have a preponderance of the singlet complex in solution. In this report, **1** is a spin-crossover compound in solution and apparently diamagnetic in the solid state.

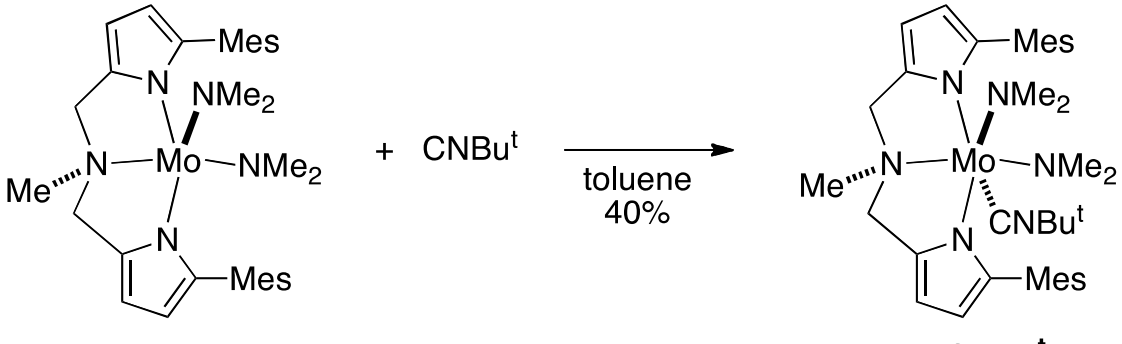

1 **1•CNBu^t**

Figure 1.3: Synthesis **1•**$CNBu^t$,of the tert-butylisonitrile adduct of **1.**

To examine the relationship between the electronic structure of **1** and its coordination number further, we prepared (Equation 1.3) the *tert*-butylisonitrile adduct $Mo(NMe_2)_2(CNBu^t)(dpma^{mes})$ (**1**•$CNBu^t$). This adduct is quite similar structurally to **1** with the $CNBu^t$ ligand *trans* to one of the dimethylamido ligands and with the donor amine of the $dpma^{mes}$ *trans* to the other NMe_2 group. The complex is high spin with $\mu_{eff} = 2.47\ \mu_B$ like the previously reported 6-coordinate $Mo(NHMe_2)(NMe_2)_2$(dpma). The isonitrile adduct of **1** was also structurally characterized (See the Appendix A for details).

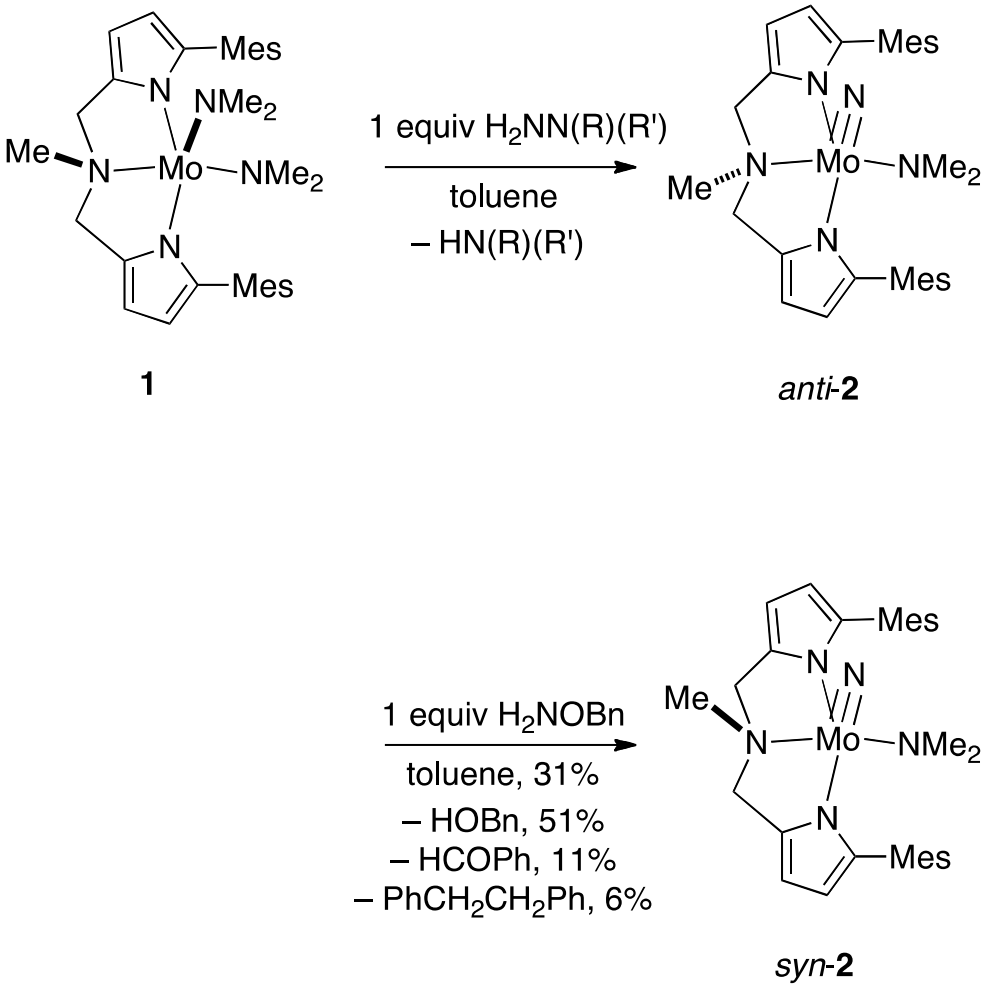

Scheme 1.2: Synthesis of *anti*-**2** and *syn*-**2** by N–N or N–O bond cleavage with isolated yields for the complexes. See Table 1.2 for hydrazines and yields of *anti*-**2**. Yields of by-products in the *O*-benzylhydroxylamine reaction are by GC-FID.

In an attempt to prepare the Mo(IV) terminal hydrazido(2–) complex, dimethylhydrazine was added to **1**. A diamagnetic product was obtained, the nitrido complex *anti*-Mo(N)(NMe_2)($dpma^{mes}$) (*anti*-**2**) shown in Scheme 1.2. The product has the nitrido nitrogen and methyl of the $dpma^{mes}$ ligand on opposite sides of the plane defined by the Mo–N1(pyrrolyl)–N2(pyrrolyl) atoms. The yield of *anti*-**2** in this reaction by ^{1}H NMR was 75%, and the isolated yield was 74% (Table 1.1).

The structure of *anti*-**2** is shown in Figure 1.4 (top). The structure of the Mo(VI) nitrido is best approximated as square pyramidal ($\tau = 0.02$).

The expectation in proceeding from the formally Mo(IV) complex **1** to the Mo(VI) complex **2** is that the bond distances should shorten. However, the Mo1-N(pyrrolyl) average distance in **2** is 2.127(3) Å, slightly longer than the 2.091(2) Å found in **1**. This lengthening of the pyrrolyl distance in **2** vs **1** may be due to the rigidity of the $dpma^{mes}$ ligand in this square planar derivative and the widening of the N(pyrrolyl)–Mo–N(pyrrolyl) angle from 129.06(7)° in **1** to 145.0(1)° in *anti*-**2**. The Mo1-N3(donor amine) distance in higher valent **2** was found to be 2.274(3) Å, whereas in **1** it was a much longer 2.401(2) Å. The Mo1-NMe_2 distance in **2** is 1.906(3) Å, which is not statistically different from the 1.917(2) Å average distance in **1**. The Mo–N(nitrido) distance in **2** was found to be 1.647(3) Å.

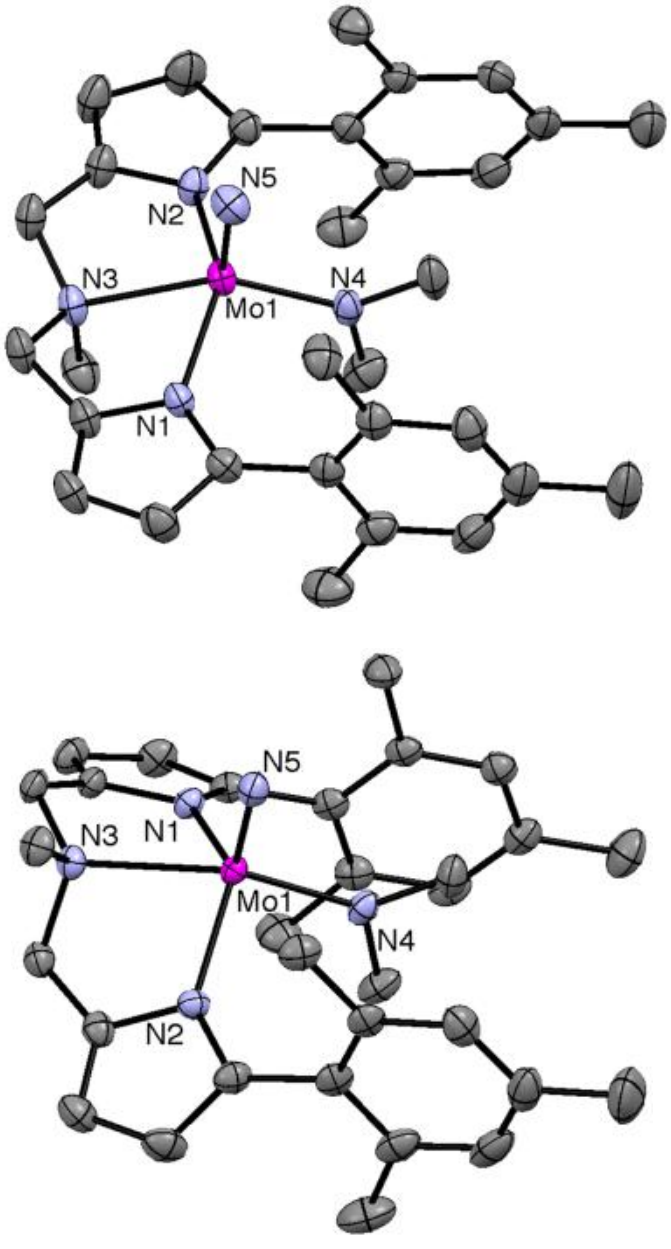

Figure 1.4: ORTEP diagram at the 50% probability level for the structures of *anti*-Mo(N)(NMe_2)($dpma^{mes}$) (*anti*-**2**, top) and *syn*-Mo(N)(NMe_2)($dpma^{mes}$) (*syn*-**2**, bottom) as determined by single crystal X-ray diffraction. H-atoms omitted.

Other 1,1-disubstituted hydrazines react with **1** to give the same product (Scheme 1.2 and Table 1.1). Consequently, only one dimethylamido in **1** is involved in the production of the nitrido.

Addition of *O*-benzylhydroxylamine (Scheme 1.2) led to formation of the *syn*-isomer of **2**, where the amine donor methyl of the $dpma^{mes}$ and nitrido nitrogen are on the same side of the Mo–N1(pyrrolyl)–N2(pyrrolyl) plane. The isomer *syn*-**2** was isolated in 31% yield. Also found in the reaction mixture were benzyl alcohol (51% yield), benzaldehyde (11% yield), and 1,2-diphenylethane (6% yield), where the yields are relative to internal standard (dodecane) from GC-FID.

The *syn*-isomer also was structurally characterized (Figure 1.4 bottom). The structure of *syn*-**2** is, like the structure of **1**, in between sp and tbp with $\tau = 0.61$. The Mo–N(pyrrolyl) and Mo–NMe_2 distances in *syn*-**2** are the same within error as in **1**. The Mo1–N3(donor) and Mo1–N5(nitrido) distances are the same as in *anti*-**2**.

Substrate (H_2NX)	%Yield of **2**[a] (^{1}H NMR)	By-product %Yield HX (GC-FID)	k_{obs} ($M^{-1}s^{-1}\bullet10^{-3}$)[c]
H_2NNMe_2	75	–[b]	873 ± 5
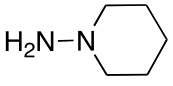	18	31	684 ± 2
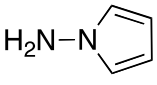	81	–[b]	146.8 ± 0.1
$H_2NN(Ph)Me$	82	91	135.8 ± 0.2
H_2NNPh_2	76	98	21.1 ± 0.1
H_2NOBn	31	51[e]	–[d]

[a]The product is **2**-*anti* except for the reaction with H_2NOBn which gave **2**-*syn*. [b]By-product yield was not determined. [c]Errors are from the fits and then propagated through the equations. [d]Reaction was too fast to measure using the methods employed here. [e]Yield given is for benzyl alcohol, but 3 by-products were identified.

Table 1.1: Rates and yields of the reactions of various substrates with 1 to form 2.

A computational study was carried out on the two isomers using Density Functional Theory with the LANL2DZ basis set as implemented in Gaussian09.[20] The difference in energy (ΔH) between the *syn* and *anti* derivatives was found to be extremely small with *syn*-**2** being more stable than *anti* by 2 kcal/mol using B3LYP as the functional. Using B3PW91 as the functional a similar value of 2 kcal/mol was found with *syn* more stable than *anti*.

Experimentally, heating *syn*-**2** in toluene at 100 °C for 24 h led to some conversion to the *anti*-**2** isomer (see Appendix A for more details); however, the conversion did not continue to completion and some decomposition also occurred. Only about 9% *anti* was produced during the heating of the *syn* isomer. Alternatively, heating *anti*-**2** did not result in detectable (^{1}H NMR) amounts of *syn*-**2**; only decomposition was observed. It seems that the energies of the isomers are very comparable but kinetic barriers hamper the equilibrium. The isomer, *syn* or *anti*, produced in the reaction of **1** and hydrazine or hydroxylamine is determined kinetically.

Since the hydrazido(1–) derivatives are unstable intermediates in the case of Mo(IV), in order to examine their structure, we prepared the Zr(IV) analogues where no bond cleavage can occur. The zirconium bis(dimethylamido) complex $Zr(NMe_2)_2(dpma^{mes})$ (**3**) is cleanly produced by addition of H_2dpma^{mes} to $Zr(NMe_2)_4$; **3** was also structurally characterized (see Appendix A). The addition of one equivalent of H_2NNMe_2 to **3** provides mixtures of the bis(hydrazido(1–)) complex $Zr(NHNMe_2)_2(dpma^{mes})$ (**4**) and a trace of a compound not fully characterized that has a ^{1}H NMR spectrum as expected for the mono(hydrazido(1–)) complex. It appears that the second addition of hydrazine may have a similar rate constant to the first. The complex **4** was prepared cleanly by addition of 2 equivalents of the hydrazine (Figure 1.5).

1.3 Mechanistic Investigations

The reaction between molybdenum-containing **1** and hydrazines was not amenable to typical pseudo-1st order conditions for the examination of the reaction kinetics. Using either the metal complex or the hydrazine in large excess led to very low yields of the nitrido product, and we were unable to isolate and characterize the products under these conditions. However, the nitrido product does not react with excess hydrazine on the timescale of the hydrazine reactions

with **1**.

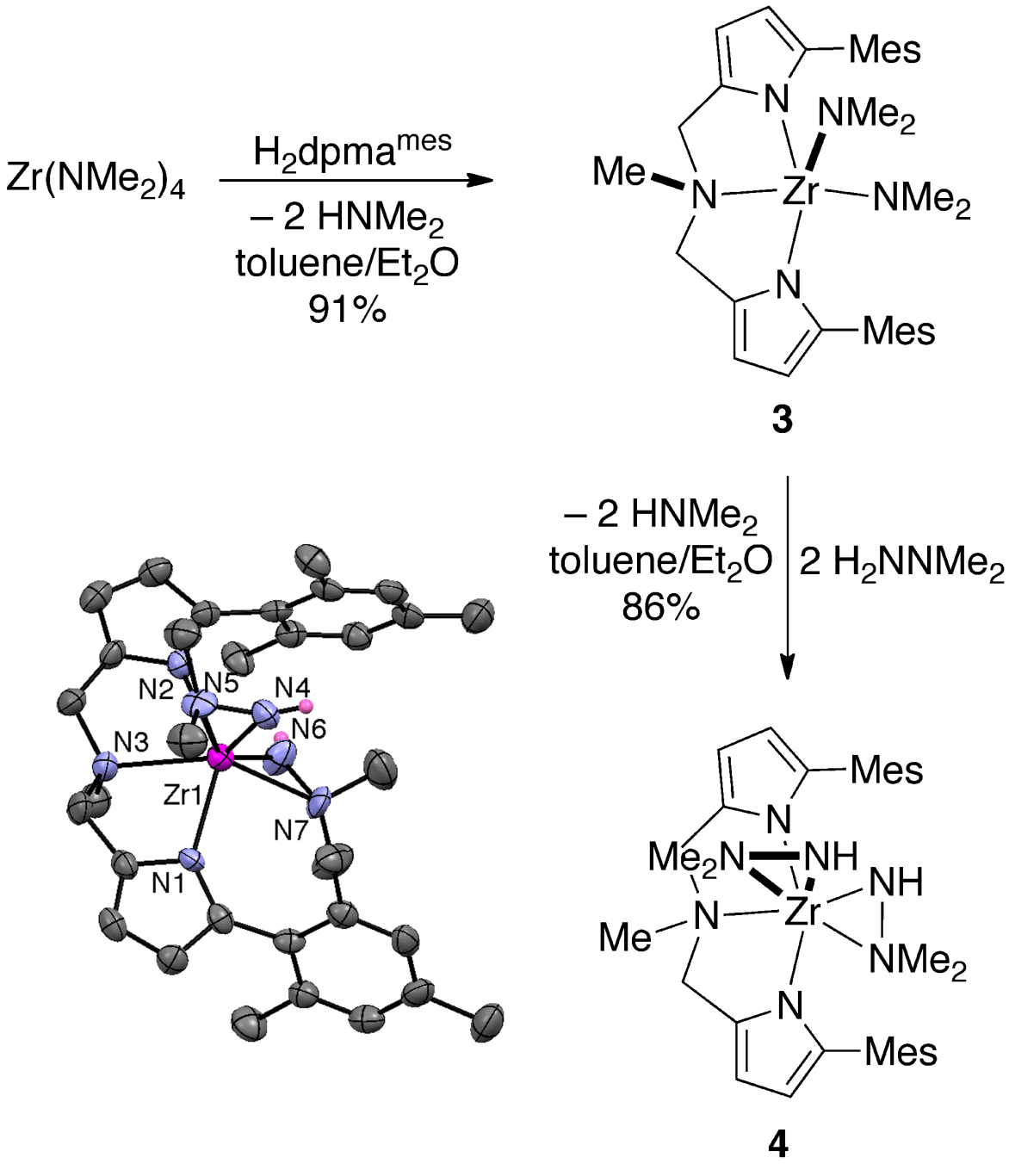

Figure 1.5: Synthetic route to the hydrazido(1–) zirconium complex **4** and ORTEP diagram at the 50% probability level for the structure of $Zr(\eta^2\text{-}NHNMe_2)_2(dpma^{mes})$ (**4**) as determined by single crystal X-ray diffraction. H-atoms (pink spheres) are omitted except on the hydrazido(1–) nitrogens N4 and N6.

Excess hydrazine or **1** in the N–N cleavage reactions leads to unidentified by-product formation; however, we were able to vary the hydrazine concentrations and examine initial rates for the loss of **1**. These experiments suggest a 1^{st} order dependence on hydrazine concentration. Similar initial rate experiments changing metal concentration suggest a 1^{st} order dependence on the concentration of **1**.

Kinetics using 1:1 hydrazine to **1** provided clean second order behaviour. Considering the 1^{st} order dependence of the reaction on hydrazine, 1^{st} order dependence on **1**, and 2^{nd} order dependence overall, the rate law is assigned as $-d[\mathbf{1}]/dt = k_{obs}[\mathbf{1}][\text{dimethylhydrazine}]$.

The reaction to form **2** was carried out with a variety of different substrates (Table 1.1). With all the hydrazine derivatives investigated, *anti*-**2** was the product. There was a dramatic affect of the substituents on the rate of nitrido formation; however, the cause of that dependence seems complex and is likely due to a mixture of factors including sterics constraints of the incoming reactant. Reactions with all of the hydrazines were followed by UV-Vis absorption spectroscopy and fit 2^{nd} order kinetics.

Using the G3 method[21] implemented in Gaussian09, we calculated the Bond Dissociation Enthalpies (BDEs) associated with some of the substrates in Table 1.1. The BDE of Me_2NNH_2 for the N–N bond was calculated as 60.2 kcal/mol, whereas the experimental BDE for this compound is 59.0 ± 2.[22] The N–N and N–O BDEs for *N*-aminopyrrole and H_2NOMe (as a model for H_2NOCH_2Ph) were calculated as 34.9 and 54.4 kcal/mol, respectively. As a result, it appears that the rate of bond cleavage is not correlated with the N–N or N–O BDE.

The only species observed by UV-Vis absorption spectroscopy for all of the hydrazine

substrates, except *N*-aminopiperidine, over the course of the reactions are the starting material **1** and the product **2**. These reactions show a clean isosbestic point (see Appendix A). However, the reaction with *N*-aminopiperidine is complicated by reactions of the piperidine by-product with starting material, which is likely the cause of the low yields for this particular substrate. All other by-products do not react on the timescales of nitrido formation with either the starting material or product.

No product inhibition was found for the hydrazine reactions except for addition of piperidine to reactions of *N*-aminopiperidine with **1**. Other by-products were tested with up to 10 equivalents of the corresponding amine and gave the same rate constant for disappearance of **1** and provided clean formation of **2**.

The reaction with *O*-benzylhydroxylamine liberates benzyl alcohol as the by-product. The nitrido product **2** does not react with benzyl alcohol. The starting material **1** does react rapidly with benzyl alcohol using a radical pathway.[22]

We examined the temperature behaviour of the rate of 1,1-dimethylhydrazine reactions with **1**. An Eyring plot of $\ln(k_{obs}/T)$ vs 1/T was linear and provided $\Delta H^{\ddagger} = +7$ kcal/mol and $\Delta S^{\ddagger} = -35$ cal/mol•K. These parameters are consistent with a very modest enthalpic barrier and a very ordered activated complex. The parameters are similar to many known activation parameters for ligand additions to metal complexes.[23]

The data above did not conclusively identify the rate-determining step in the reaction. In order to further investigate the NMe_2 for $NHNMe_2$ exchange as a possible rate-determining step, we used the zirconium complex **3** and its reaction with H_2NNMe_2 as a model. The reaction between **3** and two equivalents of dimethylhydrazine was followed by ^{1}H NMR and showed

second-order kinetics like its molybdenum analogue. Examination of the second order rate constant versus temperature for the zirconium reaction gave activation parameters, $\Delta H^{\ddagger}$ = +6.4 kcal/mol and $\Delta S^{\ddagger}$ = –45 cal/mol•K, similar to the molybdenum system.

We propose that the rate-determining step in the hydrazine reaction with **1** is the dimethylamido substitution step. In zirconium-containing **3**, the second replacement of NMe_2 has a similar rate as the first replacement with dimethylhydrazine (vide supra). A second NMe_2 replacement is not observed in the reaction with the molybdenum(IV) analogue. Since the N–N bond cleavage in the reaction of **1** with dimethylhydrazine would then be faster than the substitution of dimethylamido, reaction of the first equivalent of dimethylhydrazine with **1** gives the mono(dimethylamido) complex **2**. The nitrido **2** is then inert to NMe_2 replacement by dimethylhydrazine. In other words, the unimolecular N–N bond cleavage occurs much faster than the bimolecular reaction of hydrazine and the unobserved hydrazido(1–) intermediate $Mo(NHNMe_2)(NMe_2)(dpma^{mes})$.

In light of the data above, we propose the N–N cleavage mechanism illustrated in Scheme 1.3. (For discussions of alternative mechanisms see Appendix A.) One of the dimethylamido ligands in **1** is protolytically replaced with a hydrazido(1–) ligand. We speculate that the unobserved hydrazine adduct **A** adopts a geometry reminiscent of previously reported[18] $Mo(NMe_2)_2(NHMe_2)(dpma)$ where the donor nitrogen of $NHMe_2$ is *trans* to the donor nitrogen of the dpma ancillary.

It appears that it is this bimolecular coordination of the hydrazine (or hydroxylamine) derivative to the metal that is rate determining. The alternative rate determining steps are proton migration (conversion from **A** to **B**) or the coordination and proton migration occurring in a

concerted fashion. We assign the RDS as the coordination based on the similarity of the activation parameters to other associative substitutions.[24]

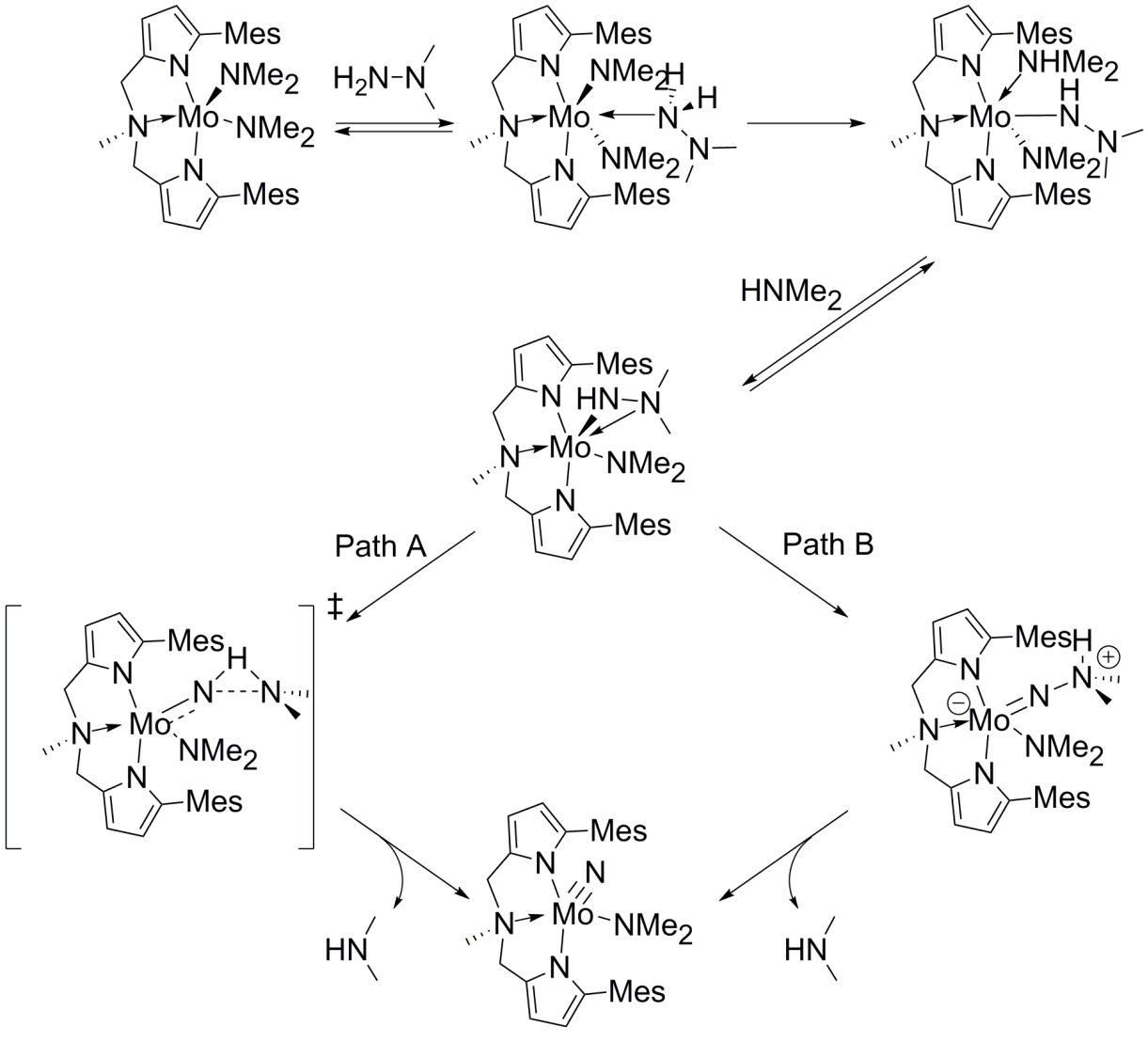

Scheme 1.3:. Proposed mechanism for the reaction of **1** with H_2NNMe_2. Mesityl groups on the dpma^{mes} ligand were omitted for clarity.

In examining various donor ligands with **1**, flat and cylindrically symmetric donors ($CNBu^t$, pyridine, DMAP, and 2-picoline) react extremely quickly with reactions being done faster than samples can be taken. Larger donors such as the hydrazone formed from benzaldehyde and 1,1-dimethylhydrazine, $Me_2NN=C(H)Ph$, reacted very slowly over the course of days as judged by disappearance of the UV-Vis bands in **1**. Again, steric constraints of the incoming donor ligand are one factor in the rate of reaction in the system.

After protolytic cleavage of a dimethylamido and dimethylamine loss, formation of the hydrazido(1–) ligand follows. The experiments with the zirconium hydrazido model suggest that the hydrazido(1–) is η^2 in this intermediate.

In the next step, the β-nitrogen of the hydrazido acts as a proton acceptor during the α,β-proton shift. The N–N bond cleavage could occur concomitant with proton migration (Path A) or through an intermediate ammonium hydrazido(2–), sometimes called a hydrazidium (Path B). (See Appendix A for additional discussion.)

The reaction mechanism proposed here is an oxidative elimination from a metal-appended nitrogen atom, where the metal is oxidized by elimination of substituents to form a metal ligand multiple bond.[i] In a process that might involve the microscopic reverse of the hydrazine cleavage reaction described, the nucleophilic addition of an amine to a nitrido with concomitant metal reduction has been reported by Meyer and coworkers.[25] In Figure 1.6 one example is shown, where tpm = tris(1-pyrazolyl)methane.[26] Several related reductive additions, where the metal center is reduced by addition of substituents to metal ligand multiple bonds have been reported.[27]

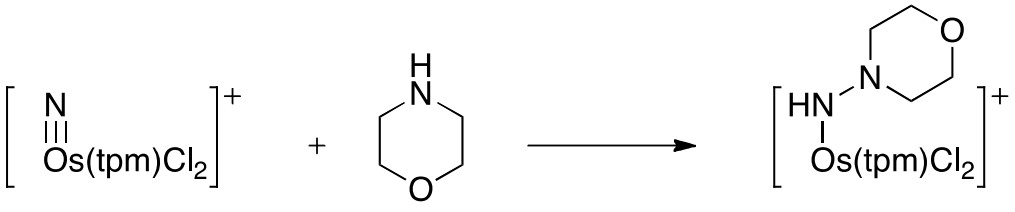

Figure 1.6: Reductive addition via nucleophilic attack of an amine on a terminal nitrido.

Whether the nitrido ends up *syn* or *anti* with respect to the methyl on the dpma^{mes} donor nitrogen may be determined by which dimethylamido is kinetically preferred for protolytic replacement in intermediate **A** of Scheme 1.3. Considering the similarity between the two dimethylamidos, we postulate that this is determined by steric interactions between the complex and hydrazine/hydroxylamine substrate leading to the difference in products observed when using hydrazines and *O*-benzylhydroxylamine. Alternatively, the sites of initial coordination for the larger H_2NNR_2 compounds could be as shown in **A**, while the smaller H_2NOBn may bind in a site similar to the isonitrile in **1•CNBu^t**, *trans* to a dimethylamido (Figure 1.3).

1.4 Conclusions

We have described a new 5-coordinate Mo(IV) complex with spin crossover behaviour in solution. The free energy barrier for the spin state change was measured as 1150 cm^{-1}. The singlet is the ground state in solution and was the only species observed in the solid, suggesting that molecular dynamics unavailable in the lattice are required for the spin equilibrium.

The Mo(IV) compound reacts in a unimolecular fashion with hydrazines and *O*-alkyl hydroxylamines to give the Mo(VI) nitrido complex, NMo(NMe$_2$)(dpma^{mes}) (**2**). Depending on the nature of the nitrogen atom donor molecule (hydrazines or *O*-benzylhydroxylamine), two different isomers of **2** were isolated, one isomer where the methyl group of the dpma^{mes} ligand is

syn to the nitrido and one where the methyl is *anti*.

We propose a mechanism where the hydrazido(1–) complex undergoes an *α,β*-proton shift either concerted with N–N bond cleavage or in a stepwise fashion with an unstable hydrazidium, ammonium hydrazido(2–), intermediate.

While the N–N cleavage mechanism proposed in Scheme 1.3 does not fall into either of the commonly discussed pathways in Scheme 1.1, there is precedent for this type of mechanism out of the peroxidase literature for O–O bond cleavage.[28] It is proposed that peroxidase uses an α,β-proton shift in a heme iron peroxide to generate a histidine-stabilized hydrogen isoperoxide complex. Cleavage of the O–O bond, which computationally occurs simultaneously with proton migration (cf. Path A in Scheme 1.3), liberates water and generates the ferryl iron(IV) with a porphyrin radical cation (Compound I).[29]

We propose a very close nitrogen analogue of the peroxidase mechanism is the low energy pathway that leads to facile N–N bond cleavage in our system and is an important possible pathway for N_2 activation in general.

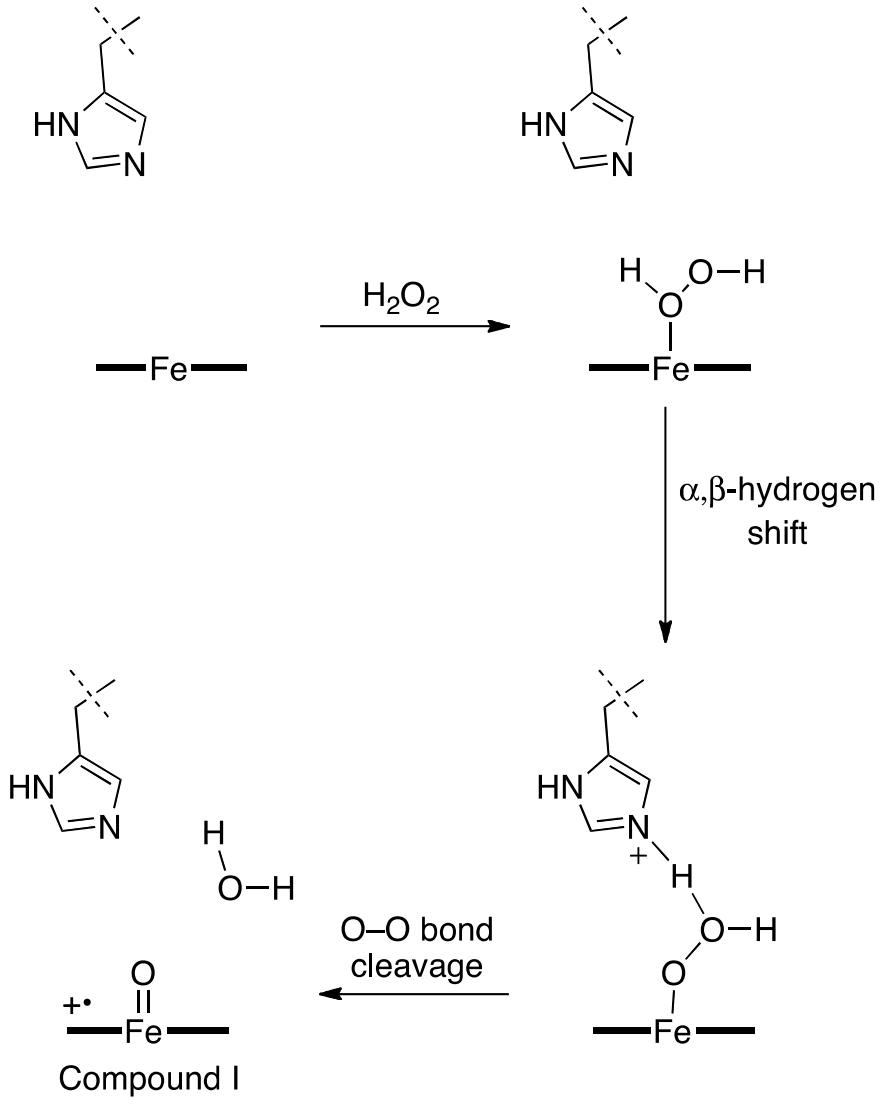

Scheme 1.4*:* Poulos-Kraut mechanism[30] for heterolytic O–O cleavage and ferryl generation in peroxidase.

1.5 Experimental

General experimental details and a more thorough discussion on how the kinetic data were collected and the results can be found in Appendix A.

H_2dpma^{mes} In a 125 mL Erlenmeyer flask methylamine hydrochloride (0.911 g, 13.5 mmol, 1 equiv.) was dissolved in formaldehyde solution (37% v/v) (2.19 g, 27.0 mmol, 2 equiv.) and

EtOH (20 mL). The solution was transferred to a 100 mL Schlenk tube, sealed, and stirred for 10 min in a 55 °C oil bath. 2-Mesitylpyrrole (5.00 g, 27.0 mmol, 2 equiv.) in EtOH (30 mL) was added to the Schlenk tube, and the headspace was evacuated. The solution continued to stir at 55 °C for 7 h, during which a white precipitate formed. The Schlenk tube was cooled to room temperature, and the precipitate was collected on a glass frit and washed with EtOH (3 × 20 mL). The solids were basified with aq. NaOH (1 M, 150 mL) and extracted with CH_2Cl_2 (3 × 100 mL). The organic layers were combined and dried under reduced pressure, yielding H_2dpma^{mes} as a white powder (3.97 g, 9.32 mmol, 69%). ^{1}H NMR (500 MHz, $CDCl_3$): 8.01 (s br, 2H, N-*H*), 6.89 (s, 4H, aromatic C-*H*), 6.07-6.05 (m, 2H, pyrrole C-*H*), 5.92-5.90 (m, 2H, pyrrole C-*H*), 3.53 (s, 4H, C*H*$_2$), 2.28 (s, 6H Ar-*p*-C*H*$_3$), 2.18 (s, 3H, NC*H*$_3$), 2.11 (s, 12H, Ar-*o*-C*H*$_3$). $^{13}C\{^1H\}$ NMR (125 MHz, $CDCl_3$): 138.3, 137.4, 130.9, 129.1, 128.0, 127.9, 108.0, 107.7, 53.5, 41.9, 21.0, 20.6. Anal. Calcd. for $C_{29}H_{35}N_3$: C, 81.84; H, 8.29; N, 9.87. Found: C, 81.53; H, 8.32; N, 9.67. Mp: 82-84 °C.

Mo(NMe$_2$)$_2$(dpma^{mes}) (1) In a glove box under an N_2 atmosphere, a 100 mL Schlenk tube was loaded with a stir bar and a solution of $Mo(NMe_2)_4$[11] (1.00 g, 36.7 mmol, 1 equiv.) in toluene/hexane (1:4, 5:20 mL). To the Schlenk tube, H_2dpma^{mes} (1.56 g, 3.67 mmol, 1 equiv.) in toluene (8 mL) was added. The headspace was evacuated, and the vessel was sealed with a Teflon stopcock. The tube was removed from the box and was placed into a 55 °C oil bath for 10 h, while stirring vigorously. After this time, the vessel was allowed to cool to room temperature and was taken back inside the dry box. The volatiles were removed in vacuo, and the solids were washed with hexane (10 mL). The solids were dissolved in a minimal amount of toluene and

held at −35 °C yielding **1** as bright green crystals (1.78 g, 2.94 mmol, 80%). Magnetic susceptibility (Evan's method, 29.7 °C): μ_{eff} = 1.178 μ_B. TOF-MS ES+ calcd (found): 608.68 (609.2). UV-Vis [toluene, 25 °C] λ_{max} in nm (ε in $cm^{-1}M^{-1}$): 643.9 (498.7), 786.9 (187.4). M.p.: 138-144 °C (d). The molecule contains a disordered toluene in the lattice as crystallized. Attempts to obtain elemental analysis were not satisfactory unless toluene was included with occupancy of 0.3. Anal. Calcd for $C_{34}H_{45}MoN_5$•$0.3C_7H_8$: C, 66.36; H, 7.52; N, 11.02. Found: C, 66.60; H, 7.26; N, 11.39.

Mo(NMe$_2$)$_2$(CNBu^t)(dpma^{mes}) (1•CNBu^t) Under an N_2 atmosphere, a scintillation vial was loaded with a stir bar, **1** (0.1 g, 0.165 mmol, 1 equiv.) and toluene (5 mL). To this, *tert*-butylisonitrile (0.1 g, 0.165 mmol, 1 equiv.) in toluene (1 mL) was added. The solution was stirred and rapidly turned dark red. After 1 h, the volatiles were removed in vacuo. The residue was extracted with toluene (2 mL). The solution was filtered through Celite and layered with an equal volume of pentane. Crystallization at −35 °C gave dark red crystals of **1**•CNBu^t in 40% yield (0.045 g, 0.066 mmol). Magnetic susceptibility (Evan's method, 28.2 °C): μ_{eff} = 2.469 μ_B. The molecule contains a toluene in the lattice as crystallized. Attempts to obtain elemental analysis were not satisfactory unless toluene was included with full occupancy. Anal. Calcd for $C_{38}H_{54}MoN_6$•C_7H_8: C, 69.03; H, 7.98; N, 10.73. Found: C, 68.89; H, 8.17; N, 10.61. Mp: 128-130 °C (dec). UV-Vis [toluene, 25 °C] λ_{max} in nm (ε in $cm^{-1}M^{-1}$): 372.2 (6588), 490 (3042). Crystals for X-ray diffraction grown from toluene gave poor structural results, and the crystals were regrown from Et_2O.

Mo(N)(NMe$_2$)(dpma^{mes}) (*anti*-2) Under an N_2 atmosphere, a scintillation vial was loaded with a stir bar, **1** (0.650 g, 1.07 mmol, 1 equiv.) and toluene (8 mL). To the stirring solution of **1**, a solution of *N*,*N*-dimethylhydrazine (0.64 g, 1.07 mmol, 1 equiv) in toluene (1 mL) was added. Upon addition, the solution turned brown and an orange precipitate formed. After 1 h, the volatiles were removed in vacuo. The residue was stirred in pentane (2 mL) for 5 min, and the suspension was filtered on a glass frit. The solids were collected and dried in vacuo yielding the title compound as an orange powder (0.459 g, 0.795 mmol, 75%). Diffraction quality crystals were grown from a concentrated toluene solution layered in pentane held at −35 °C. ^{1}H NMR (500 MHz, C_7D_8): 6.70 (s, 2H, aromatic C-*H*), 6.58 (s, 2H, aromatic C-*H*), 6.37 (d, J_{HH} = 3.0 Hz, 2H, pyrrole C-*H*), 6.17 (dd, J_{HH} = 0.5 Hz, J_{HH} = 3.0 Hz, 2H, pyrrole C-*H*), 4.53 (d, J_{HH} = 13.0 Hz, 2H, C*H*$_2$), 3.52 (s, 3H, NC*H*$_3$), 3.34 (d, J_{HH} = 12.5 Hz, 2H, C*H*$_2$), 2.43 (s, 6H, Ar-*p*-C*H*$_3$), 2.18 (s, 3H N(C*H*$_3$)$_2$), 2.12 (s, 3H N(C*H*$_3$)$_2$), 2.05 (s, 6H, Ar-*o*-C*H*$_3$), 2.04 (s, 6H, Ar-*o*-C*H*$_3$). ^{13}C{^{1}H} NMR (125 MHz, C_6D_6): 140.8, 140.2, 139.2, 138.4, 136.8, 136.6, 111.2, 106.8, 63.4, 46.5, 43.6, 21.2, 21.0, 20.9. Anal. Calcd for $C_{31}H_{39}MoN_5$: C, 64.46; H, 6.81; N, 12.12. Found: C 64.35; H, 6.72; N, 12.08. Mp: 264-270 °C (dec).

Mo(N)(NMe$_2$)(dpma^{mes}) (*syn*-2) Under an N_2 atmosphere, a scintillation vial was loaded with a stir bar, **1** (0.123 g, 0.202 mmol, 1 equiv.), and toluene (8 mL). To the stirring solution of **1**, a solution of *O*-(benzyl)hydroxylamine (0.750 mL, 0.269 M, 0.202 mmol, 1 equiv.) in toluene (1 mL) was added. Upon addition, the solution turned brown. After 2 h, the volatiles were removed in vacuo. The residue was taken up in Et_2O (5 mL) and filtered through Celite. The solution was concentrated in vacuo to 2 mL and held at −35 °C, which crystalized **2**-*syn* as orange blocks

(0.0356 g, 0.062 mmol, 30.7%). ^{1}H NMR (500 MHz, C_6D_8): 6.79 (s, 2H, aromatic C-*H*), 6.63 (s, 2H, aromatic C-*H*), 6.32 (d, J_{HH} = 3.0 Hz, 2H, pyrrole C-*H*), 6.26 (d, J_{HH} = 3.0 Hz, 2H, pyrrole C-*H*), 3.66 (dd, J_{HH} = 0.5 Hz, J_{HH} = 14.0 Hz, 2H, CH_2), 3.50 (dd, J_{HH} = 0.5 Hz, J_{HH} = 14.0 Hz, 2H, CH_2), 3.20 (d, J_{HH} = 1.0 Hz, 3H, N(CH_3)$_2$), 2.74 (s, 3H, NCH_3), 2.60 (s, 6H, Ar-*p*-CH_3), 2.50 (d, J_{HH} = 1.0 Hz, 3H N(CH_3)$_2$), 2.11 (s, 12H, Ar-*o*-CH_3). ^{13}C{^{1}H} NMR (125 MHz, $CDCl_3$): 139.72, 139.62, 137.23, 136.86, 136.54, 134.77, 128.42, 127.45, 112.15, 106.10, 63.88, 59.31, 53.13, 47.56, 21.35, 20.98, 20.84. Mp: 117-123 °C (dec). By-products of this reaction include benzyl alcohol (51.2%), benzaldehyde (10.7%) and 1,2-diphenylethane (5.9%) as determined by GC-MS/GC-FID; the yields are relative to dodecane internal standard for calibrated samples of those compounds.

Zr(NMe$_2$)$_2$(dpma^{mes}) (3) Under an N_2 atmosphere, a 100 mL Schlenk tube was loaded with a stir bar, Zr(NMe$_2$)$_4$ (0.851 g, 3.18 mmol, 1 equiv.), toluene (6 mL), and Et_2O (1 mL). To the pressure tube was added H_2dpma^{mes} (1.35 g, 3.18 mmol, 1 equiv.) in toluene (1 mL). The headspace was evacuated, and the tube was sealed with a Teflon stopcock and removed from the dry box. The solution was stirred in a 70 °C oil bath for 48 h. The tube was taken back into the dry box, and the solution was filtered through Celite. The volatiles were removed in vacuo yielding **3** as a yellow powder (1.75 g, 2.89 mmol, 91% yield). ^{1}H NMR (500 MHz, C_6D_6): 6.82-6.81 (m, 2H, aromatic C-*H*), 6.74-6.73 (m, 2H, aromatic C-*H*), 6.30 (dd, J_{HH} = 2.75 Hz, J_{HH} = 0.5 Hz, 2H, pyrrole C-*H*), 6.16 (d, J_{HH} = 3.0 Hz, 2H, pyrrole C-*H*), 4.05 (d, J_{HH} = 13.5 Hz, 2H, CH_2), 3.40 (d, J_{HH} = 13.5 Hz, 2H, CH_2) 2.59 (s, 6H, N(CH_3)$_2$), 2.28 (s, 6H, N(CH_3)$_2$),

2.26 (s, 3H, NCH_3), 2.12 (s, 6H, Ar-*o*-CH_3), 2.10 (s, 6H, Ar-*o*-CH_3), 2.02 (s, 6H, Ar-*p*-CH_3). $^{13}C\{^1H\}$ NMR (125 MHz, $CDCl_3$): 139.07, 138.61, 138.26, 136.03, 135.94, 135.92, 128.02, 127.47, 127.37, 109.25, 104.71, 59.39, 43.25, 40.63, 39.16, 21.17, 21.01, 20.75. Mp: 262-270 °C.

Zr(η^2-NHNMe$_2$)$_2$(dpma^{mes}) (4) Under an N_2 atmosphere, a scintillation vial was loaded with **3** (0.100 g, 0.166 mmol, 1 equiv.), a stir bar, and a mixture of toluene and Et_2O (1:1 v:v, 8 mL). The solution was rapidly stirred and a 0.712 M toluene solution of 1,1-dimethylhydrazine was added dropwise (466 μL, 0.332 mmol, 2 equiv.). DME (1 mL) was added. The solution stirred for 16 h, and the volatiles were removed in vacuo. **4** was obtained in 86% yield as an off-white powder (0.090 g, 1.42 mmol, 86% yield). Diffraction quality crystals of **4** were obtained from a −35 °C concentrated toluene solution layered with Et_2O. ^1H NMR (500 MHz, C_7D_8): 6.83 (br s, 2H, aromatic C-*H*), 6.74 (br s, 2H, aromatic C-*H*), 6.25 (d, J_{HH} = 3.0 Hz, 2H, pyrrole C-*H*), 6.14 (dd, J_{HH} = 1.0 Hz, J_{HH} = 3.0 Hz, 2H, pyrrole C-*H*), 4.30 (s, 1H, N*H*), 4.17 (d, J_{HH} = 13.5 Hz, 2H, CH_2), 4.10 (s, 1H, N*H*), 3.68 (d, J_{HH} = 13.5 Hz, 2H, CH_2), 2.48 (s, 3H, NCH_3), 2.30 (s, 6H N(CH_3)$_2$), 2.22 (s, 6H, N(CH_3)$_2$), 2.12 (s, 6H, Ar-*o*-CH_3), 1.91 (s, 3H, Ar-*o*-CH_3), 1.57 (s, 6H, Ar-*p*-CH_3). $^{13}C\{^1H\}$ NMR (125 MHz, C_6D_6): 140.12, 139.04, 138.91, 138.89, 136.41, 135.63, 128.54, 111.29, 108.21, 104.08, 62.57, 53.49, 50.91, 42.62, 22.44, 21.49, 21.07. Mp: 216-218 °C (dec).

APPENDIX A

APPENDIX A

A.1: General Considerations for the Experiments

Reactions and manipulations of air sensitive materials were carried out in an MBraun glovebox under a nitrogen atmosphere and/or using standard Schlenk techniques. Ethereal solvents, pentane, hexane, and toluene were purchased from Aldrich Chemical Co. and purified through alumina columns to remove water after sparging with dinitrogen to remove oxygen. Other compounds, such as formalin and methylamine hydrochloride, were purchased from commercial sources and used as received.

All NMR solvents were purchased from Cambridge Isotopes Laboratories, Inc. Deuterated toluene and benzene were distilled from sodium benzophenone ketyl. Deuterated chloroform was distilled from CaH_2 under dry a dinitrogen atmosphere. The NMR solvents were stored in the glovebox in glass containers with a stopcock. Spectra were taken on Varian instruments located in the Max T. Rogers Instrumentation Facility at Michigan State University.

A.2: Determination of Second-Order Rate Constants for Table 1.1

The reactions of **1** with various hydrazines were followed over ~3 half-lives. All kinetic data were obtained on an Evolution 600 model Thermo UV-Vis spectrometer. Temperature control was possible through a Peltier sample holder which maintained ± 0.2 °C throughout the run. Hydrazine was injected through a septum directly into an airtight UV-Vis absorption cell. Reactions were performed in toluene (3.5 mL) with constant stirring throughout the run. Single wavelength absorbance measurements were taken at 651 nm. This point was chosen due to the large difference in the absorbance of **1** (starting material) and **2-*anti*** (product) at this wavelength (ε_{651} = 621.46 for **1** vs ε_{651} = 24.23 for **2**). Absorbance data were fit to the Second-order Equation below using OriginPro 7.5 software, where Abs = absorbance, y_∞ and y_0 are floating parameters corresponding to the ending and starting absorptions respectively.[1] (The expression is only applicable when $rate = k[A]^2$ or when $rate = k[A][B]$ for [A] = [B].)[1] A minimum of 3 runs was used to obtain the rate constants in Table 1.1 of the manuscript, and the errors are at the 99% confidence level.

$$Abs = y_\infty + \frac{(y_0 + y_\infty)}{(1 + [\mathbf{1}]k_{obs}t)}$$

Shown below is one of the fits to absorption data for one of the kinetics runs where the hydrazine derivative was 1-aminopyrrole as a representative example. The black line is for the data, and the red line is the fit to the 2nd order equation above.

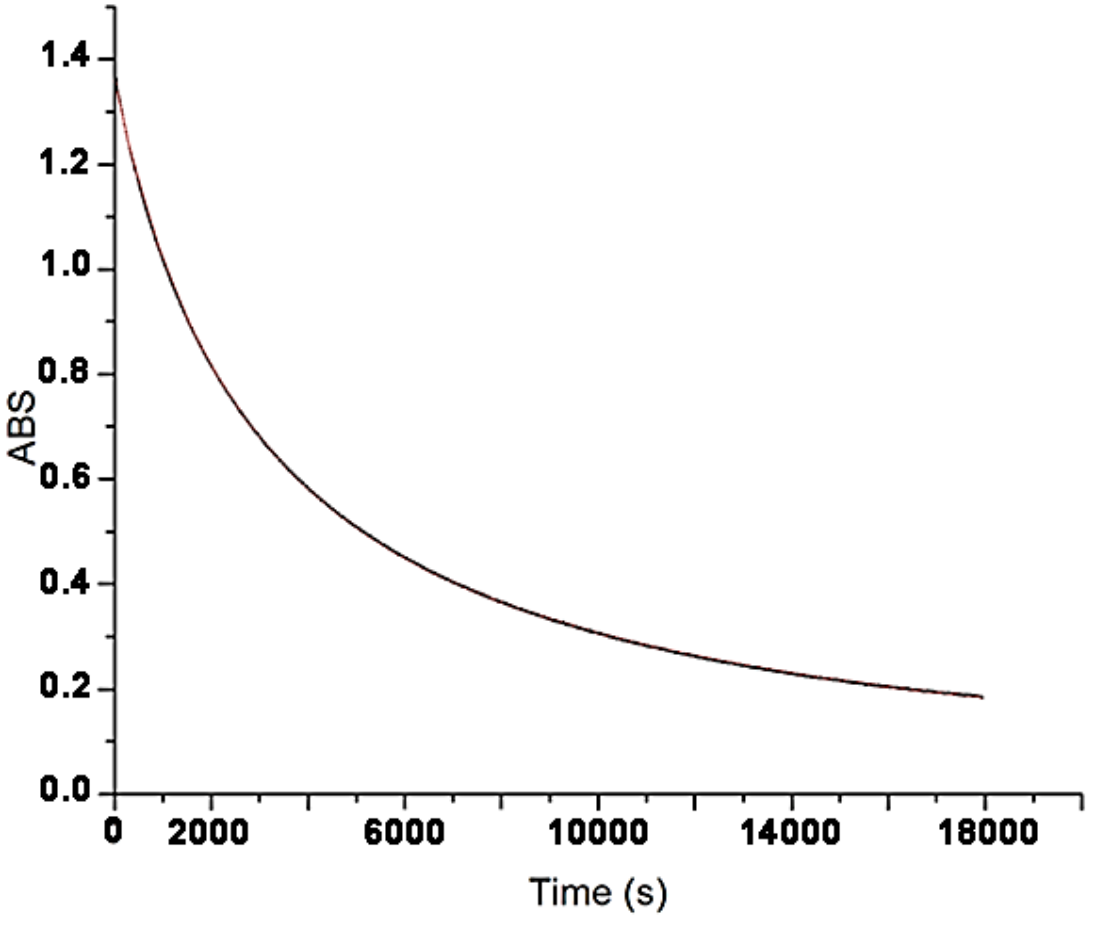

Figure A.1: A representative second order fit of 1 with disubstituted hydrazine

It is also useful to consider how well the 1st order expression fits the same curve. The first order equation used is shown below where the parameters have the same meaning as above.[1] The fit (red line in the plot) is much worse in comparison with the fit to the 2nd order expression.

$$Abs = y_\infty + (y_0 - y_\infty)exp(-k_{obs}t)$$

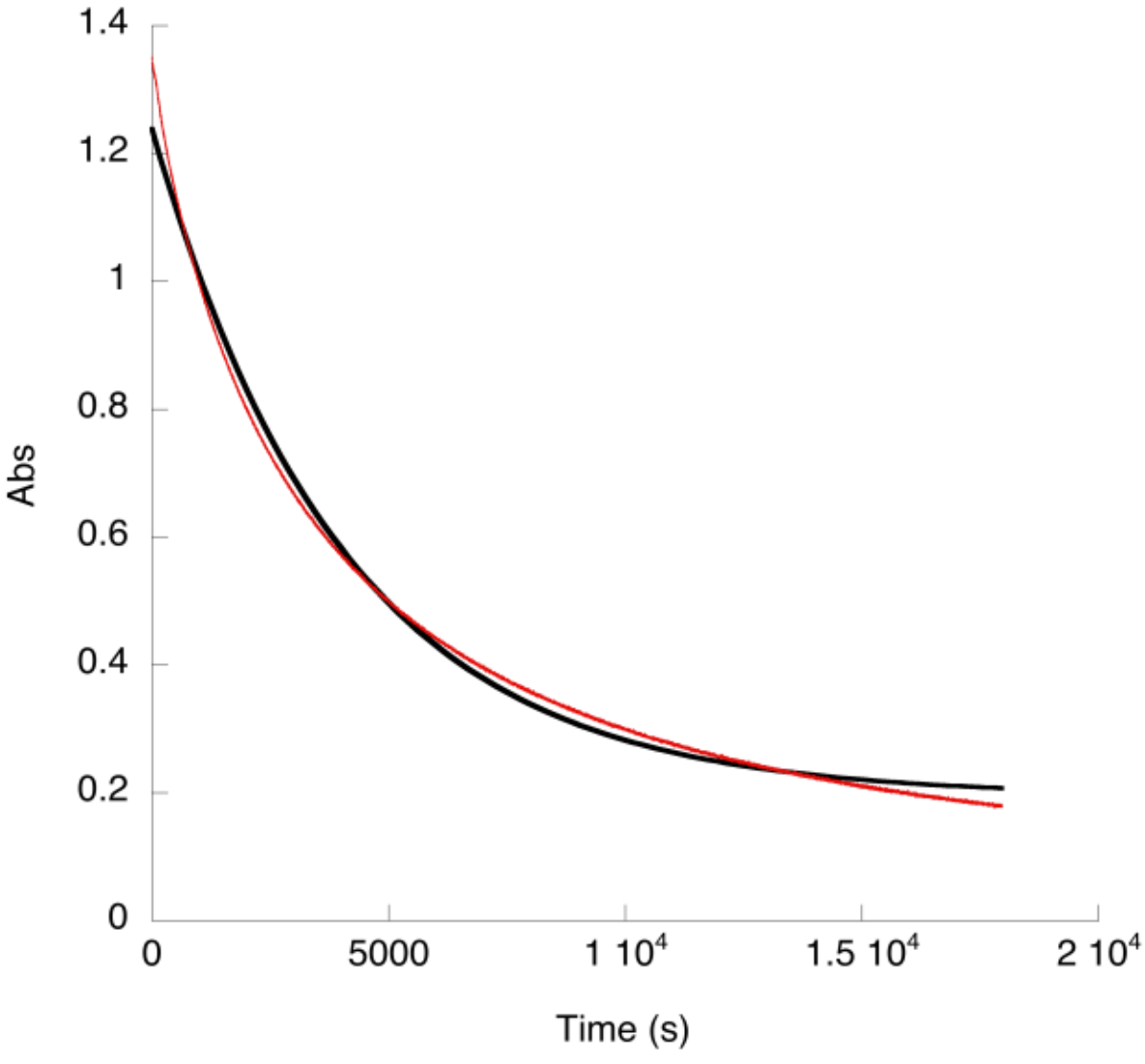

Figure A.2: A representative pseudo-1st order fit of **1** with disubstituted hydrazine

A.3: Initial Rates Experiments on 1,1-Dimethylhydrazine Concentration

To determine the order in hydrazine, considering pseudo-first order conditions were not possible with the system, we used initial rates. All kinetic data were obtained on an Evolution 600 model Thermo UV-Vis spectrometer. Temperature control was possible through a Peltier sample holder which maintained ± 0.2 °C throughout the run. 1,1-Dimethylhydrazine was injected through a septum directly into an airtight UV-Vis absorption cell. Reactions were performed in toluene (3.5 mL) with constant stirring throughout the run. Single wavelength absorbance measurements were taken at 651 nm. This point was chosen due to the large difference in the absorbance of **1** (starting material) and **2-*anti*** (product) at this wavelength (ε_{651} = 621.46 vs ε_{651} = 24.23 respectively). The data were truncated around 10% conversion of **1** as judged by the decrease from the absorbance at t = 0. The initial rate is determined from the slope of the linear fit to the line.[1] The initial absorbances, intercept of the lines, were allowed to fit and did vary slightly from run to run for this extremely reactive and air-sensitive compound even though reactions were run from stock solutions.

The [**1**] vs time plot is shown below with the linear fits.

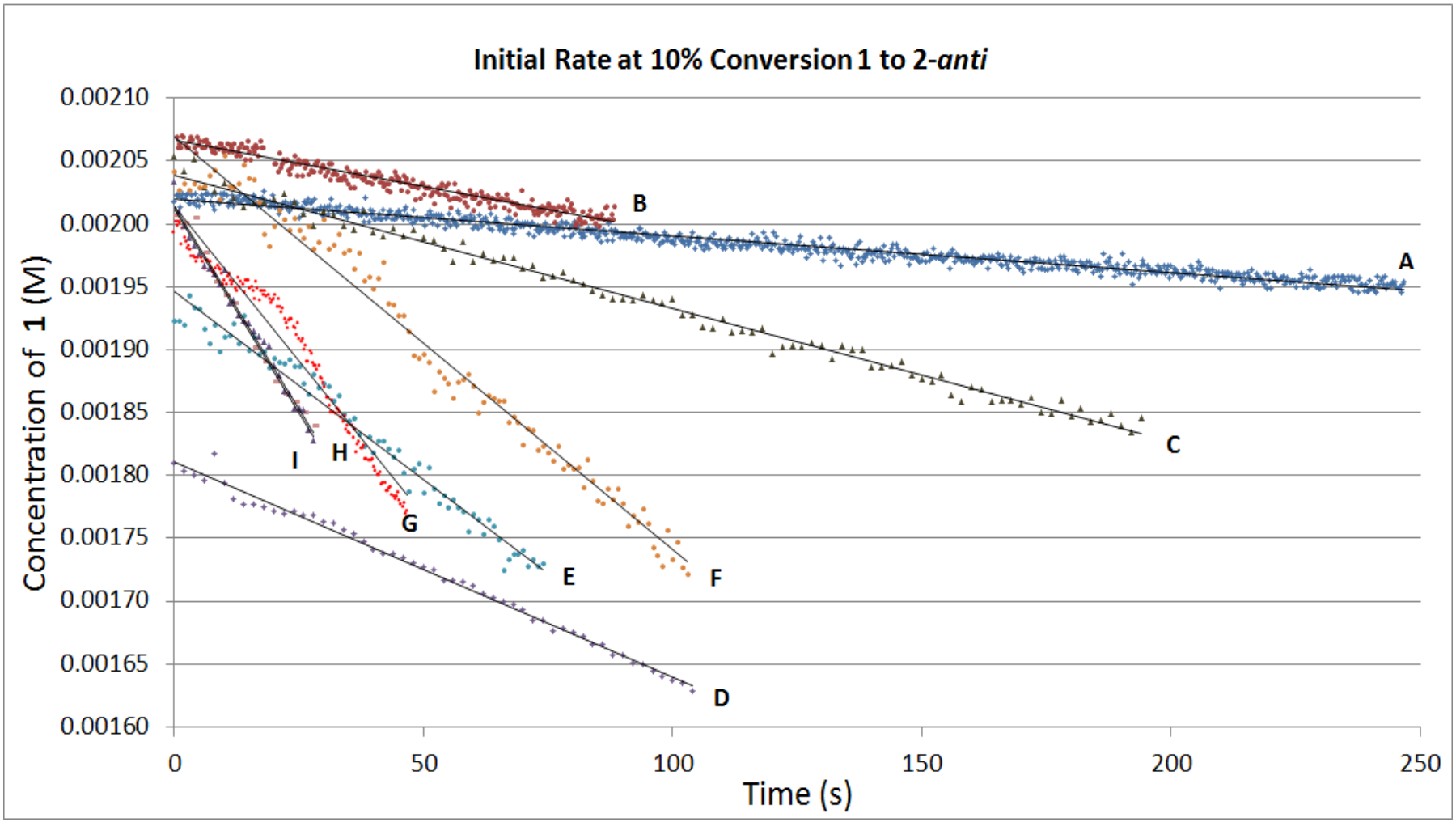

Figure A.3: Initial rate data for the conversion of 1 to 2-anti as a function of metal concentration.

The tabulated hydrazine concentrations and rates are shown in the figure and table below.

	Hydrazine Concentration (M)	Rate Conversion of 1 (M/s*10^{-6})
A	0.00012441	-0.2905
B	0.00031147	-0.7365
C	0.00093175	-1.065
D	0.00203940	-1.716
E	0.00307520	-2.996
F	0.00458054	-3.284
G	0.00487908	-4.911
H	0.00606497	-6.482
I	0.00897284	-6.456

Figure A.4: Fits of rate at 10% of conversion of **1** to **2**-*anti* along with tabulated data.

Since the reaction is cleanest when the [**1**] to [hydrazine] are 1:1 and the reaction produces unidentified by-products when the [hydrazine] goes either higher or lower than [**1**], we chose to use Run D, which has these two concentrations closest, as the most accurate run for the analysis below.

For any two reactions in the set, the following equation should apply where $rate_D$ is the rate of reaction D determined from the slopes above, $[\mathbf{1}]_D^a$ is the concentration of **1** in Run D to the power of *a*, and $[hydrazine]_D^b$ is the concentration of the hydrazine in Run D to the power of *b*.

$$\frac{rate_D}{rate_X} = \frac{k_{obs}[\mathbf{1}]_D^a[hydrazine]_D^b}{k_{obs}[\mathbf{1}]_X^a[hydrazine]_X^b}$$

If we assume that $k_{obs}[\mathbf{1}]_D^a \sim k_{obs}[\mathbf{1}]_X^a$, those terms can be eliminated. Rearrangement and using *ln* to isolate the order gives the equation below where the order in hydrazine, *b*, is related to the rates and concentrations of any two runs.

$$b = \frac{\ln\left(\frac{rate_D}{rate_X}\right)}{\ln\left(\frac{[hydrazine]_D}{[hydrazine]_X}\right)}$$

To find the orders in hydrazine relative to Run D (where the reagents are ~1:1) we applied the above expression. The run with the lowest order was Run B displaying an apparent order of 0.45; this run also had the worst R^2 factor for the fit. The highest order obtained was 1.35 for Run E.

The average order for all of the runs was $b = 0.90$, and the reaction was assigned as first order in hydrazine.

A.4: Initial Rates Experiments on 1 Concentration

As a final check on the rate law, we did briefly examine the dependence of the reaction on the concentration of **1**. The conditions and procedure were very similar to the procedure above for the initial rates experiments on hydrazine concentration. The exception being that raising the metal concentration much over that used in the hydrazine initial rates experiments leads to solutions that are too concentrated for accurate absorption measurement. Consequently, the concentrations of the hydrazine and **1** were lowered somewhat relative to those above.

The raw data are tabulated below with the initial concentration of **1** and the rate of the disappearance of the **1**. The plots and linear fits are given.

	[1] (M)	**[hydrazine] (M)**	**Rate (10^{-7})**
J	0.00122	0.000607	–3.44
K	0.00122	0.000866	–4.13
L	0.00142	0.0011	–6.52
M	0.00132	0.0011	–4.87

Table A.1: Rate dependence on the concentration of 1.

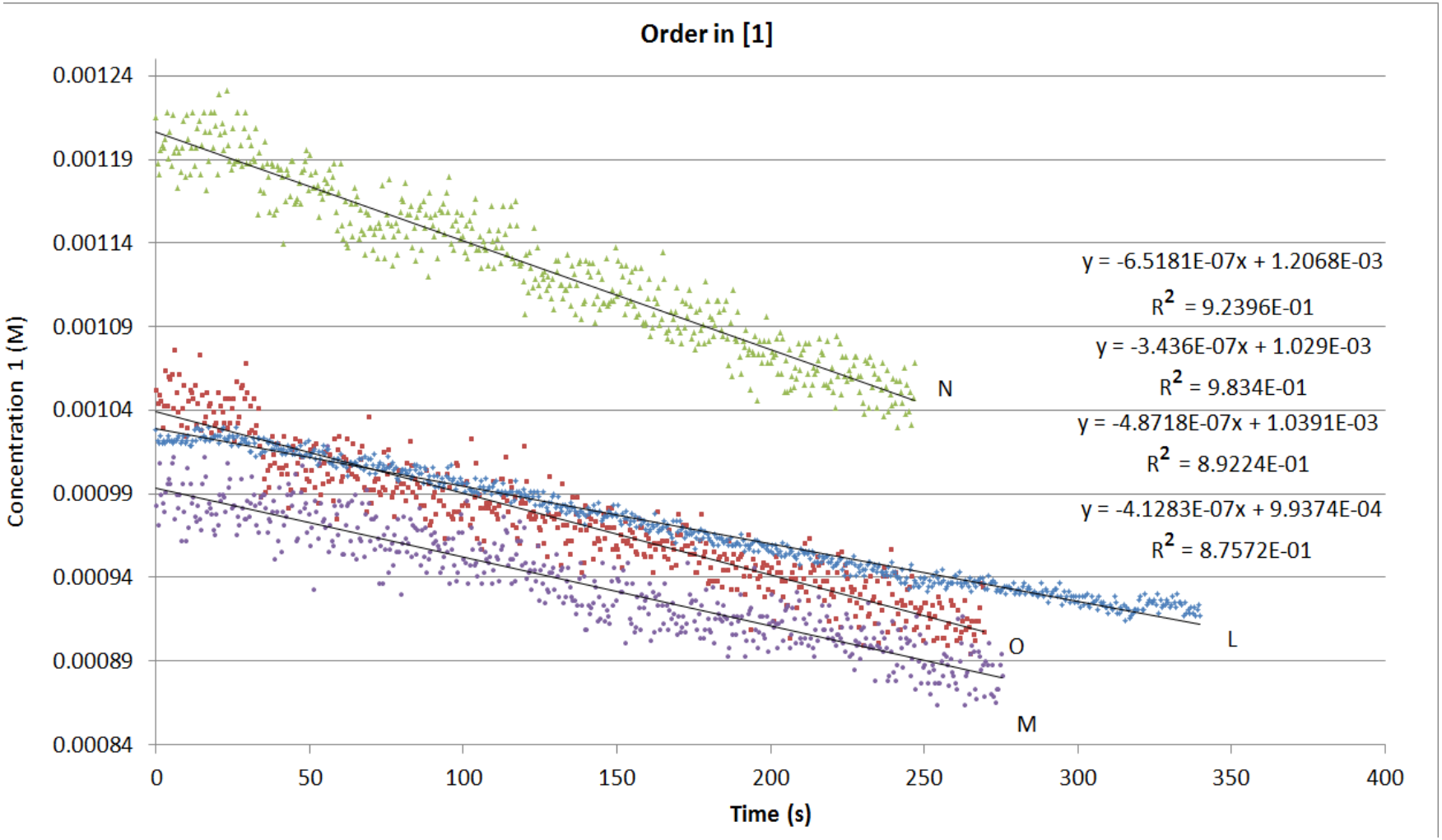

Figure A.5: Initial rate data of conversion of **1** to **2**-anti as a function of the concentration of **1**.

As before, the analysis was done using Run D, where the concentrations of **1** and hydrazine are equal, as the reference Run. We then assumed that the order in hydrazine, exponential *b*, was unity as found in the experiments described previous. This gives the expression below for the order in **1**, *a*.

$$\frac{rate_D}{rate_X} = \frac{k_{obs}[\mathbf{1}]_D^a[hydrazine]_D^b}{k_{obs}[\mathbf{1}]_X^a[hydrazine]_X^b}$$

$$a = \frac{\ln\left(\frac{rate_D}{rate_X}\right)}{\ln\left(\frac{[\mathbf{1}]_D}{[\mathbf{1}]_X}\right)}$$

Again, the metal complex is extremely reactive and there is some variation in the data. However, for the four Runs the orders in [**1**], *a* in the expression above, were found to be 0.77, 1.11, 0.97, and 1.48 for Runs J–M respectively. This gives an average order of 1.08. Based on this data, the reaction being 2^{nd} order overall, and 1^{st} order in hydrazine, the reaction was assigned as 1^{st} order in metal.

A.5: Thermal Conversion of syn-2 into anti-2

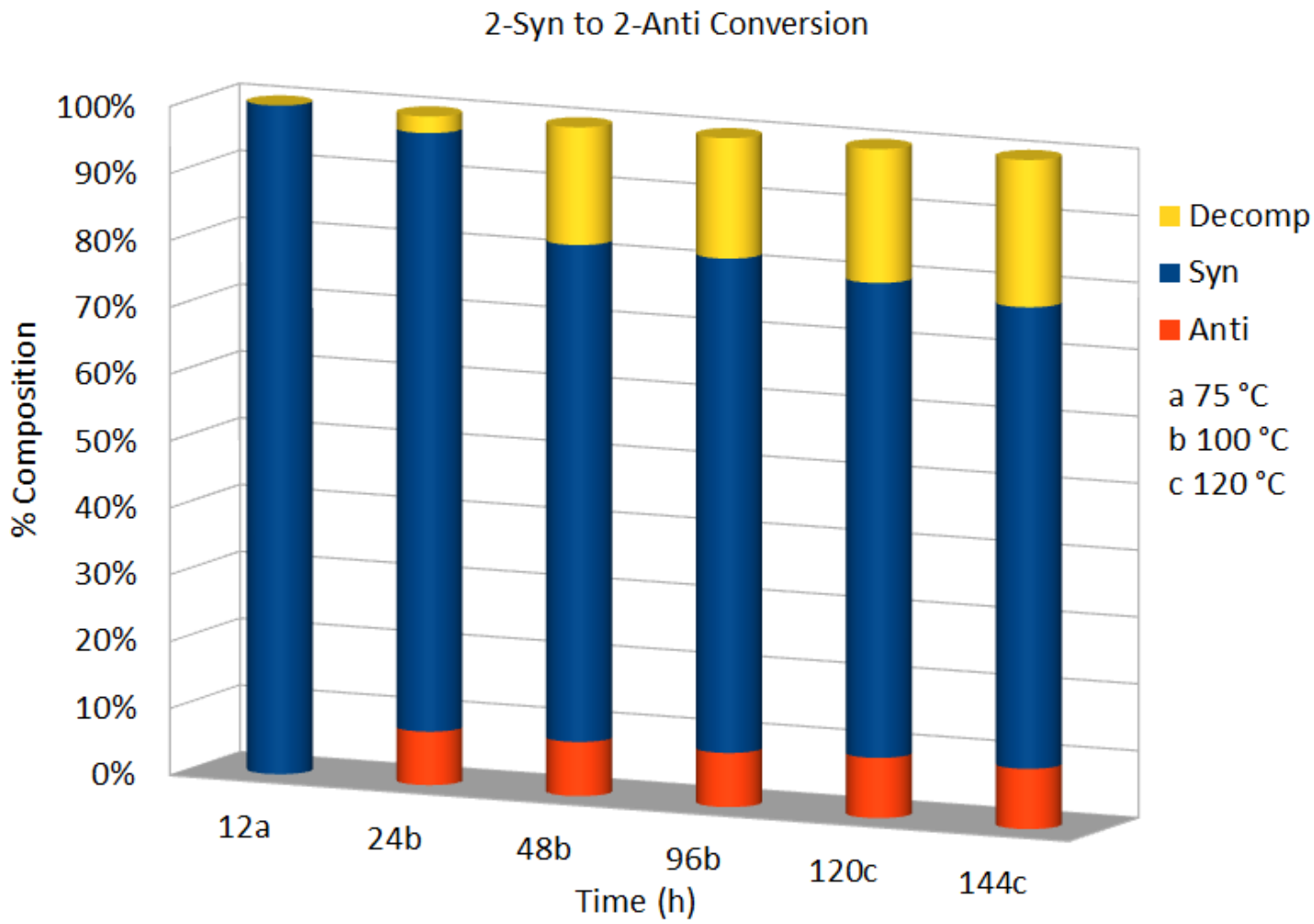

Figure A.6: Thermal conversion of **2**-syn into **2**-anti.

A.6: UV-Vis trace of anti-2 formation using H_2NNMe_2 and 1 (60 s intervals)

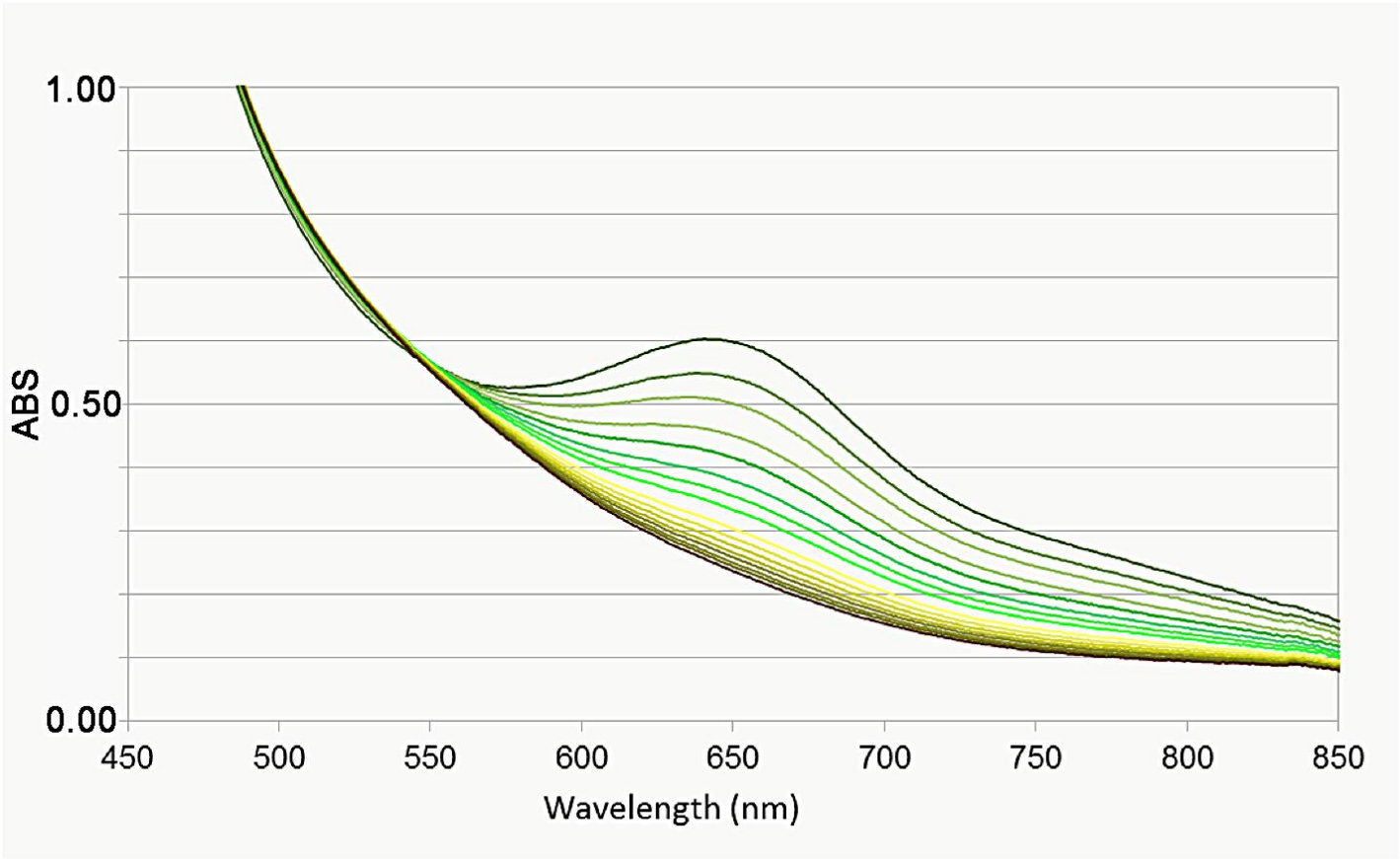

Figure A.7: UV-Vis trace of **2**-anti formation using H_2NNMe_2 and 1 (60 s intervals) showing a clear isobestic point, thus no long lived intermediates.

The trace shows an isobestic point, as do all of the substrates with **1** with the exception of *N*-aminopiperidine. It was shown independently that the piperidine by-product reacts rapidly with **1** on the time scale of the experiment, which leads to its anomalous behavior.

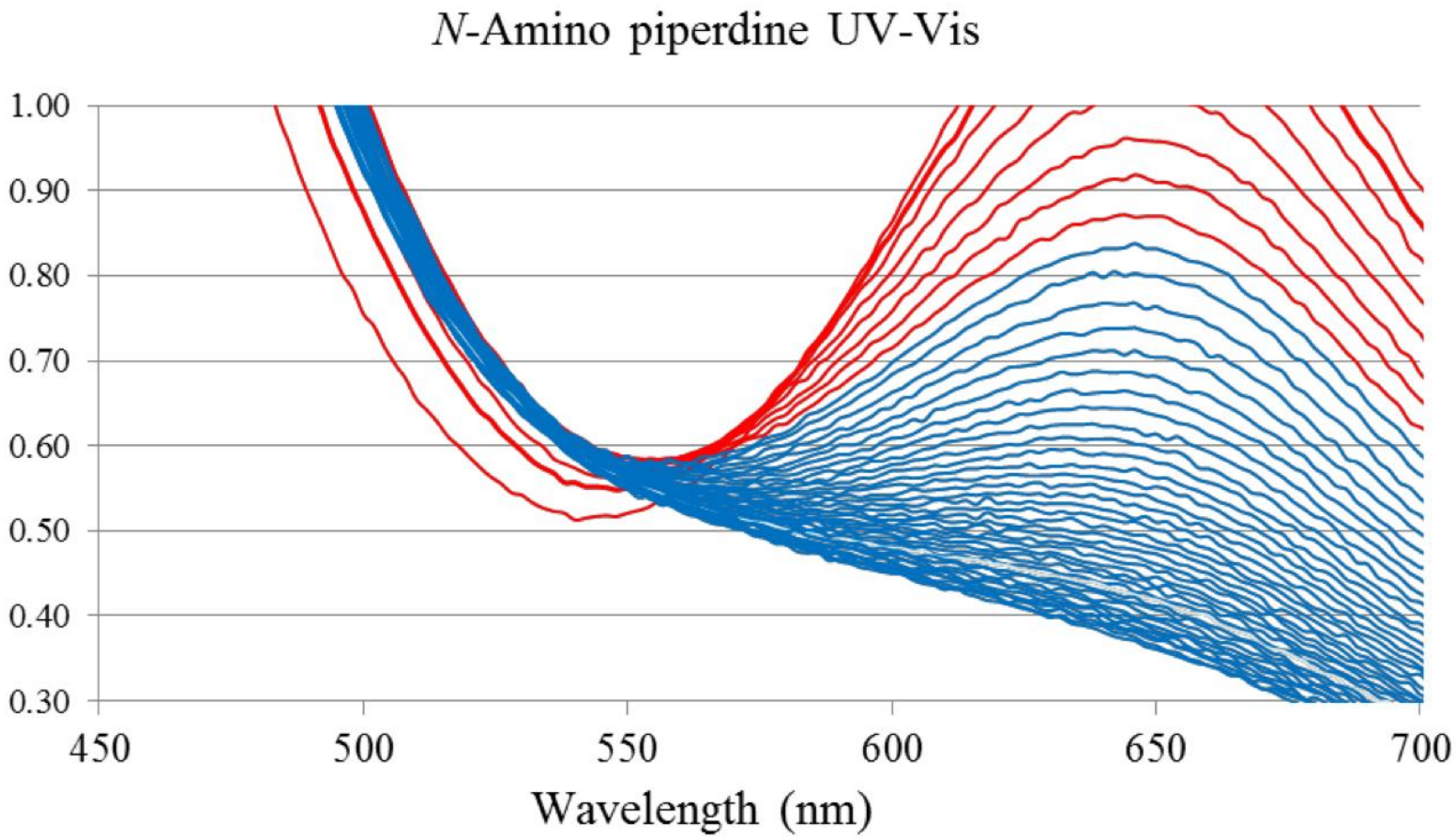

Figure A.8: UV-Vis trace of **2**-anti formation using N-Amino piperdine showing the production of other metal containing species, likely the results of product inhabition.

A.7: Powder diffraction on samples of 1

Presumably due to the high reactivity of **1** and it's tendency to retain toluene in the lattice, we had difficulty getting an adequate elemental analysis on the paramagnetic compound. One method used to examine the purity of new samples of the compound was to calculate the powder structure of the complex from the single crystal X-ray diffraction experiment and to examine the new sample by power diffraction. One such comparison is shown below.

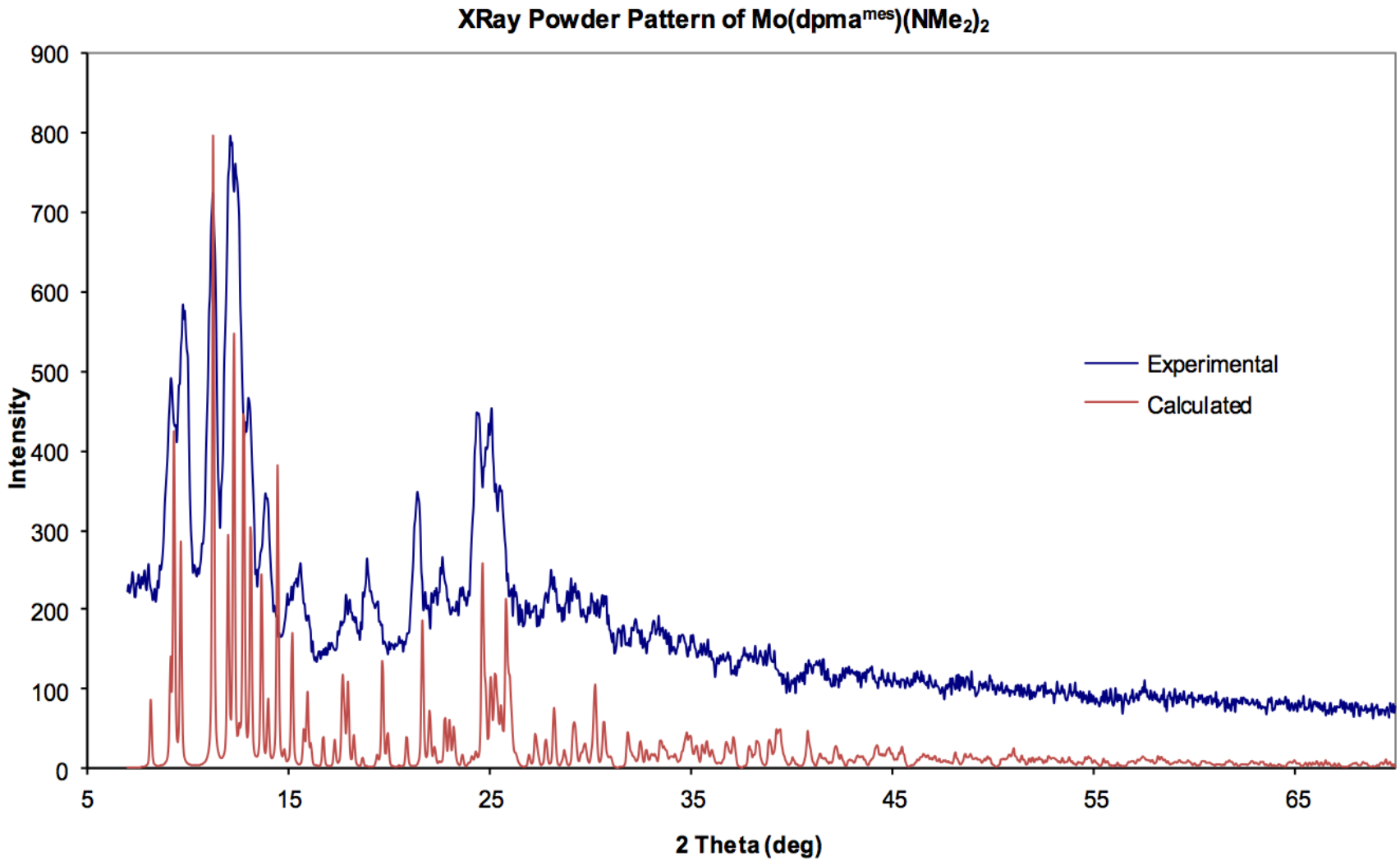

Figure A.9: Experimental and calculated X-ray powder pattern for **1.**

A.8: Eyring Plot for H_2NNMe_2 reaction with 1

The reaction of 1,1-dimethylhydrazine with **1** was carried out over as large a temperature range accessible. The Eyring plot of ln(k/T) vs 1/T is shown below with the linear fit.

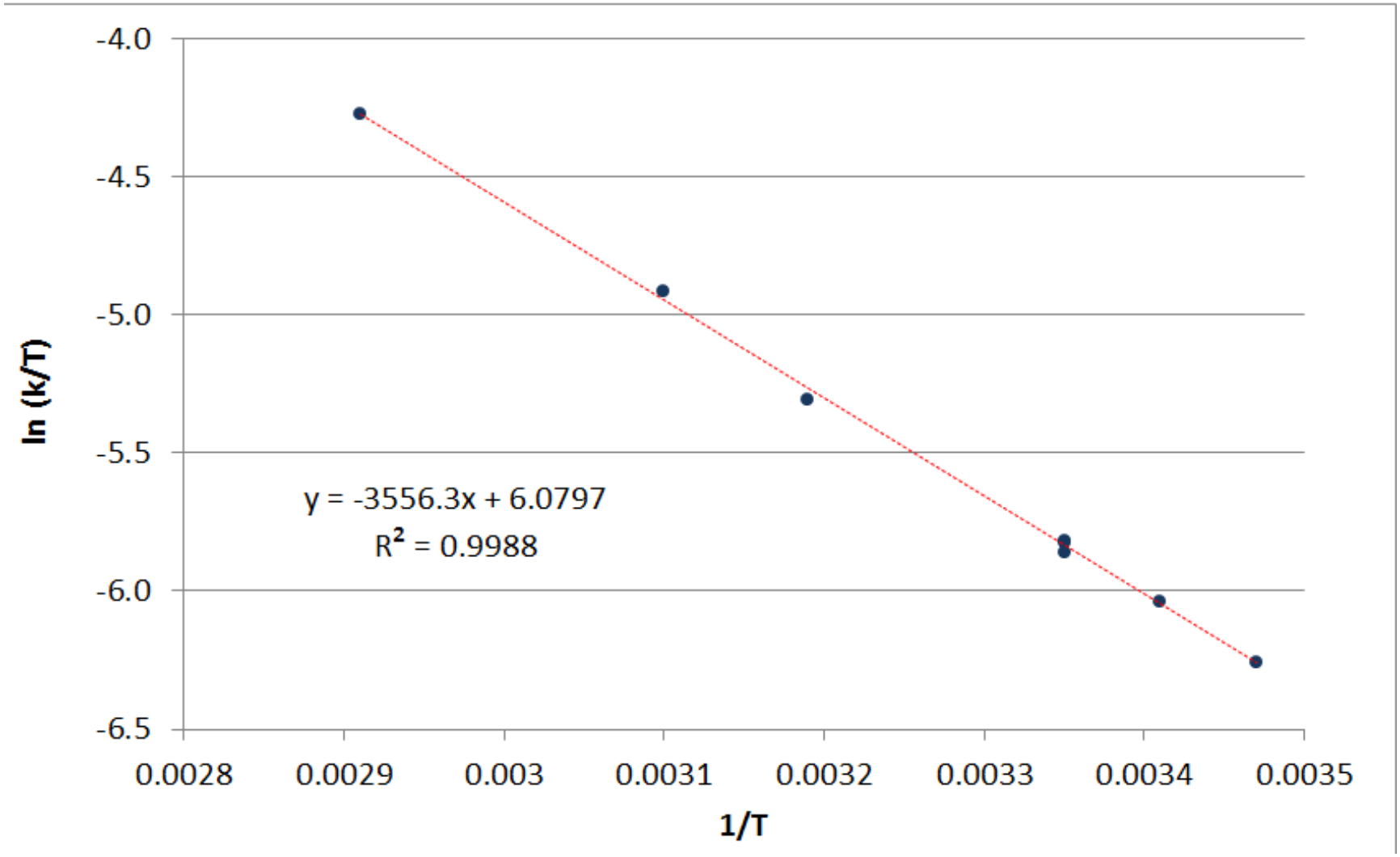

Figure A.10: Eyring plot of ln(k/T) vs 1/T with a linear fit giving activation parameters.

$$\ln\left(\frac{k}{T}\right) = \frac{\Delta S^{\ddagger}}{R} + \ln\left(\frac{k_B}{h}\right) - \frac{\Delta H^{\ddagger}}{RT} \quad (1)$$

$$\Delta H^{\ddagger} = -m \times R \quad (2)$$

$$\Delta S^{\ddagger} = R\left[b - \ln\left(\frac{k_B}{h}\right)\right] \quad (3)$$

Equation 1 above is the Eyring Equation itself, with R = gas constant, h = Planck's constant, k_B = Boltzmann constant, T = Temperature in Kelvin, and k = observed rate constant. The $\Delta H^{\ddagger}$ and $\Delta S^{\ddagger}$ are found from the slope (m) and intercept (b) of the plot using Equations 2 and 3. Using R = 1.986 cal/K•mol, k_B = 1.381 ´ 10^{-23} J/K, and h = 6.626 ´ 10^{-24} J•s, the equations set up as below.

$$D H^{\ddagger} = - (-3556.3 \times 1.986)$$
$$D H^{\ddagger} = +7.1 \text{ kcal/mol}$$

$$D S^{\ddagger} = 1.986\left[6.08 - \ln\left(\frac{1.381 \times 10^{-23}}{6.626 \times 10^{-34}}\right)\right]$$
$$D S^{\ddagger} = 1.986\left[6.08 - 23.76\right]$$
$$D S^{\ddagger} = - 35.1 \text{ cal/mol•K}$$

A.9: Additional Mechanistic Discussions

As is usually the case, there are some other mechanisms for the N–N and N–O bond cleavage reaction that are difficult to rule out entirely. Here are a few additional arguments for the mechanistic proposal and some of the other possible mechanisms considered.

Coordination/Proton Transfer as Rate Determining Step

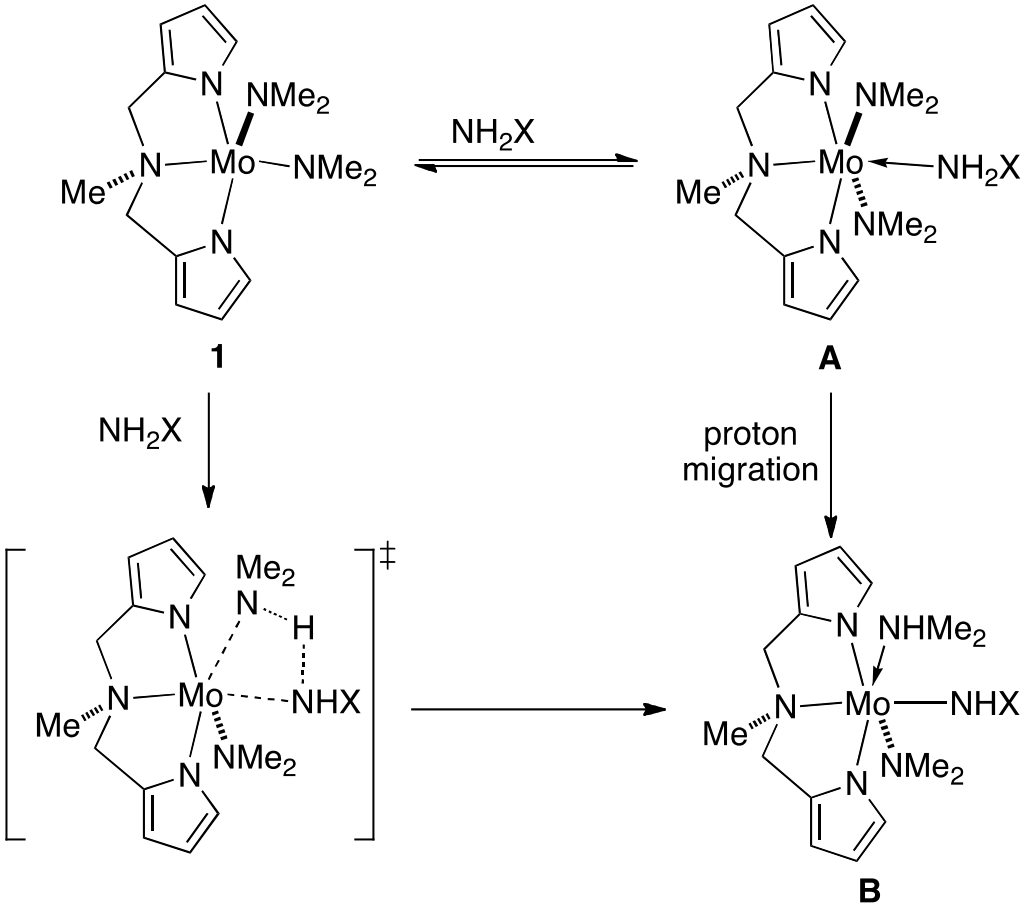

Figure A.11: α,β-proton migration as the rate determining step. Mes groups removed for clarity.

From the activation parameters, the transition state for the rate-determining step is extremely ordered. The very ordered step proposed for the rate-determining step is the addition of a ligand

(NH_2X = hydrazine or hydroxylamine) to 5-coordinate **1** in an associative process. This could occur either in conjunction with proton transfer to the dimethylamido or stepwise.

The activation parameters for ligand additions to metals in an associative process can be of similar magnitude to the parameters observed in our reaction. In our system $\Delta H^{\ddagger}$ = +7 kcal/mol and $\Delta S^{\ddagger}$ = –35 cal/mol•K. For example, the second-order, associative exchanges of $TaCl_5$•L with additional L (L = SMe_2, $SeMe_2$, $TeMe_2$) have activation parameters of $\Delta H^{\ddagger}$ = 5.5 to 5.7 ± 0.3 kcal/mol and $\Delta S^{\ddagger}$ = –25.8 to –22.7 ± 1.2 cal/mol•K. Also for reference, the associative exchange of SMe_2 to *trans*-$Pd(SMe_2)_2Cl_2$ has activation parameters of $\Delta H^{\ddagger}$ = +9.2 kcal/mol and $\Delta S^{\ddagger}$ = –18 cal/mol•K where the complex goes from 4-coordinate to 5-coordinate. Small positive enthalpies and large negative entropies of activation seem to be common for ligand association reactions in such cases.

Considering the addition of H_2NNMe_2 to the zirconium analogue of **1**, also has similar activation parameters and no possibility of doing the other steps (namely the N–N bond cleavage), we assigned the coordination of hydrazine as the rate-determining step. Whether the coordination occurs with concomitant proton transfer is unknown.

Attempts to produce the very dry $D_2NN(Me)Ph$ necessary for kinetic isotope studies did not lead to a pure isotopomer. Kinetics using about 50% labeled 1-methyl-1-phenylhydrazine did not show a kinetic isotope effect outside the error bars. However, we are uncertain as to the definitiveness of the results considering H/D-exchange in the various intermediates with the hydrazine and by-product amine may mask the KIE.

Hydrazido(2–) Formation with $HNMe_2$ Back Reaction

Another alternative pathway to **2** would involve formation of a hydrazido(2–) intermediate with loss of both dimethylamido ligands from the starting material **1**. We know that NMe_2 is present in the final product **2** regardless of the nature of X, but this may occur through loss of NMe_2 followed by regaining the NMe_2 by protonation of X in a fast step. The slow step might then be oxidative addition of N–X to the metal center through an transition state like the one below.

Hydrazido(2–) complexes like the one shown in the transition state above have been proposed and even observed in the presence of Lewis acids for Zr and Hf complexes where X = NPh_2.

However, the reaction requires the replacement of X protolytically with $HNMe_2$. We have examined reactions of **2** with a variety of potential proton donors. The position occupied by NMe_2 in **2** is flanked by two mesityl groups that seem to very competently shield the nitrogen from protonation. For example, the dimethylamido group in **2** does not react with piperidine, *N*-methylaniline, diphenylamine, or benzylalcohol under any conditions we have found. In other words, the product nitrido is quite resistant towards all of the by-products of the N–N and N–O bond cleavage reactions not only on the order of the reaction but also on the order of days!

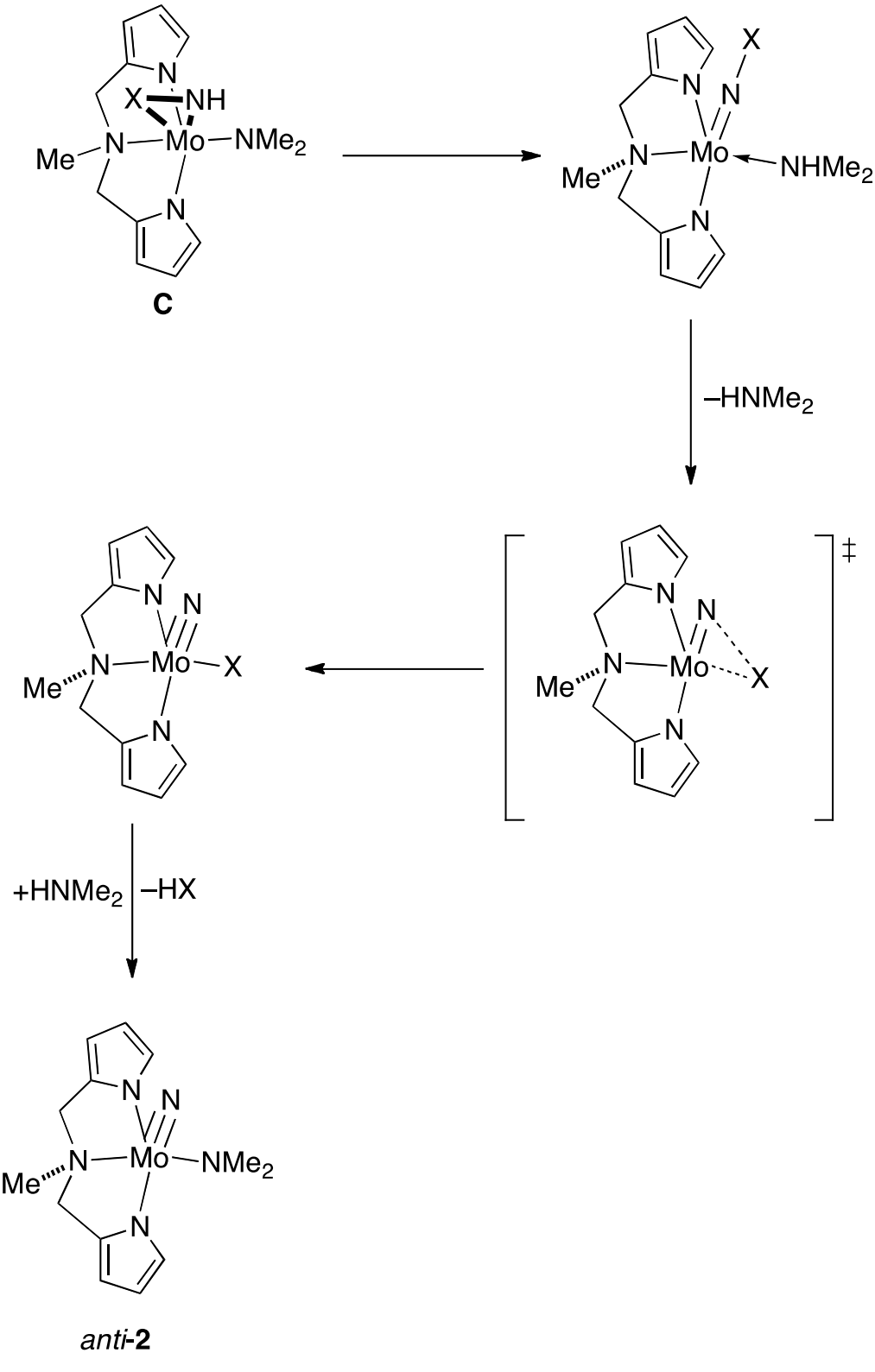

Figure A.12: Alternate mechanism of bond cleavage going through a hydrazido(2−) pathway

Consequently, it seems unlikely that X in the same position as NMe_2 in the nitrido would be readily replaced by $HNMe_2$ in a reaction fast enough that $NMo(dpma^{mes})X$ is never observed, which makes this mechanism seem unlikely. This replacement would have to occur very rapidly in the reaction regardless of X substituent as well, e.g., $HNMe_2$ would have to rapidly protonate the alkoxide intermediate to release HOBn.

Nature of the N–N bond cleavage

Because the N–N bond cleavage occurs after rate-determining hydrazine addition information as to its molecularity is more difficult to gather. However, we proffer a unimolecular bond cleavage mechanism.

If the α,β-proton migration is not unimolecular and is aided by either another metal center or by another molecule of hydrazine, that bimolecular reaction must be much faster than bimolecular reaction of the $Mo(NMe_2)(NHNMe_2)(dpma^{mes})$ intermediate with hydrazine to replace NMe_2 considering no $NMo(NHNMe_2)(dpma^{mes})$ is observed. It seemed more reasonable to assert that a proton migration, either with concomitant N–N bond cleavage or without, is unimolecular and fast. In addition, the N–N cleavage mechanism proposed is the microscopic reverse of known reactions in the literature and has analogies to known O–O bond cleavage mechanisms as discussed in the paper.

A.10: Kinetics on the reaction of $Zr(NMe_2)_2(dpma^{mes})$ (3) with H_2NNMe_2

Kinetic data for the reaction of **3** with hydrazine was obtained on a Varian 600 MHz NMR instrument. A stock solution of *N*,*N*-dimethylhydrazine (2 equiv.) in C_6D_6 was injected through a septum into an 5 mm NMR tube containing **3** (1 equiv.) in C_6D_6 (1.2 mL). The reaction was monitored by the ^1H NMR integration of the methylene resonances of **3** and **4**. There was an observed intermediate with steady-state behavior with NMR resonances suggestive of $Zr(NMe_2)(NHNMe_2)(dpma^{mes})$.

Data was fit using the OriginPro 7.5 software package to a 2nd-order equation, where Y_t is the methylene integral value for **3**, Y_∞ is the integral value at "infinite" time, and Y_0 is the initial integral value. The factor Δ_0 is the difference in concentration between dimethylhydrazine and **3** at the start of the reaction. The initial dimethylhydrazine concentration, $[hydrazine]_0$, and zirconium concentration, $[\mathbf{3}]_0$, were 0.0633 M and 0.0317 M respectively, giving $\Delta_0 = 0.0317$.

$$Y_t = \frac{Y_\infty + \left\{ Y_0 \left(1 - \frac{[\mathbf{3}]_0}{[hydrazine]_0} \right) - Y_\infty \right\} e^{-\Delta_0 k_{obs} t}}{1 - \frac{[\mathbf{3}]_0}{[hydrazine]_0} e^{-\Delta_0 k_{obs} t}}$$

The proposed reaction pathway involves reaction of **3** with hydrazine in a stepwise fashion. An intermediate assigned as mono(dimethylamido) (**I**) is observable at low concentrations (~steady state) throughout the reaction.

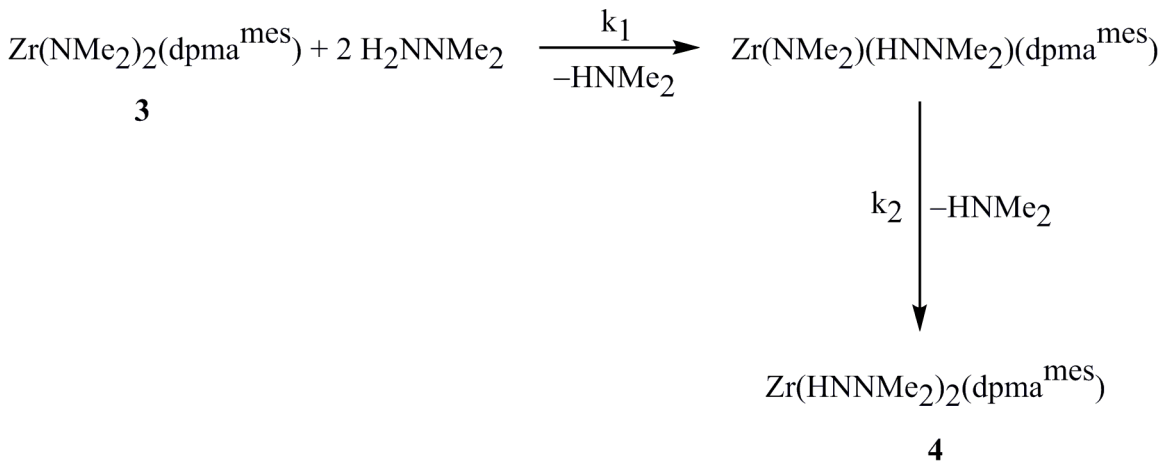

Figure A.13: Reaction of **3** with 2 equivalents of dimethylhydrazine giving **4**

If a second order rate law is applied to the formation of **4** and the steady-state approximation is used to eliminate the concentration of the intermediate **I**, it is simply found that the rate law should be $d[\mathbf{4}]/dt = k_{obs}[\mathbf{3}][\text{hydrazine}]$ consistent with experiment.

One of the 2nd-order fits is shown below as an example.

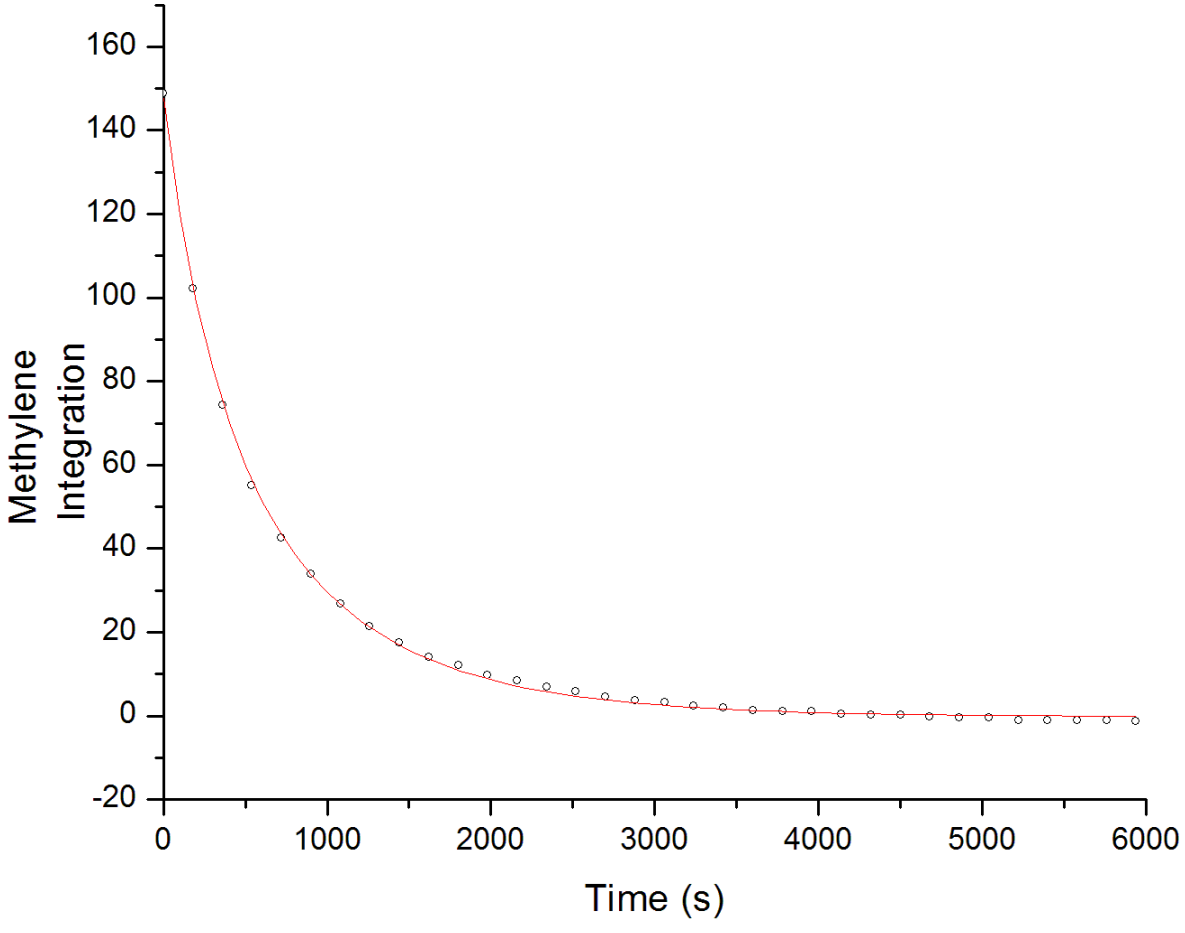

Figure A.14: A representative 2nd order fir of reaction of **3** with disubstituted hydrazine

Below is a stacked ^{1}H NMR of the methylene region in the 25 °C kinetics run. The run lasted around 20 h with traces every 20 min. The second stacked ^{1}H NMR is the same run showing the first 160 min of the reaction with traces every 2 min.

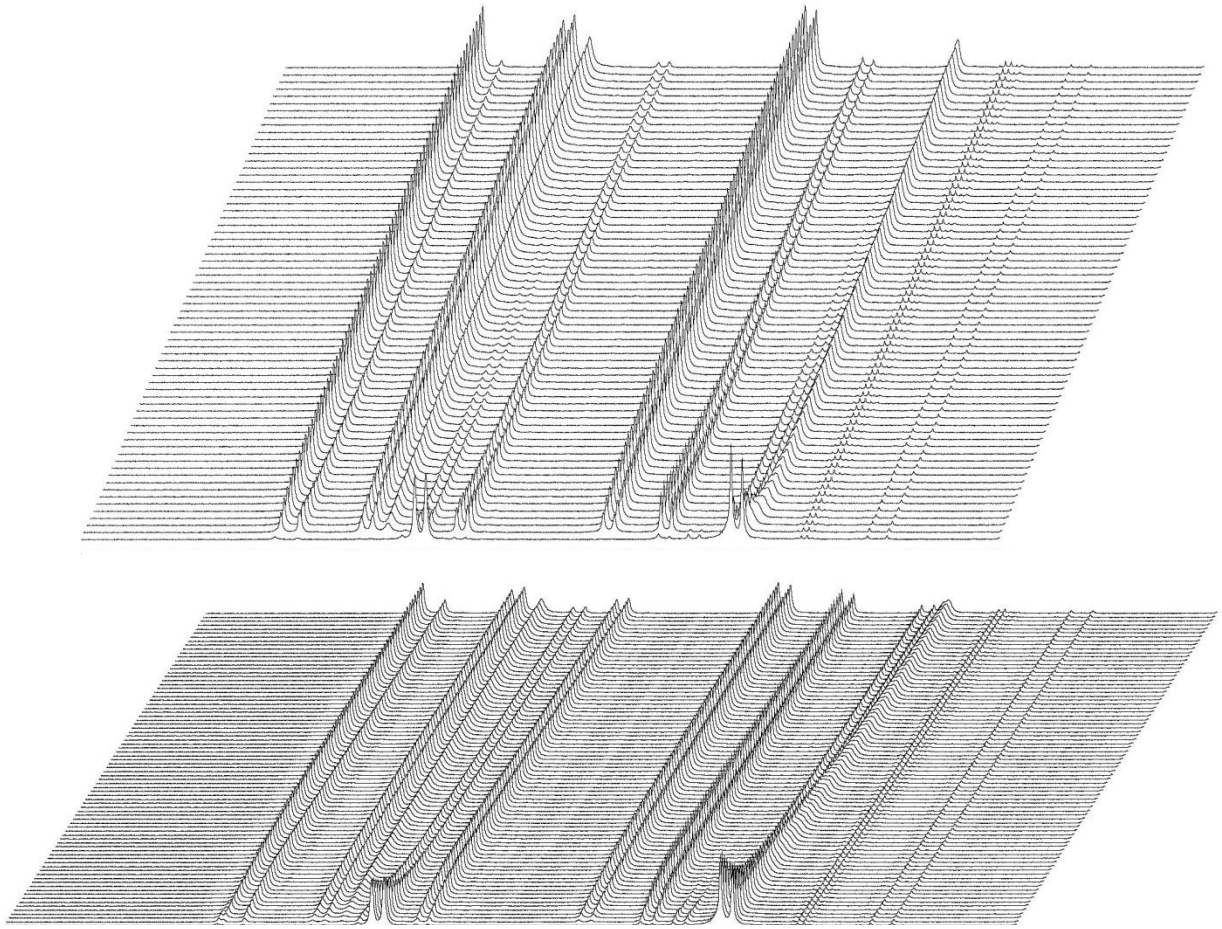

Figure A.15: Stacked 1H NMR plots of a reaction of **3** with disubstituted hydrazine over 20 h with traces taken every 20 min (top), and the first 160 min of the same run with traces taken every 2 min (bottom).

The reaction rate was examined versus temperature as well. The results are tabulated below along with a ln(k/T) vs 1/T (Eyring) plot.

Temp(°C)	k_{obs} ($\times 10^{-2}$)	Error in k_{obs} ($\times 10^{2}$)
26.54	1.736	0.017
40.71	2.191	0.061
54.41	3.449	0.037
67.68	7.434	0.137

Table A.2: Rate constants at different temperatures for the reaction of **3** with 2 equivalents of H_2NNMe_2

The calculated activation parameters from the Eyring plot are $\Delta H^{\ddagger}$ = +6 kcal/mol and $\Delta S^{\ddagger}$ = –45 cal/mol•K. These are similar to the activation parameters for the molybdenum analog of $\Delta H^{\ddagger}$ = +7 kcal/mol and $\Delta S^{\ddagger}$ = –35 cal/mol•K.

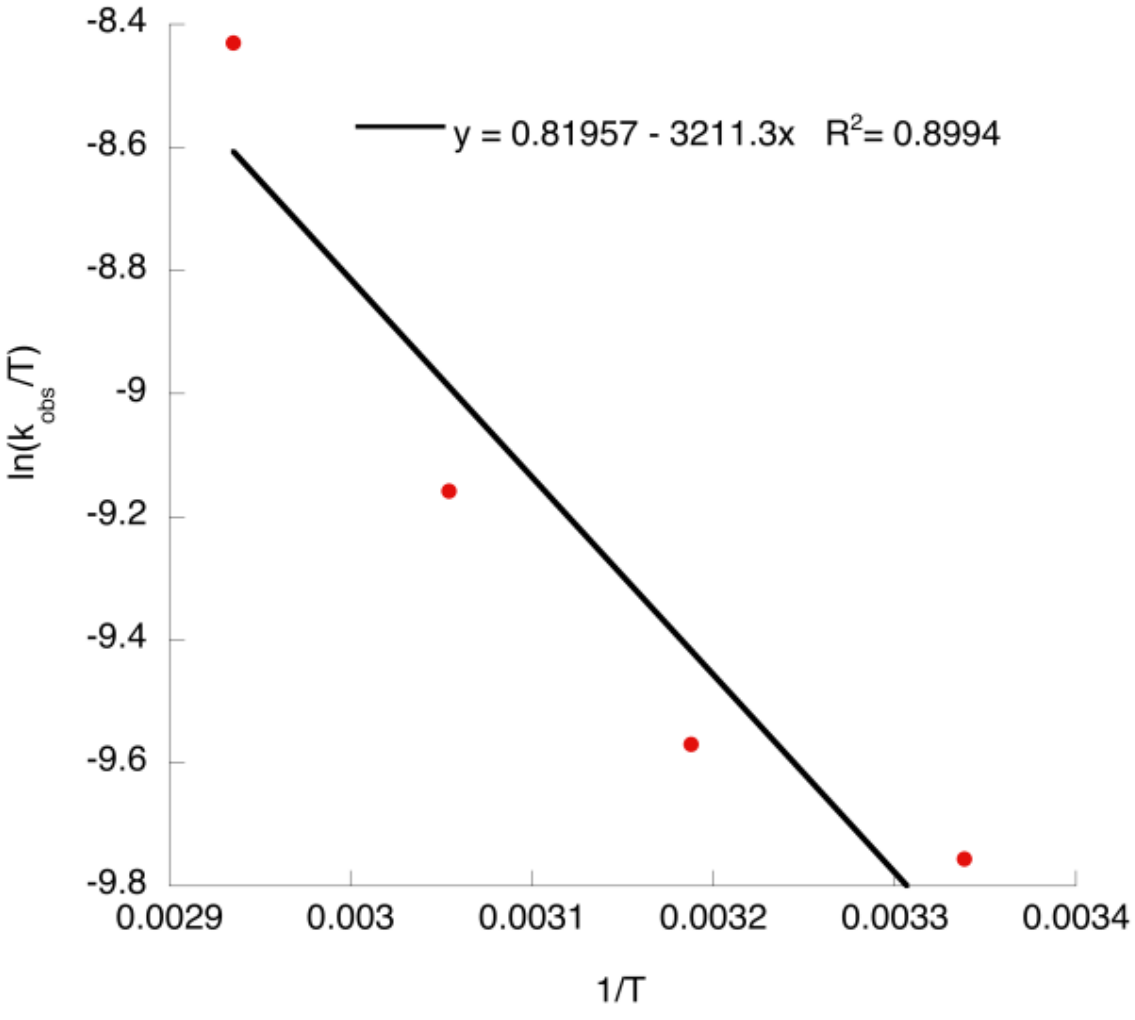

Figure A.16: Eyring plot of **3** with H_2NNMe_2

The reactions with the zirconium analog are somewhat slower and there are some differences in the structures for the two compounds, most of which are discussed in the text. An overlay of the two structures is provided below.

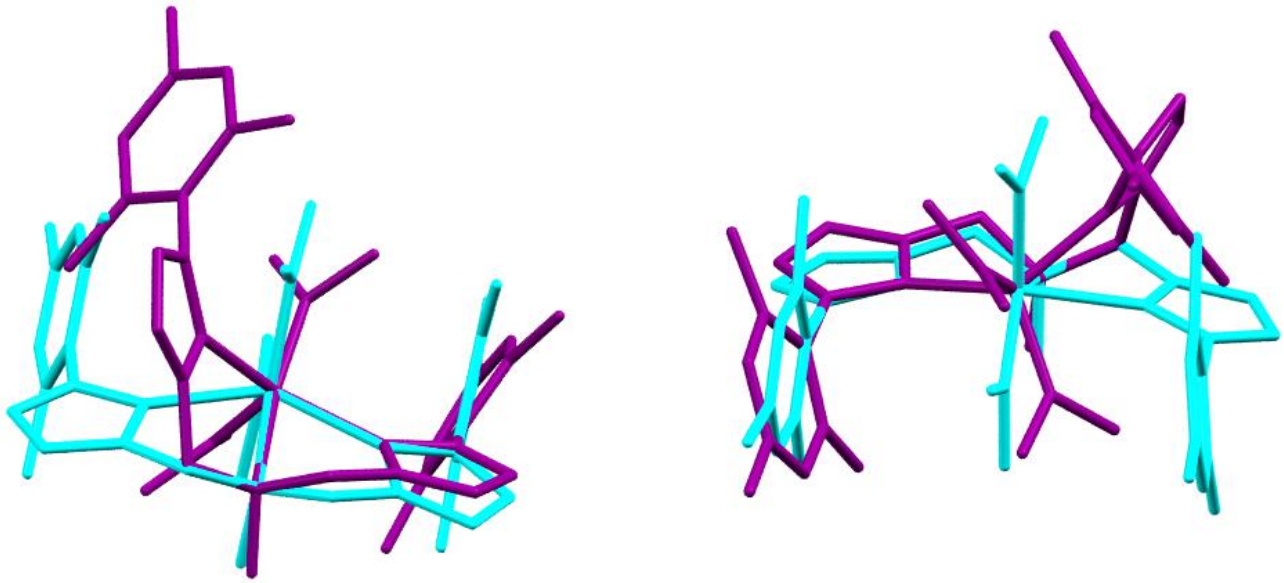

Figure A.17: Overlaid crystal structure renderings of $Mo(dpma^{mes})(NMe_2)_2$ (**1**) in purple $Zr(dpma^{mes})(NMe_2)_2$ (**3**) in blue

A.11: ^{1}H NMR Assignment of (2-syn) via HOMO Decoupling

Compound (**2**-*syn*) shows interesting couplings in its room temperature ^{1}H NMR spectrum. To investigate these small couplings a series of homo decoupled ^{1}H NMR spectra were taken. In each spectrum a single resonance was saturated resulting in a change in multiplicity of any other resonance coupled to it. This allowed the assignment of two distinguishable dimethylamido proton environments (3.20 and 2.50 ppm) with a 1 Hz coupling. These methyl protons are likely too far from the *N*-methyl protons of the dpma^{mes} ligand (5.45 Å *syn* and 5.55 Å *anti* in the solid state) to be coupling to those, and no 2D NOESY cross-peak was identified.

Furthermore, the methylene resonances from the backbone in the dpma^{mes} ligand displayed a small coupling (J_{HH} = 0.5 Hz) in addition to the geminal coupling caused by hindered rotation upon chelation (J_{HH} = 14.0 Hz). Saturation of each of the β-pyrrolyl resonances showed the origin of this coupling and allowed for the assignment pyrrolyl resonances.

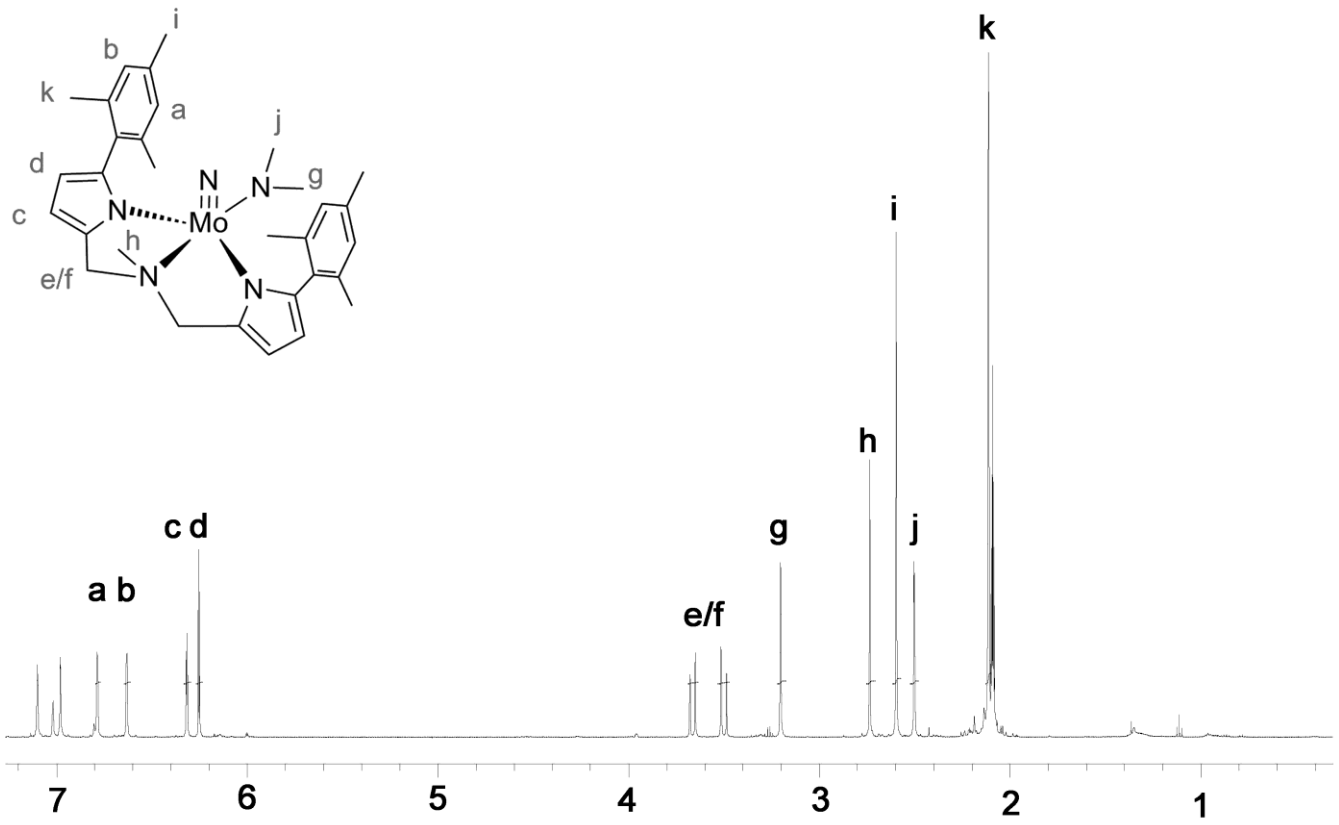

Figure A.18: ^{1}H NMR of 2-syn with the assigned proton resonanceses on the inset structure

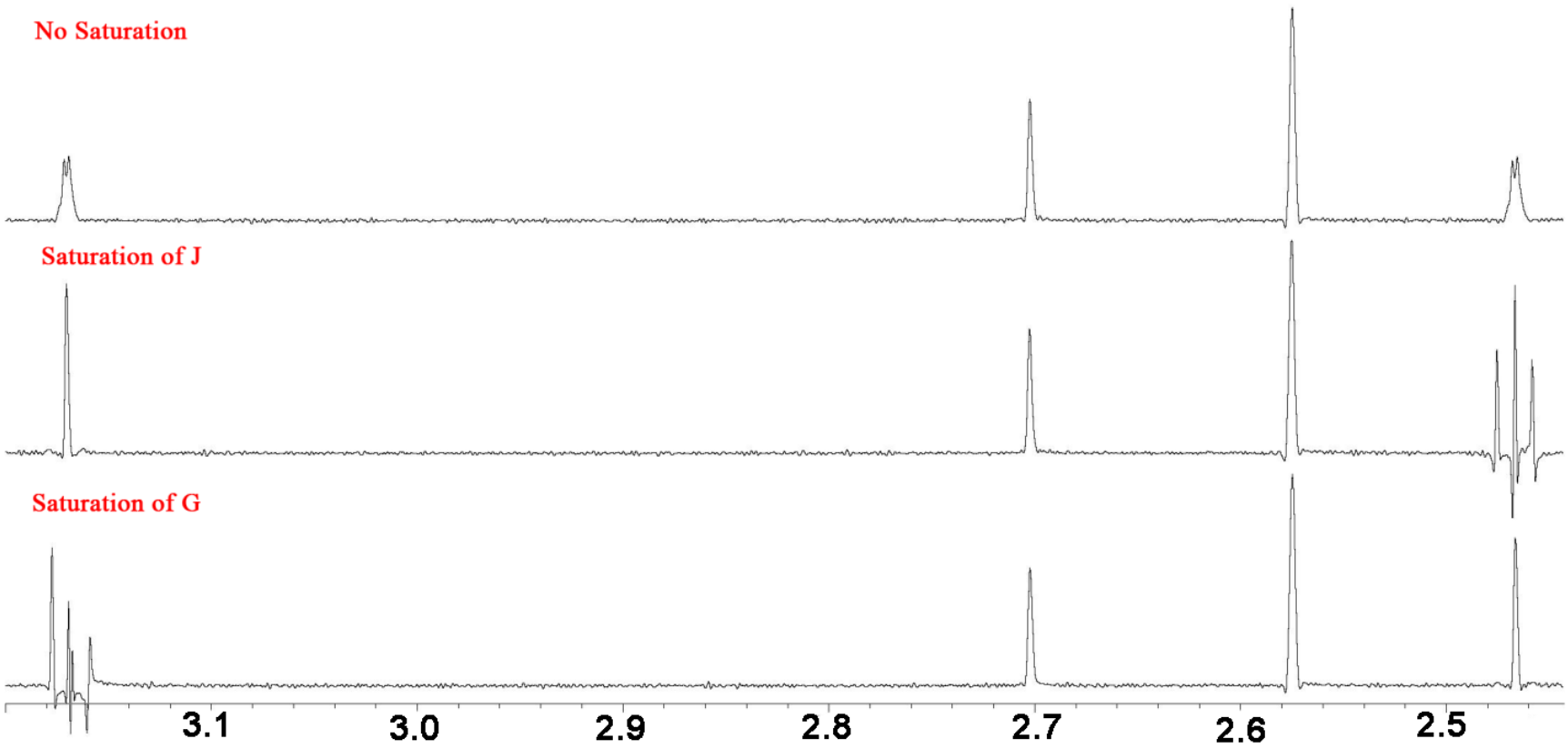

Figure A.19: A region of the homo decoupled spectra ^{1}H NMR of 2-syn showing the changing multiplicity of each peak when saturating another.

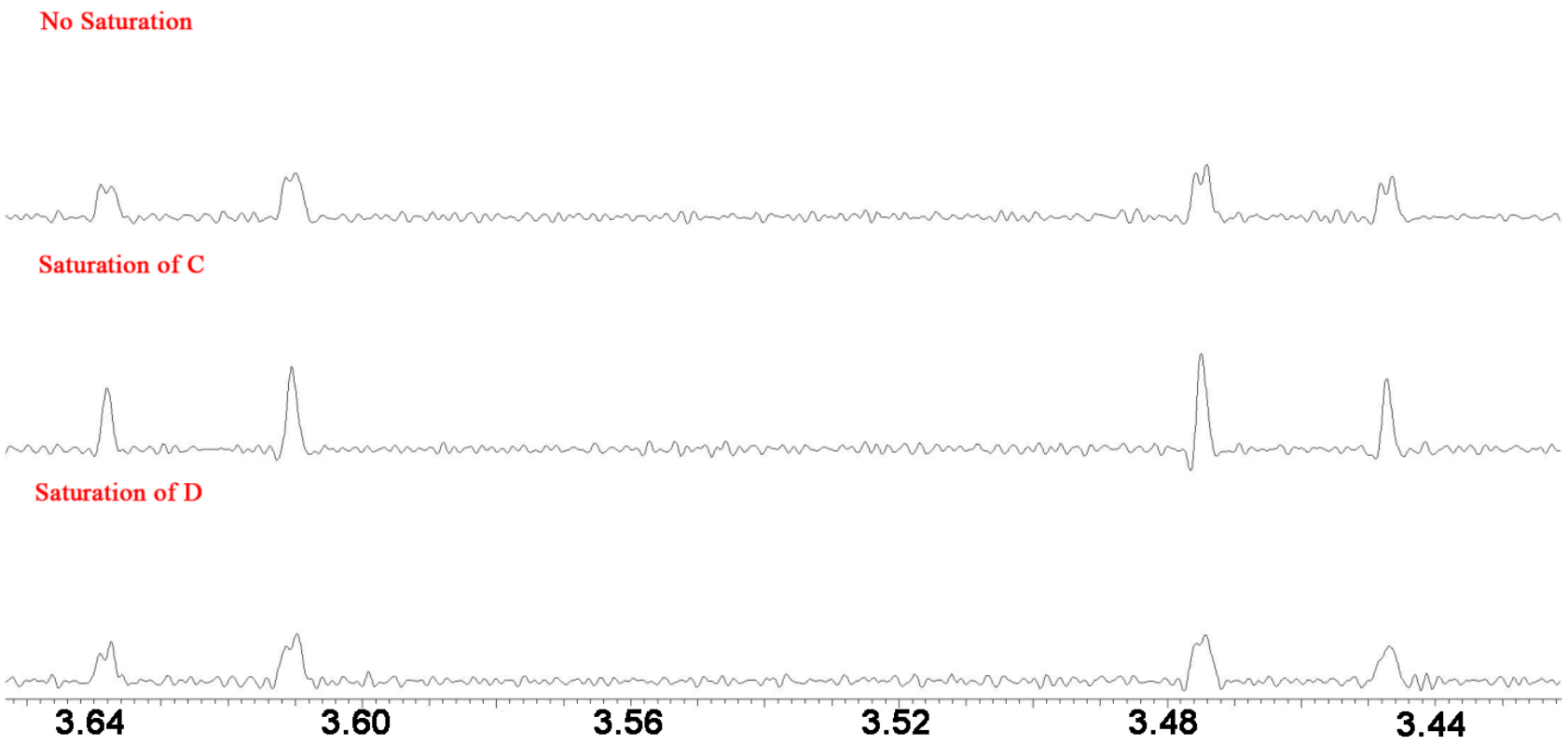

Figure A.20: A region of the homo decoupled ^{1}H NMR spectra of 2-syn showing the changing multiplicity of each peak when saturating another

REFERENCES

REFERENCES

(1) For some reviews and selected seminal papers see (a) M. D. Fryzuk, *Acc. Chem. Res.* 2009, **42**, 127. (b) P. J. Chirik, *Organometallics* 2010, **29**, 1500. (c) S. Gambarotta, J. Scott, *Angew. Chem. Int Ed* 2004, **43**, 5298. (d) N. Hazari, *Chem. Soc. Rev.* 2010, **39**, 4044. (e) Z. Jonas, P. Sobota, *Coord. Chem. Rev.* 2005, **249**, 2144. (f) K. H. Horn, N. Bores, N. Lehnert, K. Mersmann, C. Nather, G. Peters, F. Tuczek, *Inorg. Chem.* 2005, **44**, 3016. (g) A. Dreher, K. Mersmann, C. Nather, I. Ivanovic-Burmazovic, R. van Eldik, F. Tuczek, *Inorg. Chem.* 2009, **48**, 2078. (h) J.-P. F. Cherry, P. L. Diaconescu, C. C. Cummins, *Can. J. Chem.* 2005, **83**, 302. (i) G. Christian, R. Stranger, B. F. Yates, *Chem. Eur. J.* 2009, **15**, 646. (j) D. V. Yandulov, R. R. Schrock, *Science* 2003, **301**, 76. (k) R. R. Schrock, *Angew. Chem. Int. Ed.* 2008, **47**, 4415. (l) C. E. Laplaza, M. J. A. Johnson, J. C. Peters, A. L. Odom, E. Kim, C. C. Cummins, G. N. George, I. J. Pickering, *J. Am. Chem. Soc.* 1996, **118**, 8623. (m) R. A. Henderson, G. J. Leigh, C. J. Pickett, *Dalton Trans.* 1989, 425. (n) Y. Nishibayashi, *Dalton Trans.* 2012, **41**, 7447.

(2) For some reviews see (a) B. K. Burgess, D. J. Lowe, *Chem. Rev.* 1996, **96**, 2983. (b) Y. Hu, M. W. Ribbe, *Acc. Chem. Res.* 2010, **43**, 475. (c) L .C. Seefeldt, B. M. Hoffman, D. R. Dean, *Ann. Rev. Biochem.* 2009, **78**, 701.

(3) R. Schlögl, *Angew. Chem. Int Ed* 2003, **42**, 2004.

(4) In FeMo-cofactor of nitrogenase there is also a light element (1^{st} row *p*-block) in the X-ray diffraction experiments. Recent XES studies assert that the central atom in the cluster is a carbon. K. M. Lancaster, M. Roemelt, P. Ettenhuber, Y. Hu, M. W. Ribbie, F. Neese, U. Bergmann, S. DeBeer, *Science*, 2011, **334**, 974.

(5) B. M. Hoffman, D. R. Dean, L. C. Seefeldt, *Acc. Chem. Res.* 2009, **42**, 609.

(6) Hydrazido(2–) and isodiazene are two different resonance form participants for $M{=}N{-}NH_2$ ligands. The hydrazido resonance form is considered to be a dianionic ligand, and the isodiazene form is a neutral donor. The situation is very similar to Fischer versus Schrock carbenes and depends on the strength of the β-nitrogen lone pair participation. For a discussion see S. Patel, Y. Li, A. L. Odom, *Inorg. Chem.* 2007, **46**, 6373.

(7) For some examples of diazene pathways see (a) J. L. Crossland, C. G. Balesdent, D. R. Tyler, *Inorg. Chem.* 2012, **51**, 439. (b) C. T. Saouma, C. E. Moore, A. L. Rheingold, J. C. Peters, *Inorg. Chem.* 2011, **50**, 11285. (c) L. D. Field, H. L. Li, A. M. Magill, *Inorg. Chem.* 2009, **48**, 5.

(8) For some representative examples of Mo and W diazenes see (a) M. R. Smith III, T.-Y. Cheng, G. L. Hillhouse, *Inorg. Chem.* 1992, **31**, 1535. (b) M. R. Smith III, T.-Y. Cheng, G. L. Hillhouse, *J. Am. Chem. Soc.* 1993, **115**, 8638. For a few selected recent examples od diazene complexed with other metals see (c) L. D. Field, H. L. Li, S. J. Dalgarno, *Inorg.*

Chem. 2010, **49**, 6214. (d) C. T. Saouma, P. Muller, J. C. Peters, *J. Am. Chem. Soc.* 2009, **131**, 10358. (e) L. D. Field, H. L. Li, S. J. Dalgarno, P. Turner, *Chem. Commun.* 2008, 1680.

(9) (a) J. T. Ciszewski, J. F. Harrison, A. L. Odom, *Inorg. Chem.* 2004, **43**, 3605. (b) Y. Li, Y. Shi, A. L. Odom, *J. Am. Chem. Soc.* 2004, **126**, 1794. (c) Y. Li, A. Turnas, J. T. Ciszewski, A. L. Odom, *Inorg. Chem.* 2002, **41**, 6298. (d) C. Cao, J. T. Ciszewski, A. L. Odom, A. L. *Organometallics* 2001, **20**, 5011. (e) S. A. Harris, J. T. Ciszewski, A. L. Odom, *Inorg. Chem.* 2001, **40**, 1987.

(10) R, D, Rieth, N. P. Mankad, E. Calimano, J. P. Sadighi, *Org. Lett.* 2004, **6**, 3981.

(11) M. H. Chisholm, F. A. Cotton, M. W. Extine, *Inorg. Chem.* 1978, **17**, 1329-1332.

(12) S. Alvarez, M. Llunell, *Dalton Trans* 2000, 3288-3303.

(13) S. A. DiFranco, N. A. Maciulis, R. J. Staples, R. J. Batrice, A. L. Odom, *Inorg. Chem.* 2012, **51**, 1187-1200.

(14) (a) D. F. Evans, *J. Chem. Soc.* 1959, 2003. (b) D. H. Grant, *J. Chem. Ed.* 1995, **72**, 39.

(15) P. Gütlich, B. R. McGarvey, W. Kläui, *Inorg. Chem.*, 1980, **19**, 3704. Here we replace their $(\Delta\nu/\Delta_0)_{LS}$ with δ' simply because the term was fit as a single parameter. The value of δ' was found to be small, ~0.04 ppm.

(16) C. E. Krilley, P. E. Fanwick, I. P. Rothwell *J. Am. Chem. Soc.*, 1994, **116**, 5225.

(17) N. C. Mösch-Zanetti, R. R. Schrock, W. M. Davis, K. Wanniger, S. W. Seidel, M. B. O'Donoghue, *J. Am. Chem. Soc.* 1997, **119**, 11037.

(18) E. Katayev, Y. Li, A. L. Odom, *Chem. Commun.* 2002, 838.

(19) K. M. Wampler, R. R. Schrock, *Inorg. Chem.* 2007, **46**, 8463.

(20) Gaussian 09, Revision C.01, M. J. Frisch, G. W. Trucks, H. B. Schlegel, G. E. Scuseria, M. A. Robb, J. R. Cheeseman, G. Scalmani, V. Barone, B. Mennucci, G. A. Petersson, H. Nakatsuji, M. Caricato, X. Li, H. P. Hratchian, A. F. Izmaylov, J. Bloino, G. Zheng, J. L. Sonnenberg, M. Hada, M. Ehara, K. Toyota, R. Fukuda, J. Hasegawa, M. Ishida, T. Nakajima, Y. Honda, O. Kitao, H. Nakai, T. Vreven, J. A. Montgomery, Jr., J. E. Peralta, F. Ogliaro, M. Bearpark, J. J. Heyd, E. Brothers, K. N. Kudin, V. N. Staroverov, R. Kobayashi, J. Normand, K. Raghavachari, A. Rendell, J. C. Burant, S. S. Iyengar, J. Tomasi, M. Cossi, N. Rega, J. M. Millam, M. Klene, J. E. Knox, J. B. Cross, V. Bakken, C. Adamo, J. Jaramillo, R. Gomperts, R. E. Stratmann, O. Yazyev, A. J. Austin, R. Cammi, C. Pomelli, J. W. Ochterski, R. L. Martin, K. Morokuma, V. G. Zakrzewski, G. A. Voth, P. Salvador, J. J. Dannenberg, S. Dapprich, A. D. Daniels, Ö. Farkas, J. B. Foresman, J. V. Ortiz, J. Cioslowski, and D. J. Fox, Gaussian, Inc., Wallingford CT, 2009.

(21) L. A. Curtiss, K. Raghavachari, P. C. Redfern, V. Rassolov, and J. A. Pople, *J. Chem. Phys.* 1998, **109**, 7221.

(22) D. F. McMillen, D. M. Golden, *Ann. Rev. Phys. Chem.* 1982, **33**, 493.

(23) DiFranco, S. A.; Odom, A. L. manuscript in preparation.

(24) A. E. Merbach, *Pure Appl. Chem.* 1982, **54**, 1479.

(25) Compare with a related reaction where a formal M(II) nitrosyl complex is formally oxidized by addition of highly reducing V(III) through intraligand bond cleavage and formation of nitrido. (a) A. L. Odom, C. C. Cummins, J. D. Protasiewicz, *J. Am. Chem. Soc.* 1995, **117**, 6613. (b) A. L. Odom, C. C. Cummins, *Polyhedron*, 1998, **17**, 675. (c) A. S. Veige, L. M. Slaughter, E. B. Lobkovsky, P. T. Wolczanski, N. Matsunaga, S. A. Decker, T. R. Cundari, *Inorg. Chem.* 2003, **42**, 6204. Also see redox neutral hydroamination mechanistic proposals where electrocyclic reactions in the ligands are enabled by zirconium. K. Manna, M. L. Kruse, A. D. Sadow, *ACS Catalysis*, 2011, **1**, 1637.

(26) (a) M. H. V. Huynh, E.-S. El-Samanody, K. D. Demadis, T. J. Meyer, P. S. White, *J. Am. Chem. Soc.* 1999, **121**, 1403. For closely related additions of hydroxylamines to nitridos see (b) M. H. V. Huynh, T. J. Meyer, M. A. Hiskey, D. L. Jameson, *J. Am. Chem. Soc.* 2004, **126**, 3608. The reverse of the hydroxylamine cleavage, addition of an alcohol to a nitrido has also been reported (c) M. H. V. Huynh, P. S. White, K. D. John, T. J. Meyer, *Angew. Chem. Int. Ed.* 2001, **40**, 4049.

(27) Example in Figure 1.6 is from reference 26a. The hydrazido(1–), compound **4b** in the paper, was characterized as a mixture with its deprotonated hydrazido(2–) derivative in 54% yield.

(28) For some selected examples see (a) D. C. Ware, H. Taube, *Inorg. Chem.* 1991, **30**, 4605. (b) T. J. Crevier, T. M. Mayer, *J. Am. Chem. Soc.* 1998, **120**, 5595. (c) T. J. Crevier, B. K. Bennett, J. D. Soper, J. A. Bowman, A. Dehestani, D. A. Hrovat, S. Lovell, W. Kaminsky,

J. M. Mayer, *J. Am. Chem. Soc.* 2001, **123**, 1059. (d) A. G. Maestri, K. S. Cherry, J. J. Toboni, S. N. Brown, *J. Am. Chem. Soc.* 2001, **123**, 7459. (e) S. N. Brown, *J. Am. Chem. Soc.* 1999, **121**, 9752. (f) S. N. Brown, *Inorg. Chem.* 2000, **39**, 378. (g) M. H. V. Huynh, P. S. White, T. J. Meyer, *Inorg. Chem.* 2000, **39**, 2825. (h) M. H. V. Huynh, P. S. White, T. J. Meyer, *J. Am. Chem. Soc.* 2001, **123**, 9170. (i) S. B. Seymore, S. N. Brown, *Inorg. Chem.* 2002, **41**, 462.

(29) (a) J. D'Antonio, R. A. Ghiladi, *Biochemistry* 2011, **50**, 5999-6011. (b) Y. Ichikawa, H. Nakajima, Y. Watanabe, *ChemBioChem* 2006, **7**, 1582-1589. (c) I. G. Denisov, T. M. Makris, S. Sligar, *J. Biol. Chem.* 2002, **277**, 42706-42710. (d) T. Matsui, S. Ozaki, E. Liong, G. N. Phillips, Jr.; Y. Watanabe, *J. Biol. Chem.* 1999, **274**, 2838-2844. (e) H. B. Dunford, W. D. Hewson, H. Steiner, *Can. J. Chem.*, 1978, **56**, 2844-2852. (f) M. Kato, S. Aibara, Y. Morita, H. Nakatani, K. Hiromi, *J. Biochem.* 1984, **95**, 861. (g) L. Gebicka, J. Pawlak, *J. Molecular Cat. B:Enzymatic*, 1997, **2**, 185.

(30) (a) T. L. Poulos, J. Kraut *J. Biol. Chem.* 1980, **255**, 8199. (b) E. Derat, S. Shaik, *J. Phys. Chem. B* 2006, **110**, 10526.

Chapter 2: Molybdenum (IV) Promoted Radical Bond Cleavage of Alcohols

ABSTRACT

An intriguing product, 1,2 diphenylethane was recovered from the reaction of Mo(dpma^{mes})(NMe$_2$)$_2$ (**1**) and *O*-benzyl hydroxylamine. This was found to be a result of the by-product benzyl alcohol reacting with **1**. Subsequently, **1** was treated with 2 equiv. of benzyl or trityl alcohol giving organic products resulting from substitution chemistry followed by β-hydride elimination, and the C-C bond forming coupling of radicals. The Mo(VI) *bis*-oxo complex O$_2$Mo(dpma^{mes}) (**2**) is formed as a result of C-O bond cleavage. For comparison the *bis*-imido analogue Mo(NTol)$_2$(dpma^{mes}) (**3**) was independently synthesized via salt metathesis after instillation of the imidos, and was structurally characterized. ^{1}H NMR analysis of other Mo(VI) complexes bearing the dpma^{mes} ligand, *anti*-NMo(dpma^{mes})(NMe$_2$) and *syn*-NMo(dpma^{mes})(NMe$_2$) along with **1** and **3** show a link between the germinal coupling on the methylene of the ligand and the orientation of the *N*-methyl group relative to the metal-ligand multiple bond. The reaction intermediate OMo(dpma^{mes})(OBn) (**5**) was isolated from the treatment of **1** with benzyl alcohol and was structurally characterized. This asserts that the C-O bond braking is the result of two successive 1e$^-$ steps. Reaction of **1** with one or more equivalents of 1-adamantanol result in the mono-substituted paramagnetic complex Mo(dpma^{mes})(NMe$_2$)(OAd) (**6**), which has been determined to be competent for the N-N bond cleaving chemistry like that of **1**.

2.1 Introduction

In probing the reactivity of pyrrolide-supported molybdenum(IV) complexes, which were recently shown to mediate the scission of an *N*-*N* single bond, we postulated that Mo(dpma^{mes})(NMe_2)$_2$ (**1**) could also induce other bond cleavages. Expanding the substrate scope to *O*-substituted hydroxylamines yielded the products expected from *N*-*O* bond cleavage, though in drastically reduced yield (Figure 2.1).

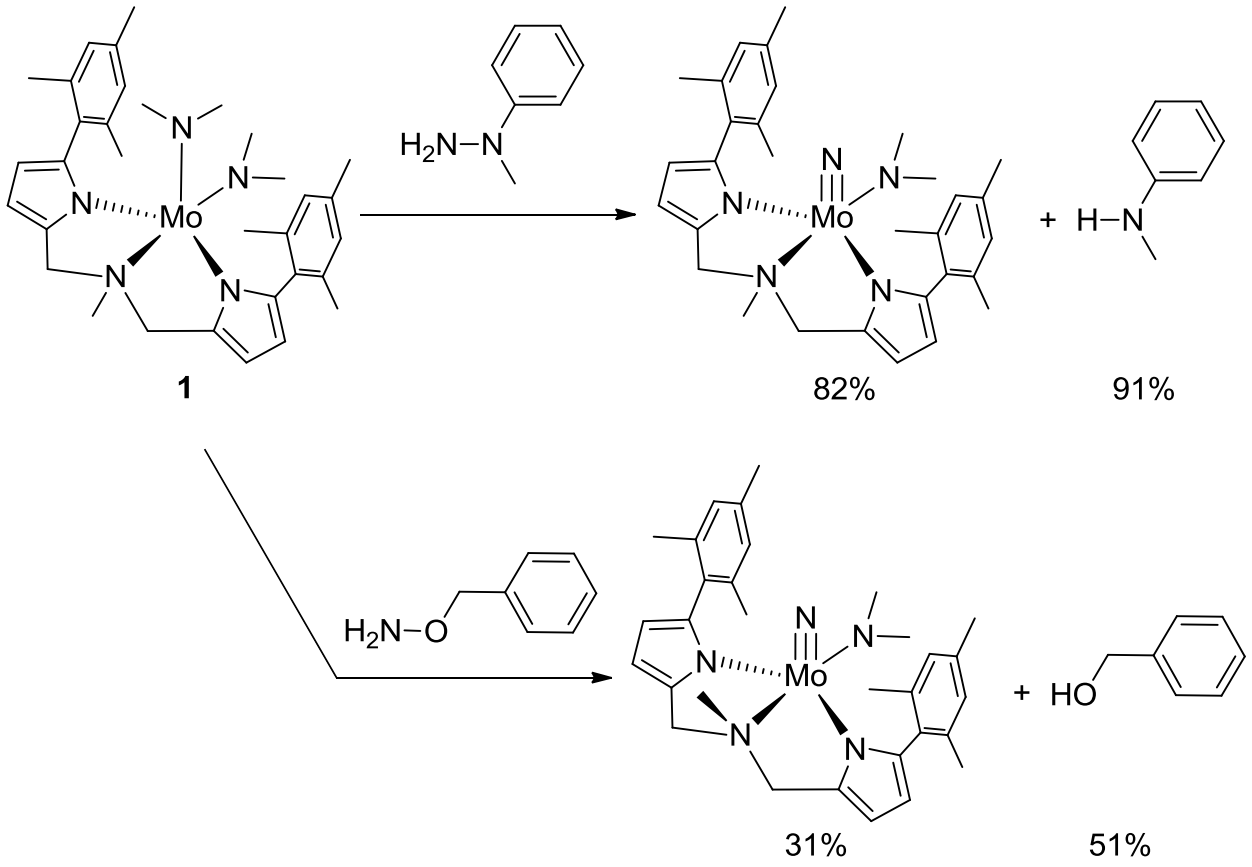

Figure 2.1: N-N and N-O bond cleavages mediated by Mo(dpma^{mes})(NMe_2)$_2$ (**1**) and the major byproduct of each reaction.

Despite the lower yield, the cleavage of hydroxylamines was much faster than the analogous cleavage of hydrazines. The heterolytic breaking of *N-N* and *N-O* bonds in these substrates are $2e^-$ processes, where the necessary electrons are supplied from the d^2 metal center and donated into a σ^* orbital based on the hydrazido(1-) or N bound hydroxylamido(1-) moiety. This pattern of reactivity is in part rationalized by the thermodynamic stability imparted by the creation of a metal-ligand multiple bond supporting the now Mo(VI), d^0 metal center.

Upon further investigation of the cleavage of *O*-benzyl hydroxylamine, two additional byproducts were identified, the results of product inhibition (Figure 2.2). Benzaldehyde was identified in the reaction mixture by GC-MS. The most likely origin of this is the ligand substitution of **1** with the benzyl alcohol produced by N-O cleavage, and subsequent β-hydride elimination. Analogous imine products (which would result from β-hydride elimination of an amide ligand) are not detected in the case of N-N bond scission of disubstituted hydrazines. In all the hydrazines substrates tried, only the piperdine formed by cleavage of *N*-amino-piperdine was competent to substitute the dimethylamide ligands of **1**.

The presence of 1,2-diphenylethane was also detected, the result of a *C-C* bond forming side reaction. This indicated that $Mo(dpma^{mes})_2(NMe_2)_2$ (**1**) was viable for *C-O* bond cleavage (Figure 2.2). ^1H NMR analysis showed a diamagnetic metal containing product, determined to be the *bis*-oxo complex $O_2Mo(dpma^{mes})$ (**2**). This result was striking, as the formation of Mo(VI) was the result of a series of two $1e^-$ processes. This shows that a homolytic pathway is also available in the Mo(IV) system, still resulting in net $2e^-$ oxidation at the metal center.

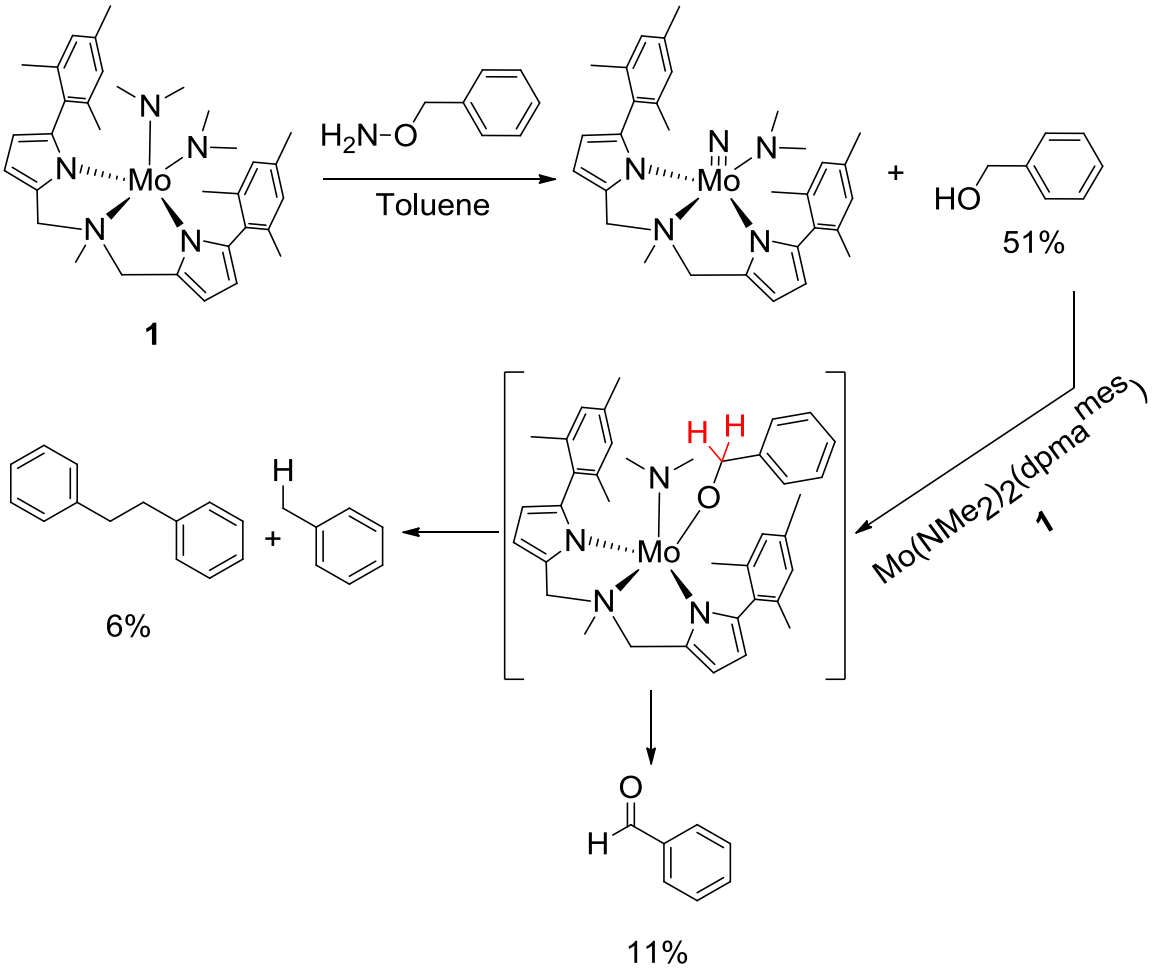

Figure 2.2: Organic byproducts identified in the reaction of **1** with *O*-benzyl hydroxylamine. Calibrated GC-FID yields are given. Toluene presumed to be created during the reaction was undetected above the background, as it was also the solvent for the reaction.

2.2 Reactivity of Mo(dpma^{mes})$(NMe_2)_2$ (1) benzyl alcohol, trityl alcohol and pinicol

To further investigate this new C-C coupling reaction, Mo(dpma^{mes})$_2$$(NMe_2)_2$ (**1**) was treated with 2 equiv. of benzyl alcohol in toluene, similar conditions used in that of hydroxylamine cleavage. The reaction rapidly turned from dark green to orange-brown, characteristic of the of the other Mo(IV) to Mo(VI) transitions seen with **1**. Both benzaldehyde from the β-hydride elimination pathway as well as 1,2 diphenylethane were produced (Table

2.1). Additionally the reaction of **1** with 2 equiv. of benzyl alcohol was conducted as an NMR tube reaction in C_6D_6, confirming the production of toluene.

Substrate[a]	**Yield of $O_2Mo(dpma^{mes})$ (2)**[b]	**Byproduct(s)**	**Yield**[c]
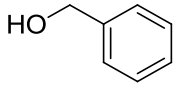	24%	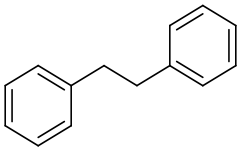	31.6%
		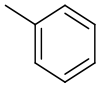	Not observed above background
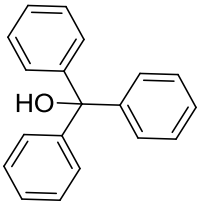	22%	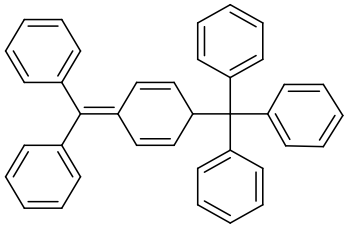	53.9%
		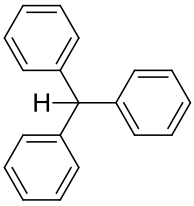	41.6%
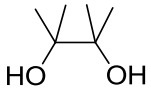	10%	–	–

a Use of 2 equiv. of substrate for benzyl and trityl, and 1 equiv. of pinicol

b Mo containing product yield determined by ^{1}H NMR

c Organic product yield determined by GC-FID relative to cymene or dodecane as an internal standard

Table 2.1: Table of substrates and organic byproducts of the molybdenum mediated C-O bond cleavage.

In an attempt to probe the substrate scope of the above reaction a variety of alcohols were screened. Simple aliphatic alcohols such as 4-methylpentan-1-ol gave complex mixtures of organic products, however low yields of **2** were identified by ^{1}H NMR. Diols, such as pinicol reacted slowly also giving low yields of the metal containing product **2**. Using 2 equiv. of triphenylmethanol proved to be most fruitful, yielding triphenylmethane and Gomberg's dimer, as quantified by GC-FID. The increased yield when using the radical stabilizing substrate triphenylmethanol, as well as the detection of a dimer of the trityl radical implicates a radical mechanism may be operative in the homolytic cleavage of C-O bonds.

2.3 Structural Comparisons and Synthesis of Mo(dpma^{mes})(NTol)$_2$ (3)

Unfortunately, the Mo(IV) hydride product formed from the β-hydride elimination of a benzyloxy ligand was not recovered, nor were the metal-containing decomposition products of this pathway. The only diamagnetic molybdenum-containing product from the reaction of **1** with benzyl or trityl alcohol recovered showed only resonances of bound dpma^{mes} in ^{1}H NMR spectroscopy.

Upon tridentate coordination, the four magnetically equivalent methylene protons of H_2dpma^{mes} split to form a characteristic pair of doublets. In the related case of *anti*-NMo(dpma^{mes})(NMe$_2$) where *N*-methyl on the ligand's backbone is on the opposite side of the plane defined by the pyrrolides as the metal-ligand multiple bond, this presents itself as a pair of doublets with a large coupling constant in toluene-d8 of J_{HH} = 12.5 Hz, and a separation of 591.3 Hz (1.18 ppm) between the two sets. Conversely, the isomer *syn*-NMo(dpma^{mes})(NMe$_2$)

with the *N*-methyl on the same side as the nitride, shows a doublet of doublets, with couplings of J_{HH} = 14.0 Hz and 82.0 Hz (0.16 ppm) (Figure 2.3).

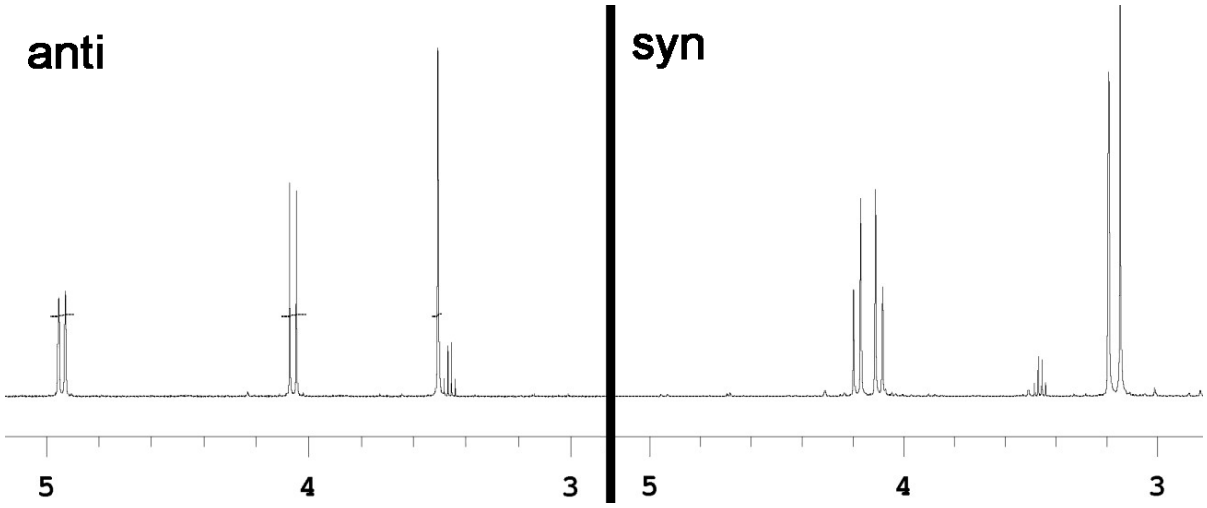

Figure 2.3: Methylene ^{1}H NMR resonances of the bound dpma^{mes} ligand where the N-methyl is *anti* or *syn* to the nitride.

To discern if these vastly different geminal couplings correspond to the *N*-methyl orientation in bound dpma^{mes}, the bis-imido analogue of **2** was independently prepared. Synthesis of *bis*-imido complexes of Mo(VI) have been well established, mainly because they are a route to the Mo(VI) alkylidene-imido complexes active for olefin metathesis (i.e. Schrock's catalyst). Reaction of $(NH_4)_2Mo_2O_7$ with the desired aniline and $SiMe_3Cl$ in the presence of DME and triethylamine affords complexes of the type $Mo(NAr)_2Cl_2(DME)$ where Ar = an aryl group.[1] For our purposes the *p*-tolyl imido was chosen for spectroscopic reasons, as well as to minimize steric congestion close to the metal center. Halide for pyrrolide substitution was

achieved in high yield by treatment of $Mo(NTol)_2Cl_2(DME)$ with 1 equiv. of H_2dpma^{mes} in toluene, in the presence of a slight excess of triethylamine (Figure 2.4).

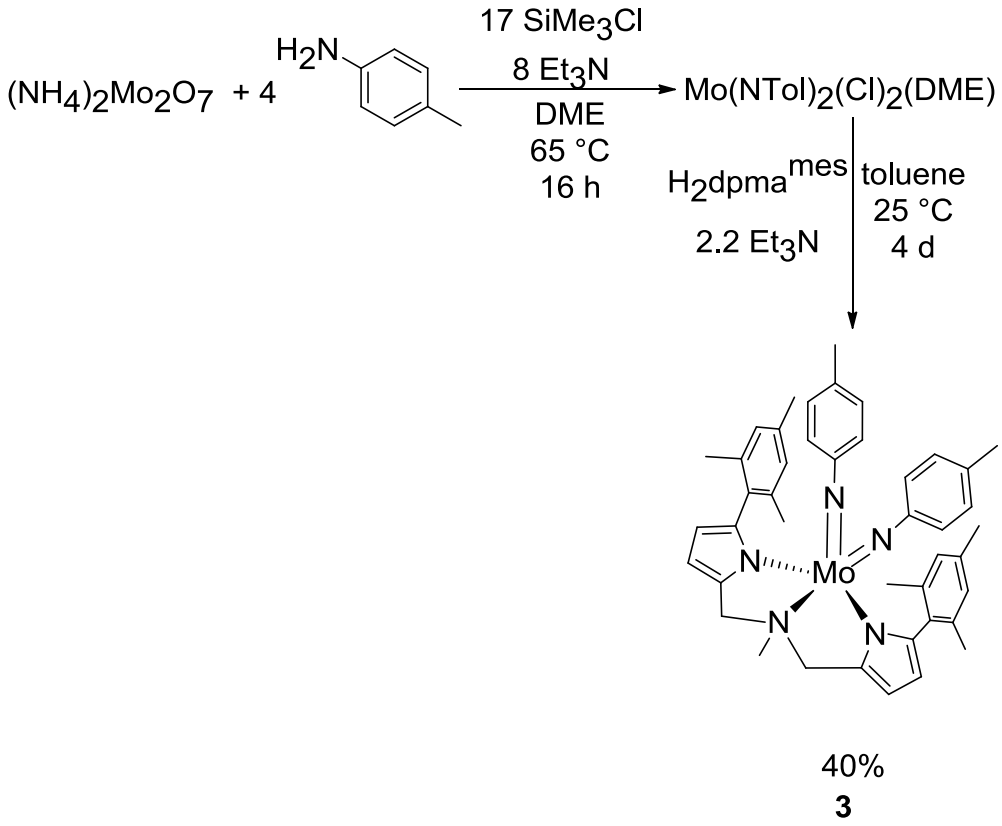

Figure 2.4: Synthesis of $Mo(NTol)_2(dpma^{mes})$ (**3**).

The single crystals of $Mo(NTol)_2(dpma^{mes})$ (**3**) grown from a concentrated ^{n}heptane solution held at −35 °C show **3** as nearly square pyramidal ($\tau = 0.12$), with one imido taking the apical position (Figure 2.5). Mo1-N4 and Mo1-N5 bond distances are 1.750(2) Å and 1.760(2) Å

respectively, and are similar to other 5 coordinate imidos of this type. Notably, the Mo1-N3 bond distance (2.281(2) Å) is nominally longer than the corresponding Mo1-N3 bond in *anti*-NMo(dpma^{mes})(NMe$_2$) (2.275(3) Å), nicely illustrating the larger *trans*-influence of an imido over an amido ligand.[2]

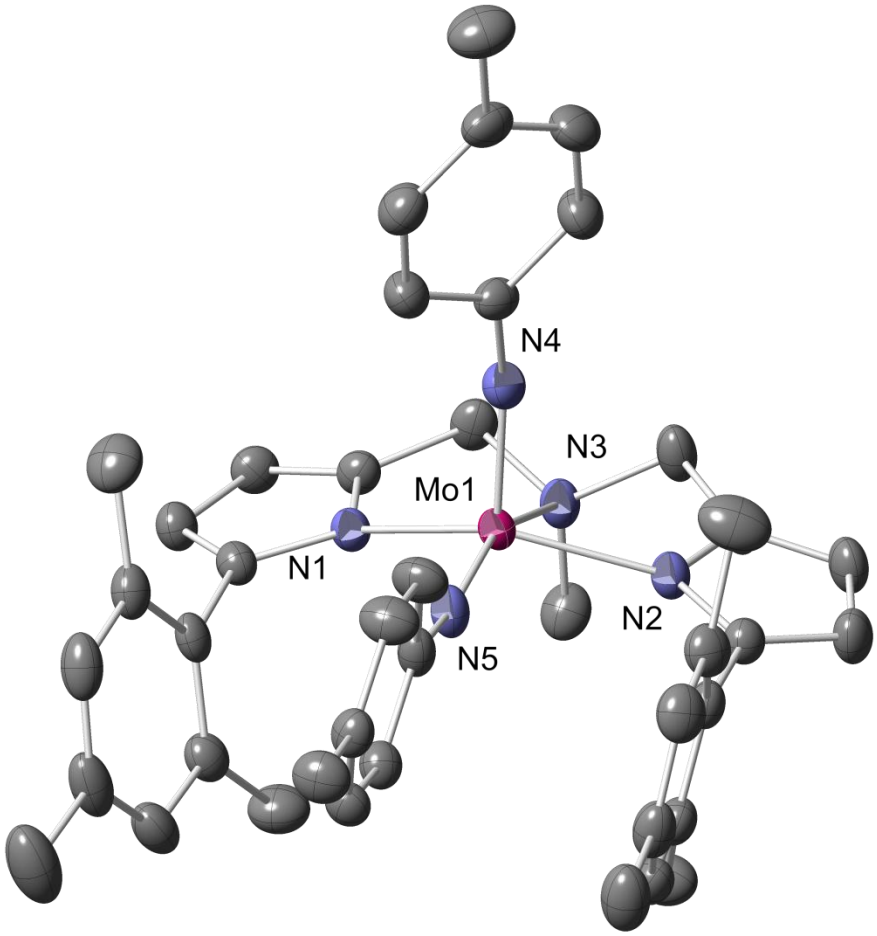

Figure 2.5: Crystal structure rendering of the Mo(VI) *bis*-imido Mo(NTol)$_2$(dpma^{mes}) (**3**). Thermal ellipsoids at 50% probability with H atoms removed for clarity.

^{1}H NMR analysis of **3** shows a set of methylene doublets for bound dpma^{mes}, of with geminal couplings of J_{HH} = 12.5 Hz and a shift between the sets of doublets of 500.0 Hz (1.0 ppm). This establishes a causal link between the solid state structure and the ^{1}H resonance multiplicity in solution for 5 coordinate Mo centers of dpma^{mes}. Unfortunately, suitable crystals of O_2Mo(dpma^{mes}) (**2**) have not been grown for structural analysis, but the above allows for the formulation of a diamagnetic Mo(VI) complex bearing only dpma^{mes} where the *N*-methyl is *syn* to an oxo bond similar to that of *syn*-NMo(dpma^{mes})(NMe_2). (Table 2.2)

Compound	***anti*-NMo(dpma^{mes})(NMe_2)**	***syn*-NMo(dpma^{mes})(NMe_2)**	**Mo(dpma^{mes})($NTol)_2$ (3)**	**O_2Mo(dpma^{mes}) (2)**
Structure	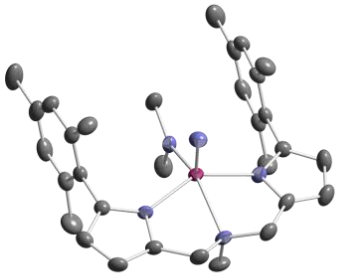	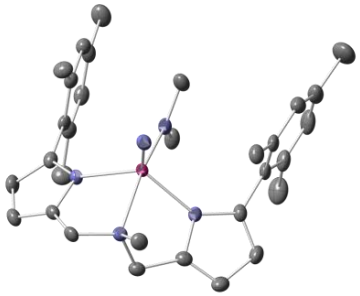	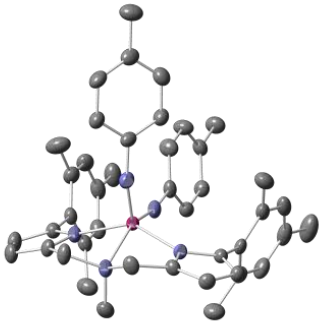	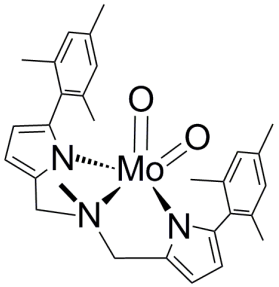
Geminal J_{HH} Coupling (Hz)	12.5	14.0	12.5	14.0
δ difference between doublets Hz (ppm)	591.3 (1.18)	82.0(0.16)	500.0(1.00)	100.5(0.20)

Table 2.2: Comparison of dpma^{mes} N-Methyl orientation toward the metal-ligand multiple bond with the geminal ^{1}H NMR coupling of the methylenes.

2.4 Radical Reactivity in Related Complexes

Though rare in the literature, cleavage of C-O bonds of a molybdenum bound ligands have been reported for alcohols. One such transformation reported by Cummins et. al.[3] involves the reaction of $Ti(NRAr)_3$ [R = $C(CD_3)_2(CH_3)$, Ar = $C_6H_3Me_2$ with $NMo(O^tBu)_3$ which expels a *tert*-butyl radical to produce a Mo-oxo species. The reaction proceeds through initial formation of a μ-Nitrido bridging a Mo(V) and Ti(IV) center as detected by ^{1}H NMR and EPR. From here hemolytic cleavage from the ^{t}butoxide ligand forms a stabilized 3° radical resulting in a $1e^-$ reduction to Mo(VI). Rapid arrangement reinstates a terminal nitride and the formation of a μ-oxo. This reaction however, differs from the observed C-O cleavage in **1** in that the starting Mo(VI) nitride is d^0 whereas **1** is d^2, thus the $1e^-$ ultimately comes from an external open shell source not the Mo center itself (Figure 2.6).

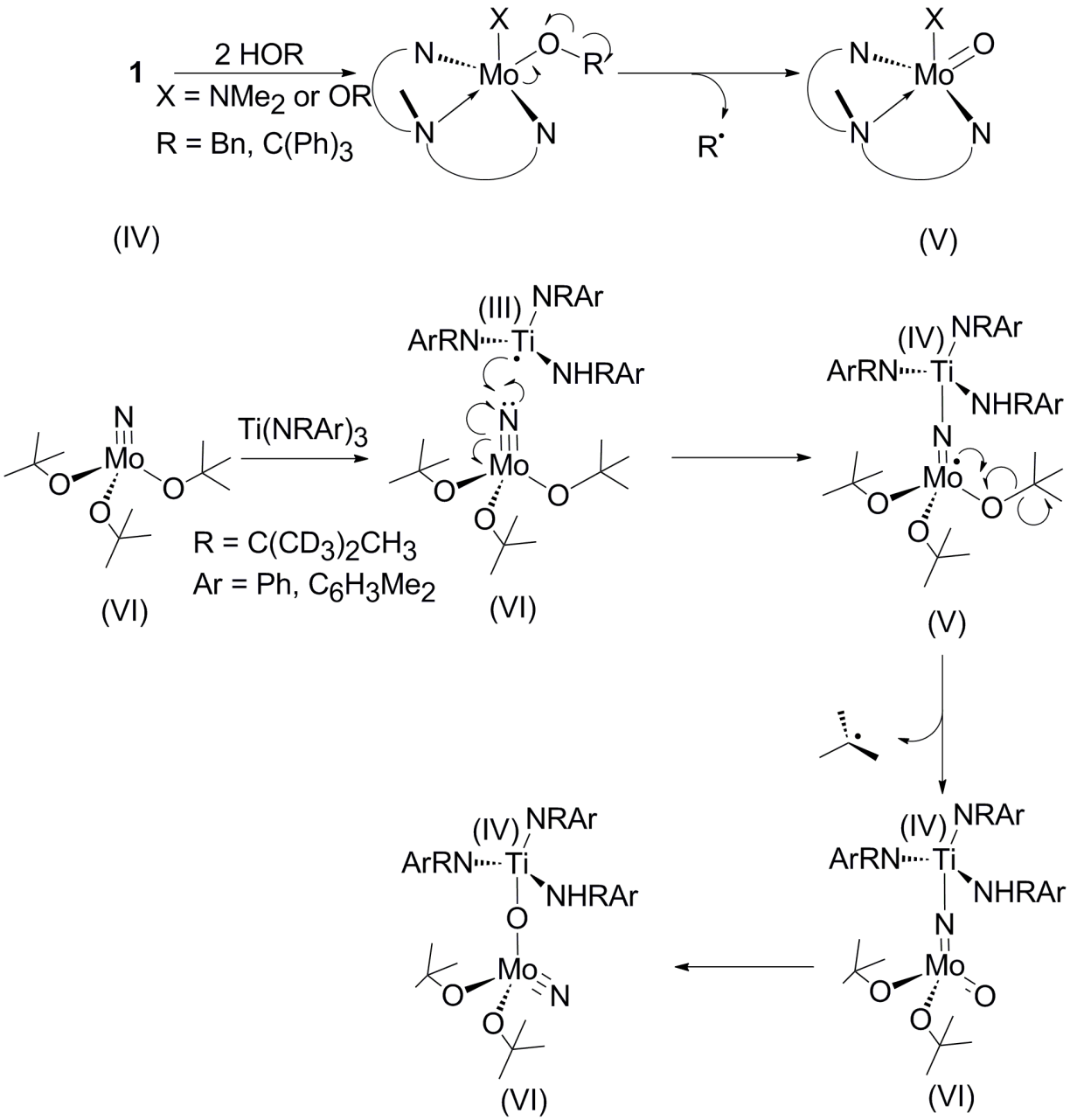

Figure 2.6: The radical forming step in the reaction of **1** with benzylic alcohols (top) along with the expulsion of a ^{t}butyl radical initiated by a Ti(III) radical source (below).

Although the radical source is titanium(III), the microscopic reverse is precedented in the case of vanadium oxo in its highest oxidation state.[4] Also reported by Cummins and coworkers attack of a Ti radical on a metal-ligand multiple bond results in one electron reduction of the vanadium center and the formation of a bridging μ-oxo. Similar to the Mo(VI) nitride system the initial step involves the bridging of the two metal centers by the multiply bounded atom, what may be described as incomplete O atom transfer.[5] However, this system does not cleave off an organic radical. In context of the reactivity seen in **1** the resulting structure may be thought of a 'titanoxide' ligand as noted by the authors. Thus, such a transformation satisfies the concept of microscopic reversibility (Figure 2.7).

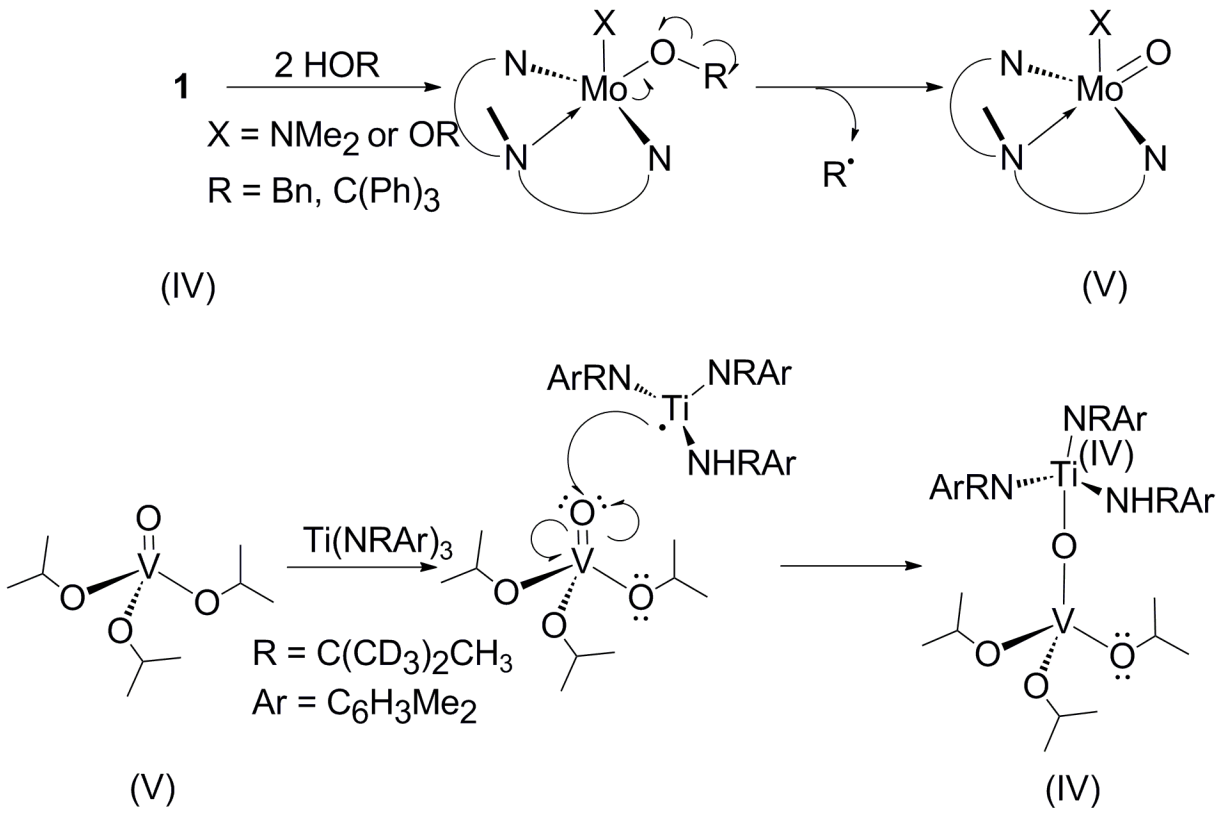

Figure 2.7: Radical attack on a terminal oxo to form a M-O-R linkage.

2.5 Reactivity of Mo(dpma^{mes})(NMe$_2$)$_2$ (1)with Phenols

In further studies aromatic alcohols were screened as substrates with **1**. Upon treatment of **1** with 2 equiv. of phenol in toluene, a rapid reaction occurred, turning the reaction mixture dark brown. Upon ^{1}H NMR analysis only free H$_2$dpma^{mes} was identified, with no metal containing, diamagnetic products detected. Crystallization of the reaction mixture from a concentrated toluene solution held at −35 °C gave single crystals suitable for diffraction.

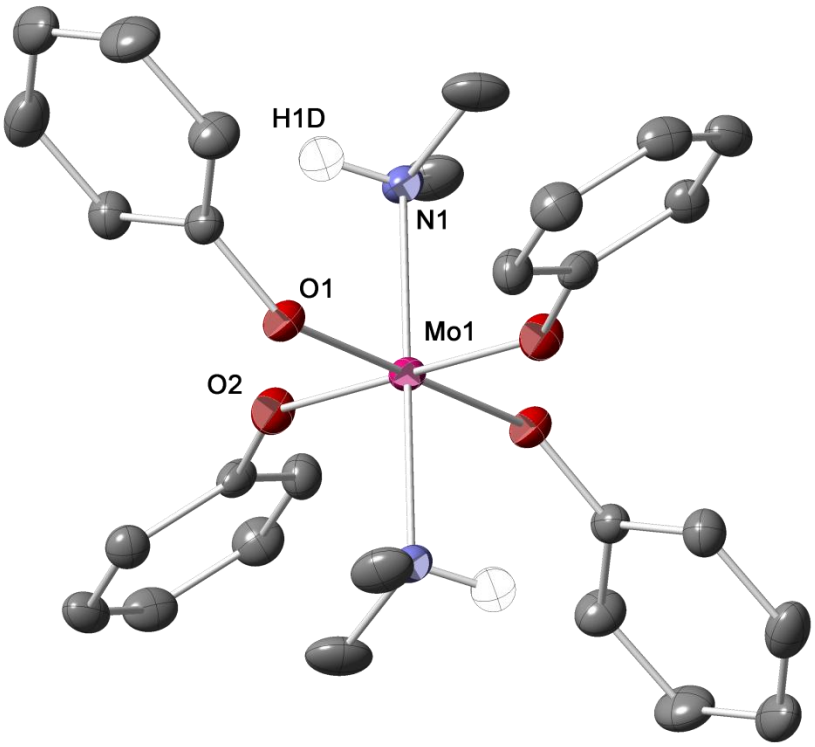

Figure 2.8: Crystal structure rendering of Mo(OPh)$_4$(HNMe$_2$)$_2$ (**4**). Thermal ellipsoids at 50% probability with carbon bound H atoms removed for clarity.

These crystals were determined to be the Mo(IV) complex $Mo(OPh)_4(HNMe_2)_2$ (**4**) (Figure 2.8). This structure is nearly identical to that of $Mo(OTol)_4(HNMe_2)_2$ and related complexes bearing *para*-substituted phenoxides previously reported by Green and coworkers.[6] Here, the reaction of $Mo(NMe_2)_4$ with 5 equiv. of cyclopentyldiene gave the compound $Mo(C_5H_5)(NMe_2)_3$ in good yield. Subsequent treatment with 4 equiv. of *p*-methyl or *p*-^{t}butyl phenol was sufficient to replace all 4 ligands via protonolysis giving a paramagnetic 6 coordinate complex in much the same way as **4**.

This finding confirmed that treatment of **1** with 2 or more equivalents of phenol decompose the Mo(IV) complex, an additional pathway dependent on the alcohol chosen.

To date phenol is the only substrate known to be able to remove the tridentate ligand from $Mo(dpma^{mes})(NMe_2)_2$ (**1**) via protonlysis.

2.6 Mechanism and Structure of $OMo(dpma^{mes})(OBn)$ (5)

Although the increase in reactivity upon stabilizing the proposed radical formed in the transition state was telling, mechanistic questions still remained. Namely, was replacement of both dimethylamide ligands necessary before bond cleavage could occur? One possible consequence of a slow ligand replacement (i.e. stepwise) and a rapid C-O bond breaking step may be the production of ethylbenzene concurrent with the formation of a mixed oxo-methylimido product (Figure 2.9). In every reaction conducted, neither ethylbenzene nor a Mo(VI) oxo/imido product was seen. This may however simply be the stability of the

dimethylamido ligand toward forming a methyl radical, as this decomposition pathway was not seen in samples of **1**.

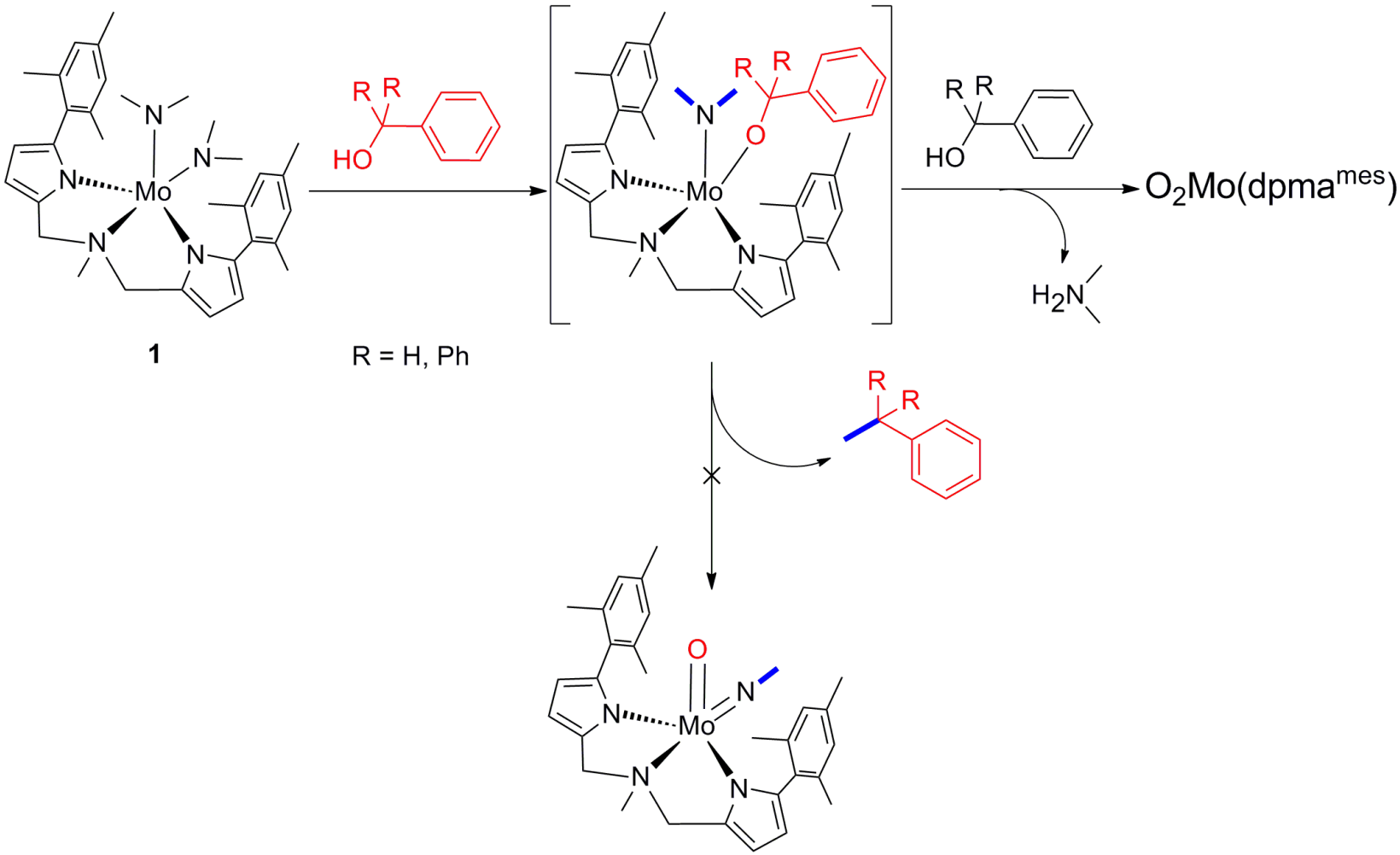

Figure 2.9: Possible products from alternate ligand substitution pathways.

Additionally, if di-substitution of dimethylamide ligands for alkoxides precedes bond cleavage, Is the cleavage step a concerted scission of two bonds or stepwise (Figure 2.10)? In other words, does Mo(IV) mediate the expulsion of radical fragments from the bound ligands or directly couple C-C bonds whilst breaking C-O bonds in alkoxides?

In attempts to purify and structurally characterize the *bis*-oxo **2**, a reaction mixture from treatment of **1** with 2 equiv. of benzyl alcohol was dried under vacuum and extracted with Et_2O. These extracts were filtered and held at −35 °C, forming a small amount of an orange precipitate after several days. This precipitate was collected and re-dissolved in minimal Et_2O, which yielded crystals after several days at −35 °C.

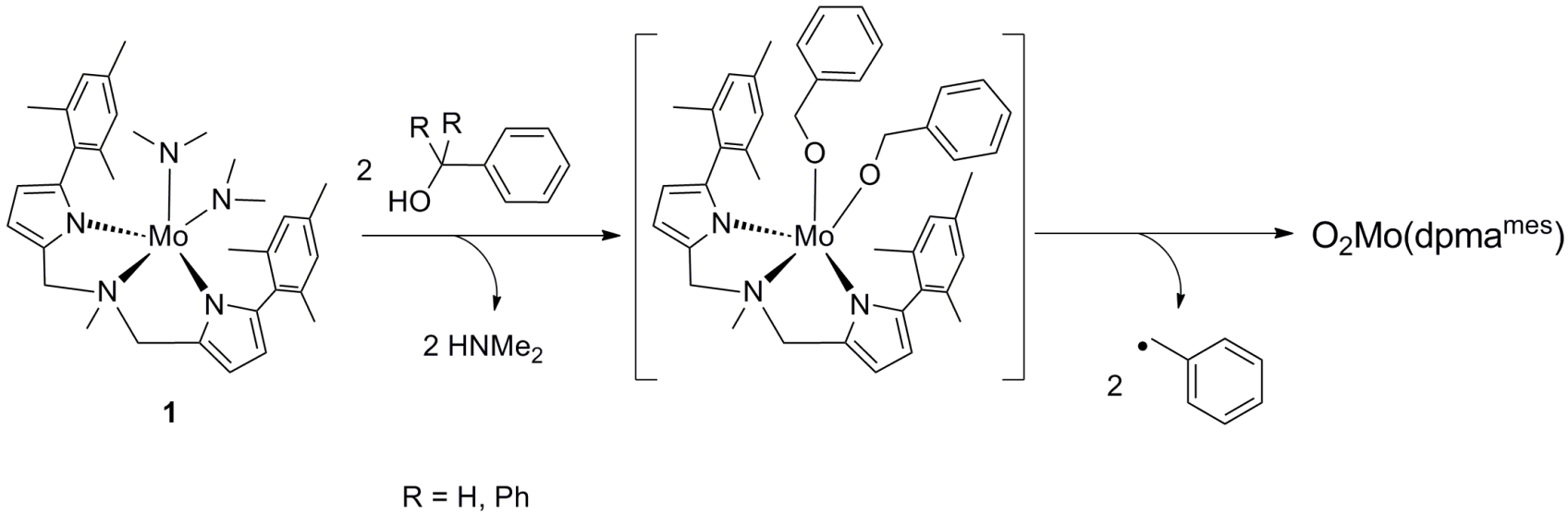

Figure 2.10: Concerted C-O bond cleavage of benzyl alcohols.

X-ray diffraction revealed the Mo(V) complex to be OMo(dpma^{mes})(OBn) (**5**) (Figure 2.11). The structure of **5** has many interesting features. Firstly, the replacement of dimethylamide by an oxo places molybdenum in the 5+ oxidation state. This signifies that stepwise $1e^-$ chemistry is occurring. The Mo1-O1 bond length of 1.677(3) Å is typical for a Mo(V) oxo. Mo-$N_{pyrrolide}$ bond lengths are 2.044(3) Å and 2.051(3) Å, slightly shorter than those in the Mo(IV) complex **1** (2.099(2) Å and 2.082(2) Å) and those in the Mo(VI) complex *syn*-NMo(dpma^{mes})(NMe_2) at 2.109(2) Å and 2.111(2) Å. Likewise a contraction of bond lengths is seen in the Mo1-N3 distance of **2** (2.248(3) Å), statistically shorter than that bond distance in *syn*-NMo(dpma^{mes})(NMe_2) (2.294(2) Å), and well shorter than the 2.401(2) Å Mo1-N3 bond distance in **1**. This trend in bond length is most likely attributed not only to the change in oxidation state of Mo center, but to the donor properties and steric effects of the other ligands accompanying the dpma^{mes}. The Mo1-O2 distance of 1.892(2)Å in **5** is similar to the molybdenum-oxygen bond in Mo(dpma^{mes})(NMe_2)(OAd) (**6**) (vida infra) at 1.858(2)Å. The dpma^{mes} framework in **5** is distorted in much the same way as it is in *syn*-NMo(dpma^{mes})(NMe_2), with a O1-Mo1-N3-C33 torsional angle of $-34.3(2)°$ as compared to $-35.6(2)°$ for N4-Mo1-N3-C33 in the nitride.

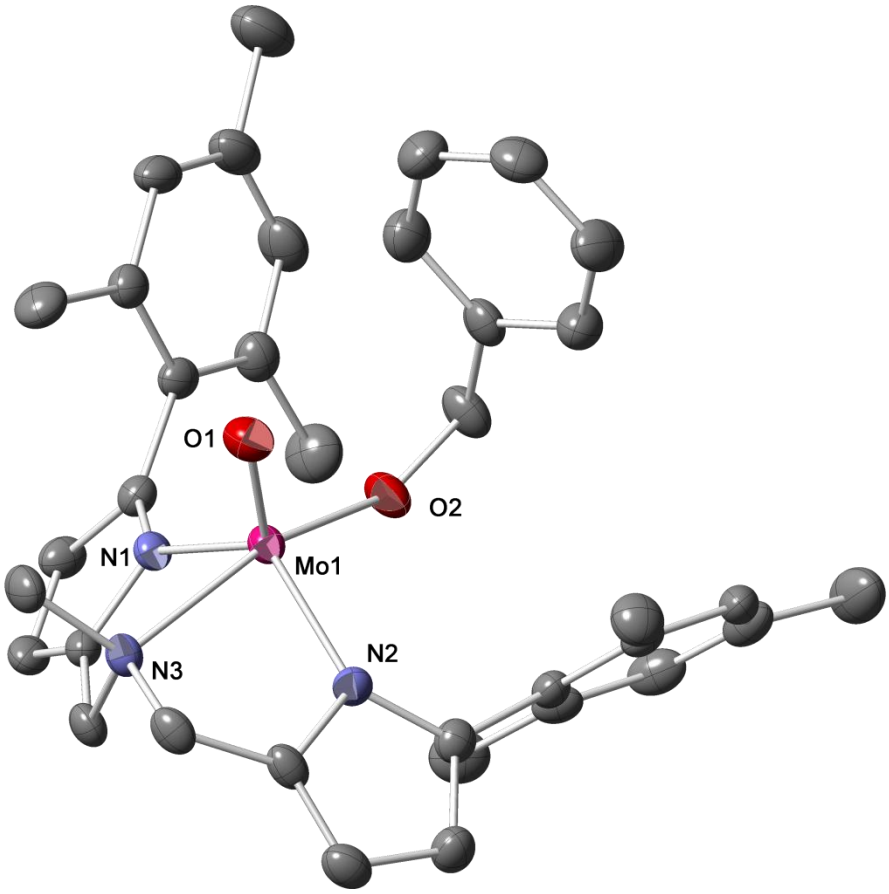

Figure 2.11: Crystal structure rendering of the Mo(V) intermediate OMo(dpma^{mes})(OBn) (**5**). Thermal ellipsoids at 50% probability with carbon H atoms removed for clarity.

Interestingly, the *N*-methyl in the ligand backbone of **5** is *syn* to the oxo bond. This implies that the stereochemistry seen in O_2Mo(dpma^{mes}) (**2**) is set before the installation of the second metal-ligand multiple bond, barring rapid and complete isomerization. Additionally, the 5-coordinate structure of **5** is closer to a square pyramidal geometry (with a continuous structure

parameter of $\tau = 0.62$) reminiscent of the structure of *syn*-NMo(dpma^{mes})(NMe_2). ($\tau = 0.61$), likely a consequence of the strong *trans*-influence common to metal-ligand multiple bonds.[7,8]

Lastly, the isolation of the intermediate **5** shows that the formation of the *bis*-oxo O_2Mo(dpma^{mes}) (**2**) is a result of stepwise C-O bond breaking via radical formation. The isolation of the mono oxo shows that C-O cleavage is not dependent upon C-C coupling. Therefore the transformation is not a concerted mechanism that directly couples the two organic fragments cleaved off of the alkoxides, as is the case in the McMurry reaction.[9]

2.7 Reactivity of Mo(dpma^{mes})(NMe_2)$_2$ (1) with 1-Adamantanol

With substantial evidence of a radical mechanism in hand, we turned our attention to another substrate, 1-adamantanol. Since moving from benzyl to trityl alcohol (thus increasing the stability of the formed radical) a modest increase in reactivity was seen, an opposite effect was expected in the case of **1** with 1-adamantanol. This is due to cage structure of the adamantly fragment prohibiting a flat sp^2 center, thus resisting radical formation on the quaternary carbon.

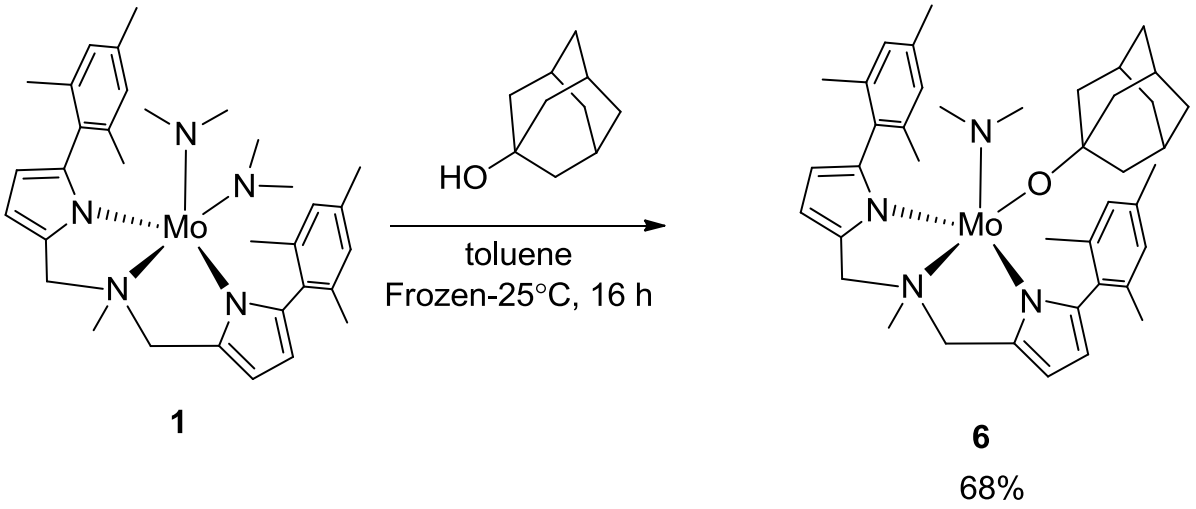

Figure 2.12: Stoichiometric reaction of **1** with 1-adamantanol yielding Mo(dpma^{mes})(NMe$_2$)(OAd) (**6**).

Treatment of **1** with 2 equiv. of 1-adamantanol in toluene affords the bright green Mo(IV) compound Mo(dpma^{mes})(NMe$_2$)(OAd) (**6**). Holding a concentrated toluene solution layered in an equal volume of pentane at −35 °C gives diffraction quality crystals in good yield. Structural analysis shows a distorted 5 coordinate Mo(IV) center between square pyramidal and trigonal bipyramidial ($\tau = 0.53$), similar to the structure of **1** (Figure 2.13).

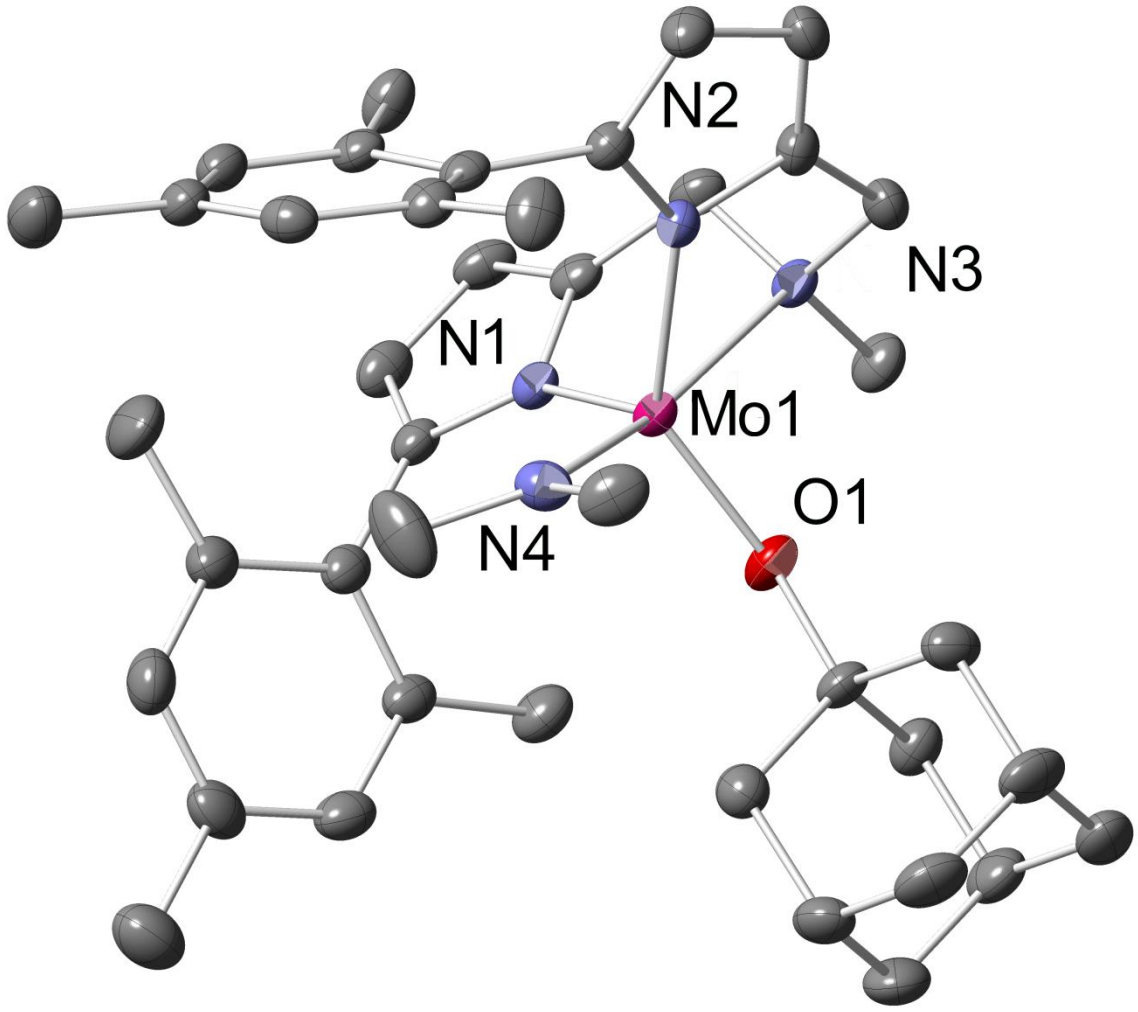

Figure 2.13: Crystal structure rendering of the Mo(IV) complex Mo(dpma^{mes})(NMe_2)(OAd) (**6**). Thermal ellipsoids at 50% probability with H atoms removed for clarity.

Reaction of **1** with a stoichiometric amount of HOAd gave **6** in 68% after crystallization (Figure 2.12). To date, substitution of both dimethylamides in **1** have been unsuccessful, with no reaction beyond mono-substitution seen even at elevated temperatures and with excess equivalents of 1-adamantanol. This ligand exchange whilst leaving the dpma^{mes} framework

intact shows yet a third substrate dependent pathway in the reactivity of Mo(dpma^{mes})(NMe_2)$_2$ (**1**) with alcohols.

Due to the similarities of Mo(dpma^{mes})(NMe_2)(OAd) (**5**) with Mo(dpma^{mes})(NMe_2)$_2$ (**1**), the magnetic properties of **5** were investigated in solution via Evan's method NMR.[10, 11] The paramagnetic nature of complex **5** varied only modestly with temperature, unlike that of **1**, with the effective magnetic moment varying from 1.07 μB to 1.21 μB over a range of 231.2-298.8 K. This does not exclude **5** from similar spin state transitions as **1**, but may suggest a higher energy barrier between S = 0 and S = 1, thus a higher crossover temperature. Despite this difference, the treatment of **5** with di-substituted hydrazines gave a 1 to 1 mixture of the *syn* and *anti* nitrido product NMo(dpma^{mes})(NMe_2) under similar reaction conditions. This argues against the spin-crossover nature of **1** being absolutely necessary for the N-N bond cleavage reaction. The treatment of Mo(dpma^{mes})(NMe_2)(OAd) (**5**) with hydroxylamines have yet to be determined and the loss of *anti* selectivity with hydrazines are still being investigated.

2.8 Conclusion

The Mo(IV) complex Mo(dpma^{mes})(NMe_2)$_2$ (**1**) has been shown to cleave the C-O bonds in benzylic alcohols, concurrent with the formation of O_2Mo(dpma^{mes}) (**2**). The use of triphenylmethanol as a substrate leads to cleaner reactions and higher conversion. Similar treatment of **1** with 1-adamantanol shows only the replacement of an amide ligand, and treatment with phenol results in decomposition of the metal complex, representing 3 pathways based on the alcohol used. These results are reflective of the stabilities of the radical (or that would be

formed) formed after C-O bond cleavage, thus evidence for their inclusion in the reaction mechanism. Isolation of the intermediate OMo(dpma^{mes})(OBn) (**5**) shows the reaction to proceed via a stepwise mechanism, where carbon-based radical fragments are expelled and later terminate by coupling to each other or abstracting H from other organics in solution. Combined with the preceding study, we now have evidence for the Mo(IV) center in **1** to cleave N-N, N-O, and C-O bonds in both a homolytic and heterolytic fashion.

2.9 Experimental

Synthesis of O_2Mo(dpma^{mes}) (2) Under an inert atmosphere a scintillation vial was loaded with **1** (80 mg, 0.132 mmol, 1 equiv.), a stir bar and toluene (10 mL). The solution was cooled for 10 min in a liquid nitrogen cooled cold well. The solution was moved to a stir plate and a toluene solution of benzyl alcohol (586 μL, 0.45 M, 0.263 mmol, 2 equiv.) was added dropwise over 5 min. The solution stirred for a further 6 h. The volatiles were removed under vacuum, and the residue was extracted with toluene (2 x 3 mL). The extracts were filtered through Celite. The solution was concentrated to 2 mL and placed in a –35 °C freezer. After 3 d the mother liquor was removed from the orange precipitate and dried under reduced pressure yielding **5**. This was taken up with minimal amounts of Et_2O and filtered through Celite. Holding a concentrated Et_2O solution at –35 °C gave crystals of OMo(dpma^{mes})(OBn) (**5**) in low yield. These crystals were filtered from solution, and the solution concentrated again. Treating Mo(dpma^{mes})$(NMe_2)_2$ with 2 equiv. of the following alcohols gave O_2Mo(dpma^{mes}) (**2**) in the following yields as judged by ^{1}H NMR: benzyl Alcohol 24%, triphenylmethanol 22% pinicol 10%. Yields of the

byproduct of C-C bond formation were determined by GC-FID calibrated with dodecane as an internal standard as given in Table 2.1. ^{1}H NMR (500 MHz, toluene-*d8*, 25 °C): 6.75 (s, 2H, Ar-*H*), 6.72 (s, 2H, Ar-*H*), 6.41 (d J_{HH} = 3.0 Hz, 2H, Pyr-*H*), 6.313 (d J_{HH} = 3.0 Hz, 2H, Pyr-*H*), 3.76 (d, J_{HH} = 14 Hz, 2H, CH_2), 3.56 (d, J_{HH} = 13.5 Hz, 2H, CH_2), 2.72 (s, 3H, N-CH_3), 2.26 (s, 6H, Ar-CH_3), 2.20 (s, 6H, Ar-CH_3), 2.12 (s, 6H, Ar-CH_3).

Synthesis of Mo(NTol)$_2$(dpma^{mes}) (3) Under an inert atmosphere a scintillation vial was loaded with Mo(Ntol)$_2$(DME)Cl$_2$ (0.126 mg, 0.27 mmol, 1 equiv.), a stir bar and toluene (5 mL). In a separate vial H$_2$dpma^{mes} (115 mg, 0.270 mmol, 1 equiv.) in toluene (5 mL) was added along with triethylamine (60 mg, 0.593 mmol, 2.2 equiv.). This solution was added to the stirring molybdenum solution. The solution stirred for 4 d forming dark solids. The volatiles were removed under vacuum. The residue was extracted with pentane until the pentane was clear. The extracts were filtered through Celite. The solution was dried under vacuum and dissolved with minimal amounts of *n*-heptane and held at –35 °C yielding crystals of **3** (79 mg, 0.108 mmol, 40% yield). ^{1}H NMR (500 MHz, toluene-*d8*, 25 °C): 6.68 (d J_{HH} = 8.5 Hz, 2H, NC$_6H_4$-CH$_3$), 6.50 (dd J_{HH} = 1 Hz J_{HH} = 8.5 Hz, 2H, NC$_6H_4$-CH$_3$), 6.14 (q J_{HH} = 8.5 Hz J_{HH} = 17.5 Hz, 4H, NC$_6H_4$-CH$_3$) 6.08 (dd J_{HH} = 1 Hz J_{HH} = 3.0 Hz, 2H, Pyr-*H*), 6.04 (s, 2H, Ar-*H*), 5.84 (s, 2H, Ar-*H*), 5.82 (d J_{HH} = 3.0 Hz, 2H, Pyr-*H*), 4.53 (d, J_{HH} = 13.5 Hz, 2H, CH_2), 3.53 (d, J_{HH} = 12.5 Hz, 2H, CH_2), 2.36 (s, 3H, N-CH_3), 2.14 (s, 6H, Ar-CH_3) 2.13 (s, 3H, NC$_6$H$_4$-CH_3), 2.06 (s, 3H, NC$_6$H$_4$-CH_3), 2.04 (s, 6H, Ar-CH_3), 1.85 (s, 6H, Ar-CH_3).

Synthesis of $Mo(OPh)_4(NMe_2)$ (4) Under an N_2 atmosphere, a scintillation vial was loaded with a stir bar, **1** (0.045 g, 0.074 mmol, 1 equiv.) and toluene (5 mL) and was cooled in a liquid nitrogen cooled cold well (10 min). The vial was removed to a stir plate and the solution stirred rapidly. To this vial phenol (0.014 g, 0.148 mmol, 2 equiv.) was added as a toluene solution (5 mL). Solution stirred 16 h turning brown. The volatiles were removed under vacuum, and the residue was extracted with pentane and filtered through Celite. Holding this concentrated pentane solution at −35 °C yielded brown crystals of **4** (as the only tractable product) suitable for diffraction in less than 10% yield.

Synthesis of $Mo(dpma^{mes})(NMe_2)(OAd)$ (6) Under an N_2 atmosphere, a scintillation vial was loaded with a stir bar, **1** (0.100 g, 0.165 mmol, 1 equiv.) and toluene (5 mL) and was cooled in a liquid nitrogen cooled cold well (10 min). To this 1-adamantanol (0.025 g, 0.165 mmol, 1 equiv.) in toluene (8 mL) was added and the reaction was allowed to come to room temperature while stirring. After 16 h the solution was dried *in vacuo* yielding a light green powder. Crystalization at from a concentrated toluene solution layered in pentane held at −35 °C gave green, hexagonal crystals suitable for diffraction in 68% yield (0.080 g, 0.112 mmol). Magnetic susceptibility (Evan's method, toluene-*d8* −42°C-+26 °C) μ_{eff} = 1.07-1.21 μ_B. UV-Vis (toluene): λ_{max}=636.0 ε=191.1, λ_{max}=765.7 ε=163.8. Mp:145-150 °C (d).

REFERENCES

REFERENCES

(1) Fox, H. H.; Yap, K. B.; Robbins, J.; Cai, S.; Schrock, R. R. *Inorganic Chemistry* **1992**, *31*, 2287–2289.

(2) Gibson, V. C.; Redshaw, C.; Clegg, W.; Elsegood, M. R. J.; Siemeling, U.; Türk, T. *Polyhedron* **2004**, *23*, 189–194.

(3) Peters, J. C.; Johnson, A. R.; Odom, A. L.; Wanandi, P. W.; Davis, W. M.; Cummins, C. C. *Journal of the American Chemical Society* **1996**, *118*, 10175–10188.

(4) Wanandi, P. W.; Davis, W. M.; Cummins, C. C.; Russell, M. A.; Wilcox, D. E. *Journal of the American Chemical Society* **1995**, *117*, 2110–2111.

(5) Woo, L. K. *Chemical Reviews* **1993**, *93*, 1125–1136.

(6) Yan, X.; Chernega, A. N.; Metzler, N.; Green, M. L. H. *Journal of the Chemical Society, Dalton Transactions* **1997**, 2091–2100.

(7) Nugent, W. A.; Mayer, J. M. *Metal-Ligand Multiple Bonds*; John Wiley & Sons: New York, 1988.

(8) Griffith, W. P. *Coordination Chemistry Reviews*, **1972**, *8*, 369–396.

(9) McMurry, J. E. *Chemical Reviews* **1989**, *89*, 1513–1524.

(10) Evans, D. F. *Journal of the Chemical Society* **1959**, 2003.

(11) Grant, D. H. *Journal of Chemical Education* **1995**, *72*, 39.

Chapter 3: Additional Reactivity of Mo(dpma^{mes})(NMe$_2$)$_2$

ABSTRACT

The Mo(IV) complex Mo(dpma^{mes})(NMe$_2$)$_2$ (**1**) which mediates the scission of *N-N*, *N-O* and *C-O* bonds decomposes in the presence of ethereal and halogenated solvents. Isolation and structural characterization of the reaction of **1** with CH_2Cl_2 shows the six-coordinate product Mo(dpma^{mes})(NMe$_2$)$_2$Cl (**2**), likely through a radical process. A high yielding synthesis of **2** has yet to be achieved. Reaction of **1** with 2 equiv. of benzylamine in the presence of CH_2Cl_2 gives the complex Mo(dpma^{mes})(NBn)(NH$_2$Bn)Cl (**3**). X-Ray diffraction shows that **3** contains a Mo-N double bond and Mo-N dative bond originating from the same amine, a unique structural feature in transition metal chemistry. Complex **1** also exhibits [1,2]-insertion chemistry into one Mo-NMe$_2$ upon treatment with excess CS_2, giving the structurally characterized thiocarbamate product, Mo(dpma^{mes})(S$_2$CNMe$_2$)(NMe$_2$) (**4**).

3.1 Introduction

Exploring the chemistry of Mo(dpma^{mes})(NMe$_2$)$_2$ (**1**) has demonstrated the bond cleaving potential of Mo(IV) complexes. As seen in di-substituted hydrazines, a $2e^-$ pathway results in N-N bond cleavage as well as direct oxidation from Mo(IV) to Mo(VI). Conversely, complex **1** promotes the C-O cleavage of alcohols via a $1e^-$ radical mechanism. Shown to be 2 discrete elementary steps. This oxidation also takes Mo(IV) to Mo(VI) while passing through a

Mo(V) intermediate. With both pathways accessible, the coordinative unsaturated complex **1** was screened with a variety of substrates, in hopes that new patterns of reactivity would emerge.

3.2 Oxidation of Mo(dpma^{mes})(NMe$_2$)$_2$ (1) in presence of Carbon-Halogen and Silicon-Halogen Bonds

The above factors lead to the extreme sensitivity of **1** towards atmospheric oxygen and water. Additionally, Mo(dpma^{mes})(NMe$_2$)$_2$ (**1**) was observed to decompose rapidly in ethereal (Et_2O, THF, DME) as well halogenated ($CHCl_3$, CH_2Cl_2, chlorobenzene). Likewise, attempts at substitution of the dimethylamides of **1** with halides by treatment with MeI or $SiMe_3Cl$ were unsuccessful, giving dark solutions predominately of paramagnetic complexes, and insoluble metal containing products.

Though the decomposition product(s) of **1** in ethers remain elusive, single crystals of an oxidized product was grown from the treatment of **1** with CH_2Cl_2. Upon mixing, a cold toluene solution of **1** rapidly turns dark brown upon treatment with 10 equiv. of CH_2Cl_2. After 1h the volatiles were removed under dynamic vacuum. The residue was extracted with Et_2O and filtered through a frit with Celite as a filtering agent. The solution was then concentrated and held at −35 °C. After several days microcrystals were harvested from solution giving Mo(dpma^{mes})(NMe$_2$)$_2$Cl (**2**) as small plates in low yield.

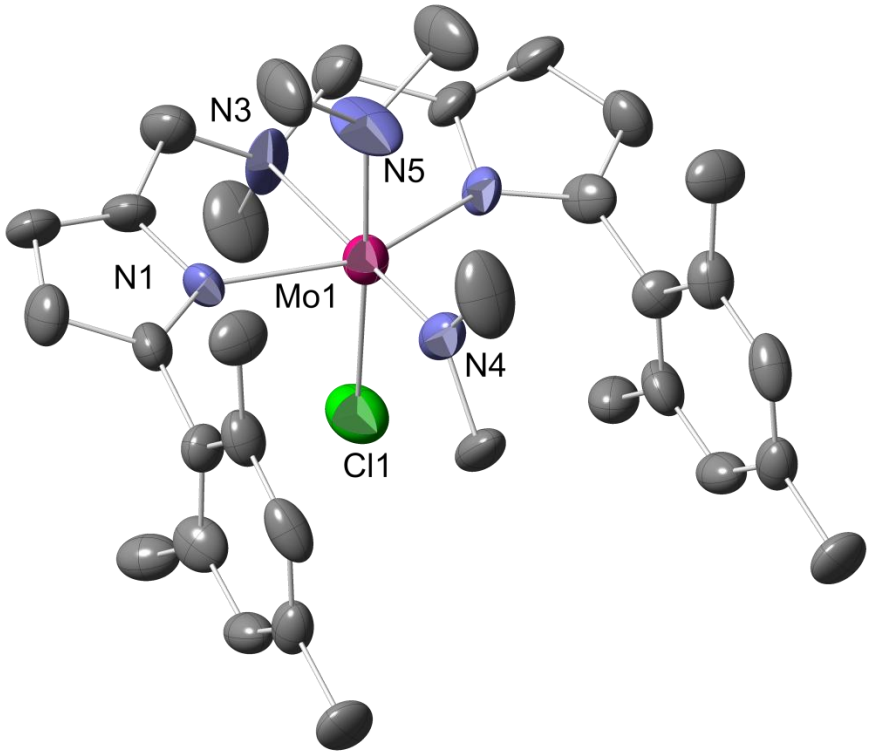

Figure 3.1: Crystal structure rendering of the oxidized product Mo(dpma^{mes})(NMe$_2$)$_2$Cl (**2**). Atom positions at 50% probability and H atoms removed for clarity.

Mo(dpma^{mes})(NMe$_2$)$_2$Cl (**2**) exhibits several interesting structural features. The distorted octahedron has bond angles of N1-Mo1-N1# 150.2(4)°, N4-Mo1-N3179.8(6)°, and N5-Mo1-Cl1 175.7(6)°. This is very similar to the 6-coordinate Mo(IV) compound Mo(NMe$_2$)$_2$(CNBu^t)(dpma^{mes}) (**1**•CNBu^t). Also as seen in (**1**•CNBu^t) the two dimethylamidos of **2**orientate themselves such that the plane defined by each C-N-C unit is orthogonal to each other. This orientation imparts *C1v* symmetry to the molecule such that the lone pair of each NMe$_2$ unit donates into different *d* orbitals. The Mo-pyrrolide bond distance of 2.109(7)Å is statistically the same as both the Mo(IV) 5-coordinate **1** and the 6-coordinate **1**•CNBu^t (however

these two bond distances are outside of esd's). Mo(dpma^{mes})(NMe_2)$_2$Cl (**2**) has two significantly different NMe_2bond lengths with a short 1.813(16)Å Mo-N4 contact *trans* to N3 and a longer 1.985(12)Å contact *trans* to Cl1, with a Mo-Cl1 bond of 2.407(4)Å.

To further our understanding of M(V) *bis*-pyrrolides attempts at a higher yielding synthesis of Mo(dpma^{mes})(NMe_2)$_2$X compounds were made. Treatment of **1** with 1 or more equiv. of *tert*-butylchloride did give **2** after crystallization, but in equally poor yields. Other halogenating oxidants such as 1,2-dibromoethane and I_2failed to give any tractable products.

3.3 Synthesis and Structure of Mo(dpma^{mes})(NBn)(H_2NBn)(Cl) (3)

The presently known reactivity of Mo(dpma^{mes})(NMe_2)$_2$ (**1**) is dominated by $1e^-$ and $2e^-$ bond cleavage reactions. Since **1** reacts with various substrates to afford N-N, N-O, and C-O bond scission, attempts to synthesize Mo(IV) amides were made to see if C-N bond breaking would follow. Treatment of **1** with 1 or 2 equiv. of benzylamine or *N*-methyl benzylamine at room temperature in toluene did not induce radical or $2e^-$ bond cleavage. Products from these reactions are paramagnetic in nature and have UV-Vis spectra consistent with Mo(IV) *bis*-amide of the form Mo(dpma^{mes})(NR_2)$_2$ where R = H, Me, or Bn. Serendipitously a reaction of **1** with 2 equiv. of benzylamine in toluene was contaminated with trace amounts of CH_2Cl_2. Crystallization of the mixture from a cold toluene solution held at −35 °C gave dark purple crystals of Mo(dpma^{mes})(NBn)(H_2NBn)(Cl) (**3**). This compound is a structural curiosity in that

it prefers one doubly bounded and one datively bonded benylimide/benzylammine ligand in the ground state as opposed to two singlelly bound amide.

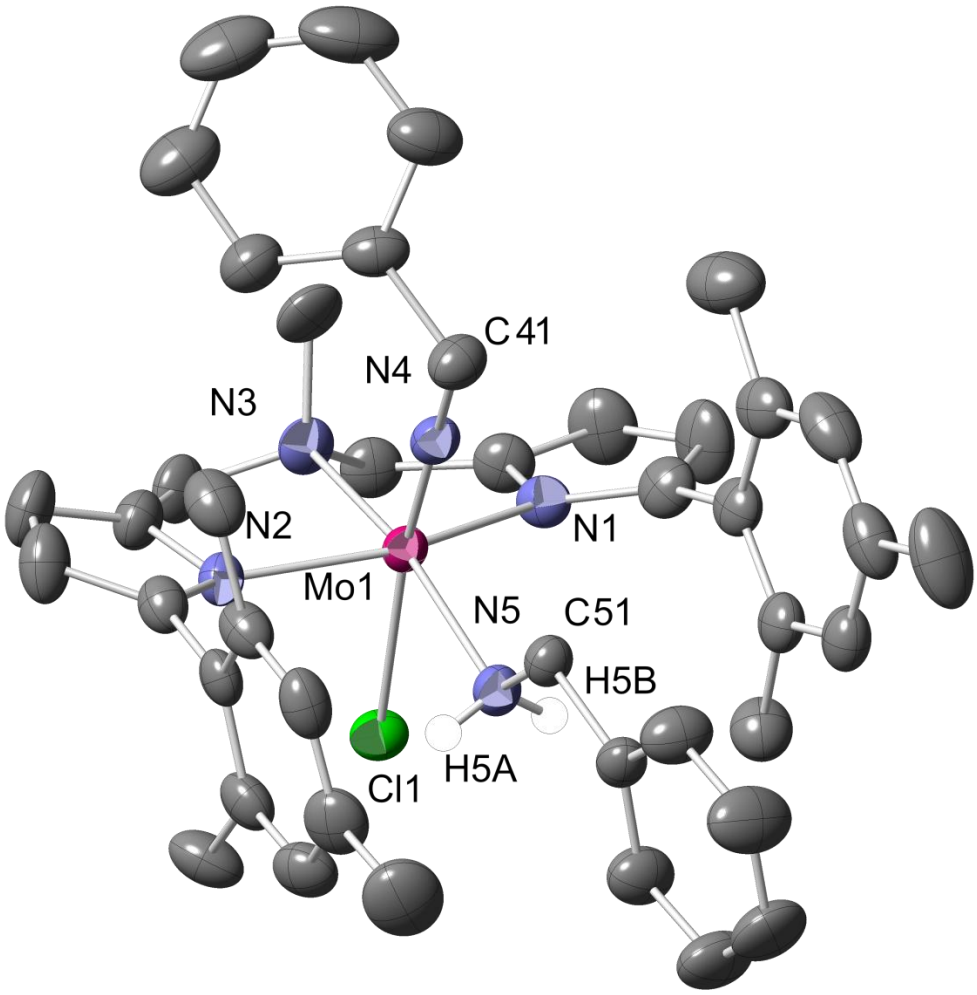

Figure 3.2: Crystal structure rendering of Mo(dpma^{mes})(NBn)(H_2NBn)(Cl) (**3**) showing a doubly and datively bonded benzylamine ligand. Thermal ellipsoids at 50% probability and non-N bound H atoms and a toluene solvent of crystallization removed for clarity.

The 6-coordinate Mo(V) complex **3** shows a octahedral coordination similar to that of **2** with bond angles defined by N1-Mo1-N2, N5-Mo1-N3, and N4-Mo1-Cl1 at 154.6(1)°, 165.4(1)°, and

169.2(1)° respectively. Mo-$N_{pyrrolide}$ distances of 2.114(2)Å and 2.137(2)Å are also typical of the other 6-coordinate Mo(V) ($dpma^{mes}$) compounds known. The Mo1-N4-C41 unit is nearly linear at 172.9(2)° with an Mo1-N4 bond distance of 1.730(2)Å. These parameters are consistent with the *bis*-arylimido $Mo(NTol)_2(dpma^{mes})$, where the two analogous angles observed are 153.3(2)° and 177.9(2)°. Likewise the Mo-N_{imido} distance of **3** is closer to the more linear of the two arylimdos of $Mo(NTol)_2(dpma^{mes})$ at 1.761(2)Å and 1.750(2)Å. Even though complex **3** is a lower formal oxidation state and has a ligand *trans* to the imido unlike the $Mo(NTol)_2(dpma^{mes})$, the imido length in **3** is markedly shorter outside of esd's. This may be due to the increased availability of the lone pair in an alkylimido nitrogen over an arylamido nitrogen. The observed Mo1-Cl1 bond of 2.525(1)Å is over 0.1Å longer than that observed in **2** suggesting an increased competitive interaction for *d*-orbitals. The Mo1-N5 linkage at 2.214(2)Å is similar to the Mo1-N3 bond (2.221(2)Å), thus was assigned it to be a dative bond. Crystal quality of **3** allowed for the refinement of the hydrogen atoms H5A and H4B.

The mechanism by which **3** forms has yet to be determined. Benzylimde for *bis*-dimethylamide substitution before oxidation by CH_2Cl_2 is likely. The structure of **3** differs from **2** in that the *N*-methyl of the $dpma^{mes}$ backbone is *anti* to the chloride ligand. If **3** was the substitution product of **2** an isomerization process would be necessary to give the observed compound. Likewise, the preference for a double and dative bond in place of two single bonds to benzylamine has not been explored. Intramolecular proton transfer from N5 to N4 likely has a

high kinetic barrier, as it would require rotation of the Mo1-N4 bond. A space filling model of **3** illustrates the highly constrained pocket formed by the flanking mesityl groups.

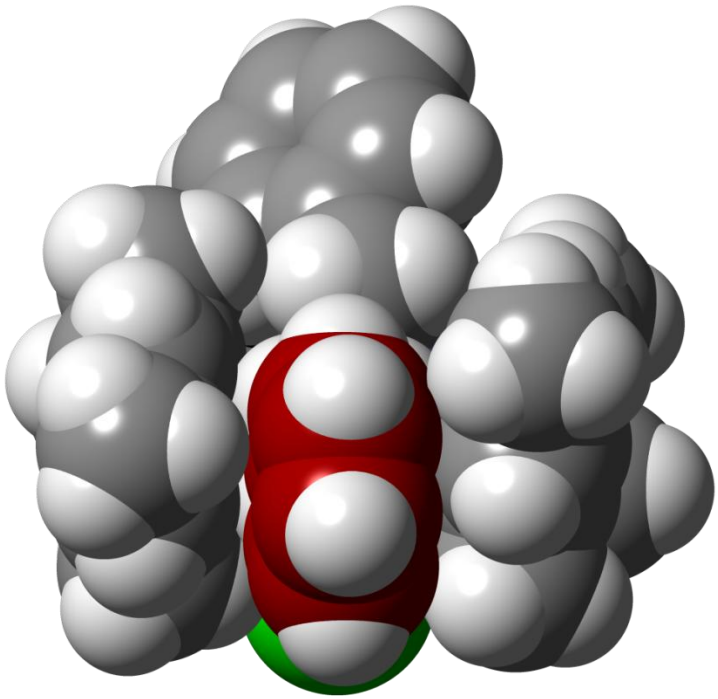

Figure 3.3 A space filling model of Mo(dpma^{mes})(NBn)(H_2NBn)(Cl) (**3**) viewed down the Mo1-N5 bond axis showing the sterically shielded benzylammine ligand (highlighted in red).

3.4 Insertions into the Metal-Amide bond of Mo(dpma^{mes})(NMe_2)$_2$ (1)

A 2002 paper by Odom and coworkers reported the insertion of an electron rich alkyne into a Mo-NMe_2 bond (Figure 3.4).[1] This departs from the reactivity of the Bradley compound Mo(NMe_2)$_4$[2] which oligermerizes 3-hexyne at room temperature. At room temperature only a

single insertion is observed with Mo(dpma)$(NMe_2)_2(NHMe_2)$ in the presence of excess alkyne. Catalytic schemes using excess alkyne and a secondary amine were unsuccessful for the hydroammination reaction, and elevated temperatures led to decomposition. It was our hope that the increased steric protection afforded by the substituted dpma framework in **1** would allow for alkyne insertion while preventing decomposition. When **1** is treated with stoichiometric amounts of 3-hexyne an orange paramagnetic product is obtained. However, to date suitable crystals and identification of this material have been unobtainable.

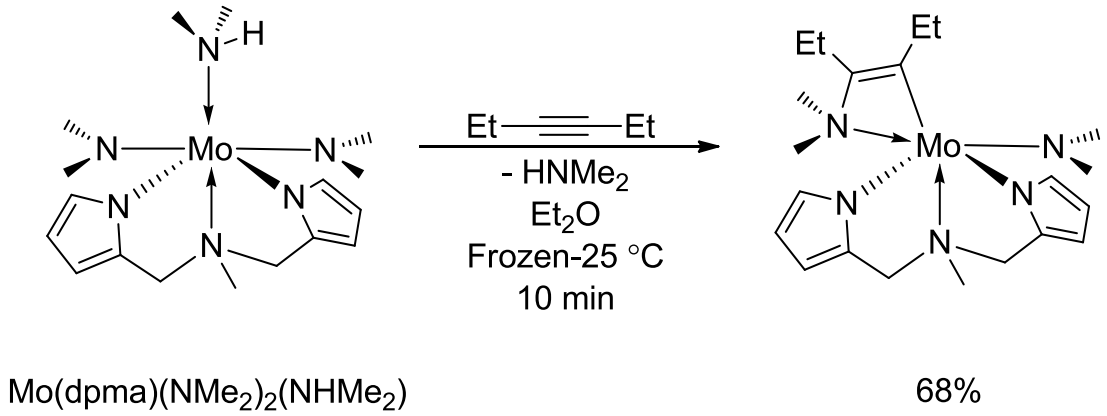

Figure 3.4: The related complex Mo(dpma)$(NMe_2)_2(NHMe_2)$ showing [1,2]-insertion of an alkyne into a Mo-NMe_2 bond.

The complex Mo($dpma^{mes}$)$(NMe_2)_2$ (**1**) does show [1,2] insertion reactivity similar to other molybdenum amides. The homoleptic $Mo(NMe_2)_4$ undergoes quantitative conversion to $Mo(S_2CNMe_2)_4$ when refluxed in benzene with CS_2.[2] Similarly Green et. al. reported multiple CS_2 insertions into Mo(η^3-C_5H_5)$(NMe_2)_3$ concurrent with a Cp hapticity shift to form Mo(η^5-C_5H_5)$(S_2CNMe_2)_3$. IR analysis of this complex suggests an $18e^-$ metal center ligated by

1 monodentate and 2 bidentate S_2CNMe_2 moieties.[3] When **1** is treated with a 10 equiv. excess of CS_2 in cold toluene the paramagnetic complex Mo(dpma^{mes})(S_2CNMe_2)(NMe_2) (**4**) immediately forms. Crystallization from a concentrated toluene solution held at -35 °C gave single crystals suitable for diffraction.

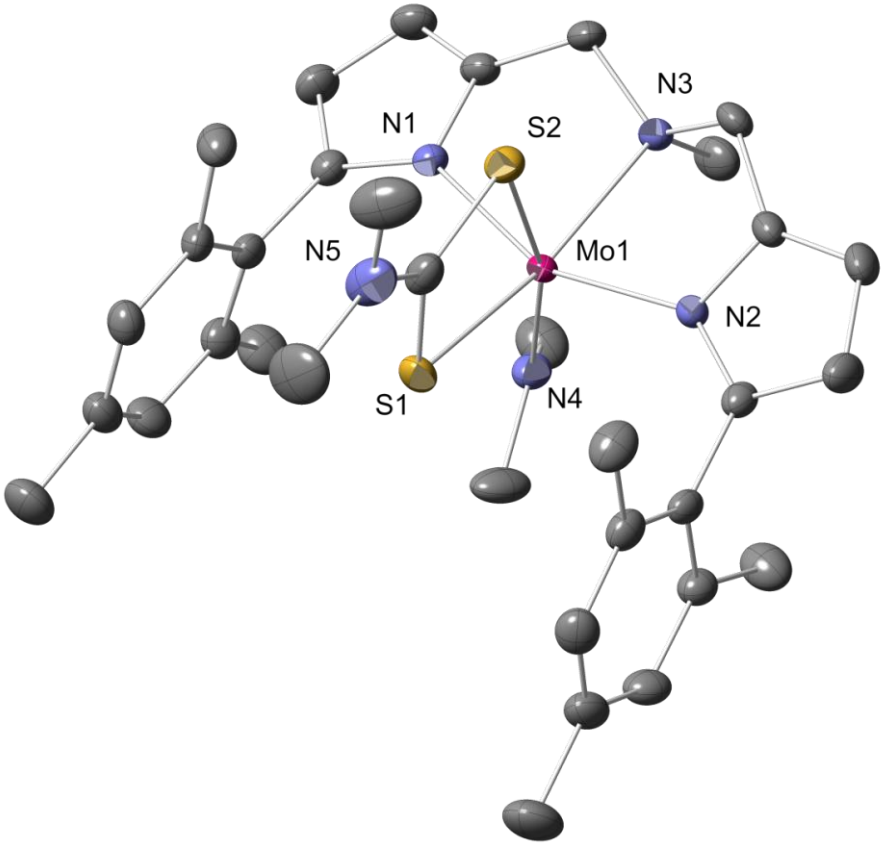

Figure 3.5: Crystal structure rendering of Mo(dpma^{mes})(S_2CNMe_2)(NMe_2) (**4**). Atom positions at 50% probability. H atoms and two toluene molecules of crystallization removed for clarity.

The 6-coordinate Mo thiocarbamate complex is best described as a distorted octahedron with the largest bond angles N1-Mo1-N2, S1-Mo1-N3, and S2-Mo1-N4 close to 180°, at 154.68(5)°, 160.62(4)°, and 162.28(5)° respectively. With a distance of 2.4434(4)Å the Mo-S1 bond *trans* to the donor ammine of $dpma^{mes}$ is shorter than the Mo-S2 bond (2.5796(4)Å) *trans* to the dimethyamide due to the greater *trans* influence of the anion. These lengths are consistent with a delocalized thiocarbimate anion bound κ^2 to molybdenum. Mo-pyrrolide bond distances of 2.123(1)Å and 2.134(1)Å are slightly longer than the 2.082(2) Å and 2.099(2)Å found in **1**. Likewise the Mo-NMe_2 bond distance in **4** of 1.936(1)Å is lengthened from the average bond distance of 1.918(2)Å seen in Mo($dpma^{mes}$)(NMe_2)$_2$ (**1**). The like **2** the Mo-N distances in **4** are consistent with the corresponding bond lengths in the 6-coordinate Mo(IV) complex Mo(NMe_2)$_2$($CNBu^t$)($dpma^{mes}$) (**1**•$CNBu^t$).

Steric analysis of complexes **1** and **4** were calculated from the crystal structures using Solid G program (For a detailed description please see Appendix B).[4] In this method the metal center is treated in some respects as a point light source. Each ligand blocks conical access to this center from incoming substrates. When a sphere of arbitrary radius is circumscribed about the complex each ligand projects a 'shadow' on its surface. The area of this 'shadow' is calculated and given as a percentage of the spheres total area. When calculated this way the higher coordinate Mo($dpma^{mes}$)(S_2CNMe_2)(NMe_2) (**4**) is sterically more shielded than Mo($dpma^{mes}$)(NMe_2)$_2$ (**1**) at 97.5% and 92.1% respectively. When subdivided the NMe_2 ligand of **4** (20.3%) is smaller than the S_2CNMe_2 unit (26.9%) by ~6.6%. Although it is unknown if the

reaction of **1** with excess CS_2 gives the mono insertion product **4** as its only product, insertion into both Mo-amide bonds seems sterically unfavored, as substrate access is greatly diminished upon mono substitution. Moreover, to a first approximation the *bis*-insertion product $Mo(dpma^{mes})(S_2CNMe_2)_2$ would have a Solid G measurement at or over 100% assuming an isosteric $dpma^{mes}$ ligand. When the area projected by each ligand is summed a value over 100% is representative of areas of the metal center shielded by more than ligand and unfavorable intramolecular close contacts between ligands. Considering **4** is coordinatively unsaturated unlike the other literature examples of CS_2 insertion into Mo-N bonds, the mono insertion observed is likely to be kinetically controlled.

3.5 Conclusions

In addition to the Mo(IV) to Mo(VI) transformations accessible through N-N, N-O, and C-O bond scission, $Mo(dpma^{mes})(NMe_2)_2$ (**1**) forms stable Mo(V) complexes through radical C-Cl bond cleavage. Further investigations of $Mo(V)(dpma^{mes})$ are merited as the framework displays rich structural chemistry. Like other molybdenum dimethylamido compounds $Mo(dpma^{mes})(NMe_2)_2$ (**1**) undergoes insertion of CS_2 into a Mo-N bond to produce a κ^2 thiocarbamate ligand.

REFERENCES

REFERENCES

(1) Katayev, E.; Li, Y.; Odom, A. L. *Chemical Communications* **2002**, *2*, 838–839.

(2) Bradley, D. C.; Chisholm, M. H. *Journal of the Chemical Society A: Inorganic, Physical, Theoretical* **1971**, 2741.

(3) Yan, X.; Chernega, A. N.; Metzler, N.; Green, M. L. H. *Journal of the Chemical Society, Dalton Transactions* **1997**, 2091–2100.

(4) Guzei, I. A.; Wendt, M. *Dalton transactions* **2006**, 3991–9.

Chapter 4: Evaluation of Donor and Steric Properties of Anionic Ligands on High Valent Transition Metals

ABSTRACT

Synthetic protocols and characterization data for a variety of chromium(VI) nitrido compounds of the general formula $NCr(NPr^i_2)_2X$ are reported, where X = NPr^i_2 (**1**), I (**2**), Cl (**3**), Br (**4**), OTf (**5**), 1-adamantoxide (**6**), $OSiPh_3$ (**7**), O_2CPh (**8**), OBu^t_{F6} (**9**), OPh (**10**), O-*p*-$(OMe)C_6H_4$ (**11**), O-*p*-$(SMe)C_6H_4$ (**12**), O-*p*-$(Bu^t)C_6H_4$ (**13**), O-*p*-$(F)C_6H_4$ (**14**), O-*p*-$(Cl)C_6H_4$ (**15**), O-*p*-$(CF_3)C_6H_4$ (**16**), OC_6F_5 (**17**), κ(O)-*N*-oxy-phthalimide (**18**), SPh (**19**), OCH_2Ph (**20**), NO_3 (**21**), pyrrolyl (**22**), 3-C_6F_5-pyrrolyl (**23**), 3-$[3,5\text{-}(CF_3)_2C_6H_3]$pyrrolyl (**24**), indolyl (**25**), carbazolyl (**26**), N(Me)Ph (**27**), κ(N)-NCO (**28**), κ(N)-NCS (**29**), CN (**30**), NMe_2 (**31**), F (**33**). Several different techniques were employed in the syntheses, including nitrogen-atom transfer for the formation of **1**. A cationic chromium complex $[NCr(NPr^i_2)_2(DMAP)]BF_4$ (**32**) was used as an intermediate for the production of **33**, which was produced by tin-catalyzed degredation of the salt. Using spin saturation transfer or line shape analysis, the free energy barriers for diisopropylamido rotation were studied. It is proposed that the estimated enthalpic barriers, Ligand Donor Parameters (LDPs), for amido rotation can be used to parameterize the donor abilities of this diverse set of anionic ligands toward transition metal centers in low *d*-electron counts. The new LDPs do not correlate well to the pK_a value of X. Conversely, the LDP values of phenoxide ligands do correlate with Hammett parameters for the *para*-substituents. Literature

data for ^{13}C NMR chemical shifts for a tungsten-based system with various X ligands plotted versus LDP provided a linear fit. In addition, the angular overlap model derived $e_\sigma + e_\pi$ values for chromium(III) ammine complexes correlate with LDP values. Also discussed is the correlation with $XTiCp^*_2$ spectroscopic data. X-ray diffraction has been used used to characterize 31 of the compounds. From the X-ray diffraction data, steric parameters for the ligands using the Percent Buried Volume and Solid Angle techniques were found.

4.1 Introduction

One of the most important methods for controlling reaction pathways in many transition metal catalyzed systems is through the steric and electronic adjustment of ancilliary ligands. Choosing from the extensive gallery of possible ligand choices is often done by (1) analogy with similar reactions already in the literature (2) picking readily available ancillaries in the investigator's laboratory or (3) making an educated guess based on experience in the field. Once some of the desired reactivity is found, reactions are optimized through similar procedures involving available ligand sets and trying to encourage hypothesized processes with slow reaction rates. Finally, a reaction may be deemed interesting enough to warrant full mechanistic investigations through experimental and computational techniques that can often lead to improved catalyst designs.

In this process of taking new reactions from conception to fruition, the donor properties and steric profiles of the ancillary ligands, along with reaction conditions, provide the major tools for optimization. Simple metrics for donor and steric properties have proven to be powerful tools for catalyst optimization, especially in late transition metal chemistry. Perhaps one of the most familiar citations in chemistry is by Chadwick Tolman published in Chemical Reviews in

1977 on steric and electronic effects in phosphine chemistry.[2] Tolman's cone angle gave a reasonable one-parameter metric for sterics. The energy of the totally symmetric carbonyl vibration in $Ni(CO)_3(PR_3)$ complexes gave a useful single-parameter metric for donor properties.

Using CO stretching frequencies to parameterize later transition metal ligand effects predates this Tolman review, however. For example, Wilkinson and co-workers in 1959 reported the IR stretching frequencies of transition metal carbonyls bearing amine/phosphine donors and reported "the resulting negative charge on the metal atom $R_3N^+–M^-$ may…be dissipated by increasing the bond orders in the M–C–O system."[3] They reported a steady rise in carbonyl stretching frequencies on replacement of phenyl groups in $(Ph_3P)_3Mo(CO)_3$ with chlorine until reaching $(Cl_3P)_3Mo(CO)_3$.[4]

Parameterization methods have been extensively used in a large variety of low-valent and late transition metal catalyses.[5] Similar quantitative measures are a mainstay of physical organic chemistry; for example, the reactivity of compounds with pendant aryl groups is often predicted or explained by parameters developed by Hammett, Taft, and others.[6] Quantitative structure-activity relationships (QSAR) have developed into a powerful tool for other areas as well, e.g., pharmaceutical design.[7]

In contrast, methods for determining donor properties of ligands on metal complexes in higher formal oxidation states are less well known. This is despite the fact that the donor properties of common ligands on earlier, higher-valent metals are likely to be quite different

from later, lower valent metals in many cases due to differences in the number and type of empty acceptor orbitals.

If the ligands in question are members of a closely related series, e.g., *para*-substituted phenoxides, one can try to draw analogies to pK_a or Hammett parameters; however, the investigator is left wondering if these are good measures for the transition metal system in question. This problem is only exacerbated if the ligands are more dissimilar, such as comparing phenoxide to iodide to indolyl. Different donor atoms, e.g., oxygen versus nitrogen, or even different hybridization of the same donor atom may affect radial extensions for the orbitals even if the frontier orbitals are of similar shape, which could lead to quite different bonding properties due to the changes in overlap integrals and energies.

While QSAR has been done on early to middle transition metal complexes, these are often studies of specific systems with limited applicability to high valent metals in general. For example, extensive QSAR has also been done in recent computationally driven studies like the one published by Jensen and coworkers on Grubbs's catalyst.[8] Steric and electronic parameterizations have been applied to metallocene[9] and nonmetallocene[10] polymerization catalysts using a variety of techniques varying from simply categorizing ligand types to numerical quantization of ligand properties. In addition, electronic influence of substituents on *ansa*-metallacene complexes has been examined in great detail.[11]

For our investigations in titanium catalysis,[12] we sought a method for the comparison of a large variety of monodentate ligands on early metals to aid in ligand design and for understanding spectroscopic and reactivity trends within various transition metal systems.

In this study, we discuss the use of a large selection of monodentate ligands on the d^0 metal complex, $NCr(NPr^i_2)_2X$, where X is an adjustable monodentate ligand. As will be shown, the synthetic versatility of this framework allows synthesis of a series of compounds for evaluation. In this manuscript, we limit the discussion to monoanionic X;[13] however, these range from common ancillaries used in organometallic chemistry like amido and alkoxide, to classical Werner-type ligands such as halides, cyanide, and thiocyanate. The system's design lends itself to a one parameter quantification of donor properties similar to the $Ni(CO)_3L$ system commonly used for late transition metal ligands. Steric metrics for the ligands are provided, and possible steric interference is discussed.

4.2 The System Used for Ligand Parameterization

The method chosen here for the experimental parameterization of ligand donor properties on high valent metal centers involves the use of chromium(VI) nitrido complexes with diisopropylamido ancillaries. All of the compounds in this study are of the type $NCr(NPr^i_2)_2X$, where X is a monoanionic ligand. These complexes are readily prepared, as will be shown in the next Section. In addition, the amido ligands display variable rotation rates dependent upon the donor properties of X. The rotation of the diisopropylamido ligand in these systems has a rate that is readily measured by ^1H NMR spectroscopy. In this study, spin saturation transfer was the standard method for ligand rotation rate determination; however, line-shape analysis can also be used and was used for some compounds (vide infra).

Since the compounds are *pseudo*-tetrahedral, the system is not orthoaxial, and the σ- and π-orbitals mix during the bonding interactions with the ligands. This is exemplified in the

Angular Overlap Model (AOM) Parameters for a rigorously tetrahedral compound by the energy of the t_2* orbital being parameterized as $e_{t_2}* = 4/3\ e_\sigma + 8/9\ e_\pi$ where the ligand's σ- and π-donor parameters both contribute to the energy of the triply degenerate orbital. Lowering the symmetry, as is done here, will lead to further mixing and a single parameter for ligand donor properties is the result.

The highest symmetry available in the nitrido compounds here would be C_{3v} with a formula of $NCrX_3$, where the chromium-nitrido bond is along the *z*-axis. In C_{3v}, the $d_{xy}/d_{x2–y2}$-orbitals comprise an *e*-set, with the p_x/p_y-orbitals having the same symmetry. These *e*-sets act as both σ- and π-acceptor orbitals for the basal amido ligands. In addition to the π-accepting *e*-set near the *xy*-plane, there is an *e*-set comprised of the d_{xz}/d_{yz}-orbitals that are involved in strong π-interactions with the nitrido.[14]

In other words, rotation of the amido ligands 90° from where they π-donate into acceptor orbitals near the *xy*-plane to where they could donate into the d_{xz}/d_{yz} orbitals along the nitrido vector causes them to compete with the very strongly donating nitrido. As a result, there is an electronic barrier to rotation around the $Cr–NPr^i_2$ bond determined by the energy difference between the geometries where the amido $CrNR_2$ plane is parallel with the Cr–N(nitrido) vector and where it is perpendicular. Increasing the donor abilities of the ligands in the basal set reduces this difference somewhat, decreasing the barrier for amido rotation through ground-state destabilization.

In short, the stronger a donor X is in a compound like $NCr(NPr^{i}_{2})_2X$, the smaller the barrier to amido rotation is expected to be. Because the σ- and π-systems are strongly mixed, the σ- and π-donor properties of X both contribute to the size of the diisopropylamido rotational barrier. We propose that this isomerization barrier can be used as a measure of the donor ability of X in high valent transition metal systems.

The above arguments can be illustrated using Density Functional Theory on the model system $NCr(NH_2)_3$ using B3LYP as the functional. Our initial exploration with this molecule used 6-31G**, but the calculations were extended to the much larger aug-cc-pVQZ basis set, which provided similar results. Optimization provided a ground state structure where all of the amido ligands are planar and the $Cr–NH_2$ planes are parallel to the nitrido vector as expected (Figure 4.1, bottom).

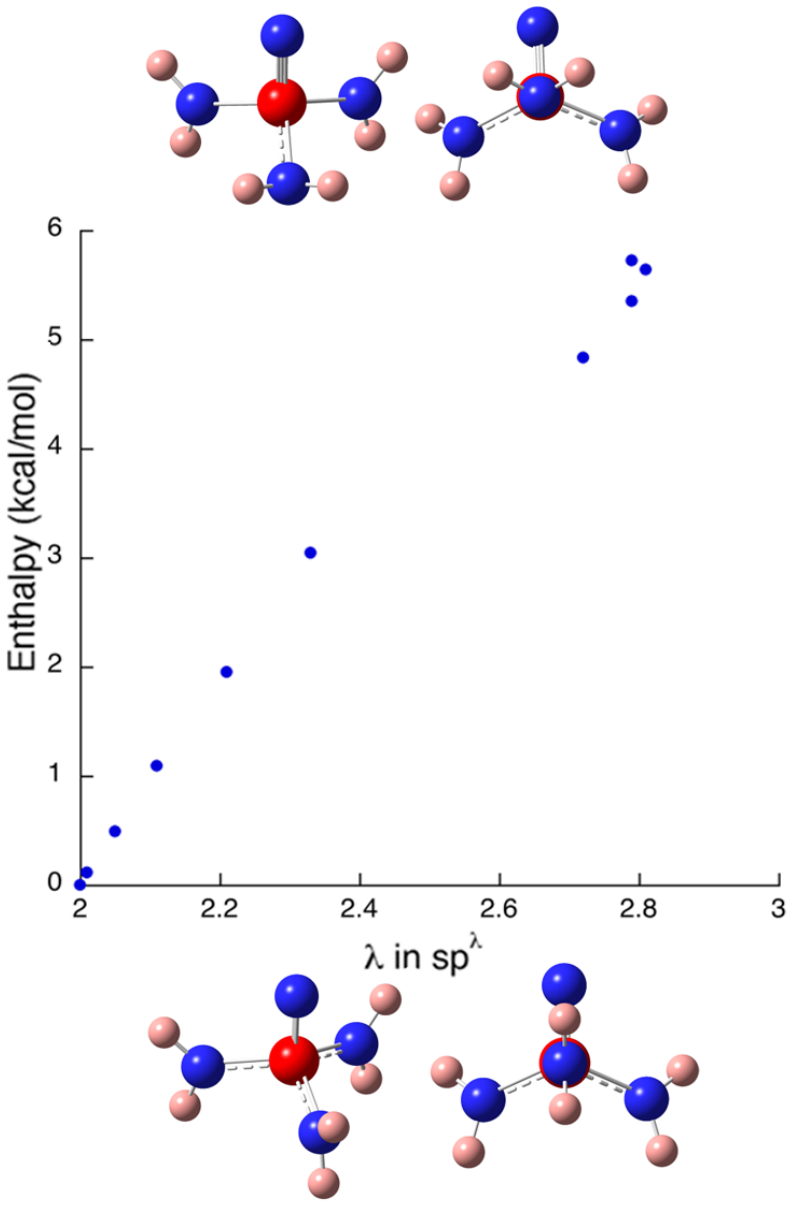

Figure 4.1. DFT B3LYP/aug-cc-pVQZ computational results for $NCr(NH_2)_3$. On the bottom are two views of the computed ground state, with the right view looking down one of the three equivalent amido-chromium vectors. In the middle is a plot of the hybridization parameter (λ) vs the calculated enthalpic energy of the complex with the ground state set to 0 kcal/mol. On the top are two views of the transition state structure found for rotation of one amido ligand, with the right view looking down the rotated amido-chromium vector.

If $NCr(NH_2)_3$ is reoptimized while restricting the dihedral angle in one of the amido ligands to induce rotation, the rotating nitrogen pyramidalizes as the lone pair on the amido approaches the nitrido π-orbitals.[15] In other words, the nitrido prohibits significant π-donation from the rotating amido when it would donate into the same orbital. The energy of the complex increases with increasing amido nitrogen hybridization parameter (λ in sp^{λ}) from $\lambda = 2$, i.e. sp^2, in the ground state to around $\lambda = 2.8$ (Figure 4.1, plot) at the transition state for the rotation.[16] From the calculations an enthalpic barrier, $\Delta H^{\ddagger}$, of 5.7 kcal/mol was found using the aug-cc-pVQZ basis set. Meanwhile, the Cr–N(nitrido) bond distance seems virtually unaffected by the rotation, varying by less than 0.01 Å over the entire course of the rotation.

The transition state for amido rotation, which had a single negative vibration, was found at 61° in the N(nitrido)-Cr–N(amido)–H dihedral. Figure 4.1 has images of the ground state and transition state structures. Also in Figure 4.1 is a plot of λ versus enthalpy. The hybridization parameter increases fairly smoothly up to the transition state, consistent with competition with the nitrido π-donation being the cause of amido pyramidalization.

The amido distance does seem to change slightly with rotation due to bond order effects with the chromium, but the relationship is complicated by electronic adjustments made by the other amido ligands. The average $Cr–NH_2$ distance in the ground state from the calculations is 1.83 Å. In the transition state, the pyramidalized (rotating) amido distance increases to 1.90 Å, but the amidos not undergoing rotation shorten their distance to chromium to 1.81 Å. As a result, the average $Cr–NH_2$ distance in the transition state is 1.84 Å, essentially identical to the ground state. In other words, rotating one ligand causes ripples of change through the other ligands. It is

these indirect changes in the amido ligands due to compensating effects around the metal that we are measuring in this study.

In the actual diisopropylamido complexes used in the experimental studies, this degree of pyramidalization may not be possible for steric reasons. However, the hybridization of the amido nitrogen in the model is illustrative of the type of electronic changes expected on rotation. Donation into the same orbitals as the strongly donating nitrido is energetically unfavorable, and, in the model at least, this competition for the metal's acceptor orbitals manifests as amido rehybridization.

In this study, the $NCr(NPr^{i}_{2})_{2}$ fragment is held constant, and the barrier to rotation of the diisopropylamido ligands in this constant fragment are what is being measured. The X substituents affect the amido barrier to rotation only indirectly, and the only changes from one complex to another are the electronic and steric components of X in $NCr(NPr^{i}_{2})_{2}X$.

This system has several advantages for this type of study. First, the compounds prepared thus far have good to excellent thermal stability. Second, the complexes are diamagnetic, allowing easy use of NMR for evaluation. Third, the Cr(VI) nitrido compounds tend to be pseudotetrahedral; we have not observed dimers with bridging X ligands in this system, for example. Fourth, ligands tend to be monodentate on the metal allowing a more uniform comparison between various ligand sets. Even ligands such as carboxylate, with a strong tendency to have higher hapticity in most complexes, only show what appear to be weak secondary interactions with the metal if any (vide infra). Fifth, the $NCr(NPr^{i}_{2})_{2}X$ complexes are readily prepared from inexpensive reagents with an extraordinary variety of X as will be described next.

4.3 Preparation of $NCr(X)(NPr^{i}_{2})_2$ Complexes and Characterization

Here, we begin by discussing a new synthetic protocol based on nitrogen-atom transfer for the formation of $NCr(NPr^{i}_{2})_3$ (**1**). All other complexes are prepared by modification of **1**. The synthetic protocols for the production of the other $NCr(X)(NPr^{i}_{2})_2$ complexes will be divided into 7 categories: protonolysis with lutidinium halides, protonolysis with HX, exchange using thallium salts, exchanges between lithium salts and the chromium phenoxide, metathesis using sodium salts, ligand exchange with lithium to zinc transmetallation, and tin(IV)-catalyzed decomposition of a cationic BF_4 salt.

4.4 Synthesis of $NCr(NPr^{i}_{2})_3$ (1) by Nitrogen Atom Transfer

The starting material for all of this chemistry is the Bradley complex, $Cr(NPr^{i}_{2})_3$, prepared on large scales from $CrCl_3$ and $LiNPr^{i}_{2}$ in ethereal solvent.[17] The 3-coordinate compound is soluble in hydrocarbons and crystallizes as large black plates. In the previously reported synthesis of nitrido $NCr(NPr^{i}_{2})_3$ (**1**), black solutions of $Cr(NPr^{i}_{2})_3$ reacted with NO gas to form orange $ONCr(NPr^{i}_{2})_3$, which was deoxygentated with vanadium(III) to form the terminal nitrido.[18]

For this work, a somewhat more straightforward synthesis was used where $Cr(NPr^{i}_{2})_3$ was treated with $NCr(OBu^{t})_3$ to give $NCr(NPr^{i}_{2})_3$ (**1**) through a nitrogen-atom transfer (Eqn 1). Yellow $NCr(OBu^{t})_3$ is available from chromyl chloride in a one-pot procedure published by

Chiu and coworkers.[19] The nitrido was readily separated from the oily $Cr(OBu^t)_3$[20] byproduct by washing with acetonitrile.

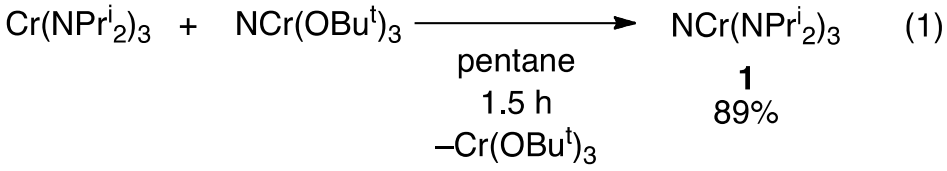

4.5 Syntheses Using Protonolysis with Lutidinium Halides

Dark beet-red **1** was converted to orange $NCr(I)(NPr^i_2)_2$ (**2**) with 2,6-lutidinium iodide using the published procedure.[21] Using procedures similar to the iodide synthesis, the chloride (**3**) and bromide (**4**) complexes were prepared. The syntheses involved the addition of anhydrous 2,6-lutidenium halide to **1** in chloroform at 60 °C (Eqn 2).

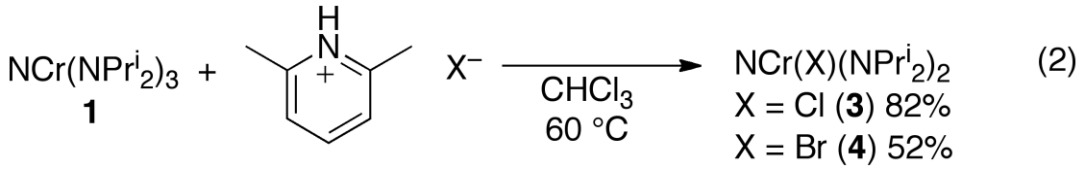

4.6 Syntheses Using Direct Protonolysis with HX

For this study, a total of 15 complexes were prepared using the direct addition of HX, where X is the new desired ancillary ligand (Eqn 3). For the synthesis of most alcohols, silanols, carboxylates, and thiolates, direct protonolysis on **1** turned out to be the most convenient and highest yielding methodology. The reactions were carried out using toluene as the solvent for all of these cases, with the exception of triflate where DME/pentane was employed.

The other conditions required for the syntheses varied widely depending on the substrate HX. Some reactions, such as with triflic acid, worked best when started at near frozen temperatures with short stirring times at room temperature. Other substrates were heating for

several days to get good conversion, e.g., the reaction with 1-adamantanol (HOAd) required heating at 90 °C for 3 days.

$$\underset{\mathbf{1}}{NCr(NPr^i_2)_3} + HX \xrightarrow[-\,HNPr^i_2]{} NCr(NPr^i_2)_2X \qquad (3)$$

X = OTf (**5**), 70%
OAd (**6**), 70%
$OSiPh_3$ (**7**), 72%
O_2CPh (**8**), 88%
OBu^t_{F6} (**9**)
OPh (**10**)
O-*p*-$(OMe)C_6H_4$ (**11**), 87%
O-*p*-$(SMe)C_6H_4$ (**12**), 92%
O-*p*-$(Bu^t)C_6H_4$(**13**), 94%
O-*p*-$(F)C_6H_4$ (**14**), 88%
O-*p*-$(Cl)C_6H_4$(**15**), 85%
O-*p*-$(CF_3)C_6H_4$ (**16**), 82%
OC_6F_5 (**17**), 76%

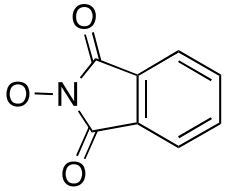

(OPth, **18**), 52%

SPh (**19**), 75%

Two of the compounds in Eqn 3, **9** and **10**, have been previously reported.[22]

4.7. Syntheses Using Exchange with Thallium Salts

Thallium salts were advantageous in several cases for the production of new $NCr(NPr^i_2)_2X$ complexes. The reactions with iodide (**2**), led to rapid precipitation of TlI, which is readily removed by filtration. The reactions were generally clean, and the use of thallium avoids unwanted reduction processes found using some other reagents (vide infra). Some obvious disadvantages for thallium are the toxicity of the metal and lack of stability with some X substituents. Thallium was employed in the preparation of five of the complexes (Eqn 4).

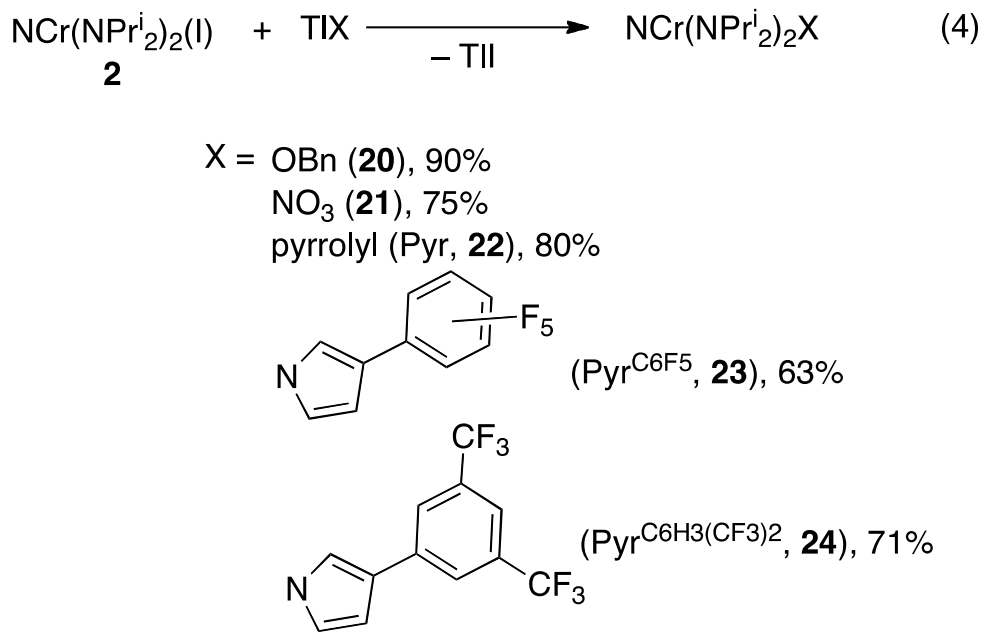

Protonolysis of **1** with HOBn proved to be slow and not very clean. Using TlOBn, NCr(NPr$^i_2$)$_2$(OBn) (**19**) was prepared in good yield from iodide **2**. Hexanes or toluene were used for the majority of these transmetallation reactions.

Likewise, commercially available $TlNO_3$ gave NCr(NPr$^i_2$)$_2$(NO_3) (**20**); in this case, THF was advantageous due to the low solubility of the thallium salt in most other solvents.

Thallium was especially useful for pyrrolyl and pyrrolyl derivatives. The thallium salts were readily available by simple reaction of TlOEt with the *NH*-pyrrole. The thallium pyrrolyls seemed at best sparingly soluble in any solvent with which they didn't react, as evinced by being ^{1}H NMR silent as saturated solutions in several solvents, but the compounds reacted readily and cleanly with the iodide **2**. The chromium complexes of pyrrolyl (**22**) and two different 3-aryl-pyrroles (**23** and **24**, Eqn 4) were prepared using this procedure.

4.8 Syntheses Using Exchange with Lithium Salts

When using lithium reagents, reduction of iodide **2** to the known μ-nitrido chromium(V) dimer[20] $[NCr(NPr^i_2)_2]_2$ was evident. Transmetallation using the phenoxide **10** was often more successful with these reagents, and this method was used to prepare the indolyl (**25**), carbazolyl (**26**), and *N*-methylanilide (**27**) complexes (Eqn 5) from their respective lithium salts. A similar method was used in the conversion of $NCr(OPh)_2(NPr^i_2)$ to $NCr(CH_2SiMe_3)_2(NPr^i_2)$ in work from the Cummins laboratory.[21]

$$\underset{\textbf{10}}{NCr(NPr^i_2)_2(OPh)} + LiX \xrightarrow[-\ LiOPh]{} NCr(NPr^i_2)_2X \qquad (5)$$

X = indolyl (**25**), 42%
carbazolyl (**26**), 35%
N(Me)Ph (**27**), 44%

4.9 Syntheses Using Exchanges with Sodium Salts

The three complexes $NCr(NPr^i_2)_2(X)$, where X = NCO (**28**), NCS (**29**), and CN (**30**), were prepared (Eqn 6) from the commercially available NaX salts and $NCr(NPr^i_2)_2(I)$ (**2**). The main difficulty with the reactions was the low solubility of these reagents in organic solvents. Acetonitrile was used as the solvent and reactions required relatively long reaction times and/or mild heating. In the case of NaCN, one equivalent of 15-crown-5 was advantageous.

$$\underset{\textbf{2}}{NCr(NPr^i_2)_2(I)} + NaX \xrightarrow[\text{acetonitrile}]{-\ NaI} NCr(NPr^i_2)_2X \qquad (6)$$

X = NCO (**28**), 60%
NCS (**29**), 52%
CN (**30**), 43% (with 15-crown-5)

4.10 Ligand Exchange with Zinc Transmetallation

For probing steric effects in the barriers to rotation (vide infra), it was desirable to synthesize the dimethylamido complex $NCr(NPr^i_2)_2(NMe_2)$ (**31**) for comparison with $NCr(NPr^i_2)_3$ (**1**). The most fruitful route (Eqn 7) we discovered to **31** involves treating $ZnCl_2$ with $LiNMe_2$ in DME/THF solvent. Presumably, a $Zn(NMe_2)_2$ solvate or perhaps an amido-containing zincate complex is prepared. This mixture does transmetallation with iodide **2** more cleanly than with the lithium salt alone. Attempts to prepare **31** directly from **2** with $LiNMe_2$ resulted largely in reduction.

$$\underset{\mathbf{2}}{NCr(NPr^i_2)_2(I)} + 8.5\ LiNMe_2/4.25\ ZnCl_2 \xrightarrow[THF/DME]{} \underset{\substack{\mathbf{31}\\ 70\ \%}}{NCr(NPr^i_2)_2(NMe_2)} \qquad (7)$$

4.11 Tin(IV)-Catalyzed Decomposition of a Cationic BF_4 Salt

Many different methods were tried in attempts to prepare the fluoro complex. Success was finally found when we generated a cationic complex by treatment of the iodo **2** with $AgBF_4$ in the presence of DMAP to form $[NCr(NPr^i_2)_2(DMAP)]BF_4$ (**32**).[12] Thermal decomposition of this complex does form small amounts of fluoride $NCr(NPr^i_2)_2(F)$ (**33**) but also gives a large amount of unidentified side-products. In one attempt to form the fluoride by transmetallation, we reacted **32** with $FSnBu^n_3$, which gives fluoro **33** relatively cleanly. Subsequently, we found that $FSnBu^n_3$ could be used catalytically. It appears that Sn(IV) complexes can catalyze the decomposition of **32**, as can some other mild Lewis acids.[23] The expected byproduct,

DMAP•BF_3, was easily detected in the ^{19}F NMR spectrum of a reaction to form **33** carried out in an NMR tube.[24]

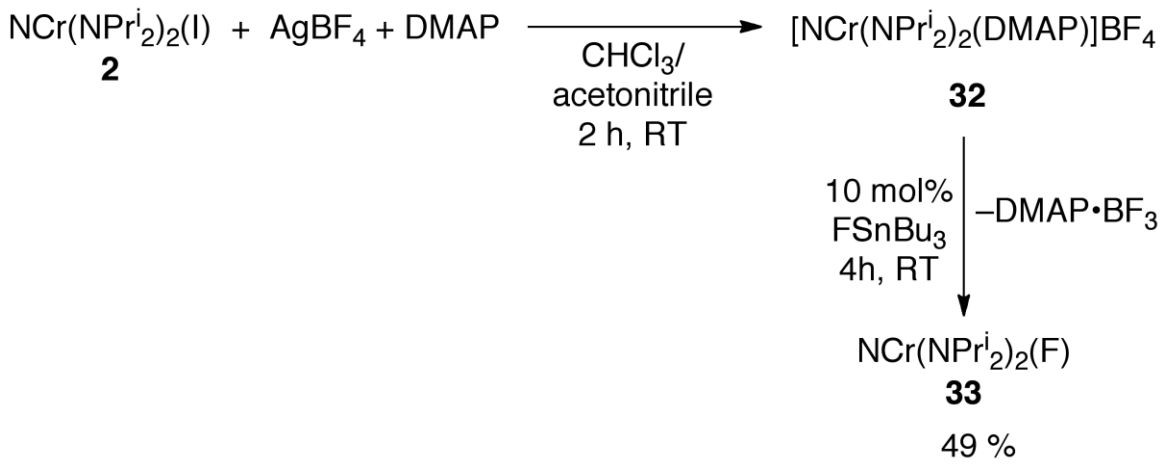

Scheme 4.1. Synthesis of NCr(NPr$^i_2$)$_2$(F) (**33**).

4.12 Single-Crystal X-ray Diffraction Studies

All of the compounds of the formula NCr(NPr$^i_2$)$_2$(X), where X is an anionic substituent, have been structurally characterized.[25] As might be expected, the Cr–N distances, both nitrido and amido, are not exceedingly sensitive to changes in X outside the error limits of the X-ray diffraction experiment. All of the compounds exhibit diisopropylamido ligands with the Cr–NC_2 amido planes parallel to the Cr–N(nitrido) vector, as expected from the electronic structure (vide supra). Discussion of the X-ray structure of each compound would be gratuitous; however, a few of the more salient features will be addressed in this section.

The structural characterization on so large a number of derivatives was carried out predominately to facilitate the steric analyses discussed below, to determine if there were any

secondary interactions (e.g., bidentate ligands), and to ascertain if any of the structural parameters might reliably correlate with the electronic and steric features.

The donor abilities of the X ligands did not have a large impact on the chromium-nitrido distance. Indeed, the nitrido distance is very similar for all the complexes measured thus far. For example, the nitrido distance in the poorly donating triflate (**5**), strongly donating and relatively small benzyloxy (**19**), and the large and strongly donating diisopropylamido (**1**) were found to be 1.543(3), 1.543(2), and 1.544(3) Å, respectively. The full range of Cr–N(nitrido) values is 1.524(3) in nitrate **21** to 1.553(4) Å in O-*p*-$(CF_3)C_6H_4$ **16**. However, there is no obvious correlation between this distance—or, for that matter, any other metric parameters investigated—and any of the steric or electronic parameters derived.

The two chromium-diisopropylamido bond distances were generally the same within error. The only exception in this list of compounds was for carbazolyl **26**, which had Cr–N(diisopropylamido) distances of 1.796(2) and 1.833(2) Å. The carbazolyl plane is tilted from the Cr–N(nitrido) vector (Figure 4.2) and, according to the space filling models, there is steric clash between the aromatic ring of the carbazolyl *anti* to the nitrido and a diisopropylamido ligand. The longer Cr–NPr^i_2 distance is associated with the amido closer to the tilted carbazolyl on the side *anti* to the nitrido (the left NPr^i_2 group in the top of Figure 4.2). However, the average Cr–NPr^i_2 distance in **26** is similar to the other compounds, and it appears that the steric influence of the carbazolyl is mostly to differentiate the two diisopropylamidos in the solid state. (The two diisopropylamido groups are equivalent in solution.)

The $NCr(NPr^i_2)_2$ molecular fragment showed some variability in its metric parameters. For example, the amido-chromium-amido angle varied from 116.1(5)° (X = N(Me)Ph **27**) to

124.9(1)° (X = CN **30**), and the average Cr–N(amido) distances varied from 1.805(3) Å (X = OTf **5**) to 1.842(2) Å (X = NPr^i_2 **1**). While attempted correlations with these metric parameters and the donor parameters are suggestive, plots of N(amido)-Cr–N(amido) angles and Cr–N(amido) distances with either the steric parameters or donor properties gleaned from the NMR data showed no strong correlations.

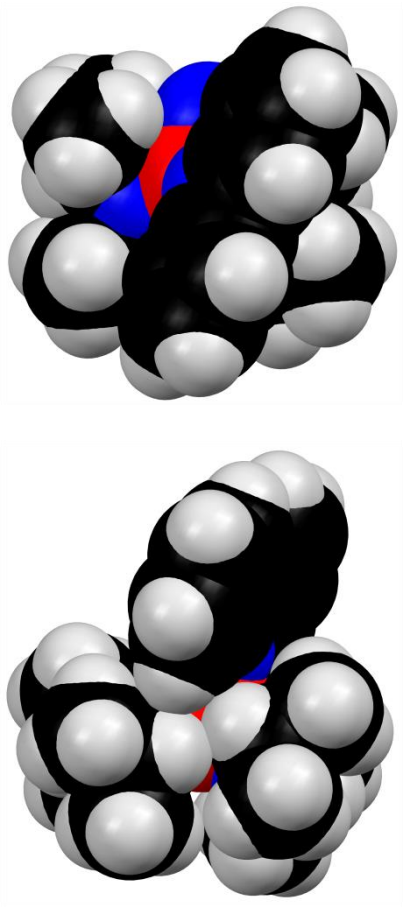

Figure 4.2. Spacefilling views of $NCr(NPr^i_2)_2$(carbazolyl) (**26**). The top view is looking down the Cr–N(carbazolyl) bond showing the tilting of the heterocyclic framework. The bottom view is *anti* to the nitrido and shows the tilted carbazolyl ring's close contacts with one of the *iso*-propyl groups.

Steric factors seem evident in the tris(diisopropylamido) complex **1** according to other data (vide infra), but it is difficult to discern this from the X-ray diffraction studies alone. The average Cr–N(amido) distance in the published structure for **1** is 1.842(3) Å. This distance in **1** is somewhat larger than many of the derivatives prepared. For example, the average Cr–N(diisopropylamido) distances for a few derivatives are: Cl **3** 1.813(2), OBn **20** 1.823(1), OAd **6** 1.822(7), N(Me)Ph **27** 1.830(2), and OTf **5** 1.805(3) Å. However, the average diisopropylamido distance in **1** is very much in line with the sterically less encumbered NMe_2 **31** with average Cr–N distances of 1.842(4) Å; incidentally, **31** was one of the compounds examined that displayed full molecule disorder in the X-ray diffraction experiments. The disorder was fully modelled.

A plot (Figure 4.3) of the average diisopropylamido distance versus the Ligand Donor Parameter (LDP) described below shows no clear correlation. This may be due to the errors in the structural parameters considering the less donating ligands (towards the right in the plot) do, generally speaking, seem to have shorter Cr–N(amido) distances and the more donating ligands seem to have generally longer distances. However, the scatter in the data is far too large to make anything resembling an accurate correlation. In fact, the shortest Cr–N(amido) averages are found for two aryloxide derivatives with moderate LDP values (vide infra) for this series.[26]

Two compounds, benzoate **8** and nitrate **21**, possibly show weak secondary interactions between Cr and the X ligand. For nitrate containing **21**, the Cr–O distance is 1.973(3) Å, and there is a possible weak interaction with a second oxygen of the nitrate nearly *trans* to the nitrido, which is quite long at over 2.7 Å. For benzoate **8**, which has a similar structure near the metal center, the short Cr–O distance is 1.924(1) Å with a possible interaction with the second carboxylate oxygen that is around 3.0 Å away. The contributions from these secondary

interactions of X to the measured donor abilities are unlikely to be large at those distances but are not known.

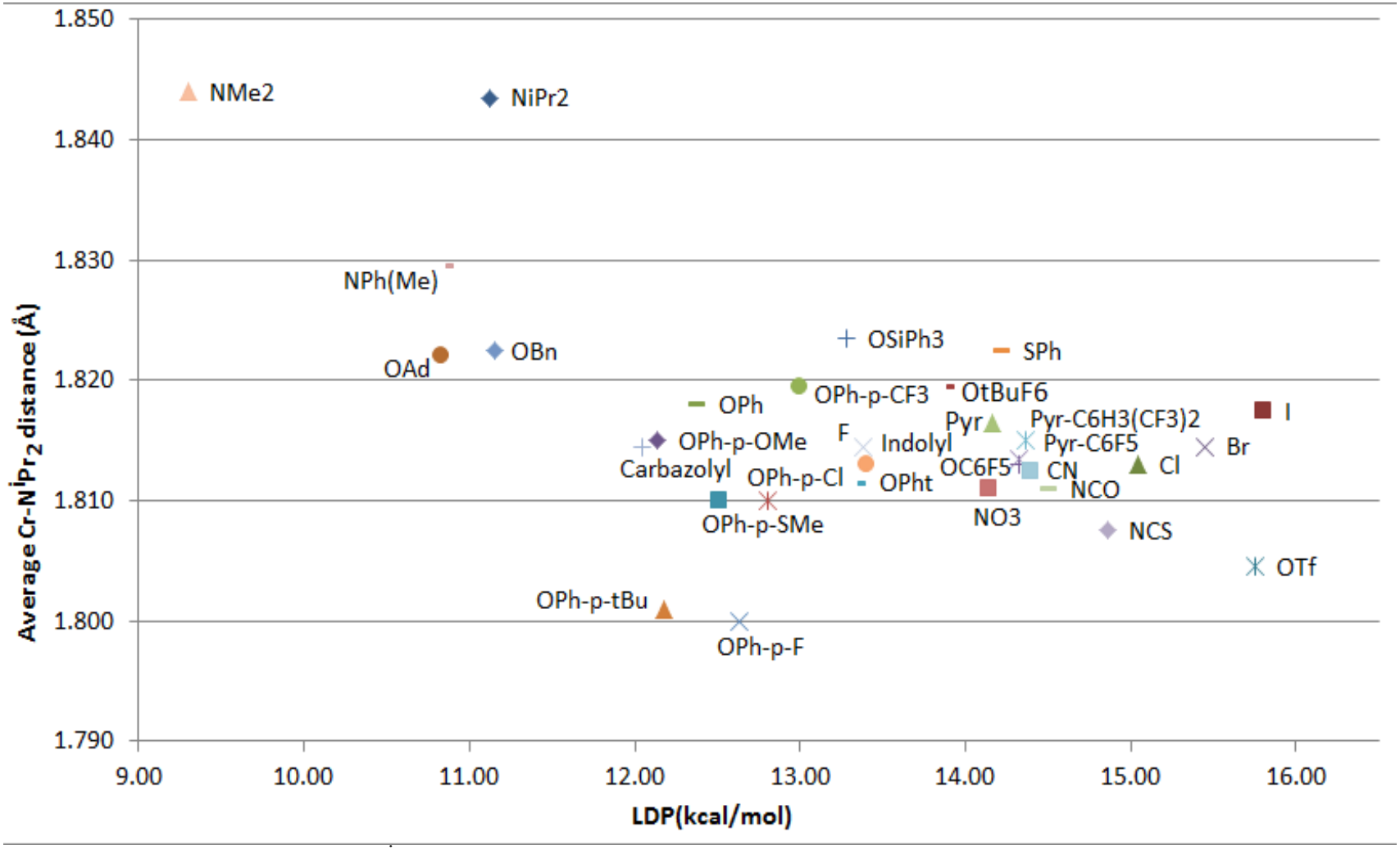

Figure 4.3. Plot of average Cr–NPr^{i}_{2} distance (Å) vs the donor ability of X (LDP in kcal/mol). For interpretation of data labels the reader is refered to Figure 3 of DiFranco, S. A.; Maciulis, N. A.; Staples, R. J.; Batrice, R. J.; Odom, A. L. *Inorganic Chemistry* **2012**, *51*, 1187–200.

4.13 Measurement of Amido Rotational Barriers and the Ligand Donor Parameters (LDP)

Most of the $NCr(NPr^i_2)_2(X)$ complexes employed in this study exhibit two distinct methyne peaks for the diisopropylamido ligands at room temperature assigned as being *syn* and *anti* to the nitrido substituent. The methyne that is *anti* is assigned as being deshielded relative to the *syn* methyne resonance on the basis of 2D NMR experiments on iodo **2** (see the Supporting Information). A few of the compounds where X is a strong donor ligand, e.g., dimethylamido and 1-adamantoxide, have the methynes at or near the coalescence point at room temperature. One of the reasons this system was chosen was that the rate of diisopropylamido rotation was easily measured by ^{1}H NMR spectroscopy. Once the rate constants were known, the Eyring equation was used to determine the free energy barriers to rotation, $\Delta G^{\ddagger}_{rot}$, relative to X.

The rate constant for the exchange of the two methynes in the isopropyls, in the majority of cases, was measured using Spin Saturation Transfer (SST) in the ^{1}H NMR.[27] The ideal temperature for the SST experiment was found to be between –56 °C and +27 °C, depending on the rate of rotation for the particular complex being studied. Detailed descriptions of how the SST experiments and error analyses were done can be found in the Supporting Information. In addition, there is a detailed discussion of how the T_1 values were found and the types of T_1 values to use in Appendix B.

For one complex, $NCr(NPr^i_2)_2(NMe_2)$ (**31**), due to instrument limitations, we were unable to reach the slow exchange temperature. Line Shape Analysis (LSA) was used to determine the barrier for the isopropyl exchange rather than SST.

The X = 1-adamantoxide **6** complex was studied using both LSA and SST for comparison. Both gave the same value to the nearest tenth of a kcal/mol at $\Delta G^{\ddagger}_{rot}$ = 12.8 kcal/mol.

It was expected that the entropy associated with the diisopropylamido rotation would be more or less constant over the series. To investigate this assertion, Eyring plots were done on several of the compounds. The plots were done over as large a temperature range allowable by the kinetics of rotation and our instrumentation. In addition, we explored compounds that varied in $\Delta G^{\ddagger}_{rot}$ and sterics as much as possible. Consequently, the Eyring plots using SST were determined for iodo **2**, benzyloxy **20**, NPr^{i}_{2} **1**, and O-*p*-SMe-C_6H_4 **12**. For these four compounds, $\Delta S^{\ddagger}_{rot}$ was found to be –9, –6, –5, and –3 cal/mol•K, respectively. Consequently, the entropy values appear to be small and negative. The entropy values were found from variable temperature (VT) experiments over temperature ranges of 47, 36, 26, and 44 K, respectively. Additional information on the entropy measurements is found in Appendix B.

It is most desirable to place the rotational barriers in terms of $\Delta H^{\ddagger}_{rot}$, to remove some of the temperature dependence associated with the measurements. Each compound had to be measured at a temperature best suited for its particular rotation kinetics in order to measure the rate constant as accurately as possible. Consequently, the SST and LSA data were collected at different temperatures for each complex.

Here, we are always measuring the kinetics for the rotation of a diisopropylamido ligand in a $NCr(NPr^{i}_{2})_2(X)$ complex. *We assume that the $\Delta S^{\ddagger}_{rot}$ values for the compounds will all be*

similar. Even in cases where the X ligand is quite large and steric effects are likely, i.e., for X = NPr^i_2, we have not observed large deviations in $\Delta S^{\ddagger}_{rot}$ values.[28]

The most reliable measurement of entropy, based on where the slow and fast exchange limits occur relative to our available instrumentation, appears to be the value for iodo **2**, which was done over a 47 K interval. As a result, –9 cal/mol•K was used as the entropy barrier for most of the compounds.[29] The only compound calculated differently is X = NMe_2 **31**, where the activation barriers were found using a different technique (LSA). The experimental barriers for **31** were determined to be $\Delta S^{\ddagger}_{rot}$ = –4 cal/mol•K and $\Delta H^{\ddagger}_{rot}$ = 9.3 kcal/mol.[30]

Under the assumption that entropy differences are minimal, a set of values approximating $\Delta H^{\ddagger}_{rot}$ is obtained. Considering the values are an approximation based on the assumption of $\Delta S^{\ddagger}_{rot}$ = –9 cal/mol•K and their uses for the purposes of this study are more dependent on their relative rather than absolute magnitudes, we call each value a Ligand Donor Parameter (LDP). The LDPs are collected in Figure 4.4 with horizontal error bars allowing quick distinguishing of ligands that are different outside error limits. The current best numerical parameters are collected in Table 4.1.

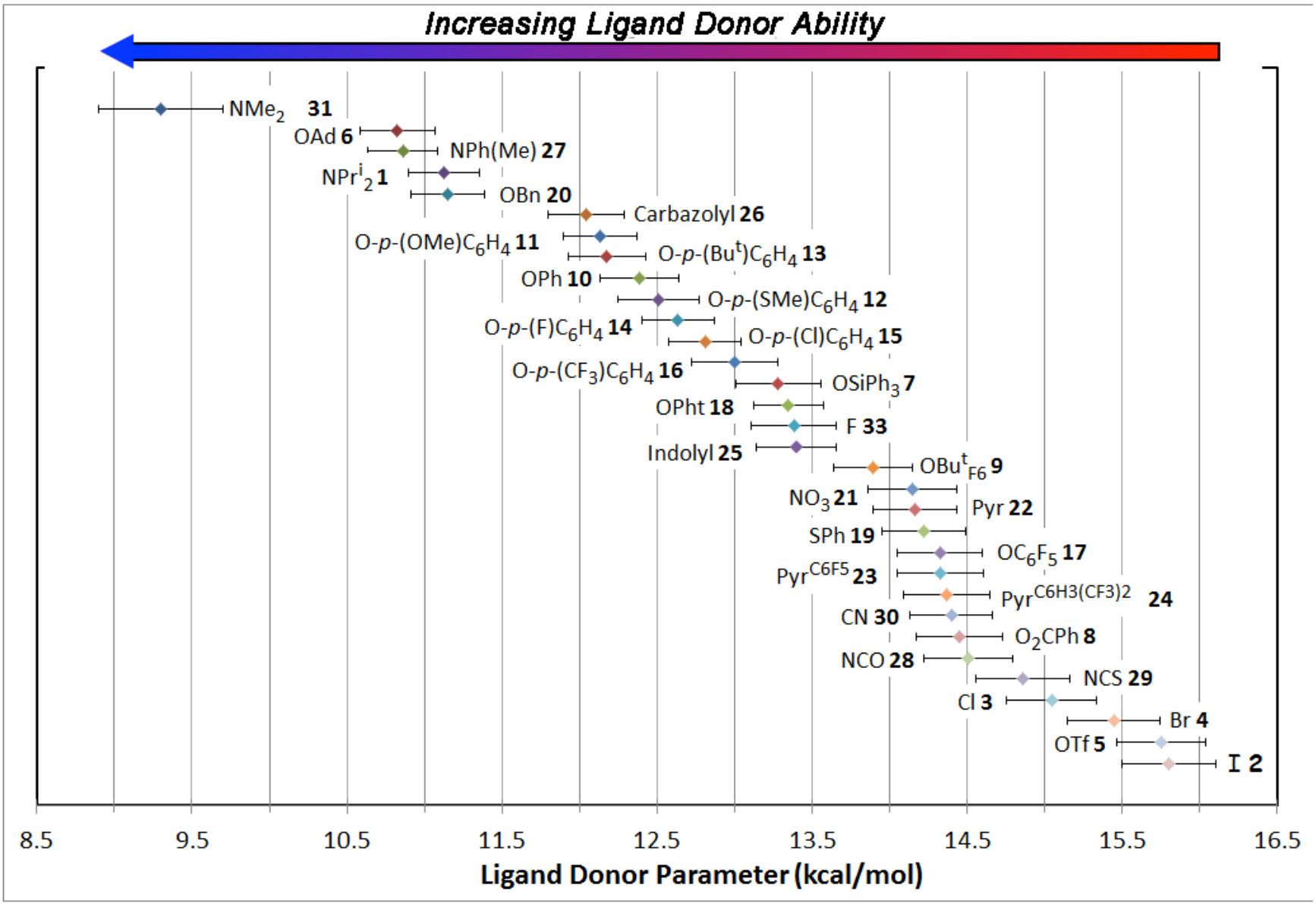

Figure 4.4. The Ligand Donor Parameters (kcal/mol) for various X in $NCr(NPr^{i}_{2})_{2}X$ with the associated errors.

The values in Figure 4.4 and Table 4.1 constitute our current best measurements on this particular series for the enthalpies of amido rotation at this time. There are a number of interesting series that one can look at qualitatively. Quantitative comparisons will be discussed in sections 4.15-4.20 after discussion of steric influences on rotational barriers.

X =	LDP[a]	$\Delta S^{\ddagger}_{rot}$[e]
NMe_2 (**31**)[29]	9.34 ± 0.32[b]	–4 ± 1[b]
OAd (**6**)	10.83 ± 0.24	
N(Me)Ph (**27**)	10.86 ± 0.23	
NPr^i_2 (**1**)	11.12 ± 0.23[d]	–5 ± 2[c]
OBn (**20**)	11.15 ± 0.23	–6 ± 5[c]
Carbazolyl (**26**)	12.04 ± 0.25	
O-*p*-(OMe)C_6H_4 (**11**)	12.14 ± 0.24	
O-*p*-(Bu^t)C_6H_4 (**13**)	12.18 ± 0.25	
OPh (**10**)	12.38 ± 0.25	
O-*p*-(SMe)C_6H_4 (**12**)	12.51 ± 0.26	–3 ± 4[c]
O-*p*-(F)C_6H_4 (**14**)	12.64 ± 0.23	
O-*p*-(Cl)C_6H_4 (**15**)	12.81 ± 0.23	
O-*p*-(CF_3)C_6H_4 (**16**)	13.00 ± 0.28	
$OSiPh_3$ (**7**)	13.28 ± 0.27	
OPht (**18**)	13.35 ± 0.23	
F (**33**)	13.39 ± 0.27	
Indolyl (**25**)	13.40 ± 0.25	
OBu^t_{F6} (**9**)	13.89 ± 0.26	
NO_3 (**21**)	14.15 ± 0.29	
Pyr (**22**)	14.16 ± 0.28	
SPh (**19**)	14.22 ± 0.27	
OC_6F_5 (**17**)	14.32 ± 0.28	
Pyr^{C6F5} (**23**)	14.33 ± 0.28	
$Pyr^{C6H3(CF3)2}$ (**24**)	14.36 ± 0.28	
CN (**30**)	14.40 ± 0.27	
O_2CPh (**8**)	14.45 ± 0.28	
NCO (**28**)	14.51 ± 0.29	
NCS (**29**)	14.86 ± 0.30	
Cl (**3**)	15.05 ± 0.29	
Br (**4**)	15.45 ± 0.30	
OTf (**5**)	15.75 ± 0.29	
I (**2**)	15.80 ± 0.30	–9 ± 5[c]

[a]Average value from at least 3 measurements. Entropy values assumed to be –9 cal/mol•K except for **31** where the variable temperature LSA value was used. [b]Value from VT LSA. [c]Value from VT SST. [d]Steric effects are quite likely contributing to this LDP. [e]Experimental entropy values in cal/mol•K. Errors are from the fits to the Eyring plots.

Table 4.1. Values for LDP (kcal/mol) and $\Delta S^{\ddagger}_{rot}$ (cal/mol•K) for **1**-**31** and **33**.

The halides are in the expected order with iodide being the least donating and fluoride the most. Looking at some monoanionic nitrogen-based heterocycles, it was found that pyrrolyl was a far poorer donor than indolyl, which was a poorer donor than carbazolyl. This is consistent with the expected availability of the nitrogen lone pair for donation in these particular heterocycles. The pyrrolyl ring's aromaticity is dependent upon use of the nitrogen lone pair to reach the 6 π-electrons required by the Hückel rule for aromaticity. As a consequence, the aromatic stabilization energy of pyrrole directly competes with π-donation, which leads to pyrrolyl being a poor π-donor.[31] For indolyl and even more so for carbazolyl, the aromaticity of the 5-membered heterocycles must compete with the 6-membered carbocycle(s) in resonance form contributions to the aromaticity.[32] As a result, the nitrogens in indolyl and carbazolyl seem to donate more strongly to the metal center than pyrrolyl due to the greater availability of their nitrogen-based lone pairs.

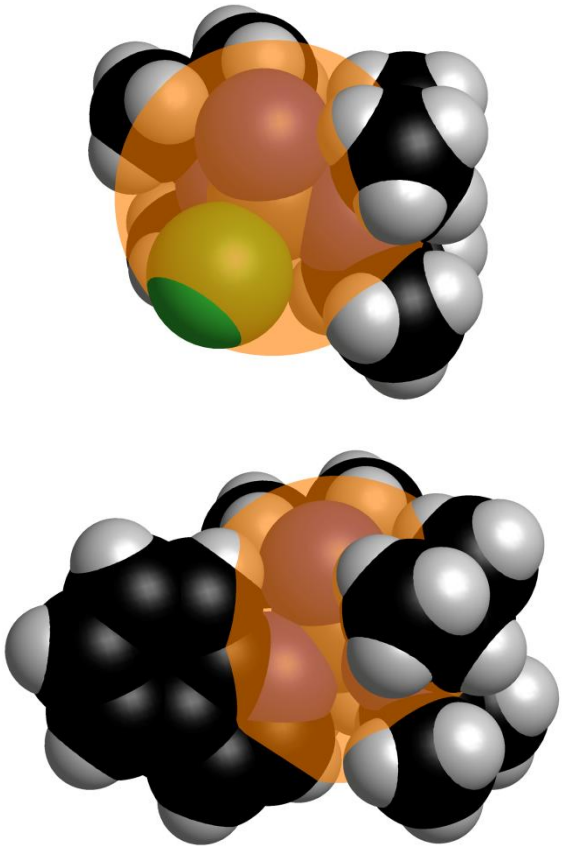

Figure 4.5. Space filling model of relatively small chloro **3** (top) and large indolyl **25** (bottom). The inscribed orange sphere shows the 3.5 Å radius limit.

The strongest donors explored thus far are dialkylamido and alkoxides, which were thought previously to be strong σ- and π-donors. The weakest donors in the series are those with poor overlap due, in all likelihood, to poor size matches between orbitals such as in iodo and thiophenolate, cf. phenolate, or where the X ligand has a competing π-system that limits π-donation such as NCS, benzoate, and pyrrolyl.

4.14 Steric Properties of the Ligands

Coming up with a single parameter for the steric properties of a diverse set of ligands is an inherently inaccurate exercise. One is using a single parameter to describe a 3-dimensional object, which unless that object is a perfect sphere is an incomplete description. However, the Tolman cone angle[1] is quite successful and gives researchers a parameter for initial optimization of reactions. More recently, Percent Buried Volume ($\%V_{bur}$) calculations have proven useful in determining steric parameters for ancillary ligand sets.[33] Encouragingly, the $\%V_{bur}$ of phosphine ligands agrees nicely with Tolman's cone angles for many standard phosphines. Furthermore, $\%V_{bur}$ are easily calculated from crystallographic data using Cavallo and coworkers web-based utility, Samb*V*ca, and have been used extensively for ligand types like *N*-heterocyclic carbenes.[34]

In order to determine the $\%V_{bur}$, the ligands are placed in a sphere so that the ligand is the Cr–X bonding distance away from the center. The sphere size is an adjustable parameter meant to approximate the size where ligands affect the primary coordination sphere of the metal. In most instances, a sphere radius of 3.5 Å is used,[35] which is the default in Cavallo's program as well as the distance used by Nolan and coworkers. In Figure 4.5, there are two examples showing space filling models; the orange sphere is 3.5 Å and shows how much of each ligand is included in the calculation. For a discussion and a plot of sphere radius's effect on $\%V_{bur}$ for a selection of ligands, see the Supporting Information. The results of the ligand parameterization using this method are shown in Figure 4.6.

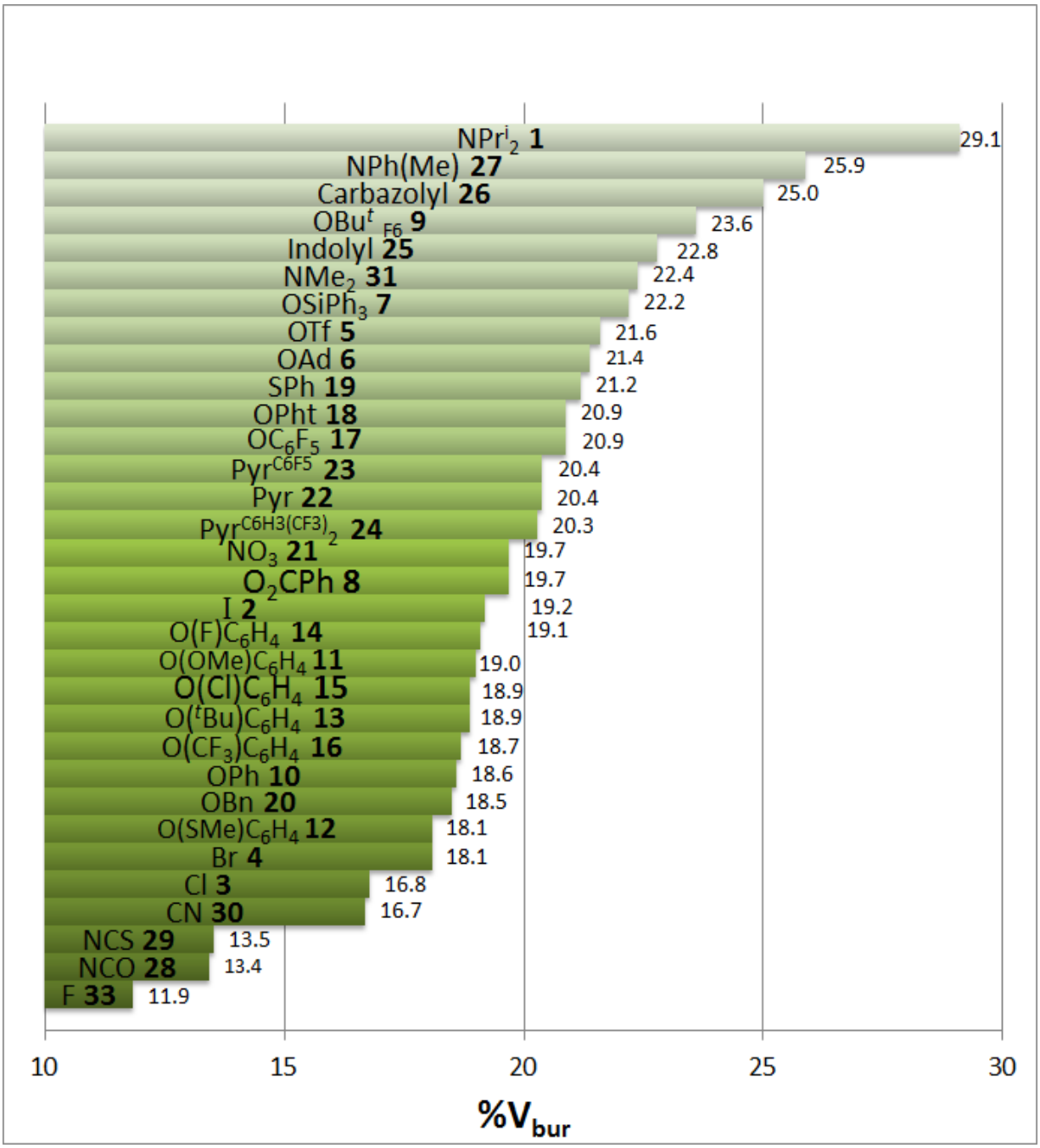

Figure 4.6. The %V_{bur} for the ligands used in this study. Values are for the percentage volume occupied by the ligand in a sphere of radius 3.5 Å from the chromium center.

In addition to $\%V_{bur}$, we also investigated another steric parameterization, the Solid Angle Steric Parameter using the Solid G program.[36] The computational technique works directly from the X-ray diffraction data. The central metal is viewed in some respects as a point source of light, and the ligands block conal access to a sphere around the molecule. An example of the Solid Angle Model is shown in Figure 4.7 for indolyl **25**, where the molecule is in a similar orientation as in the bottom of Figure 4.5. The Solid Angle Steric Parameters for the series of X ligands are shown in Figure 4.8. The x-axis values are in percentage of the sphere occupied by the X ligand.[34]

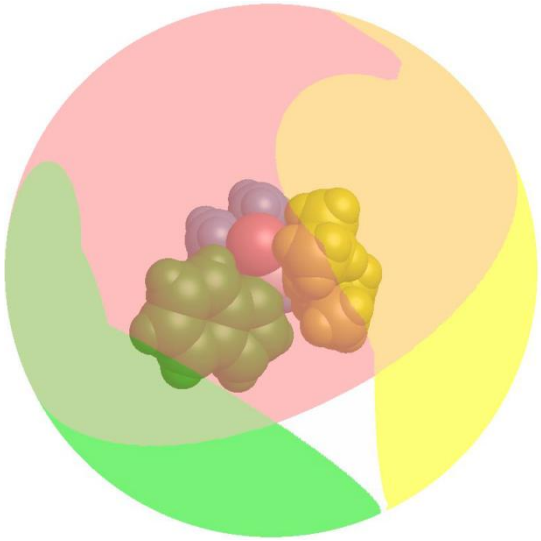

Figure 4.7. The Solid Angle Model from the Solid G program for **25** with indolyl (green), diisopropylamido (yellow and blue), and nitrido (red).

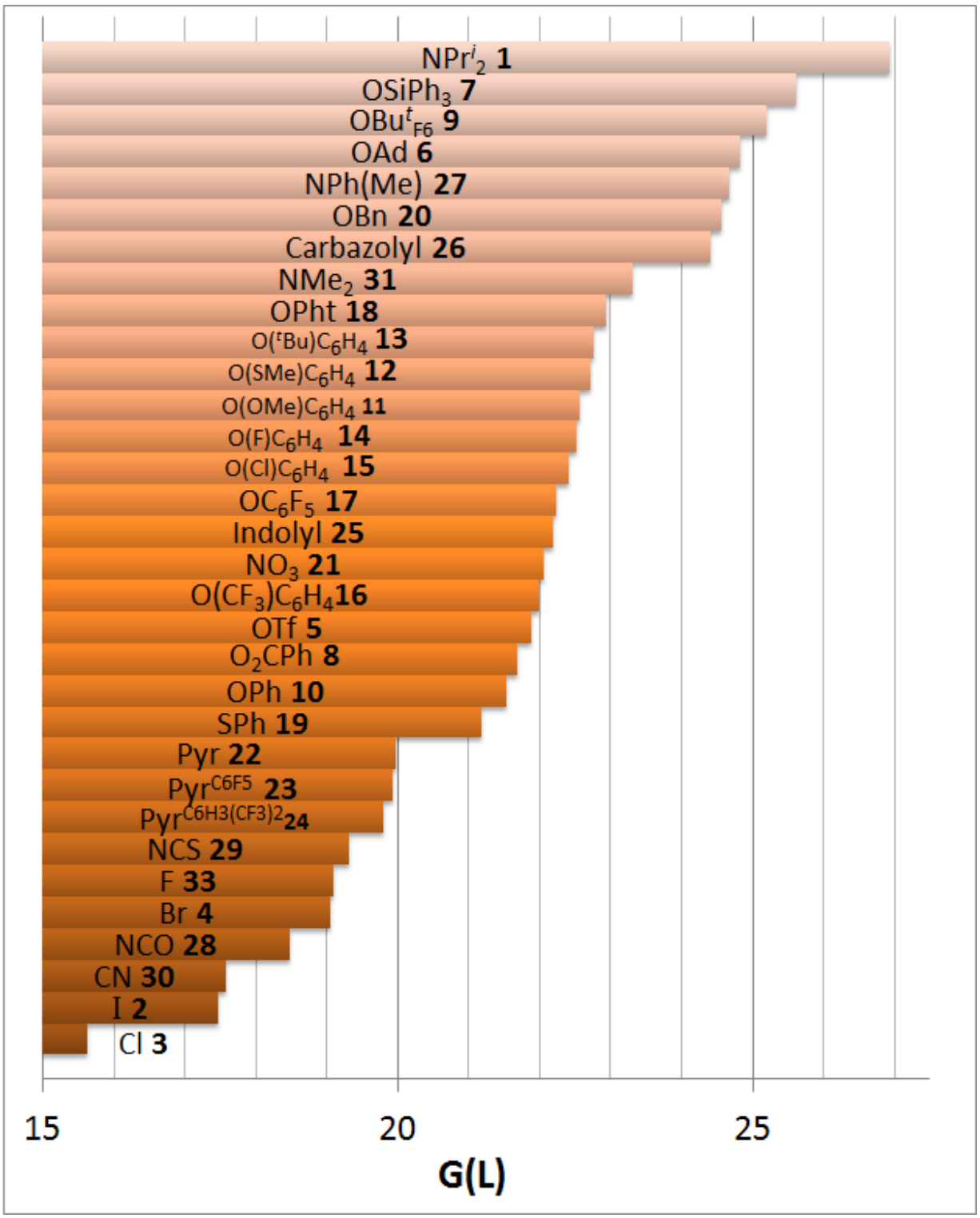

Figure 4.8. The percentage of the chromium coordination sphere shielded, $G_M(L)$, from the Solid G program for the ligands used in this study.

The orderings for many of the ligands change somewhat using the different methods. For example, the Solid G method gives a halide ordering of F > Br > I > Cl due to a mixture of bond distance and radii effects. The halide steric ordering from $\%V_{bur}$ is I > Br > Cl > F and seems to be most greatly affected by atomic radius.[37]

That the complex with X = NPr^i_2 **1** has steric influences on its rotational barrier seems likely. One would expect NPr^i_2 to be a similar or better donor than NMe_2, and yet it has a higher LDP by almost 2 kcal/mol. It appears that sterics are raising the barrier for rotation in this system, and X = NPr^i_2 is the largest ligand investigated by far using both steric metrics.

The only compound where steric effects seem certain to be playing a role in the measurement of LDP is NPr^i_2 **1**. All other compounds are assumed to have LDPs predominately associated with the electronic barrier to amido rotation as there is currently no compelling evidence to suggest otherwise. Some of the most likely ligands to have unresolved steric effects are $OSiPh_3$, OBu^t_{F6}, OAd, N(Me)Ph, indolyl, and carbazolyl, but all of these have steric metrics below NPr^i_2. If other ligands do have steric effects on the amido rotational barrier, their observed LDPs are likely upper limits, and they are electronically more donating than observed.

4.15 Applications and Comparisons with These New Electronic Parameters

We conclude the Results and Discussion Section by comparing the LDP data quantitatively with different systems from the literature. In these types of applications, the LDP values in Figure 4.4 and Table 4.1 are used much as CO stretching frequencies may be used in

alternative late transition metal applications, as arbitrary numbers (in the case of LDP inversely) proportional to the donor ability of the ligand of interest.

4.16 Comparison of LDPs with pK_a Values of the HX Compounds

First, we investigated if the LDPs found in this study correlated to the pK_a of the substituents used. As shown in Figure 4.9, there is no strong relationship. This is to be expected considering the numerous size and orbital make-up differences between the proton and the transition metal system under study.

At best, pK_a can give one a sense of the σ-donor ability of the X ligand when attached to a proton. Perhaps this is the reason for the linear correlation for pK_a and LDP that seems to exist in the plot between the heavier halides I, Br, and Cl where π-effects to the metal are likely minimal. However, pK_a would be expected to give no information on π-donor ability, which is perhaps why fluoride is not on the same line with its heavier congeners.

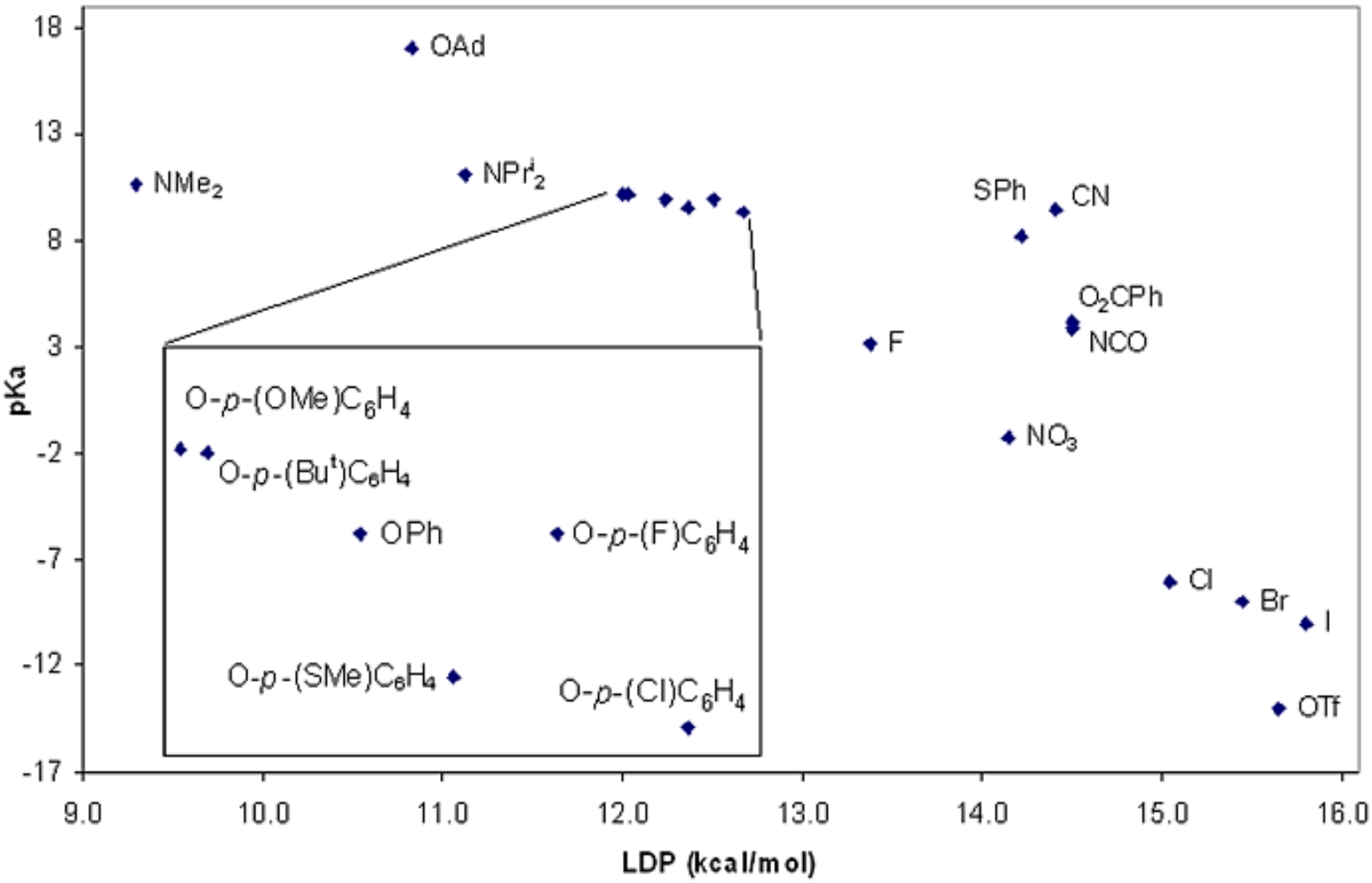

Figure 4.9. Plot of pK_a in water versus LDP. The inset is an expansion of the region containing the phenoxides.

Other closely related series, such as the phenoxides (inset in Figure 4.9) may show some trend with pK_a. However, relating ligand acidity to ligand donor ability is likely to be of dubious quality, especially if strong π-effects are present.

4.17 Phenoxides: An LDP Comparison with Hammett Parameters

Hammett parameters are a reliable and well-worn method for examining electronic effects in a variety of systems with, in large part, *para*-substitution on an arene.[5] In order to determine if there was a correlation between LDP and Hammett σ_p, we generated the set of *para*-substituted phenoxides **10**-**16**. The full range of LDP differences in the series studied from *para*-OMe to *para*-CF_3 is 12.14 to 13.00 kcal/mol with errors around 0.25 kcal/mol. While values at the extremes of this subset are different outside the errors, many of the values within the series are not distinguishable with these error limits. However, plotting this series of LDP values versus the Hammett Parameters (σ_p) for the substituents shows a good linear correlation considering the error bars on the LDP (Figure 4.10).

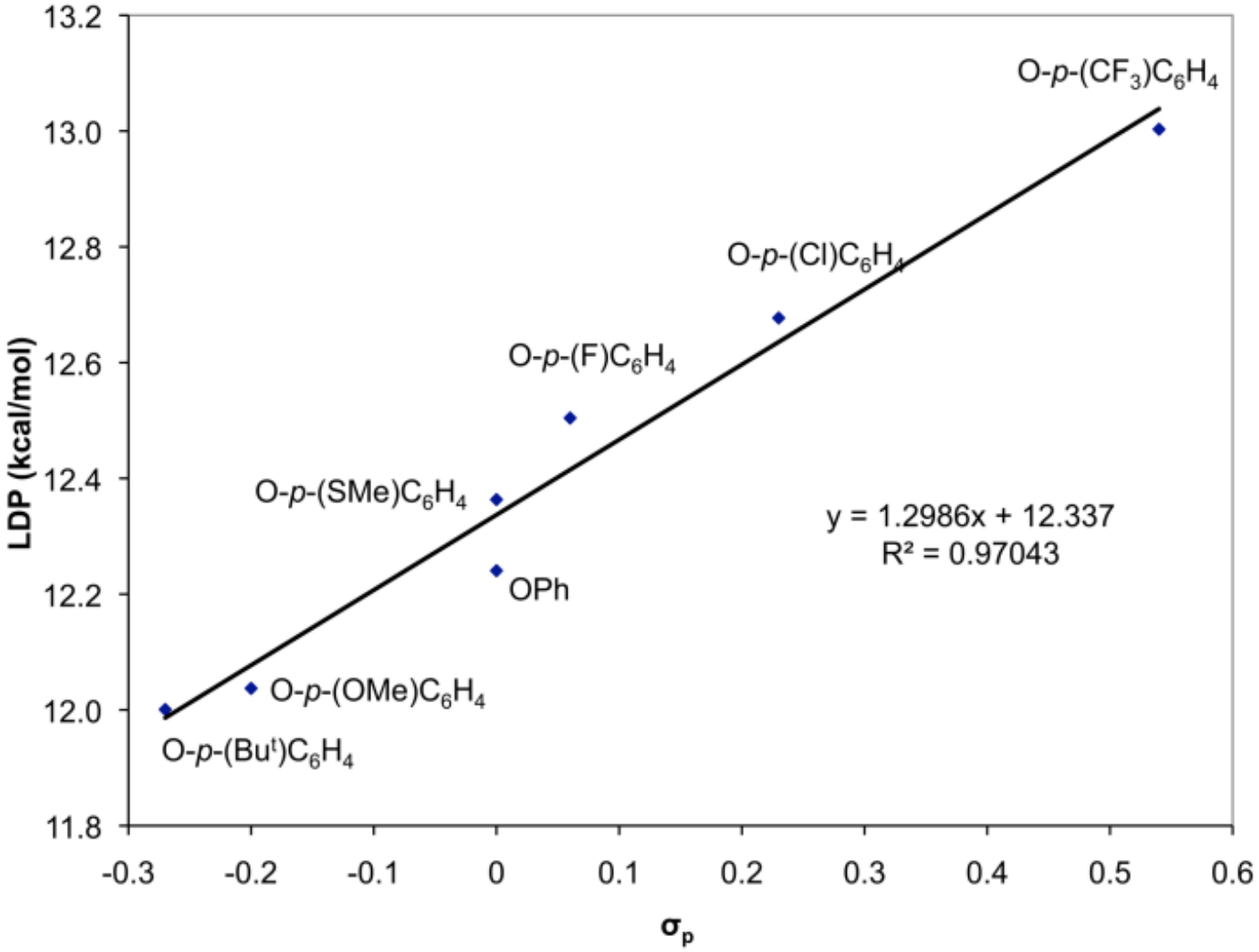

Figure 4.10. Plot of LDP vs Hammett parameters for the aryloxide complexes.

4.18 Evaluation of ^{13}C NMR Chemical Shifts in Tungsten Metallacycles using LDP

In some cases, spectroscopic data known to change with donor properties of ligands may be correlated with LDP. In 2008, our research group published a study on the reactivity and properties of an unusual class of metallacycles with tungsten-carbon double bond character.[38] Included in this study were NMR spectroscopic data for the series and reactivity in carbonyl olefination reactions for the chloride complex with various additives.

The addition of 2 equivalents of cyclooctyne to $W(NAr)_2Cl_2(DME)$ results in the formation of $W(=C_8H_{12}=C_8H_{12}=NAr)(NAr)Cl_2$ (Figure 4.11). Substitution of the chlorides for other X ligands leads to structural changes in the complexes and changes in the ^{13}C NMR chemical shift of the carbon bonded to tungsten. These changes may be viewed as being the result of differing contributions between the alkylidene-imine (left) and alkyl-amido (right) resonance forms. In the paper, we simply stated that the values for the chemical shifts changed as "might be expected" with OEt higher than O-*p*-$(OMe)C_6H_4$ higher than OC_6F_5.[37] Whereas, for chloride and triflate, also included as X ligands in the paper, it was more difficult to discern their donor properties versus these alkoxides.

Using the LDP and plotting versus the ^{13}C chemical shifts, one sees a good correlation between the ligand donor ability as measured in this work across the available ligand sets in the tungsten system and the NMR data reported (Figure 4.11).[39] The chemical shifts of the α-carbons in the metallacycles do indeed correlate with the donor abilities of the X ligands across the entire range of compounds produced in the tungsten study. The linear relationship between LDP and the ^{13}C NMR chemical shift is exceptionally good ($R^2 = 0.996$).

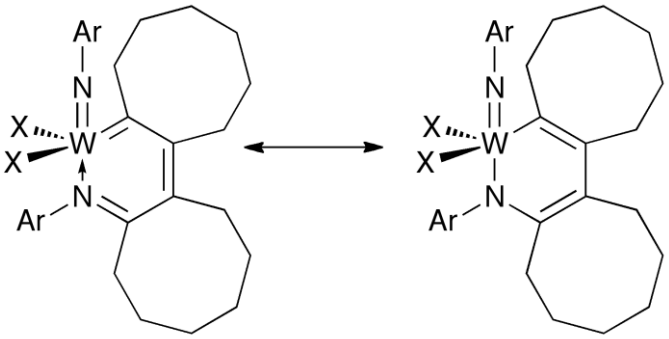

X_2 = Cl_2, $(OEt)_2$, $(OC_6H_4$-*p*-$OMe)_2$, $(OC_6F_5)_2$, (Cl)(OTf)

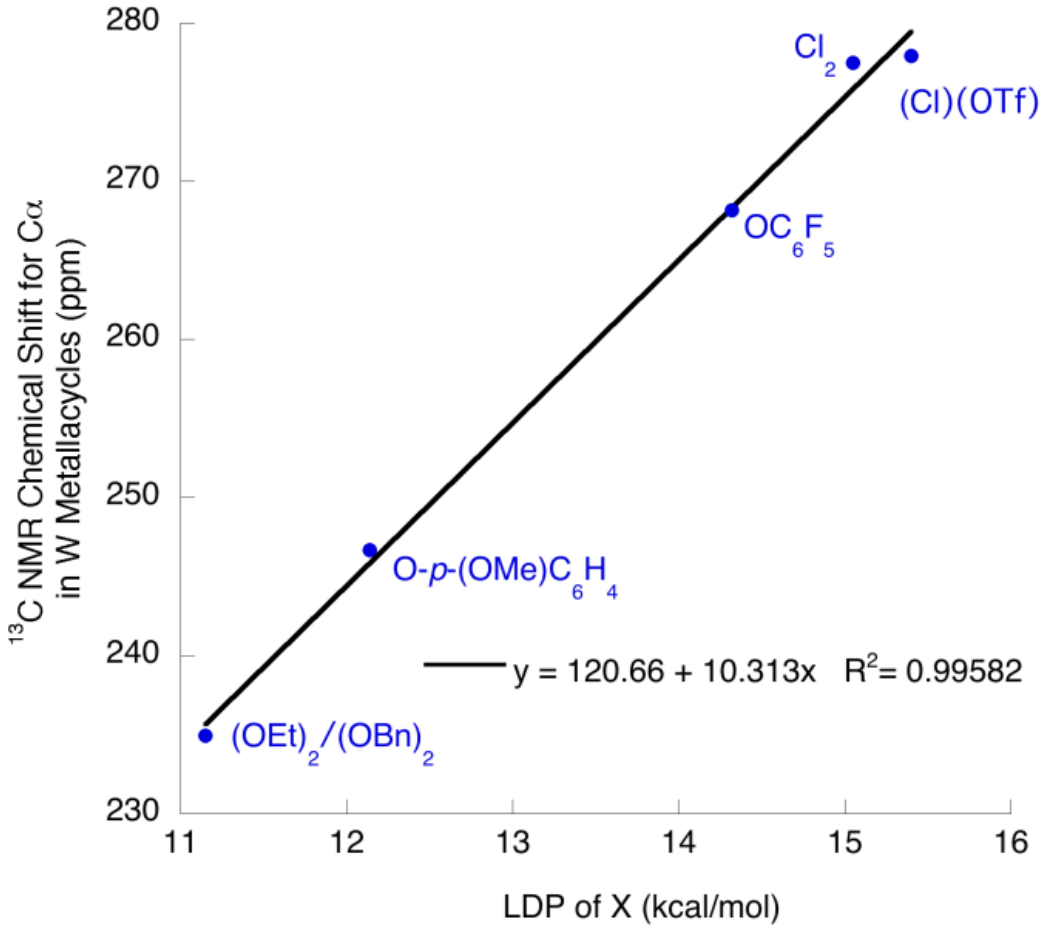

Figure 4.11. Plot of the ^{13}C NMR chemical shift for the carbon directly bonded to tungsten in W(=C_8H_{12}=C_8H_{12}=NAr)(NAr)X_2 versus the donor ability of X found in this work with a linear fit.[37-8]

4.19 Comparison Between the AOM of Cr(III) Complexes and the SST Determined Donor Values

In this study, we were able to include several classic Werner-type ligands and determine their donor properties in this Cr(VI) system. In these traditional coordination compounds, the donor properties are usually determined using visible absorption data in conjunction with Ligand Field Theory. The values can also be parameterized using the Angular Overlap Model as σ- and π-donor energies, e_σ and e_π respectively,[40] of individual X.

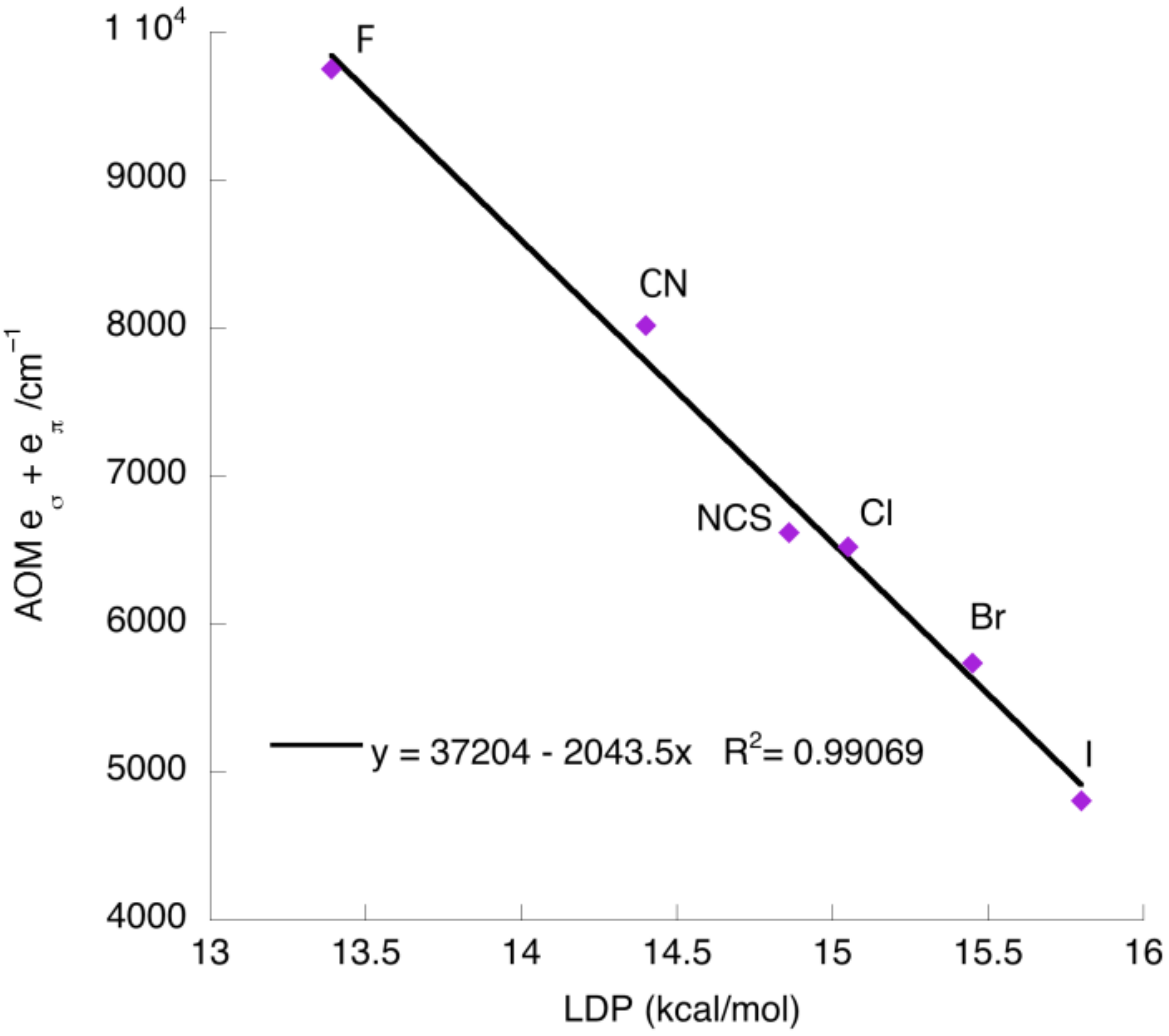

Figure 4.12. Plot of $e_\sigma + e_\pi$ for chromium(III) complexes from experimentally determined AOM values versus the LDP for X (top). Plot of e_σ (blue) and e_π (red) parameters versus the LDP for X (bottom).

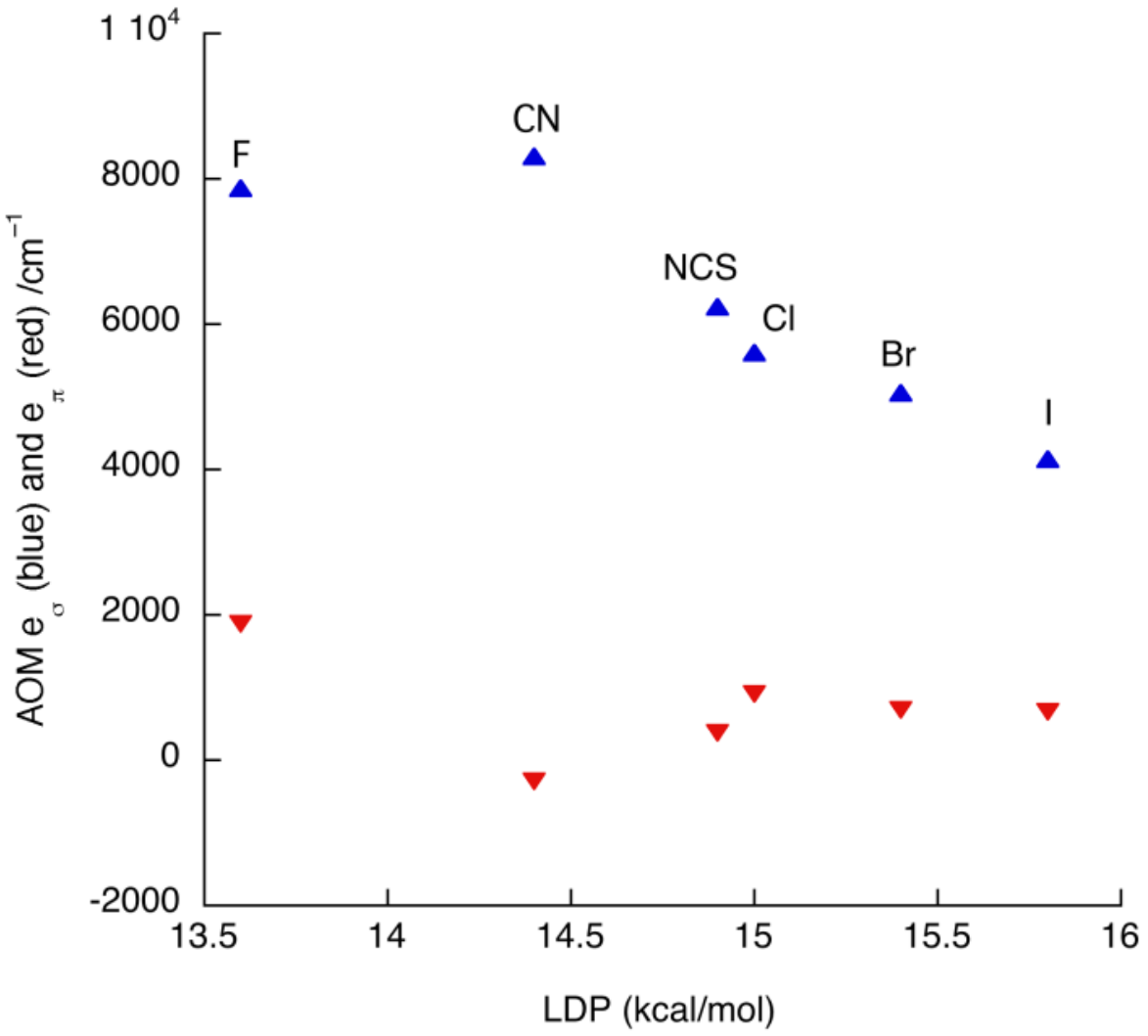

Figure 4.12 cont: Plot of $e_\sigma + e_\pi$ for chromium(III) complexes from experimentally determined AOM values versus the LDP for X (top). Plot of e_σ (blue) and e_π (red) parameters versus the LDP for X (bottom).

In Figure 4.12 is a plot of $e_\sigma + e_\pi$ for chromium(III) complexes from the experimentally determined AOM values[41] versus the donor ability of X found in this study, which shows a good

linear correlation between the two parameterization systems. Also in Figure 4.12 is a plot of the individual $e_\sigma + e_\pi$ parameters versus LDP (bottom). The correlation with either the e_σ or e_π parameter alone is not nearly as good as their sum.

4.20 Comparison Values from Electronic Spectra of Cp^*_2TiX Complexes

In 1996, Lukens, Smith, and Andersen[42] reported a "π-donor spectrochemical series for X" in Cp^*_2TiX titanium(III) compounds with a large number of X ligands. The study employed EPR and absorption spectroscopy to elucidate the electronic structure of d^1 titanium complexes. Of specific interest in the context of this paper, Andersen and coworkers report the singly occupied a_1 to b_2 energy gap, which "depends directly upon the π-donor ability of X". Mach and coworkers have since extended the system to include additional alkoxide ligands.[43]

A plot of the energy gap between a_1 (approximately nonbonding)[44] and the b_2 π-antibonding orbital (ΔE_{xz}) in Cp^*_2TiX Andersen complexes versus LDP for all X in common between the two studies is shown in Figure 4.13 (blue and red circles). In the case of X = OMe, the value for ΔE_{xz} was correlated with the LDP value for OBn in the plot (blue line). The obvious outlier is X = N(Me)Ph (red circle), which is well away from what seems to be a linear correlation between the Cp^*_2TiX spectroscopic data and LDP. Andersen and coworkers centered much of their discussion on the differences between X = N(Me)Ph and the other compounds, and this is quite obvious in Figure 4.13 as well. Also plotted in Figure 4.13 are

Mach's data (green squares) on Cp^*_2TiX, where we used our X = OAd data for their X = OBu^t example.

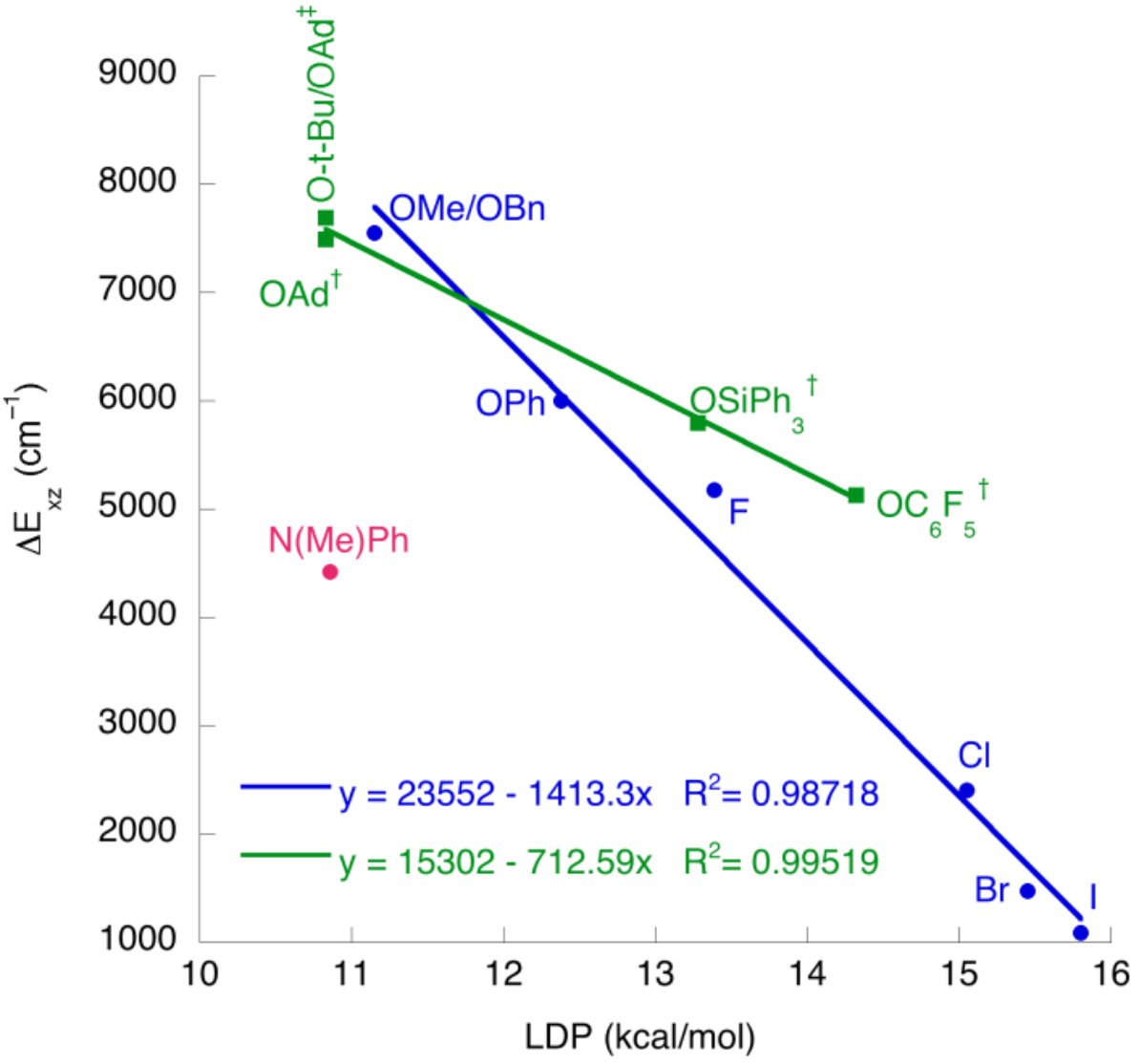

Figure 4.13. Plot of ΔE_{xz} in wavenumbers (cm^{-1}) [Andersen data[41] (red and blue circles), Mach's data[42] (green squares)] versus LDP (kcal/mol) for X. For the data represented by circles, methylcyclohexane was the solvent. The data represented by green squares were taken in either hexane (‡) or toluene (†).[45]

There are several indications that the X = N(Me)Ph in Cp^*_2TiX has little or no π-effects to the nitrogen; although there are indications of agostic effects to the methyl.[41] In the structure from X-ray diffraction, the Cp^*(centroid)–Ti–N–Me average dihedral in the X = N(Me)Ph complex is 86.9°. In other words, the large N(Me)Ph ligand rests in the plane bisecting the Cp^*-Ti-Cp^* unit, and the nitrogen lone pair is orthogonal to the empty orbital of appropriate symmetry to act as an acceptor. Consequently, the experimental Ti–N bond distance is quite long at 2.054(2) Å. This is similar to Ti–N(pyrrolyl) distances,[30] usually a much weaker donor than N(Me)Ph (vide supra). This distance is also much closer to the Ti–N single bond distance of 2.07 Å than the Ti=N distance of 1.77 Å using Pyykkö's radii.[46] In contrast, $Ti–NMe_2$ distances, where there is a strong dative π-bond, are typically ~1.90 Å.[46]

It can be concluded that the lack of correlation for X = N(Me)Ph is due to a deficiency of π-bonding in the Cp^*_2TiX system due to steric effects that do not allow the amido to reach the electronically preferred geometry, a fact readily seen in both the X-ray diffraction study and in correlations with LDP.

If one examines the X = N(H)Me complex of Cp^*_2TiX, the amide is rotated much closer to where maximal overlap with the π-acceptor orbital (b_2) would be possible. The Cp^*(centroid)–Ti–N–Me dihedral for this compound is 13.2°. However, the Ti–N bond,

1.955(5) Å, is slightly longer than the average Ti–NMe_2 bond in the CSD database.[47] This lengthened bond may be due to steric clash with the Cp* ligands.[48]

Overall, the LDP correlate fairly well with the Cp^*_2TiX spectroscopic data in cases where steric effects are not apparent, i.e., all X ligands in common between the two studies except for where the X ligand is an amido derivative.

4.21 Concluding Remarks

Changing metals, changing formal oxidation state, and other ligands on the metal can greatly alter donor properties of ligands. These types of single parameter studies should not replace full mechanistic and computational studies for systems; instead, this is a quick technique that will hopefully be useful in the discussion of properties and mechanisms for metal complexes at low *d*-electron counts. If a series of ligands for a particular system correlate well to LDP and one does not, it might indicate steric influences, hapticity differences between the chromium system here and the system under study, or other effects are important for that particular compound (for an example see X = N(Me)Ph in section 4.20 above). If the system under study does not correlate at all with LDP, there is any number of possible explanations ranging from differences in ligand donor properties, differences in metal acceptor properties, steric interactions, or simply a lack of correlation of the property being measured with ligand donor ability.

In the last segment, we attempted to correlate these new LDP values with numbers from the literature. In the cases discussed above, the values that do correlate, i.e., those other than pK_a, did so linearly. It should be kept in mind, however, that there is no reason to assume that all

correlations between LDP parameters and data determined using numerous techniques on various systems will always be linear. In addition, more involved methods than the single parameter $\%V_{bur}$ and Solid Angle methods may be required for accurate comparisons of sterics in some systems as well.

The absolute values above constitute our current best evaluations of these ligands. Improved techniques and instrumentation for the determination of ligand donor abilities in this system may lead to improved values in the future.

There are obvious ligand types that would be useful to include in a series of this type that have not yet been prepared for parameterization of their donor properties. We are continuing to expand the series presented here. Current plans include the characterization of cationic chromium(VI) nitrido systems with neutral X ligands and a selection of organometallic ligands, which are being prepared for evaluation.

Parameterizations of this type have seen some historical success in explaining reaction mechanisms and trends in reactivity. For example, Basolo, Pearson, Burdett, and many others have used the Angular Overlap Model extensively in this regard especially for later transition metal systems.[49] It is hoped that this method of ligand parameterization will be useful in catalysis studies ongoing in our group and others on high valent metal complexes.

Appendix B contains experimental details and characterization for the production of all the compounds used in the study and data for the X-ray diffraction experiments. Plot of radius versus $\%V_{bur}$ for several ligands. Details on the spin saturation transfer experiments. Details on propagation of error to find LDP values. 2D NMR on **2** and assignments. Details on $\%V_{bur}$ and Solid G calcs.

APPENDIX B

APPENDIX B

B.1 Experimental Procedures for the Preparation of Compounds

General Considerations: All reactions and manipulations were carried out in an MBraun glovebox under a nitrogen atmosphere and/or using standard Schlenk techniques. Ethereal solvents, pentane, hexanes, toluene, and benzene were purchased from Aldrich Chemical Co. and purified through alumina columns to remove water after sparging with dinitrogen to remove oxygen. HCl in diethyl ether was purchased from Aldrich Chemical Co. and used as received. The literature preparations were used for Iodo **2**,[20] OBu^{t}_{F6} **9**,[21] and OPh **10**.[21] The reagent 15-crown-5 was dried by making a toluene solution and refluxing with a Dean-Stark trap overnight. Lutidinium iodide was prepared using the literature procedure.[20] The 3-substituted pyrroles, $Hpyr^{3\text{-}C6F5}$ and $Hpyr^{C6H3\text{-}3,5\text{-}(CF3)2}$, where prepared as previously reported.[5051] (Pyrrolyl)thallium(I) was prepared similar to the literature procedure[52] using 1.1 equivalents of freshly filtered TlOEt in ether, which was added to cold pyrrole in ether. The product precipitates as a colorless solid with low solubility in common organic solvents.

All NMR solvents were purchased from Cambridge Isotopes Laboratories, Inc. Deuterated toluene and benzene were distilled from sodium benzophenone ketyl. Deuterated chloroform was distilled from calcium hydride under dry a dinitrogen atmosphere. The NMR solvents were stored in the glovebox in glass containers with a stopcock. Spectra were taken on Varian instruments located in the Max T. Rogers Instrumentation Facility at Michigan State University. These include a UNITYplus 500 spectrometer equipped with a 5 mm Pulsed-Field-Gradient (PFG) switchable broadband probe and operating at 499.955 MHz (^{1}H) and 125.77

(^{13}C), and a UNITYplus 300 spectrometer operating at 299.976 MHz(^{1}H). ^{1}H NMR chemical shifts are reported relative to residual $CHCl_3$ in $CDCl_3$ as 7.24 ppm. ^{13}C NMR chemical shifts are reported relative to $^{13}CDCl_3$ as 77.0 ppm. ^{19}F NMR chemical shifts are relative to external, neat FC_6H_5 as –113.15 ppm. The resonances for the quaternary carbons for CN, NCS, and NCO in ^{13}C NMR spectroscopy have very long relaxation times, requiring the delay time to be set to at least 15 s for the acquisition.

Computational Methods for the $NCr(NH_2)_3$ Model System: DFT calculations were done using the Gaussian03 software package.[53] The initial optimizations were done using the B3LYP functional and the 6-31G** basis set on a Macintosh computer. The amido rotation was examined by restricting an H–N–Cr–N(nitrido) dihedral angle in 10° increments from 0° (in the the ground state) to 90°, which is past the transition state for rotation. The structures were then reoptimized with B3LYP[54] and the aug-cc-pVQZ basis set[55] using the computational facilities at the High Performance Computing Center (HPCC) at MSU. The highest energy structure investigated through incrementing the dihedral had an angle of 60°; this structure was used as the approximate transition state in a Quadratic Synchronous Transit (QST) optimization to find the transition state. The transition state had a dihedral of 61° and one negative vibrational frequency associated with the amido rotation.

Synthesis of (benzyloxide)thallium(I):[56] In the dry box, a scintillation vial was loaded with benzyl alcohol (0.150 g, 1.39 mmol, 1 equiv), pentane (3 mL), and a stirbar. The solution was cooled to near frozen in a liquid nitrogen cooled cold well. The vial was moved to a stir plate, and freshly filtered TlOEt (0.349 g, 1.40 mmol, 1.01 equiv) in pentane (3 mL) was added

dropwise. The reaction was allowed to come to room temperature with stirring. After 2 h, the volatiles were removed in vacuo yielding TlOBn as a white powder (0.415 g, 1.33 mmol, 96%). ^{1}H NMR (500 MHz, C_6D_6, 25 °C): 4.92 (s, 2H, PhC*H*$_2$O), 7.06-7.09 (m, 1H, *p*-Ar-*H*), 7.19-7.21 (m, 2H, *m*-Ar-*H*), 7.23-7.25 (m, 2H, *o*-Ar-*H*). ^{13}C{^{1}H} NMR (125 MHz, C_6D_6, 25 °C): 66.58, 127.07, 127.81, 128.86, 146.53. M.p. 74-76 °C (Lit.[57] 74-78 °C).

Synthesis of 2,6-lutidenium chloride: In an oven dried 125 mL Erlenmeyer flask was loaded dry 2,6-lutidine (1.00 g, 9.33 mmol, 1 equiv.) and dry pentane (50 mL). The solution was cooled in an ice water bath. A stir bar was added to the flask, and HCl in Et_2O (10.26 mL, 1.0 M, 1.1 equiv.) was added dropwise with stirring. The bath was removed, and the mixture was allowed to come to room temperature. After 1 h the solids were collected on a glass frit and washed with pentane (3 × 10 mL). The solids were dried in vacuo yielding lutidenium chloride as an off white powder (1.27 g, 8.87 mmol, 95% yield). M.p. 237-240 °C.

Synthesis of 2,6-lutidenium bromide: In a fumehood, an oven dried 250 mL Schlenk flask with 2 side arms and one ground-glass 24/40 joint was charged with NaBr (30 g, 4.5 equiv). An inlet N_2 line (on a mercury bubbler) was connected to one of the arms. To the other side arm, Tygon tubing was attached. The other end of the Tygon tubing was connected to a glass tube. The ground glass joint was sealed with a rubber septum. The glass tube was inserted through a rubber stopper, which was placed in another 250 mL Schlenk flask. This second flask was charged with 2,6-lutidine (7.00 g, 65.3 mmol, 1 equiv.) in freshly distilled THF (60 mL) and a stir bar. The side arm of the flask containing the lutidine solution was connected via Tygon tubing to a gas trap containing a saturated NaOH aqueous solution. While vigorously stirring the lutidine solution, concentrated H_2SO_4 (5 mL, 93.8 mmol, 1.44 equiv.) was slowly added via

syringe onto the solid NaBr. After about 0.5 mL was added, the glass rod was dipped below the surface of the lutidine in THF solution. The remaining H_2SO_4 was added over a period of 10 min. After addition, the flowing N_2 was turned off, and the reaction stirred for a further 30 min during which the THF solution turned cloudy white. The suspension was then filtered on a frit and washed with pentane (3 × 20 mL). The solids were collected and dried in vacuo yielding 2,6-lutidenium bromide as a white powder (1.28 g, 6.79 mmol, 10% yield). If desired, unreacted 2,6-lutidine can be recovered from the filtrate via distillation. Exposure of the salt to air should be minimized to avoid possible hydrates. The reagent was stored in the dry box. Mp: 206-210 °C. 2,6-Lutidinium bromide can also be prepared from trimethylsilylbromide using a procedure analogous to that used for production of 2,6-lutidinium iodide.[20]

Synthesis of $NCr(NPr^i_2)_3$ ***(1)***: Under an inert N_2 atmosphere, a 250 mL Erlenmeyer flask was loaded with $Cr(NPr^i_2)_3$ (1.15 g, 3.26 mmol, 1 equiv.) and pentane (~25 mL). In a separate flask, a pentane solution (50 mL) of freshly sublimed $NCr(OBu^t)_3$ (0.931 g, 3.26 mmol, 1 equiv.) was prepared. The yellow solution of $NCr(OBu^t)_3$ was added slowly in portions over ~10 min to the rapidly stirring $Cr(NPr^i_2)_3$ solution. The solution rapidly turned beet red, and stirring was continued for 1.5 h after addition was complete. The volatiles were removed in vacuo, and acetonitrile (100 mL) was added. After stirring for 5 min, the mixture was filtered through a fritted glass funnel, and the solids were washed with acetonitrile (2 × 10 mL). The solids were transferred to a vial and dried in vacuo yielding the title compound as dark red microcrystals (1.06 g, 2.90 mmol, 89% yield). If necessary, **1** can be further purified by recrystallization from concentrated pentane solution at −35 °C. ^{1}H NMR (500 MHz, $CDCl_3$, −30 °C): 4.33 (br sept,

3H, C*H*(CH_3)$_2$), 3.42 (br sept, 3H, C*H*(CH_3)$_2$), 1.43 (br d, 14H, CH(C*H*$_3$)$_2$), 1.05 (br d, 14H, CH(C*H*$_3$)$_2$). Melting point and room temperature NMR spectroscopy were in agreement with literature values.[17a]

*Synthesis of NCr(NPr$^i_2$)$_2$(Cl) (**3**):* Under an inert atmosphere a pressure tube was loaded with **1** (0.400 g, 1.09 mmol, 1 equiv.), 2,6-lutidinium chloride (0.392 g, 2.73 mmol, 2.5 equiv.), and a stirbar. $CHCl_3$ (~35 mL) was added. The tube was sealed and removed from the drybox. The tube was set in a 60 °C oil bath, and the reaction was stirred for 12 h. The tube was taken back into the drybox, and the volatiles were removed in vacuo. The residue was extracted with pentane and filtered. The solvent was removed yielding **3** as an orange powder (0.270 g, 0.895 mmol, 82% yield). Diffraction quality crystals were obtained from a concentrated pentane solution at −35 °C. ^{1}H NMR (500 MHz, $CDCl_3$, 25 °C): 5.24 (sept, J_{HH} = 6.61, 2H, C*H*(CH_3)$_2$), 3.82 (sept, J_{HH} = 6.21, 2H, C*H*(CH_3)$_2$), 1.91 (d, J_{HH} = 6.42, 6H, CH(C*H*$_3$)$_2$), 1.49 (d, J_{HH} = 6.28, 6H, CH(C*H*$_3$)$_2$), 1.25 (d, J_{HH} = 6.33, 6H, CH(C*H*$_3$)$_2$), 1.13 (d, J_{HH} = 6.57, 6H, CH(C*H*$_3$)$_2$). ^{13}C{^{1}H} NMR (125 MHz, $CDCl_3$, 0 °C): 59.20, 57.10, 30.36, 29.92, 21.45, 19.90. Mp: 157-158 °C.

*Synthesis of NCr(NPr$^i_2$)$_2$(Br) (**4**)*: Under an inert atmosphere, a pressure tube was loaded with **1** (0.120 g, 0.328 mmol, 1 equiv.), 2,6-lutidinium bromide (0.092 g, 0.49 mmol, 1.5 equiv.), and a stirbar. $CHCl_3$ (~25 mL) was added. The tube was sealed and removed from the drybox. The tube was set in a 60 °C oil bath and stirred for 12 h. The tube was moved back into the drybox, and the volatiles were removed in vacuo. The residue was extracted with pentane and

filtered through Celite. The solvent was removed in vacuo yielding **4** as an orange powder (0.060 g, 0.17 mmol, 52% yield). Diffraction quality crystals were obtained from a concentrated pentane solution at −35 °C. ^{1}H NMR (500 MHz, $CDCl_3$, 25 °C): 5.28 (sept, J_{HH} = 6.51, 2H, C*H*$(CH_3)_2$), 3.81 (sept, J_{HH} = 6.31, 2H, C*H*$(CH_3)_2$), 1.89 (d, J_{HH} = 6.31, 6H, CH(C*H*$_3)_2$), 1.50 (d, J_{HH} = 6.26, 6H, CH(C*H*$_3)_2$), 1.28 (d, J_{HH} = 6.40, 6H, CH(C*H*$_3)_2$), 1.14 (d, J_{HH} = 6.64, 6H, CH(C*H*$_3)_2$). ^{13}C{^{1}H} NMR (125 MHz, $CDCl_3$, −5 °C): 59.34, 57.40, 30.20, 29.54, 21.29, 19.78. Mp: 160-164 °C.

*Synthesis of NCr(NPr$^{i}_2)_2$(OTf) (**5**):* Under an inert atmosphere, a scintillation vial was loaded with **1** (0.30 g, 0.82 mmol, 1 equiv.), pentane (10 mL), and a stir bar. The solution was cooled to near frozen in a liquid nitrogen cooled cold well. To the rapidly stirring solution, 1.55 M triflic acid in a DME (533 μL, 0.826 mmol, 1.01 equiv.) was added dropwise. The reaction was allowed to come to room temperature and stirred for 4 h. The volatiles were removed in vacuo, and the residue was taken up in a minimal amount of pentane (2 × 10 mL) and filtered through Celite. The filtrate was concentrated in vacuo. Cooling the pentane solution to −35 °C yielded **5** as red-orange crystals (0.238 g, 0.573 mmol, 70% yield). ^{1}H NMR (300 MHz, $CDCl_3$, 25 °C): 5.31 (sept, J_{HH} = 6.66, 2H, C*H*$(CH_3)_2$), 3.94 (sept, J_{HH} = 6.35, 2H, C*H*$(CH_3)_2$), 2.02 (d, J_{HH} = 6.35, 6H, CH(C*H*$_3)_2$), 1.48 (d, J_{HH} = 6.35, 6H, CH(C*H*$_3)_2$), 1.31 (d, J_{HH} = 6.35, 6H, CH(C*H*$_3)_2$), 1.16 (d, J_{HH} = 6.35, 6H, CH(C*H*$_3)_2$). ^{19}F NMR (564 MHz, $CDCl_3$, 25 °C): −76.65. Mp: 198 °C (sub).

*Synthesis of NCr(NPr$^{i}_{2}$)$_2$(OAd) (**6**):* Under an inert atmosphere, a pressure tube was loaded with 1-adamantanol (0.042 g, 0.27 mmol, 1 equiv.), toluene (10 mL), and a stirbar. To this solution, **1** (0.10 g, 0.27 mmol, 1 equiv.) in toluene (8 mL) was added. The pressure tube was sealed and placed in a 90 °C oil bath. The reaction stirred at this temperature for 3 d. The tube was taken back into the glove box, and the volatiles were removed in vacuo. The residue was extracted with pentane and filtered through Celite. The solution was concentrated to ~5 mL and placed in a −35 °C freezer yielding red-orange crystals of **6** (0.080 g, 0.191 mmol, 70% yield). ^{1}H NMR (500 MHz, $CDCl_3$, −40 °C): 4.75 (br sept, 2H, C*H*$(CH_3)_2$), 3.54 (br sept, 2H, C*H*$(CH_3)_2$), 2.08 (app s, 3H, Ad C*H*), 1.71 (d, J_{HH} = 2.5 Hz, 6H, Ad C*H*$_2$), 1.63 (d, J_{HH} = 5.5 Hz, 6H, CH(C*H*$_3)_2$), 1.54 (app s, 6H, Ad C*H*$_2$), 1.40 (d, J_{HH} = 5.5 Hz, 6H, CH(C*H*$_3)_2$), 1.07-1.02 (m, 12H, CH(C*H*$_3)_2$). ^{13}C{^{1}H} NMR (125 MHz, $CDCl_3$, −35 °C): 74.0, 57.4, 53.4, 47.0, 36.2, 31.0, 30.0, 29.3, 21.0, 19.5. Mp: 120-125 °C.

*Synthesis of NCr(NPr$^{i}_{2}$)$_2$(OSiPh$_3$) (**7**):* Under an inert atmosphere, a scintillation vial was loaded with **1** (0.70 g, 0.19 mmol, 1 equiv.), toluene (~5 mL), and a stirbar. A solution of $HOSiPh_3$ (0.053 g, 0.19 mmol, 1 equiv.) in toluene (5 mL) was added slowly. As the reaction stirred it gradually turned from the beet color of the starting material to orange. After 16 h, the solution was dried in vacuo. The residue was extracted with pentane and filtered through Celite. The filtrate was concentrated (~5 mL) in vacuo. The pentane solution yielded orange crystals of **7** (0.075 g, 0.14 mmol, 72% yield) at −35 °C. ^{1}H NMR (500 MHz, $CDCl_3$, 0 °C): 7.64 (d, J_{HH} = 6.34, 6H Ar-C-*H*), 7.49-7.26 (m, 9H Ar-C-*H*), 5.01 (sept, J_{HH} = 6.61, 2H, C*H*$(CH_3)_2$), 3.63

(sept, J_{HH} = 6.20, 2H, C*H*(CH_3)$_2$), 1.60 (d, J_{HH} = 6.39, 6H, CH(C*H*$_3$)$_2$), 1.39 (d, J_{HH} = 6.29, 6H, CH(C*H*$_3$)$_2$), 1.09 (d, J_{HH} = 6.53, 6H, CH(C*H*$_3$)$_2$), 1.00 (d, J_{HH} = 6.29, 6H, CH(C*H*$_3$)$_2$). ^{13}C{^{1}H} NMR (125 MHz, $CDCl_3$, 25 °C): 138.7, 135.3, 128.9, 127.2, 58.4, 55.4, 30.2, 29.5, 21.4, 20.6. Mp: 115-120 °C.

*Synthesis of NCr(NPr$^i_2$)$_2$(O$_2$CPh) (**8**):* Under an inert atmosphere a scintillation vial was loaded with **1** (0.150 g, 0.409 mmol, 1 equiv.), a stir bar, and toluene (8 mL), and placed in a liquid nitrogen cooled cold well until nearly frozen. Benzoic acid (0.050 g, 0.41 mmol, 1 equiv.) in toluene (1 mL) was added. The reaction was allowed to warm to room temperature and was stirred for 6 h. Over that time the solution changed from the beet color of the starting material to dark orange. The volatiles were removed in vacuo, and the residue was extracted with pentane (2 × 5 mL) and filtered through Celite. Concentrated solutions cooled to −35 °C yielded **8** as red-orange crystals (0.140 g, 0.360 mmol, 88% yield). ^{1}H NMR (500 MHz, $CDCl_3$, 0 °C): 8.02-8.00 (m, 2H Ar-*o*-C-*H*), 7.45-7.41 (m, 1H Ar-*p*-C-*H*), 7.37-7.34 (m, 2H Ar-*m*-C-*H*), 5.60 (sept, J_{HH} = 6.29, 2H, C*H*(CH_3)$_2$), 3.86 (sept, J_{HH} = 6.47, 2H, C*H*(CH_3)$_2$), 1.94 (d, J_{HH} = 6.31, 6H, CH(C*H*$_3$)$_2$), 1.53 (d, J_{HH} = 6.37, 6H, CH(C*H*$_3$)$_2$), 1.18 (d, J_{HH} = 6.40, 6H, CH(C*H*$_3$)$_2$), 1.13 (d, J_{HH} = 6.46, 6H, CH(C*H*$_3$)$_2$). ^{13}C NMR (125 MHz, $CDCl_3$, 0 °C): 171.5, 133.5, 131.4, 129.9, 127.9, 58.2, 57.0, 30.7, 30.1, 22.2, 21.7. Mp: 121 °C (dec).

*Synthesis of NCr(NPr$^i_2$)$_2$(O-p-(OMe)C$_6$H$_4$) (**11**):* Under an inert atmosphere, a scintillation vial was loaded with **1** (0.15 g, 0.41 mmol, 1 equiv.), toluene (5 mL), and a stirbar. The solution was frozen in a liquid nitrogen cooled cold well, then removed to a stir plate. To the

thawing solution of **1** was added a solution of HO-*p*-(OMe)C_6H_4 (0.051 g, 0.41 mmol, 1 equiv.) in toluene (5 mL) over 5 min. The reaction was stirred and was allowed come to room temperature. After 1.5 h, the orange solution was dried in vacuo. The residue was extracted with pentane and filtered through Celite. The filtrate was concentrated (~5 mL) in vacuo. Cooling concentrated pentane solutions to −35 °C yielded dark orange crystals of **11** (0.139 g, 0.356 mmol, 87% yield). ^{1}H NMR (500 MHz, $CDCl_3$, −38 °C): 6.89 (d, J_{HH} = 8.50, 2H, Ar-*m*-C-*H*), 6.71 (d, J_{HH} = 9.00, 2H, Ar-*o*-C-*H*), 4.99 (sept, J_{HH} = 6.50, 2H, C*H*$(CH_3)_2$), 3.72 (s, 3H, Ar-*p*-OC*H*$_3$), 3.71 (sept, J_{HH} = 6.50, 2H, C*H*$(CH_3)_2$), 1.82 (d, J_{HH} = 6.00, 6H, CH(C*H*$_3)_2$), 1.43 (d, J_{HH} = 6.00, 6H, CH(C*H*$_3)_2$), 1.15-1.13 (m, 12H, CH(C*H*$_3)_2$). ^{13}C NMR (125 MHz, $CDCl_3$, −35 °C): 161.3, 152.3, 117.6, 113.5, 58.0, 55.5, 54.9, 30.3, 29.9, 21.3, 21.0. Mp: 102-104 °C.

*Synthesis of NCr(NPr$^i_2$)$_2$(O-p-(SMe)C_6H_4) (**12**):* Under an inert atmosphere, a scintillation vial was loaded with **1** (0.15 g, 0.41 mmol, 1 equiv.), toluene (5 mL), and a stirbar. The solution was frozen in a liquid nitrogen cooled cold well, then removed to a stir plate. To the thawing solution was added HO-*p*-(SMe)C_6H_4 (0.057 g, 0.41 mmol, 1 equiv.) in toluene (5 mL) over 5 minutes. The reaction was stirred and allowed to come to room temperature. After 1.5 h the orange solution was dried in vacuo. The residue was extracted with pentane and filtered through Celite. The filtrate was concentrated (~5 mL) in vacuo. Cooling concentrated pentane solutions to −35 °C yielded dark orange crystals of **12** (0.153 g, 0.376 mmol, 92% yield). ^{1}H NMR (500 MHz, $CDCl_3$, −10 °C): 7.14 (d, J_{HH} = 8.64, 2H, Ar-*m*-C-*H*), 6.88 (d, J_{HH} = 8.64, 2H, Ar-*o*-C-*H*), 5.02 (sept, J_{HH} = 6.21, 2H, C*H*$(CH_3)_2$), 3.73 (sept, J_{HH} = 6.09, 2H, C*H*$(CH_3)_2$),

2.40 (s, 3H SCH_3), 1.83 (d, J_{HH} = 6.08, 6H, CH(CH_3)$_2$), 1.44 (d, J_{HH} = 6.18, 6H, CH(CH_3)$_2$), 1.14 (d, J_{HH} = 6.00, 12H, CH(CH_3)$_2$). $^{13}C\{^1H\}$ NMR (125 MHz, $CDCl_3$, −10 °C): 165.7, 130.2, 125.7, 118.2, 58.2, 55.3, 30.3, 30.0, 23.3, 21.3, 21.0, 18.6. Mp: 112-115 °C.

*Synthesis of NCr(NPr$^i_2$)$_2$(O-p-(Bu^t)C$_6$H$_4$) (**13**)*: Under an inert atmosphere, a scintillation vial was loaded with **1** (0.15 g, 0.41 mmol, 1 equiv.), toluene (5 mL), and a stirbar. The solution was frozen in a liquid nitrogen cooled cold well, then removed to a stir plate. To the thawing solution was added HO-*p*-(^{t}Bu)C$_6$H$_4$ (0.061 g, 0.41 mmol, 1 equiv.) in toluene (5 mL) over 5 min. The reaction was stirred and allowed to come to room temperature. After 1.5 h, the orange solution was dried in vacuo. The residue was extracted with pentane and filtered through Celite. The filtrate was concentrated (~5 mL) in vacuo. Cooling concentrated pentane solutions to −35 °C yielded dark orange crystals of **13** (0.16 g, 0.385 mmol, 94% yield). ^{1}H NMR (500 MHz, $CDCl_3$, −25 °C): 7.16 (d, J_{HH} = 8.62, 2H, Ar-*m*-C-*H*), 6.88 (d, J_{HH} = 8.62, 2H, Ar-*o*-C-*H*), 5.00 (sept, J_{HH} = 6.35, 2H, C*H*(CH$_3$)$_2$), 3.71 (sept, J_{HH} = 6.23, 2H, C*H*(CH$_3$)$_2$), 1.82 (d, J_{HH} = 6.18, 6H, CH(CH_3)$_2$), 1.44 (d, J_{HH} = 6.35, 6H, CH(CH_3)$_2$), 1.24 (s, 9H C(CH$_3$)$_3$), 1.13 (d, J_{HH} = 6.35, 12H, CH(CH_3)$_2$). $^{13}C\{^1H\}$ NMR (125 MHz, $CDCl_3$, −35 °C): 164.4, 141.3, 125.5, 116.5, 58.1, 58.0, 55.0, 33.9, 31.5, 30.3, 30.0, 21.2, 20.9. Mp: 188-190 °C.

*Synthesis of NCr(NPr$^i_2$)$_2$(O-p-(F)C$_6$H$_4$) (**14**):* Under an inert atmosphere, a scintillation vial was loaded with **1** (0.15 g, 0.41 mmol, 1 equiv.), toluene (5 mL), and a stirbar. The solution was frozen in a liquid nitrogen cooled cold well, then removed to a stir plate. To the thawing solution was added HO-*p*-(F)C$_6$H$_4$ (0.046 g, 0.41 mmol, 1 equiv.) in toluene (5 mL) over 5 min.

The reaction was stirred and was allowed to come to room temperature. After 1.5 h, the orange solution was dried in vacuo. The residue was extracted with pentane and filtered through Celite. The filtrate was concentrated (~5 mL) in vacuo. Cooling concentrated pentane solutions to −35 °C yielded dark orange crystals of **14** (0.136 g, 0.360 mmol, 88% yield). ^{1}H NMR (500 MHz, $CDCl_3$, −30 °C): 7.38 (d, J_{HH} = 8.63, 2H, Ar-*m*-C-*H*), 6.95 (d, J_{HH} = 8.63, 2H, Ar-*o*-C-*H*), 5.06 (sept, J_{HH} = 6.48, 2H, C*H*$(CH_3)_2$), 3.75 (sept, J_{HH} = 6.42, 2H, C*H*$(CH_3)_2$), 1.84 (d, J_{HH} = 6.35, 6H, CH(C*H*$_3)_2$), 1.45 (d, J_{HH} = 6.43, 6H, CH(C*H*$_3)_2$), 1.16-1.11 (m, 12H, CH(C*H*$_3)_2$). ^{13}C{^{1}H} NMR (125 MHz, $CDCl_3$, 0 °C): 163.2, 157.3, 117.9 (d, J_{CF} = 7.8), 114.9 (d, J_{CF} = 22.4), 58.3, 55.3, 30.3, 30.0, 21.3, 21.1. ^{19}F NMR (564 MHz, $CDCl_3$, 25 °C): –126.8. Mp: 81 °C (dec).

*Synthesis of NCr(NPr$^{i}_{2}$)$_2$(O-p-(Cl)C$_6$H$_4$) (**15**):* Under an inert atmosphere, a scintillation vial was loaded with **1** (0.15 g, 0.41 mmol, 1 equiv.), toluene (5 mL), and a stirbar. The solution was frozen in a liquid nitrogen cooled cold well, then removed to a stir plate. To the thawing solution was added HO-*p*-(Cl)C_6H_4 (0.053 g, 0.41 mmol, 1 equiv.) in toluene (5 mL) over 5 min. The reaction was stirred and was allowed to come to room temperature. After 1.5 h, the orange solution was dried in vacuo. The residue was extracted with pentane and filtered through Celite. The filtrate was concentrated (~5 mL) in vacuo. Cooling concentrated pentane solutions to −35 °C yielded dark orange crystals of **15** (0.137 g, 0.348 mmol, 85% yield). ^{1}H NMR (500 MHz, $CDCl_3$, −40 °C): 7.06 (d, J_{HH} = 8.99, 2H, Ar-*m*-C-*H*), 6.84 (d, J_{HH} = 8.76, 2H, Ar-*o*-C-*H*), 5.01 (sept, J_{HH} = 6.26, 2H, C*H*$(CH_3)_2$), 3.73 (sept, J_{HH} = 6.26, 2H, C*H*$(CH_3)_2$), 1.82 (d,

J_{HH} = 6.29, 6H, CH(CH_3)$_2$), 1.42 (d, J_{HH} = 6.04, 6H, CH(CH_3)$_2$), 1.12 (d, J_{HH} = 6.57, 6H, CH(CH_3)$_2$), 0.996 (d, J_{HH} = 6.18, 6H, CH(CH_3)$_2$). $^{13}C\{^1H\}$ NMR (125 MHz, $CDCl_3$, −20 °C): 165.3, 128.5, 123.1, 118.7, 58.3, 55.4, 44.8, 30.3, 30.1, 23.2, 21.3, 21.0. Mp: 124-125 ºC.

*Synthesis of NCr(NPr$^i_2$)$_2$(O-p-(CF$_3$)C$_6$H$_4$) (**16**):* Under an inert atmosphere, a scintillation vial was loaded with **1** (0.15 g, 0.41 mmol, 1 equiv.), toluene (5 mL), and a stirbar. The solution was frozen in a liquid nitrogen cooled cold well, then removed to a stir plate. To the thawing solution was added HO-*p*-(CF_3)C_6H_4 (0.066 g, 0.41 mmol, 1 equiv.) in toluene (5 mL) over 5 min. The reaction was stirred and was allowed to come to room temperature. After 1.5 h, the orange solution was dried in vacuo. The residue was extracted with pentane and filtered through Celite. The filtrate was concentrated (~5 mL) in vacuo. Cooling concentrated pentane solutions to −35 °C yielded dark orange crystals of **16** (0.143 g, 0.336 mmol, 82% yield). ^1H NMR (500 MHz, $CDCl_3$, 3 °C): 7.37 (d, J_{HH} = 8.58, 2H, Ar-*m*-C-*H*), 6.95 (d, J_{HH} = 8.58, 2H, Ar-*o*-C-*H*), 5.07 (sept, J_{HH} = 6.29, 2H, C*H*(CH_3)$_2$), 3.76 (sept, J_{HH} = 6.22, 2H, C*H*(CH_3)$_2$), 1.85 (d, J_{HH} = 6.04, 6H, CH(CH_3)$_2$), 1.46 (d, J_{HH} = 6.03, 6H, CH(CH_3)$_2$), 1.15 (d, J_{HH} = 3.72, 6H, CH(CH_3)$_2$), 1.02 (d J_{HH} = 6.34, 6H, CH(CH_3)$_2$). $^{13}C\{^1H\}$ NMR (125 MHz, $CDCl_3$, 3 °C): 169.1, 126.3 (quar, J_{CF} = 3.79), 117.7, 117.6, 58.5, 55.7, 30.4, 30.2, 23.3, 21.3, 21.1. ^{19}F NMR (564 MHz, $CDCl_3$, 25 °C): −64.24. Mp: 131-132 ºC. Anal. Calcd: C, 53.38; H, 7.56; N, 9.82. Found: C, 53.40; H, 7.77; N, 9.80.

*Synthesis of NCr(NPr$^{i}_{2}$)$_2$(OC$_6$F$_5$) (**17**):* Under an inert atmosphere, a scintillation vial was loaded with **1** (0.15 g, 0.41 mmol, 1 equiv.), toluene (5 mL), and a stirbar. The solution was frozen in a liquid nitrogen cooled cold well, then removed to a stir plate. To the thawing solution was added HOC_6F_5 (0.075 g, 0.41 mmol, 1 equiv.) in toluene (5 mL) over 5 minutes. The reaction was stirred and was allowed to come to room temperature. After 1.5 h, the orange solution was dried in vacuo. The residue was extracted with pentane and filtered through Celite. The filtrate was concentrated (~5 mL) in vacuo. Cooling concentrated pentane solutions to −35 °C yielded dark orange crystals of **17** (0.16 g, 0.385 mmol, 76% yield). ^{1}H NMR (500 MHz, $CDCl_3$, −20 °C): 5.12 (sept, J_{HH} = 6.50, 2H, C*H*$(CH_3)_2$), 3.81 (sept, J_{HH} = 6.50, 2H, C*H*$(CH_3)_2$), 1.87 (d, J_{HH} = 6.50, 6H, CH(C*H*$_3)_2$), 1.41 (d, J_{HH} = 6.00, 6H, CH(C*H*$_3)_2$), 1.26 (d, J_{HH} = 6.50, 6H, CH(C*H*$_3)_2$), 1.16 (d, J_{HH} = 6.00, 6H, CH(C*H*$_3)_2$). ^{13}C{^{1}H} NMR (125 MHz, $CDCl_3$, -20 ºC): 143-137, 58.7, 56.4, 30.4, 29.8, 21.6, 20.6. ^{19}F NMR (564 MHz, $CDCl_3$, 25 °C): −161.70 (dd, J_{FF} = 37.22 Hz, 13.54 Hz, 2F), −167.25 to −167.46 (m, 2F), −173.58 (tt, J_{FF} = 44.56 Hz, 13.54 Hz, 1F). Mp: 129-132 ºC.

*Synthesis of NCr(NPr$^{i}_{2}$)$_2$(OPth) (**18**)*: Under an N_2 atmosphere a scintillation vial was loaded with *N*-(hydroxy)phthalimide (HOPth, 0.081 g, 0.494 mmol, 1 equiv), $CHCl_3$ (5 mL), and a stir bar. To this slurry was added **1** (0.181 g, 0.494 mmol, 1 equiv) in $CHCl_3$ (5 mL). The solution turned orange and stirred for 16 h at room temperature. The volatiles were removed in vacuo, and the residue was extracted with toluene (3 × 5 mL). This solution was filtered through

Celite, and the filtrate was concentrated to 8 mL. Diffraction quality crystals of **18** were grown from toluene solution at −35 °C (0.110 g, 0.257 mmol, 52%). ^{1}H NMR (500 MHz, $CDCl_3$, −2 °C): 7.68-7.67 (m, 2H, Phth), 7.59-7.57 (m, 2H, Phth), 5.13 (sept, 2H, C*H*$(CH_3)_2$, J_{HH} = 6.5 Hz), 3.82 (sept, 2H, C*H*$(CH_3)_2$, J_{HH} = 6.5 Hz), 1.93 (d, 6H, CH(C*H*$_3)_2$, J_{HH} = 6.5 Hz), 1.41-1.38 (m, 12H, CH(C*H*$_3)_2$), 1.16 (d, 6H, C*H*$(CH_3)_2$, J_{HH} = 6.5 Hz). ^{13}C{^{1}H} NMR (125 MHz, $CDCl_3$, −2 °C): 20.38, 21.66, 56.10, 58.52, 122.32, 129.72, 133.30, 163.75. M.p. 179 °C (dec).

*Synthesis of NCr(NPr$^{i}_2)_2$(SPh) (**19**):* Under an inert atmosphere, a pressure tube was loaded with **1** (0.10 g, 0.27 mmol, 1 equiv.), toluene (5 mL), and a stirbar. To the stirring solution of **1** was added thiophenol (0.030 g, 0.27 mmol, 1 equiv.) in toluene (5 mL). The pressure tube was sealed, placed in a 65 °C oil bath, and stirred for 20 h. The reaction was taken back under an inert atmosphere, and the volatiles were removed in vacuo. The residue was extracted with pentane and filtered through Celite. The solution was concentrated to ~5 mL and placed in a −35 °C freezer yielding red-purple crystals of **19** (0.077 g, 0.21 mmol, 75% yield). ^{1}H NMR (500 MHz, $CDCl_3$, −4 °C): 7.62-7-60 (d, 2H, Ar-*o*-C-*H*), 7.12-7.09 (t, 2H, Ar-*m*-C-*H*), 6.99-6.96 (t, 1H Ar-*p*-C-*H*), 5.23-5.18 (sept, 2H, C*H*$(CH_3)_2$), 3.72-3.67 (sept, 2H, C*H*$(CH_3)_2$), 1.75-1.731 (d, 6H, CH(C*H*$_3)_2$), 1.49-1.47 (d, 6H, CH(C*H*$_3)_2$), 1.13-1.11 (d, 12H, CH(C*H*$_3)_2$). ^{13}C{^{1}H} NMR (125 MHz, $CDCl_3$, −4 °C): 141.95, 132.58, 127.87, 123.94, 59.00, 55.95, 30.34, 29.91, 21.96, 20.38. Mp: 118-120 ºC.

*Synthesis of NCr(NPr$^{i}_2)_2$(OBn) (**20**):* Under an inert atmosphere, a scintillation vial was loaded with **2** (0.075 g, 0.19 mmol, 1 equiv.) and hexane (10 mL). This was cooled to near

frozen in a liquid nitrogen cooled cold well. In a separate vial, TlOBn (0.065 g, 0.21 mmol, 1.1 equiv.) was slurried in THF (2 mL), and a stir bar was added. The solution of **2** was then added dropwise over 5 min to the rapidly stirring slurry. The reaction was allowed to come to room temperature and stir for 16 h, during which yellow TlI precipitated. The volatiles were removed in vacuo. The residue was extracted with pentane and filtered through Celite. The filtrate was concentrated in vacuo. Cooling a concentrated pentane solution to −35 °C yielded **20** as orange crystals (0.641 g, 0.172 mmol, 90% yield). ^{1}H NMR (500 MHz, $CDCl_3$, −45 °C): 7.55 (d, 2H, Ar-*o*-C*H*, J_{HH} = 7.0), 7.30 (app t, 2H, Ar-*m*-C*H*, J_{HH} = 7.5), 7.20 (t, 1H, Ar-*p*-C*H*, J_{HH} = 7.5), 5.47 (s, 2H, CH_2), 4.75 (sept, 2H, C*H*$(CH_3)_2$, J_{HH} = 6.0), 3.59 (sept, 2H, C*H*$(CH_3)_2$, J_{HH} = 6.0), 1.61 (d, 6H, CH(CH_3)$_2$, J_{HH} = 6.0), 1.35 (d, 6H, CH(CH_3)$_2$, J_{HH} = 6.0), 1.04 (br s, 12H, CH(CH_3)$_2$). ^{13}C{^{1}H} NMR (125 MHz, $CDCl_3$, –40 ºC): 143.9, 127.8, 127.3, 126.6, 80.3, 57.5, 54.1, 30.1, 29.4, 21.3, 20.7. Mp: 139-140 ºC. Anal. Calcd: C, 61.09; H, 9.46; N, 11.24. Found: C, 60.87; H, 9.16; N, 11.22.

*Synthesis of NCr(NPr$^{i}_2$)$_2$(NO$_3$) (**21**):* Under an inert atmosphere, a scintillation vial was loaded with $TlNO_3$ (0.203 g, 0.763 mmol, 3 equiv.), a stir bar, and THF (8 mL). To the slurry of $TlNO_3$ was added **2** (0.10 g, 0.25 mmol, 1 equiv.) in THF (5 mL). The reaction was stirred for 16 h at room temperature, after which time the volatiles were removed in vacuo. The residue was extracted with pentane (3 × 10 mL) and filtered through Celite. Removal of volatiles in vacuo yielded the title compound as a red-orange powder (0.063 g, 0.19 mmol, 75% yield). Diffraction quality crystals were obtained from a pentane at −35 °C. ^{1}H NMR (600 MHz, $CDCl_3$, 25 °C):

5.54 (sept, J_{HH} = 5.35, 2H, C*H*(CH_3)$_2$), 3.92 (sept, J_{HH} = 6.41, 2H, C*H*(CH_3)$_2$), 1.95 (d, J_{HH} = 6.21, 6H, CH(C*H*$_3$)$_2$), 1.55 (d, J_{HH} = 6.23, 6H, CH(C*H*$_3$)$_2$), 1.22 (d, J_{HH} = 6.35, 6H, CH(C*H*$_3$)$_2$), 1.13 (d, J_{HH} = 6.32, 6H, CH(C*H*$_3$)$_2$). ^{13}C{^{1}H} NMR (125 MHz, $CDCl_3$, 25 °C): 59.80, 58.12, 31.06, 30.00, 22.41, 22.03. Mp: 77 ºC (dec).

*Synthesis of NCr(NPr$^i_2$)$_2$(pyrrolyl) (**22**):* Under an inert atmosphere, a scintillation vial was loaded with **2** (0.100 g, 0.254 mmol 1 equiv.), a stir bar, and toluene (8 mL). A slurry of freshly made thallium pyrrole (0.695 g, 0.257 mmol, 1.01 equiv.) in Et_2O (5 mL) was added to the stirring solution. The reaction was allowed to stir for 20 h at room temperature, during which yellow TlI precipitated. The precipitate was removed by filatration, and the volatiles were removed in vacuo. The residue was extracted with pentane (3 × 10 mL) and concentrated in vacuo to ~5 mL. Cooling the concentrated solution to −35 °C yielded red-orange crystals of **22** (0.068 g, 0.20 mmol, 80% yield). ^{1}H NMR (500 MHz, $CDCl_3$, −10 °C): 6.94-6.81 (m, 2H, pyr-C-*H*), 6.26-6.17 (m, 2H, pyr-C-*H*), 5.10 (sept, J_{HH} = 6.09, 2H, C*H*(CH_3)$_2$), 3.77 (sept, J_{HH} = 5.52, 2H, C*H*(CH_3)$_2$), 1.83 (d, J_{HH} = 4.64, 6H, CH(C*H*$_3$)$_2$), 1.55 (d, J_{HH} = 5.03, 6H, CH(C*H*$_3$)$_2$), 1.16 (d, J_{HH} = 5.16, 6H, CH(C*H*$_3$)$_2$), 1.05 (d, J_{HH} = 4.30, 6H, CH(C*H*$_3$)$_2$). ^{13}C{^{1}H} NMR (125 MHz, $CDCl_3$, −10 °C): 129.2, 107.3, 58.0, 56.0, 30.3, 30.1, 22.0, 21.3. Mp: 125-6 ºC.

*Synthesis of NCr(NPr$^i_2$)$_2$(Pyr^{C6F5}) (**23**):* Under an inert atmosphere a scintillation vial was loaded with **2** (0.100 g, 0. 254 mmol 1 equiv.), a stir bar, and toluene (8 mL). A slurry of freshly made Tl(Pyr^{C6F5}) (0.112 g, 0.257 mmol, 1.01 equiv.) in Et_2O (5 mL) was added to the

stirring solution. The reaction was allowed to stir for 20 h at room temperature, during which yellow TlI precipitated. The precipitate was removed by filatration, and the volatiles were removed in vacuo. The residue was extracted with pentane (3 × 10 mL) and concentrated in vacuo to ~5 mL. Cooling the concentrated solution to −35 °C yielded red-orange crystals of **23** (0.080 g, 0.16 mmol, 63% yield). ^{1}H NMR (500 MHz, $CDCl_3$, 0 °C): 7.35-7.32 (m, 2H, pyr-C-*H*), 6.91-6.88 (m, 2H, pyr-C-*H*), 5.15 (sept, J_{HH} = 6.28, 2H, C*H*$(CH_3)_2$), 3.82 (sept, J_{HH} = 6.37, 2H, C*H*$(CH_3)_2$), 1.87 (d, J_{HH} = 6.07, 6H, CH(C*H*$_3)_2$), 1.57 (d, J_{HH} = 6.07, 6H, CH(C*H*$_3)_2$), 1.18 (d, J_{HH} = 6.29, 6H, CH(C*H*$_3)_2$), 1.11 (d, J_{HH} = 6.33, 6H, CH(C*H*$_3)_2$). ^{13}C{H} NMR (125 MHz, $CDCl_3$, 25 °C): 143.76 (dm, J_{CF} = 255.75 Hz), 137.90 (dm, J_{CF} = 248.5 Hz), 137.33 (dm, J_{CF} = 243.13 Hz), 130.98, 130.63, 112.47, 108.97, 58.46, 56.59, 30.37, 30.24, 22.10, 21.29. ^{19}F NMR (564 MHz, $CDCl_3$, 25 °C): −142.47 to −142.57 (m, 2F), −163.35 (t, J_{FF} = 42.86 Hz, 1F), −164.77 to −164.95 (m, 2F). Mp: 169-171 °C.

*Synthesis of NCr(NPr$^{i}_{2})_2$(Pyr$^{C6H3(CF3)2}$) (**24**):* Under an inert atmosphere, a scintillation vial was loaded with **2** (0.100 g, 0. 254 mmol 1 equiv.), a stir bar, and toluene (8 mL). A slurry of freshly made Tl(Pyr$^{C6H3(CF3)2}$) (0.124 g, 0.257 mmol, 1.01 equiv.) in Et_2O (5 mL) was added. The reaction was allowed to stir for 20 h at room temperature, during which yellow TlI precipitated. The precipitate was removed by filatration, and the volatiles were removed in vacuo. The residue was extracted with pentane (3 × 10 mL) and concentrated in vacuo to ~5 mL. Cooling the concentrated solution to −35 °C yielded red-orange crystals of **24** (0.098 g, 0.18 mmol, 71% yield). ^{1}H NMR (500 MHz, $CDCl_3$, 0 °C): 7.85 (s, 2H, Ar-*o*-C*H*), 7.49 (s, 1H, Ar-*p*-

C*H*), 7.29-7.28 (m, 1H, pyr-C*H*), 6.88-6.87 (m, 1H, pyr-C*H*), 6.52-6.52 (m, 1H, pyr-C*H*), 5.15 (sept, 2H, C*H*$(CH_3)_2$, J_{HH} = 6.0), 3.81 (sept, 2H, C*H*$(CH_3)_2$, J_{HH} =6.0), 1.86 (d, 6H, CH(C*H*$_3)_2$, J_{HH} = 6.0), 1.57 (d, 6H, CH(C*H*$_3)_2$, J_{HH} = 6.0), 1.20 (d, 6H, CH(C*H*$_3)_2$, J_{HH} = 6.0), 1.11 (d, 6H, CH(C*H*$_3)_2$, J_{HH} = 6.0). ^{13}C{H} NMR (125 MHz, $CDCl_3$, 25 °C): 138.84, 131.27 (q, J_{CF} = 32.5 Hz), 130.63, 128.45, 124.26, 123.72 (q, J_{CF} = 270.9 Hz), 121.84, 117.30 (s, br) 106.02, 58.28, 56.43, 30.37, 30.22, 21.99, 21.35. ^{19}F NMR (564 MHz, $CDCl_3$, 25 °C): −62.85 (s). Mp: 116-122 °C.

*Synthesis of NCr(NPr$^i_2)_2$(indolyl) (**25**):* Under an inert atmosphere, a scintillation vial was loaded with **10** (0.100 g, 0.278 mmol, 1 equiv.), a stir bar, and hexanes (8 mL). This was cooled to near frozen in a liquid cooled nitrogen cold well. Freshly prepared lithium indolide (0.034 g, 0.28 mmol, 1.00 equiv.), in toluene (5 mL) was added dropwise over 5 min to the thawing solution of **10**. The reaction was allowed to stir for 20 h while warming to room temperature. The volatiles were removed in vacuo. The residue was extracted with pentane (3 × 10 mL) and filtered through Celite. The filtrate was concentrated to ~5 mL and cooled to −35 °C, which provided crystals of **25**. The crystals were redissolved in cold pentane and filtered to remove remaining lithium salts. Recrystalization at –35 °C from pentane yielded pure **25** as purple crystals (0.045 g, 0.12 mmol, 42% yield). ^{1}H NMR (500 MHz, $CDCl_3$, -21 ºC) 8.06 (d, J_{HH} = 8.5, 1H, *H*-7 ind), 7.55 (d, J_{HH} = 8, 1H, *H*-4 ind), 7.37 (d, J_{HH} = 3, 1H, *H*-2 ind), 7.15 (t, J_{HH} = 6.8, 1H, *H*-5 ind), 7.03 (t, J_{HH} = 6.8, 1H, *H*-6 ind), 6.54 (d, J_{HH} = 3, 1H, *H*-3 ind), 5.18 (sept, J_{HH} = 6.50, 2H, C*H*$(CH_3)_2$), 3.74 (sept, J_{HH} = 6.50, 2H, C*H*$(CH_3)_2$), 1.73 (d, J_{HH} = 6.50,

6H, CH(CH_3)$_2$), 1.59 (d, J_{HH} = 6.50, 6H, CH(CH_3)$_2$), 1.19 (d, J_{HH} = 6.50, 6H, CH(CH_3)$_2$), 0.97 (d, J_{HH} = 6.50, 6H, CH(CH_3)$_2$). ^{13}C{^{1}H} NMR (125 MHz, $CDCl_3$, –21 ºC): 144.5, 133.4, 128.8, 120.6, 119.1, 118.7, 115.9, 102.3, 58.1, 55.8, 30.6. Mp: 194-196 °C.

*Synthesis of NCr(NPr$^i_2$)$_2$(carbazolyl) (**26**):* Under an inert atmosphere a pressure tube was loaded with **10** (0.150 g, 0.417 mmol 1 equiv.), a stir bar, and hexanes (8 mL). Freshly prepared lithium carbazolide (0.072 g, 0.42 mmol, 1.00 equiv.) in toluene (5 mL) was added to the solution of **10**. The vessel was sealed, removed from the box, and stirred in a 45 °C oil bath for 16 h. The pressure tube was taken back into the dry box, and the volatiles were removed under reduced pressure. The residue was extracted with pentane, and filtered through Celite. The filtrate was concentrated to ~5 mL and cooled to −35 °C, which provided crystals of **26**. The crystals were redissolved in cold pentane and filtered to remove remaining lithium salts. Recrystalization at –35 °C from pentane yielded pure **26** (0.063 g, 0.146 mmol, 35% yield). ^{1}H NMR (500 MHz, $CDCl_3$, −20 °C): 8.02 (d, J_{HH} = 7.58, 2H), 7.97 (d, J_{HH} = 8.33, 2H), 7.40 (d, J_{HH} = 7.71, 2H), 7.17 (d, J_{HH} = 7.28, 2H), 5.30 (sept, J_{HH} = 6.18, 2H, CH(CH$_3$)$_2$), 3.79 (sept, J_{HH} = 6.21, 2H, CH(CH$_3$)$_2$), 1.69 (d, J_{HH} = 6.07, 6H, CH(CH_3)$_2$), 1.62 (d, J_{HH} = 6.21, 6H, CH(CH_3)$_2$), 1.21 (d, J_{HH} = 6.08, 6H, CH(CH_3)$_2$), 0.96 (d, J_{HH} = 6.29, 6H, CH(CH_3)$_2$). ^{13}C{^{1}H} NMR (125 MHz, $CDCl_3$, −20 °C): 149.28, 125.02, 124.78, 119.15, 118.76, 114.96, 58.09, 55.81, 31.00, 29.47, 22.69, 22.26. Mp: 158-160 ºC.

*Synthesis of NCr(NPr$^i_2$)$_2$[N(Ph)Me] (**27**):* Under an inert atmosphere, a scintillation vial was loaded with **10** (0.150 g, 0.417 mmol 1 equiv.), a stir bar, and hexanes (8 mL). This was

cooled to near frozen in a liquid nitrogen cooled cold well. Freshly prepared lithium *N*-methyl anilide (0.047 g, 0.42 mmol, 1.00 equiv.) in toluene (5 mL) was added dropwise over 5 min. The reaction was allowed to stir for 20 h with warming to room temperature. The volatiles were removed in vacuo. The residue was extracted with pentane and filtered through Celite. The filtrate was concentrated to ~5 mL and cooled to −35 °C, which provided crystals of **27**. The crystals were recrystallized from cold pentane to obtain dark purple crystals of pure **27** (0.068 g, 0.184 mmol, 44% yield). ^{1}H NMR (500 MHz, $CDCl_3$, –10 ˚C): 7.45-7.33 (m, 2H, Ar-C-*H*), 7.32-7.24 (m, 3H, Ar-C-*H*), 5.10 (sept, J_{HH} = 6.09, 2H, C*H*$(CH_3)_2$), 3.77 (sept, J_{HH} = 5.52, 2H, C*H*$(CH_3)_2$, 1.83 (d, J_{HH} = 4.64, 6H, CH(C*H*$_3)_2$), 1.55 (d, J_{HH} = 5.03, 6H, CH(C*H*$_3)_2$), 1.16 (d, J_{HH} = 5.16, 6H, CH(C*H*$_3)_2$), 1.05 (d, J_{HH} = 4.30, 6H, CH(C*H*$_3)_2$). ^{13}C NMR (125 MHz, $CDCl_3$, −55 °C): 158.56, 127.95, 118.76, 115.46, 57.49, 53.21, 41.69, 29.99, 29.32, 22.02, 21.25. Mp: 194-6 °C.

*Synthesis of NCr(NPr$^{i}_{2})_2$(NCO) (**28**):* Under an inert atmosphere a pressure tube was loaded with sodium cyanate (0.083 g, 1.271 mmol, 5 equiv), 1,4-dioxane (8 mL), and a stir bar. To the stirring cyanate solution was added **2** (0.100 g, 0.254 mmol, 1 equiv), in acetonitrile (~8 mL). The pressure tube was sealed and placed in a 45 °C oil bath and stirred for 20 h. The tube was returned to the dry box, and the volatiles were removed in vacuo. The residue was extracted with pentane and filtered through Celite. The solution was concentrated to ~5 mL and placed in a −35 °C freezer, which yielded light orange needles of **28** (0.047 g, 0.153 mmol, 60% yield). ^{1}H NMR (500 MHz, $CDCl_3$, 25 °C): 5.04 (sept, J_{HH} = 6.34, 2H, C*H*$(CH_3)_2$), 3.81 (sept, J_{HH} = 6.28, 2H, C*H*$(CH_3)_2$), 1.90 (d, J_{HH} = 6.36, 6H, CH(C*H*$_3)_2$), 1.47 (d J_{HH} = 6.29, 6H,

$CH(CH_3)_2$), 1.23 (d, J_{HH} = 6.34, 6H, $CH(CH_3)_2$), 1.10 (d, J_{HH} = 6.50, 6H, $CH(CH_3)_2$). ^{13}C NMR (125 MHz, $CDCl_3$, 25 °C): 149.7, 58.8, 57.1, 30.549, 30.2, 21.5, 21.3. Mp: 115 □C (dec).

*Synthesis of NCr(NPr$^i_2$)$_2$(NCS) (**29**):* Under an inert atmosphere, a scintillation vial was loaded with **2** (0.100 g, 0.254 mmol, 1 equiv.), toluene (5 mL), and a stirbar. To this solution, sodium thiocyanate (0.062 g, 0.763 mmol, 3 equiv.) in acetonitrile (10 mL) was added. The reaction stirred at room temperature for 3 d. The volatiles were removed in vacuo. The residue was extracted with pentane, and filtered through Celite. Cooling concentrated pentane solutions of the crude product to −35 °C yielded yellow-orange needles of **29** (0.043 g, 0.132 mmol, 52% yield). ^1H NMR (500 MHz, $CDCl_3$, −13 °C): 5.10 (sept, J_{HH} = 6.31, 2H, $CH(CH_3)_2$), 3.86 (sept, J_{HH} = 6.40, 2H, $CH(CH_3)_2$), 1.92 (d, J_{HH} = 6.23, 6H, $CH(CH_3)_2$), 1.45 (d, J_{HH} = 6.23, 6H, $CH(CH_3)_2$), 1.28 (d, J_{HH} = 6.23, 6H, $CH(CH_3)_2$), 1.11 (d, J_{HH} = 6.29, 6H, $CH(CH_3)_2$). $^{13}C\{^1H\}$ NMR (125 MHz, $CDCl_3$, −13 °C): 189.8, 59.3, 57.9, 30.7, 30.4, 22.0, 21.6. Mp: 138-142 °C.

*Synthesis of NCr(NPr$^i_2$)$_2$(CN) (**30**):* Under an inert atmosphere, a scintillation vial was loaded with sodium cyanide (10.6 mg, 0.216 mmol, 1 equiv.) in acetonitrile (~10 mL), freshly dried 15-crown-5 (47.6 mg, 0.216 mmol, 1 equiv.), and a stir bar. After stirring for 5 min, **2** (0.085 g, 0.216 mmol, 1 equiv.) in acetonitrile (5 mL) was added. The reaction stirred at room temperature for 6 h. The volatiles were removed in vacuo, and the residue was extracted with pentane and filtered through Celite. Cooling concentrated pentane solutions of the crude product to −35 °C yielded orange crystals of **30** (28.7 mg, 0.093 mmol, 43% yield). ^1H NMR (500 MHz,

$CDCl_3$, −6 °C): 5.13 (sept, J_{HH} = 6.29, 2H, C*H*$(CH_3)_2$), 3.88 (sept, J_{HH} = 6.04, 2H, C*H*$(CH_3)_2$), 1.89 (d, J_{HH} = 5.63, 6H, CH(C*H*$_3)_2$), 1.54 (d, J_{HH} = 5.63, 6H, CH(C*H*$_3)_2$), 1.36 (d, J_{HH} = 5.84, 6H, CH(C*H*$_3)_2$), 1.13 (d, J_{HH} = 5.84, 6H, CH(C*H*$_3)_2$). ^{13}C NMR (125 MHz, $CDCl_3$, −6 °C): 143.9, 58.5, 57.9, 57.7, 31.1, 31.0, 30.7, 30.5, 23.1, 22.6, 22.4, 21.9. IR: C–N stretch appears at 2172 cm^{-1}. M.p.: 180 °C (dec).

*Synthesis of NCr(NPr$^i_2)_2$(NMe$_2$) (**31**):* Under an inert atmosphere, a vial was loaded with $ZnCl_2$ (0.293 g, 2.15 mmol, 4.23 equiv), a stirbar, and THF (15 mL). This was cooled in a liquid cooled nitrogen cold well for 10 min. The vial was moved to a stir plate, and a chilled solution of $LiNMe_2$ (0.220 g, 4.31 mmol, 8.47 equiv) in THF (4 mL) and DME (4 mL) was added dropwise. The reaction stirred for 1 h and was allowed to come to room temperature, during which the mixture turned cloudy white. To this suspension was added a solution of **2** (0.200 g, 0.509 mmol, 1 equiv) in THF (2 mL) dropwise. The reaction stirred at room temperature for 4 h and turned bright red. The volatiles were removed in vacuo. The residue was extracted with pentane and filtered through Celite. The pentane was removed in vacuo. The complex was recrystallized from a minimum of acetonitrile (~4 mL) and red crystals of **31** were isolated (0.110 g, 0.354 mmol, 70%). ^{1}H NMR (500 MHz, $CDCl_3$, 25 °C): 3.89 (sept, J_{HH} = 6.43, 4H, C*H*$(CH_3)_2$), 3.55 (s, 3H, N(C*H*$_3)_2$), 1.31 (d, J_{HH} = 6.27, 12H, CH(C*H*$_3)_2$), 1.23 (d, J_{HH} = 6.34, 12H, CH(C*H*$_3)_2$). ^{13}C{^{1}H} NMR (125 MHz, $CDCl_3$, 25 °C): 54.5, 53.7, 26.4, 25.1. Mp: 52-57 °C.

*Synthesis of NCr(NPr$^i_2)_2$(F) (**33**):* Under an N_2 atmosphere a scintillation vial was loaded with **2** (0.177 g, 0.450 mmol, 1 equiv), 4-dimethylaminopyridine (0.055 g, 0.450 mmol, 1

equiv), and a stir bar. To this vial, $CHCl_3$ (8 mL) was added, and the solution was stirred for 10 min. A solution of $AgBF_4$ (0.096 g, 0.495 mmol, 1.1 equiv) in acetonitrile (4 mL) was added over 5 min. The reaction stirred at room temperature for 1 h. The brown suspension was filtered through a glass frit with Celite as a filtering agent. The filtrate was dried in vacuo and washed with pentane (2 mL). The residue was extracted with $CHCl_3$ (2 × 5 mL). These extracts were filtered through Celite and dried under vacuum yielding $[NCr(NPr^i_2)_2(DMAP)]BF_4$ (**32**) (0.124 g, 0.261 mmol, 58%). This was used without further purification in the synthesis of **33**. ^{1}H NMR (500 MHz, $CDCl_3$, 0 °C): 8.21 (d, 2H, Ar-*H*, J_{HH} = 7.0 Hz), 6.68 (d, 2H, Ar-*H*, J_{HH} = 6.5 Hz), 5.50 (sept, 2H, C*H*$(CH_3)_2$, J_{HH} = 6.0 Hz), 3.93 (sept, 2H, C*H*$(CH_3)_2$, J_{HH} = 6.0 Hz), 3.12 (s, 6H, N(C*H*$_3)_2$) 1.86 (d, 6H, CH(C*H*$_3)_2$, J_{HH} = 6.5 Hz), 1.55 (d, 6H, C*H*$(CH_3)_2$, J_{HH} = 6.5 Hz), 1.23 (d, 6H, C*H*$(CH_3)_2$, J_{HH} = 6.5 Hz), 1.15 (d, 6H, C*H*$(CH_3)_2$, J_{HH} = 6.5 Hz). ^{19}F NMR (564 MHz, $CDCl_3$, 25 °C): –151.9 ppm. Under an N_2 atmosphere, a scintillation vial was loaded with $FSnBu^n_3$ (3.38 mg, 0.011 mmol, 10 mol%), THF (1 mL), and a stir bar. A solution of $[NCr(NPr^i_2)_2(DMAP)]BF_4$ (0.052 g, 0.109 mmol, 1 equiv.) from the previous step in THF (8 mL) was added. The reaction stirred for 4 h at room temperature. The volatiles were removed in vacuo, and the residue was extracted with pentane (2 × 5 mL) and filtered through Celite. The pentane solution was concentrated to ~5 mL under vacuum, and held at −35° C yielding **33** as red-orange crystals (0.015 g, 0.054 mmol, 49%). ^{1}H NMR (500 MHz, $CDCl_3$, 25 °C): 5.08 (sept, 2H, C*H*$(CH_3)_2$, J_{HH} = 6.5 Hz), 3.81 (sept, 2H, C*H*$(CH_3)_2$, J_{HH} = 6.0 Hz), 1.94 (d, 6H,

CH(CH_3)$_2$, J_{HH} = 6.5 Hz), 1.44 (d, 6H, CH(CH$_3$)$_2$, J_{HH} = 6.5 Hz), 1.23 (d, 6H, CH(CH$_3$)$_2$, J_{HH} = 6.0 Hz), 1.12 (d, 6H, CH(CH$_3$)$_2$, J_{HH} = 6.5 Hz). ^{13}C{^{1}H} NMR (125 MHz, $CDCl_3$, 25 °C): 21.21, 21.45, 30.15, 30.22, 56.63, 58.65. ^{19}F NMR (564 MHz, $CDCl_3$, 25 °C): −145.24. M.p. 100-102 °C.

B.2 The Effect of $\Delta S^{\ddagger}$ Choice on LDP Values

For this project we sought to put the LDP values in the form of enthalpies. In order to accomplish this, it was necessary to measure the entropy for some of the compounds using variable temperature SST in conjunction with the Eyring equation. The entropy is the intercept in such plots, and the extrapolation must often be done over a large temperature range making the uncertainty in the entropy large. Experimental entropy values were obtained for X = NPr^{i}_{2} **1** (in two solvents), OBn **20**, O-*p*-(SMe)C_6H_4 **12**, and I **2**. Most of the values are fairly small and negative, varying from –1 to –16.

The entropy for CN **30** was obtained as the large and negative value of $\Delta S^{\ddagger}$ = –16 ± 10 cal/mol•K, but the fit had a large error.

The entropy for OAd **6** was also measured experimentally, but the temperature range accessible was very small at 10 K. The value was –10 cal/mol•K, but a number determined from such a small temperature range should be considered dubious. Even the error is misleadingly small because it is a linear fit to only 3 points. LSA was also done on **6**, which gave a $\Delta G^{\ddagger}$ = 12.8 ± 1.3 kcal/mol and was very comparable to the SST value of 12.90 kcal/mol. The entropy from the LSA was –1 ±4 cal/mol•K

The most accurate experimental determination (outside of the sterically very large NPr^{i}_{2} **1** system) of the entropy was for I **2**, which was done over the largest temperature range of 47 K. The value found was $\Delta S^{\ddagger}$ = –9 ± 5 cal/mol•K, where the error was simply taken from the fit. We chose to use the Iodo value of –9 cal/mol•K as the standard entropy because it was near the

middle of the experimentally determined values, had a relatively small error for the fit, was a relatively small system unlikely to have steric effects, and the value was determined over the largest temperature range.

X =	$\Delta G^{\ddagger}$ from SST	Ave. Temp. (K)	$\Delta H^{\ddagger}$ ($\Delta S^{\ddagger} = -9$)[b]	$\Delta S^{\ddagger}_{rot}$[c] (cal/mol•K)
NMe_2 (**31**)	--	--	9.34 ± 0.32[a]	–4 ± 1[a]
OAd (**6**)	12.90±0.96	224.1	10.83 ± 0.24	–10 ± 1 (–1 ± 4)[a]
N(Me)Ph (**27**)	12.82±0.86	237.4	10.86 ± 0.23	
NPr^{i}_2 (**1**)	13.30±0.78	233.9	11.12 ± 0.23[d]	–5 ± 2 (–2 ± 3)[d]
OBn (**20**)	13.07±0.89	231.4	11.15 ± 0.23	–6 ± 5
Carbazolyl (**26**)	14.23±0.79	248.0	12.04 ± 0.25	
O-*p*-(OMe)C_6H_4 (**11**)	14.07±0.85	235.7	12.14 ± 0.24	
O-*p*-(Bu^{t})C_6H_4 (**13**)	14.24±0.88	247.1	12.18 ± 0.25	
OPh (**10**)	14.43±0.63	254.3	12.38 ± 0.25	
O-*p*-(SMe)C_6H_4 (**12**)	14.69±0.68	262.7	12.51 ± 0.26	–3 ± 4
O-*p*-(F)C_6H_4 (**14**)	14.41±0.84	232.1	12.64 ± 0.23	
O-*p*-(Cl)C_6H_4 (**15**)	14.59±0.83	233.9	12.81 ± 0.23	
O-*p*-(CF_3)C_6H_4 (**16**)	15.43±0.72	275.8	13.00 ± 0.28	
$OSiPh_3$ (**7**)	15.78±0.47	274.6	13.28 ± 0.27	
OPht (**18**)	15.76±0.56	274.3	13.35 ± 0.23	
F (**33**)	15.73±0.75	254.3	13.39 ± 0.27	
Indolyl (**25**)	15.82±0.68	274.4	13.40 ± 0.25	
OBu^{t}_{F6} (**9**)	16.19±0.51	256.9	13.89 ± 0.26	
NO_3 (**21**)	16.82±0.76	276.3	14.15 ± 0.29	
Pyr (**22**)	16.44±0.63	274.7	14.16 ± 0.28	
SPh (**19**)	16.56±0.56	270.2	14.22 ± 0.27	
OC_6F_5 (**17**)	16.76±0.55	286.8	14.32 ± 0.28	
Pyr^{C6F5} (**23**)	16.57±0.66	274.8	14.33 ± 0.28	
$Pyr^{C6H3(CF3)2}$ (**24**)	16.56±0.51	272.6	14.36 ± 0.28	
CN (**30**)	16.81±0.60	265.2	14.40 ± 0.27	–16 ± 10
O_2CPh (**8**)	16.99±0.78	279.8	14.45 ± 0.28	
NCO (**28**)	16.53±0.55	286.7	14.51 ± 0.29	
NCS (**29**)	17.79±0.31	292.3	14.86 ± 0.30	
Cl (**3**)	17.56±0.43	300.8	15.05 ± 0.29	
Br (**4**)	18.36±0.49	285.8	15.45 ± 0.30	
OTf (**5**)	18.15±0.31	301.5	15.75 ± 0.29	
I (**2**)	18.62±0.36	301.1	15.80 ± 0.30	–9 ± 5

Table B.1: Thermodynamic parameters determined for compounds **1-31**

[a]Values from LSA. [b]Enthalpy of activation for the amido rotation at that entropy value in kcal/mol. [c]Values in $CDCl_3$. [d]Value in d_8-toluene.

Above are the values from the SST fits for $\Delta G^{\ddagger}$ and the average temperatures at which the experiments were done. All the free energies are from at least three measurements. More details for how the SST experiments were carried out and how the error analysis was done are found later in the SI.

Naturally, the $\Delta H^{\ddagger}$ values shift in magnitude with the $\Delta S^{\ddagger}$ value chosen. However, the correlations with other systems, the most important aspect, do not change significantly with reasonable changes in $\Delta S^{\ddagger}$ value. The fits for the correlations in this paper are shown in the table below. Some of the R-factors for the linear fits are marginally better with $\Delta S^{\ddagger}$ = –9 cal/mol•K, the value in the paper, and some are better with $\Delta S^{\ddagger}$ = –3. The differences in the fits are quite small, however.

Correlation	**R-factor ($\Delta H^{\ddagger}$ with $\Delta S^{\ddagger}$ = –9)**	**R-factor ($\Delta H^{\ddagger}$ with $\Delta S^{\ddagger}$ = –3)**
AOM ($e\sigma$+$e\pi$)	0.991	0.988
Andersen data	0.987	0.989
Mach data	0.995	0.994
Hammett σ_p	0.969	0.993
W metallacycle ^{13}C NMR	0.996	0.998

Table B.2: R-factors of the fits of the literature data with LDP using different $\Delta S^{\ddagger}$ terms.

B.3 Steric Evaluation of Monodentate Ligands

In seeking to quantify the steric profile of each member in such a diverse set of ligands two independent methods were employed. Each method treated steric bulk differently, but gave a single parameter output as a percent. Although quantifying a 3-dimensional object in one parameter is often an incomplete description, some useful information can be extracted, especially in the case of ligands of largely different shape, where a qualitative comparison might not be intuitive.

$\%V_{bur}$ Volume Calculation

The system developed by Nolan and coworkers was chosen.[58] This methodology evaluates each ligand in isolation from the other ligands in the coordination sphere. Since the atomic positions of the ligand are taken directly from the crystal structure, ligand−ligand interactions in our system are in some ways accounted for, in that distortions in the ligand of interest as a consequence of steric crowding from the others will be reflected in the X-ray data. Likewise, metal−donor atom bond lengthening due to steric congestion close to a metal center will be accounted for, as this bond length is a major component in the calculation.

Although the system nicely describes a single ligand in its coordination environment, the incorporation of other ligands by using multiple $\%V_{bur}$ calculations is less instructive. In the instance of the tris(diisopropylamido) **1**, each of the three amides are calculated to occupy 29.1% of a 3.5 Å sphere. When added to the nitride volume of 13.76% calculated by equation 1 (*vida infra*), the total suggests that the ligand set occupies over 100% of the coordination sphere.

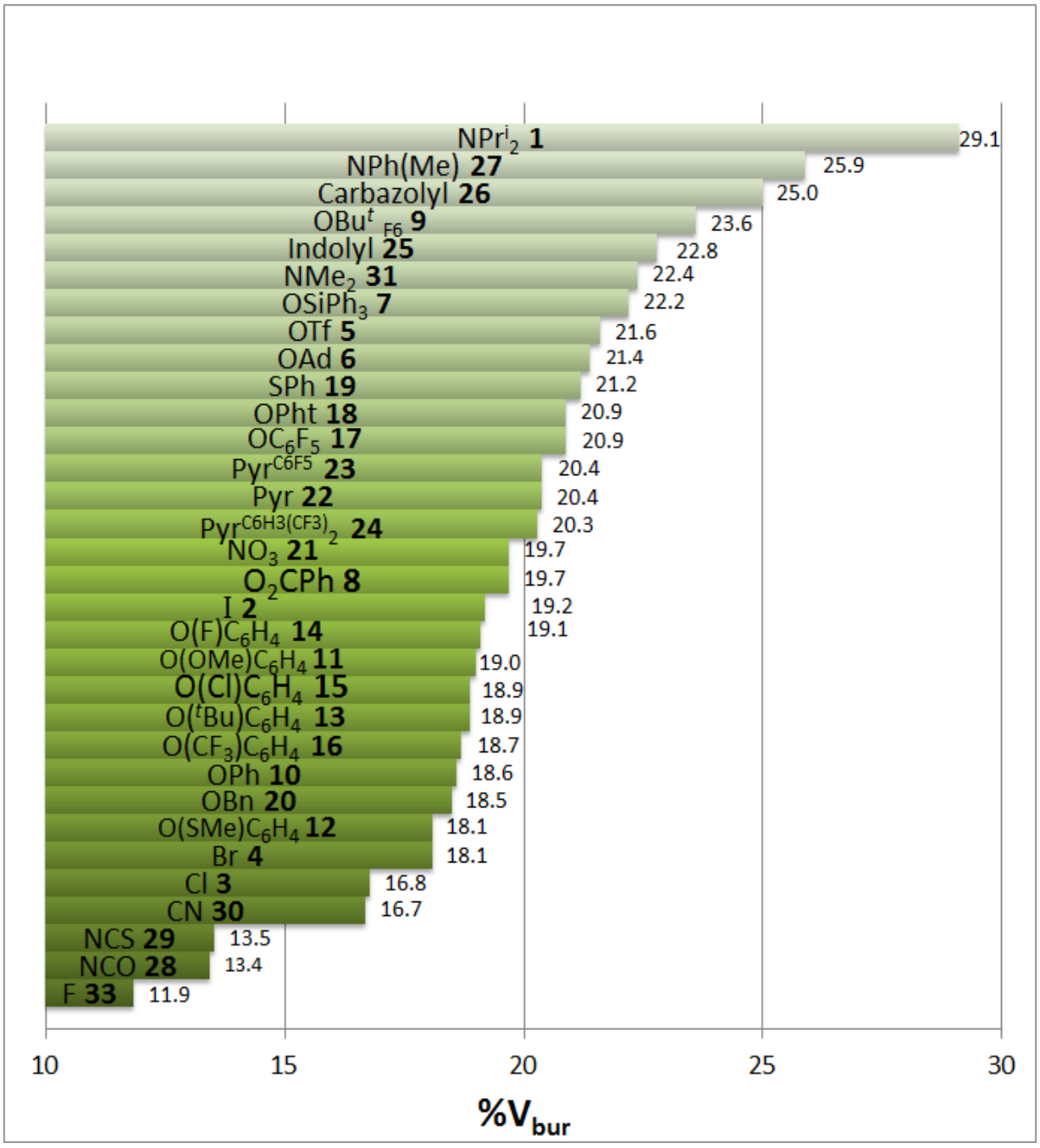

Figure B.1. %V_{bur} calculated for each ligand in **1**-**31**, and **33** in a 3.5 Å sphere.

It would be of use to identify any system specific trends in our data if parameters from our series are to be applied to other systems. One such variable may be the difference in the size of the first coordination sphere of chromium(VI) upon moving to another formal oxidation state or metal. To investigate this we looked at $\%V_{bur}$ as a function of the defined coordination sphere size for a selection of ligands.

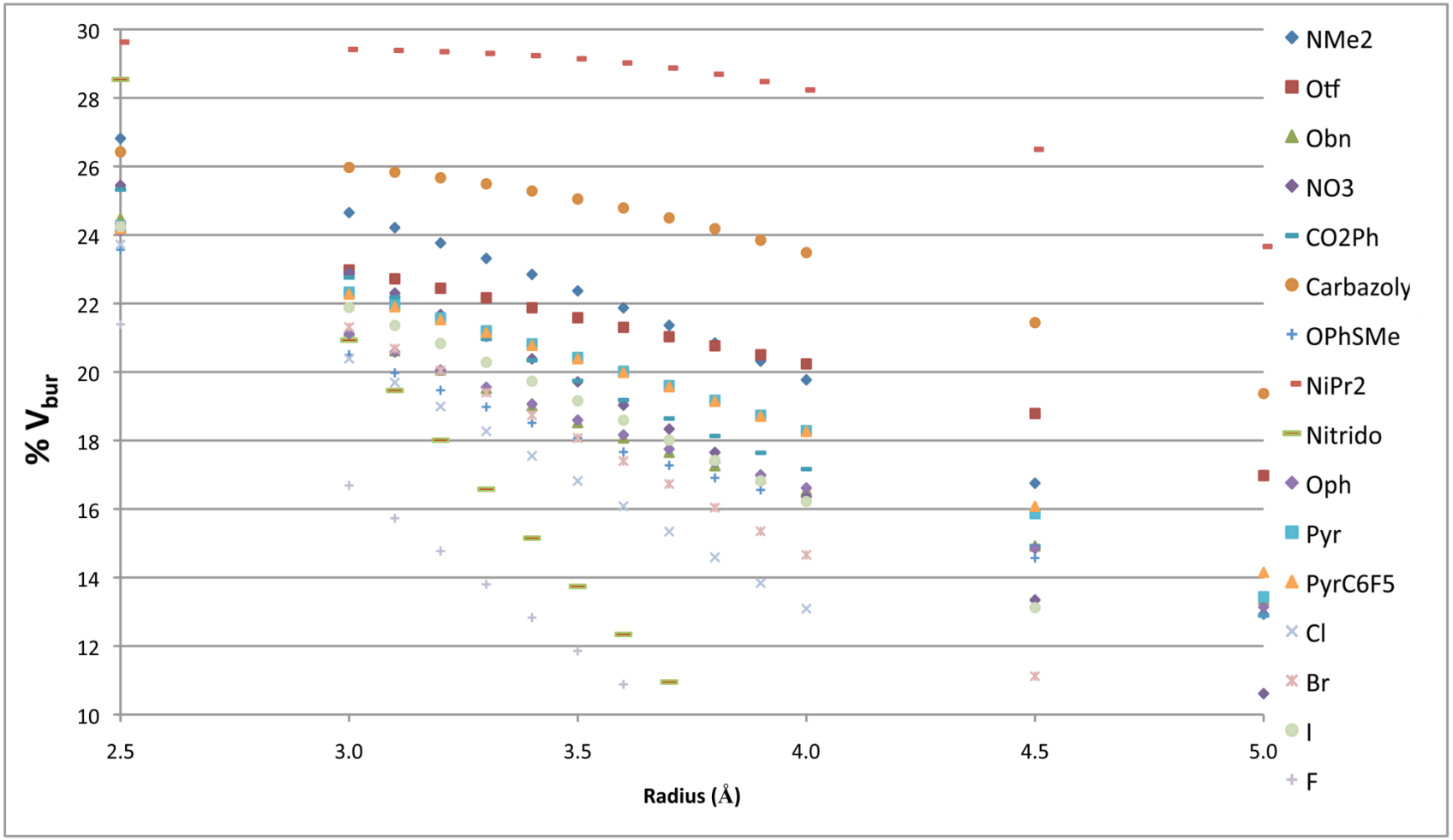

Figure B.2. $\%V_{bur}$ calculated for select ligands as a function of coordination sphere size.

Above is a plot of $\%V_{bur}$ versus the radius used in the SambVca program for 16 of the ligands used in this study. The plot in the article has the radius set to 3.5 Å, the default setting in the web application. All of the ligands evaluated certainly show significant changes in $\%V_{bur}$ with radius. In our system, many of the orderings do not change with distance but some do, e.g., OTf and NMe_2. This suggests that judicious choice of the defined coordination sphere size may be necessary if one is to extract meaningful parameters on a system by system basis.

One trend evident in the $\%V_{bur}$ is that this system assigns a smaller steric parameter than one might expect to ligands where the bulk is significantly far from the coordinated metal. Surprisingly, this regime determined $OSiPh_3$ to be the same size or a slightly *smaller* ligand than NMe_2 at 22.2% and 22.4%, respectively. The effect of coordination sphere size and the distance from the steric bulk to the coordinated metal are nicely illustrated in compounds **8** and **21**, determined to have the same $\%V_{bur}$ of 19.7%.

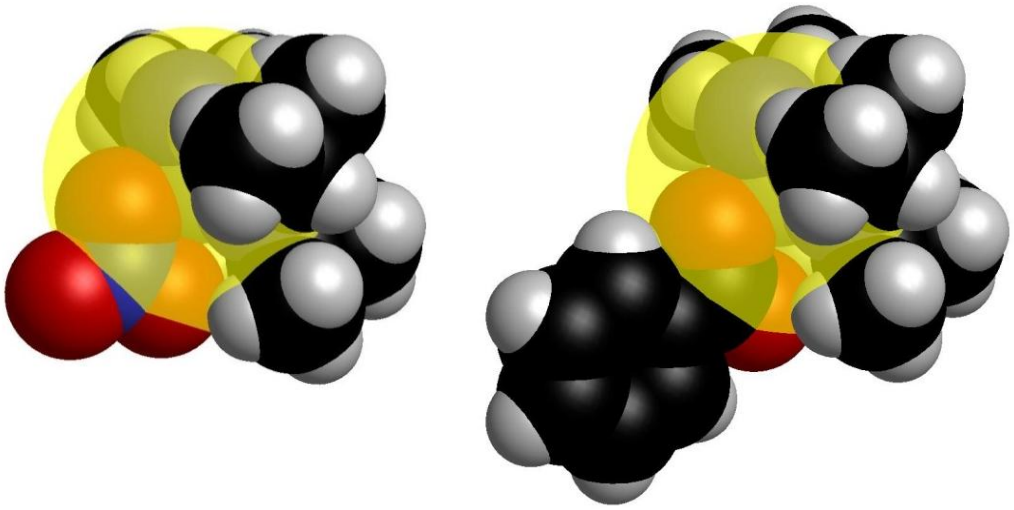

Figure B.3. Space-filling models of **8** and **21** with a coordination sphere (yellow) with a radius of 3.5 Å

Although NO_3 and O_2CPh ostensibly are different sizes, in terms of the occupation of a 3.5 Å coordination sphere they look identical to the metal center.

$\%V_{bur}$ Volume Calculation Procedure

General procedure: To assess the ligand sterics, the $\%V_{bur}$ was calculated using the SambVca web-based application.[59] Prior to upload all atoms not in the ligand of interest were removed from the .cif file. The default coordination sphere of 3.5 Å was used as well as the default mesh size of 0.050 Å. Hydrogen atoms were included in each volume calculation. For each compound the crystallographically determined Cr–X bond distance was input to define the distance of the coordinating atom to the center of the sphere. The volume for each input atom was defined by the Bondi radius scaled by a factor of 1.17 Å.

Amides and Heterocycles: For compounds **1**, **21-26**, and **30** the coordinating atom was input to define the distance to the center of the sphere as above. To define the Cr–X bond axis the atoms α to the X atom were used.

Phenoxides, Alkyoxides, and Triflate: For compounds **5-20** the crystallographic positions were imported into a Gaussview3. The ligand was rotated along the Cr–X bond axis 180° from the observed N≡Cr-X-Y torsion angle (where X is the coordinating atom and Y is any atom α to it). A new set of atom coordinates was generated from this, and the new position of Y, Y′ was manually input into the original list of positions. This new list was opened in Mercury and saved as an .xyz file, allowing it to be further altered so that the new atom Y′ position was defined as 'X', an atom with zero volume (i.e. a point in space equidistant from the coordinating atom as the α atom, but rotated 180°). In addition, all other atoms not included in the ligand of interest were removed from the file. This was then uploaded to the SambVca application and the positions of Y and Y′ were used to define the Cr–X bond axis. By defining Y′ as an 'X' atom no additional volume was introduced into the ligand.

Halides and Pseudohalides: For the $\%V_{bur}$ of compounds **2-4**, **27-29** and **33** SambVca was not used since the application did not define all the atom types required, or the evaluation of single atom ligands was problematic. For these calculations a formula for the calculation of the volume of two intersecting spheres (Equation 1) was used

$$Vol = \frac{\pi(R+(r-d^2))(d^2+2dr-3r^3+2dR+6rR-3R^3)}{12d} \qquad \textbf{Equation 1}$$

where R is the radius of the coordination sphere (3.5 Å), r is the Bondi radius scaled by 1.17 of the coordinating atom, and d is the crystallographically determined Cr–X bond distance, giving the volume occupied in the intersection of two spheres. This volume was then divided by the

volume of a complete sphere with radius 3.5 Å to give the $\%V_{bur}$. For pseudohalides, only the volume of coordinating atom was taken into account, as the rest of the ligand falls outside of the 3.5 Å sphere of enclosure. Calculation on the chloride **3** using this method agreed with the SambVca application, which defines the Cl radius.

Steric Evaluation using Solid G

In addition to the $\%V_{bur}$ calculations, where each ligand is treated individually, another independent steric parameter was used. The Solid-G program was selected as it evaluates the sterics of the entire ligand set using solid angles.[60] For each compound, the crystallographically determined atom positions were imported as an .xyz file. For compounds **6**, **9**, **13**, **16**, and **31** with disordered structures, the conformations that had the highest refined occupancies were selected for evaluation. Table 4 of the output file gave G(L), the percentage of the sphere shielded by each ligand, in addition to the solid angle Omega(L) in Steradians, and the equivalent cone angle.

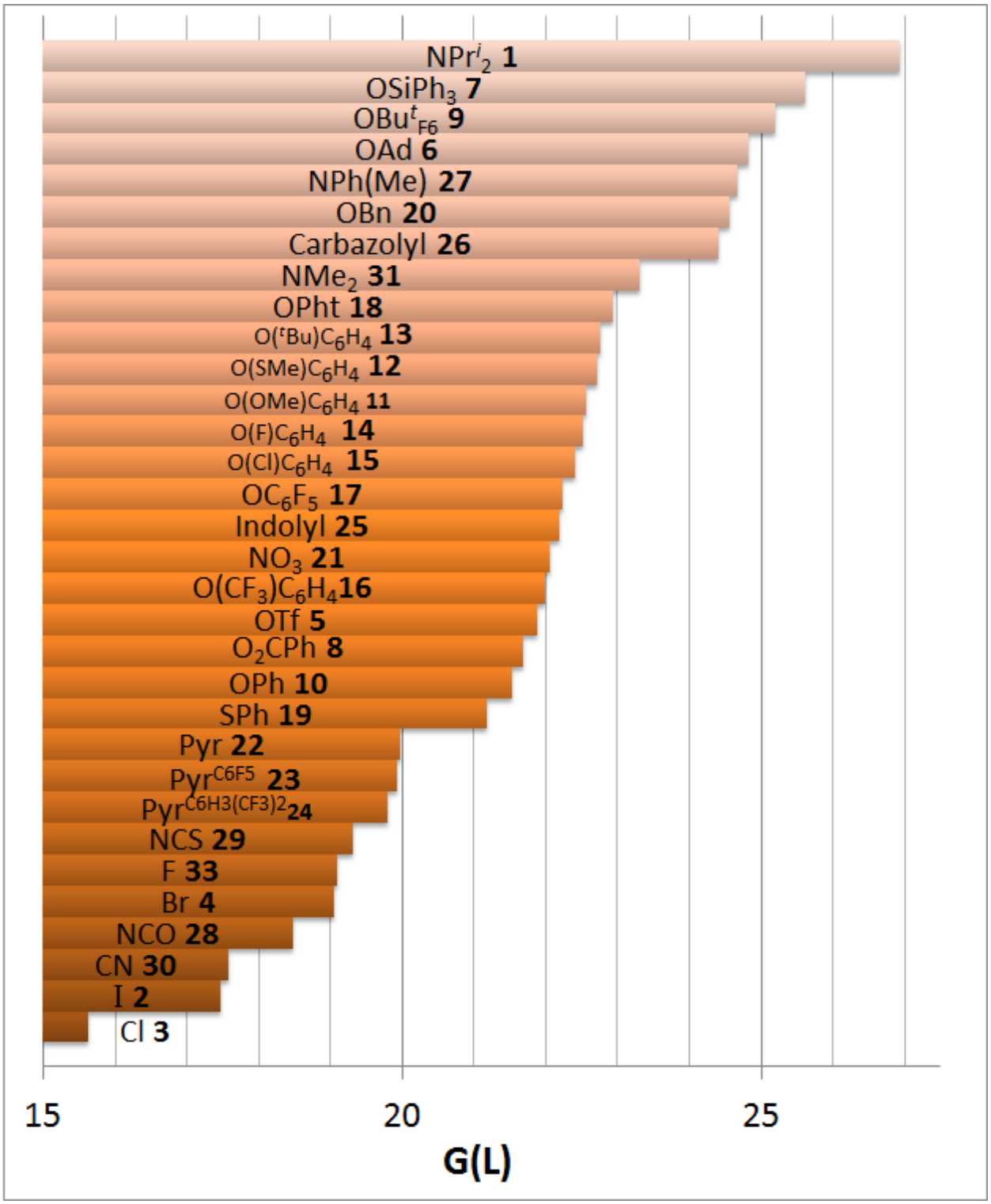

Figure B.4. Percentage of the sphere shielded by a given ligand as calculated by Solid G

Additionally, the G (complex) gave the amount of the sphere shielded as if all the ligands were treated as one. The difference between G (complex) and the sum of each of the individual ligand G(L)'s, SUM (G(L)), is due to areas of overlap of multiple ligands. The G (complex) was subtracted from 100 to give the available free space around the metal center as a percentage.

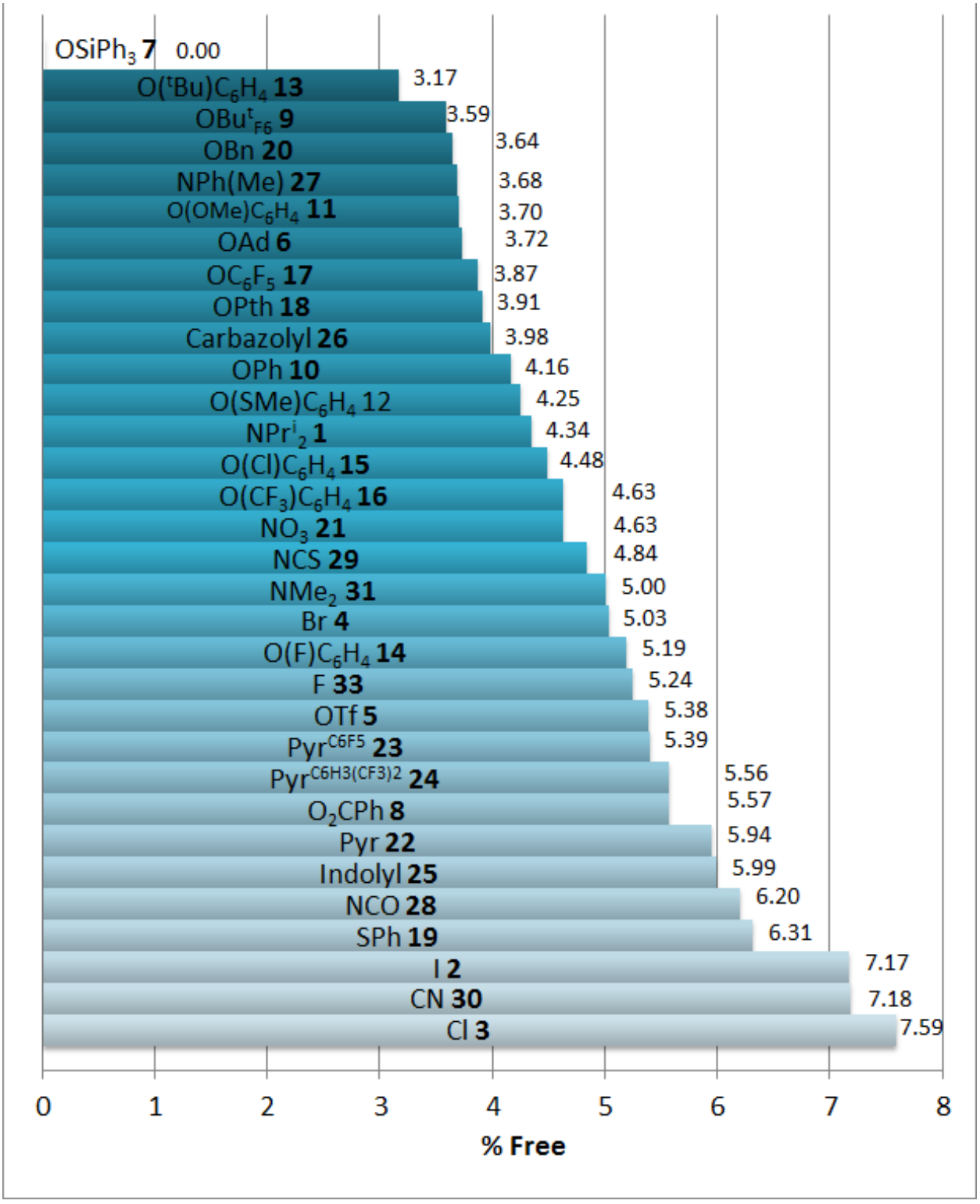

Figure B.5. Percentage of free space not shielded any ligand of $NCr(NPr^{i}_{2})_{2}(X)$

Concluding Remarks

As stated before, the property of sterics is complex and often under-described in quantitative terms using a single parameter. Using both Solid G and $\%V_{bur}$ with such a vast array of ligands highlights some of the inherent shortcomings in describing a 3-dimensional object in one number. That being said, both systems seem to have a place in steric discussions. It is suspected that, while $\%V_{bur}$ may accurately predict the steric environment close to a metal thus being applicable for intramolecular processes, the Solid G parameter may be more useful in describing intermolecular reactions such as substrate binding.

B.4 ^{1}H NMR assignment of 2

Spectral Assignment of NCr(X)(NPr$^{i}_{2}$)$_2$ Complexes with Iodo **2** as an Example

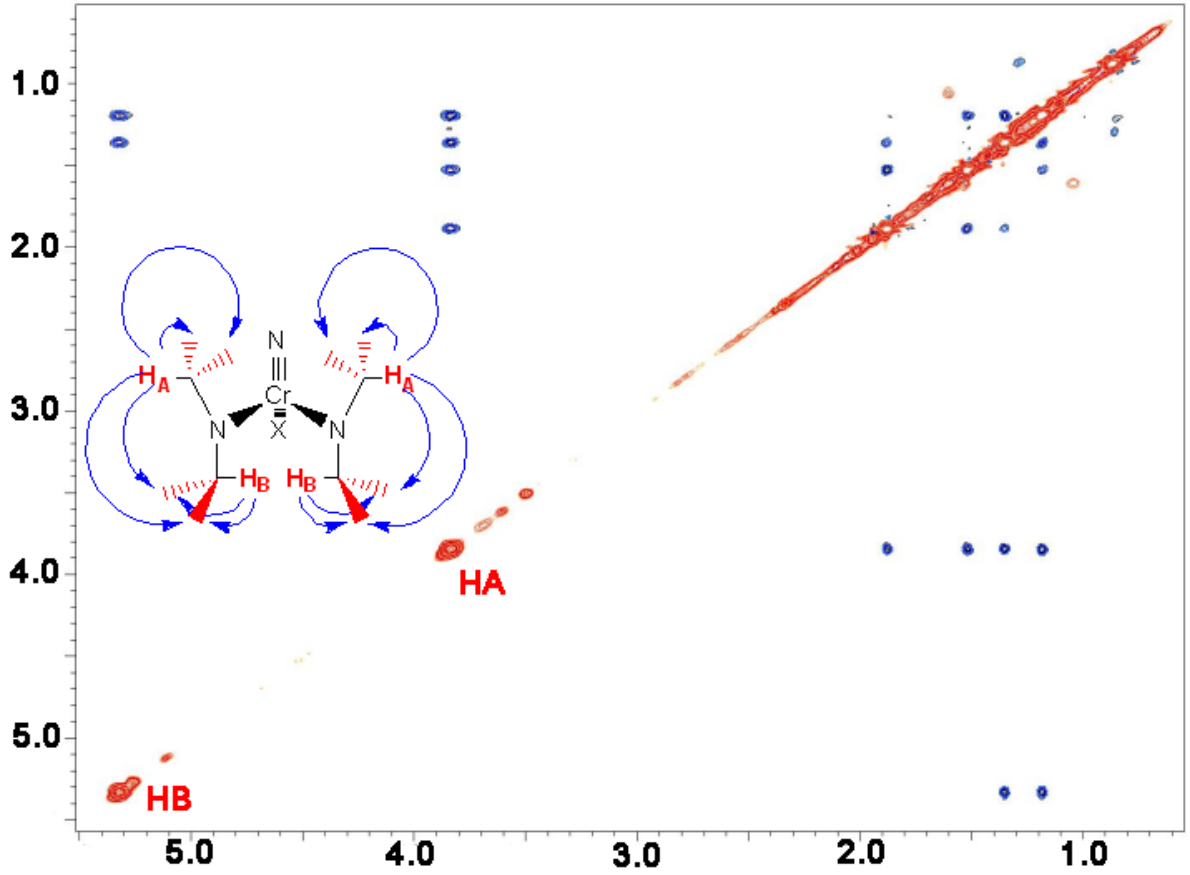

Figure B.6: 2D NOESY of **2** at –60 °C

Assignment of the chemical shifts for H_A and H_B of $NCr(NPr^i_2)_2I$ (**2**) are based upon the 2D NOESY spectrum above. In the spectrum, positive resonances are in red, while negative are in blue. Thus, for this small molecule, red cross-peaks represent exchange and blue cross-peaks represent NOE's. The blue arrows on the structure show observed NOE interactions between the methyne and methyl protons. The resonance at 3.834 ppm is assigned to H_A since it shows NOE interactions with all four methyl resonances. H_B is assigned to 5.346 ppm and has two NOE interations.

The above spectrum is of **2** at –60 °C, where no chemical exchange (due to amido rotation) between the methyne peaks occurs. There is free rotation about the N—C bond bearing H_A allowing interaction with all methyl groups, both *syn* and *anti*, with the *syn* methyne. H_B cannot rotate as freely around the N–C bonds to larger steric constraints *anti* to the nitrido due to the N–Cr–amido angles. In other words, rotating the *anti iso*-propyl group to where the methyl is under the metal is sterically more difficult, which makes the conformation with hydrogen of the *iso*-propyl group adjacent to the metal strongly preferred.

As a result, the methynes H_B do not come within the NOE limit of ~5 Å for the methyl groups *syn* to the nitrido. Furthermore, it is plausible that since H_B spends more time closer to the metal center, it experiences a greater downfield shift due to the deshielding zone near the metal center.

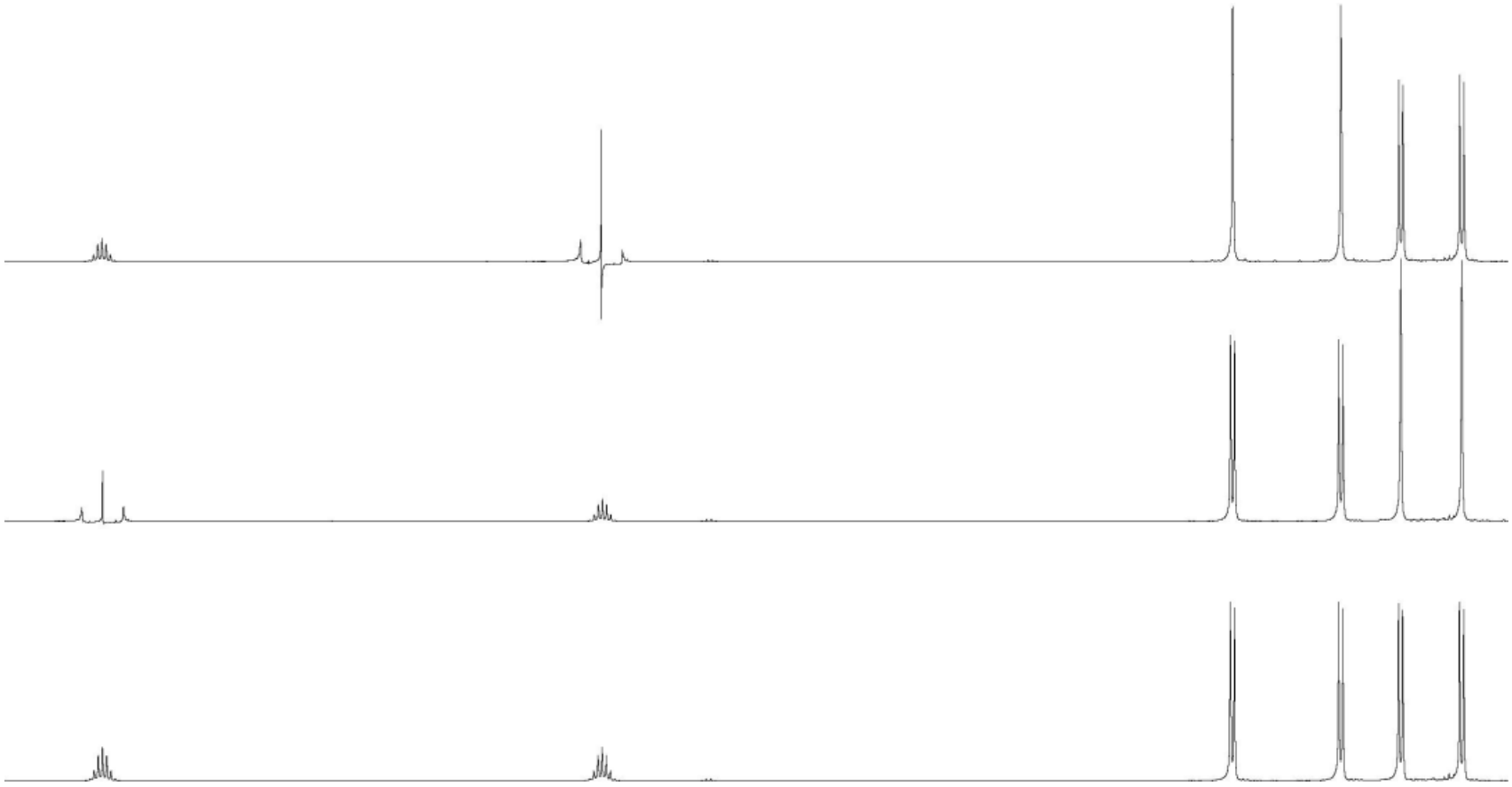

Figure B.7: ^{1}H Homodecoupling Experiment of **2** at 25 ˚C

The above spectra indicate the coupling of the methyne proton with the methyl protons on the isopropyl groups. Both the homodecoupling experiment and the 2D NOESY experiment are in agreement in assignment of the methyne and methyl protons. The methyne peak at 5.316 ppm is deshielded due to being closer to the chromium center, and the two more shielded doublet peaks, at 1.148 ppm and 1.335 ppm, are *anti* to the nitrido, where they spend more time pointed away from the metal center. The *iso*-propyl group *syn* to the nitrido is freely rotating and has a methyne peak at 3.783 ppm. The methyls of the *iso*-propyl group *syn* to the nitrido spend more time pointed toward the metal center and are therefore deshielded relative to the other doublets at 1.519 ppm and 1.852 ppm.

In short, the less shielded (higher ppm) methyne septet and more shielded (lower ppm) methyl doublets are assigned to the diisopropyl groups *anti* to the nitrido. The more shielded methyne septet and less shielded methyl doublets are assigned to the diisopropyl groups *syn* to the nitrido.

B.5 Spin Saturation Magnetization Transfer Experiment

General Considerations for the SST

The rate constant for the exchange of the two methynes in the isopropyls, in the majority of cases, was measured using Spin Saturation Transfer (SST) in the ^{1}H NMR.[61] The ideal temperature for the SST experiment was found to be between –56 °C and +27 °C depending on the rate of rotation for the particular complex being studied. A methanol standard was used to measure the temperature of the probe before and after each experiment. The T_1 values for the compounds were determined using the inversion recovery method. The concentration of the analyte was 0.02-0.03 M in $CDCl_3$ for all of the compounds, and solutions were degassed.

Sample Preparation

Since T_1's are concentration dependent, it is important to have a consistent concentration for all experiments. In all the cases, the goal was to maintain a concentration between 0.0222 M and 0.0333 M. The solution was dispensed into an oven dried JY tube and sealed. The sample was then degassed using the freeze-pump-thaw method.

General Considerations for SSMT Experiment

For temperatures colder and warmer than room temperature, the sample was allowed 15 min to equilibrate to the new temperature before the experiment began. After every spin saturation magnetization experiment, a methanol standard was placed into the NMR and left to equilibrate at the set temperature for 15 minutes before the temperature was measured. The number reported for the barrier of rotation is the average of at least 3 runs attempted at the same temperature (within 1-2 °C).

The Experiment

First, a standard ^{1}H NMR spectrum was obtained followed by determination of the 90° pulse width of the exchanging peaks (the methyne peaks in this case). The sample was scanned with the new pulse width with 64 transients, shimmed, and referenced. Then the T_1 of the septets was determined using the inversion recovery method. The T_1 value is used to set the saturation delay and for calculating the rate of exchange. Now the spin saturation magnetization experiment can be started. A quality non-spinning ^{1}H spectrum was acquired with 64 transients using the newly acquired 90° pulse width. The spectrum was expanded upon the region of the two methynes, and two experiments were performed. One experiment was carried out in which one methyne was saturated, and, in the second experiment, an offsite point was saturated as a control that is equidistant from exchanging resonance in order to compensate for decoupler sidebands. The peak to be saturated was set to the decoupler frequency. It was made sure that the offsite point chosen did not lie on a peak of exchange. Saturation power was set to -4, the saturation delay was set to $5 \times T_1$ value and the experiment was acquired with 64 transients. Integration of the peak with saturation and without saturation was performed and used to determine the rate of exchange between the methynes using the equation below.

$$k_{obs} = \frac{1}{T_1}\left(\frac{M_0}{M} - 1\right)$$

where M_{OA} is integration before spin saturation magnetization transfer and M_A is after integration after exchange. Then the T_1 of the exchanging peak was determined using the

inversion recovery method. By knowing the temperature of the experiment the barrier of rotation of the compound can be determined using the Eyring equation shown below.

$$k_{obs} = \kappa\left(\frac{k_B T}{h}\right)e^{-\Delta G^{\ddagger}/RT}$$

Where k_b is the Boltzmann constant, T is temperature (K), h is Plank's constant, κ is the transmission coefficient (assumed to be 1), k_{obs} is the rate of exchange determined using equation above, and R is the gas constant (1.987×10^{-3} kcal·mol^{-1}·K^{-1}).

Control Experiments

To test the consistency of the values under different conditions, several control experiments were carried out involving solvent, NMR field, and the effect of paramagnetic impurities.

The effect of solvent on the barrier was examined. The free energy barrier for amido rotation in NCr(NPr$^{i}_{2}$)$_3$ (**1**) was measured in both $CDCl_3$ and d_8-toluene; the values for $\Delta G^{\ddagger}_{rot}$ determined in these two solvents were quite close at 12.6 and 12.5 kcal/mol. In addition, the value for NCr(NPr$^{i}_{2}$)$_2$(OBu$^{t}_{F6}$) (**9**) in $CDCl_3$ was found to be 16.1 kcal/mol, which was consistent with the literature value in C_6D_6 of $\Delta G^{\ddagger}_{rot}$ = 16 kcal/mol.[62]

The consistency of the SST values at different fields was also explored using NCr(NPr$^{i}_{2}$)$_2$(I) (**2**) as the analyte. The standard experiments for the compounds in this paper were performed on a 500 MHz instrument. For **2** at that field, the measured barrier was $\Delta G^{\ddagger}_{rot}$ = 18.2 kcal/mol. The same compound at 300 MHz had a measured barrier of 18.3 kcal/mol.

To test the effect of possible paramagnetic impurities, a common paramagnetic relaxation agent, $Cr(acac)_3$, was added in high concentration. In $CDCl_3$, the SST experiment was carried out on $NCr(NPr^i_2)_2(I)$ (**2**) in the presence of 9 equivalents of $Cr(acac)_3$, which gave $\Delta G^{\ddagger}_{rot}$ = 18.4 versus 18.2 kcal/mol in the absence of the paramagnetic compound. Consequently, small amounts of paramagnetic impurites possibly present are unlikely to have a significant effect on these SST measurements.

B.6 Propagation of Error in the Spin Saturation Transfer Experiments

The equation for the relating the experimental observables to the rate constant, k, is Eqn 1 below. In Eqn 1, M_{0A} is the integral before irradiation, which was set to 100, and M_A is the observed integral after irradiation. The T_1 were found the inversion recovery method, and the error in T_1 is that calculated by the Varian software VNMR 61c or VNMR J22d, both software packages gave very similar results. The error in the integrals were set to 0.1 with the integration of the peak before irradiation set to 100. The error in temperature, ε_T, was ±1 °C.[63] The propagation of error in this system, error in k (ε_k), is found using Eqn 2.

$$k = \frac{1}{T_1}\left(\frac{M_{0A}}{M_A} - 1\right) \quad (1)$$

$$\varepsilon_k = k\sqrt{\left(\frac{\varepsilon_{1/T_1}}{T_1}\right)^2 + \left(\frac{\varepsilon_{M_{0A}/M_A}}{M_{0A}/M_A}\right)^2} \quad (2)$$

Where, $\varepsilon_{1/T1}$ and $\varepsilon_{M0A/MA}$ are found using Eqns 3 and 4, respectively.

$$\varepsilon_{1/T_1} = \frac{1}{T_1}\sqrt{\left(\frac{\varepsilon_{T_1}}{T_1}\right)^2} \quad (3)$$

$$\varepsilon_{M_{0A}/M_A} = \sqrt{\left(\frac{\varepsilon_{M_{0A}}}{M_{0A}}\right)^2 + \left(\frac{\varepsilon_{M_A}}{M_A}\right)^2} = \sqrt{1\times10^{-6} + \left(\frac{0.1}{M_A}\right)^2} \quad (4)$$

The free energy of the amido rotation was found using the Eyring equation in the form shown in Eqn 5. The error in ΔG was calculated as shown in Eqn 6.

$$\Delta G = RT\ln\left(\frac{k_B}{h}\right) + RT\ln T - RT\ln k \quad (5)$$

$$\varepsilon_{\Delta G} = \sqrt{\left(\varepsilon_T R\ln\left(\frac{k_B}{h}\right)\right)^2 + (R\varepsilon_{T\ln T})^2 + (R\varepsilon_{T\ln k})^2}$$

$$\varepsilon_{T\ln T} = T\ln T\sqrt{\left(\frac{\varepsilon_T}{T\ln T}\right)^2 + \left(\frac{\varepsilon_T}{T}\right)^2} \quad (6)$$

$$\varepsilon_{T\ln k} = T\ln k\sqrt{\left(\frac{\varepsilon_k}{k\ln k}\right)^2 + \left(\frac{\varepsilon_T}{T}\right)^2}$$

T_1s, Apparent T_1s, and NOE Effects of Exchanging Resonances

In spin saturation magnetization experiments involving exchange between two sites, the rate is determined by the ratio of the fractional decrease in integration of one site in the presence of saturation of the other relative to its T_1. In a system experiencing two site exchange, the relaxation of the spins for peak A is dependent on the rate of decay from the excited state A* to the ground state A; the same is true for peak B. When $T_{1A} = T_{1B}$, the rate of relaxation is the same. In this case, the T_1 of the peak experiencing exchange is measured before saturation.[64,65,66] But if T_{1A} and T_{1B} differ more than ~30% or if more than two peaks are experiencing exchange, the T_1 of the peak experiencing exchange in the presence of saturation is measured, which is known as the apparent T_1.[67,68] In essence, the apparent T_{1app} is the average T_1 for the two exchanging sites.

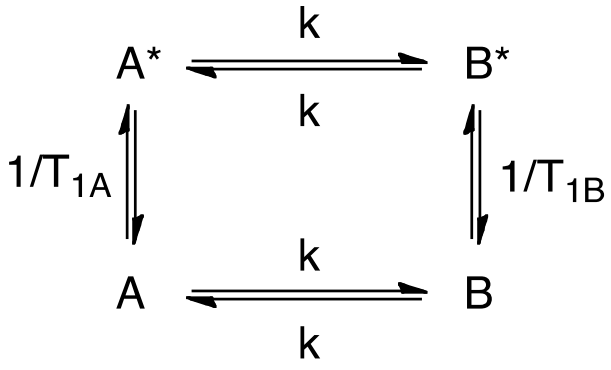

Figure B.8: Kinetic Scheme for Two-Site Exchange

In our chromium nitrido system, both T_1 and apparent T_1 of the less shielded septet were measured, e.g., the septet at 5.32 ppm in iodo **2** (see below).

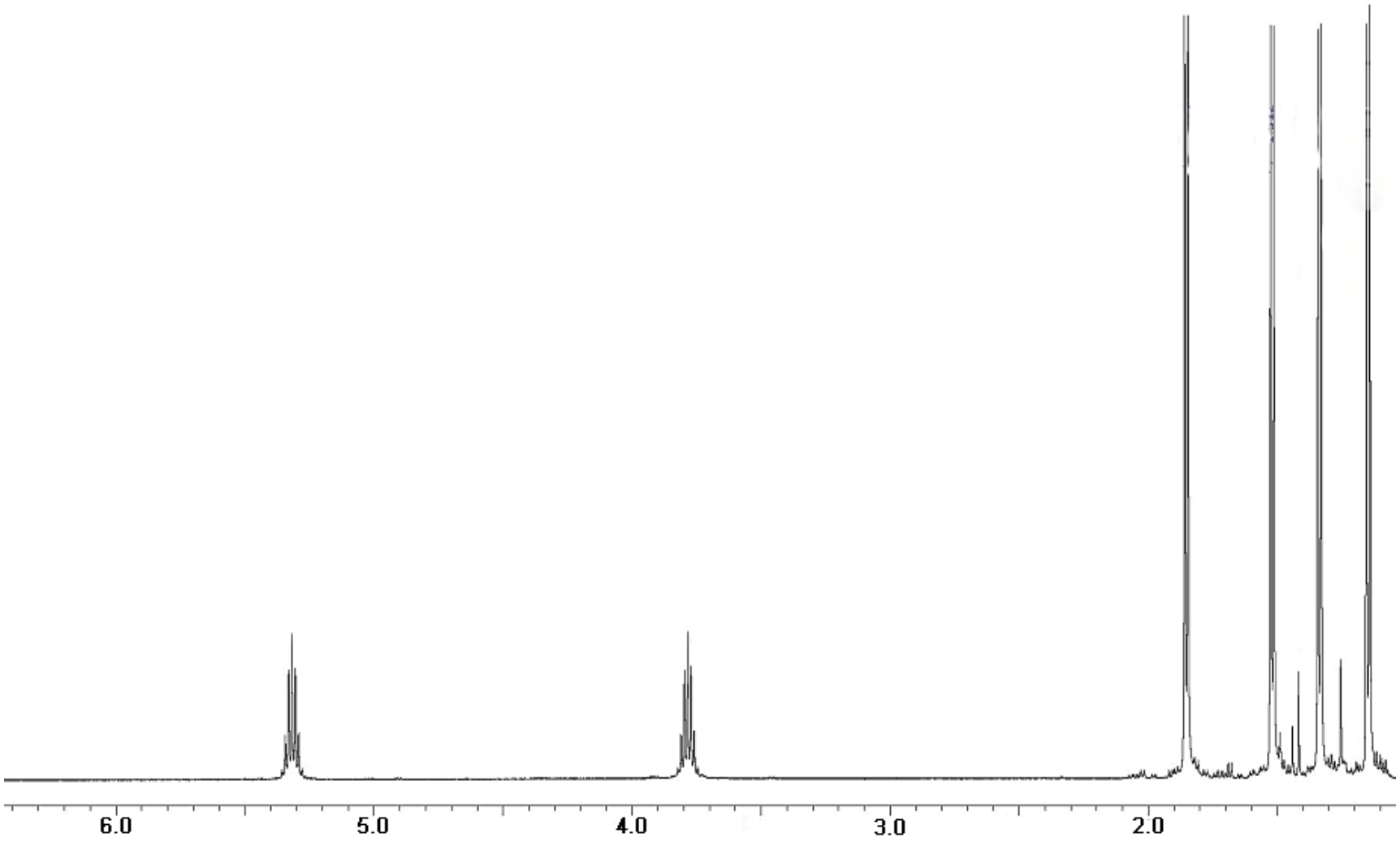

Figure B.9: ^{1}H NMR Spectrum of NCr(NPr$^{i}_{2}$)$_2$I (**2**) at 25 ˚C

This peak was chosen because it is easily saturated in a selective fashion without effecting the peak due to the exchanging site. Data for both the T_1 and apparent T_1 of the peak at 5.316 ppm are shown below for **2**. The relationship between T_1 and apparent T_1 (T_{1app}) is

$$T_{1app} = \frac{M_z^A(\infty)}{M_z^A(0)} T_1 \quad (1)$$

where $M_z(\infty)$ is the intensity (or integrated area) of the resonance upon saturation (applied for, at least, $5 \times T_1$) of the exchanging site and $M_z(0)$ is the intensity of the resonance with no saturation.

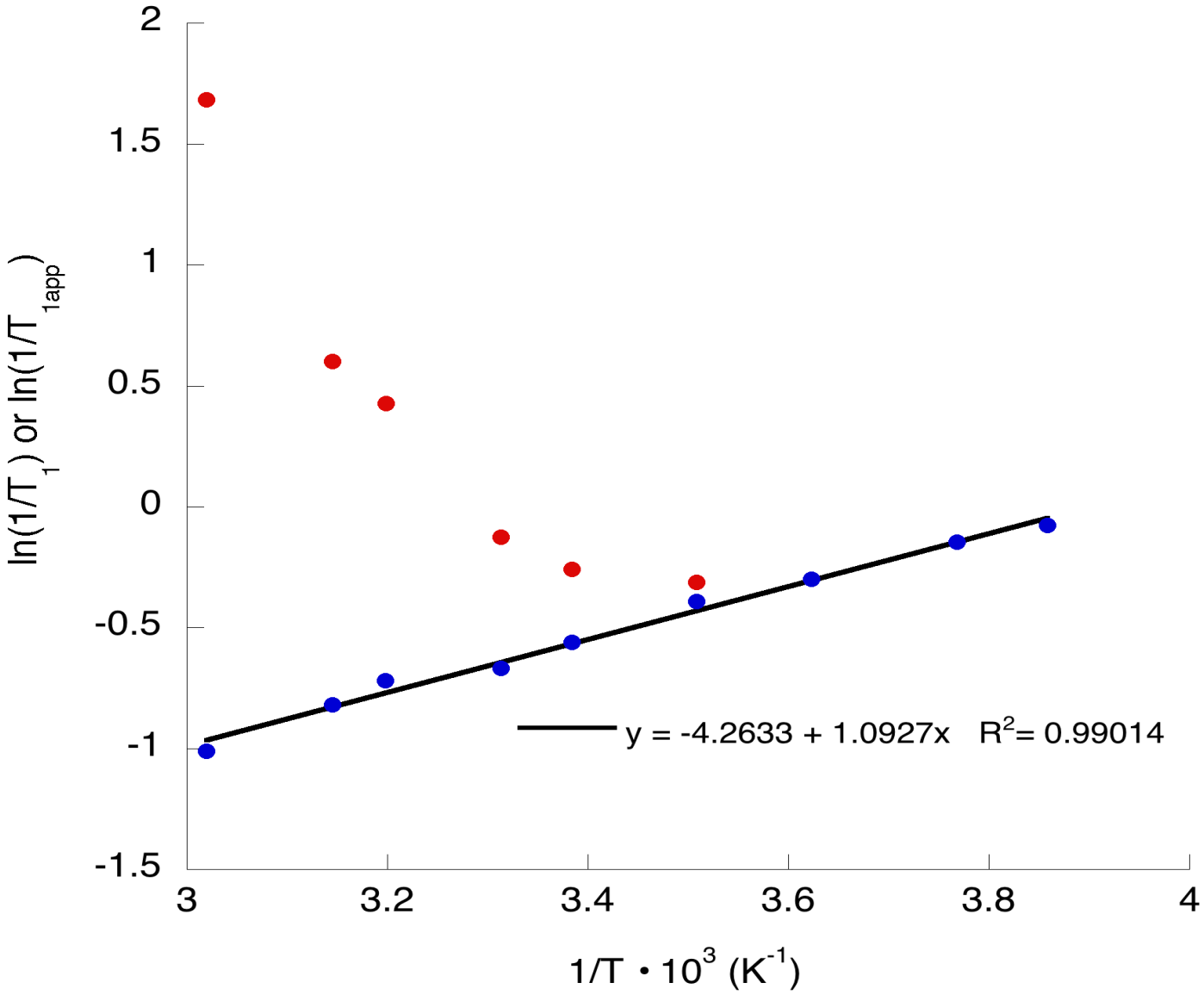

Figure B.10: ln(1/T_1) (blue) and ln (1/apparent T_1) (red) of **2** at different temperatures

At 285 K and below the molecule does not experience exchange of the isopropyl groups as seen by the lack of change in chemical shifts and linewidths of the exchanging sites. At this extreme, Eqn 1 above simplifies so that $T_{1app} = T_1$. This was observed in our experiments (see plot above) as a region to the right in the plot (large 1/T) where the red and blue points converge at the same line. In this region, the Kinetic Scheme is dominated by the vertical equilibria because there is no chemical exchange.

Above 335 K, exchange becomes fast on the NMR timescale ($k >> \delta_a - \delta_b$) and individual peaks are not observable. In the temperature regime where the exchange can be measured, T_1 increases with temperature. The opposite is observed for the apparent T_1, as would be expected from Eqn 1. In this region, the Kinetic Scheme is dominated by chemical exchange, the horizontal equilibria.

Between 285 and 335 K, the $T_{1app} \neq T_1$, and T_{1app} becomes linked with the exchange process. In other words, the entire Kinetic Scheme becomes relevant, and the horizontal and vertical equilibria all have similar rates. Use of apparent T_1 in cases of this type, where T_{1A} and T_{1B} have very similar values that are also similar to the exchange rate, leads to a situation where it can be difficult to extricate the exchange rate from the T_1 value. They become linked.

The relationship between T_1 and temperature should be linear when 1/Temp versus $\ln(1/T_1)$ is plotted (see the graph above) provided that the apparent T_1 is not contaminated by exchange processes.[19] As shown, this is the case for T_1 (blue points) but it is not the case for

T_{1app} (red points). Presumably, the deviation from linearity in the plot above for T_{1app} is due to it becoming linked with the chemical exchange (amido rotation) process.

Another possible complication to getting very accurate exchange values is that NOE effects in the saturated site and the exchange site can interfere with the measurement of the chemical exchange kinetics. We examined our system using 2D NOESY spectroscopy, and NOE effects between the chemically exchanging sites measured in the SST were negligible. It is possible to separate the NOE and exchange phenomena using this technique, which fortunately was unnecessary for our system.

REFERENCES

REFERENCES

(1) Tolman, C. A. *Chem. Rev.* **1977**, *77*, 313.

(2) Abel, E. W.; Bennett, M. A.; Wilkinson, G. *J. Chem. Soc.* **1959**, 2323.

(3) For other seminal work on CO stretches being used for electronic evaluation see (a) Nyholm, R. S.; Short, L. N. *J. Chem. Soc.* **1953**, 2670. (b) Cotton, F. A. *Inorg. Chem.* **1964**, *3*, 702. (c) Abel, E. W.; Stone, F. G. A. *Q. Rev. Chem. Soc.* **1969**, *23*, 325. (d) Poilblanc, R.; Bigorgne, M. *Bull. Soc. Chim. Fr.* **1962**, 1301. (e) Strohmeier, W.; Muller, F. J. *Chem. Ber.* **1967**, *100*, 2812. For a recent paper showing effects other than metal electron density can effect these CO stretching frequencies see (f) Valyaev, D. A.; Brousses, R.; Lugan, N.; Fernandez, I.; Sierra, M. A. *Chem. Eur. J.* **2011**, *17*, 6602.

(4) For a few representative examples see (a) Maldonado, A. G.; Hageman, J. A.; Mastroianni, S.; Rothenberg, G. *Adv. Synth. Cat.* **2009**, *351*, 387. (b) Hageman, J. A.; Westerhuis, J. A.; Frühauf, H.-W.; Rothenberg, G. *Adv. Synth. Cat.* **2006**, *348*, 361. (c) Burello, E.; Rothenberg, G. *Int. J. Mol. Sci.* **2006**, *7*, 375. (d) Maldonado, A. G.; Rothenberg, G. *Chem. Soc. Rev.* **2010**, *39*, 1891. (e) Mikhel, I. S.; Garland, M.; Hopewell, J.; Mastroianni, S.; McMullin, C. L.; Orpen, A. G.; Pringle, P. G. *Organometallics* **2011**, *30*, 974. (f) Birkholz, M.-N.; Freixa, Z.; van Leeuwen, P. W. N. M. *Chem. Soc. Rev.* **2009**, *38*, 1099. (g) Gillespie, J. A.; Dodds, D. L.; Kamer, P. C. J. *Dalton Trans* **2010**, *39*, 2751. (h) Fey, N. *Dalton Trans.* **2010**, *39*, 296. (i) Dröge, T.; Glorius, F. *Angew. Chem. Int. Ed.* **2010**, *49*, 6940.

(5) For a review see Hansch, C.; Leo, A.; Taft, R. W. *Chem. Rev.* **1991**, *91*, 165.

(6) For some selected recent reviews see (a) Sprous, D. G.; Palmer, R. K.; Swanson, J. T.; Lawless, M. *Current Topics Med. Chem.* **2010**, *10*, 619. (b) Verma, R. P.; Hansch, C. *Chem. Rev.* **2009**, *109*, 213. (c) Michaelidou, A. S.; Hadjipavou-Litina, D. *Chem. Rev.* **2005**, *105*, 3235. (d) Lipinski, C. A.; Lombardo, F.; Dominy, B. W.; Feeney, P. J. *Adv. Drug Delivery Reviews* **2001**, *46*, 3.

(7) Occhipini, G.; Bjørsvik, H.-R.; Jensen, V. R. *J. Am. Chem. Soc.* **2006**, *128*, 6952.

(8) For a few examples see (a) Möhring, P. C.; Coville, N. J. *Coord. Chem. Rev.* **2006**, *250*, 18. (b) Silveira, F.; de Sá, D. S.; da Rocha, Z. N.; Alves, M. C. M.; dos Santos, J. H. Z. *X-Ray Spectrometry* **2008**, *37*, 615. (c) Kozimor, S. A.; Yang, P.; Batista, E. R.; Boland, K. S.; Burns, C. J.; Christensen, C. N.; Clark, D. L.; Conradson, S. D.; Hay, P. J.; Lezama, J. S.; Martin, R. L.; Schwarz, D. E.; Wilkerson, M. P.; Wolfsberg, L. E. *Inorg. Chem.* **2008**, *47*, 5365.

(9) Redshaw, C. *Dalton Trans.* **2010**, *39*, 5595.

(10) Zachmanoglou, C. E.; Docrat, A.; Bridgewater, B. M.; Parkin, G.; Brandow, C. G.; Bercaw, J. E.; Jardine, C. N.; Lyall, M.; Green, J. C.; Keister, J. B. *J. Am. Chem. Soc.* **2002**, *124*, 9525.

(11) (a) Swartz, D. L., II; Staples, R. J.; Odom, A. L. *Dalton Trans.* **2011**, *40*, 7762. (b) Swartz, L. D, II; Odom, A. L. *Organometallics* **2006**, *25*, 6125.

(12) Some cationic complexes using this framework with neutral ligands in place of X have already been prepared and many others are being developed. It is hoped that this series will allow more overlap with the Tolman ligand maps, which involve mostly neutral ligands. One such complex, **32**, is used as an intermediate to the fluoride reported here. Unpublished results DiFranco, S.; Maciulis, N.; Odom, A. L.

(13) The orbital labels are an approximation. In actuality, because the d_{xy}/d_{x2-y2} and d_{xz}/d_{yz} e- sets have the same symmetry, they will mix as well.

(14) In the calculations, two minima can sometimes be found in the model: one where the lone pair is *syn* to the nitrido and one where it is *anti*. The *anti* isomer is typically the global minimum, which is what is used here.

(15) The hybridization at nitrogen was calculated by taking the calculated angles around the nitrogen and dividing by 3 to get an average hybridization for all the bonds. From the average angle, Coulson's equation for the Directionality Theorem, $\cos W_{ij} = - \frac{1}{(l_i l_j)^{1/2}}$, can be used to get the hybridization parameter. In this case where we are simply looking at the average angle, effectively average orbital hybridization, the equation can be simplified to $l = - \frac{1}{\cos W}$ for looking at equivalent hybrids. (a) McWeeny, R. *Coulson's Valence*, **1979**, Oxford University Press: Oxford. (b) Weinhold, F.; Landis, C. R. *Valency and Bonding*, **2005**, Cambridge University Press: Cambridge.

(16) (a) Bradley, D. C.; Hursthouse, M. B.; Newing, C. W.; Welch, A. J. *Chem. Commun.* **1971**, 411. (b) Bradley, D. C.; Copperthwaite, R. G. *Inorg. Synth.* **1978**, *18*, 112. (c) Bradley, D. C.; Newing, C. W. *Chem. Commun.* **1970**, 219.

(17) (a) Odom, A. L.; Cummins, C. C.; Protasiewicz, J. D. *J. Am. Chem. Soc.* **1995**, *117*, 6613. For related nitrosyl deoxygenation studies see (b) Veige, A. S.; Slaughter, L. M.; Lobkovsky, E. B.; Matsunaga, N.; Decker, S. A.; Cundari, T. R.; Wolcanski, P. T. *Inorg. Chem.* **2003**, *42*, 6204.

(18) Chiu, H.-T.; Chen, Y.-P.; Chuang, S.-H.; Jen, J.-S.; Lee, G.-H.; Peng, S.-M. *Chem. Commun.* **1996**, 139.

(19) The byproduct $Cr(OBu^t)_3$ is believe to be a soluble dimer. Bradley, D. C.; Mehrotra, R.; Rothwell, I.; Singh, A., *Alkoxo and Aryloxo Derivatives of Metals*, Academic Press: San Diego, 2001.

(20) Odom, A. L.; Cummins, C. C. *Organometallics* **1996**, *15*, 898.

(21) Odom, A. L.; Cummins, C. C. *Polyhedron* **1998**, *17*, 675.

(22) For a similar decomposition of a DMAP containing BF_4 salt see Huynh, K.; Rivard, E.; Lough, A. J.; Manners, I. *Chem. Eur. J.* **2007**, *13*, 3431. In addition, the tetraalkyltin $SnBu^n_3$(allyl), which we had on hand, was an active catalyst. It is likely that Sn(IV) is acting as a mild Lewis acid in the reaction, and other acids may catalyzed the decomposition of **32**.

(23) The chemical shift in the ^{19}F NMR of the byproduct in the reaction to produce **33** was identical to the product of the reaction between 1 equivalent each of BF_3•OEt_2 and DMAP in the same solvent.

(24) In this work, 31 of the compounds have been structurally characterized; this number includes the previously reported structures for $NCr(NPr^i_2)_3$ (**1**) and $NCr(NPr^i_2)_2(I)$ (**2**). The only compound not structurally characterized is compound **32**, which was only used as an intermediate in production of the fluoride **33**.

(25) For related studies on aryloxides where no correlation was found between M–O–Ar angle and M–O bond distance see (a) Steffey, B. D; Fanwick, P. E., Rothwell, I. P. *Polyhedron* **1990**, *9*, 963-968. (b) Howard, W. A.; Trnka, T. M.; Parkin, G. *Inorg. Chem.* **1995**, *34*, 5900. (c) Wolczanski, P. T. *Polyhedron* **1995**, *14*, 3335. For systems where alkoxide bond angle does seem to correlate with bond distance see (d) Tomaszewski, R.; Arif, A. M.; Ernst, R. D. *J. Chem. Soc., Dalton Trans.* **1999**, 1883-90. (e) Huffman, J. C.; Moloy, K. G.; Marsella, J. A.; Caulton, K. G. *J. Am. Chem. Soc.* **1980**, *102*, 3009.

(26) (a) Jarek, R. L.; Flesher, R. J.; Shin, S. K. *J. Chem. Ed.* **1997**, *74*, 978. (b) Perrin C. L.; Thoburn, J. D.; Kresge, A. J. *J. Am. Chem. Soc.* **1992**, *114*, 8800. (c) Dahlquist, F. W.; Longmuir, K. J.; Du Vernet, R. B. *J. Mag. Resonance* **1975**, *17*, 406.

(27) We measured the variable temperature SST data for X = Pr^i in two different solvents. In toluene, the activation parameters for rotation were found to be $\Delta H^{\ddagger}$ = 12.4 kcal/mol and $\Delta S^{\ddagger}$ = –2 cal/mol•K over a temperature range of 30 °C. In $CDCl_3$, the usual solvent employed for the studies in this paper, the activation parameters for rotation were found to be $\Delta H^{\ddagger}$ = 11.6 kcal/mol and $\Delta S^{\ddagger}$ = –5 cal/mol•K over a temperature range of 26 °C. The value of $\Delta H^{\ddagger}$ = 11.12 ± 0.23 kcal/mol in Table 4.1 is from multiple measurements, consistent with the majority of data in that table.

(28) The amido entropic barriers found here are quite similar to values in the literature for organic amides of various types. For example, the amide rotational barrier in nicotinamide was measured using several different techniques and values from –3 to –10 cal/mol•K were obtained. Olsen, R. A.; Liu, L.; Ghaderi, N.; Johns, A.; Hatcher, M. E.; Mueller, L. J. *J. Am. Chem. Soc.* **2003**, *125*, 10125. For some other examples see Drakenberg, T.; Dahlqvist, K.-I.; Forsén, S. *J. Phys. Chem.* **1972**, *76*, 2178.

(29) Because the value for the NMe_2 derivative was found using a different technique from all the other values, we view its absolute value relative to all the other LDP numbers with

some suspicion. However, we have little doubt in its placement as the most donating ligand investigated in this study.

(30) This can be seen in the metal-nitrogen bond distances of pyrrole versus dialkylamidos. See Harris, S. A.; Ciszewski, J. T.; Odom, A. L. *Inorg. Chem.* **2001**, *40*, 1987 and references therein for examples.

(31) For a mixed experimental theoretical treatment of aromaticity in indoles and pyrroles see (a) Hou, D.-R.; Wang, M.-S.; Chung, M.-W.; Hsieh, Y.-D.; Tsai, H.-H. G. *J. Org. Chem.* **2007**, *72*, 9231. For a review on aromaticity of heterocycles see (b) Balaban, A. T.; Oniciu, D. C.; Katritzky, A. R. *Chem. Rev.* **2004**, *104*, 2777.

(32) For a review concerning the application of $\%V_{bur}$ see Clavier, H.; Nolan, S. P. *Chem. Commun.* **2010**, *46*, 841.

(33) (a) Hillier, A. C.; Sommer, W. J.; Yong, B. S.; Petersen, J. L.; Cavallo, L.; Nolan, S. P. *Organometallics* **2003**, *22*, 4322. (b) Poater, A.; Cosenza, B.; Correa, A.; Giudice, S.; Ragone, F.; Scarano, V.; Cavallo, L. *Eur. J. Inorg. Chem.* **2009**, 1759. (c) http://www.molnac.unisa.it/OMtools/sambvca.php

(34) It is certainly possible that no single parameter steric scheme will accurately encompass the influences of a diverse set of ligands like the one found here even if the methodologies are applicable to a relatively narrow group like phosphines and *N*-heterocyclic carbenes. Included in the Supporting Information is a plot of sphere radius versus $\%V_{bur}$ for some ligands. As might be expected, the ligands show different maxima and some of the lines do cross, suggesting the ideal radius is likely system and application dependent. The values here are intended to give a rough measure of sterics for the various ligands.

(35) Guzei, I. A.; Wendt, M. *Dalton Trans.* **2006**, 3991.

(36) The online program for $\%V_{bur}$, Samb*V*ca, does not include all of the halides, and some of these were calculated using an overlapping spheres methods at the appropriate distances. See Supporting Information for details.

(37) (a) Lokare, K. S.; Odom, A. L. *Inorg. Chem.* **2008**, *47*, 11191. See also (b) Lokare, K. S.; Ciszewski, J. T.; Odom. A. L. *Organometallics* **2004**, *23*, 5386.

(38) The value used in the plot for the mixed X ligand set (Cl)(OTf) is the average of the two SST values for the two different ligands. The SST value for OBn was used as the parameter for the ethoxide ligand.

(39) A note of caution for the use of AOM values, the e_π values are often found using the assumption that e_π for NH_3 is equal to zero due to over-parameterization within the AOM model. The validity of this assumption has been called into question for some coordination complexes, most notably Pt(II) where the e_π value for NMe_3 was determined to be well above zero. It is not believed that NH_3 actually does have π-effects; instead, this is

attributable to the e_π parameter not being truly zero within the model. For further discussion see reference 39 and (a) Chang, T.-H.; Zink, J. I. *J. Am. Chem. Soc.* **1987**, *109*, 692. (b) Bridgeman, A. J.; Gerlock, M. *Prog. Inorg. Chem.* **1997**, *45*, 179. (c) Schaffer, C. E.; Anthon, C.; Bendix, J. *Coord. Chem. Rev.* **2009**, *253*, 575.

(40) AOM values were taken from Hoggard, P. E. *Structure and Bonding* **2004**, *106*, 37, which were calculated from splittings in spin-allowed transitions of the corresponding Cr(III) ammine complexes.

(41) Lukens, W. W., Jr.; Smith, M. R., III; Andersen, R. A. *J. Am. Chem. Soc.* **1996**, *118*, 1719.

(42) (a) Gyepes, R.; Varga, V.; Horacek, M.; Kubista, J.; Pinkas, J.; Mach, K. *Organometallics* **2010**, *29*, 3780. (b) Varga, V.; Cisarova, I.; Gyepes, R.; Horacek, M.; Kubista, J.; Mach, K. *Organometallics* **2009**, *28*, 1748.

(43) That the quantity measured is exclusively determined by the π-donor ability of X is of course an approximation. The a_1 is weakly σ-bonding but largely nonbonding. The b_2 orbital is orthogonal and its energy is largely determined by the π-bonding of X. For a discussion of the bonding see Lauher, J. W.; Hoffmann, R. *J. Am. Chem. Soc.* **1976**, *98*, 1729.

(44) The data for X = N(Me)Ph was not used in determining the linear fit to the Andersen data (blue line) shown in Figure 4.10. The exact cause for the two different slopes of the Andersen and Mach data fits is unknown; however, there are several small differences in the data sets like different solvents, slightly different instrumentation, and possible differences in concentration. In addition, the Andersen data are relative to Cp^*_2TiH as $\Delta E_{xz} = 0$, and we did not adjust the baseline in the Mach data similarly. If the data from the two groups are taken all together and linearly fit, the line obtained is y = 20761 – 1205x with a much worse R^2 of 0.93 versus the R^2 = ~0.99 obtained fitting the data from the two groups independently. This fit for Mach's data is for only four points from the four new alkoxides in common between our study and Mach's reports. In addition, one of the four points was done with a substitution in the LDP value, *tert*-butoxide for 1-adamantoxide.

(45) Calculated using Year 2009 single-, double- and triple-bond covalent radii from a private communication. (a) http://www.chem.helsinki.fi/~pyykko/ (b) Pyykkö, P.; Atsumi, M. *Chem. Eur. J.* **2009**, *15*, 12770.

(46) The average Ti–NMe_2 bond in CSD version 5.32 Nov 2010 is 1.897 Å. It should be noted, however, that the majority of those complexes are Ti(IV), and the distance in titanium(III) $Me(H)NTiCp^*_2$ may be somewhat longer just due to the difference in oxidation state. There are a few Ti–NH_2 cyclopentadienyl complexes in the CSD database, which should allow the Ti–N bond to shorten if electronically favorable. These do tend to have slightly shorter titanium-amido bond distances. For example, amidobis[1,3-bis(trimethylsilyl)cyclopentadienyl]titanium(III) has a Ti–NH_2 distance of 1.933(3) Å. (a) Sofield, C. D.; Walter, M. D.; Andersen, R. A. *Acta Cryst. C* **2004**, *60*, M465. The

compound $H_2NTiCp^*_2$ has a Ti–N distance of 1.944(2) Å. (b) Brady, E.; Telford, J. R.; Mitchell, G.; Lukens, W. *Acta Cryst C* **1995**, *51*, 558. Neither of these NH_2 complexes has a statistically significant difference in the Ti–N distance from the value in $Me(H)NTiCp^*_2$, however.

(47) The methyl group is rotated in the $Me(H)N–TiCp^*_2$ complex so that the amido methyl is directed at one of the Cp* ligands. The Solid-G program calculates the G(gamma) value to be 3.03 in this compound, which is a measure of how much of the sphere is shielded by more than one ligand. For the complex $Me(Ph)N–TiCp^*_2$, were the amido methyl and phenyl groups rest between the Cp*s, the G(gamma) value is 2.19, suggesting there is less ligand overlap. In other words, the small amido is nesting with the methyls of the Cp* groups in order to reach this electronically preferred but sterically encumbered position. For the structure of $Me(Ph)NTiCp^*_2$ see: Feldman, J.; Calabrese, J. C. *Chem. Commun.* **1991**, 1042.

(48) For examples see (a) Basolo, F.; Pearson, R. G. *Mechanisms of Inorganic Reactions*, 2nd Ed.; Wiley & Sons: New York, 1967. (b) Burdett, J. K. *Adv. Inorg. Chem. Radiochem.* **1978**, *21*, 113. (c) Jordan, R. B. *Reaction Mechanisms of Inorganic and Organometallic Systems*, 2nd Ed.; Oxford University Press: New York, 1998.

(49) Swartz, D. S. II; Staples, R. J.; Odom, A. L. *Dalton Trans.* **2011**, *40*, 7762.

(50) (a) Candy, C. F.; Jones, R. A.; Wright, P. H. *J. Chem. Soc. C* **1970**, 2563. (b) Candy, C. F.; Jones, R. A. *J. Org. Chem.* **1971**, *36*, 3993.

(51) Gaussian 03, Revision C.02, M.J. Frisch, G.W. Trucks, H.B. Schlegel, G.E. Scuseria, M.A. Robb, J.R. Cheeseman, J.A. Montgomery, Jr., T. Vreven, K.N. Kudin, J.C. Burant, J.M. Millam, S.S. Iyengar, J. Tomasi, V. Barone, B. Mennucci, M. Cossi, G. Scalmani, N. Rega, G.A. Petersson, H. Nakatsuji, M. Hada, M. Ehara, K. Toyota, R. Fukuda, J. Hasegawa, M. Ishida, T. Nakajima, Y. Honda, O. Kitao, H. Nakai, M. Klene, X. Li, J.E. Knox, H.P. Hratchian, J.B. Cross, V. Bakken, C. Adamo, J. Jaramillo, R. Gomperts, R. E. Stratmann, O. Yazyev, A.J. Austin, R. Cammi, C. Pomelli, J.W. Ochterski, P.Y. Ayala, K. Morokuma, G.A. Voth, P. Salvador, J.J. Dannenberg, V.G. Zakrzewski, S. Dapprich, A.D. Daniels, M.C. Strain, O. Farkas, D.K. Malick, A.D. Rabuck, K. Raghavachari, J.B. Foresman, J. V. Ortiz, Q. Cui, A.G. Baboul, S. Clifford, J. Cioslowski, B.B. Stefanov, G. Liu, A. Liashenko, P. Piskorz, I. Komaromi, R.L. Martin, D.J. Fox, T. Keith, M.A. Al-Laham, C.Y. Peng, A. Nanayakkara, M. Challacombe, P.M.W. Gill, B. Johnson, W. Chen, M.W. Wong, C. Gonzalez, and J.A. Pople, Gaussian, Inc., Wallingford CT, 2004.

(52) (a) Becke, A. D. *Phys. Rev. A* **1988**, *38*, 3098. (b) Lee, C. T.; Yang, W. T.; Parr, R. G. *Phys. Rev. B* **1988**, *37*, 785.

(53) For the lighter elements, this basis set is found in the G03 software. For chromium, see the Basis Set Exchange website https://bse.pnl.gov/bse/portal. For the reference on the chromium basis see Balabanov, N. B.; Peterson, K. A. *J. Chem. Phys* **2005**, *123*, 064107.

(54) Burke, P. J.; Matthews, R. W.; Gillies, D. G. *Dalton Trans* **1980**, 1439.

(55) Sidgwick, N. V.; Sutton, L. E. *J. Chem. Soc.* **1930**, 1461

(56) Clavier, H.; Nolan, S. P. *Chem. Commun* **2010**, *46*, 841-861.

(57) https://www.molnac.unisa.it/OMtools/sambvca.php

(58) Guzei, I. A.; Wendt, M. *Dalton Trans* **2006**, 3991–3999.

(59) (a) Jarek, R. L.; Flesher, R. J.; Shin, S. K. *J. Chem. Ed.* **1997**, *74*, 978. (b) Perrin C. L.; Thoburn, J. D.; Kresge, A. J. *J. Am. Chem. Soc.* **1992**, *114*, 8800. (c) Dahlquist, F. W.; Longmuir, K. J.; Du Vernet, R. B. *J. Mag. Resonance* **1975**, *17*, 406.

(60) Odom, A. L.; Cummins, C. C. *Polyhedron* **1998**, *17*, 675.

(61) Van Geet, A. L. *Analytical Chem* **1968**, *40*, 2227. For a more recent study see Findeisen, M.; Brand, T.; Berger, S. *Mag. Reson. Chem.* **2007**, *45*, 175.

(62) Forsen, S., Hoffman, R. A. *J. Chem. Phys.* **1963**, *39*, 2892-2901.

(63) Jarek, R. L., Flesher, R. J., Shin, S. K. *J. Chem. Educ.* **1997**, *74*, 978-982.

(64) Dahlquist F. W., Longmuir, K. J., Du Vernet, R. B. *J. Magn. Reson.* **1975**, *17*, 406-410.

(65) Perrin, C. L., Johnston, E. R. *J. Magn. Reson.* **1979**, *33*, 619-626.

(66) Mann, B. E. *J. Magn. Reson*. **1977**, *25*, 91-94.

(67) Klochkov, V. V.; Shaikhutdinov, R. A.; Khairutdinov, Klimovitskii, E. N.; Findelsen, M.; Berger, S. *Appl. Mag. Reson.* **2003**, *24*, 97.

Chapter 5: Synthesis, Structure, and Hapticity Changes in Chromium (VI) Nitrido Complexes Bearing Cp and Related Ligands.

ABSTRACT

Synthesis and characterization of new chromium(VI) nitride compounds of the form $NCr(NPr^i_2)_2X$, where X = Cp (**3**), indenyl (**4**), and fluorenyl (**5**) are reported. Crystal structures of complexes **1**-**3** show an η^1-interaction to X in the solid state. Evaluation of the donor properties of X is parameterized by measurement of the free energy of rotation about the Cr-amide bond, and is reported as the LDP. Treatment of **3** and **5** with benzoic acid gives $NCr(NPr^i_2)(O_2CPh)(Cp)$ (**6**) and $NCr(NPr^i_2)(O_2CPh)(Fluorenyl)$ (**7**) respectively. A crystal structure of **6** shows a Cp hapticity change from η^1 to η^3 upon replacement of an amide ligand from **3**. IR carbonyl stretches of the benzoate ligand of **6** show it to be κ^1. Also reported is the synthesis and structure of a cationic chromium(VI) compound $[NCr(NPr^i_2)_2DBN]I$ (**2**) used in the synthesis of **4** and **5**, as well as thallium indenidide**.** LDP's of complexes **2**, **4** and **5** are also reported. Steric analysis of all **2**-**6** are reported as a $\%V_{bur}$ as well using the method of solid G.

5.1 Introduction

Perhaps the quintessential organometallic complex, cyclopentyldienyl appended transition metals have been known since the 1950's.[1] Interest in metallocene complexes, however has not waned, due in part to their high catalytic activity in a variety applications. Common in once such

application, the polymerization of olefins,[2] researchers have successfully employed Cp and derivative ligands to support early transition metal based Ziegler-Natta systems. Moreover, tuning of the highly amendable Cp framework has allowed for control over reaction parameters, which give rise to specific tacticity,[3,4] poly despersity,[5] and the formation of co-block polymers.[6]

Recently, our work[7] with chromium(VI) nitrido complexes led us to draw a parallel to the titanium and zirconium(IV) catalysts frequently used in olefin polymerizations (Figure 5.1).

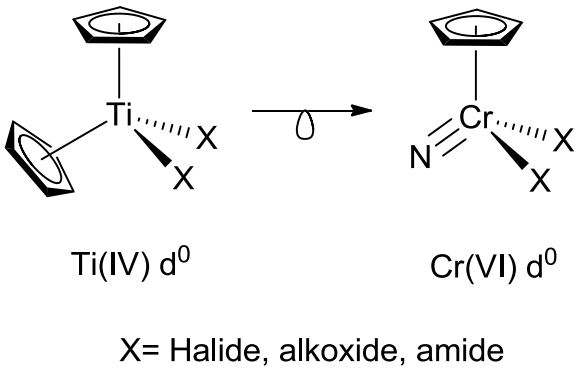

Figure 5.1: A Ti(IV) *bis*-Cp complex and an isolobal chromium nitride.

Both nitride and the η^5-cyclopentadieneyl anion require three orbitals to accommodate 2σ and 4π electrons. In the case of Cr(VI) the more electronegative nitride may support a more electron deficient, formally d^0 metal center. Furthermore, the sterically smaller nitride (*vide infra*) may provide better metal access to incoming substrates. Lastly, substituting nitride in place of one Cp ligand in a metallocene might have interesting structural consequences due in part to the much stronger trans influence of a metal-ligand multiple bond.[8, 9] Thusly, we felt complexes of the form $NCr(Cp)(X)_2$ warranted additional study.

5.2 Synthesis and Structure of NCr(NPr$^{i}_{2}$)$_2$(η^1-Cp) 3

Access into high valent chromium nitrides of the form NCr(X)$_3$ was achieved through a facile nitrogen atom transfer reaction onto Cr(NPr$^{i}_{2}$)$_3$.[10] Subsequent treatment with Lutidenium Iodide gave NCr(NPr$^{i}_{2}$)$_2$(I) (**1**) as reported by Cummins and coworkers.[11] Substitution of the halide ligand using 3 equivalents of NaCp gave NCr(NPr$^{i}_{2}$)$_2$(η^1-Cp) cleanly in good yield (Figure 5.2).

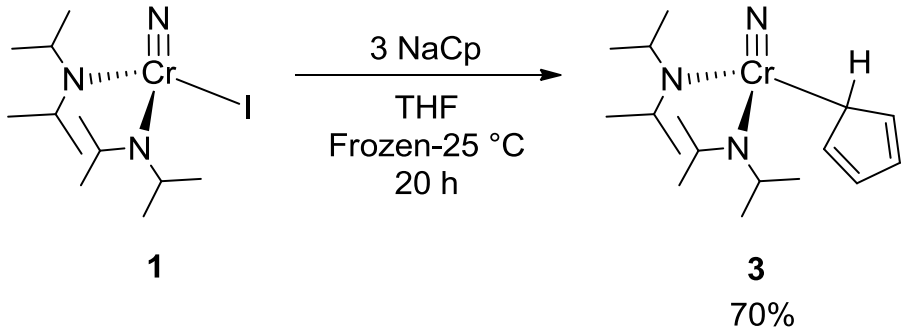

1 **3**
70%

Figure 5.2: Synthesis of NCr(NPr$^{i}_{2}$)$_2$(η^1-Cp).

^{1}H NMR analysis of **3** shows a sharp singlet corresponding to the aromatic protons of Cp, which does not resolve even at −30 °C. Single crystal Xray diffraction of **3** is consistent with an η^1-Cp, with double bond character localized between C2-C3 and C4-C5 (Figure 5.3). This C2-C5 moiety is very similar in bond lengths to that of free C_5H_6, suggesting that the Cp ring of **3** is not largely aromatic (Figure 5.4).[12] C1 adopts a typical tetrahedral arrangement with a bond length to chromium of 2.115(2) Å, considerably shorter than the other Cr-C interatomic distances (Figure 5.4). This bond distance is also significantly shorter than those in all other

crystallographically characterized examples of η^1-Cp complexes of chromium (2.195(2) Å[13] and 2.262(5) Å).[14] This is likely due to the higher oxidation state of **3** in comparison to the η^1, η^5 bis-Cp complexes of Cr(II).

Furthermore planarity of the 5 member ring is maintained in the η^1 coordination mode as judged by the angle between the planes defined by C1 C2 C5 and C2 C3 C4 C5, intersecting at just 3.5° (often reported in indenide literature as the hinge angle).[15]

Coordination in a η^1 fashion maintains a $16e^-$, assuming strong π-donation from the diisopropylamide ligand to a d^0 Cr center. This situation puts additional interaction with the Cp ligand in direct competition with strong amide donors as well as the strongly π-donating nitrido.

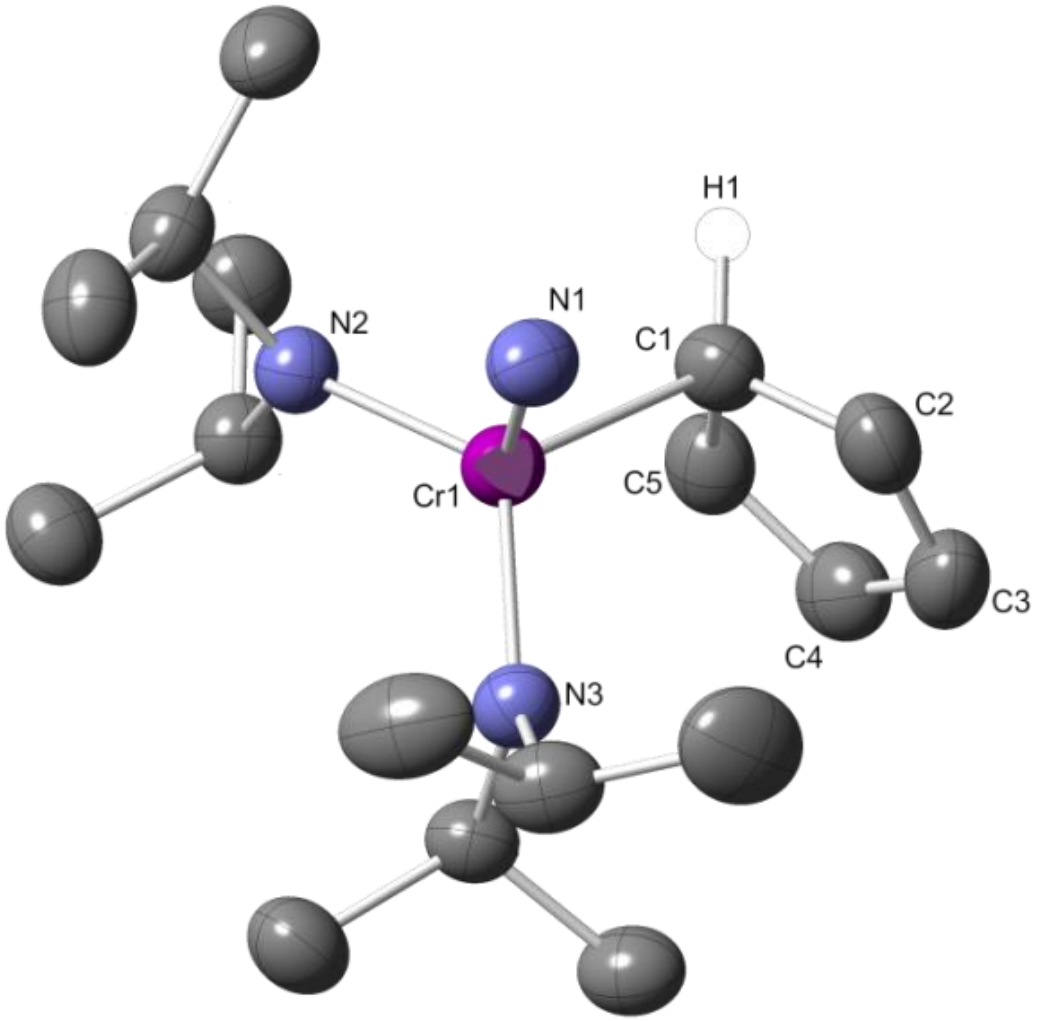

Figure 5.3: A crystal structure rendering of $NCr(NPr^{i}_{2})_2(\eta^{1}\text{-Cp})$ **3**. Thermal ellipsoids at 50% probability and H atoms removed except for calculated H on C1.

5.3 Synthesis of $[NCr(NPr^{i}_{2})_2DBN][I]$ (2), $NCr(NPr^{i}_{2})_2(Ind)$ (4), and $NCr(NPr^{i}_{2})_2(Flu)$ (5) and Synthesis and Structure of Thallium(I)indenide

We were similarly interested in the electronic and structural features of indenyl and fluorenyl complexes of Cr(VI) nidrides. Synthesis of these complexes through similar methods as **3** proved to be low yielding. Production of **4** and **5** was achieved by using the cationic Cr(VI) complex $[NCr(NPr^{i}_{2})_2DBN][I]$ (**2**).

Compound **2** is generated in high yield by treatment of **1** with one equivalent of 1,5-Diazabicyclo[4.3.0]non-5-ene (DBN), which readily displaces an iodine ligand into the outer coordination sphere (Figure 5.5).

Diffraction quality crystals of **2** were grown from a cold THF solution. Analysis shows a Cr-N4 bond length of 1.9728(18) Å. This contact is surprisingly short for a formally dative bond when compared to the average Cr-N amide bond length in 2 (1.8156 Å) and the Cr-N pyrrolide bond distance in $NCr(NPr^{i}_{2})_2(Pyr)$ (1.946(2) Å) where little π-bonding to empty d orbitals is observed.

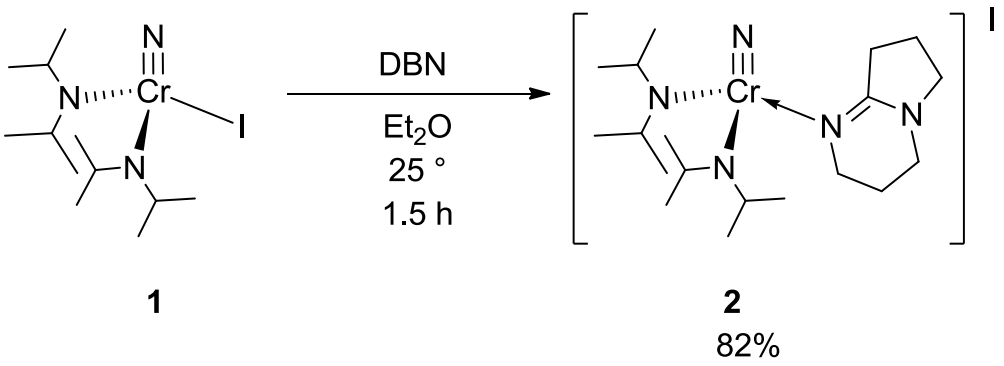

Figure 5.5: Synthesis of $[NCr(NPr^{i}_{2})_2DBN][I]$ (**2**).

^{13}C NMR analysis shows a downfield shift of the imine carbon resonance in **2** when compared to free DBN (169.30 ppm and 160.16 ppm respectively). This deshielding effect suggests that a resonance form that delocalizes cationic charge from the Cr(VI) on the carbon is a significant contributor to the structure of **2**. Consequences of the I^- anion on the properties of **2** are unknown but are currently being investigated.

Synthesis of $NCr(NPr^{i}_2)_2$(ind) (**4**) (ind = indenide) was realized by a salt metathesis reaction of **2** with a slight excess of Tl indenide in THF (Figure 5.6).

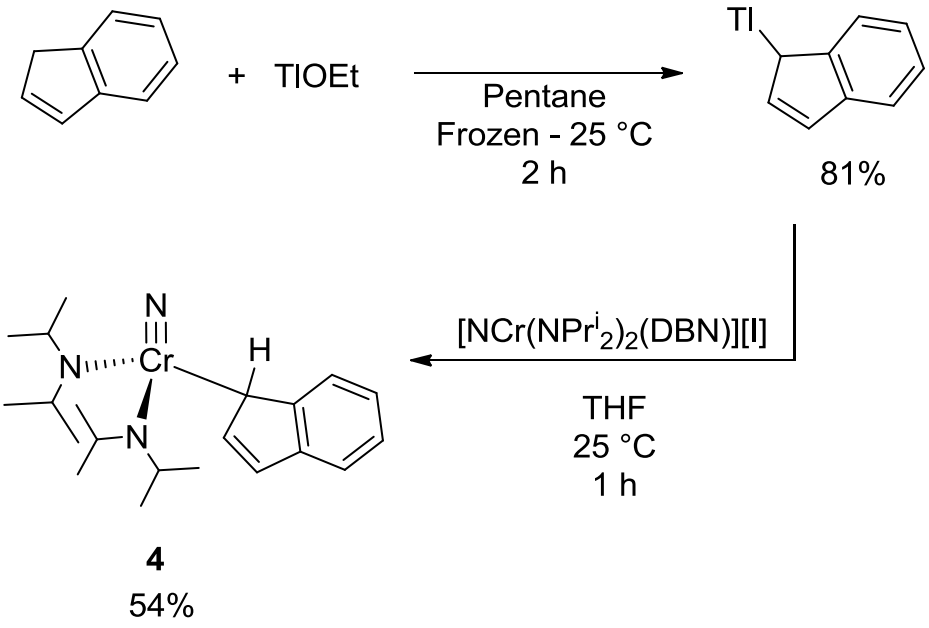

Figure 5.6: Synthesis of **4** using thallium(I) indenide.

Thallium indenide was first generated by reaction of thallium(I) ethoxide with freshly distilled indene in pentane. The yellow-orange powder was unstable at room temperature for extended periods and readily precipitated Tl metal. Interestingly, the bulk solid was observed to be thermochromic, shifting from yellow to orange in the temperature range −35 °C – 25 °C. This property has also been briefly noted by Janiak for the related TlCp.[16]

In attempt to determine the structural nature of this effect, crystals of Tlind were grown from a concentrated THF solution held at −35 °C as yellow needles. Single crystal diffraction carried out at 173 K revealed an asymmetric unit containing 2 atoms of thallium, 2 disordered indenides, and one unbound THF as a solvent of crystallization. Indenides appear to be bound η^1 via the 5 member ring to one Tl (with an average bond distance of 2.99 Å), with the six member ring

datively bound to the other Tl. This differs significantly from the known crystal structures of $TlCp$[17] and $TlCp^*$[18], both η^5 polymeric half sandwich complexes with average Tl-Cp bond distances of 2.73 Å and 2.96 Å respectively. Crystals of Tlind also exhibit a close inter atomic distance between Tl centers of 3.6207 (17) Å, shorter than the sum of the Bondi radii for Tl (3.92 Å).[19]

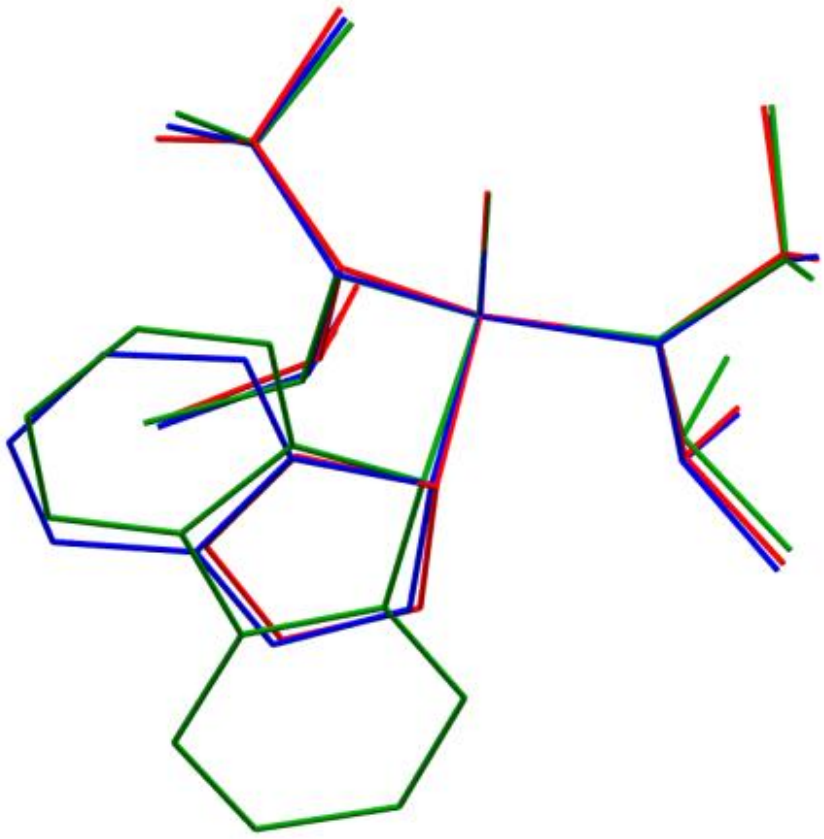

Figure 5.7. Overlaid structures of $NCr(NPr^i_2)_2(X)$ where X = Cp (**3)** (red), Indenyl (**4**) (blue), and fluorenyl (5) (green).

Unfortunately, variable temperature data collection was unsuccessful, bound by the lower limit of our instrumentation, and by poor diffraction intensity at higher temperatures. The asymmetric unit however remained unchanged when the crystal was cycled from 298 K back to 173 K,

which may rule out the exclusion of the solvent of crystallization as giving rise to the thermochromicity.

Similarly $NCr(NPr^i_2)_2$(flu) (**5**) (flu = fluorenyl) was synthesized in moderate yield from the reaction of **2** with one equiv. of LiFlu generated *in situ* from stoichiometric amounts of fluorene and ^{n}BuLi in THF.

5.4 Structures of $NCr(NPr^i_2)_2$(Ind) (4) and $NCr(NPr^i_2)_2$(Flu) (5) and Steric Evaluation

Compounds **4** and **5** show structural similarities to **3** in the solid state, with the bound 5 member ring adopting an η^1 configuration in each (Figure 5.7). Alternating bond lengths within the 5 member rings of **4** and **5** are similar to those of Cp suggesting the localization of multiple bonding character typical of the η^1 binding mode. Likewise the sp^3 hybridization around C1 suggests this binding mode as all the carbons in an aromatic η^5 Cp must be sp^2. Summarized in Table 5.1, Cr-C bond lengths to the bound carbon is the same within ESDs for each, and thus not a reliable indicator of the electronic differences within the series.

Compound	Cr-C1 distance (Å)	Avg. Bond angle around C1	$\%V_{bur}$	$G_m(L)$
$NCr(NPr^i_2)_2(Cp)$ (**3**)	2.115(2)	109.3°	24.88	20.87
$NCr(NPr^i_2)_2(Ind)$ (**4**)	2.108(4)	109.3°	25.19	22.31
$NCr(NPr^i_2)_2(Flu)$ (**5**)	2.102(7)	109.4°	26.73	23.48
$NCr(NPr^i_2)(O_2CPh)(Cp)$ (**6**)	2.228(3)	119.73°[a]	36.08	31.83

[a] Only H1-C1-C2, H1-C1-C5, and C2-C1-C5 angles included.

Table 5.1: Chromium-carbon bond distances and average angle around C1 in compounds **3-5**. Steric parameters of $\%V_{bur}$ and $G_m(L)$ of the X ligand, both as percentages.

Granted the binding of each ligand may be similar, the overall steric environment in **3-5** varies. To quantify this property, two individual methods were used in describing the added bulk away from the metal center.

In addressing sterics, the Tolman cone angle[20] traditionally used to evaluate ligand size has expounded upon in recent years with the need to describe unsymmetrical and unusually shaped ligands. One such system developed by Nolan and coworkers places the ligand of interest the correct bond distance (in this case crystallographically determined) from the center point of a sphere.[21] This sphere represents the first coordination sphere of a given metal, usually with a radius of 3.5 Å. Atomic radii of each atom within this 3.5 Å sphere are then used to calculate the

total volume of space occupied by the ligand. This is then compared to the total volume of the sphere and given as a single parameter, the percentage buried volume ($\%V_{bur}$).

Additionally, the sterics in compounds **3-5** were evaluated using the system of Soild Angles.[22] In this treatment the crystollographically determined positions of each compound are inscribed in a sphere of arbitrary radius. The metal center is treated analogous to a point source of light. Each ligand blocks a given amount of this 'light', casting a 'shadow' that is projected on the inside of the sphere. This area is compared to the total area of the sphere and is also given as a single parameter as a percentage, $G_m(L)$.

Results of these analyses summarized in Table 5.1 illustrate the differences within the ligand series as well as between the two systems of steric evaluation. Expectedly both systems track with increasing ring sizes. However, $\%V_{bur}$ only increases moderately, as not all of the the extended ring system of **4** and **5** are within the defined 3.5 Å coordination sphere. Likewise, the small increase seen in the Solid G analysis suggests that the subtle differences in sterics, and thus substrate access to a metal center are non-trivial, since large changes in reactivity are seen among catalysts bearing a series of Cp and derivative ligands.

5.5 LDP determination of compounds 3-5

With compounds **3-5** in hand we sought to evaluate the electronic differences between η^1-Cp, indenyl, and fluorenyl. Although they are sterically different (*vida supra*), the similar bond distances and exclusively σ-bonded coordination mode allows for a good comparison of their relative donor abilities to be made.

In C_{3v} compounds such as those above the similar symmetry of the d_{xy} and $d_{x^2-y^2}$ with the p_x and p_y orbitals form an pair of e-sets, assuming a z-axis along the Cr-nitrido bond vector. These orbitals act to accept σ and π electron density from the three ligands in the basal plane of $NCr(NPr^i_2)_2(X)$. Since the strongly donating nitride also π-donates into the d_{xy} /$d_{x^2-y^2}$ e-set, a situation arises whereas a 90° rotation of a basal ligand places π electrons in direct competition to donate into the same set of orbitals. This is manifested in a kinetically unfavorable barrier to bond rotation along the Cr-NPr^i_2 bond. To date all solid (ground) state geometries of $NCr(NPr^i_2)_2X$ compounds have diisoproplylamido ligands aligned such that the plane defined by $C_{methine}$-N-$C_{methine}$ is nearly parallel to the Cr-nitrido bond (the defined z-axis). The observed barrier of rotation along either Cr-NPr^i_2 therefore approximates the energy difference between the ground state geometry and one in which a 90° rotation of the NPr^i_2 ligand causes the unfavorable competition with the multiply bonded nitrido. It has further been established that greater donor ability of the X ligand in the basal set slightly attenuates this energy difference via ground state destabilization.

To quantify the effect of the X ligand on the system the barrier to Cr-amide rotation was observed in solution. The 1D ^1H NMR technique of Spin Satuaration Magnetic Transfer (SSMT)[23, 24] was employed to gauge the kinetics of the interchange between the magnetically inequivalent methine resonances of the NPr^i_2 ligand. Assuming an entropy of the $\Delta S^{\ddagger} = -9$ cal/mol K for each compound (experimentally derived for other $NCr(NPr^i_2)_2X$ compounds) the

enthalpy of the transition state of amide rotation, $\Delta H^{\ddagger}$ was used as a measure of the donor ability of X, defined as the Ligand Donor Parameter (LDP). Due to orbital mixing, σ and π contributions from the X ligand are also mixed (as in the case in most real world catalytic systems). This methodology has been shown to give a single, meaningful parameter of electronic donation in a highly diverse series of anionic monodentate ligands.

Although the above system does not give a definitive amount, as absolute ligand donor ability could/should vary from system to system, the relative ordering in such series is chemically relevant. Below are the experimentally derived LDPs of **3**-**5** (Table 5.2).

	Compound	LDP (kcal/mol)
(4)	$NCr(NPr^{i}_{2})_2(ind)$	13.76±0.270
(3)	$NCr(NPr^{i}_{2})_2(Cp)$	13.91±0.277
(5)	$NCr(NPr^{i}_{2})_2(flu)$	14.16±0.301

Table 5.2. Experimentally determined LDP values of **3**-**5**.

The following series of η^1-bound five member rings of Cyclopentadienyl, indenyl, and fluorenyl has closely spaced LDPs, giving the ordering of donor ability as Ind>Cp>Flu. However, these values are indistinguishable within experimental errors. This however does not impugn the usefulness of this type of donor evaluation, as small changes in the LDP in the test complexes can translate into significant differences in reactivity. LDP values on the order of 13.8 to 14.2 kcal/mol places the donor ability of these ligands similar to pyrrolyl (also bound η^1)

which has little π-donor ability from the bound N. In comparison, the indenlyl ligand is very similar to OBu^{t}_{F6} (LDP = 13.89±0.26), typically regarded as an electron poor alkoxide.

Slight variation in the series may be attributed to the available resonance structures in 5 member and higher ring systems. Furthermore the increased steric interaction of the larger rings may increase the barrier of rotation making the LDP parameter a lower bound to the donor ability.

5.6 Synthesis, Structure and LDP determination of $NCr(NPr^{i}_{2})(O_2CPh)(\eta^3\text{-Cp})$ 6

We were further interested in the substitution reactivity of compounds **3**-**5**. Treatment of **3** with excess lutidenium iodide and other halogenating agents did not yield mono or bis-halide products, even at elevated temperatures. Substitution of a single diisopropylamide ligand is possible by treatment of **3** with 1 equiv. of benzoic acid (Figure 5.8) yielding clean $NCr(NPr^{i}_{2})(O_2CPh)(\eta^3\text{-Cp})$ after crystallization from toluene layered with pentane. Attempts at multiple substitutions with additional benzoic acid led to no reaction.

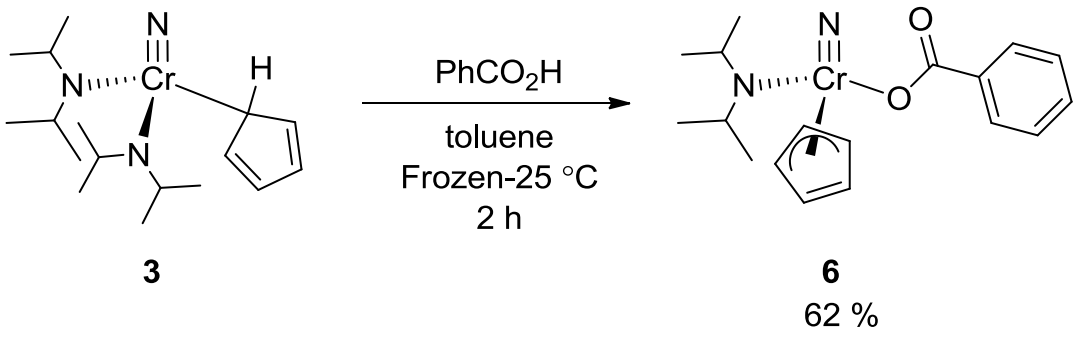

Figure 5.8: Synthesis of compound $NCr(NPr^{i}_{2})(O_2CPh)(\eta^3\text{-Cp})$ **6**.

Upon substitution a hapticity change in the Cp ligand was observed in the X-ray structure of **6** which crystalized as enantiomers in the space group $P2_1/c$ (Figure 5.9). Carbon atoms C1, C2,

and C3 adopt a geometry reminiscent of a π-allyl system, with C4 and C5 acting as an olefinic unit. This configuration was first described by Huttner and coworkers in the complex $W(CO)_2(Cp)_2$.[25]

Bond distances within the 5 member ring as well as interatomic distances to the bound metal are given in Figure 5.4, showing much closer contacts from the Cr to the carbons of the allylic unit. Planes defined by C1, C2, C3 and C2, C3, C4, C5 intersect at a 2.4° angle (as compared to 19.6° the corresponding atoms in $W(CO)_2(Cp)_2$) showing little deformation of the ring from planarity. In light of this planarity despite the distribution in chromium-carbon distances, the Cp of **6** might be best described as in a 'slipped' η^3 bonding mode. In drawing the analogy to a bonding mode more often encountered with indenyl ligands, a commonly used metric can be used to describe the amount of 'slippage' versus an idealized pentohapto mode. Defined by the equation below, where M-C(X) is metal-carbon distance.[15] The Cp in **6** has a of ΔM-C = 0.215 Å, whereas typical η^5 complexes have a ΔM-C under 0.1 Å.

$$\Delta M - C = \left(\frac{M - C(3) + M - C(4)}{2}\right) - \left(\frac{M - C(2) + M - C(5)}{2}\right)$$

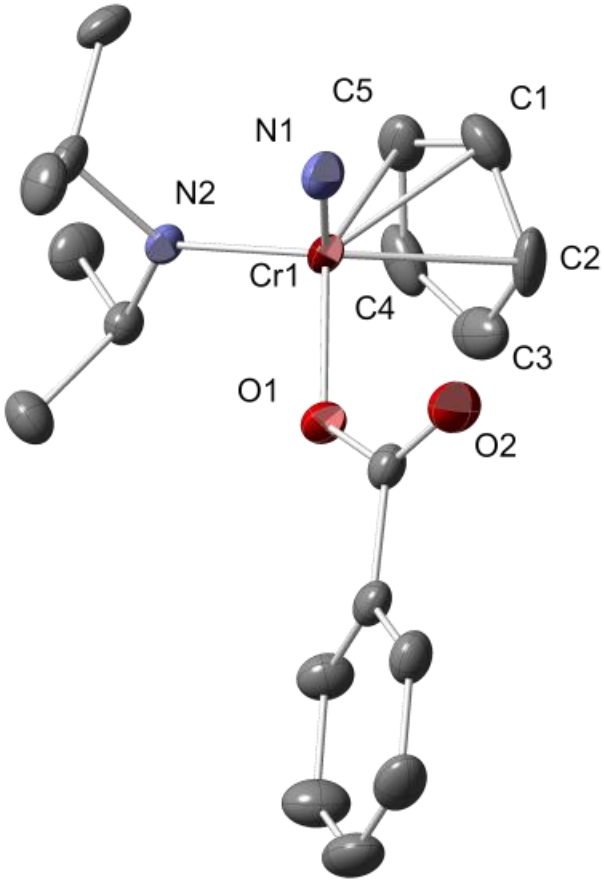

Figure 5.9. A crystal structure rendering of $NCr(NPr^{i}_{2})(O_2CPh)(\eta^3\text{-Cp})$ (**6**). Thermal ellipsoids at 50% probability. Hydrogen atoms omitted ford for clarity.

Moreover similarities to can be drawn to $W(CO)_2(Cp)_2$ as the authors note the 6π aromatic system of an η^5-Cp is broken to maintain an $18e^-$ complex rather than dissociation of a CO ligand. While formally a $16e^-$ complex, compound **6** shows a preference not to adopt an η^5 configuration realizing a full $18e^-$. This is not so surprising when viewed in the context of other nitride complexes of Cr(VI) such as the previously reported $NCr(NPr^{i}_{2})_2(O_2CPh)$, where the benzoate ligand remains κ^1, maintaining a $16e^-$ electronic structure.

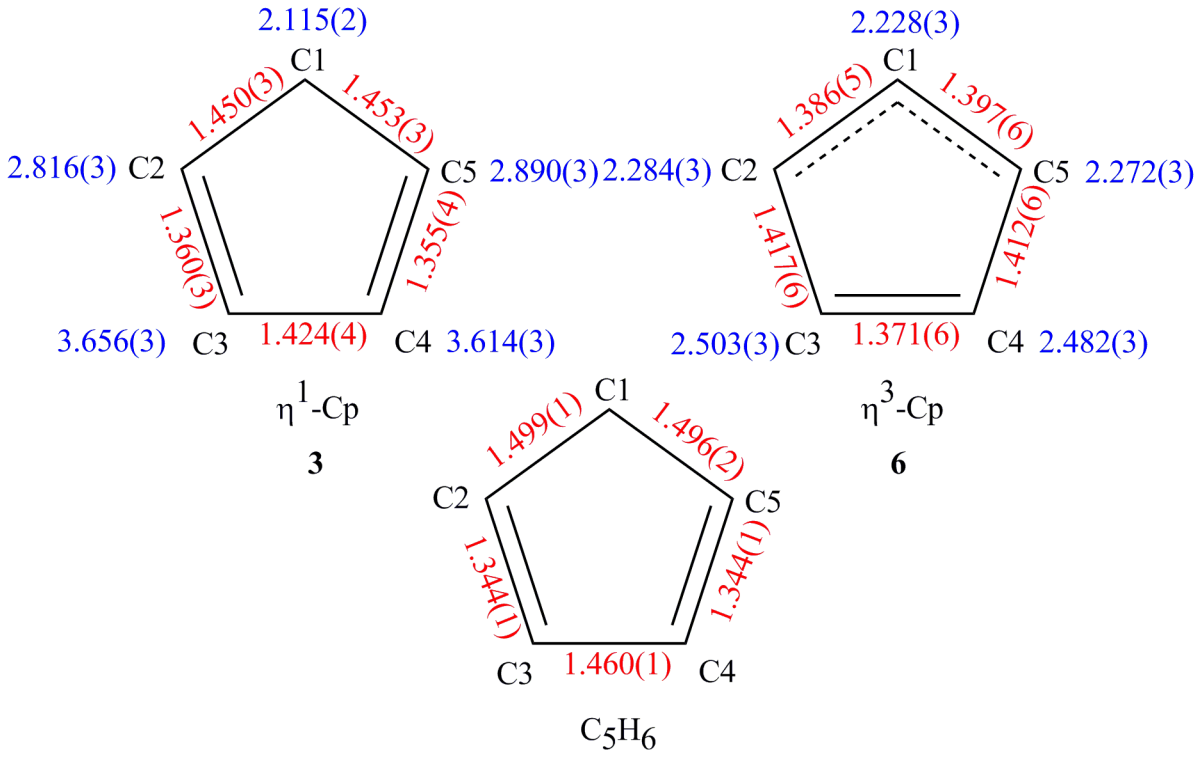

Figure 5.4. Crystallograpically determined interatomic Cr-C distances (blue) and C-C bond distances (red) in compounds **3** and **6**, with free C_5H_6 for comparison.

Furthermore, the benzoate ligand in complex **6** also remains κ^1 in the solid state with a Cr-O1 distance of 1.928(2) Å and a Cr-O2 distance of 3.169(2) Å (compared to $NCr(NPr^i_2)_2(O_2CPh)$, with Cr-O1 and Cr-O2 distances of 1.924(1) Å and 2.9664(15) Å respectively).

5.7: FT-IR Studies of $NCr(NPr^i_2)_2(O_2CPh)$ and $NCr(NPr^i_2)(O_2CPh)(\eta^3\text{-Cp})$ (6)

As seen in compounds of this type ligand bond distances are not always reliable to judge the nature of interactions to the metal. As such we investigated the coordination of the benzoate ligand in **6** by FT-IR spectroscopy. It has been noted by Deacon and Phillips that the stretches of

a metal bound carboxlate can be used to judge its denticity.[26] In this system a Δ value is determined by the difference of the symmetric, $\nu_s(CO_2^-)$ and asymmetric stretch, $\nu_a(CO_2^-)$ according the the formula below.

$$\Delta = [\nu_a(CO_2^-) - \nu_s(CO_2^-)]$$

Comparison of this value to the determined Δ value of the corresponding sodium or potassium salt of the ligand are made. Monodentate carboxalate ligands exhibit a Δ greater than their ionic (sodium) salts.[27] Likewise, bidentate ligands are marked by their significantly lower Δ values.

To identify these stretches isotopolagues of $NCr(NPr^i_2)_2(O_2CPh)$ and $NCr(NPr^i_2)(O_2CPh)(\eta^3$-Cp) (**6**) were synthesized, with a ^{13}C label at the carbonyl carbon on the benzoate ligand. Values of Δ in both cases were less than the measured $\Delta_{NaO2CPh}$ = 179.3 cm^{-1} (at 295.1 cm^{-1} and 223.7 cm^{-1} respectively) assigning both as κ^1. This is in agreement with the single crystal data, however both are solid state measurements. Attempts at solution IR measurements of the same type were unsuccessful due to solubility issues with the above complexes and the reference sodium benzoate.

5.8 Hapticity Shift as a function of π-loading in 6

Overall the Cp hapticity shift is consistent with the determined LDP values for the diisopropylamide and benzoate ligands, along with the penchant for Cr(VI) nitrides to adopt a $16e^-$ configuration. With LDP values of 11.12±0.23 and 14.45±0.28 kcal/mol respectively, much less electron density is donated to the metal in the case of a κ^1 benzoate. Although the additive effects of LDP are still under investigation, to a first approximation dividing the 2 values

suggests that the amide is about 1.3 times a better donor than benzoate. Thus replacement of NPr^{i}_{2} with O_2CPh would result in a more electron deficient metal center. Since the complex also contains a ligand capable of a hapticity shift (which upon doing so increases its formal contribution in electron counting) the η^3-Cp may be compensating for the loss of electron density.

Related complexes bearing multiple cyclopentyldienyl ligands of the form $M(Cp)_3X$ where M = Ti, Zr, or Hf and X = H, CH_3, OH, or NH_2, have been investigated by Bursten and coworkers.[28] The DFT calculations have determined that the resulting hapticity of the Cp is dependent on the ligand X, with lower hapticities favored as the π-donor ability of X increases. Such competition for orbital occupation can be described as π-loading, with filled-filled orbital interactions destabilizing coordinately saturated complexes.

The Mo(IV) complex $Mo(\eta^3\text{-Cp})(NMe_2)_3$ described by M. L. H. Green and coworkers displays a similar hapticity shift in the Cp ring upon ligand substitution.[29] Upon replacement of one dimethylamide ligand by a much less donating alkoxide[1] ligand the Cp moiety adopts an η^5 coordination. Assuming each amide formally donates $3e^-$, whereas alkoxides only contribute $1e^-$, an $18e^-$ complex is maintained after the transformation to $Mo(\eta^5\text{-Cp})(NMe_2)_2(OR)$ where R = Pr^{i} or Bu^{t}. Such an effect may be thought of as 'π-unloading', with a hapticity shift compensating for loss of electron density.

Moreover, the complex $Mo(\eta^3\text{-}Cp)(NMe_2)_3$ undergoes [1,2]-insertion of CS_2 giving the complex $Mo(\eta^5\text{-}Cp)(S_2CNMe_2)_3$, with a κ^1 and two κ^2 thiocarbamate ligands. Resulting in an $18e^-$ complex (assuming 1σ and 2π electrons from each κ^2-thiocarbamate ligand), the compound avoids a $20e^-$ configuration by not binding the last S moiety. This is very similar to the case of **6**, where increased hapticity (thus a greater electronic donation) of Cp out competes a ligand capable of κ^1 or κ^2 coordination.

Additionally, replacement of the bulky amide in complex **6** for the less sterically demanding benzoate relaxes congestion around the metal and may allow for the larger sterics of a higher hapticity Cp. As before both the methods of Solid G and $\%V_{bur}$ (31.83 and 36.08% respectively) suggests that the η^3-Cp in **6** is much bigger than the η^1-Cp of **3**. A $\%V_{Bur}$ of 36.08% places η^3-Cp as the largest ligand thus far encountered in our investigations of $NCr(NPr^i_2)_2(X)$ complexes, with the next largest being N^iPr_2 (29.1%). This is due not only to Cp's size but its proximity to the metal in **6**, as the large but distal sterics of $OSiPh_3$ have $\%V_{bur}$ of 22.2% (Figure 5.10). Comparing the $G_m(L)$ of **3** and **6** gives an increase of 10.96. To put this number into perspective a bound Cl ion has a $G_m(L)$ of 15.14.

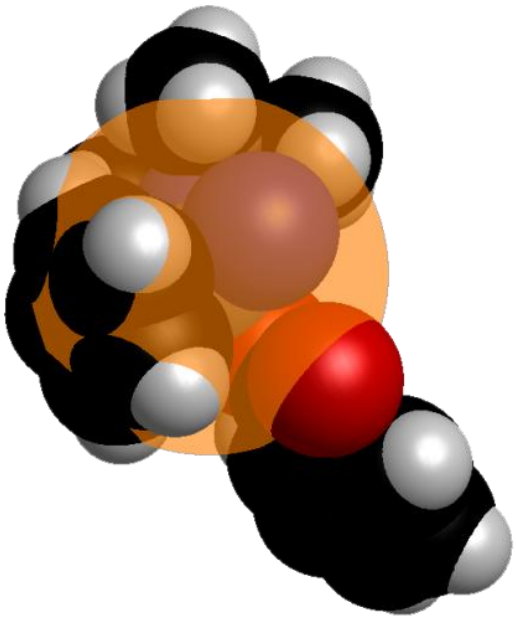

Figure 5.10: A space filling representation of NCr(NPr^i_2)(O_2CPh)(η^3-Cp) (**6**). The inscribed orange sphere with radius 3.5 Å approximating the 1st coordination sphere.

Since complex **6** also shows magnetically inequivalent resonances for the NPr^i_2 methines, SSMT was conducted giving a LDP of 16.53±0.30 kcal/mol. This comparatively large barrier to amide rotation is a function both of the new Cp coordination mode but also the loss one of the electron donating NPr^i_2 ligands. However, when compared to the LDP of NCr(NPr^i_2)$_2$(O_2CPh) (14.45±0.28 kcal/mol), only one ligand in the basal set has changed (i.e. replacement of NPr^i_2 by η^3-Cp).

Attempts at the synthesis of the indenyl analogue of **6** yielded only intractable products. Limited success in the synthesis of NCr(NPr^i_2)(O_2CPh)(flu) (**7**) through the same methods as **6** was low yielding. Attempts at isolation and purification via crystallization have yet to be

successful; however, the crude product was suitable to be evaluated by SSMT. The observed LDP of 14.68±0.30 kcal/mol is significantly greater than that of $NCr(NPr^{i}_{2})_2$(flu), it is drastically lower than that of compound **6**. Currently the relationship between contributions from multiple ligands as well as the alteration of the model system are not well understood. It is our hope that these effects can be derived from comparisons of compounds bearing two or more ligands in common from within in our series.

5.9 Conclusion

A series of complexes of the form $NCr(NPr^{i}_{2})_2$(X) whereas X = Cp (**3**), indenyl (**4**), and fluorenyl (**5**) were synthesized and structurally characterized, each having an η^1 interaction to the metal. In doing so a new reagent thallium indenylide was synthesised and structurally characterized. Additionally, the cationic Cr(VI) complex [$NCr(NPr^{i}_{2})_2$DBN][I] (**2**) proved to be a useful synthon, as well as an interesting compound which will be fully reported on elsewhere. Sterics in 3-**5** were evaluated by the method of Solid G and $\%V_{Bur}$ with both systems showing the expected trend of increasing size Cp<indenyl<fluorenyl. Compounds **3-5** were also evaluated via the method of SSMT giving LDPs of 13.91±0.277, 13.76±0.270 and 14.16±0.301 respectively. This suggests that the strength of donor abilities toward low valent metals nominally follows Ind>Cp>Flu although these are equivalent with error. Substitution of a diisopropylamide ligand on **3** affords the compound $NCr(NPr^{i}_{2})(O_2CPh)$(Cp) (**6**), which shows a slipped η^3-Cp in the solid state. This structural change can explained in terms of π-loading on the chromium center. FT-IR analysis reveals a κ^1 benzoate ligand in **6** and the related compound $NCr(NPr^{i}_{2})_2(O_2CPh)$, both in agreement with their solid state X-ray structures. Additional

investigations are underway to understand the individual ligand contributions to the overall measured LDPs.

5.10 Experimental

Synthesis of thallium(I) indenylide Under an inert atmosphere a scintillation vial was loaded with freshly distilled indene (1.48 g, 12.71 mmol, 1 equiv.), 8 mL pentane and a stir bar. The solution was cooled 10 min in a liquid nitrogen cooled cold well. To this vial thallium(I) ethoxide (3.17 g, 12.71 mmol, 1 equiv.), was added as a pentane solution (1 mL) and the solution turned yellow. The reaction was stirred 2 h at which time the volatiles were removed under vacuum. The solid was titrated twice with Et_2O, and left under dynamic vacuum for several hours yielding Thallium Indenylide as an orange-yellow powder (3.28 g, 10.27 mmol, 81% yield). Diffraction quality crystals were grown from a concentrated THF solution of 1 held at −35 °C. Mp: 114 °C (dec.)

Synthesis of [NCr(NPr$^{i}_{2}$)$_2$(DBN)][I] (2) Under an N_2 atmosphere a 125 mL Erlenmeyer flask was loaded with NCr(NPr$^{i}_{2}$)$_2$(I) (2.05 g, 5.20 mmol, 1 equiv.) a stirbar and 50 mL Et_2O. To this an Et_2O (10 mL) solution of DBN (0.646 g, 5.20 mmol, 1 equiv.) was added drop wise to the flask over 5 min. The solution stirred for 1.5 h during which time the product precipitated. The suspension was filtered on a glass frit and the washed with pentane (2 × 10 mL). The solids were collected and dried under reduced pressure yielding **2** as an orange powder (2.195 g, 4.24 mmol, 82% yield). Diffraction quality crystals were grown from a concentrated THF solution of **2** held at −35 °C. ^{1}H NMR (500 MHz, $CDCl_3$, 25 °C): 5.32 (sept. J_{HH} = 6 Hz, 2H, $(CH_3)_2CH$), 3.87 (sept. J_{HH} = 6.5 Hz, 2H, $(CH_3)_2CH$), 3.75 (t J_{HH} = 7.5 Hz, 2H, DBN), 3.63 (t J_{HH} = 5 Hz, 2H,

DBN), 3.48 (t J_{HH} = 6 Hz, 2H, DBN), 3.10 (t J_{HH} = 8 Hz, 2H, DBN), 2.11-2.04 (multi., 4H, DBN), 1.80 (d J_{HH} = 6 Hz, 6H, $(CH_3)_2CH$), 1.52 (d J_{HH} = 6.5 Hz, 6H, $(CH_3)_2CH$), 1.30 (d J_{HH} = 6.5 Hz, 6H, $(CH_3)_2CH$), 1.19 (d J_{HH} = 6.5 Hz, 6H, $(CH_3)_2CH$). $^{13}C\{^1H\}$ NMR (125 MHz, $CDCl_3$, 25 °C): 169.30, 59.44, 57.41, 55.15, 47.56, 43.68, 36.26, 30.89, 30.97, 22.79, 22.29, 20.50, 18.36. Anal. Calcd. for $C_{19}H_{40}CrIN_5$: C, 44.10; H, 7.79; N, 13.53. Found: C, 44.02; H, 7.63; N, 13.47. Mp: 168-170 °C.

Synthesis of $NCr(NPr^i_2)_2(Cp)$ (3) Under an inert atmosphere a scintillation vial was loaded with $NCr(NPr^i_2)_2(I)$ (**1**) (0.257 g, 0.654 mmol, 1 equiv.), 8 mL THF, and a stirbar. The solution was cooled to near frozen in a liquid nitrogen cooled cold well. To this a 2.0 M THF solution of sodium cyclopentadienide (0.98 mL, 1.96 mmol, 3 equiv.) was added, and the solution was rapidly stirred for 20 h. The volitiles were removed in vacuo, and the residue was extracted with pentane (2 × 10 mL) and filtered through Celite. The volitiles were removed under vacuum yielding **3** as a brown powder. Diffraction quality crystals were obtained from a concentrated pentane solution of **3** held at −35 °C (0.152 g, 0.459 mmol, 70% yield). ^1H NMR (500 MHz, $CDCl_3$, −30 °C): 6.14 (s, 5H, C_5H_5), 4.89-4.85 (sept, 2H, $CH(CH_3)_2$), 3.59-3.55 (sept, 2H, $CH(CH_3)_2$), 1.72-1.71 (d, 6H, $CH(CH_3)_2$), 1.43-1.41 (d, 6H, $CH(CH_3)_2$), 1.05-1.01 (m, 12H, $CH(CH_3)_2$). $^{13}C\{^1H\}$ NMR (125 MHz, $CDCl_3$, −30 °C): 114.73, 57.98, 54.87, 30.25, 30.17, 23.10, 17.49. Anal. Calcd. for $C_{17}H_{33}CrN_3$: C, 61.60; H, 10.03; N, 12.68. Found: C, 61.59; H, 9.97; N, 12.65. Mp: 90-92 °C (sub).

Synthesis of NCr(NPr$^{i}_{2}$)$_2$(indenyl) (4) Under an inert atmosphere a scintillation vial was loaded with **2** (0.122 g, 0.237 mmol, 1 equiv.), 4 mL THF, and a stirbar. To this a THF solution (5 mL) of freshly prepared thallium(I) indenylide (0.076 g, 0.237 mmol, 1 equiv.) was added. The reaction stirred rapidly for 1 h. The volatiles were removed under reduced pressure. The residue was extracted with pentane until the extracts were clear. The extracts were filtered on a fritted funnel with Celite as a filtering agent. The pentane solution was concentrated under reduced pressure to 5 mL and held at −35 °C yielding crystals of **4** (0.049 g, 0.128 mmol, 54%). ^{1}H NMR (500 MHz, $CDCl_3$, 25 °C): 7.53-7.50 (multi, 2H, C_9H_9), 6.98-6.95 (multi, 3H, C_9H_9), 5.58 (s br. 2H C_9H_9), 4.75 (sept J_{HH} = 6.4 Hz, 2H, $CH(CH_3)_2$), 3.41 (sept J_{HH} = 6.1 Hz, 2H, $CH(CH_3)_2$), 1.39 (dd J_{HH} = 6.1 Hz J_{HH} = 13.9 Hz, 12H, $CH(CH_3)_2$), 0.97 (d J_{HH} = 6.3 Hz, 6H, $CH(CH_3)_2$), 0.83 (d J_{HH} = 6.1 Hz, 6H, $CH(CH_3)_2$). Mp: 138-140 °C.

Synthesis of NCr(NPr$^{i}_{2}$)$_2$(fluorenyl) (5) Under an inert atmosphere a scintillation vial was loaded with a fluorene (0.048 g, 0.287 mmol, 1 equiv.), a stir bar, and THF (8 mL). The vial was cooled in liquid nitrogen cooled cold well for 10 min. The vial was moved to a stir plate. To the rapidly stirring solution an ^{n}BuLi (0.179 mL, 0.287 mmol, 1 equiv.) was added drop wise over 5 min as a 1.6 M solution in hexane. The reaction was allowed to come to room temperature and stirred for 30 min, turning bright yellow. To the vial a solution of **2** (0.149 g, 0.287 mmol, 1 equiv.) in THF (5mL) was added. The reaction stirred for an additional 2 h. The volitiles were removed under vacuum. The residue was extracted with pentane until the extracts were clear. The extracts were filtered on a fritted funnel, with Celite as a filtering agent. The pentane

solution was concentrated under reduced pressure to 5 mL and held at −35 °C yielding crystals of **5** (0.039 g, 0.092 mmol, 32%). ^{1}H NMR (500 MHz, $CDCl_3$, 25 °C): 7.79 (d, J_{HH} = 8.9 Hz, 2H, $C_{13}H_9$), 7.74 (d, J_{HH} = 8.9 Hz, 2H, $C_{13}H_9$), 7.25 (t, J_{HH} = 7 Hz, 2H, $C_{13}H_9$), 7.15 (t, J_{HH} = 7.4 Hz, 2H, $C_{13}H_9$), 4.67 (s br., 1H, $C_{13}H_9$), 4.55 (sept J_{HH} = 6.4 Hz, 2H, $CH(CH_3)_2$), 3.43 (sept J_{HH} = 6.2 Hz, 2H, $CH(CH_3)_2$), 1.44 (d J_{HH} = 6.3 Hz, 6H, $CH(CH_3)_2$), 1.32 (d J_{HH} = 6.3 Hz, 6H, $CH(CH_3)_2$), 0.98 (d J_{HH} = 6.3 Hz, 6H, $CH(CH_3)_2$), 0.76\ (d J_{HH} = 6.3 Hz, 6H, $CH(CH_3)_2$).

Synthesis of NCr(NPr$^{i}_2$)(O_2CPh)(Cp) (6) Under an inert atmosphere a scintillation vial was loaded with **3** (0.178 g, 0.537 mmol, 1 equiv.), a stir bar, and toluene (4 mL). The vial was moved to a liquid nitrogen cooled cold well for 10 min. The reaction was stirred vigorously and benzoic acid (0.066 mg, 0.537 mmol, 1equiv.) in toluene (6 mL) was added drop wise over 5 min. The solution turned dark red and was allowed to stir at room temperature for 2 h. The volatiles were removed under reduced pressure and the residue was dissolved in 2 mL of toluene. The solution was filtered and layered with an equal volume of pentane and held at −35 °C yielding crystals of **6** (0117 g, 0.333 mmol, 62%). ^{1}H NMR (500 MHz, $CDCl_3$, 13 °C): 7.95 (dd J_{HH} = 8.25 Hz, J_{HH} = 1.5 Hz , 2H, Ar-*H*), 7.41 (tt J_{HH} = 7.0 Hz, J_{HH} = 2.5 Hz, 1H, Ar-*H*), 7.34 (t J_{HH} = 7.5 Hz, 2H, Ar-*H*), 6.14 (s, 5H, C_5H_5), 5.56 (sept. J_{HH} =6.0 Hz ,1H, $NCH(CH_3)_2$), 4.31 (sept. J_{HH} = 6.0 Hz ,1H, $NCH(CH_3)_2$), 2.11 (d J_{HH} = 6.0 Hz ,3H, $NCH(CH_3)_2$), 1.75 (d J_{HH} = 6.0 Hz ,3H, $NCH(CH_3)_2$), 1.29 (d J_{HH} = 6.0 Hz ,3H, $NCH(CH_3)_2$), 1.11 (d J_{HH} = 6.0 Hz ,3H,

NCH(CH_3)$_2$). $^{13}C\{^1H\}$ NMR (125 MHz, $CDCl_3$, 13 °C): 170.74, 135.26, 130.77, 129.66, 127.83, 108.22, 73.71, 63.71, 31.06, 29.83, 20.64, 20.15. FT-IR (KBr): 1639.2 cm^{-1}, 1415.5 cm^{-1}.

General Procedure for FT-IR Denticity Determination All FT-IR analysis was done on a Mattson Galaxy Series FTIR 3000 spectrometer. Samples were prepared by pressing ~10 mg of each compound into anhydrous KBr. The symmetric and asymmetric carbonyl stretches were identified by comparison to its isotopologue, ^{13}C labeled at the carbonyl carbon. Difference between the stretches in the sample were compared to the difference in the symmetric (ν_s = 1415.5 cm^{-1}) and asymmetric (ν_a = 1594.8 cm^{-1}) stretches in a sample of sodium benzoate in KBr, which had a value for $\Delta_{NaO2CPh}$ of 179.3 cm^{-1}.

REFERENCES

REFERENCES

(1) Kealty, T. J.; Pauson, P. L. *Nature* **1951**, *168*, 1039–1040.

(2) McKnight, A. L.; Waymouth, R. M. *Chemical Reviews* **1998**, *98*, 2587–2598.

(3) Miller, S. A.; Bercaw, J. E. *Organometallics* **2004**, *23*, 1777–1789.

(4) Brintzinger, H. H.; Fischer, D.; Mülhaupt, R.; Rieger, B.; Waymouth, R. M. *Angewandte Chemie International Edition in English* **1995**, *34*, 1143–1170.

(5) Resconi, L.; Cavallo, L.; Fait, A.; Piemontesi, F. *Chemical Reviews* **2000**, *100*, 1253–1346.

(6) Coates, G. W. *Chemical Reviews* **2000**, *100*, 1223–1252.

(7) DiFranco, S. A.; Maciulis, N. A.; Staples, R. J.; Batrice, R. J.; Odom, A. L. *Inorganic Chemistry* **2012**, *51*, 1187–200.

(8) Coe, B. J.; Glenwright, S. J. *Coordination Chemistry Reviews* **2000**, *203*, 5–80.

(9) Dehnicke, K.; Strahle, J. *Angewandte Chemie International Edition in English* **1981**, *20*, 413–426.

(10) Alyea, E. C.; Basi, J. S.; Bradley, D. C.; Chisholm, M. H. *Chemical Communications* **1968**, 495.

(11) Odom, A. L.; Cummins, C. C. *Organometallics* **1996**, *15*, 898–900.

(12) Haumann, T.; Benet-Buchholz, J.; Boese, R. *Journal of Molecular Structure* **1996**, *374*, 299–304.

(13) Jandciu, E. W.; Kuzelka, J.; Legzdins, P.; Rettig, S. J.; Smith, K. M. *Organometallics* **1999**, *18*, 1994–2004.

(14) Abernethy, C. D.; Clyburne, J. A. C.; Cowley, A. H.; Jones, R. A. *Journal of the American Chemical Society* **1999**, *121*, 2329–2330.

(15) Zargarian, D. *Coordination Chemistry Reviews* **2002**, *233-234*, 157–176.

(16) Janiak, C. *Journal fur praktische Chemie Chemiker-Zeitung* **1998**, *340*, 181–183.

(17) Frasson, E.; Menegus, F.; Panattoni, C. *Nature* **1963**, *199*, 1087.

(18) Kraus, H. J.; Otto, H.; Werner, H. *Journal of Organometallic Chemistry* **1986**, *315*, C57–C60.

(19) Bondi, A. *Journal of Physical Chemistry* **1965**, *68*, 441–451.

(20) Tolman, C. A. *Chemistry Reviews* **1976**, *77*, 313–348.

(21) Clavier, H.; Nolan, S. P. *Chemical Communications* **2010**, *46*, 841–61.

(22) Guzei, I. A.; Wendt, M. *Dalton Transactions* **2006**, 3991–9.

(23) Jarek, R. L.; Flesher, R. J.; Shin, S. K. *Journal of Chemical Education* **1997**, *74*, 978–982.

(24) Perrin, C. L.; Thoburn, J. D.; Kresge, A. J. *Journal of the American Chemical Society* **1992**, *114*, 8800–8807.

(25) Huttner, G.; Brintzinger, H. H.; Bell, L. G. *Journal of Organometallic Chemistry* **1978**, *145*, 329–333.

(26) Deacon, G. B.; Phillips, R, J. *Coordination Chemistry Reviews* **1980**, *33*, 227–250.

(27) Nakamoto, K. *IR and Raman spectra of Inorganic and Coordination Compounds 4ed*; 1986.

(28) Palmer, E. J.; Bursten, B. E. *Polyhedron* **2006**, *25*, 575–584.

(29) Yan, X.; Chernega, A. N.; Metzler, N.; Green, M. L. H. *Journal of the Chemical Society, Dalton Transactions* **1997**, 2091–2100.

Chapter 6: Synthesis, Structure, and LDP Determination of Organometallic Ligands on Chromium(VI) Nitrido Complexes

ABSTRACT

In expanding the series ligand parameterization using a Cr(VI) nitride platform complexes of the form $NCr(NPr^{i}_{2})_2(X)$ where X = CH_2SiMe_3 (**4**), $CH_2CMe_2(Ph)$ (**5**), CH_2CMe_3 (**6**), $CCSi(Pr^{i}_{3})$ (**7**), and $CC^{t}Bu$ (**8**) were synthesized. Using the technique of Spin Saturation Magnetization Transfer the kinetics of diisopropylamide rotation were determined and used to parameterize the donor ability of the organometallic ligand X. This ligand Donor Parameter (LDP) is given for complexes **4-8** and the known $NCr(NPr^{i}_{2})_2(CH_2SiMe_2(Ph))$ (**3**). Crystal structures of compounds **3-8** were used to quantify the sterics of each X ligand using the method of Percent Buried Volume and Solid Angle techniques. The complex $[NCr(NPr^{i}_{2})_2(C_2Ph)]_2$ (**9**) was also synthesized and structurally characterized showing a cumulated 4 carbon chain between two metal centers.

6.1 Introduction

In an effort to expand the scope of the preceding studies into the electronic and steric profiles of commonly used ligands, our attention turned toward X-type ligands bound through a metal carbon bond. Metal alkyls and aryls show many interesting features specific to ligand of the type. Our interest in this study had two main goals. Firstly, to find the effect of the hybridization of the bound carbon on the ligand's donor properties. Secondly, to determine if substituting a non-carbon atom β to the bound carbon had a measurable effect on its donor ability

toward a metal center. Well studied in the realm of organic chemistry, placement of a Si atom adjacent to a carbocation stabilizes the positive charge through hyperconjugation (Figure 6.1).[1]

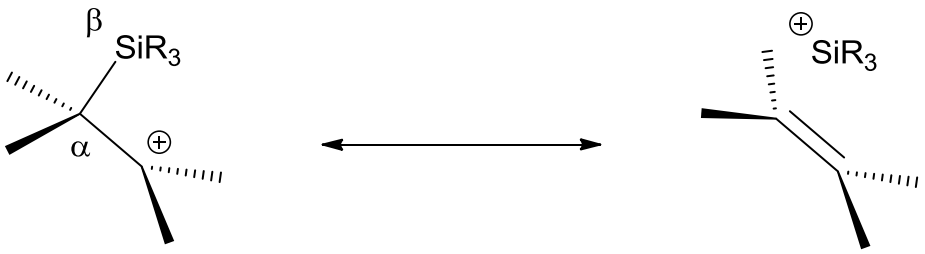

Figure 6.1: Hyperconjugation as seen in β-substituted carbocations.

Such stabilization may also be gained by orbital overlap of the empty p orbital of the carbocation with the larger filled σ orbital of a Si-C bond. Dubbed the β atom effect, the effect of a silicon atom in this position on a transition metal bound ligand is less well known despite been employed in many common organometallic ligands. Although Si is less electronegative than C any inductive effect is thought to be overshadowed by a larger resonance effect,[2] where the Si can go hypervalent, competing for the electron density donating into the transition metal. It follows that this may weaken the metal carbon linkage to some degree (Figure 6.1).

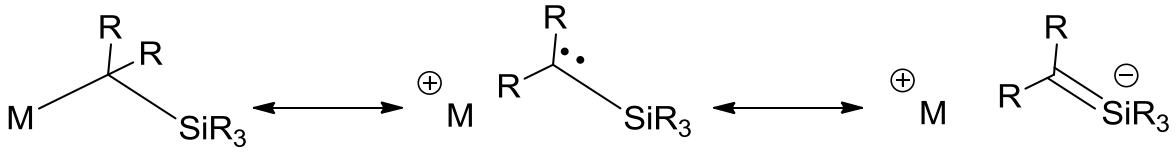

Figure 6.2: The ylide like resonance forms possible in β-silicon substituted metal alkyls.

Additionally, metal-carbon linkages are common in the intermediates and transition states of many metal-catalyzed organic transformation. Perhaps most notably M-C bonds are sequentially made and broken in group 10 cross-coupling chemistry, ubiquitous in modern

organic synthesis.[3] In rationally designing more efficient catalyst systems, knowing the nature of M-C bonded intermediates (i.e. measuring relative bond strengths) may be useful in preventing yield attenuating side reactions and catalyst decomposition pathways. The possible utility of measuring a standardized parameter such as the Ligand Donor Parameter (LDP) for these metal-carbon bonds is twofold.

Although there are very important differences between the late metals typically employed in cross-coupling and the early metals most relevant to or previous studies, we felt a series of LDP's measured on a d^0 system would be applicable to d^8 metal alkyl complexes. While the presence of metal based electrons occupying d orbitals may impede the usefulness of LDP with π –donor ligands such as amides and alkoxides, carbon bound organometallic ligands are σ only. As measured, LDP mixes σ and π electron donation from the ligand into one parameter. To a first approximation the LDP's of complexes bearing ligands with no π contribution will likely be invariant in correlations to known systems with d-orbital occupancy.

Perhaps more ambitiously, there has been a push in recent years toward developing early transition metal analogues to platinum group metals that can catalyze the cross-coupling of organic substrates. One such proof of concept system by Heyduk and coworkers uses zirconium bearing redox active ligands as a stand in for palladium. Here redox chemistry on the formally d^0 metal supports the oxidative addition[4] and reductive elimination[5] steps typically seen by the Pd(0)/Pd(II) redox couple in more orthodox systems. While more conventional early metal systems are known to react via σ bond metathesis[6] (yielding products as if oxidative addition and

reductive elimination were happening concurrently), this is a concerted reordering of bonds, thus unlikely to be useful in directed coupling of two different substrates.

To this end, a series of commonly employed organometallic ligands were affixed a Cr(VI) nitride complex of the form $NCr(NPr^{i}_{2})_{2}(X)$ so that their electronic and steric profiles could be quantified.

6.2 Synthesis of $NCr(NPr^{i}_{2})_{2}(X)$ X = Alkyl Complexes

Complexes of the type $NCr(NPr^{i}_{2})_{2}(X)$ where X is the monodentante, monoanionic ligand of interest are accessible through a variety of established methods.[7] In general complexes of this type bearing organometallic (i.e. carbon bound) X-type ligands are less stable than those bearing amide, halides, and alkoxydes. Specifically, two main decomposition products have been seen in the synthesis of virtually all of the $NCr(NPr^{i}_{2})_{2}(X)$ compounds reported; from trace amounts to the major product of reaction.

Firstly, the highly electron deficient Cr(VI) center in such complexes is prone to reduction by reagents appropriate in other systems for simple substitution chemistry. First described by Odom and coworkes,[8] $1e^{-}$ reduction to Cr(V) results in the bridging of nitridos between molecules, giving $[Cr(\mu\text{-}N)(NPr^{i}_{2})_{2}]_{2}$. This product was first seen as a decomposition product of thermally unstable Cr(VI) alkyls, and then intentionally synthesized with Na amalgam (Figure 6.3).

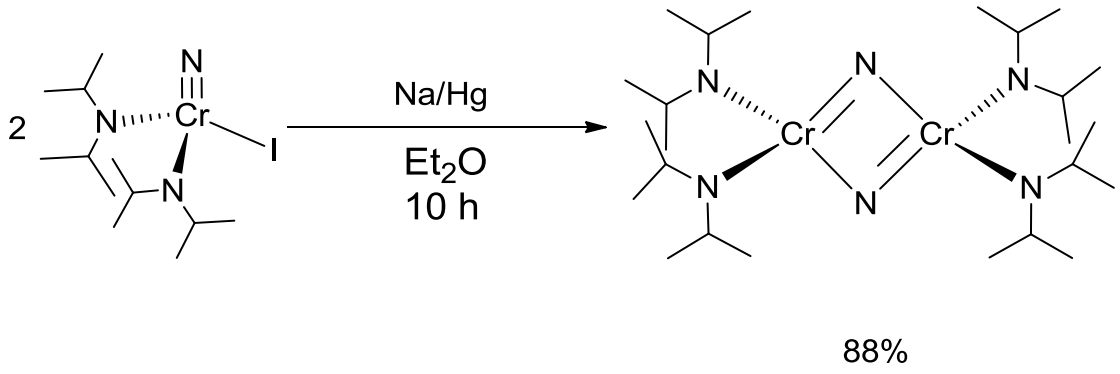

Figure 6.3: Synthesis of $[Cr(\mu\text{-}N)(NPr^{i}_{2})_2]_2$, the Cr(V)-Cr(V) dimer by reduction with sodium amalgam.

The reducing power of many lithium and sodium alkyl reagents was found to be sufficient to reduce typical Cr(VI) nidrido starting materials appropriate for similar metathesis reactions with lithiumi alkyoxide or amide reagents. This issue was sidestepped by disfavoring electron transfer by using less polar solvents, lowering temperatures, and using more electron rich Cr(VI) alkyoxides as synthons in place of Cr(VI) halides. Thus judicious choice of both the reagent used to install the X ligand as well as the Cr(VI) nitride source is necessary.

Secondly, the imine product *N*-(propan-2-ylidene)propan-2-amine was recovered in many failed syntheses of Cr(VI) alkyls. We surmise that this is likely the result of the abstraction of the methine proton on one NPr^{i}_{2} ligand by the incoming carbanion, as the corresponding product of Li- or Na-alkyl protonalysis was also observed. Conversely, this product may be formed after the desired substitution has occurred, thus an endemic limitation of our system with specific X ligands.

In circumventing these synthetic pitfalls we found that the preparation of organometallic Cr(VI) nitridos are highly sensitive to reaction conditions, such as solvent, temperature, time, and the transmetallation reagents chosen.

One of the earliest Cr(VI) alkyls known was prepared by the Cummins group using $CH_2SiMe_2(Ph)$, commonly known as the silyneophyl[9] ligand (Figure 6.4).[8,10] Using this as a starting point, the neophyl ligand,[11] $CH_2CMe_2(Ph)$ ligand was installed (Figure 6.4).

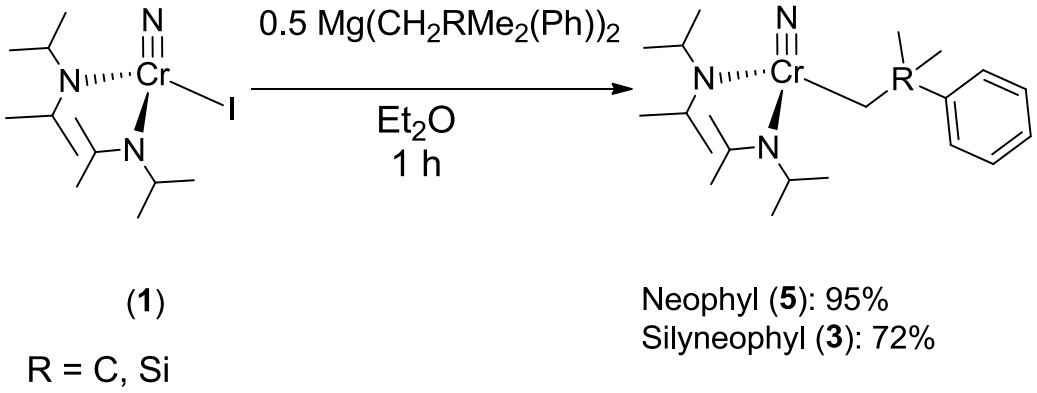

Figure 6.4: Synthesis of $NCr(NPr^i_2)_2(CH_2SiMe_2(Ph))$ (**3**) and $NCr(NPr^i_2)_2(CH_2CMe_2(Ph))$ (**5**).

The synthesis of $NCr(NPr^i_2)_2(CH_2CMe_3)$ (**6**) and its silicon substituted analogue $NCr(NPr^i_2)_2(CH_2SiMe_3)$ (**4**) were accessible through the above procedure, however yield and purity was low, as $NCr(NPr^i_2)_2(I)$ (**1**) is reduced to the Cr(V) dimer under the attempted conditions. Instead for **4** and **6** the use of the more electronically rich alkoxides $NCr(NPr^i_2)_2(OPh)$ (**2**)[10] and $NCr(NPr^i_2)_2(OAd)$ where Ad = 1-adamantanyl were a more

advantageous starting materials with the reducing neopentyl[12] and trimethylsilymethyl lithium (Figure 6.5).

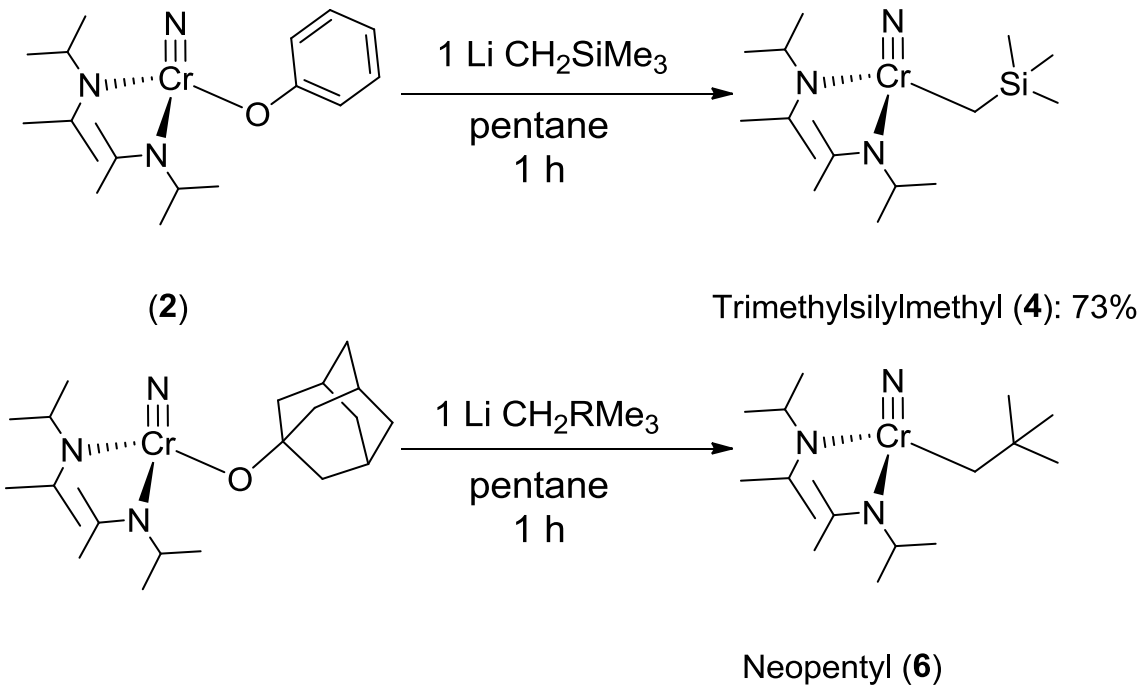

Figure 6.5: Synthesis of $NCr(NPr^{i}_{2})_2(CH_2CMe_3)$ (**6**) and $NCr(NPr^{i}_{2})_2(CH_2SiMe_3)$ (**4**).

6.3 Synthesis of $NCr(NPr^{i}_{2})_2(X)$ X = Alkynyl Complexes

In expanding our series, alkynyl substituents were installed onto Cr(VI) to judge the effect of hybridization of the bound C atom upon overall ligand donor ability. The Cr-alkynyl complexes $NCr(NPr^{i}_{2})_2(CC^{t}Bu)$ (**8**) and $NCr(NPr^{i}_{2})_2(CCSi(Pr^{i}_{3}))$ (**9**) were synthesized in good yield from treatment of **2** the corresponding lithium alkynyls (Figure 6.6).

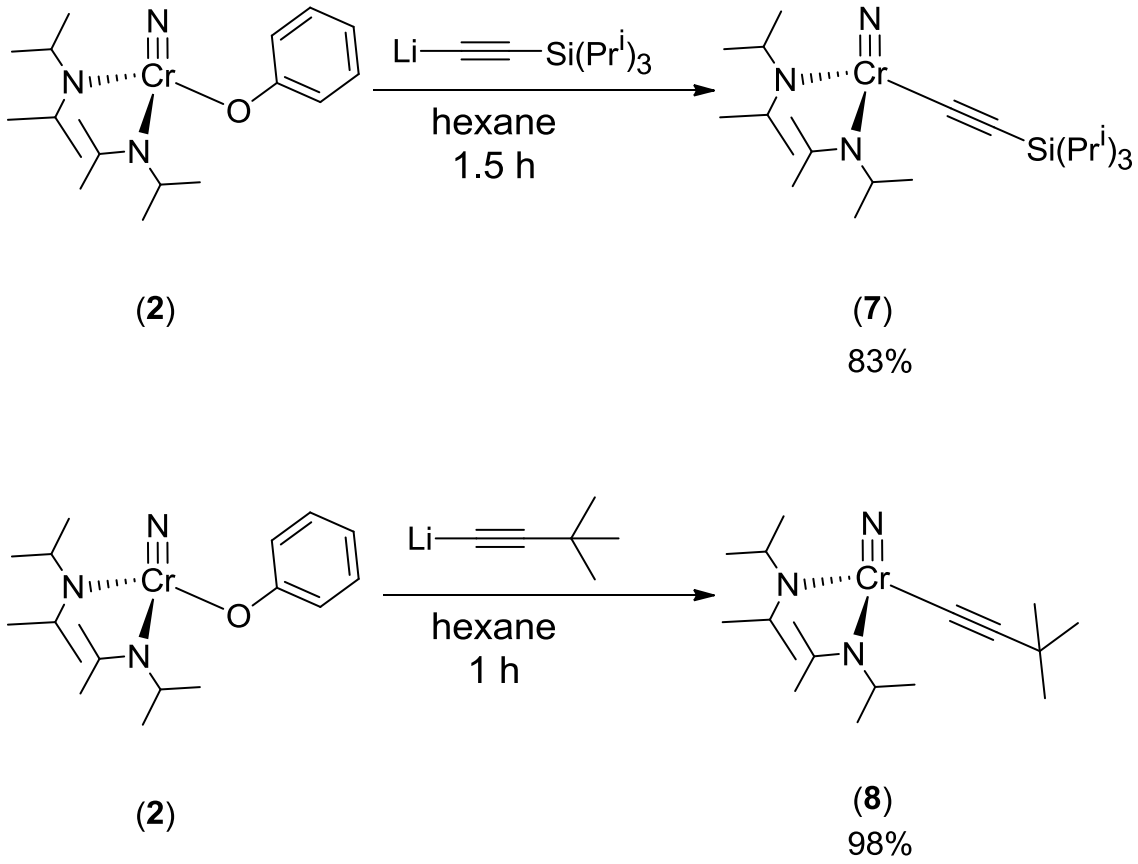

Figure 6.6: Synthesis of NCr(NPr$^i_2$)$_2$(CC^{t}Bu) (**8**) and NCr(NPr$^i_2$)$_2$(CCSi(Pr$^i_3$)) (**7**).

6.4 Synthesis and Structure of [NCr(NPr$^i_2$)$_2$(C$_2$Ph)]$_2$ (9)

Interestingly, a similar reaction to those above with an *in situ* generated Li-alkynyl of phenyl acetylene gave the dimer [Cr(μ-N)(NPr$^i_2$)$_2$]$_2$, as well as various other intractable metal containing species. An alternative synthetic strategy using a presumed *in situ* generated zincate also failed give the desired product, but gave an intriguing product found to be [NCr(NPr$^i_2$)$_2$(C$_2$Ph)]$_2$ (**9**) (Figure 6.7).

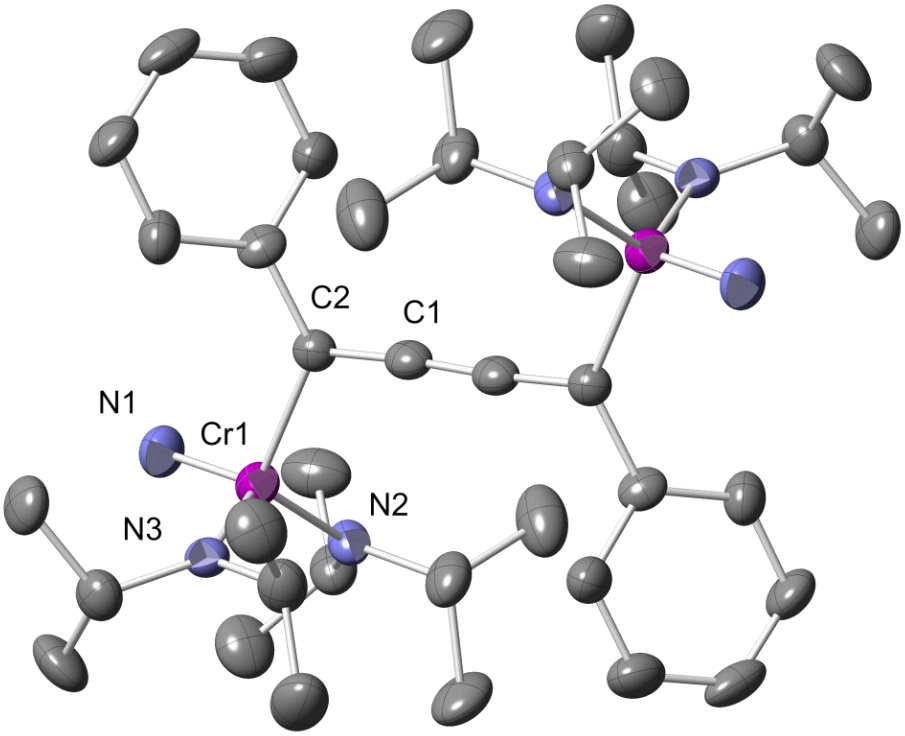

Figure 6.7: A crystal structure rendering of $[NCr(NPr^{i}_{2})_2(C_2Ph)]_2$ (**9**) showing a dimeric structure symmetric about the midpoint of the bridging allenyl moiety. Atom positions shown at 50% probability with H atoms removed for clarity.

As seen in other syntheses using Zn(II) or Mg(II) as transmettalating reagents for Cr(VI), both do not give appreciable amounts of the desired $NCr(NPr^{i}_{2})_2(X)$ product when a halide source is present (i.e. Grignard reagents of the form MgRX where X = Cl or Br will selectively transmetallate a halide ligand to $NCr(NPr^{i}_{2})_2(I)$ (**1**) or $NCr(NPr^{i}_{2})_2(OPh)$ (**2**) in most cases). This has also been observed with Zn reagents generated in situ from $ZnCl_2$. In fact, treatment of **1** with 1 equiv. of $ZnCl_2$ gives $NCr(NPr^{i}_{2})_2(Cl)$ in nearly quantitative yield.

To promote transfer of the desired R group, $ZnCl_2$ was treated with 2.02 equiv. of (phenylethynyl)lithium in cold THF. Transmetalation onto Zn(II) ostensibly creates the dialkynyl zincate, which upon reaction with **1** produces an unusual Cr(VI)-Cr(VI) dimer bridged through a cumulated ligand ligand.

A concentrated Et_2O solution held at –35 ºC yielded small orange crystals of **9** in the space group P1-, with half of the symmetric dimer in the asymmetric unit. Each Cr1-C2 bond length is 2.017(5) Å, statically shorter than the average corresponding Cr-C(sp^3) bonds of **3**-**6** at 2.047 Å and longer than the Cr-C(sp) bonds of **7**-**8** at 1.986 Å (*vida infra*). The bridging ligand consists of four nearly linear C atoms, with a torsional angle of C2-C1-C1'-C2' of 180°. Bond angles in the linkages of C2-C1-C1' and C2'-C1'-C1 are 174.75° and symmetric about the molecules' inversion center, midway between C1 and C1'. The C-C bonds are best described as double bonds, with a length of 1.324(4) Å between C2 and C1 and 1.270(6) Å between C1 and C1'. These bonds are characteristic of an allene like structure closely matching the corresponding lengths seen in Ph(H)C=C=C=C(H)Ph of 1.343(6) Å and 1.322(6) Å for terminal C=C bonds and 1.256(6)Å for the internal C=C linkage.[13] This alternation of longer Csp^2-Csp bonds with the shorter interior Csp-Csp bond has been noted in the case of butatrienes.[14]

Although the reaction by which **9** forms is currently not fully understood at present, the C_4 diacetylene moiety has been known to undergo redox chemistry when bound to transition metals.[15]

6.5 LDP Determination of $NCr(NPr^{i}_{2})_2(X)$ Organometallic Complexes

With a broad ranging series of $NCr(NPr^{i}_{2})_2(X)$ compounds in hand, the kinetics of diisopropylamide rotation for the complexes bearing various organometallic ligands were evaluated via the method of Spin Saturation Magnetization Transfer as outlined in Chapter 4.[7] Assuming a $\Delta S^{\ddagger}$ of −9 cal/mol K the Ligand Donation Parameters (LDPs) derived for **3-8** are shown in Table 6.1.

With an LDP of 13.30±0.26 kcal/mol compound **7** is the most donating (i.e. has the lowest barrier to amide rotation) of all the organometallic ligands surveyed. This value places the alkynyl $CCSi(Pr^{i}_{3})$ as donating as the siloxide ligand $OSiPh_3$ (13.28±0.27 kcal/mol). Although the coordinated oxygen of $OSiPh_3$ has a lone pair of appropriate symmetry to donate into the empty d orbitals of Cr(VI) the Lewis acidic Si atom is thought to compete for this density, lowering the amount of π-donation (thus LDP) relative to other alkoxides.[16]

It is not surprising that **7** and the alkynyl $NCr(NPr^{i}_{2})_2(CC^{t}Bu)$ (**8**) (LDP = 13.73±0.14 kcal/mol) were relatively better donors than most organometallic ligands in the study, despite being bound via an sp carbon versus an less electronegative sp^3 carbon. Scholarship into the nature of metal-acetylide bonding has shown that the filled d orbital-π* interactions which play an important part in the bonding of the isoelectronic cyanide ligand are not predominate with acetylides.[17] Studies using a variety of techniques have suggested acetylide ligands act as weak π-donors toward metal centers with d orbital vacancies.[18,19] Homoleptic Cr(III), Fe(II), and

Co(III) complexes bearing alkynyl ligands have been prepared by Long and coworkers which show three strong charge transfer bands, assigned as one LMCT and two MLCT, suggesting alkynyls ability to also act as a π-donor.[20] In the case of Cr(III) the authors propose an estimate of the ligand field splitting parameter of Δ_o = 20,200 cm^{-1}, putting $CCSiMe_3$ after methyl (Δ_o = 20,800 cm^{-1})[21] but before chloride (Δ_o = 18,700 cm^{-1})[22] in the spectrochemical series. This value differs significantly from that of cyanide (Δ_o = 26,600 cm^{-1})[23] also suggesting a π-donating as opposed to a π-accepting role. Computational work by Floriani and coworkers on dinuclear transition metal species bridged by an C^{2-} unit also suggests that this behavior is more typical for early first row transition metals than for late, as the empty d orbitals are of a more appropriate energy to interact with the filled π-orbitals of the ligand.[24] As it relates to complex **7** and **8,** the predominate metal-ligand π interaction (if any) is of the ligand acting as a π-donor as there is formally no metal based electron density to back donate.

Graphically represented in Figure 6.8, the majority of **3-8** exhibited donor abilities closely spaced and within experimental error of each other. Of note however, the silyl analogues **3** and **4** were nominally stronger donors than their carbon congeners **5** and **6**. This might be a manifestation of the electronegativity differences between a carbon ligated methylene and a silyl ligated methylene playing more of a role in the LDP than hypervalent or hyperconjugated resonance structures.

Likewise, the expected trend in hybridization (i.e. more electronegative C atoms would be weaker donors) is not seen within the series beyond error. In fact the presumed most electronegative C_{sp} bound ligands (**7** and **8**) are at the stronger donating end of the series. This

may be due to π-effects as previously discussed, suggesting this added effect may trump the effect of the change in electronegativity of C with hybridization.

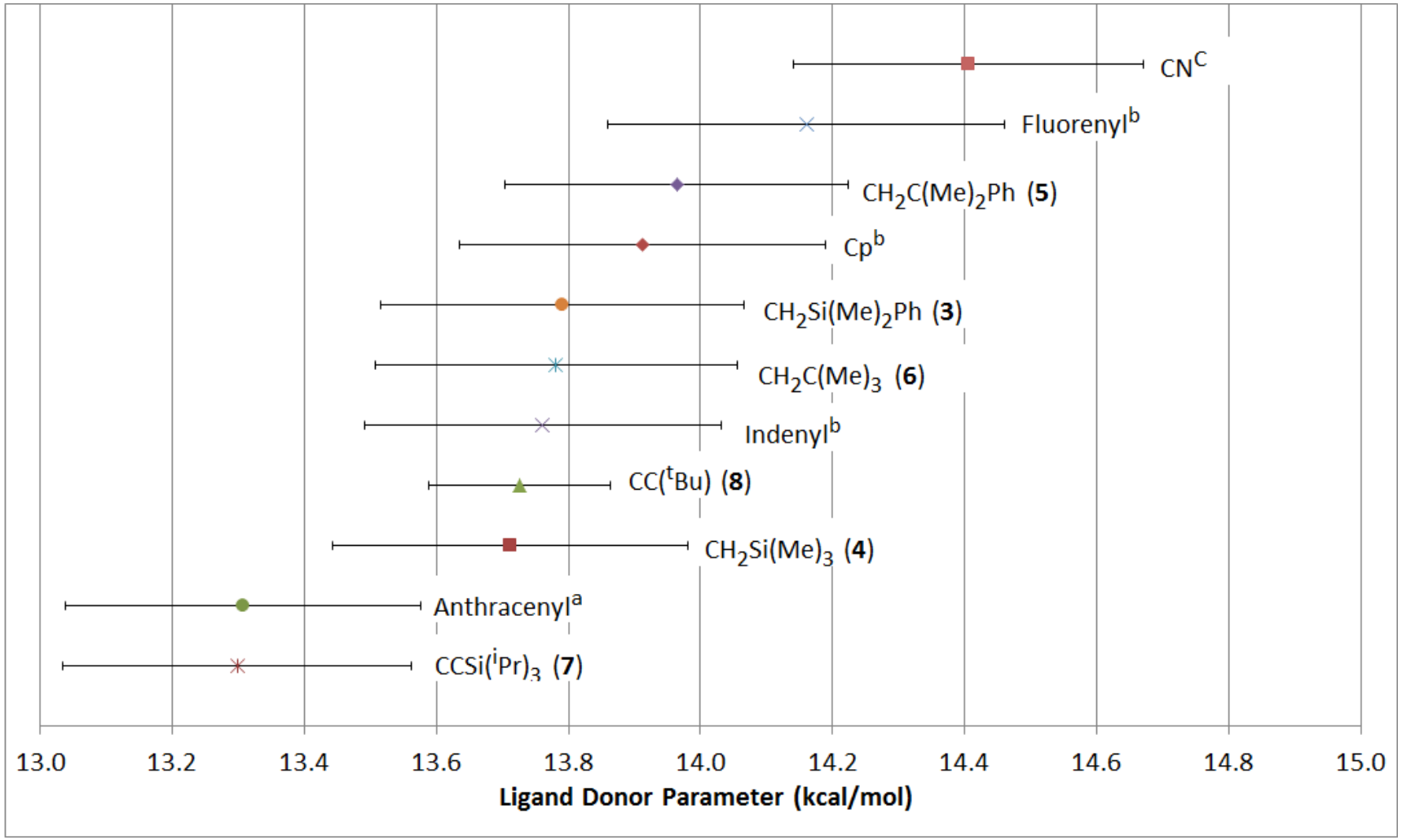

[a] Proposed but not fully characterized. [B] See Chapter 5. [C] See Chapter 4.

Figure 6.8: Ligand Donation Parameters of all C-bound X-type ligands evaluated with associated experimental errors. Lower barriers of amide rotation (stronger donors) displayed on the left.

Compound	LDP (kcal/mol)[a]	Cr1-C1 Bond Length (Å)	%V_{bur}	G_m(L)
$NCr(NPr^i_2)_2(CCSi(Pr^i_3))$ (**7**)	13.30±0.26[b]	1.997(7)	17.31	18.15
$NCr(NPr^i_2)_2(CH_2SiMe_3)$ (**4**)	13.71±0.27	2.046(2)	24.35	22.67
$NCr(NPr^i_2)_2(CC^tBu)$ (**8**)	13.73±0.14[b]	1.979(8)	17.43	18.57
$NCr(NPr^i_2)_2(CH_2CMe_3)$ (**6**)	13.78±0.27	2.061(3)	24.12	21.87
$NCr(NPr^i_2)_2(CH_2SiMe_2(Ph))$ (**3**)	13.79±0.28	2.041(5)	23.94	22.35
$NCr(NPr^i_2)_2(CH_2CMe_2(Ph))$ (**5**)	13.96±0.26	2.040(3)	24.62	24.75
$[NCr(NPr^i_2)_2(C_2Ph)]_2$ (**9**)	-	2.017(5)	-	-

[a] LDP calculated from the average of three SSMT runs. [b] LDP calculated from the average of six SSMT runs.

Table 6.1: Ligand Donation Parameter, Cr1-C1 bond distance, and the steric parameters $\%V_{bur}$ and G_m(L) of compounds **3-9**.

6.6 Structure and Steric Analysis of $NCr(NPr^{i}_{2})_2(X)$ Complexes

Like most of the previously synthesized $NCr(NPr^{i}_{2})_2(X)$ complexes those bearing organometallic ligands crystalize well from cold concentrated pentane solutions, sans for the highly lipophilic neopentyl compound (**6**). Along with the previously reported **3**, single crystal X-ray diffraction of **4-8** was collected to provide structural as well as quantitative steric assessment of each X ligand.

As is the case with the other X-type ligands previously evaluated, no correlation was seen between Cr1-C donar atom bond length and LDP *throughout the series*, reiterating that caution is necessary in comparing the relative donor properties of ligands solely by crystallographic parameters.

Structural comparison of **4** and **6** suggest that that Si for C substitution at the β has little effect upon the solid state structure. The average Cr-$N^{i}Pr_2$ bond distance in **4** of 1.815(3) Å is indistinguishable within ESD to that of **6** at 1.822(3) Å. Cr-C bond distances of 2.046(2) Å in **4** and 2.061(3) Å in **6** are statistically different, and do follow the initial expectation that stronger donors will have shorter Cr1-C bonds. The trimethylsilymethyl compound **4** has a N1-Cr1-C1-Si1 dihedral angle of 1.64(2)°, slightly smaller than the corresponding dihedral angle of the neopentyl **6** at −12.02(3)°. This structural similarity, especially of distal steric bulk in the *tert*-Si of C suggests that the barriers to rotation reported do not contain significantly different steric components when comparing **4** and **6**.

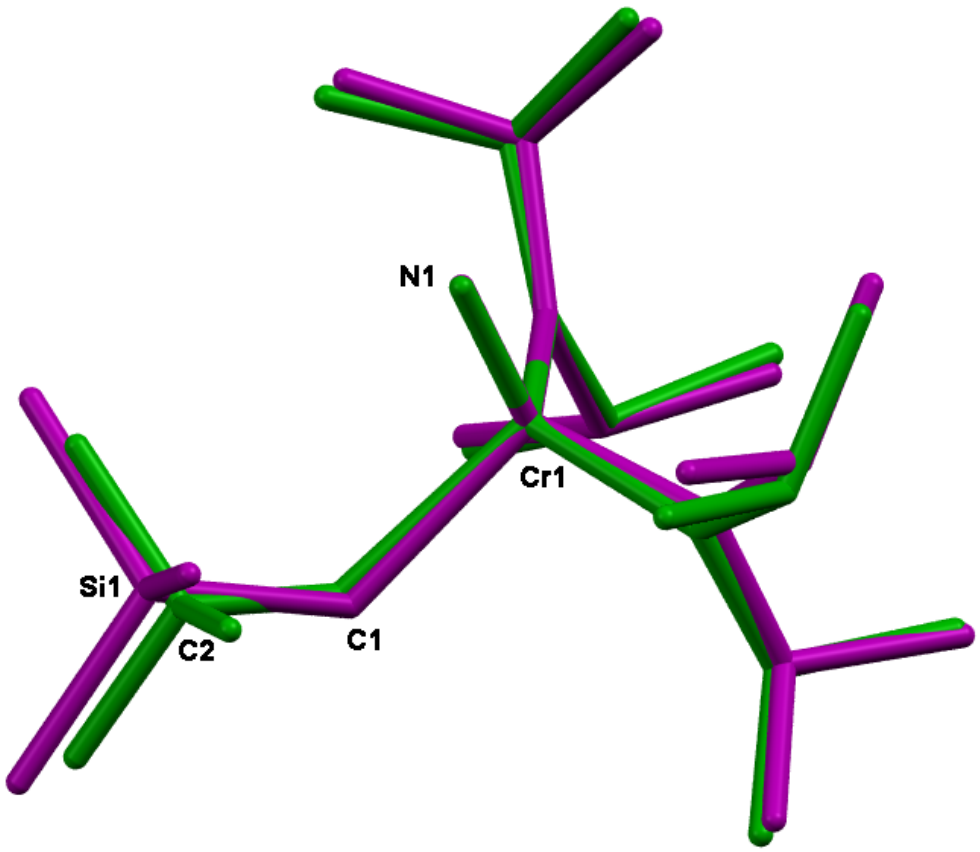

Figure 6.9: Crystal structure overlay of $NCr(NPr^{i}_{2})_2(CH_2SiMe_3)$ (**4**) (green) and $NCr(NPr^{i}_{2})_2(CH_2CMe_3)$ (**6**) (purple) showing a close structural similarity between the complexes.

The structures of the silyneophyl **3** and neophyl **5** complexes exhibit much less agreement upon the phenyl for methyl substitution on C2/Si1. Complexes **3** and **5** have nearly identical Cr1-C1 bond lengths but differing N1-Cr1-C1-C2/Si1tortional angles of 6.1(3)° and -26.22(3)° respectively. This change in orientation may be a manifestation of the unsymmetrical bulk held closer to Cr1 in **5** than in **3** due to the relatively shorter C1-C2 bond distance in **5** (1.535(5) Å) versus the C1-Si1 bond distance in **3** (1.832(4) Å).

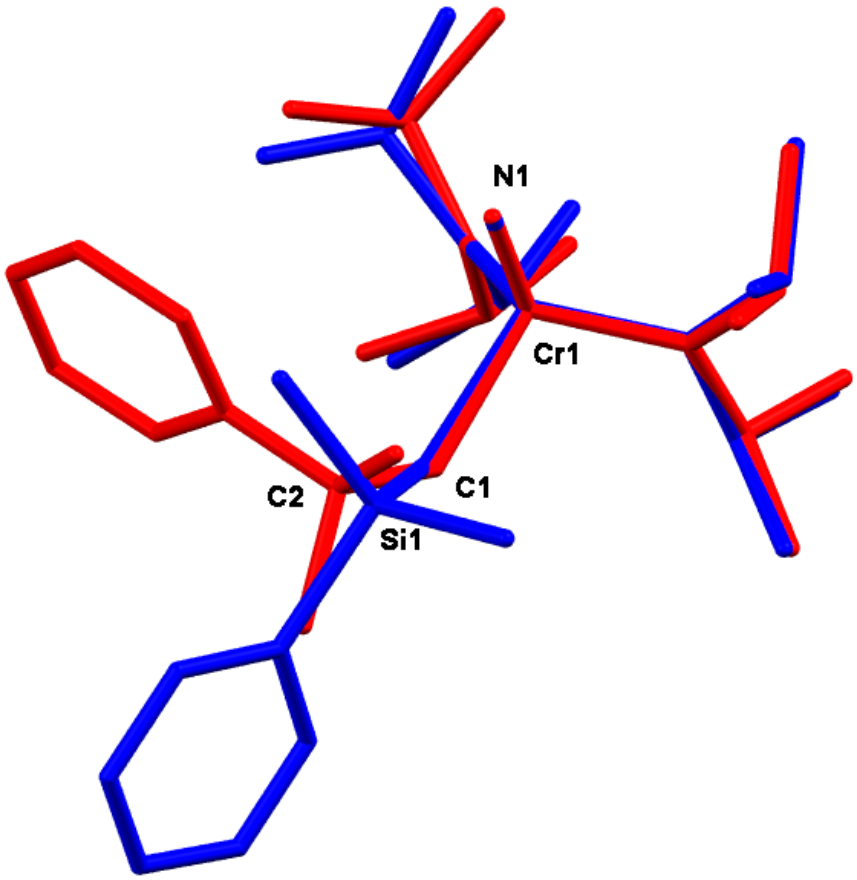

Figure 6.10: Crystal structure overlay of $NCr(NPr^{i}_{2})_2(CH_2SiMe_2(Ph))$ (**3**) (blue) and $NCr(NPr^{i}_{2})_2(CH_2CMe_2(Ph))$ (**5**) (red).

To address the overall steric profile of **3-8** quantitatively, two separate methods were employed using the atomic positions gained from single crystal x-ray diffraction. For an in depth discussion of the method of solid angles using the Solid G[25] program**,** and a calculation of occupied volume, $\%V_{bur}$[26] please refer to Appendix B. Tabulated data are listed in Table 6.1.

When addressing the amount of space occupied by each alkyl or alkynyl ligand via the method of $\%V_{bur}$, a sphere of 3.5 Å is circumscribed around the metal center approximating the

first coordination sphere of the Cr(VI) center. The volume of this sphere occupied by the constituents of a given ligand are then compared to the total volume and given as a percentage. This regime sharply discriminates between ligands like the CC^{t}Bu in **8 (**17.43%**)** and the neopentyl of **6** (24.12%). Although they both contain a *tert*-butyl moiety, and CC^{t}Bu even contains one more C atom it occupies a significantly lower percentage. This is due to the linear orientation of the CC^{t}Bu placing the bulk of the sterics outside the sphere of enclosure, in spite of the shorter Cr-C1 bond distance in the alkynyl relative to the alkyl. Illustrated in Figure 6.11, this rift is apparent for the other alkynyls and alkyls in the series. When compared to other ligands treated in the same manner (Chapter 4 and Appendix B), the common alkyl ligands tested rank among some of the largest in terms of $\%V_{bur}$ falling between OBu$^{t}_{F6}$ (23.6%) and NMe(Ph) (25.9%). Conversely, the alkynyls tested, sit at the low end of all the ligands tested, about the size of chloride (16.8%).

When approached from a solid angle standpoint, the description of sterics is geared toward substrate access to the metal center. By treating the Cr(VI) center as a point source of light each bound ligand casts a 'shadow' on an arbitrarily sized sphere inscribing the complex.

The area of this shadow is calculated and also given as a percentage of the total area of the sphere. The steric parameter calculated in this way by the Solid G program for **3-8** are shown in Figure 6.12. While the alkynyl substituents are still smaller, the effect of moving steric bulk distal to the metal is attenuated. In the context of other ligands examined organometallic ligands span the range of G(L), from CCSi(Pr$^{i}_{3}$) (18.15%) comparable to CN (17.08%) to neophyl (24.75%) like the large OBu$^{t}_{F6}$ (24.71%).

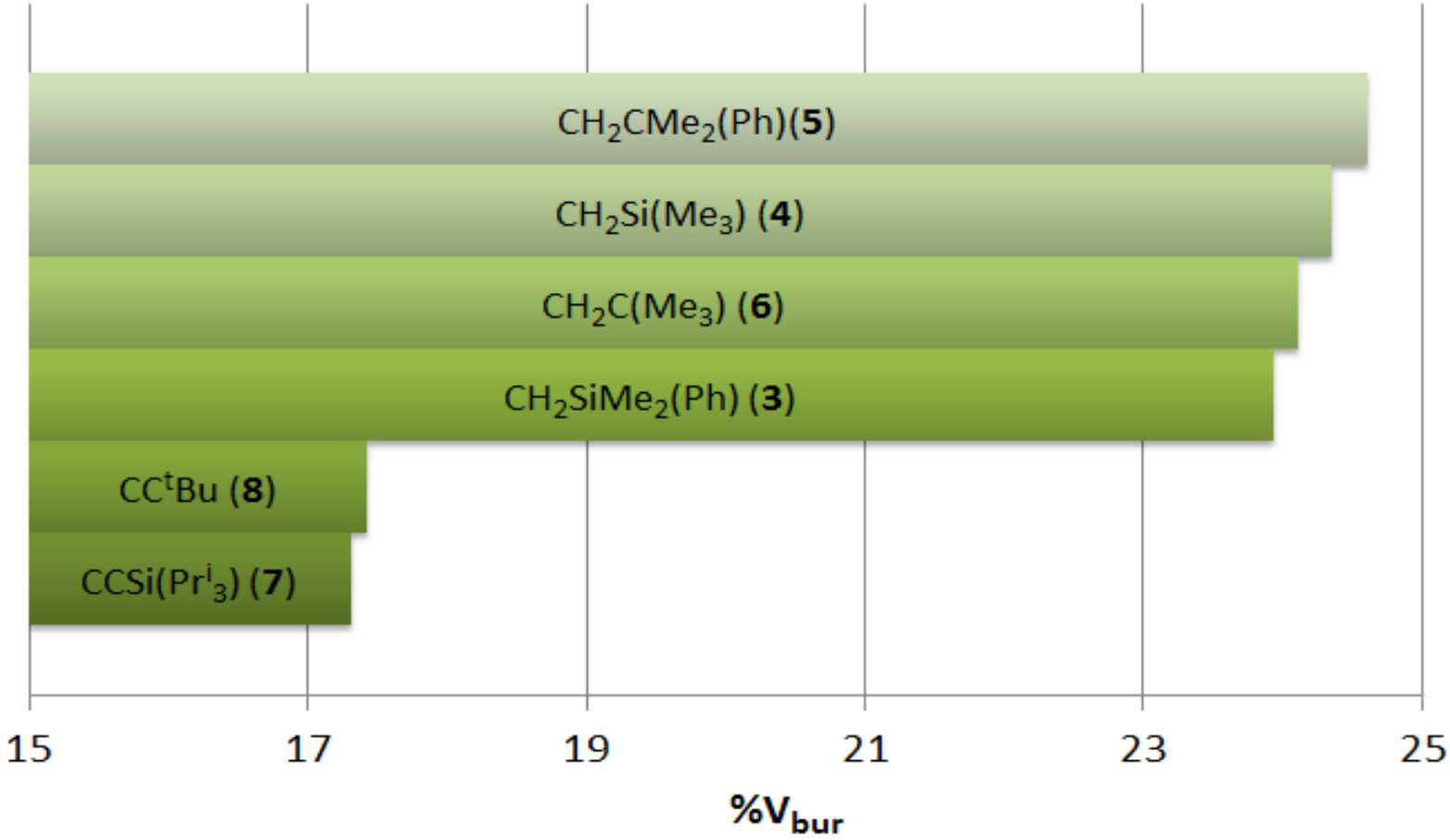

Figure 6.11: $\%V_{bur}$ Calculated for each ligand in **3-8** in a 3.5 Å sphere.

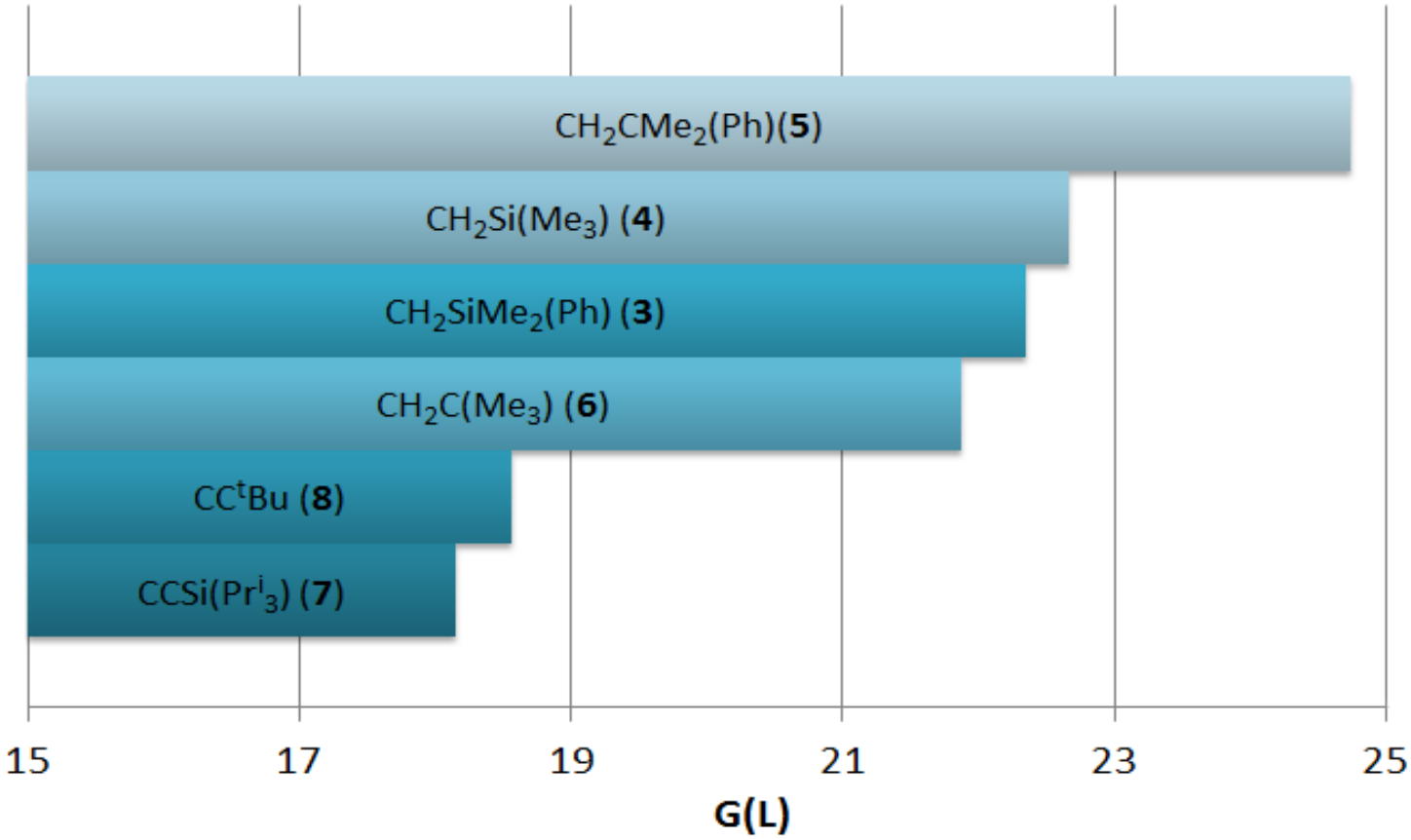

Figure 6.12: Percentage of the sphere shielded by the C bound ligand in **3-8** as calculated by Solid G.

6.7 Conclusion

The above $NCr(NPr^i_2)_2(X)$ complexes bearing Cr-C linkages round out a fairly comprehensive series of common monoanionic, mondentate ligands evaluated in both electronics and sterics. Though our system mixes both σ and π effects into a single parameter the subset of alkyl complexes are σ only, thus their LDP may find broader usage across transition metals of various d-counts. In realizing the series, new synthetic methodologies for problematic substitution reactions have been developed. LDP determinations on complexes **3-8** give the following order of increasing donor ability $CH_2CMe_2(Ph)<CH_2SiMe_2(Ph)<CH_2CMe_3<CC^tBu$ $CH_2SiMe_3<CCSi(Pr^i_3)$.

An obvious omission to the above study is the inclusion of an organometallic ligand bound through an sp^2 carbon, namely that of an aryl ring. While attempts at installing a phenyl substituent (or a *meta*-disubstituted phenyl substituent) gave only the previously mentioned products of decomposition, limited success has be achieved by treating $NCr(NPr^i_2)_2I$ with 1 equiv. of di(anthracen-9-yl)magnesium in 7:1 (v:v) hexane:THF. LDP determination on the resulting compound presumed to be $NCr(NPr^i_2)_2(anth)$ where anth = 2-anthycenyl gave a value of 13.31±0.27 kcal/mol. This places 2-anthycenyl near $CCSi(Pr^i_3)$ at 13.30±0.26 kcal/mol and incongruent to the expected trend that ligand donation is inversely related to electronegativity and follows $Csp^3>Csp^2>Csp$. As seen in $NCr(NPr^i_2)_2(X)$ where $X = NPr^i_2$, a steric limit exists where a one to one comparison between ligands breaks down when their bulk becomes

appreciably large. Since the LDP parameter is empirically derived from the kinetics of amide rotation any hindrance to this molecular motion will also be included. The above studies make the assumption that the barrier to diisopropylamide bond rotation is a function of the Cr-NPr^i_2 bond order and that any steric hindrance (thus increase to that barrier) is negligible or consistent for all the compounds. Though crystals of $NCr(NPr^i_2)_2$(anth) suitable for diffraction have not yet been obtained, it is reasonable to assume a large steric bulk by either measure, Solid G or $\%V_{bur}$. However, even if the sterically large 2-anthrycenyl hindered rotation this would serve to *increase* the LDP, artificially making the ligand look like a worse donor. This is the opposite of what is observed. Like was suggested for alkynyl ligands donation of ligand based π-electrons may account for this aberration warranting further study.

6.8 Experimental

Synthesis of $NCr(NPr^i_2)_2(CH_2SiMe_3)$ (**4**) In a 20 mL scintillation vial equipped with a stir bar was loaded with $NCr(NPr^i_2)_2$(OPh) (**2**) (0.050 g, 0.140 mmol, 1.0 equiv.) and 8 mL of pentane. This solution was placed into a liquid nitrogen cooled cold well to cool for 5 min. To this cold, stirring solution was added 0.139 mL of 1.0 M $LiCH_2SiMe_3$ dropwise. The solution was allowed to warm up to room temperature and stir for 1 h. The solution turned from orange-red to a yellow-brown color. The pentane solution was cooled and then filtered through Celite to remove LiOPh. The solution was concentrated *in vacuo* and placed in a freezer yielding yellow-orange crystals (0.036 g, 0.10 mmol, 73%). ^{1}H NMR (500 MHz, $CDCl_3$, 1.67 ºC): 4.93 (sept, J_{HH} = 6.0 Hz, 2H, C*H*$(CH_3)_2$), 3.52 (sept, J_{HH} = 6.0 Hz, 2H, C*H*$(CH_3)_2$), 1.60 (d, J_{HH} = 6.5 Hz, 6H,

$CH(CH_3)_2$), 1.41 (d, J_{HH} = 6.0 Hz, 6H, $CH(CH_3)_2$), 1.14 (d, J_{HH} = 6.5 Hz, 6H, $CH(CH_3)_2$), 1.12 (d, J_{HH} = 6.5 Hz, 6H, $CH(CH_3)_2$), 0.056 (s, 9H, $Si(CH_3)_3$), -0.033 (s, 2H, $CH_2Si(CH_3)_3$). $^{13}C\{^1H\}$NMR (125 MHz, $CDCl_3$, 10 ºC): 56.1, 53.5, 30.8, 29.4, 29.0, 22.4, 20.1, 1.6. ^{29}Si NMR (119.16 MHz, $CDCl_3$, 25 ºC): 2.078 (s, $CH_2Si(CH_3)_3$). Mp: 90-92 ºC.

Synthesis of $NCr(NPr^i_2)_2(CH_2C(Me)_2Ph)$ (**5**) A 20 mL scintillation vial equipped with a stir bar was loaded with **1** (0.020 g, 0.10 mmol, 1 equiv.) and 2 mL of diethylether. This solution was placed into a liquid nitrogen cooled cold well to cool for 5 min. To this cold stirring solution was added a cold solution of $Mg(CH_2C(Me)_2Ph)_2$ (0.011 g, 0.04 mmol, 0.7 equiv.) in 2 mL of diethylether dropwise. This was allowed to warm to room temperature and stir for 1.5 h. A white solid precipitated, and the solution turned yellow-brown. The solvent was removed *in vacuo* and the brown solid dissolved in hexane. The solution was cooled to –35 ºC and filtered through Celite to remove MgI_2. The solution was concentrated *in vacuo* and placed in a freezer yielding yellow-orange crystals (0.019 g, 0.048 mmol, 95% yield). ^1H NMR (500 MHz, $CDCl_3$, 25 ºC): 7.33 (d, J_{HH} = 7.5 Hz, 2H, *ortho*), 7.13 (app t, J_{HH} = 8.0 Hz, 2H, *meta*), 6.98 (app t, J_{HH} = 7.0 Hz, 1H, *para*), 4.74 (sept, J_{HH} = 6.5, 2H, $CH(CH_3)_2$), 3.40 (sept, J_{HH} = 6.5 Hz, 2H, $CH(CH_3)_2$), 1.49 (s, 6H, $C(CH_3)_2Ph$), 1.47 (s, 2H, $CH_2C(CH_3)_2Ph$), 1.45 (d, J_{HH} = 6.0 Hz, 6H, $CH(CH_3)_2$), 1.32 (d, J_{HH} = 6.0 Hz, 6H, $CH(CH_3)_2$), 1.05 (d, J_{HH} = 6.0 Hz, 6H, $CH(CH_3)_2$), 1.01 (d, J_{HH} = 6.0 Hz, 6H, $CH(CH_3)_2$). $^{13}C\{^1H\}$ NMR (125 MHz, $CDCl_3$, 25 ºC): 154.7, 127.7, 125.5, 124.5, 64.7, 55.8, 53.3, 39.6, 32.0, 31.0, 28.9, 22.7, 19.7. Mp: 71-73 ºC.

Synthesis of NCr(NPr$^{i}_{2}$)$_2$(CH$_2$CMe$_3$) (**6**) A 20 mL scintillation vial equipped with a stir bar was loaded with NCr(NPr$^{i}_{2}$)$_2$(OAd) (0.027g, 0.065 mmol, 1.0 equiv.) and 4 mL of pentane. This was placed into a liquid nitrogen cold well to cool for five min. To this cold stirring solution was added LiCH$_2$CMe$_3$ (0.005 g, 0.065 mmol, 1.0 equiv.) in 3 mL of cold ether dropwise. Over a period of 1 h a white solid precipitated. The solution was pumped dry, and the product was dissolved in pentane. The pentane solution was cooled to –35 ºC and filtered through Celite to remove LiOAd. The solution was concentrated in vacuo and stored in the freezer yielding crystals of **6**. ^{1}H NMR (500 MHz, CDCl$_3$, 2 ºC): 4.85 (sept, J_{HH} = 6.5 Hz, 2H, C*H*(CH$_3$)$_2$), 3.49 (sept, J_{HH} = 6.5 Hz, 2H, C*H*(CH$_3$)$_2$), 1.58 (d, J_{HH} = 6.0 Hz, 6H, CH(C*H*$_3$)$_2$), 1.41 (d, J_{HH} = 6.0 Hz, 6H, CH(C*H*$_3$)$_2$), 1.26 (s, 2H, C*H*$_2$C(CH$_3$)$_3$), 1.14 (d, J_{HH} = 6.5 Hz, 6H, CH(C*H*$_3$)$_2$), 1.11 (d, J_{HH} = 6.0 Hz, 6H, CH(C*H*$_3$)$_2$), 1.09 (s, 9H, CH$_2$C(C*H*$_3$)$_3$).

Synthesis of NCr(NPr$^{i}_{2}$)$_2$(CCSiPr$^{i}_{3}$) (**7**) A 20 mL scintillation vial equipped with a stir bar was loaded with **2** (0.050 g, 0.140 mmol, 1.0 equiv.) and 5 mL of hexane. This was placed in a liquid nitrogen cooled cold well to cool for 5 min. To this cold stirring solution was added a cold solution of LiCCSiPr$^{i}_{3}$ (0.026 g, 0.140 mmol, 1.0 equiv.) in 5 mL of hexane. The reaction was allowed to warm up to room temperature and stir for 1.5 h. The solution was cooled to –35 ºC and filtered through Celite to remove LiOPh. This solution was concentrated in vacuo and then placed in the freezer yielding orange crystals (0.052, 0.115 mmol, 83% yield). ^{1}H NMR (500 MHz, CDCl$_3$, –18 ºC): 5.05 (sept, J_{HH} = 6.0 Hz, 2H, C*H*(CH$_3$)$_2$), 3.72 (sept, J_{HH} = 6.5 Hz, 2H,

C*H*(CH_3)$_2$), 1.80 (d, J_{HH} = 6.0 Hz, 6H, CH(C*H*$_3$)$_2$), 1.48 (d, J_{HH} = 6.5 Hz, 6H, CH(C*H*$_3$)$_2$), 1.25 (d, J_{HH} = 6.5 Hz, 6H, CH(C*H*$_3$)$_2$), 1.10 (d, J_{HH} = 6.5 Hz, 6H, CH(C*H*$_3$)$_2$), 1.00 (br s, 21H, Si(C*H*(C*H*$_3$)$_2$)$_3$. ^{13}C{^{1}H} NMR (125 MHz, $CDCl_3$, –20 ºC): 150.4, 119.0, 57.5, 55.8, 30.6, 30.4, 21.9, 21.4, 18.8, 11.4. ^{29}Si NMR (119.16 MHz, $CDCl_3$, 25 ºC): –6.108 (s, CC*Si*^{i}Pr$_3$). Mp: 109-110 ºC.

Synthesis of NCr(NPr$^i_2$)$_2$(CC^{t}Bu) (**8**) In a 20 mL scintillation vial equipped with a stir bar was loaded **2** (0.037 g, 0.102 mmol, 1.0 equiv.) and 7 mL of hexanes. This was placed in a liquid nitrogen filled cold well to cool for five min. To this cold stirring solution was added a cold solution of LiCC^{t}Bu (0.009 g, 0.1 mmol, 1.0 equiv.) in 2 mL of ether. The reaction was allowed to warm to room temperature and stir for 1 h. Over this period, the solution turned from dark-red to light orange-red. Then the solvent was removed *in vacuo*. The product was dissolved in pentane, chilled, and filtered through Celite to remove LiOPh. The cold solution was concentrated and placed in a freezer at –35 ºC yielding bright red-orange crystals (0.035 g, 0.101 mmol, 98% yield). ^{1}H NMR (500 MHz, $CDCl_3$, 1 ºC): 5.07 (sept, J_{HH} = 6.5 Hz, 2H, C*H*(CH_3)$_2$), 3.69 (sept, J_{HH} = 6.0 Hz, 2H, C*H*(CH_3)$_2$), 1.80 (d, J_{HH} = 6.5 Hz, 6H, CH(C*H*$_3$)$_2$), 1.46 (d, J_{HH} = 6.5 Hz, 6H, CH(C*H*$_3$)$_2$), 1.25 (d, J_{HH} = 6.5 Hz, 6H, CH(C*H*$_3$)$_2$), 1.17 (s, 9H, C(C*H*$_3$)$_3$), 1.10 (d, J_{HH} = 6.0 Hz, 6H, CH(C*H*$_3$)$_2$). ^{13}C{^{1}H} NMR (125 MHz, $CDCl_3$, 25 ºC): 127.0, 114.7, 57.4, 55.6, 31.7, 30.6, 30.3, 28.9, 21.7, 21.1. Mp: 110-112 ºC.

Synthesis of $[NCr(NPr^{i}_{2})_2(C_2Ph)]_2$ (9) Under an N_2 atmosphere a 25 mL Erlynmeyer flask was loaded with a stir bar (phenylethynyl)lithium (0.073 g, 0.679 mmol, 2 equiv.) and THF (8 mL). The flask was cooled in a liquid nitrogen cooled cold well for 10 min. The flask was removed and stirred on a plate vigorously. To this $ZnCl_2$ (0.046 g, 0.340 mmol, 1 equiv.) was added as a solid. The solution came to room temperature and stirred for 1h. To the stirring mixture was added **1** (0.134 g, 0.340 mmol, 1 equiv.) in THF (5 mL). The reaction stirred for 12 h. The volatiles we removed under reduced pressure. The residue was extracted with pentane until the extracts were clear. The combined extracts were filtered through a fritted funnel using Celite as a filtering agent. The filtrate was dried under reduced pressure and dissolved in minimal amounts of Et_2O (~5 mL) held at −35 °C yielding small orange crystals of **9** in low yield.

Synthesis of $LiCCSi(^{i}Pr)_3$ In a 20 mL scintillation vial equipped with a stir bar was loaded tri(*iso*propyl)silylacetylene (0.20 g, 1.1 mmol, 1 equiv.) and 8 mL of hexane. The solution was placed in a liquid nitrogen cooled cold well. To this cold stirring solution was added 1.6 M *n*-butyl lithium in hexanes (0.625 mL, 1.10 mmol, 1.0 equiv.) by syringe. The solution was allowed to warm to room temperature and stir for 1 h. The solvent was removed *in vacuo* leaving a sticky oil. This was used directly in the next reaction. (0.181 g, 0.9 mmol, 87.4% yield). This is a slight modification of the literature procedure.[27]

Synthesis of $LiCC^{t}Bu$ In a 20 mL scintillation vial equipped with a stir bar was loaded 3,3-dimethyl-1-butyne (0.100 g, 1.21 mmol, 1 equiv.) and 5 mL of hexane. This solution was cooled for 5 min in a liquid nitrogen cooled cold well. To this cold stirring solution was added 1.6 M *n*-butyl lithium in hexanes (0.760 mL, 1.21 mmol, 1.0 equiv.) and was allowed to warm to room

temperature and stir for 1 h. Over this period the solution turned cloudy and a white precipitate formed. The solvent was removed *in vacuo* leaving a white solid. (0.101 g, 1.1 mmol, 96% yield). The melting point matched the reported literature value.[28]

REFERENCES

REFERENCES

(1) Wierschke, S. G.; Chandrasekhar, J.; Jorgensen, W. L. *Journal of the American Chemical Society* **1985**, *107*, 1496–1500.

(2) Varga, V.; Císařová, I.; Gyepes, R.; Horáček, M.; Kubišta, J.; Mach, K. *Organometallics* **2009**, *28*, 1748–1757.

(3) Jana, R.; Pathak, T. P.; Sigman, M. S. *Chemical reviews* **2011**, *111*, 1417–92.

(4) Blackmore, K. J.; Ziller, J. W.; Heyduk, A. F. *Inorganic chemistry* **2005**, *44*, 5559–61.

(5) Haneline, M. R.; Heyduk, A. F. *Journal of the American Chemical Society* **2006**, *128*, 8410–1.

(6) Crabtree, R. H. *The Organometallic Chemistry of the Transition Metals, 5th Edition*; 5th ed.; Wiley, 2009.

(7) DiFranco, S. A.; Maciulis, N. A.; Staples, R. J.; Batrice, R. J.; Odom, A. L. *Inorganic Chemistry* **2012**, *51*, 1187–200.

(8) Odom, A. L.; Cummins, C. C. *Organometallics* **1996**, *15*, 898–900.

(9) Collier, M. R.; Lappert, M. F.; Pearce, R. *Journal of the Chemical Society, Dalton Transactions* **1973**, 445.

(10) Odom, A. L.; Cummins, C. C. *Polyhedron* **1998**, *17*, 675–688.

(11) Andersen, R. A.; Wilkinson, G. *Journal of the Chemical Society, Dalton Transactions* **1977**, 809.

(12) Schrock, R. R.; Fellmann, J. D. *Journal of the American Chemical Society* **1978**, *100*, 3359–3370.

(13) van den Hoek, W. G. M.; Kroon, J.; Kleijn, H.; Westmijze, H.; Vermeer, P.; Bos, H. J. T. *Journal of the Chemical Society, Perkin Transactions 2* **1979**, 423.

(14) Almenningen, A.; Bastiansen, O.; Trætteberg, M.; Olsen, G. E.; Pedersen, C.; Toft, J. *Acta Chemica Scandinavica* **1961**, *15*, 1557–1562.

(15) Kaim, W. *Inorganic chemistry* **2011**, *50*, 9752–65.

(16) Wolczanski, P. T. *Polyhedron* **1995**, *14*, 3335–3362.

(17) Manna, J.; John, K. D.; Hopkins, M. D. *AdV. Organomet. Chem.* **1995**, *38*, 79.

(18) Lichtenberger, D. L.; Renshaw, S. K.; Wong, A.; Tagge, C. D. *Organometallics* **1993**, *12*, 3522–3526.

(19) Lichtenberger, D. L.; Renshaw, S. K.; Bullock, R. M. *Journal of the American Chemical Society* **1993**, *115*, 3276–3285.

(20) Berben, L. a; Long, J. R. *Inorganic chemistry* **2005**, *44*, 8459–68.

(21) Bühmer, W.-H.; Madeja, K.; Kurras, E.; Rosenthal, U. *Zeitschrift für anorganische und allgemeine Chemie* **1979**, *458*, 69–73.

(22) Hatfield, W. E.; Fay, R. C.; Pfluger, C. E.; Piper, T. S. *Journal of the American Chemical Society* **1963**, *85*, 265–269.

(23) Alexander, J. J.; Gray, H. B. *Journal of the American Chemical Society* **1968**, *90*, 4260–4271.

(24) Belanzoni, P.; Re, N.; Sgamellotti, A.; Floriani, C. *Journal of the Chemical Society, Dalton Transactions* **1997**, 4773–4782.

(25) Guzei, I. A.; Wendt, M. *Dalton transactions* **2006**, 3991–9.

(26) Clavier, H.; Nolan, S. P. *Chemical communications* **2010**, *46*, 841–61.

(27) Li, J.; Zhang, K.; Zhang, X.; Huang, K.-W.; Chi, C.; Wu, J. *The Journal of Organic Chemistry* **2010**, *75*, 856–63.

(28) Miller, M. J.; Lyttle, M. H.; Streitwieser, A. *The Journal of Organic Chemistry* **1981**, *46*, 1977–1984.

Chapter 7: Synthesis, Structure, and Ligand Evaluation of Cationic Chromium(VI) Nitrido Complexes.

ABSTRACT

Synthesis and characterization of cationic Cr(VI) nitride complexes of the form $[NCr(NPr^{i}_{2})_2(L)][A]$ where L = THF, DMAP, HMPA, qunicludine, ^{t}BuNC, DBN, $P(Me)_2Ph$, NHC and A = I, OTf, BF_4, PF_6, SbF_6, BPh_4, and BAr^{F}_{4} are reported. New synthetic methodologies were developed to access $[NCr(NPr^{i}_{2})_2(L)][A]$ compounds including displacement of iodine from $NCr(NPr^{i}_{2})_2I$ (**1**), halide abstraction using silver salts of weakly coordinating anions, substitution of L, and substitution of A. The neutral complex $NCr(NPr^{i}_{2})_2(PzB(Et_3))$ (**10**) bearing a mono pyrazolyl borate is also reported. The kinetics of diisopropylamide rotation was measured via Spin Saturation Magnatization Transfer in the ^{1}H NMR for each complex to assess the donor abilities of L. Collected into a single parameter, the Ligand Donor Parameter (LDP) of each are reported. In order to correct these LDP's for differing anions between each complex a series of $[NCr(NPr^{i}_{2})_2(DBN)][A]$ compounds were made where A = I, OTf, BF_4, PF_6, SbF_6, BPh_4, and BAr^{F}_{4}, and a linear correction factor applied giving the donor series $PzB(Et_3)$>THF>NHC>DMAP>^{t}BuNC>DBN>HMPA>$P(Me)_2Ph$>quin. When $NCr(NPr^{i}_{2})_2I$ (**1**) was treated with DMAP iodine was displaced into the outer sphere producing $[NCr(NPr^{i}_{2})_2(DMAP)][I]$ (**4-I**) in a temperature dependent equilibrium, favoring cation formation at low temperature. The LDP was determined for $[NCr(NPr^{i}_{2})_2(DMAP)][I]$ (**4-**

I) in $CDCl_3$, CD_3CN, and THF-*d8* with LDP increasing with increasing dielectric constant of the solvent. The compounds [NCr(NPr^i_2)$_2$(DBN)][I] (**2-I**), [NCr(NPr^i_2)$_2$(quin)][PF_6] (**3**), [NCr(NPr^i_2)$_2$(DMAP)][BF_4] (**4-BF_4**), [NCr(NPr^i_2)$_2$(NHC)][PF_6] (**5**), [NCr(NPr^i_2)$_2$(HMPA)][PF_6] (**6**), and [NCr(NPr^i_2)$_2$(THF)][PF_6] (**8**) are structurally characterized via single crystal x-ray diffraction and give evidence for cationic charge delocalization onto the ligands. The steric profiles of **2-I, 3-6** and **8** were calculated through the methods of $\%V_{bur}$ and Solid G. Lastly, Cr-N_{ligand} bond distances were discussed as a function of LDP for the X- and L-type ligands bound through nitrogen.

7.1 Introduction

In the development of transition metal chemistry formal oxidation state assignments have provided a solid foundation in describing metal-ligand bonding interactions. However, with increasing ligand complexity and ligands with multiple coordination modes, a need arose to classify covalent interactions toward metal ions based upon the origin of the electrons involved. Introduced by M. L. H. Green, the Covalent Bond Classification Method (CBC method) provided such a construct, dividing metal-ligand interactions into permutations of 3 categories, X-type, L-type, and Z-type.[1]

The L-type interaction is a dative interaction where the $2e^-$ forming the bond are provided from the ligand. Often these ligands are neutral molecules with the electrons originating from occupied orbitals such as a non-bonding lone pair (PR_3 ,NH_3, CO) or σ a interaction to

double bond (C_2H_4, side on N_2, aromatic systems). X-type interactions are those involving singly occupied orbitals (radicals) where $1e^-$ is provided from the metal and $1e^-$ from the ligand (Cl, H, alkyls). Lastly, Z-type interactions are also defined as dative interactions with both electrons originating from the metal donating into an empty ligand based orbital of a Lewis acid (BF_3, AlR_3).

Much work has, and will continue to go into expanding these qualitative concepts in a quantitative fashion. Systematic evaluations of ligand properties in the literature however, have been predominated of L-type ligands. Perhaps the most notable example of ligand parameterization followed an observation by Wilkinson and coworkers that successive substitutions in the R groups of the phosphine in $(R_3P)_3Mo(CO)_3$ perturbs the bond orders in the Mo-CO moiety, which can be quantified by an increase in the IR stretching frequency of the carbonyl.[2]

In his seminal work Chadwick Tolman profiled both the steric and electronic properties of commonly used phosphines. This exhaustive study was predicated upon the previously mentioned observation that perturbations in the symmetric IR stretch of a carbonyl in $Ni(CO)_3L$ varied regularly with the nature of L. This construct allowed for the unprecedented ordering of L-type ligands used in catalytic systems based on their donor strength toward late transition metals in a quantitative way. Tolman's work also addressed the issue of ligand sterics within the aforementioned series. To quantitate the size of the various L groups the concept of ligand cone angle was developed. In this formalism a cone whose vertex lies at the metal center is

circumscribed around the ligand. The cone angle is thus described as the angle of the smallest cone which fully encapsulates the ligand.

While incredibly useful for its intended purpose, Tolman's assessment focused exclusively on L-type ligands evaluated on low valent Pt group metals, largely due to their ease of synthesis and the rapid data collection afforded by IR. This methodology limited the platform for electronic parameterization to L-type ligands, and moreover only phosphines in the initial studies. Additionally, the concept of cone angle was also designed around phosphine ligands. As more elaborate and highly asymmetrical ligands have been developed, the metric of cone angle has struggled to adequately describe their 'size' in one parameter.

More recently there has been electronic evaluations of N-heterocyclic carbene ligands (NHC's) by the groups of Crabtree[3,4] and Nolan[5] using a (NHC)Ir$(CO)_2$Cl system. Although the Ir(I) system shows good linear correlation to Tolman's original work this system still relies on the installation of CO ligands as a reporting unit. Furthermore, to correlate to "Tolman's electronic parameter" (TEP) based off the A_1stretching mode of CO, the average of the 2 CO stretching frequencies of (NHC)Ir$(CO)_2$Cl are used, as the synthetic route to complexes of the type do not produce C_2 symmetric systems. DFT investigations by Gusev comparing both $NiCO_3L$ and various Ir(I) systems suggest that the average stretching of (L)Ir$(CO)_2$X complexes does not linearly correlate to the average CO bond distance, thus may not be an appropriate measure of metal to ligand back-bonding and the overall electronic 'richness' of the metal.[6] Furthermore, although metrics such as TEP may be meaningful within a series, direct comparisons to other series (i.e. phosphines to NR_3 ligands or NHC's) may breakdown.

Similar ligand parameterizations have been conducted by experimental methods beyond IR stretching frequencies, including electrochemical[7,8] and electronic spectrum analysis. Notably, a 1996 report by Anderson et. al. evaluated a series of π-donor, monodentate X-type ligands using the Cp^*_2TiX platform.[9] This departure toward early d^1 metals employed EPR and absorption spectroscopy, circumventing the need to install a 'reporting group'.

Powerful in their own right, when examining these disparate methods in the context of each other, inter system comparisons become tenuous at best and indiscernible at worst. Often an insufficient amount of ligands overlap between series. Furthermore, the utility of computational methods of parameterization are dependent on the extent they describe real-world phenomena. Empirical data is essential to their development and is not always obtainable for the ligand in question.

Recently the steric and electronic profiles of a wide set of monodentate X-type ligands were experimentally evaluated using a Cr(VI) nitride system.[10] Compounds of the form $NCr(NPr^i_2)_2X$ were synthesized in good yields, and the rotation kinetics of the diisopropylamide group were used to probe the ligand donor ability (LDP) of the X ligand via the method of Spin Saturation Magnetization Transfer (SST) in the ^1H NMR.[11-12]

Analogous Cr(VI) cations have been synthesized of the form $[NCr(NPr^i_2)_2L][A]$ where L is a $2e^-$ donor and A is an anion. Herein we report the LDP and steric profiles of several L-type ligands featuring O, P, N and C donor atoms using the method of SST as before. This provides a quantitative series that spans both X- and L-type ligands reported as a single parameter (LDP),

facilitating direct comparison along the continuum. Furthermore, a general procedure for future ligand parameterization studies has been delineated using facile data collection via readily available ^{1}H NMR spectroscopy. The chromium nitride platform employed proves to be highly amenable to a wide variety of reagents and synthetic strategies. Beyond the scope of this work we hope the model will facilitate ligand parameterization for other researchers who are curious about their own specialized monodentate ligand, be it X- or L-type.

7.2 Synthesis of Chromium Starting Materials

Access into complexes of the form $[NCr(NPr^{i}_{2})_{2}L][A]$ where L is a $2e^{-}$ donor and A is a weakly-coordinating anion can be achieved through various synthetic routes. Using the method of Bradley and coworkers, $Cr(NPr^{i}_{2})_{3}$ can be obtained in high yield using anhydrous $CrCl_{3}$ and $LiNPr^{i}_{2}$.[13] Chiu and coworkers published a one-pot synthesis of $NCr(O^{t}Bu)_{3}$ starting from chromyl chloride.[14] A stoichiometric mixture of $Cr(NPr^{i}_{2})_{3}$ and $NCr(O^{t}Bu)_{3}$ results in complete N-atom transfer affording $NCr(NPr^{i}_{2})_{3}$ in high yield.[15] Subsequent treatment of $NCr(NPr^{i}_{2})_{3}$ by 2,6-lutidenium iodide in chloroform gives $NCr(NPr^{i}_{2})_{2}I$ (**1**) as reported by Cummins.[16]

7.3 Synthesis of Cr(VI) Cations

Synthesis of $[NCr(NPr^{i}_{2})_{2}L][A]$ was accomplished through a variety of techniques and will be addressed individually. In general Cr(VI) cations seem more sensitive to temperature, solvent, and reagents than their Cr(VI) nitride counterparts. However, in situ synthesis from

known precursors proved to be adequate for the SST experiment, allowing electronic evaluation of in-isolatable species.

Synthesis by displacement of an X-type ligand

While typical syntheses of $NCr(NPr^{i}_{2})_2X$ complexes were performed in non-polar (toluene) or weakly polar (Et_2O) solvents, preliminary experiments using largely insoluble sodium or silver salts required the use of THF and DME. Analysis of these reaction mixtures showed a trace amount of a then unidentified chromium bisdiisopropylamide compound. Subsequent investigations revealed that strongly coordinating solvents could act as $2e^-$ donors and displace the iodide of $NCr(NPr^{i}_{2})_2I$ (**1**) into the outer sphere. When a stoichiometric amount of DBN was added to $NCr(NPr^{i}_{2})_2I$ (**1**) in Et_2O an orange precipitate rapidly formed, found to be $[NCr(NPr^{i}_{2})_2DBN][I]$ **2-I** when isolated in 82% yield (Figure 7.1).

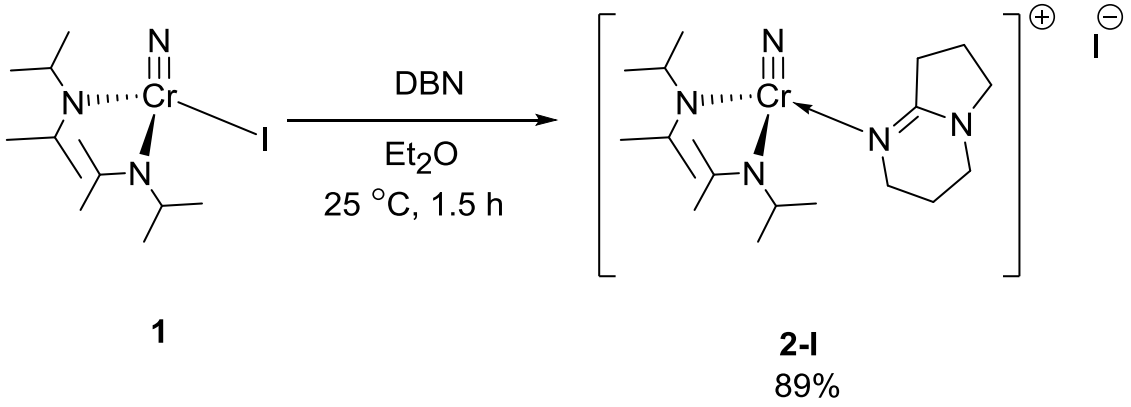

Figure 7.1: Synthesis of $[NCr(NPr^{i}_{2})_2DBN][I]$ **2-I**.

Curiously, the same reaction ran in THF gave a mixture of **1** and **2-I** when evaporated to dryness, and using pentane as a solvent failed to give more than a trace amount of the product. This suggests that L-type for X-type ligand substitution in these systems is reversible as well as solvent dependent.

Synthesis by halide abstraction

While the synthesis of **2-I** was straightforward other complexes of the form $[NCr(NPr^{i}_{2})_2L][A]$ with other L-type ligands were not satisfactorily generated by halide displacement. It is likely that some of the L ligands chosen for study are either not competent to initially displace the iodide of **1**, or that the product generated is unstable toward the back reaction. As such replacement of an outer sphere iodide with a counter ion traditionally viewed as 'non-coordinating'[17] was sought to alleviate this restriction. Treatment of **1** with 1 equiv. of 4-Dimethylaminopyridine (DMAP) in chloroform followed by the addition of 1.1 equiv. of $AgBF_4$ in acetonitrile produced $[NCr(NPr^{i}_{2})_2DMAP][\ BF_4]$ **4** in 58% yield after crystallization from a concentrated toluene solution held at −35 °C (Figure 7.2).

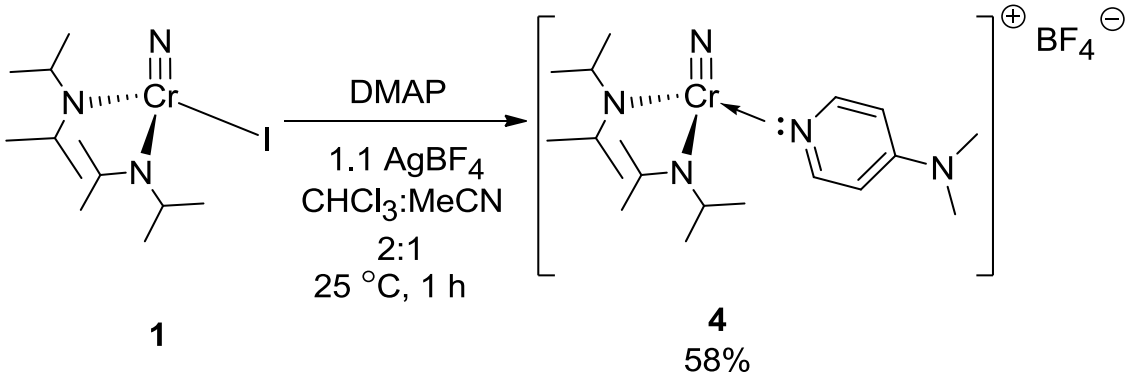

Figure 7.2: Synthesis of $[NCr(NPr^{i}_{2})_2DMAP][\ BF_4]$ **4** using silver tetrafluoroborate.

Attempted syntheses with other L-type ligands using $AgBF_4$ and similar conditions resulted largely in decomposition into insoluble products. Synthesis where L = quinuclidine (quin) was successful by switching counter ions, using silver hexafluorophosphate for halide abstraction (Figure 7.3).

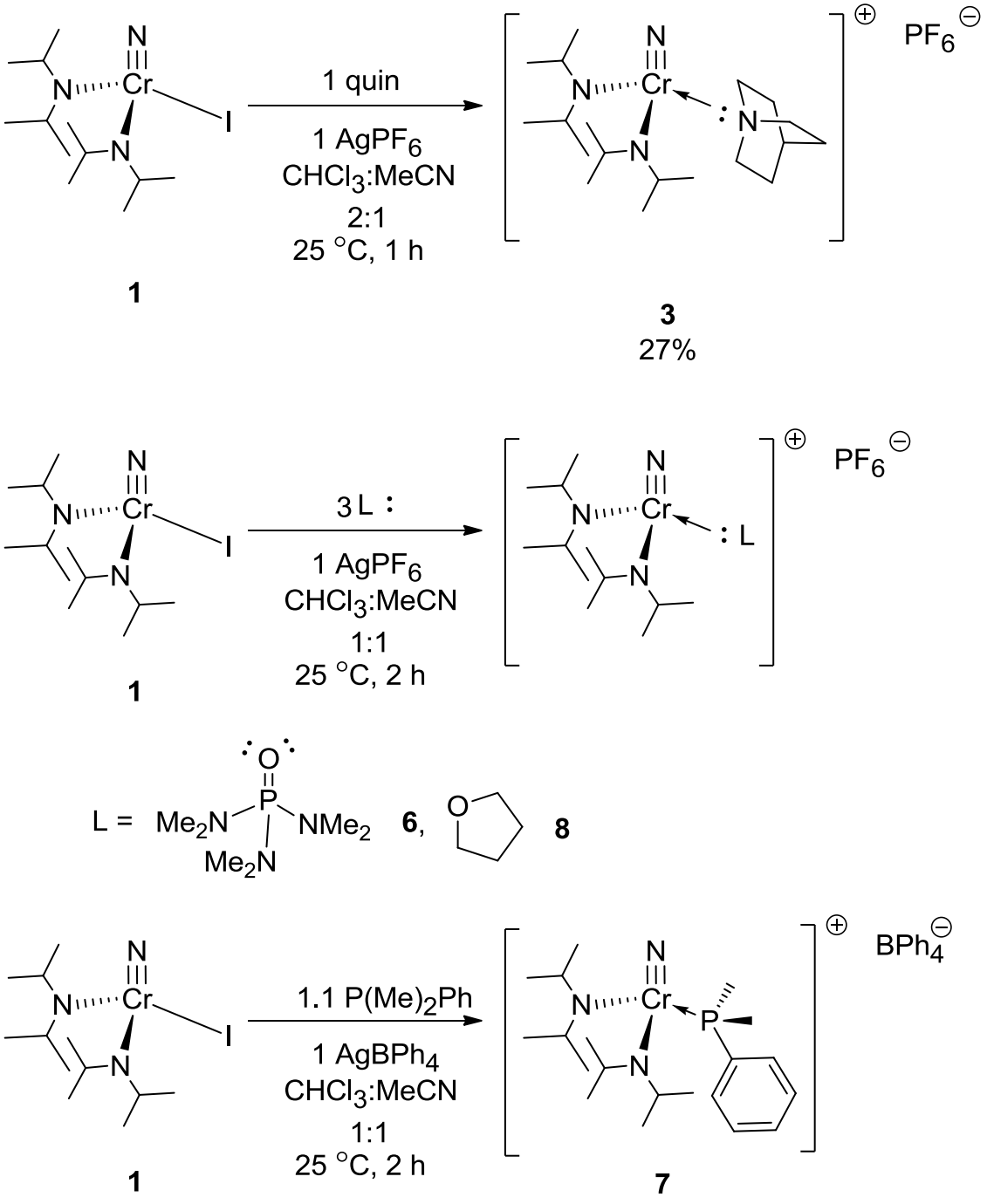

Figure 7.3: Synthesis of compounds **3** and **6-8** using $AgPF_6$ to abstract a halide from **1.**

Compounds of the form $[NCr(NPr^i_2)_2L][A]$ where L = hexamethylphosphoramide (HMPA) **6** and THF **8** we also accessible using $AgPF_6$ (Figure 7.3). While reaction of **1** with

$P(Me)_2Ph$ followed by treatment with $AgPF_6$ did give the desired product, treatment with 1 equiv. of $AgBPh_4$ resulted in a much cleaner reaction yielding $[NCr(NPr^i_2)_2P(Me)_2Ph][BPh_4]$ (**7**). Greater yields of **6** and **7** were obtained by using an excess of the desired ligand, as the Ag(I) ion scavenged some of the L reactant in solution. Unlike the quinuclidine in **3** or the DMAP in **4** residual HMPA or $P(Me)_2Ph$ was readily removed by evaporation or lyophilzation with the reaction solvent. Synthesis of $[NCr(NPr^i_2)_2THF][PF_6]$ **8** was also attempted using 10 equiv. of THF and with THF as a solvent. Although product was formed, compound **8** is able to polymerize any excess THF giving poor yields and complicating purification.

For completeness of our series a representative *N*-heterocyclic carbine ligand was sought. 1,3-dimethylimidizoium iodide was obtained by treatment of *N*-methylimidazole with MeI.[18] Generation of persistent (Arduengo) carbenes are typically obtained from such precursors by in situ deprotonation using a strong base such as KO^tBu.[19,20,21] Treatment of *N*,*N*-dimethylimidizoium iodide with KO^tBu followed successively by the addition of **1** and silver salts failed to give the desired product, yielding $NCr(NPr^i_2)_2O^tBu$ as the only tractable product. Instead, deprotonation of 1,3-dimethylimidizoium iodide by 1 equiv. benzyl potassium gave only toluene as a byproduct. After 2 h the carbene in toluene solution was filtered through celite in a fritted funnel to remove KI and any unreacted benzyl potassium. Addition of the filtrate to **1** followed by the addition of 1.1 equiv. $AgPF_6$ gave $[NCr(NPr^i_2)_2NHC][PF_6]$ **5** in 40% isolated yield (Figure 7.4).

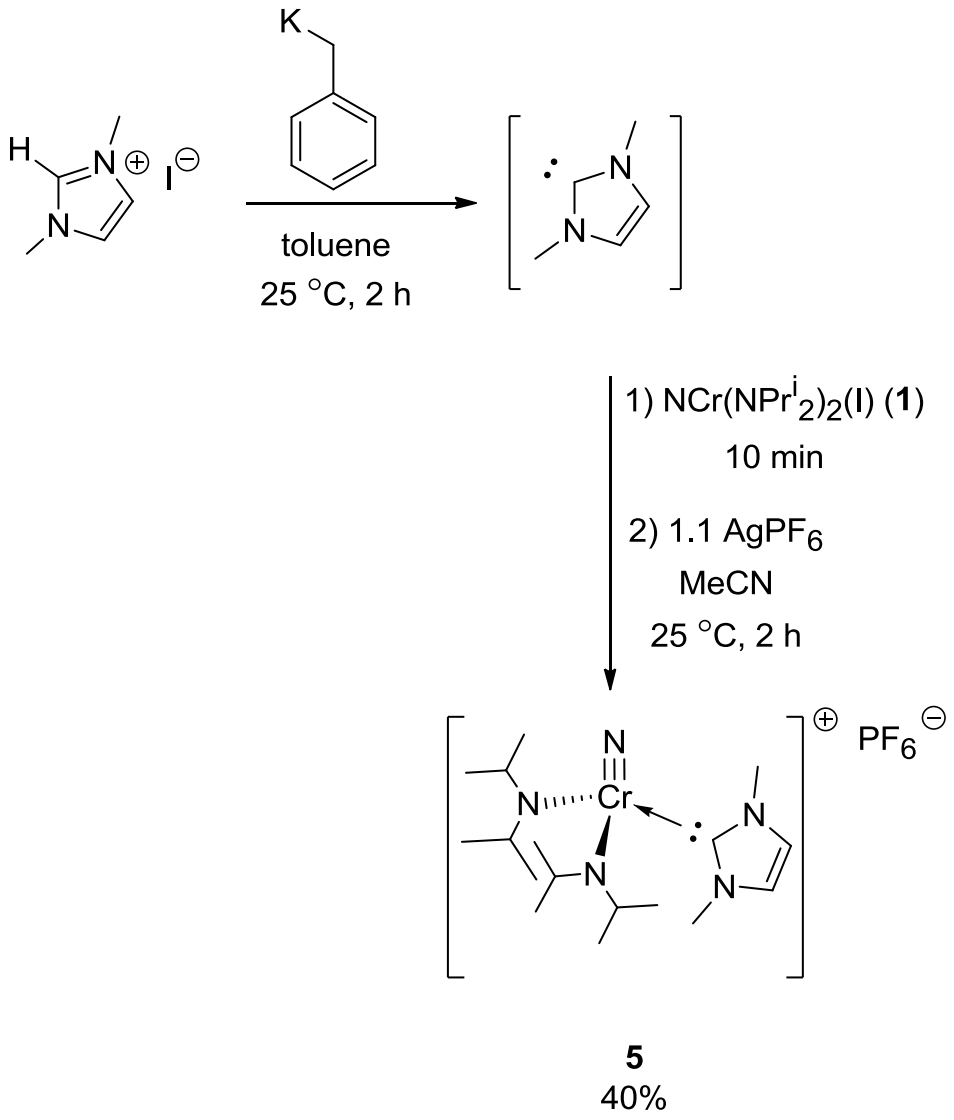

Figure 7.4: In situ generation of a persistent carbene and its reaction with **1** to make [NCr(NPr$^i_2$)$_2$NHC][PF$_6$] **5** .

Synthesis by substitution of A

Although many L-type ligands form stable complexes with the PF_6 anion suitable for evaluation, the target [NCr(NPr$^i_2$)$_2$DMAP][PF$_6$] could not be obtained by halide abstraction or by ligand exchange. Additionally, the effect of the counter ion upon LDP was unknown. Thus a

series of [NCr(NPr$^{i}_{2}$)$_2$L][A] complexes was synthesized where L is held constant and A is a variety of weakly-coordinating anions. For this study the L chosen was DBN, as it readily produces **2-I** where A is an outer sphere iodide. The [NCr(NPr$^{i}_{2}$)$_2$DBN] cation also forms stable complexes with BF_4, PF_6, SbF_6, and BPh_4 by treating **2-I** with 1 equiv. of the corresponding sodium salt (Figure 7.5).

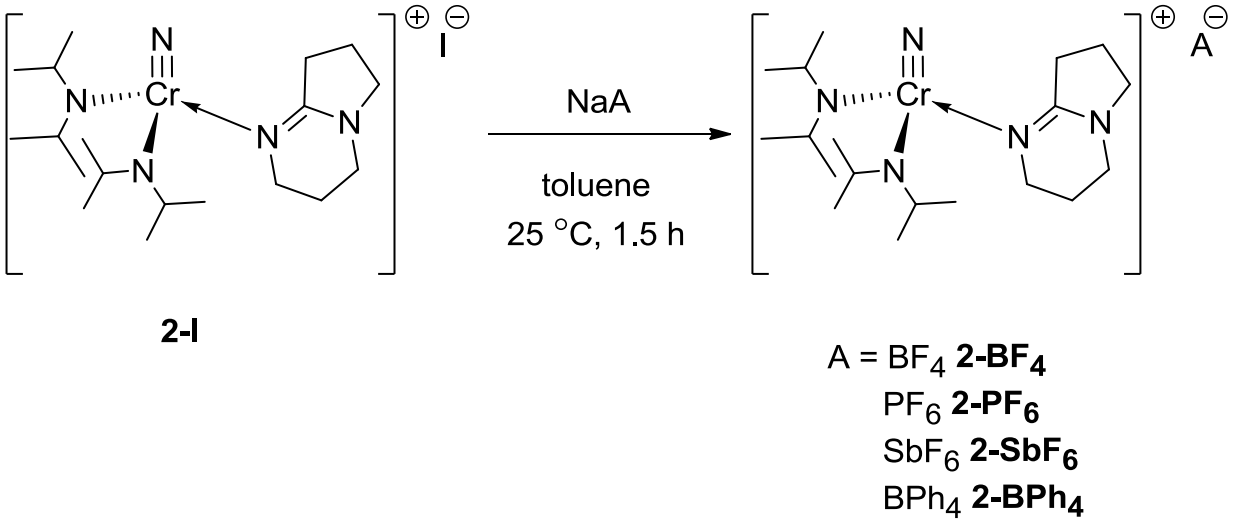

Figure 7.5: Counter ion substitution of **2-I** using sodium salts

The compound [NCr(NPr$^{i}_{2}$)$_2$DBN][OTf] (**2-OTf**) was synthesized by treatment of **2-I** with excess NBu_4OTf in toluene. This represents a unique example of Cr(VI) cation, as the DBN ligand is not displaced by triflate in solution to produce the previously described NCr(NPr$^{i}_{2}$)$_2$OTf (Figure 7.6).

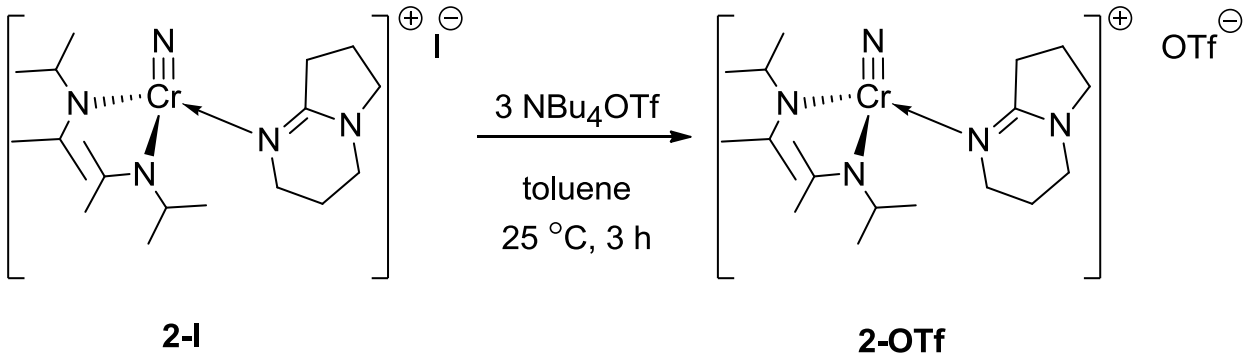

Figure 7.6: Synthesis of **2-OTf** by anion exchange with an ammonium salt.

Lastly, treatment of **2-I** with one equiv. of silver tetrakis[(3,5-trifluoromethyl)phenyl]borate ($Ag(BAr^{F}_{4})$)[22] in toluene afforded the highly lipophilic $[NCr(NPr^{i}_{2})_{2}DBN][BAr^{F}_{4}]$ **2-BAr$^{F}_{4}$** (Figure 7.7).

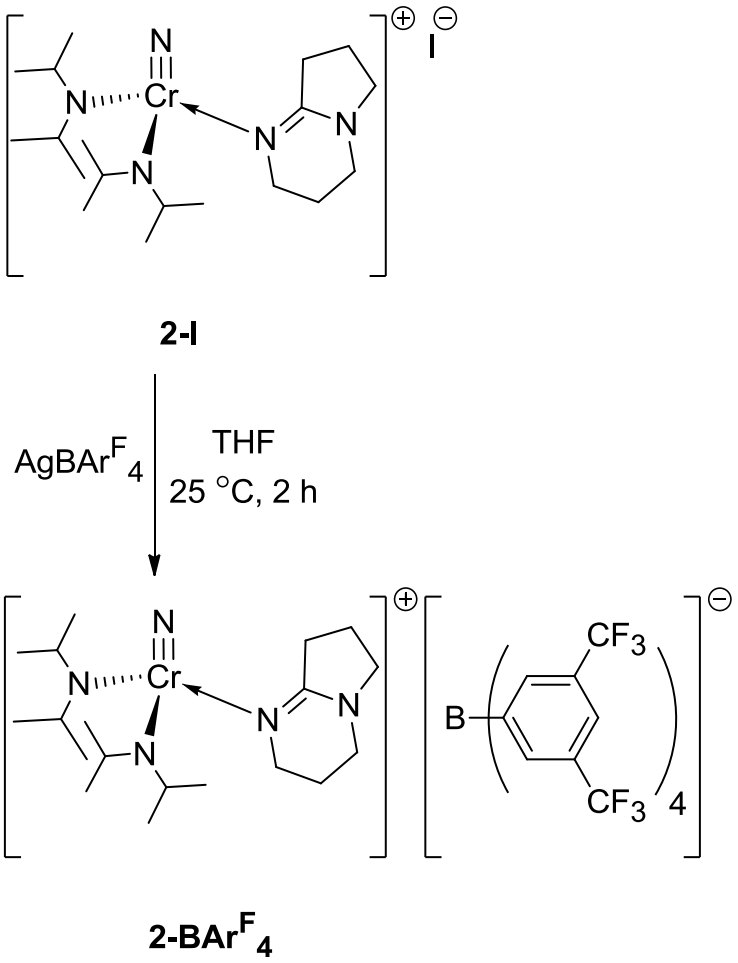

Figure 7.7: Synthesis of **2- BAr$^F_4$** by anion exchange with an Ag(BAr$^F_4$.

Synthesis by substitution of L

In the generation of the series of Cr(VI) cation with various weakly-coordinating counterions it was noticed that some ligand-counterion combinations are inaccessible by the treatment of NCr(NPr$^i_2$)$_2$I (**1**) with the appropriate silver slat in the presence of the L-type ligand. Attempts at synthesis of these molecules by directly substituting a coordinated L with another (stronger) L-type ligand gave only trace amounts of the desired product, and quickly

decomposed upon isolation. This suggests that these combinations are kinetically accessible but are thermodynamically unstable complexes (Figure 7.8).

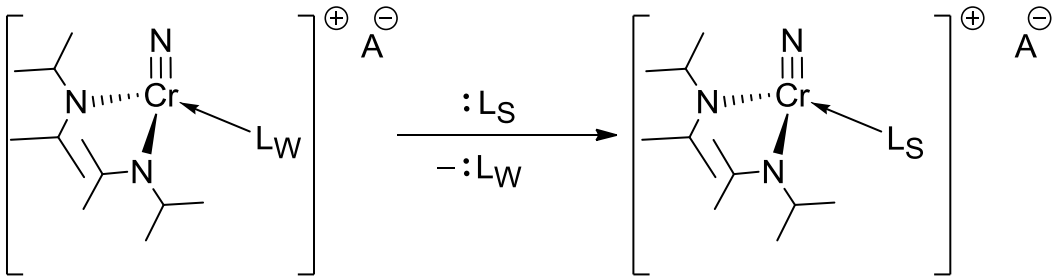

Figure 7.8: Displacement of a weaker donating ligand (L_W) by a stronger neutral donor (L_S).

One such exchange reaction however, yielded the desired product in situ. Treatment of **2-I** in with an excess of *tert*-butlyisonitrile (^{t}BuNC) in chloroform afforded a mixture of [NCr(NPr$^i_2$)$_2$DBN][I] **2-I** and a complex presumed to be [NCr(NPr$^i_2$)$_2$(^{t}BuNC)][I] (**9**) as determined by ^{1}H NMR.

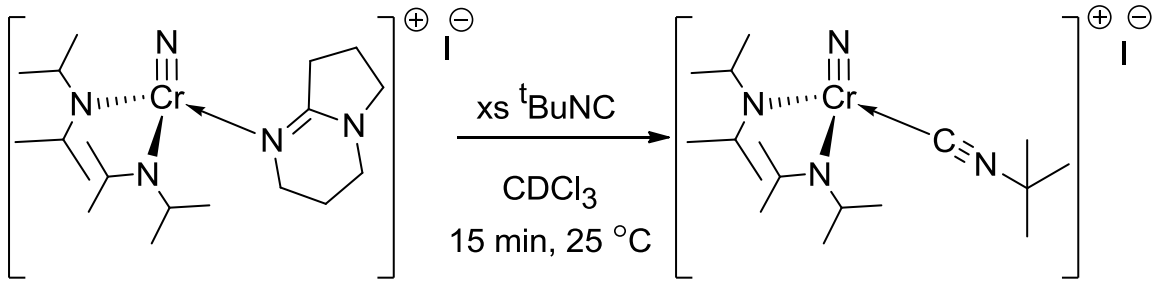

2-I **9**

Figure 7.9: In situ synthesis of [NCr(NPr$^i_2$)$_2$(^{t}BuNC)][I] (**9**) by ligand substitution.

Further analysis via FT-IR on this this mixture showed the CN stretch of both unbound (2140.6 cm^{-1}) and coordinated (2254.3 cm^{-1}) ^{t}BuNC. Isoelectronic to the CO ligand, a reduction of the CN stretching frequency is typically observed upon isonitrile coordination to transition metals due to filled d-orbital donation into ligand π*. In **9** however the increase observed is likely due to the removal of electron density from a ligand based σ* orbital to form the Cr-C bond, along with the (formal) lack of d-electrons which typically back-donate to populate the ligand π* orbital.[23] Thus far attempts to isolate **9** have been unsuccessful, leading to insoluble decomposition products and residual NCr(NPr$^{i}_{2}$)$_2$I (**1**). When isolated coordinated nitrile and isonitrile complexes like **9** may be invaluable to the further development of this model, providing an independent metric of metal center electronics via their IR stretching frequencies.

7.4 Synthesis of Zwitterionic Cr

Due to their widespread use in transition metal chemistry, a model for the trispyrazolylborate (Tp) ligand was sought. A monodentate pyrazolylborate was chosen for consistency's sake for evaluation on the chromium nitride platform. Sodium triethylpyrazolylborate[24] was added to **2-I** in THF to afford NCr(NPr$^{i}_{2}$)$_2$(PzB(Et$_3$)) (**10**).

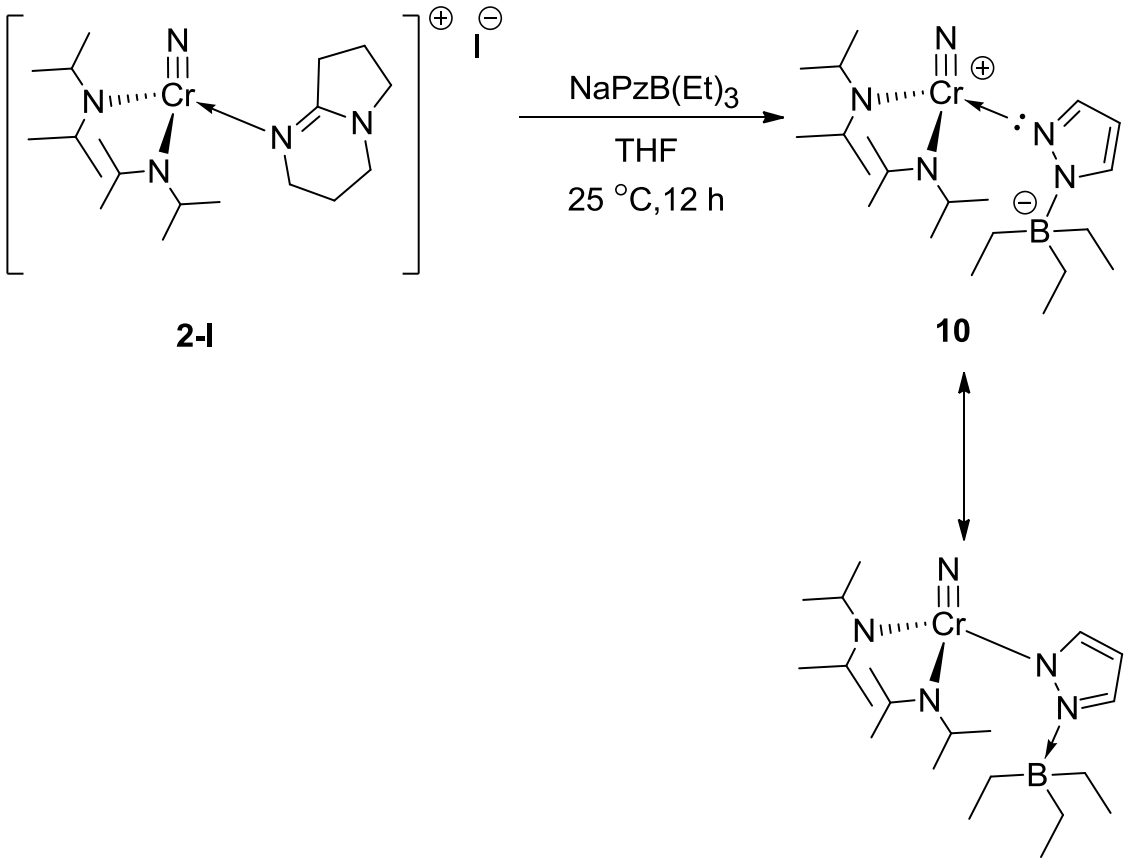

Figure 7.10: Synthesis of $NCr(NPr^{i}_2)_2(PzB(Et_3))$ (**10**) with resonance structures.

While Tp and similar pyrazolyl borate ligands are formally regarded as a (1-) anion[25] Zwitterionic resonance structures of **10** exist, placing a cationic charge on chromium with a dative bond to a trivalent pyrazolyl nitrogen.

7.5 LDP determination of Cr(VI) Cations

With a fairly comprehensive series of $[NCr(NPr^{i}_2)_2L][A]$ complexes where L is bound through an N, O, C or P atom, the kinetics of diisopropylamide inchange were used quantify the electronic ligand donation to the metal center in **2-10** via the method of Spin Saturation Magnetization Transfer (SST)[11,12,26] in the ^{1}H NMR as outlined in Chapter 4. Assuming an

entropy for the rotation of $\Delta S^{\ddagger}$ of -9 cal/mol K as determined for $NCr(NPr^{i}_{2})_2X$ complexes[9] the Cr-(NPr^{i}_{2}) bond enthalpy denoted $\Delta H^{\ddagger}$ was calculated for **2**-**10**, and presented in Table 7.1 as the Ligand Donation Parameter (LDP).

Unlike the previously reported X-type ligands which were measured at room temperature down to -48 °C, SST measurements on the series of neutral donors generally required temperatures above room temperature (up to +47 °C) to obtain satisfactory results. This large temperature range of -48 °C to +47 °C was predicated on the molecular dynamics of the $NCr(NPr^{i}_{2})_2$ moiety with each specific ligand. As donor ability of X or L decreases bond order between Cr and NPr^{i}_{2} increases slowing rotation and the chemical exchange of the methine protons. Since accurate measurement of the kinetics of site exchange depends largely on the difference in the ^{1}H NMR integration between the resonances of the two sites, a balance is needed. If the site exchange is too fast both sites are saturated or can give a signal obscured by the signal to noise of the baseline. If exchange is too slow the error associated with the integration is as large as the measurement itself. A judicious choice of temperature for accurate results can be estimated by a comparison to the other ligands already in the series. Thus the constraint of temperature let us determine *a priori* that the series of L-type ligands were far worse donors than the anions previously tested.

Unfortunately, this also sets a technical limit on the L-type ligands we are able to evaluate. To obtain adequate site exchange for the poorest donating of all the ligands thus far studied, the sample of $[NCr(NPr^{i}_{2})_2quin][PF_6]$ (**3**) required heating to near the boiling point of

the NMR solvent ($CDCl_3$). This precludes SST measurement on any ligand more poorly donating than quinuclidine unless a higher boiling solvent (and a solvent correction) is used.

Compound	LDP (kcal/mol)	Corrected LDP (kcal/mol)[a]
$NCr(NPr^i_2)_2(PzB(Et_3))$ (**10**)	14.35±0.30	-
$[NCr(NPr^i_2)_2THF][PF_6]$ (**8**)	15.28±0.30	15.61±0.30
$[NCr(NPr^i_2)_2NHC][PF_6]$ (**5**)	15.37±0.30	15.70±0.30
$[NCr(NPr^i_2)_2DMAP][BF_4]$ (**4**)	15.37±0.30	16.08±0.30
$[NCr(NPr^i_2)_2{}^tBuNC][I]$ (**9**)	15.85±0.30	16.87±0.30
$[NCr(NPr^i_2)_2HMPA][PF_6]$ (**6**)	16.55±0.32	16.88±0.32
$[NCr(NPr^i_2)_2P(Me)_2Ph][BPh_4]$ (**7**)	16.95±0.32	17.33±0.32
$[NCr(NPr^i_2)_2quin][PF_6]$ (**3**)	18.67±0.32	19.01±0.32

a See Table 7.2 for a list of corrective factors added to each LDP based upon anion

Table 7.1: Corrected and uncorrected Ligand Donor Parameters of **3-10**.

Suitably, the series of L-type ligands had much higher barriers to diisopropylamide rotation than the majority of X-type ligands previously tested. In fact most were worse donors than the poorest anions in the $NCr(NPr^i_2)_2X$ system where X = iodide (15.80±0.30 kcal/mol), triflate (15.65±0.29 kcal/mol) and bromide(15.45±0.30 kcal/mol).

Interestingly, $NCr(NPr^{i}_{2})_2(PzB(Et_3))$ (**10**) with an LDP of 14.35±0.30 kcal/mol, acted characteristically of a poorly donating anion, much like OC_6F_5 (14.32±0.28 kcal/mol) or the electron deficient pyrrole $Pyr^{C6H3(CF3)2}$ (14.36. ±0.28 kcal/mol). As such, the resonance form which places cationic charge β to the coordinated atom (i.e. an electron deficiency on at the 2-position nitrogen of the pyrazole ring) may be the dominate resonance form leading to poor electronic donation from a anionic ligand.

7.6 Counter Ion Effect and Correction

The series of LDP presented in Table 7.1 however was compiled from SST measurements on complexes with varying anions as well as ligands. Though they are all poorer donors than the anions tested, the ordering within the series appears problematic. Suspiciously compounds **4** and **5** both have LDP's of 15.37±0.30 kcal/mol. This seems counterintuitive that an NHC would be as strongly donating as a heterocyclic amine in DMAP. Thus a correction was sought to normalize these numbers, and allow for direct comparison in spite of the inability to synthesize some ligand-anion pairs.

To this end a series of complexes all bearing the DBN ligand was made using a variety of weakly coordinating anions. Presented in Table 7.3 the LDP's of each complex (**2-A**) was measured as above. Upon inspection the experimental LDP of **(2-BAr^{F}_{4})** is more than 1 kcal/mol greater than **(2-I)** at 16.44±0.30 and 15.42±0.30 kcal/mol respectively. This energy difference is approximately the difference in the LDP's of OC_6F_5 and $OSiPh_3$ or F and OPh anionic ligands. Although a small numerical difference, an energy of this magnitude in LDP can translate to largely different chemical properties and patterns of reactivity when the ligand is

used in catalytic processes. For example studies by Swartz et. al. showed that the Ti(IV) catalyzed hydroamination of 1-phenylpropyne with aniline is over 3.5 times faster when using a 3-substitued bispyrrolide ligand (Table 7.2).[27, 28] As previously reported this specific 3-subsitituted pyrrolide has an LDP just 0.2 kcal/mol greater than unsubstituted pyrrolyl (although they are 'indistinguishable' within experimental error).

Hydroamination Catalyst	K_{obs}(× 10^{-7} s^{-1})	Comparable Ligand	LDP (Kcal/mol)
$Ti(NMe_2)_4$	866±94	NMe_2	9.34±0.32
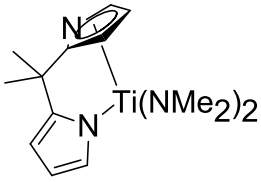	1976±130	Pyr	14.16±0.28
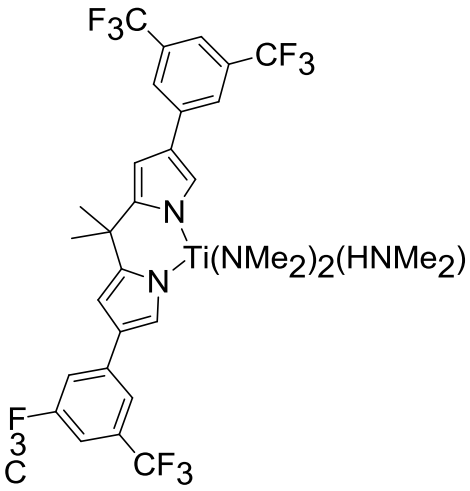	6963±582	$Pyr^{C6H3(CF3)2}$	14.36±0.28

Table 7.2: Evaluation of Ti(IV) Hydroamination Catalysts and their corresponding ligands evaluated by the LDP method.

Within the LDP's of **2-A** complexes a general trend immerges as LDP increases with larger (less-coordinating) cations, implying closer bound cation-anion pairs reduce the barrier to amide rotation in complexes of the same L. In other words, as charge separation increases Cr-diisopropylamide bond order increases, as cationic charge builds at the metal center. In exploring this phenomenon the average radius of each anion was tabulated from a listing of all the structures deposited in the Cambridge Structure Database[29] containing an uncoordinated anion of interest, as at present only **2-I** has been suitable to structurally characterize. Bond length and angle data was used in conjunction with the atomic radii reported by Bondi[30] to calculate the

radius of the smallest sphere possible which completely encloses the anion. This approximation is tabulated in Table 7.2 and graphically presented below.

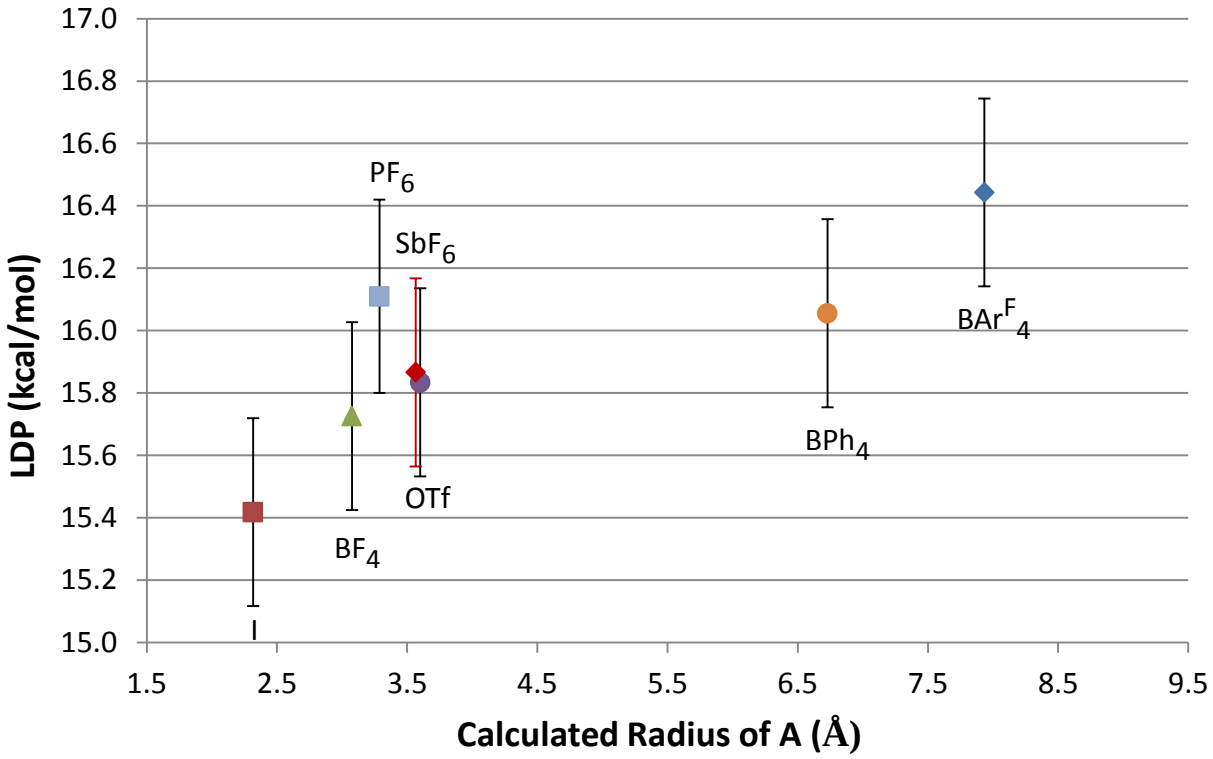

Figure 7.11: LDP's of [NCr(NPr$^{i}_{2}$)$_2$DBN][A] (**2-A**) complexes versus the approximated anion size.

Figure 7.11 shows a general approach toward an asymptote in the LDP of [NCr(NPr$^{i}_{2}$)$_2$DBN][A] (**2-A**) complexes. Thus to quantify the anion perturbation upon LDP a linear correction was applied using [NCr(NPr$^{i}_{2}$)$_2$DBN][BAr$^{F}_{4}$] **(2-BAr$^{F}_{4}$)** as an endpoint, assuming total dissociation between the anion and the chromium nitride cation. By subtracting the LDP's of each [NCr(NPr$^{i}_{2}$)$_2$DBN][A] complex the from that of **2-BAr$^{F}_{4}$** an corrective factor was calculated for each anion as given in Table 7.3.

Compound	LDP (kcal/mol)	Corrective Factor (kcal/mol)	Calculated Anion Radius (Å)
$[NCr(NPr^{i}_{2})_2DBN][I]$ (**2-I**)	15.42±0.30	1.025	2.32
$[NCr(NPr^{i}_{2})_2DBN][BF_4]$ **(2-BF_4)**	15.73±0.30	0.718	3.08
$[NCr(NPr^{i}_{2})_2DBN][OTf]$ **(2-OTf)**	15.83±0.30	0.609	3.60
$[NCr(NPr^{i}_{2})_2DBN][SbF_6]$ **(2-SbF_6)**	15.87±0.30	0.577	3.57
$[NCr(NPr^{i}_{2})_2DBN][BPh_4]$ **(2-BPh_4)**	16.06±0.30	0.387	6.73
$[NCr(NPr^{i}_{2})_2DBN][PF_6]$ **(2-PF_6)**	16.11±0.31	0.334	3.29
$[NCr(NPr^{i}_{2})_2DBN][BAr^{F}_{4}]$ **(2-BAr^{F}_{4})**	16.44±0.30	-	7.93

Table 7.3: Ligand Donor Parameters for $[NCr(NPr^{i}_{2})_2DBN][A]$ (**2-A**) complexes with anion corrective factors and calculated anion radii.

These factors are then added to the experimentally determined LDP of the various L-type ligands based upon the anion employed. In this way we can project what the LDP of each $[NCr(NPr^{i}_{2})_2L][A]$ complex would be if anion A were the BAr^{F}_{4} anion.

This works well to a first approximation, as the corrected LDP places DMAP as a worse donor than the NHC. Barring the strongly donating NHC and THF this correction places all the L-type ligands worse than the tested X-type ligands. Furthermore, this system places the strongest donor as NHC (**5**) and the poorest as a tertiary amine (**3**).

7.7 In situ generation, temperature dependent equilibrium, and solvent effect on LDP.

Although the counter anion correction is appropriate for comparison and implementation of our system, information *about* the system can be gleaned from the synergistic effect of ligand and anion. With an (uncorrected) LDP of 15.42±0.30 kcal/mol it is self-consistent that DBN can displace iodine (15.80±0.30 kcal/mol) to form thermodynamically stable **2-I**.

In a set of related studies $NCr(NPr^{i}_{2})_2I$ (**1**) was treated with excess DMAP in an NMR tube in $CDCl_3$**.** Although the corrected LDP for DMAP based on $[NCr(NPr^{i}_{2})_2DMAP][BF_4]$ (**4-BF_4**) is 16.08±0.30 kcal/mol, the DMAP ligand is competent to displace the iodine into the outer sphere creating a mixture of $[NCr(NPr^{i}_{2})_2DMAP][I]$ (**4-I**) and $NCr(NPr^{i}_{2})_2I$ + DMAP based on temperature (*vida infra*). Separately a sample of $[NCr(NPr^{i}_{2})_2DMAP][BF_4]$ (**4-BF_4**) was treated with 1 equiv. of AgOTf in toluene. This gave a complex mixture which contained unreacted $[NCr(NPr^{i}_{2})_2DMAP][BF_4]$ (**4-BF_4**), $[NCr(NPr^{i}_{2})_2DMAP][OTf]$ (**4-OTf**), and $NCr(NPr^{i}_{2})_2OTf$ in a roughly 1:2:6 ratio, along trace amounts of $NCr(DMAP)_4OTf$ and other unidentified side products. Together these experiments show that in our system DMAP with an uncorrected LDP of 15.37±0.30 kcal/mol can displace an iodide ligand (15.80±0.30 kcal/mol) but resists displacement by triflate anions (15.75±0.29 kcal/mol) forming an equilibrium mixture between $[NCr(NPr^{i}_{2})_2DMAP][OTf]$ (**4-OTf**) and $NCr(NPr^{i}_{2})_2OTf$ (Figure 7.12). Although triflate and iodide are indistinguishable within error, the pattern of reactivity with DMAP may show a manifestation of the 0.05 kcal/mol discrepancy in their LDP parameters.

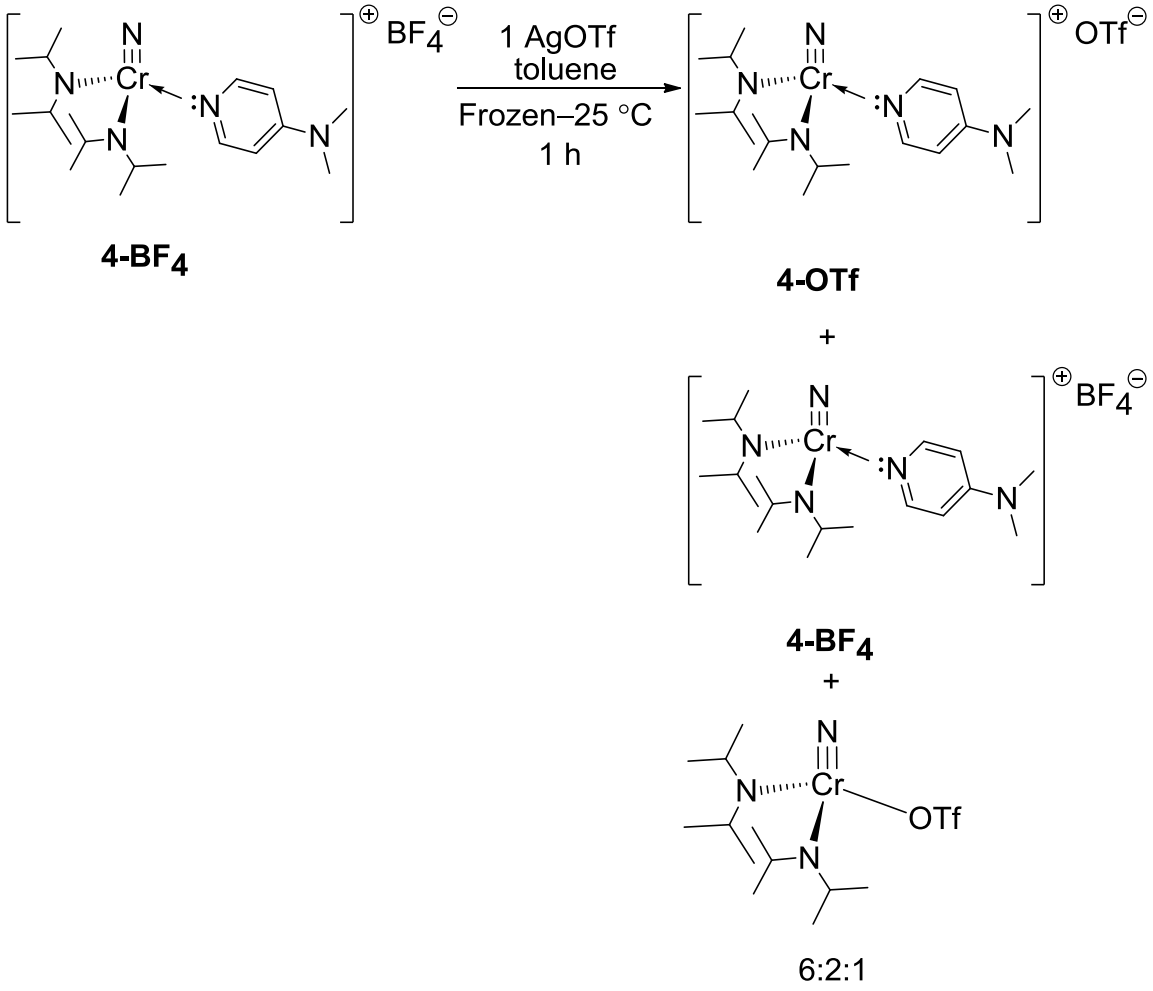

Figure 7.12: Reaction of $[NCr(NPr^{i}_2)_2DMAP][BF_4]$ (**4-BF_4**) with silver triflate

In situ generation of $[NCr(NPr^{i}_2)_2DMAP][I]$ (**4-I**) by treating $NCr(NPr^{i}_2)_2I$ (**1**) with 1 equiv. DMAP in $CDCl_3$ was monitored via ^1H NMR. This gave a mixture of $[NCr(NPr^{i}_2)_2DMAP][I]$ and $NCr(NPr^{i}_2)_2I$ (**1**) in a ratio based upon the solution's temperature (Figure 7.12).

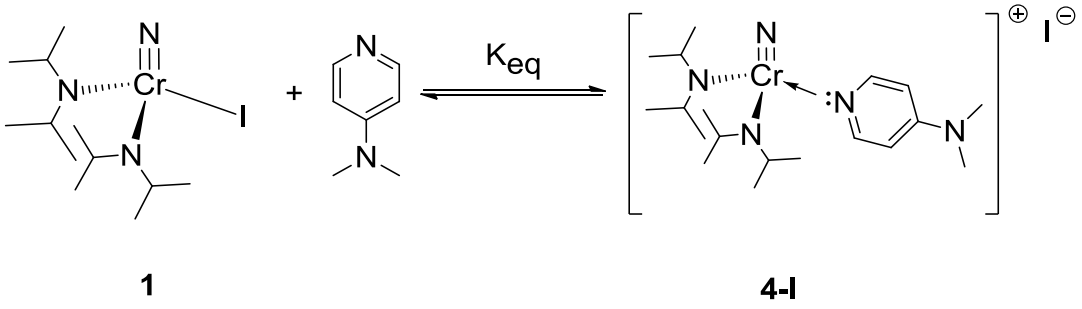

1 **4-I**

Figure 7.13: NCr(NPr$^{i}_{2}$)$_2$I (**1**) and [NCr(NPr$^{i}_{2}$)$_2$DMAP][I] (**4-I**) in a temperature dependent equilibrium.

Data was collected from -41 °C to +27 °C in $CDCl_3$ and -30 °C to +20 °C in actetonitrile-*d3*. In both instances this equilibrium mixture showed no memory, as the temperature was cycled back between temperatures giving the same results (Table 7.4). In both solvents the equilibrium shifts favoring the cation at low temperature. This behavior may be linked to the solvents dielectric constant as the $K_{eq(CD3CN)}>K_{eq(CDCl3)}$ at any given temperature. Furthermore, as temperature increases the dielectric constant of both solvents decrease, with acetonitrile going from 39.7-39.1 on the range 5-60 °C and chloroform going from 6.5-3.7 on the range of -61.5-100 °C.[31,32] In testing this hypothesis temperature dependent equilibrium data was sought in THF-*d8*. Although this caused [NCr(NPr$^{i}_{2}$)$_2$DMAP][I] (**4-I**) formation, ^{1}H NMR spectroscopy at 25 °C showed no **1** present. Inspection of the NMR tube showed **4-I** precipitating from solution, precluding the accurate measurement of an equilibrium constant. Other solvents resulted in either decomposition of **1** (DMSO) or the inability to support Cr(VI) cation formation (toluene).

Acetonitrile-*d3*		Chloroform-*d1*	
Temperature (°C)	$K_{eq(CD3CN)}$	Temperature (°C)	$K_{eq(CDCl3)}$
−30.4	0.243	−41.1	0.236
−14.5	0.173	−30.7	0.134
−3.7	0.109	−4.2	0.068
7.8	0.015	10.8	0.029
20.3	0.005	14.9	0.004
-	-	27.1	0.001

Table 7.4: Temperature based equilibrium of $NCr(NPr^i_2)_2I$ (**1**) and $[NCr(NPr^i_2)_2DMAP][I]$ (**4-I**) in various solvents.

From a synthetic standpoint the balance of solubility versus solvent polarity seems general to the other Cr(VI) cations with L-type ligands. Synthesis (and purification) of $[NCr(NPr^i_2)_2DBN][I]$ (**2-I**) by precipitation from a mixture of **1** with DBN in Et_2O proceeded smoothly, although incompletely. While changing the solvent to THF produced more **2-I** the increased solubility of **2-I** in THF prohibited precipitation making isolation from **1** difficult. Conversely, in pentane complex **1** was very soluble whereas **2-I** is completely insoluble but would not form in such low polarity conditions.

Although solubility issues precluded the determination of an equilibrium constant of the in situ generated $[NCr(NPr^i_2)_2DMAP][I]$ (**4-I**) in THF-*d8*, the LDP was measured giving a

barrier to rotation of 15.77±0.30 kcal/mol. When compared to the LDP of [NCr(NPr$^{i}_{2}$)$_2$DMAP][I] (**4-I**) in acetonitrile-*d3* of 15.98±0.28 kcal/mol the DMAP ligand appears to be a stronger donor in THF. Attempts to obtain an LDP for (**4-I**) in $CDCl_3$, unfortunately were unsuccessful as a suitable temperature is not available where both enough of the compound is generated in the equilibrium and the kinetics of diisopropylamide rotation are fast enough to measure. However, if we use the corrected LDP for DMAP (ostensibly what we would observe for the compound [NCr(NPr$^{i}_{2}$)$_2$DMAP][BAr$^{F}_{4}$]) and *subtract* the corrective factor for the iodide anion a reasonable estimate for [NCr(NPr$^{i}_{2}$)$_2$DMAP][I] (**4-I**) in $CDCl_3$ can be made at 15.07 kcal/mol. These LDP figures track well with the dielectric constants of the three solvents (Table 7.5).

Solvent	LDP (kcal/mol)	Dielectric Constant[a]
Acetonitrile	15.98±0.28	37.5
Tetrahydrofuran	15.77±0.30	7.58
Chloroform	15.07[b]	4.81

a Dielectric constants are given at 25 °C. b Calculated from anion corrections.

Table 7.5: LDP's of [NCr(NPr$^{i}_{2}$)$_2$DMAP][I] (**4-I**) in each solvent along with their dielectic constants.

Such a large solvent dependence of LDP is unique to the cationic complexes with neutral donors, as little to no solvent dependence was observed when evaluating anionic ligands. A

previous SST measurement of $NCr(NPr^{i}_{2})_2OBu^{t}_{F6}$ by the Cummins group placed the free energy of diisopropylamide rotation at $\Delta G^{\ddagger}$ = 16 kcal/mol at room temperature in C_6D_6.[16] Assuming the same entropy term of $\Delta S^{\ddagger}$ = -9 cal/mol K this translates to an LDP of 13.54 kcal/mol versus an LDP of 13.89±0.26 kcal/mol when evaluated in $CDCl_3$. This is likely within error but still follows the observed trend as benzene's dielectric constant is 2.27 at 25 °C.

Further work in this area is needed to fully understand and correct for the solvents effect upon LDP.

7.8 Structure of Cr(VI) Cations

In addressing the steric profiles of the L-type ligands single crystal X-ray structures of **2-I, 3-6** and **8** were obtained via the slow evaporation of concentrated solutions of each at -35 °C. Generally the chromium nitride cationic complexes do not crystalize as well as the neutral $NCr(NPr^{i}_{2})_2X$ complexes previously investigated. Chromium-$N_{nitrido}$ bond distances for the Cr(VI) cations range from 1.533(2) Å to 1.546(2) Å and show no significant difference from the Cr-$N_{nitrido}$ $NCr(NPr^{i}_{2})_2X$ complexes. Similarly, the average Cr-NPr^{i}_{2} bond distance was 1.813(3) Å in the Cr(VI) cations, close to the average bond distance observed in the neutral complexes. As before no correlation between the Cr-N_{nitrdo} bond distance or the average Cr-NPr^{i}_{2} bond distance and the LDP value was observed. Several structural features of these complexes are worth noting and will be discussed individually below.

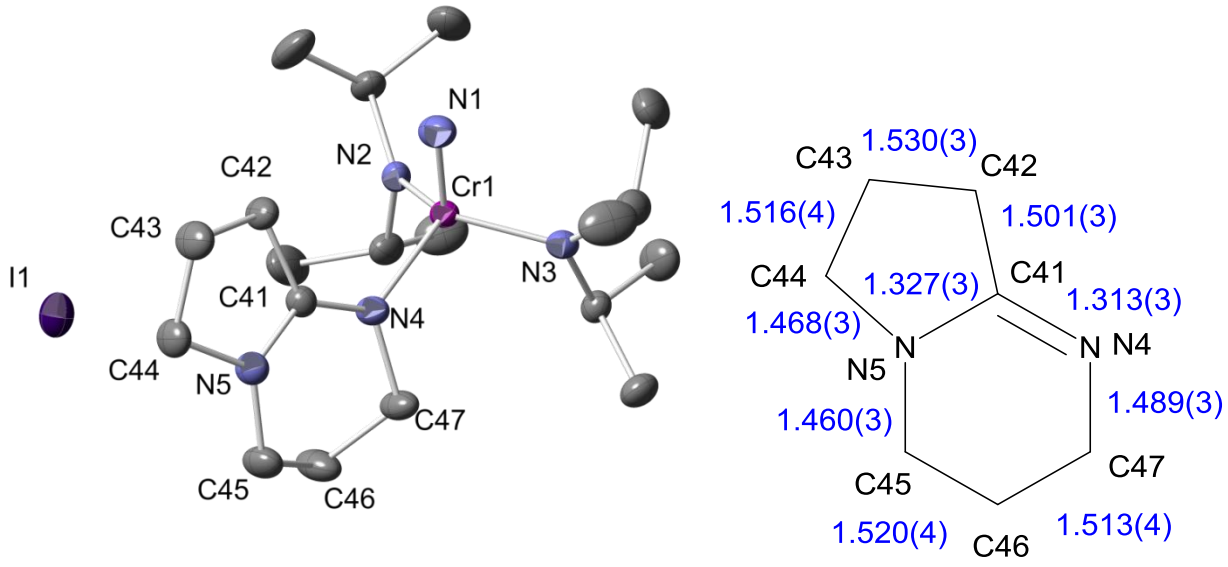

Figure 7.14: Crystal structure rendering of [NCr(NPr$^{i}_{2}$)$_2$DBN][I] (**2-I)** with thermal probabilities at 50% and H atoms omitted for clarity. Bond lengths within the DBN ligand are shown in the inset in Å (blue).

The complex [NCr(NPr$^{i}_{2}$)$_2$DBN][I] (**2-I)** represents the only Cr(VI) cation of this type to be isolated and structurally characterized with an iodine counter ion. The Cr-N3 bond distance of 1.973(2) Å is markedly short for a formally dative bond, approaching that of the analogous Cr-N bond distance of 1.966(4) Å observed in NCr(NPr$^{i}_{2}$)$_{22}$Pyr$^{C6H3(CF3)2}$. Comparison to the structurally characterized 9-hydroxymethyl-1,5-Diazabicyclo[4.3.0]non-5-ene[33] show that the N4-C41 bond in **2-I** is lengthened while the N5-C41 bond has shortened from the corresponding bond lengths (1.279 Å and 1.343 Å respectively). Likewise the analogous N4-C41 bond length in DBN·HCl (protonated at the 1 position of DBN i.e. N4) is 1.377 Å, with the N5-C41 bond shortened to 1.269 Å. These lengths suggest an intermediary between the two structures and provide evidence of a resonance structure in **2-I** that places cationic charge on N5 (Figure 7.15).

Additionally the ^{13}C NMR of **2-I** shows a downfield shift of the imine carbon resonance when compared to free DBN (169.30 ppm and 160.16 ppm respectively) suggesting a deshielding of this position. Further study of the ^{13}C NMR of the DBN ligand may be instructive among the entire series of **2-A** complexes as it may correlate to the observed LDP's.

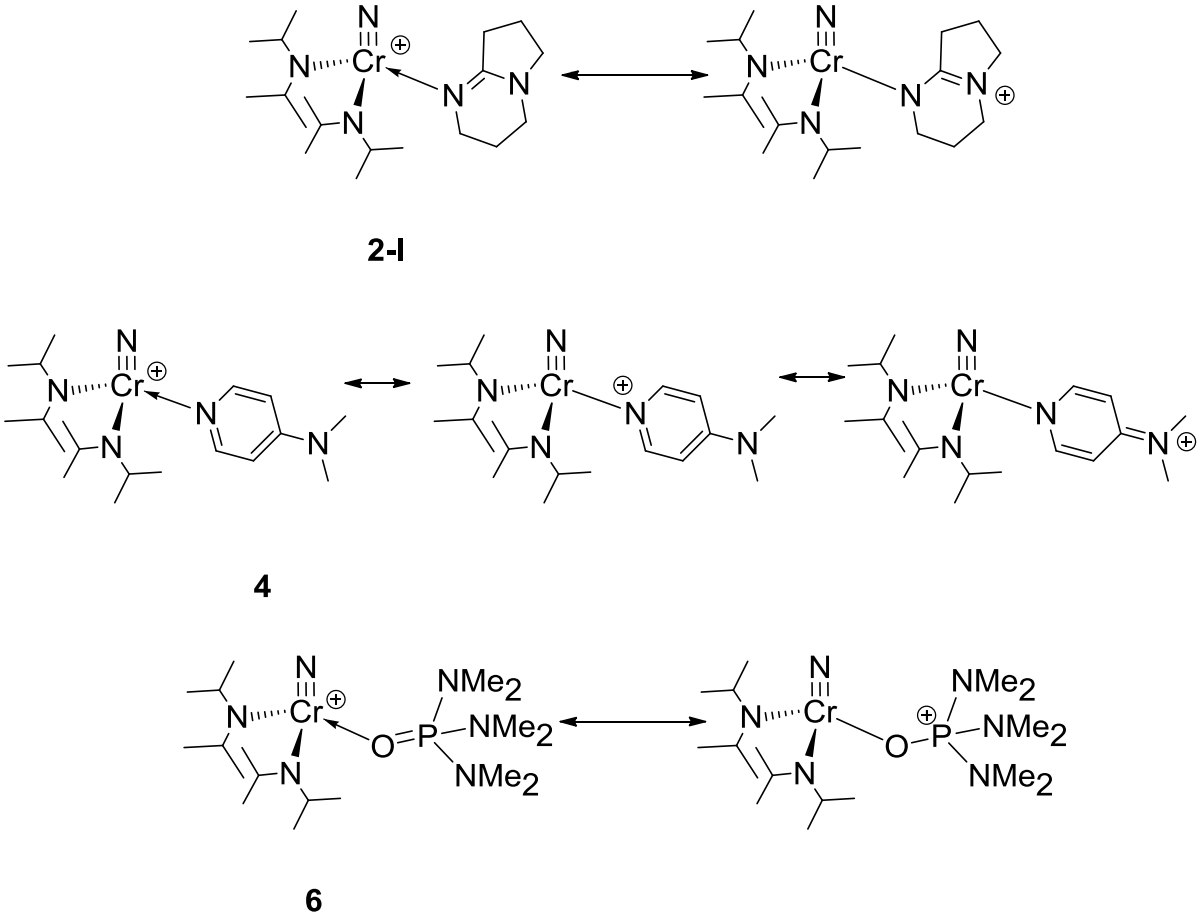

Figure 7.15: Resonance structures of **2-I**, **4-BF$_4$**, and **6**. Weakly coordinating anion omitted for clarity.

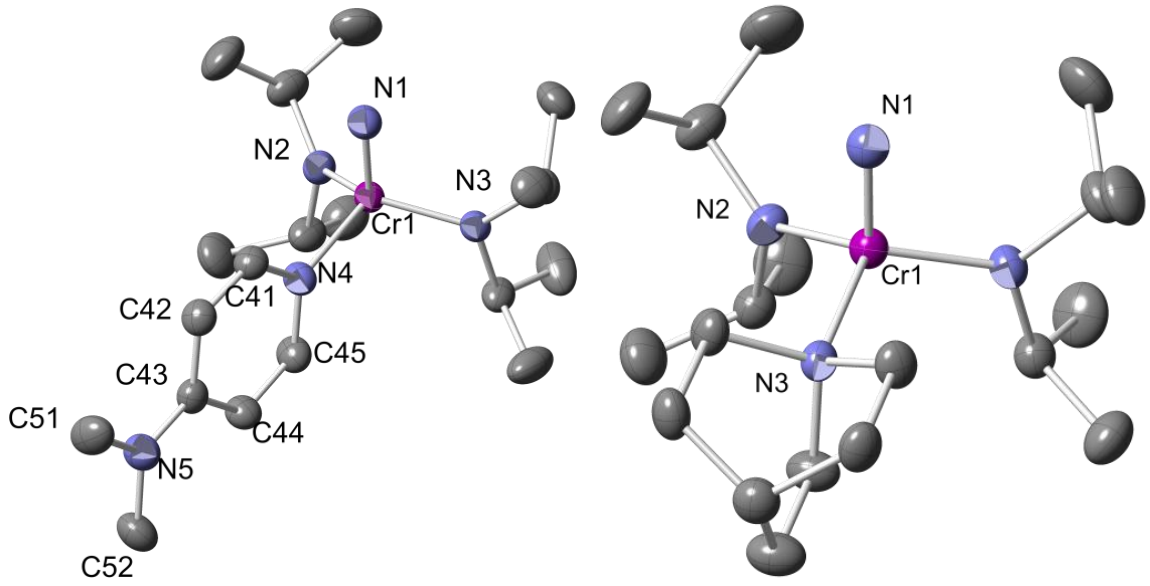

Figure 7.16: Crystal structure renderings for the cations of [NCr(NPr$^{i}_{2}$)$_2$DMAP][BF_4] (**4-BF_4**) (left) and [NCr(NPr$^{i}_{2}$)$_2$quin][PF_6] (**3**) (right). Atom positions at 50% probability. H atoms and a solvent of crystallization (toluene) removed in the case of **4-BF_4**.

Although both are bound to chromium through a sp^2 nitrogen, compound **4-BF_4** has a significantly longer Cr-N4 bond length to that of **2-I** at 2.001(2) Å. Some bond localization within the 6-membered ring of DMAP is observed with slightly shorter C41-C42 (1.359(4)Å) and C45-C44 (1.354(4)Å) bonds compared to 1.381(3)Å and 1.375(4)Å in free DMAP.[34] Additionally, the C41-N4 (1.359(3)Å) and C45-N4 (1.357(3)Å) distances are lengthened from those of unbound DMAP at 1.337(3)Å and 1.335(4)Å). Bond contraction is also observed in the C43-N5 bond length of **4-BF_4** at 1.342(3)Å versus the 1.367(3)Å for the corresponding bond in DMAP. These bond lengths are similar to those in 4-Dimethylaminopyridine hydrochloride

dehydrate, with localized bonding with the ring and a contracted C-NMe_2 bond length corresponding to C43-N5 of 1.340(3) Å.[35] Compound **4-BF_4** maintains co-planarity of the 6 membered ring and the NMe_2 group with a dihedral angle defined by C42-C43-N5-C51 of 2.46°. ^{1}H NMR of **4-BF_4** shows a single resonance for the *N*-methyl groups of DMAP at 0 °C (the lowest temperature obtained), as does the related **4-I** down to −40 °C suggesting a low barrier to rotation about the Cr1-N4 bond. Like **2-I** it is likely that the cationic charge of **4-BF_4** is delocalized onto the ligand (Figure 7.15) affording stability to the molecule.

Unlike **2-I** and **4-BF_4**, [NCr(NPr^i_2)$_2$quin][PF_6] (**3**) exhibits a crystallographic mirror plane along the N1-Cr1-N3 plane. The Cr-N3 bond distance in **3** of 2.068(4) Å is statistically shorter than the other chromium sp^2 nitrogen bonds evaluated. Though electronegativity increases with increasing *s*-character, the less electronegative sp^3 nitrogen of **3** is the weakest donating of all N bound ligands tested. The hybridization of nitrogen does not appear to be a predominate factor in the LDP's or bond lengths to each ligand. Moreover, LDP and bond lengths within **2-I**, **3**, and **4-BF_4** do not correlate to pKa values for the conjugate acids of DBN, quinicludine, and DMAP. As was noted in Chapter 4, metal-ligand bond lengths are not predictive of LDP's in the NCr(NPr^i_2)$_2$X and [NCr(NPr^i_2)$_2$L][A] systems, reiterating the need for multifaceted approaches toward ligand evaluation .

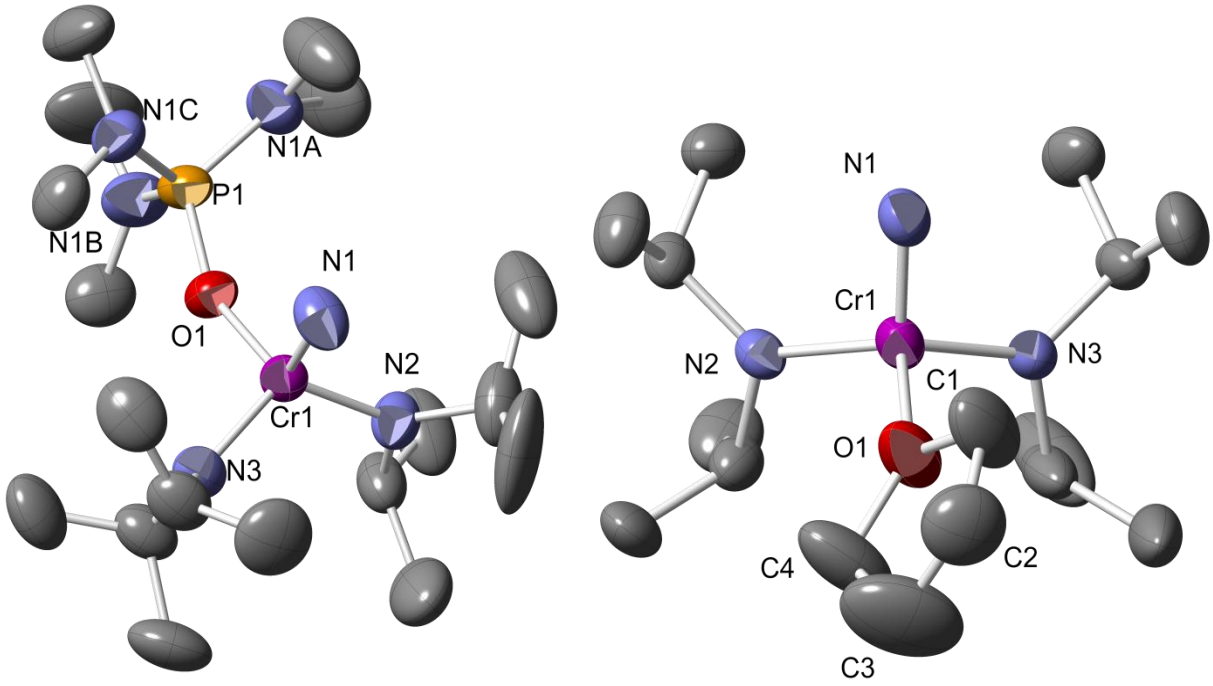

Figure 7.17: Crystal structure renderings of the cation of $[NCr(NPr^{i}_{2})_2(HMPA)][PF_6]$ **6** (left) and $[NCr(NPr^{i}_{2})_2(THF)][PF_6]$ **8** (right). Atom positions at 50% probability and H atoms removed for clarity.

The oxygen bound ligands in $[NCr(NPr^{i}_{2})_2(HMPA)][PF_6]$ **6** and $[NCr(NPr^{i}_{2})_2(THF)][PF_6]$ **8** contain especially short Cr1-O1 bond lengths bond at 1.888(4) Å and 1.957(4) Å respectively. These bonds represent the closest Cr-O contacts crystallographically known for formally dative interactions. As shown in Figure 7.15 a likely resonance structure in **6** delocalizes cationic charge onto phosphorus. This manifests as a weakening of the P-O bond which averaged 1.517(4) Å in the crystal structure of **6** as compared to 1.478(2)Å in unbound HMPA.[36] Further evidence for charge delocalization comes from the

^{31}P NMR resonance of bound HMPA in **6** at 37.86 ppm, shifted downfield of free HMPA 29.30 ppm when added into the same sample.

Unlike **6** complex **8** has no stable resonance forms that can delocalize the cationic charge residing on the metal center. However, complex **8** is competent to polymerized THF, likely by ring opening an oxonium species.[37,38] Inspection of the ^{1}H NMR resonances of the coordinated THF in **8** shows a downfield shift of 0.426 ppm for the protons attached to C1/C4 and 0.303 ppm for the protons on C2/C3 when compared to unligated THF. As before this effect is consistent with oxonium formation via the transfer of positive charge from the chromium onto the ligand.[39]

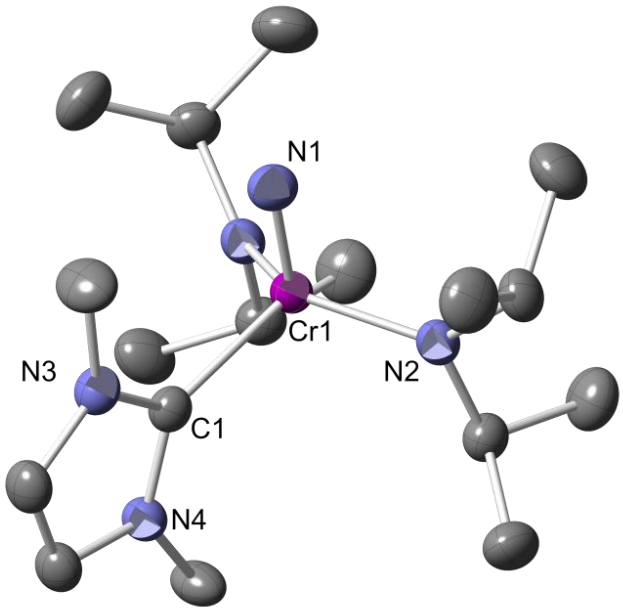

Figure 7.18: Crystal structure rendering of the cation of [NCr(NPr$^{i}_{2}$)$_2$NHC][PF$_6$] (**5**). Atomic positions at 50% probability and H atoms removed for clarity.

[NCr(NPr$^{i}_{2}$)$_2$NHC][PF$_6$] (**5**) is of particular interest as it is the first structurally characterized chromium N-heterocyclic carbene known in the Cr(VI) oxidation state.

Crystalizing in the space group Pnma, the compound has a mirror plane bisecting the molecule down the plane of the NHC and adopts a distorted tetrahedral geometry about the chromium center. The plane defined by the 5-membered NHC ring is parallel to the Cr-$N_{nitrido}$ axis, with a dihedral angle defined by N1-Cr1-C1-N3 of 0.00°.Complex **5** has a Cr-C1 bond length of 2.081(4) Å, 0.111 Å longer than predicted by Pyykkö's table of covalent radi for a chromium carbon single bond.[40] This length is markedly shorter than the Cr(0) NHC's reported (which average 2.143 Å), and most Cr(II) and Cr(III), averaging 2.126 Å and 2.158 Å respectively. A 2011 paper by Wang and coworkers reports the Cr(V) nitride $NCrPh_2(IMP)_2$, where IMP = 1,3-diisopropyl-4,5-dimethylimidazole-2-yl-idene.[41] This complex has an average Cr-C_{IMP} bond length of 2.111(2) Å, statistically longer than that in **5**. The ^{1}H NMR of complex **5** has equivalent resonances for the methyl groups on N3 and N4 at room temperature indicating a low barrier to rotation about the Cr-C1 bond at this temperature.

7.9 Steric Analysis of Cr(VI) Cations

In quantitatively addressing the overall steric profile of the $[NCr(NPr^i_2)_2L][A]$ complexes structurally characterized two separate methods were employed using the atomic positions gained from the single crystal x-ray diffraction of **2-I, 3-6** and **8**. For an in depth discussion of the method of solid angles using the Solid G[42] program**,** and a calculation of occupied volume, $\%V_{bur}$[43] please refer to Appendix B. Tabulated data for each complex are listed in Table 7.6.

Compound	$\%V_{bur}$	$G_m(L)$
$[NCr(NPr^i_2)_2THF][PF_6]$ (**8**)	20.4	18.4
$[NCr(NPr^i_2)_2NHC][PF_6]$ (**5**)	25.0	23.4
$[NCr(NPr^i_2)_2DMAP][BF_4]$ (**4-BF$_4$**)	20.8	19.1
$[NCr(NPr^i_2)_2DBN][I]$ (**2-I**)	25.3	22.8
$[NCr(NPr^i_2)_2HMPA][PF_6]$ (**6**)	22.8	24.3
$[NCr(NPr^i_2)_2quin][PF_6]$ (**3**)	26.8	22.6

Table 7.6: The steric parameters %Vbur and Gm(L) of $[NCr(NPr^i_2)_2L][A]$ complexes, both given as a percent.

When addressing the amount of space occupied by each L-type ligand via the method of $\%V_{bur}$, a sphere of 3.5 Å is circumscribed around the metal center approximating the first coordination sphere of the Cr(VI) center. The volume of this sphere occupied by the constituents of a given ligand are then compared to the total volume and given as a percentage. For this treatment the anion of each complex was ignored, as none showed any close contacts to the Cr(VI) cation.

The calculated $\%V_{bur}$ of the L-type ligands span a relatively narrow range when viewed in context of the anionic ligands already reported. On the small end THF at 20.4% is identical to that calculated for pyrrolide. While most of the L-type ligands presented here are largely planer,

the ridged structure of quinicudine places it as the second largest ligand evaluated among anions and neutral donors, with a $\%V_{bur}$ of 26.8%. Only NPr^{i}_{2} at 29.1% was larger. Although 1,3 dimethyl imidazolide was chosen as it is the smallest 1,3 disubstituted NHC available, the 25.0% buried volume suggests some steric interaction may hinder the diisopropylamide rotation in **5** This may also be the case with DBN (25.3%) as noted before with the anionic carbazolyl ligand (25.0%). In fact among the two series, the L-type ligands presented here represent 4 of the 10 largest ligands evaluated by $\%V_{bur}$.

When approached from a solid angle standpoint, the description of sterics is focused more on access to the metal center by an incoming substrate. By treating the Cr(VI) center as a point source of light each bound ligand casts a 'shadow' on an arbitrarily sized sphere inscribing the complex. The area of this 'shadow' is calculated and also given as a percentage of the total area of the sphere. The steric parameter $G_m(L)$ calculated in this way by the Solid G program for **2-I, 3-6** and **8** are shown in Table 7.6.

Unlike the series of $\%V_{bur}$ the $G_m(L)$ parameters span a large range, with THF (18.4%) similar in size to that of Br (18.6%) to HMPA (24.3%) the 4^{th} largest ligand evaluated similar to that of 1-adamantoxy (24.3%). Additionally, the ordering of ligand size in $G_m(L)$ within the series of HMPA>NHC>DBN>quin>DMAP>THF differs from that calculated by $\%V_{bur}$, quin>DBN>NHC>HMPA>DMAP>THF. This reordering is likely attributed to the different way in which each system treats steric bulk distal to the metal center. For example, while HMPA contains more non-hydrogen atoms than quinuclidine, the majority of the bulk in the NMe_2

groups is held over 3.5 Å away from the metal center, thus is not included in the in $\%V_{bur}$ calculation. Quinuclidine however is bound through a tertiary nitrogen, placing much of the bulk with the sphere of enclosure leading to a larger $\%V_{bur}$ (Figure 7.19). Conversely, when calculated in by the Solid G the branched HMPA ligand shields more of the metal center than the compact quinuclidine ligand.

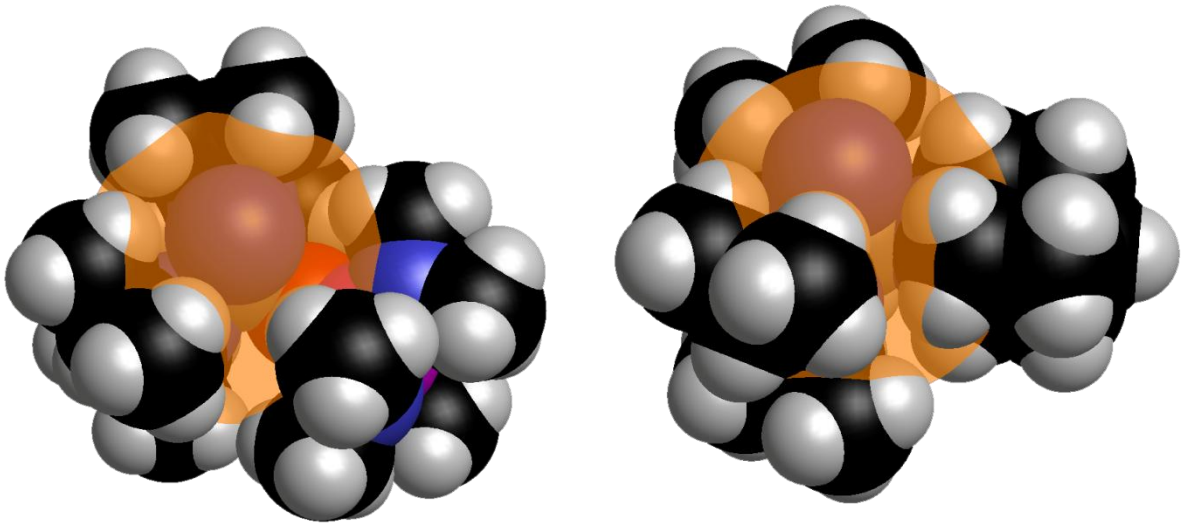

Figure 7.19: Space filling models of $[NCr(NPr^{i}_{2})_2HMPA][PF_6]$ (**6**) (left) and $[NCr(NPr^{i}_{2})_2quin][PF_6]$ (**3**) (right) with a 3.5 Å radius sphere approximating the first coordination sphere of the Cr(VI) center.

7.10 Series of Nitrogen bound ligands

With the addition of **2-I**, **3** and **4-BF_4** fourteen complexes of the form $NCr(NPr^i_2)_2(X)$ or $[NCr(NPr^i_2)_2L][A]$ where X or L are bound by a nitrogen atom have been synthesized, structurally characterized, and evaluated by the LDP methodology. This subset spans the range of observed LDP's, with NMe_2 being the strongest donor evaluated and quinuclidine the weakest, at 9.34±0.32 kcal/mol and 19.01±0.32 kcal/mol respectively. Furthermore, the series of N-bound ligands also covers a wide range of steric profiles. When evaluated by $\%V_{bur}$ the largest ligand evaluated was NPr^i_2 (29.1%) ranging to the second smallest ligand NCO at 13.4%. When evaluated by the Solid G system NPr^i_2 remains the largest ligand at 26.4%, with NCO (18.0%) also remaining the smallest N-bound ligand (although now the fourth smallest in the entire series). The crystallographically determined $Cr\text{-}N_{ligand}$ bond lengths are equally as varied, with a difference of 0.225 Å between the longest and shortest contact observed. (Table 7.7). Of the observed bond lengths the longest belongs to $[NCr(NPr^i_2)_2quin][PF_6]$ (the worst donor), and the shortest to $NCr(NPr^i_2)_3$ or within error $NCr(NPr^i_2)_2NMe_2$ (the best donor).

Compound	LDP (Corrected) (kcal/mol)	Cr-N Bond distance (Å)
$NCr(NPr^{i}_{2})_3$	11.12±0.23	1.842(3)
$NCr(NPr^{i}_{2})_2NMe_2$	9.34±0.32	1.845(6)
$NCr(NPr^{i}_{2})_2N(Me)Ph$	10.86±0.23	1.889(2)
$NCr(NPr^{i}_{2})_2$indolyl	13.40±0.24	1.933(2)
$NCr(NPr^{i}_{2})_2Pyr^{Fc}$ a	13.45±0.27	1.938(3)
$NCr(NPr^{i}_{2})_2$Pyr	14.16±0.28	1.946(2)
$NCr(NPr^{i}_{2})_2$NCS	14.86±0.30	1.946(2)
$NCr(NPr^{i}_{2})_2$carbazolyl	12.04±0.25	1.947(2)
$NCr(NPr^{i}_{2})_2Pyr^{C6F5}$	14.33±0.28	1.951(1)
$NCr(NPr^{i}_{2})_2Pyr^{C6H3(CF3)2}$	14.36±0.28	1.966(4)
$[NCr(NPr^{i}_{2})_2$DBN][I] (**2-I**)	15.42±0.30 (16.44±0.30)	1.973(2)
$NCr(NPr^{i}_{2})_2NCO$	14.51±0.29	1.980(3)
$[NCr(NPr^{i}_{2})_2$DMAP][BF_4] (**4-BF_4**)	15.37±0.30 (16.08±0.30)	2.001(2)
$[NCr(NPr^{i}_{2})_2$quin][PF_6] (**3**)	18.67±0.32 (19.01±0.32)	2.067(4)

a See Chapter 8

Table 7.7: Cr1-N1 bond lengths and LDP's of all structurally characterized $NCr(NPr^{i}_{2})_2(X)$ and $[NCr(NPr^{i}_{2})_2L][A]$ complexes with ligands bound through nitrogen.

Traditional thinking has argued that metal-ligand bond lengths should correlate to bond order. The series above provides a unique opportunity to investigate that argument, as bond lengths and the empirically derived electronic nature of the Cr-N_{ligand} bonds are known quantitatively. Although our LDP parameter is a measurement of the *Cr-NPr$^{i}_{2}$ bond order* and not the Cr-N_{ligand} bond order, a one-to-one correlation exists. Since both bond orders are of non-integer value the numerical value is less important than the ordering since no zero-point exists (i.e. we would have to designate one Cr-N_{ligand} bond length as having a bond order of exactly 1). Below the series of N-bound ligands is presented graphically (Figure 7.20).

The dataset shows a loose linear correlation between LDP and bond length running through the best and worse donors of the series. Although the NCr(NPr$^{i}_{2}$)$_2$ fragment is largely isosteric among the compounds the steric influence of the ligand be the source of deviation from the trend line. The LDP as defined is dependent on the rotation of very bulky diisopropylamide ligands. When the X or L in question is sufficiently large steric influence may cause an increase in the observed NPr$^{i}_{2}$ barrier of rotation in addition to the barrier imposed by the Cr-NPr$^{i}_{2}$ bond order. This may or may not be included in the entropy term ($\Delta S^{\ddagger}$) which has not been independently determined for all compounds.

Curiously, the data points furthest off the line are that of carbazolyl and NPr$^{i}_{2}$, the largest by far and third largest of all ligands evaluated by the $\%V_{bur}$ system. When these two points are excluded from the graph the R^2 value increases to 0.95. Though NPr$^{i}_{2}$ is also the largest by Solid

G carbazolyl is nominally bigger than NMe_2. This may indicate that in fact $\%V_{bur}$ is a better measure of intermolecular processes (i.e. bond rotation) than Solid G, as argued in Appendix B. When comparing the solid state Cr-N_{ligand} bond lengths of NMe_2 and NPr^i_2 they are indistinguishable within esd. Their LDP's however are ~1.78 kcal/mol different. From a purely electronic standpoint one might expect NPr^i_2 to be more electron rich by the increased inductive effect of an extend carbon change, and thus a better donor than NMe_2 toward a d^0 metal center. This follows as the pKa of NPr^i_2 (11.05) is greater than that of NMe_2 (10.64).[44] However, the opposite ordering in LDP's is observed, as the measurement is taken in solution with molecular dynamics occurring. It is very likely that the large difference in LDP (stemming from the larger barrier to rotation) is steric in origin and that in the absence of this effect the LDP of NPr^i_2 would be slightly lower or equal to that of NMe_2. The same argument may be true of the other members of the series to a lesser extent. Where this threshold of sterics exists merits further study, but may be a system specific effect.

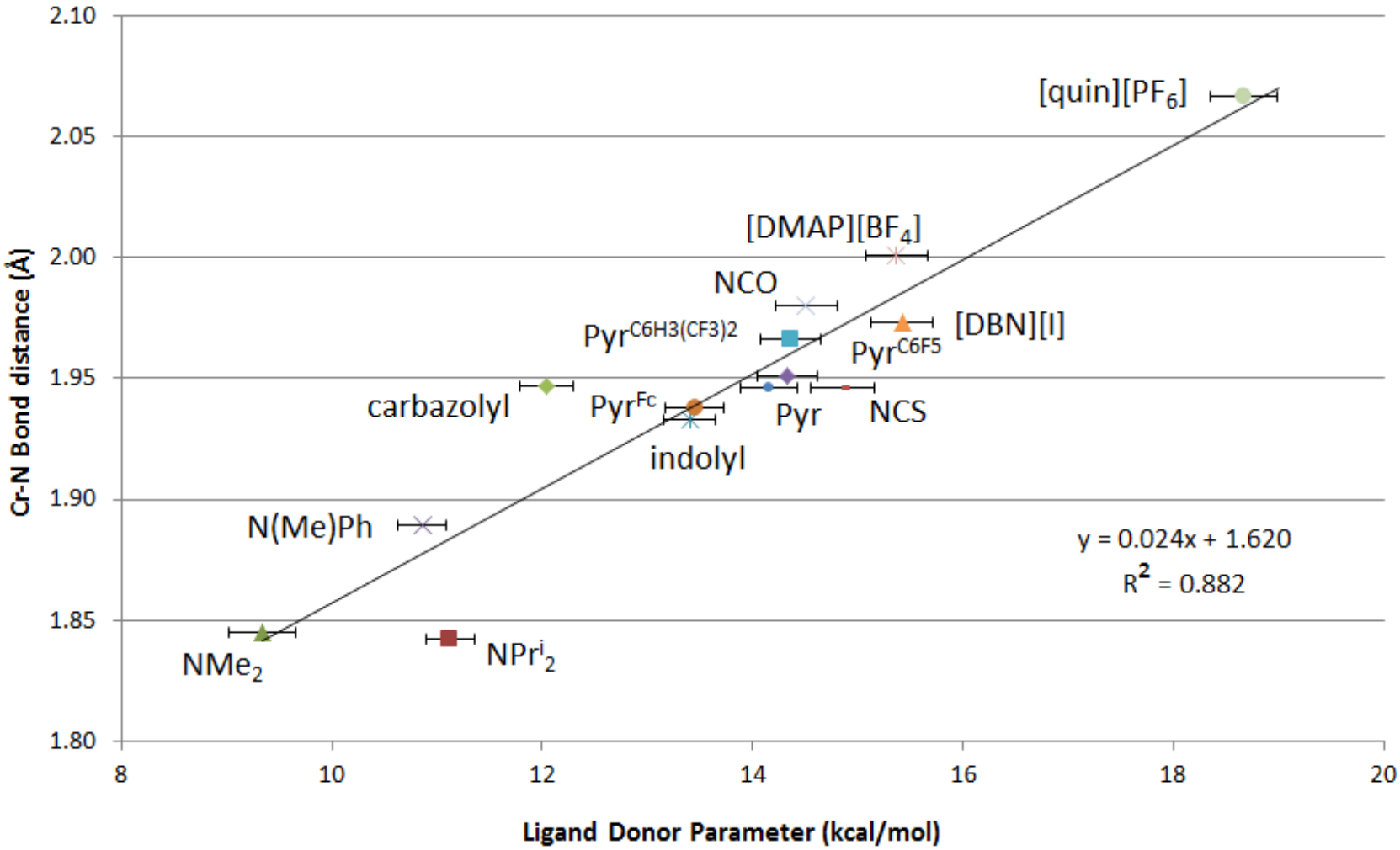

Figure 7.20: LDP values versus the crystallographically determined bond lengths from chromium to the ligated nitrogen atom.

7.11 Conclusion

In expanding the methodology for electronically parameterizing ligand donor abilities of neutral donors several cationic Cr(VI) complexes bearing L-type ligands were synthesized. New synthetic methods were developed including displacement of iodine from $NCr(NPr^i_2)_2I$ (**1**), halide abstraction using silver salts of weakly coordinating anions, substitution of L, and substitution of A to form complexes of the type $[NCr(NPr^i_2)_2(L)][A]$ where L = THF, DMAP, HMPA, qunicludine, ^{t}BuNC, DBN, $P(Me)_2Ph$, NHC and A is an dissociated anion. Also, the complex $NCr(NPr^i_2)_2(PzB(Et_3))$ (**10**) bearing a mono pyrazolyl borate was synthesized. The kinetics of diisopropylamide rotation was measured via Spin Saturation Magnatization Transfer in the ^{1}H NMR for each complex. In correcting these LDP's for anion effects a series of $[NCr(NPr^i_2)_2(DBN)][A]$ compounds were made where A = I, OTf, BF_4, PF_6, SbF_6, BPh_4, and BAr^F_4, and a linear correction factor applied giving the donor series $PzB(Et_3)$>THF>NHC>DMAP>^{t}BuNC>DBN>HMPA>$P(Me)_2Ph$>quin. When $NCr(NPr^i_2)_2I$ was treated with DMAP iodine was displaced into the outer sphere producing $[NCr(NPr^i_2)_2(DMAP)][I]$ in a temperature dependent equilibrium, favoring cation formation at low temperature. The LDP was determined for $[NCr(NPr^i_2)_2(DMAP)][I]$ in $CDCl_3$, CD_3CN, and THF-*d8* with LDP increasing with increasing dielectric constant of the solvent. Compounds **2-I, 3-6** and **8** were structurally characterized via single crystal x-ray diffraction, showing short Cr-O bonds and giving evidence for cationic charge delocalization onto the ligands. The steric profiles of **2-I, 3-6** and **8** were calculated through the methods of $\%V_{bur}$ and Solid G. Lastly, $Cr\text{-}N_{ligand}$

bond distances were discussed as a function of LDP for the X- and L-type ligands bound through nitrogen.

7.12 Experimental

Procedure for Equilibrium Studies Under an N_2 atmosphere a JY tube was loaded with **1** (26.3 mg, 0.067 mmol, 1 equiv.)**,** 4-Dimethylaminopyridine (8.17 mg, 0.067 mol, 1equiv.) and a deuterated solvent (0.75 mL). The tube was sealed with a teflon stopcock and shaken to ensure mixing. The tube was removed from the drybox and was degased using the freeze-pump-thaw method. ^{1}H NMR measurements were taken on a Varian Inova 500 MHz spectrometer. At each data point the temperature was allowed to stabilize for 10 min. After collection the temperature of the spectrometer was taken with a methanol or ethylene glycol standard allowed to equilibrate for 10 min.[45] After initial collection the high and low temperature data points were taken again to ensure that a fully reversible equilibrium was occurring. Concentrations of **1** and **4-I** were measured by the relative proportions of the integrals of their methine resonances normalized to the initial concentration. This was fit to the following equation to find the Keq at each temperature.

$$K_{eq} = \frac{\left[\mathrm{NCr}\left(\mathrm{NPr^i_2}\right)_2(\mathrm{DMAP})\right][\mathrm{I}]}{[\mathrm{NCr}(\mathrm{NPr^i_2})_2\mathrm{I}][\mathrm{DMAP}]}$$

[NCr(NPr$^{i}_{2}$)$_2$(DMAP)][I] (4-I) ^{1}H NMR (500 MHz, $CDCl_3$, -25 °C): 8.49 (d J_{HH} = 6.8 Hz, 2H, $NC_5H_4N(CH_3)_2$), 6.68 (d J_{HH} = 6.6 Hz, 2H, $NC_5H_4N(CH_3)_2$), 5.81 (sept J_{HH} = 5.9 Hz, 2H, $N(CH(CH_3)_2)_2$), 3.90 (sept J_{HH} = 6.1 Hz, 2H, $N(CH(CH_3)_2)_2$), 3.11 (s, 6H, $NC_5H_4N(CH_3)_2$), 1.83 (d J_{HH} = 6.5 Hz, 6H, $N(CH(CH_3)_2)_2$), 1.52 (d J_{HH} = 6 Hz, 6H, $N(CH(CH_3)_2)_2$), 1.22 (d J_{HH} = 6 Hz, 6H, $N(CH(CH_3)_2)_2$), 1.15 (d J_{HH} = 6 Hz, 6H, $N(CH(CH_3)_2)_2$).

^{1}H NMR (500 MHz, CD_3CN, -30 °C): 8.26 (d J_{HH} = 6.3 Hz, 2H, $NC_5H_4N(CH_3)_2$), 6.84 (d J_{HH} = 6.1 Hz, 2H, $NC_5H_4N(CH_3)_2$), 5.61 (sept J_{HH} = 6.2 Hz, 2H, $N(CH(CH_3)_2)_2$), 4.19 (sept J_{HH} = 5.9 Hz, 2H, $N(CH(CH_3)_2)_2$), 3.24 (s, 6H, $NC_5H_4N(CH_3)_2$), 2.01 (d J_{HH} = 5.6 Hz, 6H, $N(CH(CH_3)_2)_2$), 1.69 (d J_{HH} = 6.1 Hz, 6H, $N(CH(CH_3)_2)_2$), 1.36 (d J_{HH} = 6.1 Hz, 6H, $N(CH(CH_3)_2)_2$), 1.26 (d J_{HH} = 6.1 Hz, 6H, $N(CH(CH_3)_2)_2$).

^{1}H NMR (500 MHz, THF, 25 °C): 8.10 (d J_{HH} = 3 Hz, 2H, $NC_5H_4N(CH_3)_2$), 6.50 (d J_{HH} = 3.5 Hz, 2H, $NC_5H_4N(CH_3)_2$), 5.37 (sept J_{HH} = 5.5 Hz, 2H, $N(CH(CH_3)_2)_2$), 3.86 (sept J_{HH} = 5 Hz, 2H, $N(CH(CH_3)_2)_2$), 2.96 (s, 6H, $NC_5H_4N(CH_3)_2$), 1.82 (d J_{HH} = 5 Hz, 6H, $N(CH(CH_3)_2)_2$), 1.54 (d J_{HH} = 5 Hz, 6H, $N(CH(CH_3)_2)_2$), 1.33 (d J_{HH} = 5 Hz, 6H, $N(CH(CH_3)_2)_2$), 1.18 (d J_{HH} = 5.5 Hz, 6H, $N(CH(CH_3)_2)_2$).

Synthesis of [NCr(NPr$^{i}_{2}$)$_2$(DBN)][I] (2-I) Under an N_2 atmosphere a 125 mL Erlenmeyer flask was loaded with **1** (2.05 g, 5.20 mmol, 1 equiv.) a stirbar and 50 mL Et_2O. To this an Et_2O (10

mL) solution of DBN (0.646 g, 5.20 mmol, 1 equiv.) was added drop wise to the flask over 5 min. The solution stirred for 1.5 h during which time the product precipitated. The suspension was filtered on a glass frit and the washed with pentane (2 × 10 mL). The solids were collected and dried under reduced pressure yielding **2-I** as an orange powder (2.195 g, 4.24 mmol, 82% yield). Diffraction quality crystals were grown from a concentrated THF solution of **2-I** held at −35 °C. ^{1}H NMR (500 MHz, $CDCl_3$, 25 °C): 5.32 (sept. J_{HH} = 6 Hz, 2H, $(CH_3)_2CH$), 3.87 (sept. J_{HH} = 6.5 Hz, 2H, $(CH_3)_2CH$), 3.75 (t J_{HH} = 7.5 Hz, 2H, DBN), 3.63 (t J_{HH} = 5 Hz, 2H, DBN), 3.48 (t J_{HH} = 6 Hz, 2H, DBN), 3.10 (t J_{HH} = 8 Hz, 2H, DBN), 2.11-2.04 (multi., 4H, DBN), 1.80 (d J_{HH} = 6 Hz, 6H, $(CH_3)_2CH$), 1.52 (d J_{HH} = 6.5 Hz, 6H, $(CH_3)_2CH$), 1.30 (d J_{HH} = 6.5 Hz, 6H, $(CH_3)_2CH$), 1.19 (d J_{HH} = 6.5 Hz, 6H, $(CH_3)_2CH$). $^{13}C\{^{1}H\}$ NMR (125 MHz, $CDCl_3$, 25 °C): 169.30, 59.44, 57.41, 55.15, 47.56, 43.68, 36.26, 30.89, 30.97, 22.79, 22.29, 20.50, 18.36. Anal. Calcd. for $C_{19}H_{40}CrIN_5$: C, 44.10; H, 7.79; N, 13.53. Found: C, 44.02; H, 7.63; N, 13.47. Mp: 168-170 °C.Anal. Calcd. for $C_{19}H_{40}CrIN_5$: C, 44.10; H, 7.79; N, 13.53. Found: C, 44.02; H, 7.63; N, 13.47. Mp: 168-170 °C

General Synthesis of [NCr(NPr$^{i}_2$)$_2$(DBN)][A] A=BF_4, PF_6, SbF_6 (2-BF_4, 2-PF_6, 2-SbF_6)

Under an N_2 atmosphere a scintillation vial was loaded with **2-I** (1 equiv.), a stirbar and toluene (5 mL). To this solution the desired sodium salt was added drop wise as a toluene solution (5 mL) over 5 min. The reaction was stirred vigorously for 1.5 h at which time the reaction mixture

was filtered through Celite. The volatiles were removed under vacuum yielding **2** as an orange powder.

[NCr(NPr$^{i}_{2}$)$_2$(DBN)][BF$_4$] (2-BF$_4$)

^{1}H NMR (300 MHz, $CDCl_3$, 25 °C): 5.20 (sept. J_{HH} = 6.3 Hz, 2H, $(CH_3)_2CH$), 3.87 (sept. J_{HH} = 6.3 Hz, 2H, $(CH_3)_2CH$), 3.68 (t J_{HH} = 7.3 Hz, 2H, DBN), 3.52-3.46 (multi, 2H, DBN), 3.39 (t J_{HH} = 6.9 Hz, 2H, DBN), 3.08 (t J_{HH} = 7.9 Hz, 2H, DBN), 1.89-1.78 (multi., 4H, DBN), 1.80 (d J_{HH} = 6.3 Hz, 6H, $(CH_3)_2CH$), 1.52 (d J_{HH} = 6.3 Hz, 6H, $(CH_3)_2CH$), 1.27 (d J_{HH} = 6.3 Hz, 6H, $(CH_3)_2CH$), 1.18 (d J_{HH} = 6.3 Hz, 6H, $(CH_3)_2CH$). ^{19}F NMR (282 MHz, $CDCl_3$, 25 °C):-153.50.

[NCr(NPr$^{i}_{2}$)$_2$(DBN)][PF$_6$] (2-PF$_6$)

^{1}H NMR (500 MHz, $CDCl_3$, 30 °C): 5.33 (sept. J_{HH} = 6.5 Hz, 2H, $(CH_3)_2CH$), 3.88 (sept. J_{HH} = 6 Hz, 2H, $(CH_3)_2CH$), 3.74 (t J_{HH} = 7.5 Hz, 2H, DBN), 3.64 (t J_{HH} = 5.5 Hz, 2H, DBN), 3.50-3.43 (multi, 4H, DBN), 3.11 (t J_{HH} = 8 Hz, 2H, DBN), 2.10-2.02 (multi., 2H, DBN), 1.81 (d J_{HH} = 6.5 Hz, 6H, $(CH_3)_2CH$), 1.53 (d J_{HH} = 6 Hz, 6H, $(CH_3)_2CH$), 1.31 (d J_{HH} = 6 Hz, 6H, $(CH_3)_2CH$), 1.20 (d J_{HH} = 6.5 Hz, 6H, $(CH_3)_2CH$). ^{19}F NMR (282 MHz, $CDCl_3$, 25 °C):-70.87, -73.39.

[NCr(NPr$^{i}_{2}$)$_2$(DBN)][SbF$_6$] (2-SbF$_6$)

^{1}H NMR (500 MHz, $CDCl_3$, 25 °C): 5.19 (sept. J_{HH} = 6.5 Hz, 2H, $(CH_3)_2CH$), 3.87 (sept. J_{HH} = 6.5 Hz, 2H, $(CH_3)_2CH$), 3.75-366 (multi, 4H, DBN), 3.49-3.43 (multi, 2H, DBN), 3.09 (t J_{HH} = 8 Hz, 2H, DBN), 2.02-1.95 (multi., 2H, DBN), 1.80 (d J_{HH} = 6 Hz, 6H, $(CH_3)_2CH$), 1.53 (d J_{HH} = 6.5 Hz, 6H, $(CH_3)_2CH$), 1.26 (d J_{HH} = 6.5 Hz, 6H, $(CH_3)_2CH$), 1.19 (d J_{HH} = 6 Hz, 6H, $(CH_3)_2CH$). ^{19}F NMR (282 MHz, $CDCl_3$, 25 °C):-72.19, -74.68.

Synthesis of [NCr(NPr$^{i}_{2}$)$_2$(DBN)][BPh$_4$] (2-BPh$_4$) Under an N_2 atmosphere a scintillation vial was loaded with **2-I** (0.044 g, 0.085 mmol, 1 equiv.), a stirbar and toluene (5 mL). To this solution sodium tetraphenylborate (0.029 g, 0.02 mmol, 1 equiv.) in toluene (5 mL) was added. The reaction was stirred for 1.5 h. The volatiles were removed under vacuum. The residue was extracted with diethyl ether (5 mL) and filtered through a frit of Celite. The remaining residue was extracted with THF (8 mL) and filtered through Celite. The organic extracts were combined causing precipitate to form. The solids were collected on a frit and dried under vacuum giving **2-BPh$_4$** as an orange powder. (0.038 g, 0.053 mmol, 62% yield). ^{1}H NMR (500 MHz, $CDCl_3$, 25 °C): 7.39 (s br., 8H, $B(C_6H_5)_4$), 7.01 (t J_{HH} = 7 Hz, 8H $B(C_6H_5)_4$), 6.87 (t J_{HH} = 6.5 Hz, 8H $B(C_6H_5)_4$), 4.92 (sept. J_{HH} = 6.5 Hz, 2H, $(CH_3)_2CH$), 3.84 (sept. J_{HH} = 6 Hz, 2H, $(CH_3)_2CH$), 3.14 (t J_{HH} = 7.5 Hz, 2H, DBN), 2.97-2.92 (multi, 4H, DBN), 2.58 (t J_{HH} = 5.5 Hz, 2H, DBN), 1.89-1.81 (multi, 2H, DBN), 1.78 (d J_{HH} = 6.5 Hz, 6H, $(CH_3)_2CH$), 1.52 (d J_{HH} = 6.5 Hz, 6H, $(CH_3)_2CH$), 1.39-1.33 (multi, 2H, DBN), 1.18 (dd J_{HH} = 3 J_{HH} = 3 Hz, 12H, $(CH_3)_2CH$).

$^{13}C\{^{1}H\}$ NMR (125 MHz, $CDCl_3$, 25 °C):169.08, 136.24, 125.49, 121.65, 59.36, 57.35, 54.68, 46.75, 42.76, 36.24, 30.84, 30.08, 22.28, 22.17, 19.74, 18.06.

Synthesis of [NCr(NPr$^{i}_{2})_2$(DBN)][OTf] (2-OTf) Under an N_2 atmosphere a scintillation vial was loaded with **2-I** (0.050 g, 0.097 mmol, 1 equiv.), a stirbar and toluene (8 mL). The solution was rapidly stirred and tetrabutlyammonium triflate (0.113 g, 0.290 mmol, 3 equiv.) was added as a solid. The vial was stirred 3 h at which time the volatiles were removed under vacuum. The residue was washed with diethyl ether (2 × 3 mL) to remove unreacted starting materials. The residue was extracted with THF (2 × 5 mL) and filtered through Celite. The volatiles were removed under vacuum yielding **2-OTf** as an orange powder (0.XXX g, 0.XXX mmol, XX% yield). ^{1}H NMR (500 MHz, $CDCl_3$, 25 °C): 5.30 (sept. J_{HH} = 6.5 Hz, 2H, $(CH_3)_2CH$), 3.90 (sept. J_{HH} = 6.5 Hz, 2H, $(CH_3)_2CH$), 3.78 (t J_{HH} = 7.5 Hz, 2H, DBN), 3.63-3.59 (multi, 2H, DBN), 3.49 (t J_{HH} = 5.5 Hz, 2H, DBN), 3.37-3.33 (multi, 2H, DBN), 3.13 (t J_{HH} = 8 Hz, 2H, DBN), 2.03-1.97 (multi., 2H, DBN), 1.84 (d J_{HH} = 6.5 Hz, 6H, $(CH_3)_2CH$), 1.56 (d J_{HH} = 6.5 Hz, 6H, $(CH_3)_2CH$), 1.32 (d J_{HH} = 6.5 Hz, 6H, $(CH_3)_2CH$), 1.22 (d J_{HH} = 6.5 Hz, 6H, $(CH_3)_2CH$). ^{19}F NMR (282 MHz, $CDCl_3$, 25 °C):−78.32.

Synthesis of [NCr(NPr$^{i}_{2})_2$(DBN)][BAr$^{F}_{4}$] (2-BAr$^{F}_{4}$) Under an N_2 atmosphere a scintillation vial was loaded with **2-I** (0.038 g, 0.074 mmol, 1 equiv.), a stirbar, and toluene (5 mL). To the rapidly stirring solution silver tetrakis(3,5-bis(trifluoromethyl)phenyl)borate (0.072 g, 0.074 mmol, 1 equiv.) was added in THF (5 mL). The reaction stirred for 2 h, and the volatiles were removed under vacuum. The residue was extracted with toluene until the toluene was clear. The

extracts were filtered through Celite and then dried under vacuum yielding **(2-BAr$^{F}_{4}$)** as an orange powder. (0.XXX g, 0.XXX mmol, XX% yield). ^{1}H NMR (500 MHz, $CDCl_3$, 25 °C): 7.67 (s br., 8H, $B(C_6H_3(CF_3)_2)_4$), 7.52 (s, 4H, $B(C_6H_3(CF_3)_2)_4$), 4.98 (sept. J_{HH} = 6.5 Hz, 2H, $(CH_3)_2CH$), 3.84 (sept. J_{HH} = 6 Hz, 2H, $(CH_3)_2CH$), 3.56 (t J_{HH} = 7.5 Hz, 2H, DBN), 3.50 (t J_{HH} = 7.5 Hz, 2H, DBN), 3.29-321 (multi, 4H, DBN), 3.14-3.04 (multi, 4H, DBN), 1.77 (d J_{HH} = 6 Hz, 6H, $(CH_3)_2CH$), 1.53 (d J_{HH} = 6 Hz, 6H, $(CH_3)_2CH$), 1.15 (dd J_{HH} = 6.3 Hz J_{HH} = 5.1 Hz, 12H, $(CH_3)_2CH$).

Synthesis of [NCr(NPr$^{i}_{2}$)$_2$(Quin)][PF$_6$] (3) Under an N_2 atmosphere a scintillation vial was loaded with **1** (0.108 mg, 0.275 mmol, 1 equiv.), a stirbar, and chloroform (8 mL). To this quinuclidine (0.031 g, 0.275 mmol, 1 equiv.) was added as a solid. The solution stirred for 5 min at which time silver hexafluorophosphate (0.069 g, 0.275 mmol, 1 equiv.) in acetonitrile (4 mL) was added drop wise over 10 min. The reaction stirred for 2 h forming a tan precipitate. The reaction was filtered, and filtrate was collected. The volitiles were removed under vacuum. The residue were washed with pentane (3 mL) and then extracted with toluene until the extracts were clear. The extracts were filtered through Celite and concentrated under vacuum to half their volume. The concentrated toluene solution was held at −35 °C yielding crystals of **3 (**0.039 g, 0.074 mmol, 27% yield). ^{1}H NMR (500 MHz, $CDCl_3$, 25 °C): 5.49 (sept J_{HH} = 6.3 Hz, 2H, $N(CH(CH_3)_2)_2$), 3.98 (sept J_{HH} = 6.3 Hz, 2H, $N(CH(CH_3)_2)_2$), 3.32 (t, J_{HH} = 8.1 Hz, 6H, $N(CH_2CH_2)_3CH$), 1.94 (d J_{HH} = 6.6 Hz, 6H, $N(CH(CH_3)_2)_2$), 1.88-1.78 (multi, 6H,

$N(CH_2CH_2)_3CH$), 1.48 (d J_{HH} = 6.6 Hz, 6H, $N(CH(CH_3)_2)_2$), 1.37 (d J_{HH} = 6.6 Hz, 6H, $N(CH(CH_3)_2)_2$), 1.27 (s, 1H, $N(CH_2CH_2)_3CH$), 1.23 (d J_{HH} = 6.3 Hz, 6H, $N(CH(CH_3)_2)_2$). ^{19}F NMR (282 MHz, $CDCl_3$, 25 °C): –72.08, –72.61. Mp: 218-221°C

Synthesis of $[NCr(NPr^i_2)_2(DMAP)][BF_4]$ (4-BF_4) Under an N_2 atmosphere a scintillation vial was loaded with **1** (0.177 g, 0.450 mmol, 1 equiv), 4-dimethylaminopyridine (0.055 g, 0.450 mmol, 1 equiv.), and a stir bar. To this vial, $CHCl_3$ (8 mL) was added, and the solution was stirred for 10 min. A solution of $AgBF_4$ (0.096 g, 0.495 mmol, 1.1 equiv.) in acetonitrile (4 mL) was added over 5 min. The reaction stirred at room temperature for 1 h. The brown suspension was filtered through a glass frit with Celite as a filtering agent. The filtrate was dried in vacuo and washed with pentane (2 mL). The residue was extracted with $CHCl_3$ (2 × 5 mL). These extracts were filtered through Celite and dried under vacuum yielding **4** (0.124 g, 0.261 mmol, 58% yield). Diffraction quality crystals of **4** were obtained by holding a concentrated toluene solution of **4** at −35 °C. ^{1}H NMR (500 MHz, $CDCl_3$, 0 °C): 8.21 (d, 2H, Ar-H, J_{HH} = 7.0 Hz), 6.68 (d, 2H, Ar-H, J_{HH} = 6.5 Hz), 5.50 (sept, 2H, $CH(CH_3)_2$, J_{HH} = 6.0 Hz), 3.93 (sept, 2H, $CH(CH_3)_2$, J_{HH} = 6.0 Hz), 3.12 (s, 6H, $N(CH_3)_2$) 1.86 (d, 6H, $CH(CH_3)_2$, J_{HH} = 6.5 Hz), 1.55 (d, 6H, $CH(CH_3)_2$, J_{HH} = 6.5 Hz), 1.23 (d, 6H, $CH(CH_3)_2$, J_{HH} = 6.5 Hz), 1.15 (d, 6H, $CH(CH_3)_2$, J_{HH} = 6.5 Hz). ^{19}F NMR (282 MHz, $CDCl_3$, 25 °C): –151.9 ppm.

Synthesis of [NCr(NPr$^{i}_{2}$)$_2$(NHC)][PF$_6$] (5) Under an N_2 atmosphere a scintillation vial was loaded with 1,3 dimethylimidazolium iodide (0.070 g, 0.312 mmol, 1.0 equiv.), a stir bar, and toluene (2 mL). In a separate vial benzyl potassium (0.041 g, 0.312 mmol, 1 equiv.) was slurried in toluene (8 mL). The suspended benzyl potassium was added to the imidazolium salt dropwise over 5 min. The combined mixture stirred vigorously for 2 h, turning from redish to clear with an off white precipitate. The solution was filtered through Celite to remove KI and any unreacted starting materials. The filtrate was then added to a new vial containing **1** (0.123, 0.312 mmol, 1 equiv.) and a stir bar. The solution stirred for 10 min and lightened slightly. To this solution, $AgPF_6$ (0.087 g, 0.343 mmol, 1.1 equiv.) in acetonitrile (4 mL) was added over 5 min. The reaction stirred for 2 h, forming a tan precipitate. The volatiles were removed in vacuo and the residue was extracted with Et_2O (3 × 5 mL). These extracts were filtered through Celite and the volatiles were removed under vacuum. Crystals of **5** were grown from the concentrated dichloromethane of **5** held at −35° C (0.063 g, 0.125 mmol, 40%). ^{1}H NMR (500 MHz, $CDCl_3$, 25 °C): 7.39 (s, 1H, NHC-*H*), 7.29 (s, 1H, NHC-*H*), 5.46 (sept J_{HH} = 6.5 Hz, 2H, N(C*H*$(CH_3)_2)_2$), 4.07 (s, 6H, NHC-(C*H*$_3)_2$), 3.98 (sept J_{HH} = 6.5 Hz, 2H, N(C*H*$(CH_3)_2)_2$), 1.74 (d J_{HH} = 6 Hz, 6H, N(CH(C*H*$_3)_2)_2$), 1.71 (d J_{HH} = 6 Hz, 6H, N(CH(C*H*$_3)_2)_2$), 1.31 (d J_{HH} = 6.5 Hz, 6H, N(CH(C*H*$_3)_2)_2$), 1.26 (d J_{HH} = 6.5 Hz, 6H, N(CH(C*H*$_3)_2)_2$). ^{13}C{^{1}H} NMR (125 MHz, $CDCl_3$, 25 °C): 260.6, 244.0, 124.5, 59.6, 57.9, 39.4, 31.2, 30.5, 23.0. ^{19}F NMR (282 MHz, $CDCl_3$, 25 °C):-71.80, −74.32. ^{31}P (202 MHz, $CDCl_3$, 25 °C):-143.78 (sept J_{PF} = 711.04 Hz, *P*F_6). Mp: 218-221 °C (dec.).

Synthesis of [NCr(NPr$^{i}_{2}$)$_2$(HMPA)][PF$_6$] (6) Under an N_2 atmosphere a scintillation vial was loaded with **1** (0.118 g, 0.300 mmol, 1 equiv.), a stirbar, and chloroform (5 mL). To the solution hexamethylphosphoramide (0.054 g, 0.300 mmol, 1 equiv.) was added. After stirring 5 min a solution of silver hexafluorophosphate (0.083 g, 0.330 mmol, 1.1 equiv.), and hexamethylphosphoramide (0.108 g, 0.600 mmol, 2 equiv.) in acetonitrile (5 mL) was added drop wise over 10 min. The reaction was stirred for 2 h. The volatiles were removed under vacuum. The residue was extracted with diethyl ether until the extracts were clear. The extracts were filtered through Celite, and concentrated under vacuum to 5 mL. The concentrated solution was held at −35° C yielding orange needles of **6** (0.056 mg, 0.095 mmol, 31.6%). ^{1}H NMR (500 MHz, $CDCl_3$, 25 °C): 5.24 (sept J_{HH} = 6 Hz, 2H, N(C*H*$(CH_3)_2)_2$), 3.93 (sept J_{HH} = 6 Hz, 2H, N(C*H*$(CH_3)_2)_2$), 2.68 (d J_{HH} = 10 Hz, 18H, OP(NC*H*$_3)_2)_3$), 1.94 (d J_{HH} = 6 Hz, 6H, N(CH(C*H*$_3)_2)_2$), 1.43 (d J_{HH} = 6.5 Hz, 6H, N(CH(C*H*$_3)_2)_2$), 1.25 (d J_{HH} = 6.5 Hz, 6H, N(CH(C*H*$_3)_2)_2$), 1.20 (d J_{HH} = 6 Hz, 6H, N(CH(C*H*$_3)_2)_2$). ^{19}F NMR (282 MHz, $CDCl_3$, 25 °C):-71.48, −74.00. ^{31}P (121 MHz, $CDCl_3$, 25 °C):37.86 (s, O*P*$(NCH_3)_2)_3$), -143.11 (sept J_{PF} = 675.3, *P*F_6).

Synthesis of [NCr(NPr$^{i}_{2}$)$_2$(P(Me)$_2$Ph)][PF$_6$] (7) Under an N_2 atmosphere a scintillation vial was loaded with **1** (0.090 g, 0.229 mmol, 1 equiv.), a stir bar, and acetonitrile (5 mL). To this dimethyl(phenyl)phosphine (0.035 g, 0.252 mmol, 1.1 equiv.) in acetonitrile (1 mL) was added, and the solution stirred for 5 min. A solution of silver tetraphenylborate (0.098 g, 0.229 mmol, 1 equiv.) in acetonitrile (3 mL) was added drop wise over 5 min. The reaction stirred for 2 h. The

volatiles were removed under vacuum. The residue was extracted with THF until the extracts were clear. The extracts were filtered through Celite and concentrated to ~3 mL. The solution was then dropped into hexane (10 mL) slowly forming a precipitate. The precipitate was collected on a frit, and dried under vacuum yielding **7** (0.XXX g, 0.XXX mmol, XX% yield). ^{1}H NMR (300 MHz, $CDCl_3$, 25 °C): 7.51 (s br., 8H, $B(C_6H_5)_4$), 7.43 (t br. J_{HH} = 9 Hz, 2H, $P(CH_3)_2C_6H_5$), 7.35 (s br., 2H, $P(CH_3)_2C_6H_5$), 7.32 (s br., 1H, $P(CH_3)_2C_6H_5$), 7.05 (s br., 8H, $B(C_6H_5)_4$), 6.89 (s br., 4H, $B(C_6H_5)_4$), 4.81 (sept J_{HH} = 6.6 Hz, 2H, $N(CH(CH_3)_2)_2$), 3.80 (sept J_{HH} = 6.3 Hz, 2H, $N(CH(CH_3)_2)_2$), 3.51-3.44 (multi, 6H $P(CH_3)_2Ph$), 1.14 (d J_{HH} = 6 Hz, 6H, $N(CH(CH_3)_2)_2$), 1.04 (d J_{HH} = 6 Hz, 6H, $N(CH(CH_3)_2)_2$), 0.86 (d J_{HH} = 7.2 Hz, 6H, $N(CH(CH_3)_2)_2$), 0.76 (d J_{HH} = 6.3 Hz, 6H, $N(CH(CH_3)_2)_2$). ^{11}B (96 MHz, $CDCl_3$, 25 °C):-6.62.

Synthesis of $[NCr(NPr^{i}_2)_2(THF)][PF_6]$ (8) Under an Under an N_2 atmosphere a scintillation vial was loaded with **1** (0.196 g, 0.498 mmol, 1 equiv.), a stirbar, and chloroform (5 mL). To this tetrahydrofuran (0.036 g, 0.498 mmol, 1 equiv.) was added, and the reaction was placed in a liquid N_2 cooled cold well for 10 min. A separate vial was loaded with $AgPF_6$ (0.127 g, 0.503 mmol, 1.01 equiv.), THF (3 drops) and acetonitrile (5 mL). The acetonitrile solution was added dropwise to the stirring chloroform solution over 5 min. After stirring an additional 15 min the volitiles were removed under vacuum. The residue was extracted with chloroform (~5 ml) and filtered through Celite on a fritted funnel. The solution was dried under vacuum and the residue extracted with Et_2O until the extracts were clear. The combine extracts were filtered through

Celite on a fritted funnel and dried under reduced pressure giving **8** as an orange powder. A saturated pentane solution (5mL) of **8** with cholorform (3 drops) was held at -35 °C giving orange needles suitable for diffraction. ^{1}H NMR (300 MHz, $CDCl_3$, -40 °C): 5.57 (s br., 2H, $N(CH(CH_3)_2)_2$), 4.15 (s, 4H, THF) 4.03 (s br., 2H, $N(CH(CH_3)_2)_2$), 2.14 (s, 4H, THF), 1.98 (d J_{HH} = 5.5 Hz, 6H, $N(CH(CH_3)_2)_2$), 1.47 (d J_{HH} = 5.5 Hz, 6H, $N(CH(CH_3)_2)_2$), 1.35 (d J_{HH} = 5 Hz, 6H, $N(CH(CH_3)_2)_2$), 1.18 (d J_{HH} = 5.5 Hz, 6H, $N(CH(CH_3)_2)_2$).

Synthesis of [NCr(NPr$^{i}_2)_2$(^{t}BuNC)][I] (9) Under an N_2 atmosphere a scintillation vial was loaded with **2-I** (0.110 g, 0.213 mmol, 1 equiv.), a stirbar, and THF (8 mL). To this *tert*-butyl isonitrile (0.019 g, 0.234 mmol, 1.1 equiv.) in THF (1 mL) was added. The reaction stirred vigorously for 1.5 h. The volatiles were removed under vacuum. The residue was titrated with pentane (2 × 5 mL) yielding an orange powder (0.XXX g, 0.XXX mmol, XX% yield). ^{1}H NMR (500 MHz, $CDCl_3$, 25 °C): 5.31 (sept J_{HH} = 6.4 Hz, 2H, $N(CH(CH_3)_2)_2$), 3.86 (sept J_{HH} = 6.4 Hz, 2H, $N(CH(CH_3)_2)_2$), 1.80 (d J_{HH} = 6.4 Hz, 6H, $N(CH(CH_3)_2)_2$), 1.52 (d J_{HH} = 6.4 Hz, 6H, $N(CH(CH_3)_2)_2$), 1.29 (d J_{HH} = 6.4 Hz, 6H, $N(CH(CH_3)_2)_2$), 1.19 (d J_{HH} = 6.4 Hz, 6H, $N(CH(CH_3)_2)_2$). FT-IR (N≡C): 2254.3 cm^{-1}

Synthesis of [NCr(NPr$^{i}_2)_2$(PzB(Et$_3$)) (10) Under an N_2 atmosphere a scintillation vial was loaded with **2-I** (0.194 g, 0.375 mmol, 1 equiv.), a stir bar, amd THF (8 mL). To this Sodium triethylpyrazolylborate (0.071 g, 0.375 mmol, 1 equiv.) in THF (3 mL) was added drop wise over 5 min. The reaction was stirred for 12 h. The volatiles were removed under vacuum. The residue

was extracted with pentane until the extracts were clear. These extracts were filtered through Celite and the volitiles removed under vacuum. The product was dissolved in benzene (2 mL) and frozen solid. The frozen solution was lyophilized under dynamic vacuum yielding **10** and a red orange powder (0.XXX g, 0.XXX mmol, XX% yield). ^{1}H NMR (500 MHz, $CDCl_3$, 25 °C): 7.67 (d J_{HH} = 1.7 Hz, 2H, $N_2C_3H_3$), 6.18 (t J_{HH} = 1.7 Hz, 1H, $N_2C_3H_3$) 5.59 (sept J_{HH} = 6.5 Hz, 2H, $N(CH(CH_3)_2)_2$), 3.76 (sept J_{HH} = 6.35 Hz, 2H, $N(CH(CH_3)_2)_2$), 1.79 (d J_{HH} = 6 Hz, 6H, $N(CH(CH_3)_2)_2$), 1.54 (d J_{HH} = 5.5 Hz, 6H, $N(CH(CH_3)_2)_2$), 1.15 (d J_{HH} = 6.5 Hz, 6H, $N(CH(CH_3)_2)_2$), 0.95 (d J_{HH} = 6.5 Hz, 6H, $N(CH(CH_3)_2)_2$), 0.63 (s br., 9H, $B(CH_2CH_3)_3$), 0.29-0.15 (multi, 6H, $B(CH_2CH_3)_3$).

REFERENCES

REFERENCES

(1) Green, M. L. H. *Journal of Organometallic Chemistry* **1995**, *500*, 127–148.

(2) Abel, E. W.; Bennett, M. A.; Wilkinson, G. *Journal of the Chemical Society (Resumed)* **1959**, 2323.

(3) Chianese, A. R.; Li, X.; Janzen, M. C.; Faller, J. W.; Crabtree, R. H. *Organometallics* **2003**, *22*, 1663–1667.

(4) Perrin, L.; Clot, E.; Eisenstein, O.; Loch, J.; Crabtree, R. H. *Inorganic Chemistry* **2001**, *40*, 5806–5811.

(5) Kelly III, R. A.; Clavier, H.; Giudice, S.; Scott, N. M.; Stevens, E. D.; Bordner, J.; Samardjiev, I.; Hoff, C. D.; Cavallo, L.; Nolan, S. P. *Organometallics* **2008**, *27*, 202–210.

(6) Gusev, D. G. *Organometallics* **2009**, *28*, 763–770.

(7) Lever, A. B. P. *Inorganic Chemistry* **1990**, *29*, 1271–1285.

(8) Lever, A. B. P. *Inorganic Chemistry* **1991**, *30*, 1980–1985.

(9) Lukens, W. W.; Smith, M. R.; Andersen, R. A. *Journal of the American Chemical Society* **1996**, *118*, 1719–1728.

(10) DiFranco, S. A.; Maciulis, N. A.; Staples, R. J.; Batrice, R. J.; Odom, A. L. *Inorganic Chemistry* **2012**, *51*, 1187–200.

(11) Jarek, R. L.; Flesher, R. J.; Shin, S. K. *Journal of Chemical Education* **1997**, *74*, 978–982.

(12) Dahlquist, F. .; Longmuir, K.; Vernet, R. B. D. *Journal of Magnetic Resonance (1969)* **1975**, *17*, 406–410.

(13) Alyea, E. C.; Basi, J. S.; Bradley, D. C.; Chisholm, M. H. *Chemical Communications* **1968**, 495.

(14) Chiu, H.-T.; Chen, Y.-P.; Chuang, S.-H.; Jen, J.-S.; Lee, G.-H.; Peng, S.-M. *Chemical Communications* **1996**, 139.

(15) DiFranco, S. a; Maciulis, N. a; Staples, R. J.; Batrice, R. J.; Odom, A. L. *Inorganic Chemistry* **2012**, *51*, 1187–200.

(16) Odom, A. L.; Cummins, C. C. *Polyhedron* **1998**, *17*, 675–688.

(17) Honeychuck, R. V.; Hersh, W. H. *Inorganic Chemistry* **1989**, *28*, 2869–2886.

(18) Benac, B. L.; Burgess, E. M.; Arduengo, A. J. *Organic Syntheses* **1986**, *64*, 92.

(19) Arduengo, A. J.; Dias, H. V. R.; Harlow, R. L.; Kline, M. **1992**, *53*, 5530–5534.

(20) Abernethy, C. D.; Clyburne, J. A. C.; Cowley, A. H.; Jones, R. A. *Journal of the American Chemical Society* **1999**, *121*, 2329–2330.

(21) Herrmann, W. A.; Elison, M.; Fischer, J.; Köcher, C.; Artus, G. R. J. *Chemistry - A European Journal* **1996**, *2*, 772–780.

(22) Coucouvanis, ed. D. *Inogranic Syntheses*; John Wiley & Sons, Inc., 2002; Vol. 33.

(23) Cotton, F. A.; Zingales, F. *Journal of the American Chemical Society* **1961**, *83*, 351–355.

(24) Ghosh, P.; Hascall, T.; Dowling, C.; Parkin, G. *Journal of the Chemical Society, Dalton Transactions* **1998**, *87*, 3355–3358.

(25) Trofimenko, S. *Chemical Reviews* **1993**, *93*, 943–980.

(26) Perrin, C. L.; Thoburn, J. D.; Kresge, A. J. *Journal of the American Chemical Society* **1992**, *114*, 8800–8807.

(27) Shi, Y.; Hall, C.; Ciszewski, J. T.; Cao, C.; Odom, A. L. *Chemical Communications* **2003**, 586–587.

(28) Swartz II, D.; Staples, R. J.; Odom, A. L. *Dalton transactions* **2011**, *40*, 7762.

(29) Allen, F. H. *Acta Crystallogr.* **2002**, *B58*, 380–388.

(30) Bondi, A. *Journal of Physical Chemistry* **1965**, *68*, 441–451.

(31) Philippe, R.; Piette, A. M. *Bulletin des Sociétés Chimiques Belges* **2010**, *64*, 600–627.

(32) Hill, W. W.; Rosenzweig, S.; Franck, E. U. *Berichte der Bunsengesellschaft für Physikalische Chemie* **1990**, *94*, 564–568.

(33) Dijkink, J.; Eriksen, K.; Goubitz, K.; van Zanden, M. N. A.; Hiemstra, H. *Tetrahedron: Asymmetry* **1996**, *7*, 515–524.

(34) Ohms, U.; Guth, H.; Treutmann, W.; Dannöhl, H.; Schweig, A.; Heger, G. *The Journal of Chemical Physics* **1985**, *83*, 273.

(35) Chao, M.; Schempp, E.; Rosenstein, D. *Acta Crystallographica Section B Structural Crystallography and Crystal Chemistry* **1977**, *33*, 1820–1823.

(36) Mitzel, N. W.; Lustig, C. *Journal of the Chemical Society, Dalton Transactions* **1999**, 3177–3183.

(37) Rosenberg, B. A.; Ludvig, E. B.; Gantmakher, A. R.; Medvedev, S. S. *Journal of Polymer Science Part C: Polymer Symposia* **2007**, *16*, 1917–1929.

(38) Vofsi, D.; Tobolsky, A. V. *Journal of Polymer Science Part A: General Papers* **1965**, *3*, 3261–3273.

(39) Bégué, J. P.; Bonnet-Delpon, D. *Organic Magnetic Resonance* **1980**, *14*, 349–355.

(40) Pyykkö, P.; Atsumi, M. *Chemistry (Weinheim an der Bergstrasse, Germany)* **2009**, *15*, 186–97.

(41) Wang, J.; Tan, G.; An, D.; Zhu, H.; Yang, Y. *Zeitschrift für Anorganische und Allgemeine Chemie* **2011**, *637*, 1597–1601.

(42) Guzei, I. a; Wendt, M. *Dalton transactions* **2006**, 3991–9.

(43) Clavier, H.; Nolan, S. P. *Chemical Communications* **2010**, *46*, 841–61.

(44) Boyle, M.; Thorn, V. M.; Quinones, N. Q. *Journal of the American Chemical Society* **1957**, *256*, 1955–1958.

(45) Van Geet, A. L. *Analytical Chemistry* **1968**, *40*, 2227–2229.

Chapter 8: Synthesis and Evaluation of 3-Ferrocenylpyrrole as a Ligand

ABSTRACT

A new synthesis for 3-ferrocenyl pyrrole is reported using a palladium catalyzed cross coupling method. Metallation onto thallium(I) using TlOEt and subsequent reaction with $NCr(NPr^{i}_{2})_2(I)$ affords $NCr(NPr^{i}_{2})_2(Pyr^{Fc})$ in 70% yield. X-ray diffraction studies on $NCr(NPr^{i}_{2})_2(Pyr^{Fc})$ reveal an η^1-bound pyrrolide in the solid state. Steric analysis was conducted using the $\%V_{bur}$ and Solid G steric parameters giving 20.5% and 19.95%, respectively. The Ligand Donation Parameter (LDP) was determined via the method of SSMT and determined to be 13.45±0.27 kcal/mol. Attempts at chemical oxidation of the ferrocenyl moiety failed with various silver salts, returning only the protonated $HPyr^{Fc}$.

8.1 Introduction

Undoubtedly, chemical mechanism plays a central role in optimizing catalyzed transformations. In the case of transition metals, the nature of the metal employed and the supporting ligand ultimately determine the observed reactivity. Lumped under the ubiquitous and broad terms of *Sterics* and *Electronics*, these characteristics can be manipulated to great effect by judicious choice of supporting ligands. It is through rational design of these two ligand properties that allows for faster reaction times, milder conditions, lower catalyst loadings, and larger substrate scopes in many transformations.

Specifically, we are interested in optimizing early transition metal mediated hydroamination; the formal addition of an N-H moiety across an unsaturated bond and related

reactions. It has been determined that one viable pathway for d^0 Ti(IV) to catalyze such reactions proceeds through the [2 + 2] cycloaddition of an alkyne to an in situ generated Ti-imido bond (Figure 8.1).[1,2] Dubbed the Bergman mechanism, this pathway shares several similarities to the related reaction of olefin metathesis, catalyzed by a d^0 molybdenum or tungsten center.[3] Here the reactivity of a metal ligand multiple bond is also exploited to form a 4 membered metallacyclic intermediate. These [2 + 2]-cycloadditions, orbitally disallowed in traditional organic chemistry are accessible by use of the metal's d manifold.[4]

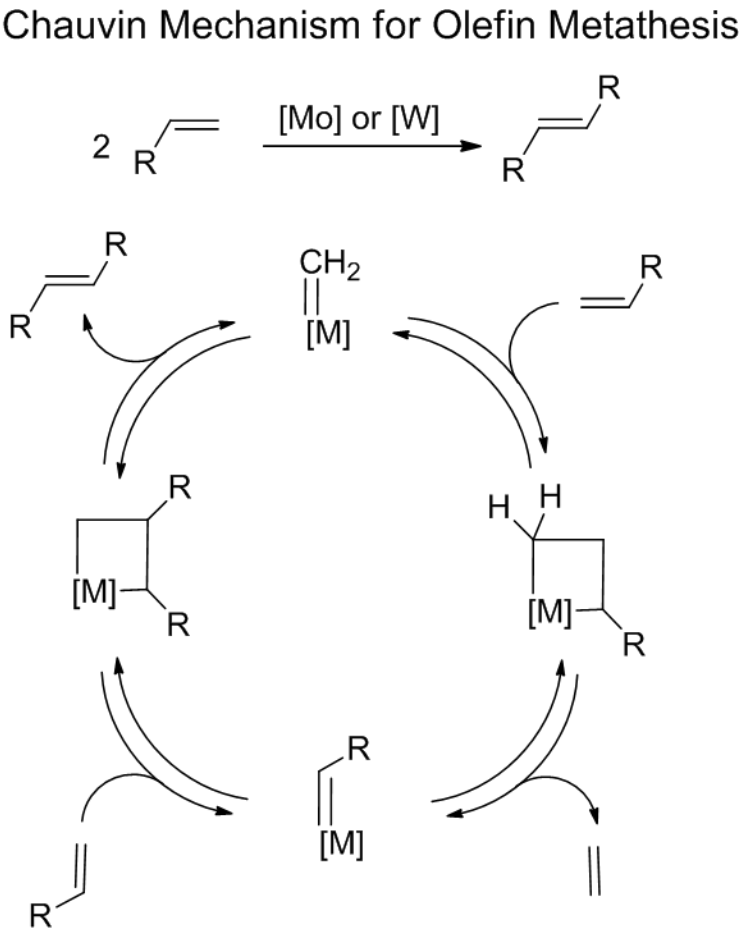

Figure 8.1: The Chauvin and Bergman mechanisms for transformations catalyzed by d^0 transition metals, both containing a [2+2]-cycloaddition step to a metal ligand multiple bond.

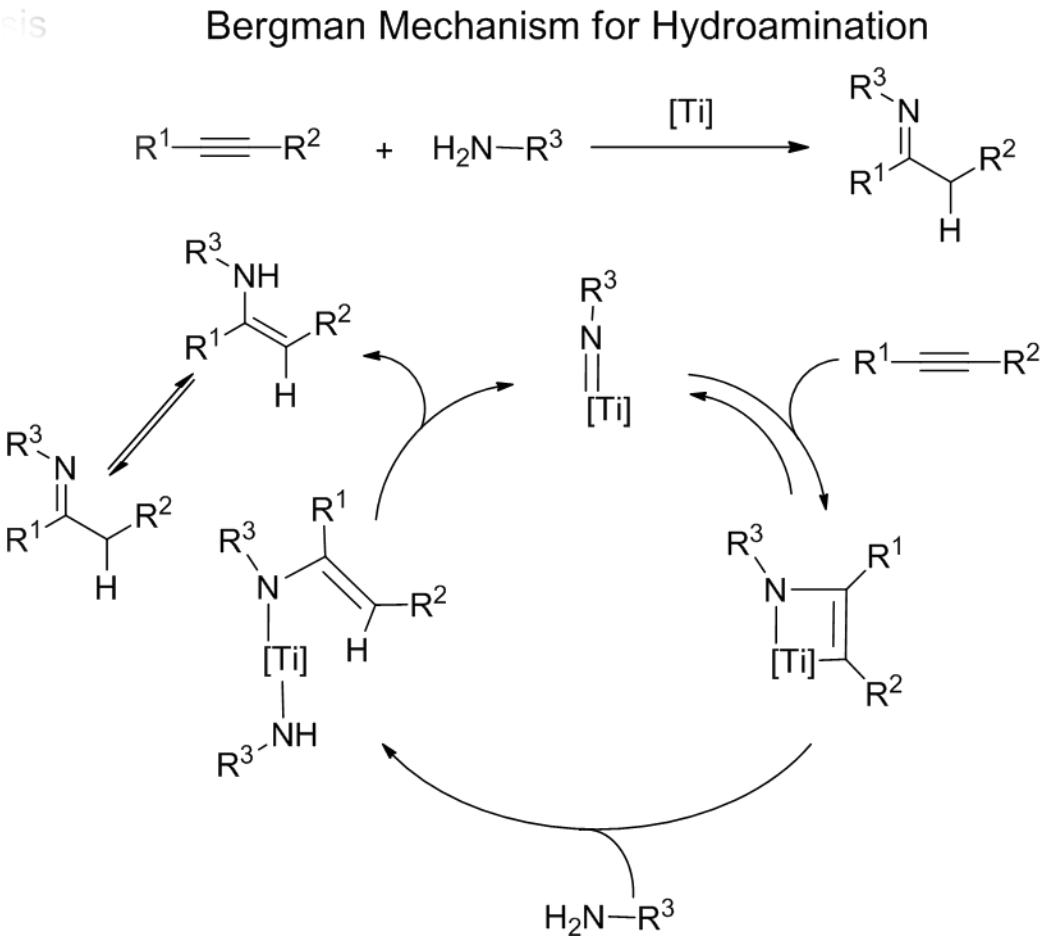

Figure 8.1(cont'd): The Chauvin and Bergman mechanisms for transformations catalyzed by d^0 transition metals, both containing a [2+2]-cycloaddition step to a metal ligand multiple bond.

Studies done by Schrock and coworkers have shown that increasing the Lewis acidity of the metal center (i.e. a more electron poor Mo(VI) or W(VI) center) greatly increases the rate by which olefin metathesis occurs.[5] In some cases this accelerated rate allows for the transformation of substrates inert to previous catalysts. Due to the similarities between the Chauvin mechanism of olefin metathesis and the Bergman mechanism of hydroamination, an analogous effect was envisioned in the latter case.

8.2 Electron Deficient Pyrrolides in Catalysis

Studies by the Odom lab demonstrate that pyrrolide supported Ti(IV) catalysts are competent to add primary amines across a wide range of alkynes.[6] Kinetic data suggests that the simple dipyrrolylmethane appended $Ti(dpm)_2(NMe_2)_2$ (where dpm is 5,5-dimethyldipyrrolylmethane[7]) shows higher rates of catalysis than that of sterically similar Cp and indolyl-based systems (Figure 8.2).[8]

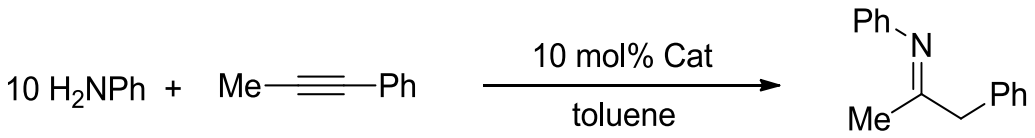

$$-\frac{d[1-\text{phenylpropyne}]}{dt} = k_{obs}t$$

Catalyst	Temperature (°C)	K_{obs}(× 10^{-7} s^{-1})
$Ti(NMe_2)_4$	75	866±94
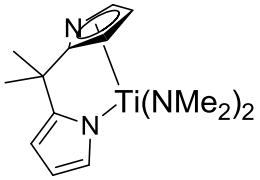	75	1976±130
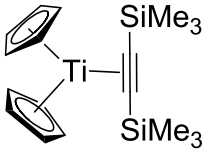	75	20±16

Figure 8.2: The hydroamination of 1-phenylpropyne with aniline under pseudo-first order conditions with vaious catalysts.

Catalyst	Temperature (°C)	$K_{obs}(\times 10^{-7}\ s^{-1})$
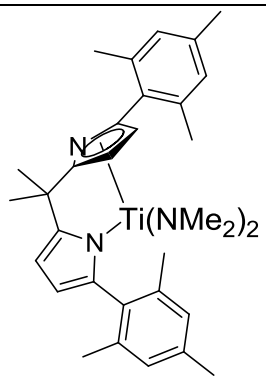	75	403±80
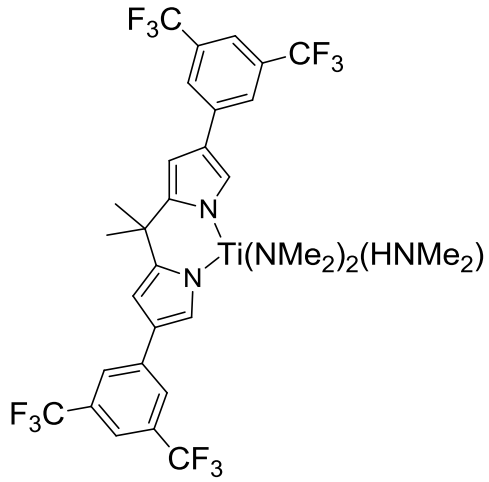	75	6963±582

Figure 8.2(cont'd): The hydroamination of 1-phenylpropyne with aniline under pseudo-first order conditions with vaious catalysts.

Catalyst	Temperature (°C)	K_{obs}(× 10^{-7} s^{-1})
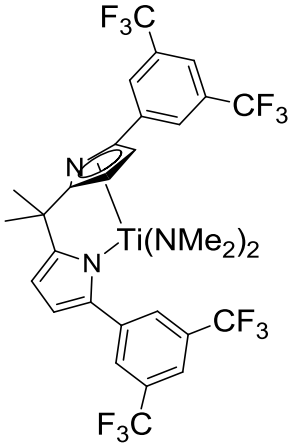	75	780±30
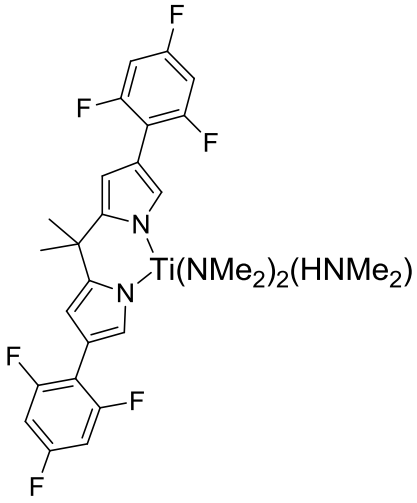	75	6225±614

Figure 8.2(cont'd): The hydroamination of 1-phenylpropyne with aniline under pseudo-first order conditions with vaious catalysts.

Moreover, homoleptic Ti(IV) bearing dimethylamide ligands are sluggish to catalyze the hydroamination of 1-phenylpropyne with aniline under similar conditions. This is arguably a manifestation of the same effect as seen in electron poor olefin metathesis catalysts, and

confirmed by comparison of the LDP of dimethylamide and pyrrolide (9.34±0.32 and 14.16±0.28 kcal/mol respectively).[9] One rationalization for the greatly reduced donor ability of pyrrolyl versus other amides is that lone pair normally localized on the N in traditional amides is delocalized over a 5 atom ring, and contributes to the aromaticity of pyrrole (Figure 8.3). This creates a situation where the π-donation from the N into empty metal d orbitals would dearomatize the 5 membered pyrrolide ligand at an energy cost approaching the aromatic stabilization energy of pyrrole (c.a. 24 kcal/mol). Additionally, significant anionic charge is localized on the α and β-positions of the pyrrolide ion. This is manifest in the organic heterocycle chemistry of pyrrole, as the α position is the preferred nucleophilic site.[10]

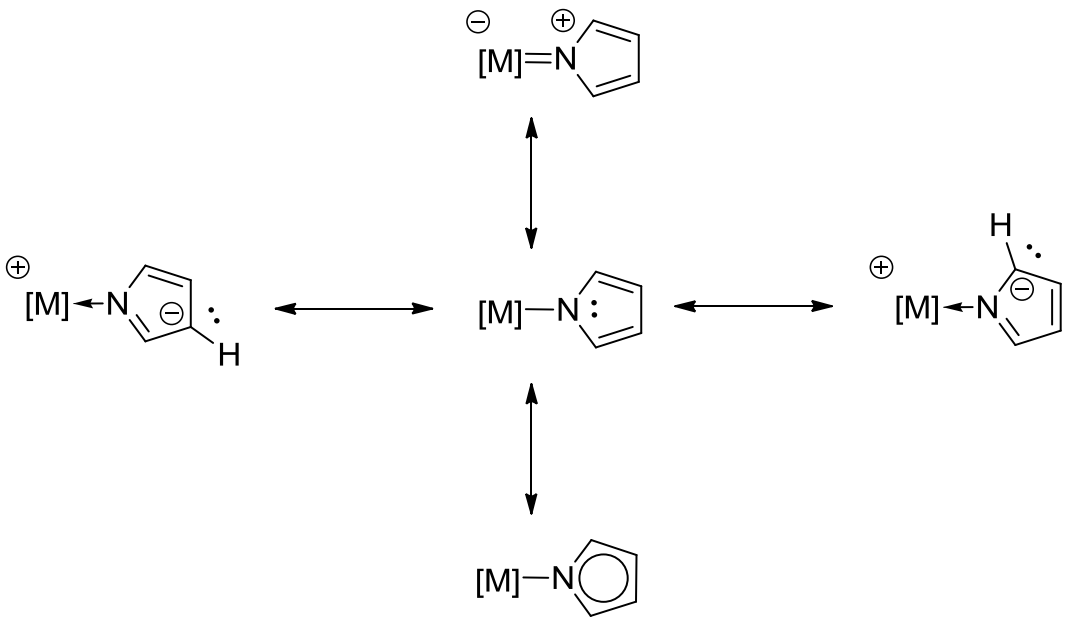

Figure 8.3: Limiting resonance structures of an η^1 bound pyrrolide to a metal capable of accepting pπ-dπ donation ranging from ligand to metal charge transfer (top) to a fully aromatic pyrrolyl (bottom).

Further exploiting this effect for greater catalyst performance, a systematic study was conducted using 2-substituted pyrroles. Synthesis of such pyrroles was facilitated by a modified Negishi coupling, a method first reported by Sadaghi and coworkers.[11] Installation of electronically withdrawing aryl moieties, as well as isosteric (yet largely electronically neutral) substituents was achieved in moderate to high yields (Figure 8.4).

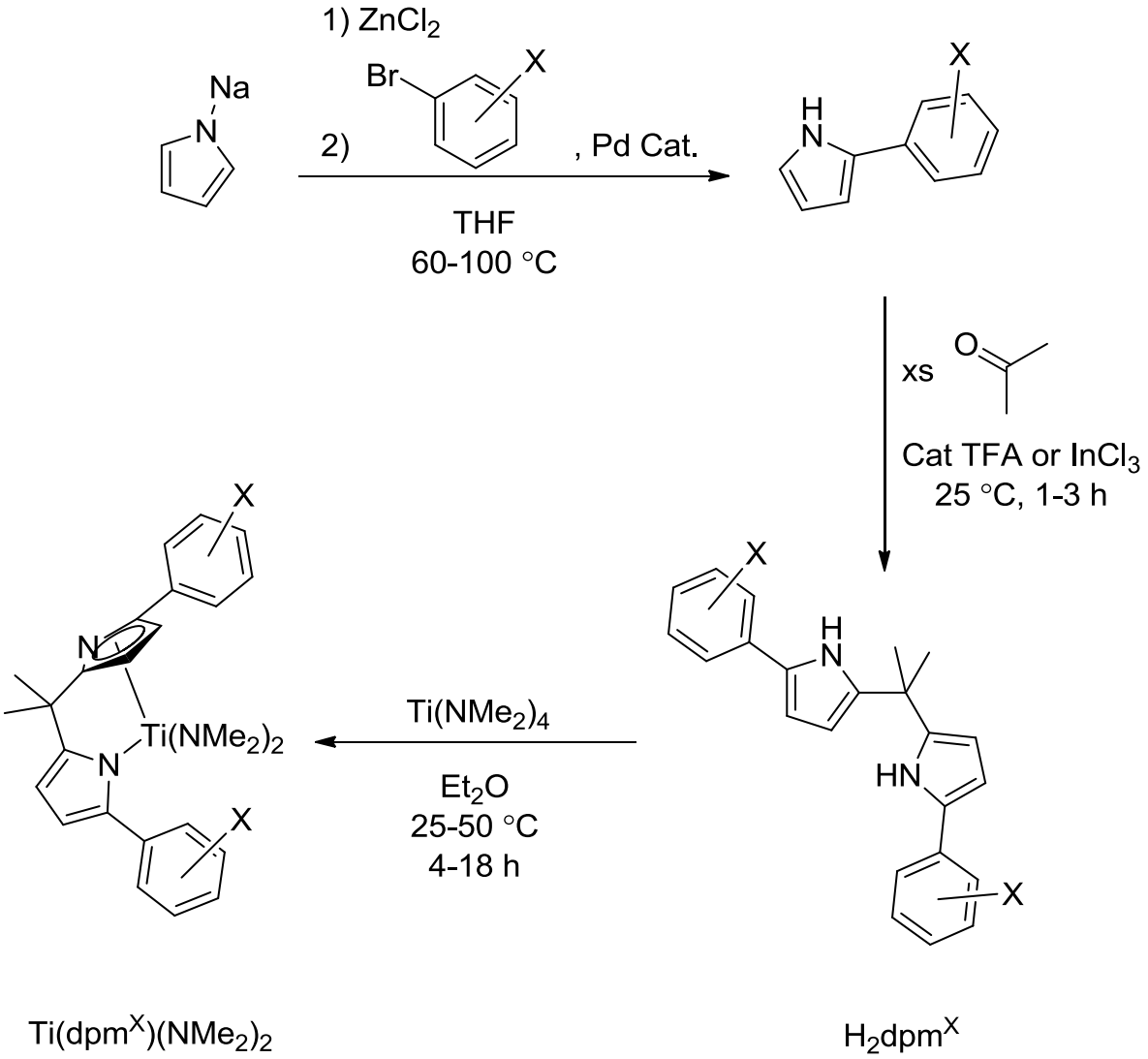

Figure 8.4: Synthesis of 2-aryl pyrroles, condensation into the bidentate ligand H_2dpm^X, and transamination onto titanium(IV)

These 2-substituted pyrroles were easily fabricated into ligands with the dpm framework via an acid-catalyzed condensation reaction with acetone (Figure 8.4). Kinetic profiles of a test hydroamination reaction under pseudo-first order conditions revealed that the increased steric inhibition caused by these appended dpm ligands offsets any increase in reactivity that incorporation of electron-deficient groups has.[12]

With this balance of sterics and electronics in mind, attention was focused on synthesis of 3-substituted, electron poor-pyrroles, which proved to be much less accessible than their 2-substituted isomers. Although similar kinetic studies on the hydroamination reaction do show an increase in the rate constant, the difficulty in synthesis and purification of 3-substituted dpm ligands precludes their practical adoption.[13]

Moreover, the observed rate increase was moderate at best, as was the variability between electron-deficient pyrroles bearing different 3-aryl rings. As reflected in their LDP values, perfluoronated Pyr^{C6F5} and the bistrifluoromethyl substituted pyrrolyl, $Pyr^{C6H3(CF3)2}$ (14.33±0.28 and 14.36±0.28 kcal/mol respectively) are indistinguishable within error. Similarly, the complexes $Ti(NMe_2)_2(dpm^{C6H3(CF3)2})$ and $Ti(NMe_2)_2(dpm^{C6H2F3})$ exhibit equivalent rate constants with the 99% confidence limit for the hydroamination reaction tested.

In light of the above study,[12] we surmised that the optimal place for the elaboration of pyrrolyl moieties in the dpm framework is at the 3-position of pyrrole due to steric congestion around the substrate binding pocket. Additionally, while the reaction rate did increase roughly three-fold, the effect of inductively removing electronic density from bound pyrrolides upon reaction rates fell short of our expectations. In turn, focus shifted to methods of creating

electronically poor pyrroles that would communicate this deficiency to the metal center via resonance.

8.3 Redox Active Ligands Bearing Cationic Charge

One such class of ligands that may fit the criteria desired, redox active ligands, has recently come into favor in a variety of applications. While supporting unprecedented redox chemistry in a wide variety of main group[14-15] and early[16] to late transition metals[17], our interest in these ligands is somewhat different. Redox active ligands, which can electronically communicate cationic charge to low valent metal centers, can increase their Lewis acidity dramatically. Sadow and coworkers have cited a related effect in the intramolecular hydroaminiation of alkenes, in which cationic charge is localized on the d^0 metal of the zwitterionic complex $[\{PhB(C_5H_4)(Ox^{Me2})_2\}Zr(NMe_2)_2]$.[18-19]

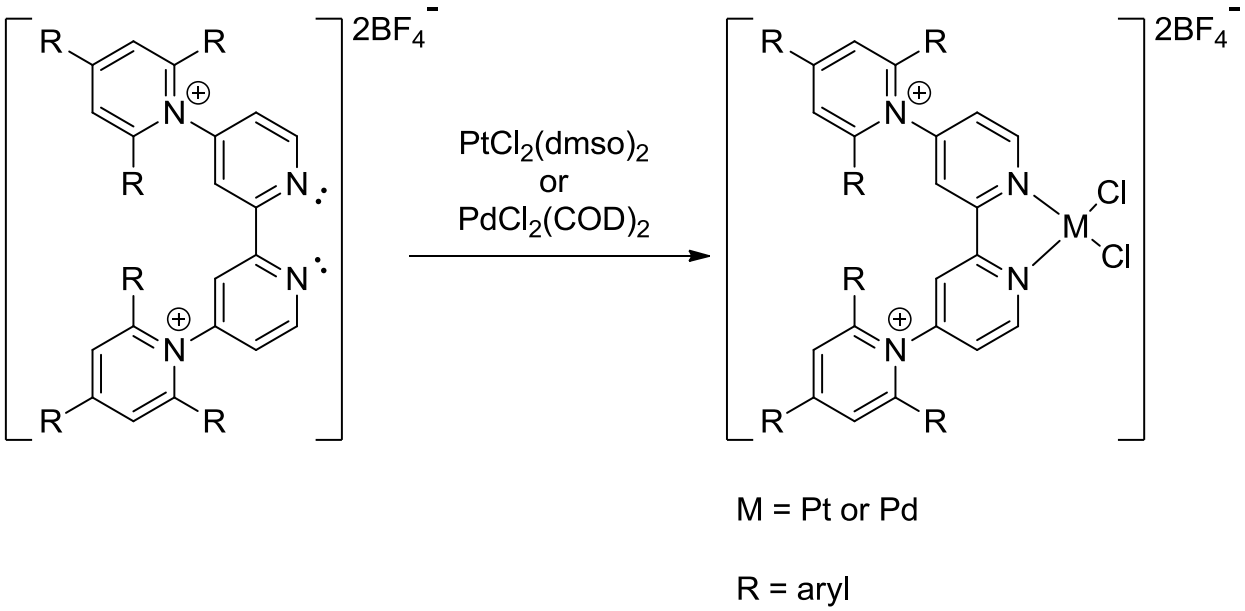

Figure 8.5: Representative synthesis of transition metal complexes bearing ligands that have cationic charge.

The Sanford lab has been investigating one such framework for Pt and Pd catalyzed H/D exchange in arenes and oxidation chemistry.[20] Computational studies have implicated a protonated (thus cationic) ligand as the active catalyst for the C-H activation in the conversion of methane to methanol.[21] Here dicationic, bidentate bipyridyl ligands support the highly electrophilic group 10 metal centers necessary for high reactivity without the need for an acidic medium (Figure 8.5).

8.4 3-Ferrocenylpyrrole

Due to the large number of pyrrolide supported titanium complexes active for hydroamination, as well as the synthetic versatility of substituted pyrroles into bi- and tridentate

ligands, we thought the incorporation of redox active units onto known architectures would be fruitful.

The redox couple of ferrocene/ferrocenium was chosen due to its presumed stability in typical reaction conditions. Moreover in a related 1996 communication by Wakatsuki et. al., a Ti(IV) complex bearing a ferrocenyl moiety in conjugation with the metal center shows unique reactivity upon oxidation.[22] Here titanocene derivatives were appended with ferrocenyl units placed in conjugation with the metal via alkynyl units. Upon treatment with 2 equiv. of the 1 e^- oxidant $AgPF_6$ the Ti-alkynyl yielded $TiCp_2F_2$ as well as a coupled alkynylferrocene compound (Figure 8.6).

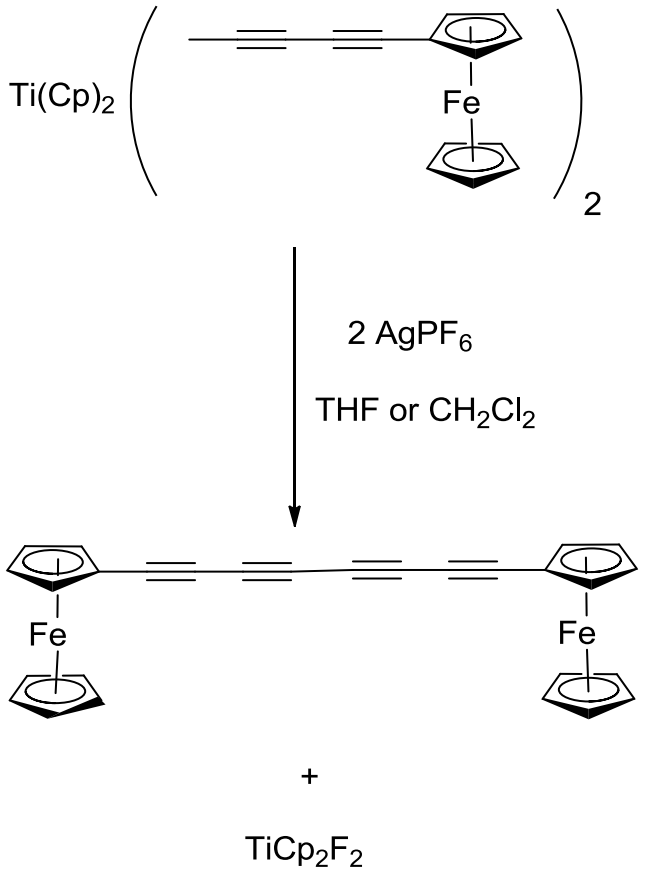

Figure 8.6: The non-classical reductive elimination of two alkynylferrocene ligands induced by chemical oxidation.

It was our hope that Ti(IV) supported by a bi- or tridentate ligand framework such as dpm would be stable toward elimination, yet still delocalize the cationic charge of a ferrocenium moiety in the 3-position, similar to the ferrocenyldiketonates of Brown and coworkers.[23]

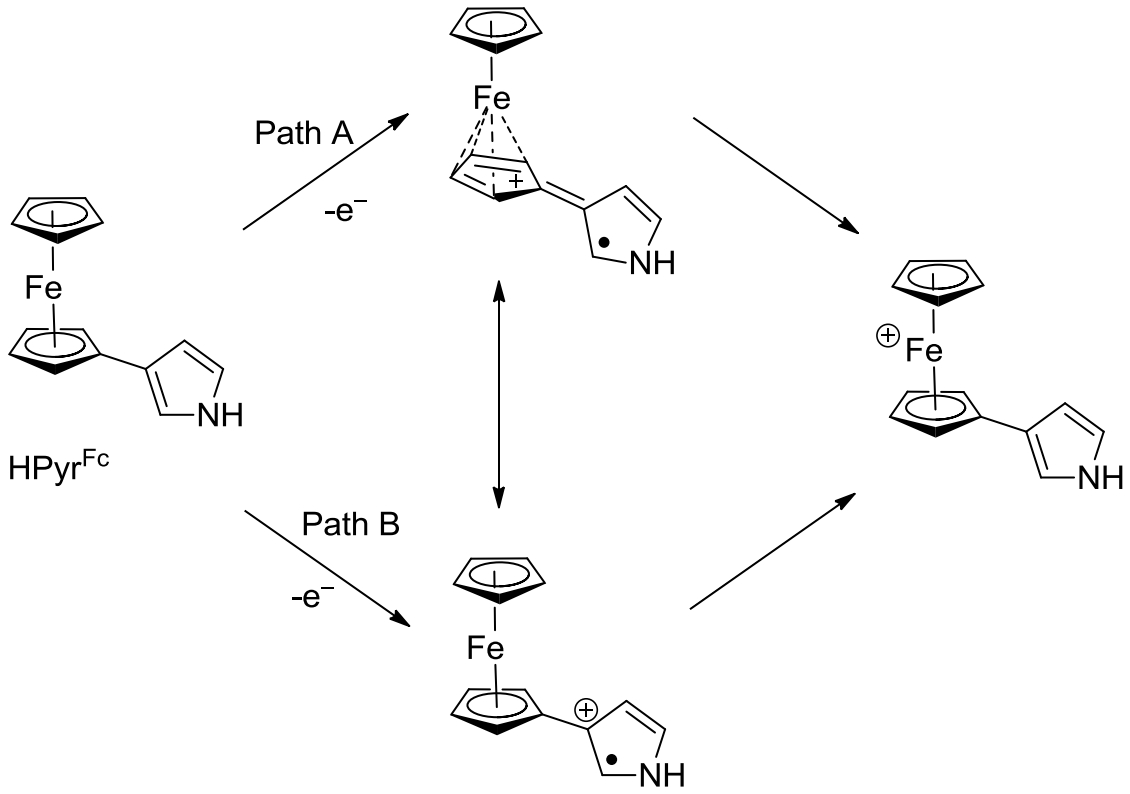

Figure 8.7: Resonance contributors in $HPyr^{Fc}$ upon $1e^-$ oxidation.

3-Ferrocenylpyrrole has already been reported[24] and is used in polymer applications.[25] The oxidation potential of $HPyr^{Fc}$ is decreases with respect to unsubstituted ferrocene, possibly due to the delocalization of charge through the π-system. The site of initial oxidation may be from ferrocene (Path A) or pyrrole (Path B). Though $HPyr^{Fc}$ is much easier to oxidize than free pyrrole, it has yet to be determined. Electron delocalization results in a planar structure described as 'fulvalene'-like by the authors. Furthermore, the effect of N-metallation on the resonance structures of $HPyr^{Fc}$ is unknown, but may lead to pyrrolide displaying characteristics indicative of an L type ligand as opposed to an anionic X type ligand.

8.5 Synthesis of 3-Ferrocenylpyrrole

Synthesis of 3-ferrocenylpyrrole was first attempted via the method outlined by Rose and coworkers (Figure 8.5).[24] Although this method did produce the desired product, it was very low yielding and required an excess of toxic KCN, chromatography using a benzene eluent, and reduction using pyrophoric DiBAl-H; thus an improved method was sought out. At the outset, cross-coupling strategies were very attractive due their direct nature.

Initial attempts sought to couple mono-borylated ferrocene with a brominated, protected pyrrole generated by reaction with NBS. This compound proved hard to separate from β-brominated, and multiply brominated *N*-TIPS-pyrrole,[25] and was highly unstable towards the typical cross-coupling conditions involving ferrocene.[26-27] Mono-borylated ferrocene[28] can be converted to bromo-ferrocene by treatment with *N*-bromosuccinimide, circumventing the difficulty in accessing monohalogenated ferrocene through more traditional routes. However, the coupling between the brominated ferrocene and the previously reported 3-BPin-*N*-Boc-pyrrole gave only trace amounts of the desired product (Figure 8.8).

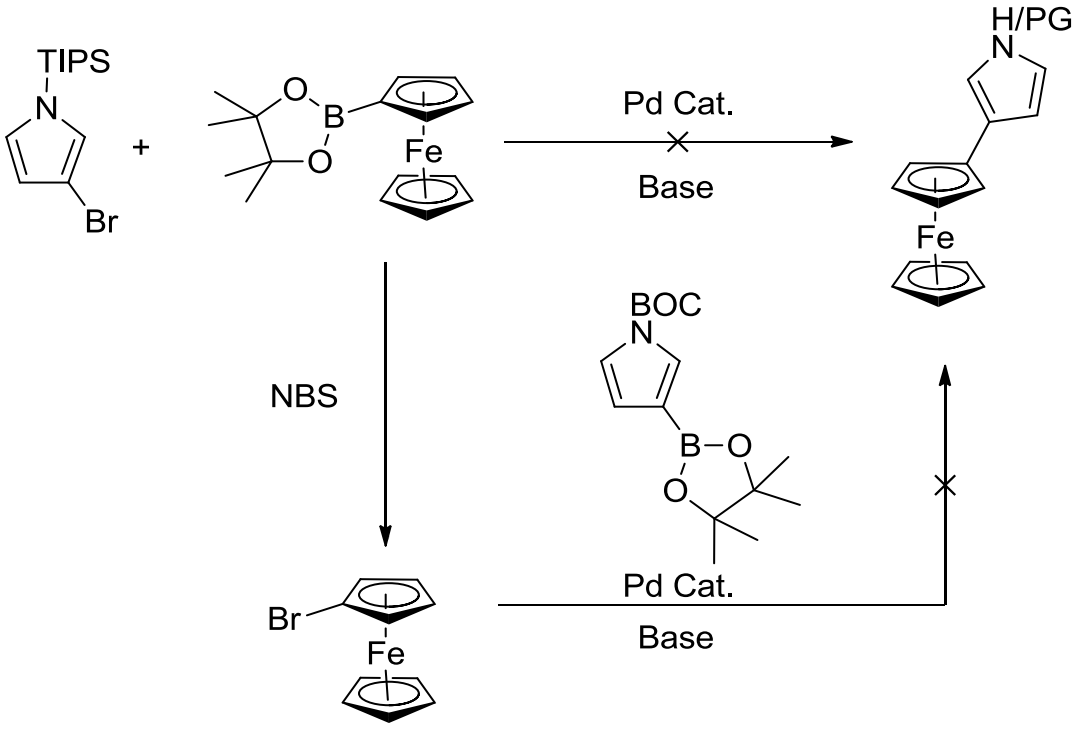

Figure 8.8: Failed cross coupling strategies in the production of HPyr^{Fc}.

A succinct albeit moderate yielding synthesis for 3-ferrocenylpyrrole was finally achieved through the Pd catalyzed cross coupling with of 3-BPin-*N*-Boc-pyrrole and iodo-ferrocene (Figure 8.9). High yielding synthesis of iodoferrocene was accomplished using the method of Kubiak, through treatment of a small excess of ferrocene with *tert*-butyllithium in cold THF, followed by the slow addition of I_2 in toluene.[29] The basic biphasic system employed was sufficient to partially remove the BOC protecting group from 3-BPin-*N*-Boc-pyrrole as well as 3-ferrocenyl-*N*-BOC-pyrrole during the reaction. An excess of 3-BPin-*N*-Boc-pyrrole (from 1.5-2 equiv.) was necessary for good yields, although unreacted 3-BPin-*N*-Boc-pyrrole as well as 3-BPin-*N*-H-pyrrole were seen in GC-FID traces taken after 12 h. Thus far extended reaction times have not increased conversion. Likewise, the premature deprotection of 3-BPin-*N*-Boc-pyrrole before coupling is exacerbated by elevated temperatures, lowering yields. 3-ferrocenyl-

N-BOC-pyrrole was purified by column chromatography on silica with 9:1 hexane:ethyl acetate as an eluent. Deprotection was achieved by treatment of 3-ferrocenyl-*N*-BOC-pyrrole with 3 equiv. of sodium methoxide in 1:1 (v/v) THF:methanol at room temperature for 45 min giving 3-ferrocenyl-pyrrole in near quantitative yield.

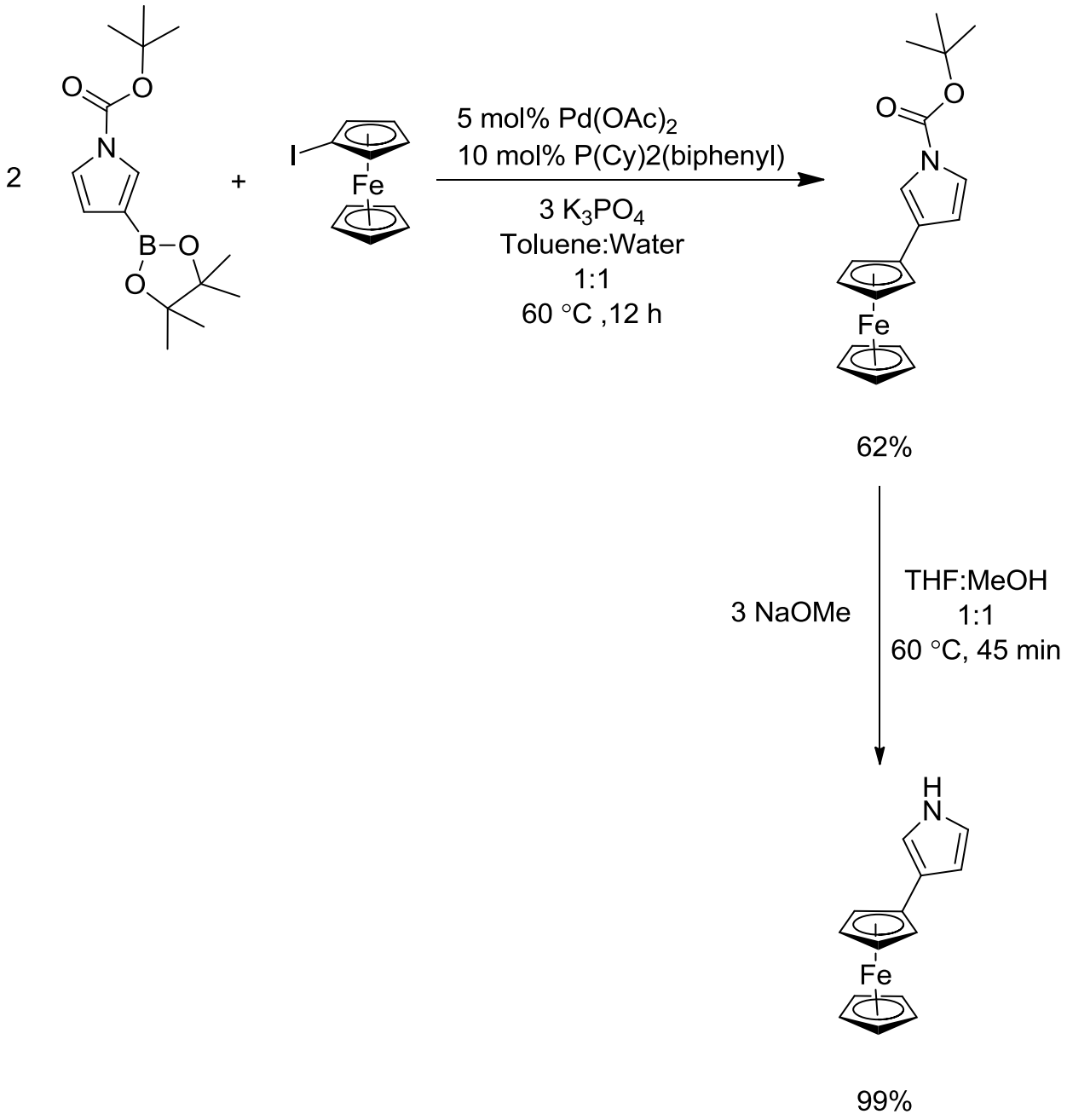

Figure 8.9: A new synthesis for 3-Ferrocenyl-*N*-BOC-pyrrole using Pd catalyzed cross-coupling and subsequent deprotection.

8.6 Synthesis of $NCr(NPr^{i}_{2})_{2}(Pyr^{Fc})$

Analogous to the synthesis of other pyrrolide compounds of the form $NCr(NPr^{i}_{2})_{2}(Pyr^{X})$, the thallium(I) salt of the pyrrolide was first generated by treating freshly purified $HPyr^{Fc}$ with 1.05 equiv. thallium(I)ethoxide in cold diethylether. After 3 h the volatiles were removed under reduced pressure, and the residue was titrated with pentane (3 × 1 mL). A stoichiometric amount of $NCr(NPr^{i}_{2})_{2}(I)$ was added in THF, affording $NCr(NPr^{i}_{2})_{2}(Pyr^{Fc})$ as a red-orange powder in 70% yield (Figure 8.10). Further purification via crystallization from pentane held at −35 °C gave crystals suitable for diffraction.

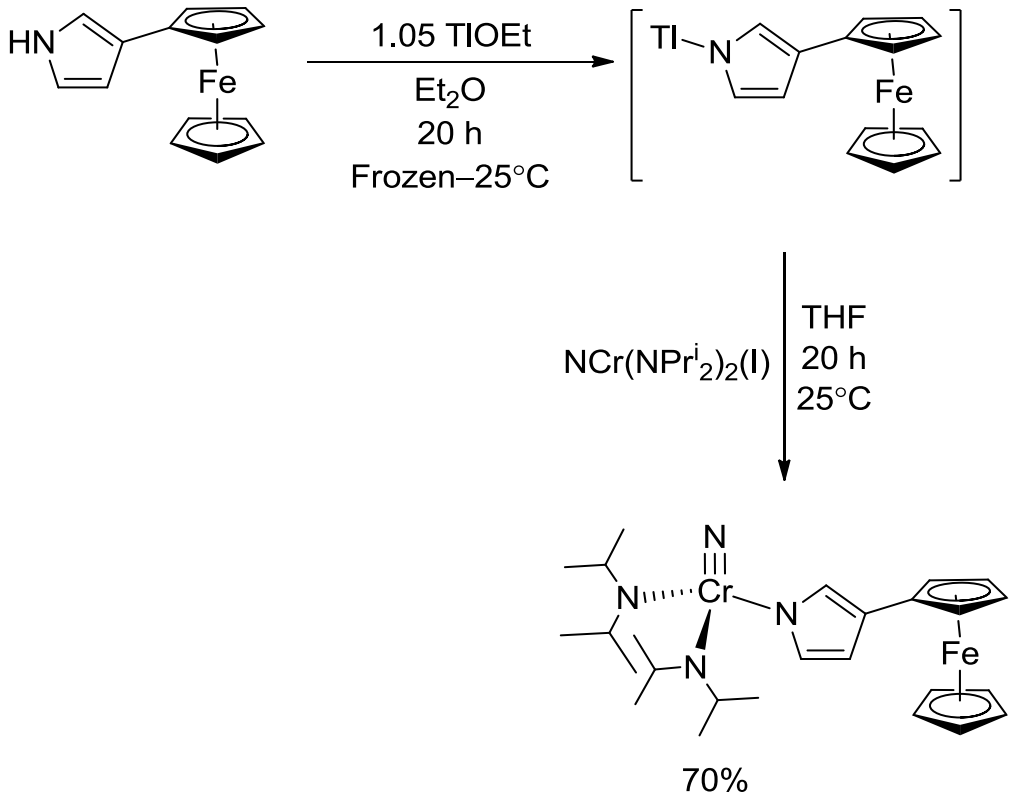

Figure 8.10: Synthesis of $NCr(NPr^{i}_{2})_2(Pyr^{Fc})$ using an in situ generated thallium(I) transmetalating reagent.

8.7 Structure and Steric Evaluation of $NCr(NPr^{i}_{2})_2(Pyr^{Fc})$

Single crystal X-ray diffraction shows an η^1-bound pyrrolide, akin to other known $NCr(NPr^{i}_{2})_2(X)$ complexes, where X = pyrrolyl and 3-substituted pyrrolyl (Figure 8.11). The determined Cr-Pyr^{Fc} bond distance of 1.938(3) Å is just within error of the Cr-Pyr bond distance (1.946(2) Å) in the unsubstituted pyrrolide, but significantly different than that of the Cr-Pyr^{C6F5} and Cr-$Pyr^{C6H3(CF3)2}$ bond lengths (1.951(1) Å and 1.966(4) Å respectively). Although Cr-X bond lengths in the previously reported ligand series are not indicative of the corresponding LDP

values, as they are complicated by other factors, this ordering makes sense for the subseries of structurally similar pyrrolides (Figure 8.12). Namely, the most donating pyrrolyl, Pyr^{Fc} (vida supra) has a bond length statistically shorter than the next two most donating pyrrolides, Pyr and Pyr^{C6F5}, whose Cr-N bond lengths are the same within ESD, and whose LDP values overlap accounting for experimental error. Of the pyrrolyls examined, the poorest donating, Cr-$Pyr^{C6H3(CF3)2}$, has both a statically longer bond length and larger LDP value than that of $NCr(NPr^{i}_{2})_2(Pyr^{Fc})$. This trend also follows that ferrocenyl substituents are generally regarded as electron donating, whereas trifluoromethyl-substituted aryls tend to be withdrawing in organic systems. Curiously, the Cr-Pyr^{Fc} bond distance is identical to the Cr-indolyl distance (1.933(2) Å) of $NCr(NPr^{i}_{2})_2$(indolyl), as well as overlapping LDP values.

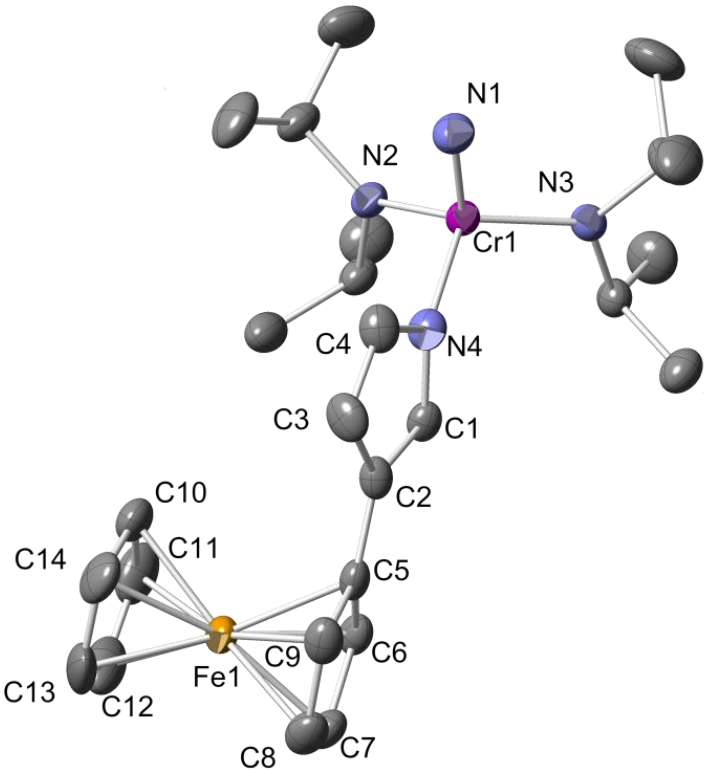

Figure 8.11: Crystal structure rendering of $NCr(NPr^{i}_{2})_2(Pyr^{Fc})$ with thermal ellipsoids at 50% probability. H atoms removed for clarity.

Features within the Pyr^{Fc} unit are largely unremarkable for substituted ferrocene, with $Fe1\text{-}Cp_{centroid}$ distances of 1.645 Å and a $Cp_{centroid}\text{-}Fe1\text{-}Cp_{centroid}$ angle of 177.15°. The dihedral angle defined by C1-C2-C5-C6 at −19.06° is relatively shallow as compared to other known 3-ferrocenyl pyrroles, suggesting a larger amount of communication between the π systems on the adjoining 5 membered rings in $NCr(NPr^{i}_{2})_2(Pyr^{Fc})$. Likewise, the C2-C5 linkage is 1.466(6) Å, slightly shorter than the $Cp\text{-}CH_2$ bond distance in

$FeCp(C_5H_4(CH_2C(CH_2OH)_2CH_3))$ at 1.501(1) Å, implying some amount of double bond character.

Compound	LDP (kcal/mol)	$\%V_{Bur}$	$G_m(L)$
$NCr(NPr^i_2)_2(Pyr^{Fc})$	13.45±0.27	20.5	19.95
$NCr(NPr^i_2)_2(Pyr)$	14.17±0.27	20.4	19.47
$NCr(NPr^i_2)_2(Pyr^{C6F5})$	14.08±0.28	20.4	19.44
$NCr(NPr^i_2)_2(Pyr^{C6H3(CF3)2})$	14.25±0.28	20.3	19.30

Table 8.1: LDP and steric parameters of pyrrolyl compounds.

The sterics of $NCr(NPr^i_2)_2(Pyr^{Fc})$ were also evaluated by the method of Solid G[30] and $\%V_{bur}$[31] and are summarized in Table 8.1. At the defined radius of 3.5 Å, approximating the first coordination sphere, the $\%V_{bur}$ parameter of $NCr(NPr^i_2)_2(Pyr^{Fc})$ is largely unaffected regardless of the 3-substitution as the entirety of the Fc unit is outside the area of enclosure, such is the case for all the 3-substituted pyrrolides examined. Slight differences may reflect the closer Cr1-pyrrolyl bond distances, lending to more of the ligand being enclosed in the first coordination sphere. This is a very promising feature in terms of implementation of the PyrFc ligand into real catalyst systems, as the sterics are largely unaffected regardless of the 3-substituant used to tune the electronics. Comparisons, among the $G_m(L)$ parameter reflect only a

modest shielding of the metal center upon substituting bound pyrrolyl, likely due to the Fc moiety overlapping area already shielded by a diisopropylamide ligand. Again, this bodes well for applications where barriers to substrate binding upon increased sterics may become an issue.

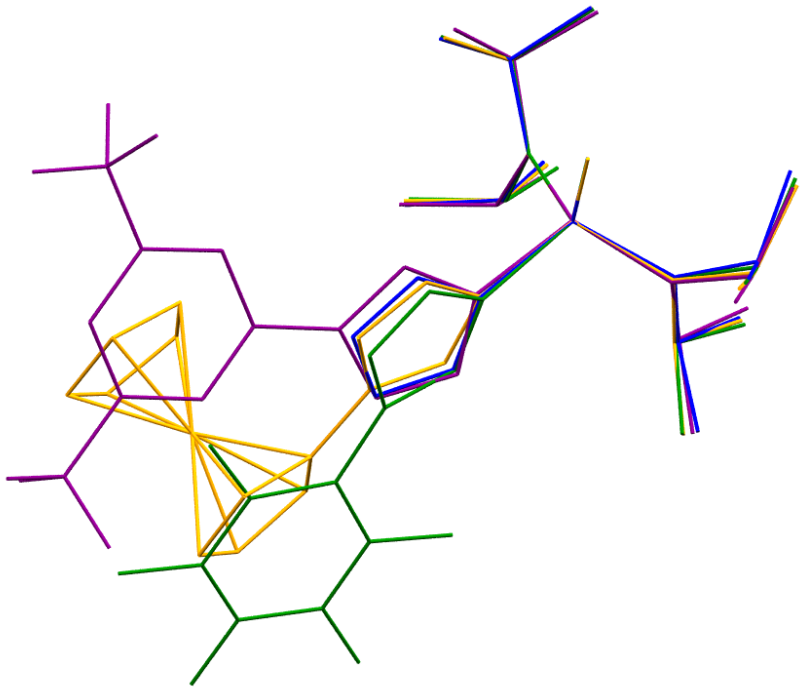

Figure 8.12: Overlaying crystal structures of $NCr(NPr^{i}_{2})_{2}(Pyr)$ (blue), $NCr(NPr^{i}_{2})_{2}(Pyr^{Fc})$ (orange), $NCr(NPr^{i}_{2})_{2}(Pyr^{C6F5})$ (green), and $NCr(NPr^{i}_{2})_{2}(Pyr^{C6H3(CF3)2})$ (purple) showing similarities in the orientation of the pyrrolyl based ligand.

8.8 LDP Determination of $NCr(NPr^{i}_{2})_{2}(Pyr^{Fc})$

In addressing the effect of redox changes at the iron site upon the d^{0} Cr center, a baseline determination of the donor ability of the ferrocenyl(II)pyrrolide ligand was needed. Through the method of Spin Saturation Magnetization Transfer as discussed earlier, the LDP was found to be

13.45±0.27 kcal/mol. This places the overall donor ability above that of unsubstituted pyrrolide (14.17±0.27 kcal/mol) and close to that of indolyl (13.76±0.27 kcal/mol). This decrease in the barrier of amide rotation clearly shows that the electron donating effect of ferrocenyl (with a Hammett parameter of $\sigma_p = -0.15$) in the 3-position of a bound pyrrolyl inductively perturbs the electronics of the metal center. Assuming the Hammett parameters are an accurate assessment of the Fc unit's effect on the *pyrrolyl* ring, it is not necessary that these correlate with the observed LDPs. LDPs are a reflection of the overall electronics at the metal, and are likely complicated by structural features, such as ligand conformation, other molecular motions, and orbital overlap. Additionally, the observed LDP is a function of *all* the ligands in the basal set. Granted the two diisopropylamide groups are consistent among the test compounds, the contribution of subtle changes in Cr-NPr^i_2 bonding induced by the variable X ligand cannot be experimentally separated. Although absolute correlation with Hammett parameters and other linear free-energy relationships developed for organic systems fail to predict ligand donation, they are qualitatively useful in making predictions in closely related subsets of the ligands explored thus far.

Making this assumption, it follows that upon oxidation the ferrocenium substituent would likely be inductively withdrawing from the pyrrolyl ring as judged by the change in sign of its Hammett parameter ($\sigma_p = 0.29$) as compared to that of ferrocene. Our real hope was that any resonance effects in combination with inductive effects would lead to a very electron deficient system, putting cationic charge on the metal center via delocalization from iron(III) through the pyrrolyl linkage.

8.9 Attempted Chemical Oxidation of $NCr(NPr^{i}_{2})_2(Pyr^{Fc})$

The chemical oxidation of $NCr(NPr^{i}_{2})_2(Pyr^{Fc})$ was attempted using silver(I) salts of $AgPF_6$, $AgSbF_6$, and $AgB(Ph)_4$ in various solvents. Unfortunately, no oxidized products were identified. While a rapid color change from orange to deep purple did occur, all chromium-containing products were either insoluble or paramagnetic, suggesting Cr(V). Interestingly, significant amounts of the *N*-H pyrrole, $HPyr^{Fc}$ were recovered along with *N*-(propan-2-ylidene)propan-2-amine, both likely β-hydride elimination products from a diisopropylamide ligand of $NCr(NPr^{i}_{2})_2(Pyr^{Fc})$. While discouraging, conditions may be found which yield the desired product through milder oxidants or electrochemical means.

8.10 Conclusions

A new cross-coupling synthesis of 3-ferrocenyl pyrrole is reported, one which affords higher yield (62%) and utilizes milder reagents. Transmetallation from thallium(I) gives the test complex $NCr(NPr^{i}_{2})_2(Pyr^{Fc})$, which was structurally characterized. Steric analysis was conducted using the $\%V_{bur}$ and Solid G steric parameters giving 20.5% and 19.95%, respectively. The Ligand Donation Parameter (LDP) was determined via the method of SSMT and determined to be 13.45±0.27 kcal/mol, placing Pyr^{Fc} as slightly more donating than pyrrole. Thus far attempts at chemical oxidation of the ferrocenyl moiety induce decomposition, yielding only protonated Pyr^{Fc}. Multidentate ligands containing 3-ferrocenyl pyrrole may ultimately prove stable in Ti complexes, competent to catalyze the hydroamination reaction.

8.11 Experimental

Synthesis of 3-ferrocenyl-*N*-BOC-pyrrole Under an inert atmosphere of N_2 a 1L Schlenk tube was loaded with 3-BPin-*N*-BOC-pyrrole (4.32 g, 14.74 mmol, 1.9 equiv.), K_3PO_4 (4.94 g, 23.27 mmol, 3 equiv.), toluene (10 mL) and a stirbar. In a separate 50 mL Erylenmeyer flask a 20 mL of a toluene solution of $Pd(OAc)_2$ (87.0 mg, 0.388 mmol, 0.05 equiv.) and [1,1'-biphenyl]-2-yldicyclohexylphosphine (272 mg, 0.775 mmol, 0.1 equiv.) was mixed. After 5 min the toluene solution was added to the Schlenk tube, and iodoferrocene (2.42 g, 7.76 mmol, 1 equiv.) was added. The tube was sealed with a Teflon stopcock and removed from the drybox. The stopcock was replaced by a septum under flowing N_2**.** Distilled water (30 mL) was degassed through 3 freeze-pump-thaw cycles and cannulated into the Schlenk tube. The septum was replaced by the Teflon stopcock, and the headspace was evacuated. The tube was placed in a 60 °C oil bath for 12 h with very vigorous stirring. The tube was removed from the oil bath and allowed to cool to room temperature, at which time the solution was filtered through a fritted funnel full of silica. The filtrate was rotovapped to near dryness. The residue was extracted with Et_2O (3 × 75 mL) and brine, and dried over Na_2SO_4. The solution was concentrated and loaded onto a silica column using 9:1 (v/v) hexane:ethyl acetate as an eluent. The product containing fractions were rotovapped to dryness, yielding 3-ferrocenyl-*N*-BOC-pyrrole as an orange powder (1.68 g, 4.78 mmol, 61.7%). ^{1}H NMR (500 MHz, $CDCl_3$, 25 °C): 7.17 (s br.,1H, Pyr-*H*), 6.31 (s br., 1H, Pyr-*H*), 6.18 (s br., 1H, Pyr-*H*), 4.44 (s br., 2H, Cp'-*H*), 4.20 (s br., 2H, Cp'-*H*), 4.04 (s, 5H, C_5H_5), 1.59 (s, 9H, O-C(CH_3)$_3$). MP 86-70 °C.

Deprotection of 3-ferrocenyl-*N*-BOC-pyrrole A 100 mL round bottom flask was loaded with 3-ferrocenyl-*N*-BOC-pyrrole (1.68 g, 4.78 mmol, 1 equiv.), a stirbar, methanol (20 mL) and THF (20 mL). To the stirring round bottom flask, sodium methoxide (0.775 g, 14.35 mmol, 3 equiv.) was added. The reaction stirred for 45 min. The volatiles were removed under reduced pressure, and the residue was titrated with pentane (3 × 5 mL). 3-ferrocenyl-*N*-H-pyrrole ($HPyr^{Fc}$) was recovered in near quantitative yield. Spectroscopy and melting point of the 3-ferrocenyl-*N*-H-pyrrole was identical to those reported in literature.

Synthesis of $NCr(NPr^{i}_{2})_2(Py^{Fc})$ Under an inert N_2 atmosphere a scintillation vial was loaded with $HPyr^{Fc}$ (0.090 g, 358 mmol, 1 equiv.), Et_2O (10 mL), and a stirbar. The vial was cooled in a liquid N_2 cooled cold well for 10 min. The vial was removed from the cold well, and thallium(I)ethanolate (0.094 g, 0.376 mmol, 1.05 equiv.) was added dropwise. The mixture was rapidly stirred for 3 h. The volatiles were removed under vacuum, and the residue was titrated with pentane (3 × 1 mL). The residue was dissolved in THF (5 mL), and $NCr(NPr^{i}_{2})_2(I)$ (0.141 g, 0.358 mmol, 1 equiv.) was in an additional 5 mL of THF. The reaction stirred for 20 h at room temperature, with a yellow precipitate of thallium(I)iodide forming. The reaction mixture was evaporated to dryness, and extracted with Et_2O until the ether ran clear. The extracts were filtered through a fritted funnel with Celite as a filtering agent. The volitiles were removed under vacuum affording $NCr(NPr^{i}_{2})_2(Pyr^{Fc})$ as a red-orange powder (0.130 g, 0.251 mmol, 70%). Further purification via crystallization from a concentrated pentane solution held at −35 °C gave crystals suitable for diffraction. ^{1}H NMR (500 MHz, $CDCl_3$, 4 °C): 6.93 (t J_{HH} = 1.5 Hz, 1H,

Pyr-*H*), 6.82 (t J_{HH} = 2.0 Hz, 1H, Pyr-*H*), 6.25-6.24 (m, 1H, Pyr-*H*), 5.09 (sept J_{HH} = 6.0 Hz, 2H, NC*H*$(CH_3)_2$), 4.40 (t J_{HH} = 1.7 Hz, 2H, Cp'-*H*), 4.01 (t J_{HH} = 1.7 Hz, 2H, Cp'-*H*), 3.96 (s, 5H, C_5H_5), 3.77 (sept J_{HH} = 6.0 Hz, 2H, NC*H*$(CH_3)_2$), 1.84 (d J_{HH} = 6.1 Hz, 6H, NCH(C*H*$_3)_2$), 1.56 (d J_{HH} = 6.35 Hz, 6H, NCH(C*H*$_3)_2$), 1.17 (d J_{HH} = 6.35 Hz, 6H, NCH(C*H*$_3)_2$), 1.08 (d J_{HH} = 6.6 Hz, 6H, NCH(C*H*$_3)_2$). ^{13}C {^{1}H} NMR (125 MHz, $CDCl_3$, 4 °C) 129.86, 125.41, 120.41, 106.80, 83.14, 69.25, 67.03, 65.69, 57.99, 55.91, 30.26, 30.15, 21.88, 21.44.

REFERENCES

REFERENCES

(1) Bisamides, Z.; Walsh, P. J.; Baranger, A. M.; Bergman, R. G. *Journal of the American Chemical Society* **1992**, *114*, 1708–1719.

(2) Baranger, A. M.; Walsh, P. J.; Bergman, R. G. *Journal of the American Chemical Society* **1993**, *115*, 2753–2763.

(3) *Makromol* **1970**, *141*, 161–176.

(4) Jorgensen, K. A. *Karl Anker Jørgensen (Eds .) Cycloaddition Reactions in Organic Synthesis*.

(5) Schrock, R. R. *Chemical Reviews* **2002**, *102*, 145–79.

(6) Odom, A. L. *Dalton Transactions* **2005**, 225–33.

(7) Littler, B. J.; Miller, M. A.; Hung, C.; Wagner, R. W.; Shea, D. F. O.; Boyle, P. D.; Lindsey, J. S.; Carolina, N. *Journal of Organic Chemistry* **1999**, *64*, 1391–1396.

(8) Shi, Y.; Hall, C.; Ciszewski, J. T.; Cao, C.; Odom, A. L. *Chemical Communications* **2003**, 586–587.

(9) DiFranco, S. A.; Maciulis, N. A.; Staples, R. J.; Batrice, R. J.; Odom, A. L. *Inorganic Chemistry* **2012**, *51*, 1187–200.

(10) Hauptmann, S.; Eicher, T. *The Chemistry of Heterocycles*; 2003; pp. 3–527.

(11) Rieth, R. D.; Mankad, N. P.; Calimano, E.; Sadighi, J. P. *Organic letters* **2004**, *6*, 3981–3.

(12) Swartz, D. L.; Odom, A. L. *Organometallics* **2006**, *25*, 6125–6133.

(13) Swartz II, D.; Staples, R. J.; Odom, A. L. *Dalton Transactions* **2011**, *40*, 7762.

(14) Myers, T. W.; Kazem, N.; Stoll, S.; Britt, R. D.; Shanmugam, M.; Berben, L. a *Journal of the American Chemical Society* **2011**, *133*, 8662–72.

(15) Myers, T. W.; Berben, L. *Inorganic chemistry* **2012**, *51*, 1480–8.

(16) Nguyen, A. I.; Blackmore, K. J.; Carter, S. M.; Zarkesh, R. a; Heyduk, A. F. *Journal of the American Chemical Society* **2009**, *131*, 3307–16.

(17) Kaim, W. *Inorganic Chemistry* **2011**, *50*, 9752–65.

(18) Manna, K.; Ellern, A.; Sadow, A. D. *Chemical Communications* **2010**, *46*, 339–41.

(19) Manna, K.; Xu, S.; Sadow, A. D. *Angewandte Chemie International Ed. in English* **2011**, *50*, 1865–8.

(20) Emmert, M. H.; Gary, J. B.; Villalobos, J. M.; Sanford, M. S. *Angewandte Chemie International Ed. in English* **2010**, *49*, 5884–6.

(21) Kua, J.; Xu, X.; Periana, R. A.; Goddard, W. A. *Organometallics* **2002**, *21*, 511–525.

(22) Hayashi, Y.; Osawa, M.; Kobayashi, K.; Wakatsuki, Y. *Chemical Communications* **1996**, *2*, 1617.

(23) Dulatas, L. T.; Brown, S. N.; Ojomo, E.; Noll, B. C.; Cavo, M. J.; Holt, P. B.; Wopperer, M. M. *Inorganic Chemistry* **2009**, *48*, 10789–99.

(24) Rose, T. L.; Kon, A. B. *Inorganic Chemistry* **1993**, *32*, 781–782.

(25) Inagaki, T.; Hunter, M.; Yang, X. Q.; Skotheim, T. A.; Okamoto, Y. *Journal of the Chemical Society, Chemical Communications* **1988**, 126.

(26) Mamane, V. *Mini-Reviews in Organic Chemistry* **2008**, *5*, 303–312.

(27) Knapp, R.; Rehahn, M. *Journal of Organometallic Chemistry* **1993**, *452*, 235–240.

(28) Datta, A.; Köllhofer, A.; Plenio, H. *Chemical Communications* **2004**, 1508–9.

(29) Goeltz, J. C.; Kubiak, C. P. *Organometallics* **2011**, *30*, 3908–3910.

(30) Guzei, I. A.; Wendt, M. *Dalton Transactions* **2006**, 3991–9.

(31) Clavier, H.; Nolan, S. P. *Chemical Communications* **2010**, *46*, 841–61.